

Synthetic and Mechanistic Investigations into Photoredox Catalysis

By

Megan Amelia Cismesia

A dissertation submitted in partial fulfillment
of the requirements for the degree of

Doctor of Philosophy

(Chemistry)

at the

UNIVERSITY OF WISCONSIN–MADISON

2015

Date of final oral examination: 07/28/2015

The dissertation is approved by the following members of the Final Oral Committee:

Tehshik P. Yoon, Professor, Chemistry

Randall H. Goldsmith, Assistant Professor, Chemistry

Clark R. Landis, Professor, Chemistry

Jennifer M. Schomaker, Associate Professor, Chemistry

Shannon S. Stahl, Professor, Chemistry

Synthetic and Mechanistic Investigations into Photoredox Catalysis

By

Megan Amelia Cismesia

Under the supervision of Professor Tehshik P. Yoon
at the University of Wisconsin–Madison

Abstract

One of the main areas of research in the Yoon group is the development of new methods using on visible light photoredox catalysis. Moreover, we are interested in studying the mechanisms of these transformations in order to understand how to optimize conditions and design new reactivity. The research herein includes the development of two synthetically useful photoredox catalyzed methodologies and the investigation of chain processes in photoredox reactions. Chapter 2 discusses the development of an intramolecular hetero-Diels–Alder reaction of bis(enones). In Chapter 3, the reductive cyclization of nitroarenes to form hydroxamic acids is described. Finally, Chapter 4 details the investigation of chain propagation in three prototypical photoredox reactions, each with a different reactive intermediate (radical cation, radical anion, neutral radical). Evidence for chain processes are given through the measurement of quantum yields and calculation of chain lengths.

Acknowledgements

I would not have been able to achieve my Ph.D. without the help of many people, and as such, I thank everyone who has been there for me these past five years. To my advisor – Prof. Tehshik Yoon, thank you letting me join your research group. Your guidance and involvement over the years have made me the chemist that I am today. I will take everything I learned from you on to my future adventures. Also, I will wait eagerly for the ReYoonion when the group can meet up together again.

To all the other professors – Thank you for all the help over the years through my requirements, supergroup meetings, recommendations, etc. Special thanks to my committee members (Prof. Clark Landis, Prof. Shannon Stahl, Prof. Jen Schomaker, Prof. Randy Goldsmith) for being a part of my thesis defense.

To all who work in the chemistry department – Thank you for all the support over the years. Thanks to the wonderful instrumentation staff (Dr. Charlie Fry, Dr. Martha Vestling, Dr. Ilia Guzei, Dr. Rob McClain) who were there for me when I needed help with the instruments. Thank you for maintaining great facilities; my research would have been much more difficult without all of your work. And a special thanks to Kat Myhre for helping me out with so much along the way to graduation.

To the Yoonicorn (a.k.a. Yoon group members) – You have been a great group of people to work alongside. Thanks for making a stressful time in my life enjoyable. You have been not only good coworkers but also great friends. My Group Fun Folder is full of a lot of great memories: mandatory fun, boat trips, pont chats, burritos, etc. Special thank you to Laura Havens, Dani Schultz, Liz Tyson, Travis Blum and Kaz Skubi for always being there for me to

talk about life or science, making me laugh, or just listening when I needed to talk. Also, thank you Anna Hurtley for making me a “welcome addition” to the Yoon group.

To my friends – Over the past few years, I have made many great friends here in Madison. Thank you to Janelle Steves, Alicia Phelps, Laura Havens, Jackie Powell and the rest of the girls’ night gang. You have made these past five years wonderful. Thanks for listening to me complain about grad school life and making me laugh about it all. And then I would also like to thank my best friend, Kat Katsma for her endless words of encouragement and support throughout my graduate studies. I am blessed to have you as my bestie, and I cannot wait for the Kat and Megan Adventures that lie in the future.

To my family – I would not be where I am without you. Thank you for supporting me throughout my entire life and especially during graduate school. To my brother, Jeff, thank you for being there for me whenever I needed you and for being a great role model to me. Thank you to my parents (Dan and Char) for instilling in me the importance of an education. I am very grateful for your support through my entire education and consider it one of the greatest gifts you have ever given me. I love you.

Table of Contents

Abstract	i
Acknowledgements	ii
Table of Contents	iv
List of Schemes	ix
List of Figures	xii
List of Tables	xv
Chapter 1. Studying Mechanism in Transition Metal Photoredox Catalysis	1
1.1 Introduction	2
1.2 Photocatalyst Quenching Studies	3
1.2.1 Electrochemical measurements of the photocatalyst and substrate	3
1.2.2 Bond dissociation energies of the substrates and additives	7
1.2.3 Spectroscopic quenching studies	10
1.2.4 Quenching fraction	15
1.3 Non-Quenching Photocatalyst Studies	17
1.4 Intermediate Studies	21
1.4.1 Characterization of reactive intermediates	21
1.4.2 Transition state studies	26
1.5 Rate Data and Isotope Effects Studies	27
1.5.1 Rate data and kinetic isotope effects	27
1.5.2 Isotopic labeling studies	29
1.6 Chain Propagation Studies	30
1.6.1 Light dependence studies	30
1.6.2 Additive effect studies	31
1.6.3 Crossover studies and kinetic isotope effects	32
1.6.4 Quantum yield measurements and chain length calculations	34
1.7 Conclusion	36

1.8 References	37
Chapter 2. Visible Light Photocatalysis of Radical Anion Hetero-Diels–Alder Cycloadditions	48
2.1 Introduction	49
2.2 Results and Discussion	50
2.3 Conclusions	56
2.4 Contributions	56
2.5 Experimental	57
2.5.1 General experimental information	57
2.5.2 Preparation of bis(enone)substrates	57
2.5.3 Experimental details for the hetero-Diels–Alder cyclization of bis(enone) substrates	65
2.5.4 Experimental details for the functionalization of cycloadduct 2.4	73
2.5.5 Stereochemical determinations	76
2.6 References	76
Chapter 3. Reductive Cyclizations of Nitroarenes to Hydroxamic Acids by Visible Light Photoredox Catalysis	80
3.1 Introduction	81
3.2 Results and Discussion	82
3.3 Conclusions	87
3.4 Experimental	88
3.4.1 General experimental information	88
3.4.2 Preparation of nitroarene substrates	88
3.4.3 Experimental details for the reductive cyclization of nitroarenes	99
3.4.4 Experimental details for the cleavage of C–O and N–O bonds	108
3.5 References	109
Chapter 4. Characterizing Chain Processes in Visible Light Photoredox Catalysis	113
4.1 Introduction	114

4.2 Results and Discussion	117
4.2.1 Photoinitiated radical cation reaction	117
4.2.2 Photoinitiated radical anion reaction	122
4.2.3 Photoinitiated neutral radical reaction	128
4.2.4 Light/Dark experiments	133
4.3 Conclusions	135
4.4 Experimental	135
4.4.1 General experimental information	135
4.4.2 Determination of light intensity	136
4.4.2.1 Determination of the light intensity at 436 nm	136
4.4.2.2 Determination of fraction of light absorbed at 436 nm for the ferrioxalate solution	137
4.4.3 Analysis of [4+2] Diels–Alder reaction	138
4.4.3.1 Proposed mechanism	138
4.4.3.2 Determination of quantum yield	139
4.4.3.3 Absorbance of catalyst	140
4.4.3.4 Lifetime measurement	141
4.4.3.5 Stern–Volmer quenching rate data	141
4.4.3.6 Simple quenching experiment	143
4.4.3.7 Chain length calculation	144
4.4.3.8 Light/dark experiment	144
4.4.3.9 Non-photochemical [4+2] reaction	145
4.4.4 Analysis of [2+2] cycloaddition reaction	146
4.4.4.1 Determination of quantum yield	146
4.4.4.2 Absorbance of catalyst	147
4.4.4.3 Stern–Volmer quenching rate data	147
4.4.4.4 Simple quenching experiment	149
4.4.4.5 Chain length calculation	149

4.4.4.6 Light/dark experiment	150
4.4.5 Analysis of α -alkylation of aldehydes reaction	151
4.4.5.1 Determination of quantum yield	151
4.4.5.2 Absorbance of catalyst	152
4.4.5.3 Stern–Volmer quenching rate data	152
4.4.5.4 Simple quenching experiment	153
4.4.5.5 Chain length calculation	154
4.4.5.6 Light/dark experiment	154
4.4.6 <i>N,N</i> -dimethyl- <i>p</i> -toluidine studies	155
4.4.6.1 Stern–Volmer quenching data	155
4.4.6.2 Time course experiments	156
4.4.6.3 Experiments without Ru(bpy) ₃ Cl ₂	157
4.4.6.4 Determination of enantioselectivity	158
4.5 References	160
Appendix A. Dihydroxylation and Aminohydroxylation of Alkenes	167
A.1 Introduction	168
A.2 Results and Discussion	170
A.2.1 Dihydroxylation of alkenes by cyclic peroxides	170
A.2.2 Aminohydroxylation of styrene by cyclic hydroxylamines	176
A.3 Conclusions and Future Directions	179
A.4 Experimental	180
A.4.1 Synthesis of phthaloyl peroxide A.10	180
A.4.2 General method for the dihydroxylation of styrene	180
A.4.3 Synthesis of aminohydroxylating reagents A.27, A.29–A.32	180
A.4.4 General method for the aminohydroxylation of styrene	181
A.5 References	181

Appendix B. Brønsted Acid Catalysis using Cysteic Acids	183
B.1 Introduction	184
B.2 Results and Discussion	184
B.3 Conclusions and Future Directions	189
B.4 Experimental	190
B.4.1 Synthesis of cysteic acids	190
B.5 References	191
Appendix C. ^1H and ^{13}C NMR spectra for new compounds	192
C.1 List of Compounds from Chapter 2	193
C.2 List of Compounds from Chapter 3	218
Appendix D. X-Ray crystallographic data	247
D.1 Compound 2.4	249
D.2 Compound 2.24	260

List of Schemes**Chapter 1**

Scheme 1-1.	Redox potentials of Ru(bpy) ₃ ²⁺ vs. SCE in MeCN	4
Scheme 1-2.	Oxidative [2+2] cycloaddition of anethole	5
Scheme 1-3.	Photocatalytic thiol-ene reaction and proposed redox mediator mechanism	6
Scheme 1-4.	Proposed PCET mechanism of the ketyl-olefin coupling	8
Scheme 1-5.	C–H arylation of benzylic ethers and the proposed mechanism	9
Scheme 1-6.	Proposed HAT mechanism in thiol-ene reaction	10
Scheme 1-7.	Coupling of ethers and imines and proposed mechanism	12
Scheme 1-8.	Amination of nitrogen heterocycles	13
Scheme 1-9.	Fluorination of aryl ethers	13
Scheme 1-10.	Debromination of vicinal dibromides	14
Scheme 1-11.	Hydrodebromination of glucosides and the proposed mechanism	18
Scheme 1-12.	Proposed mechanism of phenol oxidation and cyclization with styrenes	19
Scheme 1-13.	Alkylation of indoles	21
Scheme 1-14.	Amidation of keto acid 1.63	22
Scheme 1-15.	Radical clock experiment	23
Scheme 1-16.	Aldehyde cleavage TEMPO trapping experiment and proposed mechanism	24
Scheme 1-17.	Evidence for a carbocation and radical-polar mechanism in the ATRA reaction	25
Scheme 1-18.	Hydroamination of styrenes and the proposed intermediate	26
Scheme 1-19.	Proposed mechanism for hydrodebromination of glucosides	27
Scheme 1-20.	Proposed mechanism of the α -amino radical addition	28
Scheme 1-21.	Isotopic labeling experiments and the proposed mechanism	29
Scheme 1-22.	Generic reaction scheme involving both chain propagation and closed cycle	30
Scheme 1-23.	Evidence for chain propagation and proposed mechanism	33

Scheme 1-24. Quantum yield and chain length for eqs 1-3, 1-4, and 1-5	36
Chapter 2	
Scheme 2-1. Photocatalytic [2+2] and [4+2] cycloadditions	50
Scheme 2-2. Proposed mechanism for regioselective hetero-Diels–Alder cycloaddition of unsymmetrical bis(enone) 2.19	54
Scheme 2-3. Diastereoselective functionalization of 2.4	55
Chapter 3	
Scheme 3-1. Preparation of hydroxamic acids by reduction and cyclization of nitroarenes	82
Scheme 3-2. Origin of overreduction of 3.6	86
Scheme 3-3. Manipulation of <i>N</i> -Boc hydroxamic acids	87
Chapter 4	
Scheme 4-1. Generalized mechanism for oxidative photoredox reactions	115
Scheme 4-2. Chain and closed mechanism for a radical cation Diels–Alder cycloaddition	118
Scheme 4-3. Calculating quantum yield for photocatalytic radical cation Diels–Alder cycloaddition	120
Scheme 4-4. Calculating chain length for chemically induced radical cation Diels–Alder cycloaddition	122
Scheme 4-5. Mechanistic proposal for the radical anion [2+2] cycloaddition	123
Scheme 4-6. Mechanistic proposal for organocatalytic photoredox α -alkylation of aldehydes	128
Scheme 4-7. Quantum yield measurement for the organocatalytic photoredox α -aldehyde alkylation	130
Scheme 4-8. Proposed mechanism of the [4+2] radical Diels–Alder reaction between anethole (4.1) and isoprene (4.2)	138
Scheme 4-9. [4+2] Reaction between anethole and isoprene	139
Scheme 4-10. Aminium initiated [4+2] reaction between anethole and isoprene	145
Scheme 4-11. [2+2] Cycloaddition of bis(enone) 4.6	146
Scheme 4-12. Asymmetric α -alkylation of octanal by diethyl bromomalonate	151
Scheme 4-13. Asymmetric α -alkylation of octanal in the absence of Ru(bpy) ₃ Cl ₂	157

Scheme 4-14. Conversion of 4.10 into the corresponding hydrazone	158
Appendix A	
Scheme A-1. Regioselective aminohydroxylation of styrene	168
Scheme A-2. Possible formation of 4 stereoisomers in the aminohydroxylation of styrene	169
Scheme A-3. Dihydroxylation of alkenes by cyclic peroxides	169

List of Figures

Chapter 1

- Figure 1-1.** Structure of Ru(bpy)₃Cl₂ (**1.1**[Cl₂]) and Ir(ppy)₂(dtbpy)(PF₆) (**1.2**[PF₆]) 2
- Figure 1-2.** (A) Typical luminescence quenching experiment plot 11
(B) Stern–Volmer plot
- Figure 1-3.** Comparison of rates of the alkylation reaction in the presence and absence of *N,N*-dimethyl-*p*-toluidine 17
- Figure 1-4.** Comparison of the precatalyst **1.66** and the proposed catalyst **1.67** 20
- Figure 1-5.** General example of a positive (A) and negative (B) light/dark experiment 31

Chapter 4

- Figure 4-1.** UV-vis absorption spectrum for Ru(bpz)₃(BArF)₂ at 4×10^{-4} M in CH₂Cl₂ 120
- Figure 4-2.** Stern–Volmer quenching studies for (A) *i*-Pr₂NEt, (B) LiBF₄, and (C) enone **4.6**. 125
- Figure 4-3.** Phosphorescence intensity during reaction 127
- Figure 4-4.** Effect of exogenous co-catalytic reductive quencher 132
- Figure 4-5.** “Light/dark” experiments for (A) the radical cation [4+2] cycloaddition, (B) radical anion [2+2] cycloaddition, and (C) photoredox aldehyde alkylation reaction 134
- Figure 4-6.** Absorbance of the ferrioxalate actinometer solution 138
- Figure 4-7.** Absorbance of a 4×10^{-4} M solution of Ru(bpz)₃(BArF)₂ in CH₂Cl₂ 140
- Figure 4-8.** Absorbance of a 4×10^{-6} M solution of Ru(bpz)₃(BArF)₂ in CH₂Cl₂ 140
- Figure 4-9.** Stern–Volmer quenching experiment of Ru(bpz)₃(BArF)₂ and anethole. For anethole, $k_q = 1.4 \times 10^9 \text{ M}^{-1} \text{ s}^{-1}$. 142
- Figure 4-10.** Stern–Volmer quenching experiment of Ru(bpz)₃(BArF)₂ and isoprene. No quenching observed. 142
- Figure 4-11.** Phosphorescence intensity of the reaction over 90 s with (red line) and without (blue line) anethole. For this reaction, $Q = 0.96$. 144
- Figure 4-12.** Light/dark experiment 145
- Figure 4-13.** Absorbance of a 1.0×10^{-3} M solution of Ru(bpy)₃Cl₂ in MeCN 147

Figure 4-14. Stern–Volmer quenching of Ru(bpy) ₃ Cl ₂ and <i>i</i> -Pr ₂ NEt. For the amine, $k_q = 7.8 \times 10^6 \text{ M}^{-1} \text{ s}^{-1}$.	148
Figure 4-15. Stern–Volmer quenching of Ru(bpy) ₃ Cl ₂ and LiBF ₄ . No quenching observed.	148
Figure 4-16. Stern–Volmer quenching of Ru(bpy) ₃ Cl ₂ and the bis(enone) 4.6 starting material. No quenching observed.	148
Figure 4-17. Phosphorescence intensity of the reaction over 90 s with (red line) and without (blue line) <i>i</i> -Pr ₂ NEt. For this reaction, $Q = 0.50$.	149
Figure 4-18. Light/dark experiment	150
Figure 4-19. Absorbance of a $2.5 \times 10^{-3} \text{ M}$ solution of Ru(bpy) ₃ Cl ₂ in DMF	152
Figure 4-20. Phosphorescence intensity of the reaction over 90 s with (red line) and without (blue line) organocatalyst 4.12 . For this reaction, $Q = 0.10$.	154
Figure 4-21. Light/dark experiment	155
Figure 4-22. Stern–Volmer quenching of Ru(bpy) ₃ Cl ₂ and <i>N,N</i> -dimethyl- <i>p</i> -toluidine. For the amine, $k_q = 3.9 \times 10^8 \text{ M}^{-1} \text{ s}^{-1}$.	155
Figure 4-23. Time course of the reaction with (blue line) and without (red line) <i>N,N</i> -dimethyl- <i>p</i> -toluidine.	157
Figure 4-24. SFC chromatogram of racemic hydrazone 4.19	159
Figure 4-25. SFC chromatogram of 4.19 (90% ee) from 4.13 that was synthesized using the standard conditions reported by MacMillan	159
Figure 4-26. SFC chromatogram of 4.19 (88% ee) from 4.13 that was synthesized using the method with <i>N,N</i> -dimethyl- <i>p</i> -toluidine.	160
Appendix A	
Figure A-1. Enantioselective ligand screen	174
Figure A-2. Different alkenes and peroxides investigated	176
Appendix B	
Figure B-1. Structure of the cysteic acids	185

Appendix D

- Figure D-1.** A molecular drawing of yoon15. All H atoms are omitted. 251
- Figure D-2.** The two stereoisomers of yoon15 superimposed (one molecule had to be inverted). All H atoms are omitted. 251
- Figure D-3.** A molecular drawing of yoon27. The H atoms on the non-chiral C atoms are omitted. 262

List of Tables

Chapter 1

Table 1-1.	Ketyl-olefin coupling reported by Knowles	7
Table 1-2.	Comparison of photocatalysts for the hydroxylation of arylboronic acids	15

Chapter 2

Table 2-1.	Optimization of [4+2] cycloaddition 2.3	51
Table 2-2.	Scope of the photocatalytic [4+2] cycloaddition	53

Chapter 3

Table 3-1.	Optimization studies for photocatalytic hydroxamic acid synthesis	83
Table 3-2.	Scope studies for hydroxamic acid synthesis	85

Appendix A

Table A-1.	Preliminary metal catalyst screen for the dihydroxylation of styrene	171
Table A-2.	Copper screen for the dihydroxylation of styrene	172
Table A-3.	Peroxide equivalent screen	173
Table A-4.	Copper metal screen with ligand A.15	175
Table A-5.	Metal catalyst screen in the aminohydroxylation of styrene	177
Table A-6.	Investigation of the protecting group of the oxidant	178
Table A-7.	Stoichiometric use of copper salts and the effect of temperature	179

Appendix B

Table B-1.	Solvent screen for the reduction of imines	186
Table B-2.	Alteration of the <i>N</i> -terminus of the cysteic acid catalyst	187
Table B-3.	Alteration of the <i>C</i> -terminus of the cysteic acid catalyst	188
Table B-4.	Examination of dipeptide catalysts	189

Appendix D

Table D-1.	Crystal data and structure refinement for yoon15	252
Table D-2.	Atomic coordinates ($\times 10^4$) and equivalent isotropic displacement parameters ($\text{\AA}^2 \times 10^3$) for yoon15. $U(\text{eq})$ is defined as one third of the trace of the orthogonalized U^{ij} tensor.	253

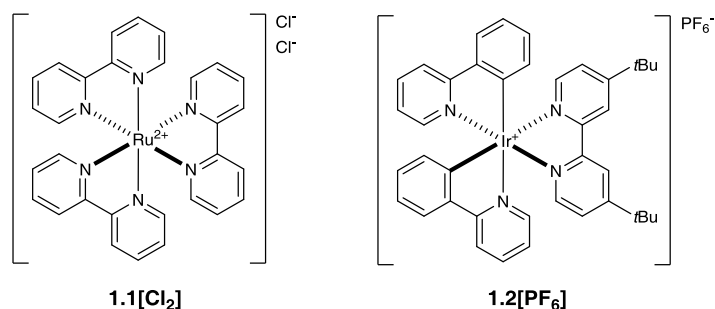
Table D-3.	Bond lengths [\AA] and angles [$^{\circ}$] for yoon15	254
Table D-4.	Anisotropic displacement parameters ($\text{\AA}^2 \times 10^3$) for yoon15. The anisotropic displacement factor exponent takes the form: $-2p^2 [h^2 a^{*2} U^{11} + \dots + 2 h k a^* b^* U^{12}]$	257
Table D-5.	Hydrogen coordinates ($\times 10^4$) and isotropic displacement parameters ($\text{\AA}^2 \times 10^3$) for yoon15	258
Table D-6.	Torsion angles [$^{\circ}$] for yoon15	259
Table D-7.	Crystal data and structure refinement for yoon27	263
Table D-8.	Atomic coordinates ($\times 10^4$) and equivalent isotropic displacement parameters ($\text{\AA}^2 \times 10^3$) for yoon27. $U(\text{eq})$ is defined as one third of the trace of the orthogonalized U^{ij} tensor.	264
Table D-9.	Bond lengths [\AA] and angles [$^{\circ}$] for yoon27	265
Table D-10.	Anisotropic displacement parameters ($\text{\AA}^2 \times 10^3$) for yoon27. The anisotropic displacement factor exponent takes the form: $-2p^2 [h^2 a^{*2} U^{11} + \dots + 2 h k a^* b^* U^{12}]$	267
Table D-11.	Hydrogen coordinates ($\times 10^4$) and isotropic displacement parameters ($\text{\AA}^2 \times 10^3$) for yoon27	268
Table D-12.	Torsion angles [$^{\circ}$] for yoon27	269

Chapter 1. Studying Mechanism in Transition Metal Photoredox Catalysis

1.1 Introduction

Although organic photochemistry has been a subject of study for over a century,¹ its use in synthesis has been relatively limited. This may in part be due to the fact that most organic molecules absorb only ultraviolet (UV) light. Synthetic photochemical reactions therefore require high-energy light sources and often do not tolerate a variety of photosensitive functional groups. One increasingly common strategy to avoid these issues is the use of a photocatalyst that can absorb lower-energy light and transfer the chemical potential to the desired substrate. By using a photocatalyst that absorbs strongly in the visible region of the electromagnetic spectrum, selective irradiation of only the photocatalyst can be achieved, thereby minimizing unproductive side reactions. Several classes of visible light photocatalysts have been used for organic transformations, including transition metal complexes, organic dyes, and semiconductors, but the most commonly utilized photocatalysts in synthetic contexts have been transition metal polypyridyl complexes such as Ru(bpy)₃Cl₂ and Ir(ppy)₂(dtbpy)(PF₆) (Figure 1-1).

Figure 1-1. Structure of Ru(bpy)₃Cl₂ (**1.1**[Cl₂]) and Ir(ppy)₂(dtbpy)(PF₆) (**1.2**[PF₆])



The photophysical properties of these transition metal photocatalysts have been investigated in depth, as they are also widely studied for applications related to solar energy conversion.² As such, the absorbance and emission spectra, lifetime, and redox potential data are known for numerous complexes.² The availability of detailed photophysical characterization data for a large

variety of complexes has been an important benefit for the design of photocatalytic transformations.³ Even though the field of visible light photoredox catalysis has seen a resurgence of interest with a concomitant expansion of new photoinitiated synthetic methods,⁴ the interaction between transition metal photocatalyst and organic reaction components has not been as thoroughly characterized. While there have been few in-depth mechanistic studies on transition metal photocatalysis in organic synthesis to date, several techniques have been used to investigate individual portions of these multifaceted reactions. These have included physical organic techniques that have become standard methods to probe a range of catalytic reactions, as well as more specialized analyses unique to photochemistry. A better understanding of the mechanistic details of these photoredox reactions is needed to guide the further optimization and design of novel reactivity. This review chapter will address mechanistic studies, including both spectroscopic and traditional physical organic experiments, of transition metal catalyzed photoredox reactions in organic chemistry.

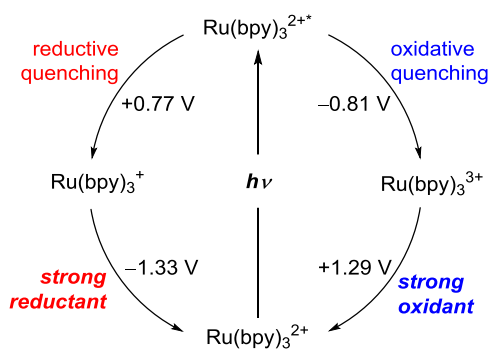
1.2 Photocatalyst Quenching Studies

1.2.1 Electrochemical measurements of the photocatalyst and substrate

Photoredox mechanisms start with absorption of a photon by the photocatalyst, generating an excited state. This excited state can then be quenched *via* an electron transfer event, generating a species that is either reduced or oxidized by one electron. One of the attractive features of using transition metal based photocatalysts such as $\text{Ru}(\text{bpy})_3^{2+}$ is the ability of the photoexcited complex to act as either a reductant ($\text{Ru}^{2+*/3+} = -0.81 \text{ V vs. SCE}$) or an oxidant ($\text{Ru}^{2+*/+} = +0.77 \text{ V vs. SCE}$) in its excited state. Quenching of the excited state thus provides access to both $\text{Ru}(\text{bpy})^+$ (-1.33 V vs. SCE) as a strong reductant or $\text{Ru}(\text{bpy})_3^{3+}$ ($+1.29 \text{ V vs. SCE}$) as a strong

oxidant (Scheme 1-1).^{2a} Because the electrochemical potentials of most of these photoactive complexes are known, it is possible to determine which compounds in the reaction can undergo electron transfer based on their redox properties. Indeed, most reports in the photoredox literature use electrochemical measurements to rationalize which components in the reaction undergo single electron transfer (SET) with the photocatalyst. This section details how electrochemical experiments have been used to support mechanistic hypotheses regarding electron transfer in photoredox catalysis.

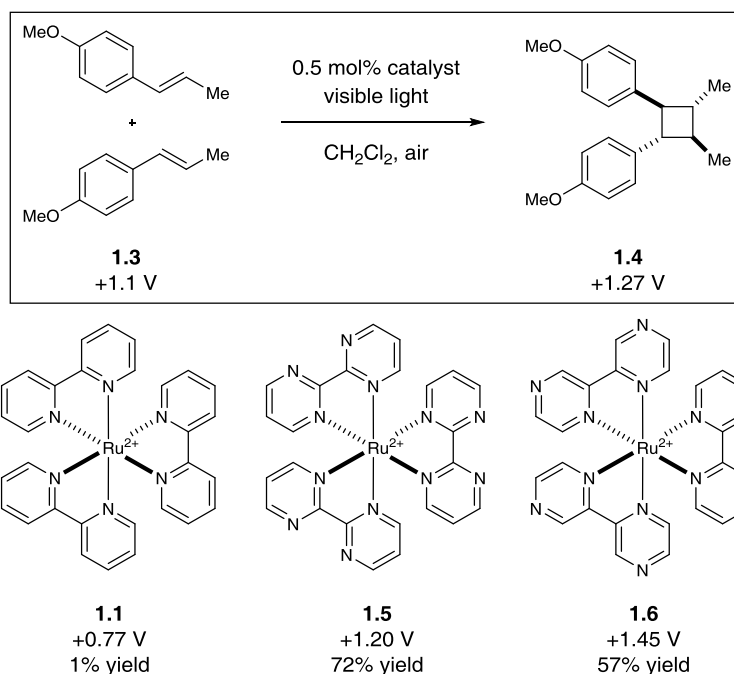
Scheme 1-1. Redox potentials of $\text{Ru}(\text{bpy})_3^{2+}$ vs. SCE in MeCN



For example, Yoon and coworkers used oxidation potentials to choose the best photocatalyst for the radical cation initiated [2+2] cycloadditions (Scheme 1-2).⁵ While optimizing the dimerization of anethole **1.3**, $\text{Ru}(\text{bpy})_3^{2+}$ (**1.1**) yielded essentially no product, which was unsurprising as the oxidation potential of **1.1** is lower than the substrate **1.3** (+1.1 V vs. SCE). On the other hand, $\text{Ru}(\text{bpz})_3^{2+}$ (**1.6**) yielded a moderate amount of product (57%), though the reaction did not proceed to complete conversion. The authors hypothesized that the oxidation potential of $\text{Ru}(\text{bpz})_3^{2+}$, at +1.45 V vs. SCE, was high enough to also oxidize the cycloaddition product **1.4** (+1.27 V vs. SCE) and enable cycloreversion back to the monomer **1.3**. In order to avoid cycloreversion, the authors used a catalyst with an intermediate oxidation potential between the starting material and the product; $\text{Ru}(\text{bpm})_3^{2+}$ (**1.5**), with an oxidation potential of

+1.20 V vs SCE, yielded 72% of **1.4**. Moreover, the reaction carried out with **1.5** at 0 °C resulted in complete consumption of the **1.3** and 81% isolated yield of **1.4**.

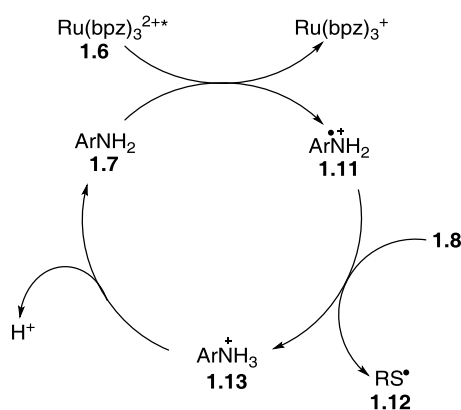
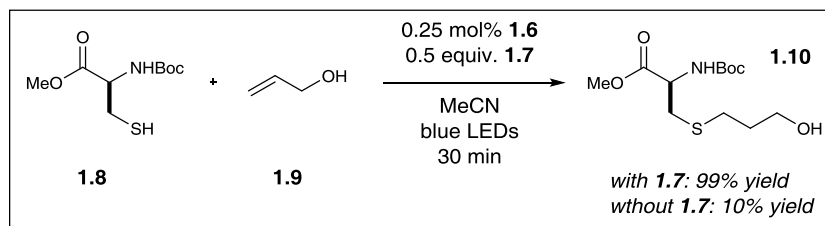
Scheme 1-2. Oxidative [2+2] cycloaddition of anethole



Redox potentials have also been used to explain the effects of additives on a photochemical system. In another report from the Yoon group, the rate of a photocatalytic thiol-ene reaction was observed to be dramatically enhanced in the presence substoichiometric amounts of *p*-toluidine **1.7** (Scheme 1-3).⁶ The authors hypothesized that **1.7** (+0.72 V vs. SCE) was functioning as a redox mediator, minimizing the difference in redox potentials between the photocatalyst (Ru*(bpz)₃²⁺, +1.4 V vs. SCE) and the thiol (*ca.* +0.50 V vs. SCE), which can explain the original slow reactivity. While the oxidation of thiol **1.8** by the photocatalyst is thermodynamically feasible, it is kinetically slow; a redox mediator replaces the kinetically slow step with two much faster steps and therefore increases the overall rate of the reaction. As a redox mediator, the aniline additive is faster than the thiol at quenching the photocatalyst,

forming $\text{Ru}(\text{bpz})_3^+$ and the corresponding aniline radical cation **1.11**. Then, **1.11** abstracts a hydrogen atom from the thiol to form the reactive thiyl radical species **1.12**.

Scheme 1-3. Photocatalytic thiol-ene reaction and proposed redox mediator mechanism

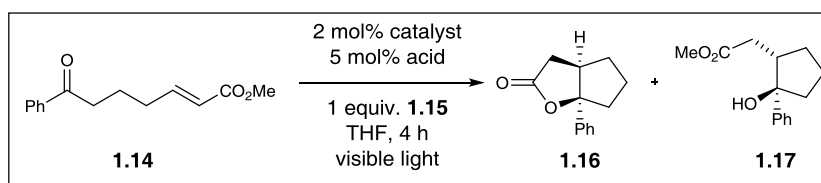


To investigate this hypothesis, the authors compared the oxidation potential of a variety of additives against the yield obtained in the thiol-ene reaction between **1.8** and **1.9**. They observed a maximum increase in reactivity when the additive's oxidation potential was between +0.70 and +0.90 V vs. SCE. The oxidation potentials for the highest yielding additives were midway between the potentials for the catalyst and the thiol substrate, evidence for the authors' redox mediator hypothesis. In this case, electrochemical measurements are suitable evidence for SET interactions between the photocatalyst and organic substrate. Nevertheless, in more complicated electron transfer mechanisms (*vide infra*), simple redox potentials cannot always account for reactivity and other parameters must be explored.

1.2.2 Bond dissociation energies of the substrates and additives

In addition to simple photoinduced electron transfer (PET), the excited state of a photocatalyst can also be quenched *via* proton-coupled electron transfer (PCET), in which an electron and a proton are both transferred to an organic substrate in a single, concerted step. This mechanism of photoactivation can allow redox chemistry to be performed on substrates whose redox potentials are outside of the functioning range of the catalyst. In cases of PCET, it is more informative to examine the bond dissociation energies (BDE) of a substrate for assessing quenching of the photocatalyst.⁷ The BDEs of a substrate are compared to the formal BDEs (an energy thermodynamically similar to normal BDEs) of a photocatalyst/acid combination as there is no bond breaking between the photocatalyst and acid, and if the formal BDE values are close to the BDE of the substrate, then the reaction becomes kinetically feasible. For example, Knowles and coworkers have described an intramolecular ketyl-olefin coupling of substrate **1.14** that is proposed to proceed through a PCET reduction of the ketyl moiety of **1.14**. This protocol employs Ru(bpy)₃²⁺ as the photocatalyst, catalytic amounts of diphenyl phosphoric acid, and Hantzsch ester **1.15** as the terminal reductant (Table 1-1).^{7a}

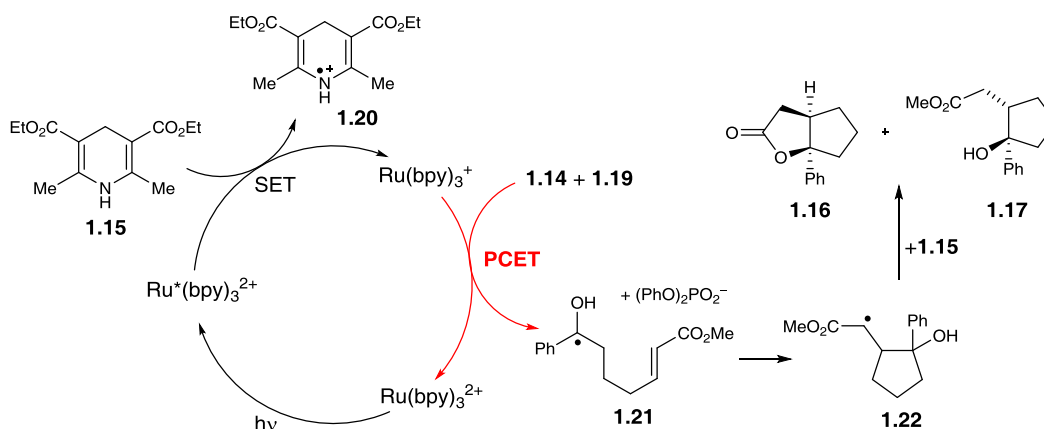
Table 1-1. Ketyl-olefin coupling reported by Knowles



photocatalyst	acid catalyst	BDE (kcal/mol)	% yield (1.16 : 1.17)
Ru(bpy) ₃ (BArF) ₂	none	-	0 (n/a)
Ru(bpy) ₃ (BArF) ₂	lutidine·HBF ₄ (1.18)	35	0 (n/a)
Ru(bpy) ₃ (BArF) ₂	(PhO) ₂ PO ₂ H (1.19)	33	78 (4.6:1)
Ir(ppy) ₂ (dtbpy)(PF ₆)	1.18	31	74 (4.9:1)

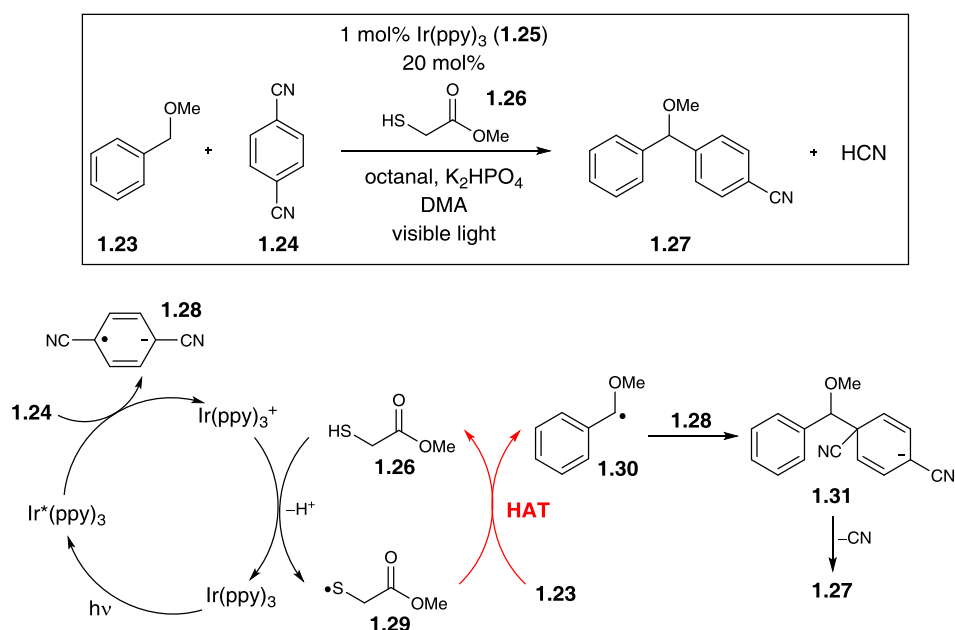
The mechanistic cycle (Scheme 1-4) begins with photoexcitation and quenching of $\text{Ru}(\text{bpy})_3^{2+}$ with **1.15**. The proposed PCET (in red) involves $\text{Ru}(\text{bpy})_3^+$, Brønsted acid **1.19**, and the ketone substrate, which forms ketyl radical **1.21** that undergoes cyclization and further reduction to afford the final products **1.16** and **1.17**. The authors rule out stepwise proton and electron transfer events based on electrochemical and $\text{p}K_a$ data. The reduction potential of acetophenone (similar to **1.14**) is -2.48 V vs. Fc and has a $\text{p}K_a$ of -0.1 in MeCN. The reduction potential of the photocatalyst ($\text{Ru}^{+/2+}$, $E_{1/2} = -1.71$ V vs Fc) is too positive to directly reduce the ketone through SET, and the $\text{p}K_a$ of **1.15** ($\text{p}K_a$ ca. 13 in MeCN) is too low to enable substantial protonation of the ketone. As evidence for the proposed PCET, the authors calculate the BDE of acetophenone to its ketyl radical is 26 kcal/mol and the formal BDE of $\text{Ru}(\text{bpy})_3^+$ in conjunction with acid **1.15** is 33 kcal/mol, in the range for a kinetically feasible reaction. Furthermore, the authors demonstrate that weaker acids (lutidine• HBF_4 , $\text{p}K_a = 14.1$ in MeCN) that did not work with $\text{Ru}(\text{bpy})_3^+$ were reactive with the more reducing **1.2**[PF_6] (-1.89 V vs. Fc) because the calculated BDE is 31 kcal/mol (as compared to 35 kcal/mol with **1.1**[BArF_2]). These BDE calculations show that a PCET reduction of the ketone is feasible, while stepwise protonation and electron transfer is thermodynamically inaccessible.

Scheme 1-4. Proposed PCET mechanism of the ketyl-olefin coupling



Bond dissociation energies have also been used to interrogate a hydrogen atom transfer (HAT) pathway.⁸ In a study by MacMillan and coworkers, the authors propose a HAT mechanism in the arylation of C–H bonds of benzylic ethers.^{8a} The proposed mechanism (Scheme 1-5) begins with the excited state of the photocatalyst quenched by cyanobenzene **1.24** to afford $\text{Ir}(\text{ppy})_3^+$, which with base performs oxidation and deprotonation of the co-catalytic thiol **1.26** to produce thiyl radical **1.29**.⁹ HAT (in red) occurs between **1.29** and the benzylic ether **1.23** to regenerate the thiol catalyst and form the reactive coupling partner **1.30**. The authors show that the HAT step is kinetically feasible because the S–H BDE of **1.26** *ca.* 87 kcal/mol is more stable than the C–H BDE of **1.24** = 85.8 kcal/mol.

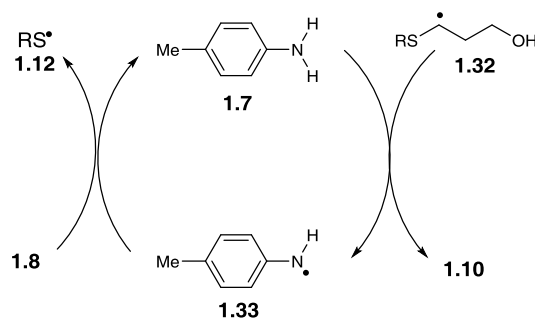
Scheme 1-5. C–H arylation of benzylic ethers and the proposed mechanism



Conversely, Yoon used the BDE of N–H to reject a HAT mechanism in the previously discussed thiol-ene reaction (Scheme 1-3).⁶ Prior to determining the aniline additive was acting as a redox mediator, one hypothesis was that **1.7** was acting as an H-atom shuttle between radical thiol-ene product **1.10** and thiol **1.8** (Scheme 1-6). To probe this pathway, the authors compared

the BDE of N–H bonds in a variety of aniline additives to the thiol-ene yield obtained. No trend was observed, and the authors subsequently ruled out a HAT mechanism.

Scheme 1-6. Proposed HAT mechanism in thiol-ene reaction



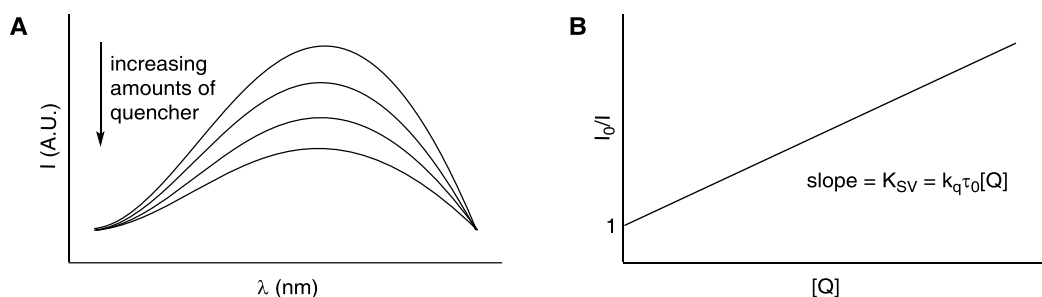
As demonstrated above, electrochemical measurements and BDE calculations have been used to investigate whether certain mechanisms (SET, PCET, HAT) are reasonable explanations for observed photocatalytic reactivity. While these data suggest potential interaction with the photocatalyst, they are not directly measuring such a process. Spectroscopic quenching studies, explored further in the next section, provide more compelling evidence for an interaction between the photocatalyst and substrate.

1.2.3 Spectroscopic quenching studies

In the absence of external quenchers, the triplet excited state of a photocatalyst can relax to the ground state through radiative (phosphorescence) or non-radiative (internal conversion) pathways. A chemical species that can quench the photocatalyst reduces the amount of radiative and non-radiative relaxation that occurs; this effect results in a concentration-dependent diminution of the phosphorescence of the photocatalyst in the presence of quencher. Figure 1-2A shows a typical plot of the phosphorescence intensity decreasing with increasing amounts of quencher added. This technique is frequently used in photochemistry to determine the identity of

the excited state quencher.^{7a,7c,8b,10–27} The reduction of the lifetime value of the photocatalyst can also indicate the quencher in a given system.²⁸

Figure 1-2. (A) Typical luminescence quenching experiment plot (B) Stern–Volmer plot



Furthermore, the decrease in phosphorescence of the photocatalyst in the presence of a quencher (Q) is directly related to the rate of the quenching event. This relationship is commonly expressed in the form of the Stern–Volmer equation (eq 1-1).

$$\frac{I_0}{I} = 1 + k_q\tau_0[Q] \quad \text{eq1 - 1}$$

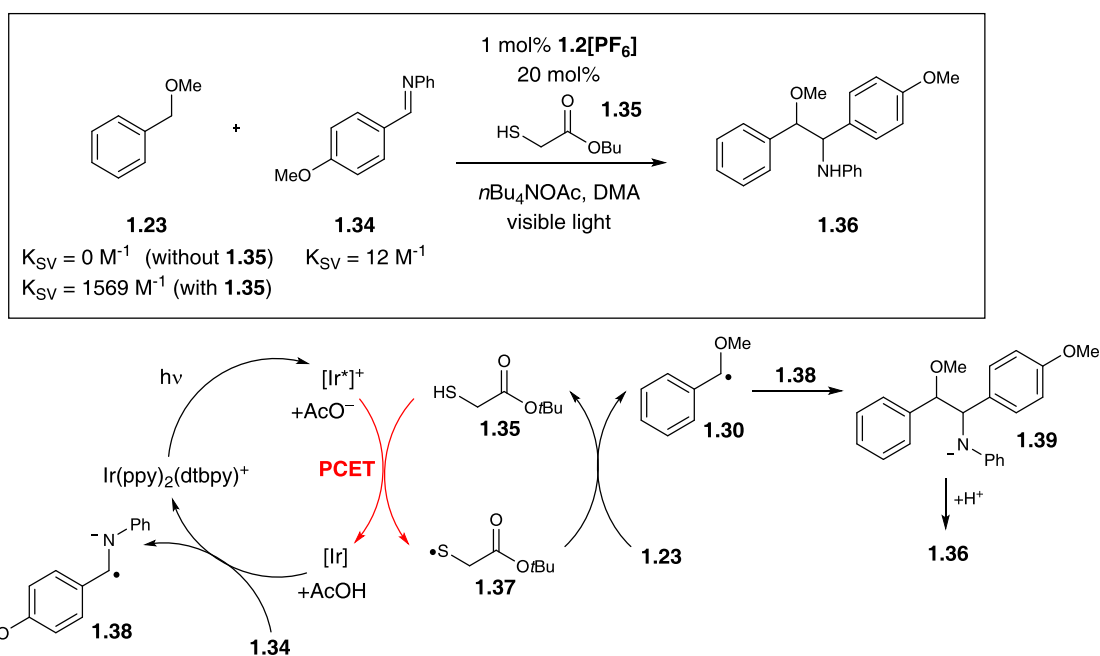
I_0 is the luminescence intensity in the absence of quencher, I is the luminescence intensity in the presence of the quencher, k_q is the rate of quenching, τ_0 is the lifetime of the photocatalyst in the absence of quencher, $[Q]$ is the concentration of the quencher.

A plot of concentration of quencher ($[Q]$) vs. the ratio of change in phosphorescence (I_0/I) results in a straight line (Figure 1-2B);²⁹ the slope, known as the Stern–Volmer constant (K_{SV}) is the product of the bimolecular quenching rate (k_q) and the lifetime of the photocatalyst excited state (τ_0). These plots are often used to determine either K_{SV} or k_q for the reaction components, and can be especially useful in more complex reactions that have more than one possible quencher.

For example, MacMillan used Stern–Volmer quenching data as evidence for PCET quenching of the photocatalyst excited state. MacMillan and coworkers reported the coupling of benzylic ethers and imines and proposed that the catalytic cycle begins with the quenching of the

photocatalyst **1.2**[PF₆] through PCET with thiol and base (Scheme 1-7).^{8b} In order to gain evidence for this proposal, the authors conducted a variety of Stern–Volmer quenching experiments. Luminescence quenching of **1.2**[PF₆] in the presence of thiol **1.39** was not observed, but upon addition of Bu₄NOAc, a K_{SV} of 1569 M⁻¹ was measured. The authors also observed quenching of the excited photocatalyst by benzalaniline; however, the measured K_{SV} of 12 M⁻¹ is two orders of magnitude smaller than the thiol/base combination and is unlikely to be catalytically relevant. Altogether, the Stern–Volmer quenching data provided good evidence for a PCET mechanism.

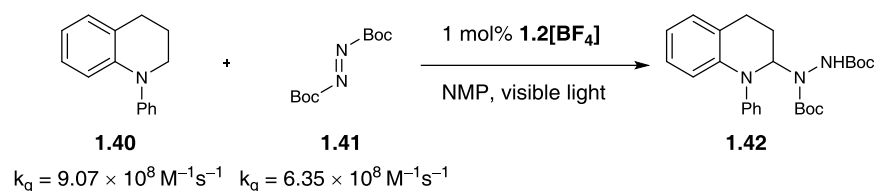
Scheme 1-7. Coupling of ethers and imines and proposed mechanism



However, Stern–Volmer quenching experiments are not always conclusive. While investigating the mechanism of C–H amination of nitrogen heterocycles,³⁰ Nishibayashi and coworkers conducted a Stern–Volmer study indicating that both the heterocycle **1.40** and the aminating agent **1.41** were able to quench the excited state of the photocatalyst (Scheme 1-8). Moreover, the rates of quenching were on the same order of magnitude ($9.07 \times 10^8 \text{ M}^{-1}\text{s}^{-1}$ for

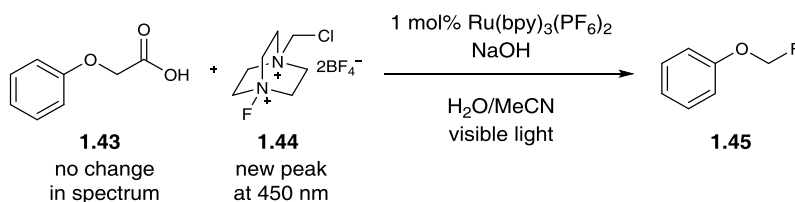
1.40 and $6.35 \times 10^8 \text{ M}^{-1}\text{s}^{-1}$ for **1.41**), which indicated that both **1.40** and **1.41** compete for catalyst quenching and complicate the mechanistic analysis.

Scheme 1-8. Amination of nitrogen heterocycles



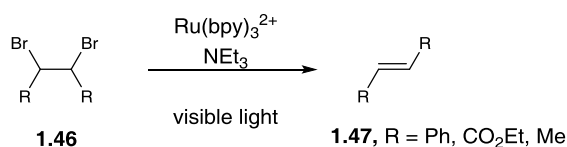
Absorption techniques such as transient absorption or steady state absorption spectroscopy can also be used to study the photocatalyst quenching. In a report from Sammis and Paquin on the decarboxylative radical fluorination of aryloxyacetic acids,³¹ the authors used transient absorption spectroscopy to determine both the identity of the quencher and the operative mechanism (SET or energy transfer). The overall reaction involves carboxylic acid **1.43** and Selectfluor[®] (**1.44**) in the presence of $\text{Ru}(\text{bpy})_3^{2+}$ and NaOH (Scheme 1-9). There was no change in the excited state absorption difference spectrum³² of $\text{Ru}(\text{bpy})_3^{2+}$ with the addition of substrate **1.43**, ruling out a quenching pathway involving the carboxylic acid. However, there was a change in the spectrum in the presence of Selectfluor[®], showing a growth of a new distinct band centered at 450 nm that did not correlate to the known spectra of $\text{Ru}(\text{bpy})_3^{2+}$ or its excited state and was thus assigned potentially as a new ruthenium species ($\text{Ru}(\text{bpy})_3^{3+}$) or a reduced version of Selectfluor[®]. The authors concluded that Selectfluor[®] quenches $\text{Ru}(\text{bpy})_3^{2+*}$ through an oxidative quenching mechanism involving the generation of $\text{Ru}(\text{bpy})_3^{3+}$.

Scheme 1-9. Fluorination of aryl ethers



Willner and coworkers used a combination of luminescence quenching and absorption spectroscopy to probe the mechanism of the debromination of vicinal dibromides to form alkenes.^{12b} The reaction involves dibromides (**1.46**), triethylamine and $\text{Ru}(\text{bpy})_3^{2+}$ as the photocatalyst (Scheme 1-10).

Figure 1-8. Debromination of vicinal dibromides



First, luminescence quenching experiments revealed that the dibromides in this study did not quench the excited state, $\text{Ru}^*(\text{bpy})_3^{2+}$. Instead, the photocatalyst excited state is quenched by triethylamine to form $\text{Ru}(\text{bpy})_3^+$, which is seen by the growth of a band at 510 nm in the absorption spectrum over time. Steady state illumination of the photocatalyst in the presence of both triethylamine and the dibromide resulted in no peak at 510 nm, consistent with a mechanism involving reduction of the dibromide by $\text{Ru}(\text{bpy})_3^+$. More detailed information was obtained using laser flash photolysis experiments that tracked the decay of $\text{Ru}(\text{bpy})_3^+$ in both the presence and absence of dibromide **1.46**. The Ru(I) decay is faster in the presence of the dibromide, indicating a faster regeneration of $\text{Ru}(\text{bpy})_3^{2+}$ through oxidation of the $\text{Ru}(\text{bpy})_3^+$ with **1.46**. Additionally, the authors noticed a difference in the rates of decay of $\text{Ru}(\text{bpy})_3^+$ with different dibromides that corresponded well with the measured quantum yields.³³ A faster decay of Ru(I) implies that reduction of the dibromide is quicker, which would increase the overall quantum efficiency of the reaction. This analysis informed the authors that the reaction rate is greatly dependent upon each substrate.

1.2.4 Quenching fraction

Luminescence quenching and absorption data have been used to determine the identity of the photocatalyst excited state quencher and its mechanism of quenching. To understand the efficiency of the quencher, the quenching fraction (f) can be calculated. The quenching fraction compares the excited state quenching rate for an exogenous quencher (Q) to other modes of quenching or relaxation of the photocatalyst excited state. The calculation for the quenching fraction for Q is shown in eq 1-2.

$$f = \frac{k_q[Q]}{\tau_0 + k_q[Q] + k_{q'}[Q'] + \dots} \quad \text{eq 1 - 2}$$

Q' represents a compound in the reaction that non-productively quenches the excited state of the photocatalyst.

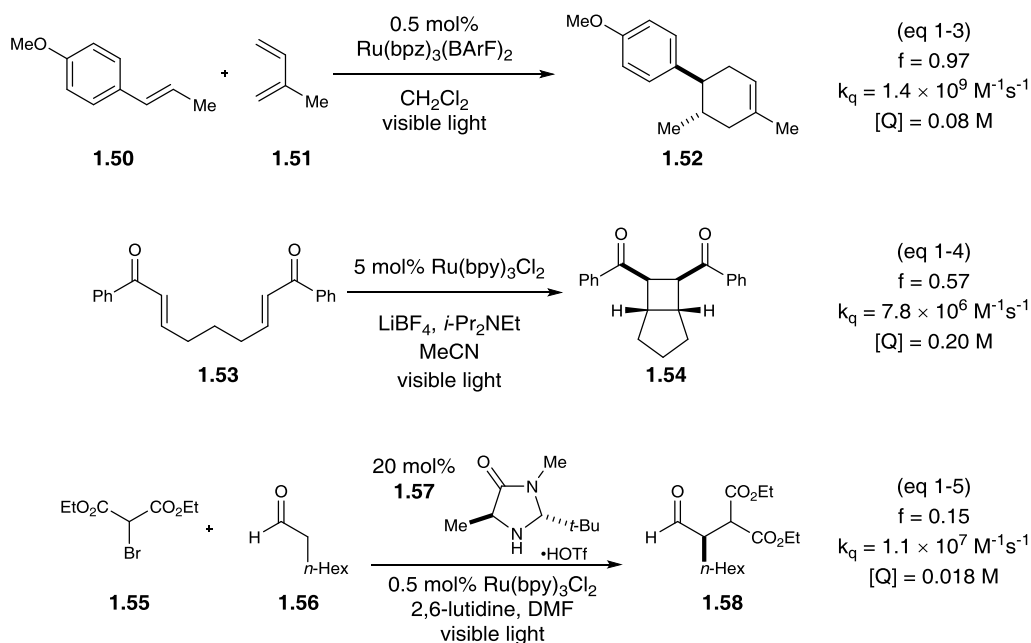
As the equation shows, the quenching fraction is dependent upon both the rate of quenching and the concentration of the quencher. In a study on the hydroxylation of arylboronic acids reported by Scaiano,¹⁸ the authors compared two photocatalysts, Ru(bpy)₃Cl₂ and the organic dye methylene blue (Table 1-2). Their analysis uses the calculation of quenching fractions (0.06 for Ru(bpy)₃Cl₂ and 0.71 for methylene blue) to explain the difference in reactivity between the two photocatalysts (after 7 h, 58% isolated yield for Ru(bpy)₃Cl₂, 94% for methylene blue). This difference in f between the two catalysts is attributed to the rate of quenching (k_q for *i*-Pr₂NEt) for Ru(bpy)₃Cl₂ being two orders of magnitude slower than for methylene blue.

Table 1-2. Comparison of photocatalysts for the hydroxylation of arylboronic acids

photocatalyst	% yield (7 h)	f	k_q (M ⁻¹ s ⁻¹)
Ru(bpy) ₃ Cl ₂	58	0.06	6.21×10^6
methylene blue	94	0.71	2.44×10^8

c1ccc(cc1)B(O)O (1.48) $\xrightarrow[\text{MeCN/H}_2\text{O, O}_2, \text{visible light}]{1 \text{ mol\% photocatalyst, } 5 \text{ equiv. } i\text{-Pr}_2\text{NEt}}$ c1ccc(cc1)O (1.49)

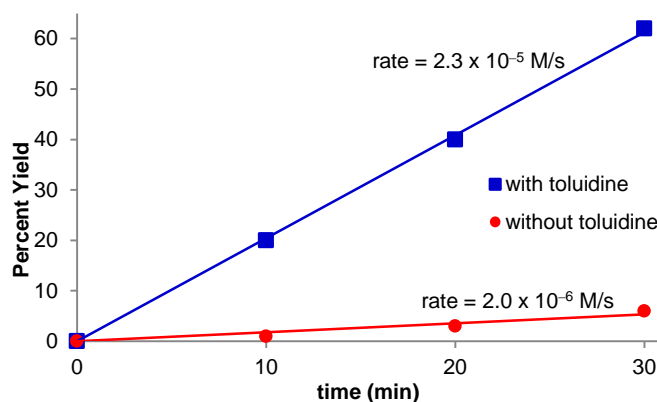
Another study on the quenching fraction of photoredox reactions by the Yoon group^{15b} calculates f for three previously reported reactions: 0.97 for the Diels–Alder between anethole **1.50** and isoprene **1.51** (eq 1-3),³⁴ 0.57 for the cyclobutanation of bis(enone) substrate **1.53** (eq 1-4),³⁵ and 0.15 for the α -alkylation of aldehyde **1.56** (eq 1-5).^{16a}



In comparison, the quenching fraction for the Diels–Alder reaction is much higher than the α -alkylation reaction due to both a faster rate of quenching and a larger concentration of quencher. The cyclobutanation reaction, while having a similar k_q to the α -alkylation reaction, has a larger quenching fraction due to its much larger quencher concentration. In order to increase the quenching fraction for eq 1-5, either the concentration of the quencher must be increased or the identity of the quencher must be changed to one with a larger k_q . As the concentration of the quencher (an enamine formed *in situ* from **1.56** and **1.57**) is proportional to the concentration of the catalyst, the authors proposed that the addition of an exogenous quencher with a larger k_q than the enamine ($k_q = 1.1 \times 10^7 \text{ M}^{-1}\text{s}^{-1}$) would increase efficiency. Indeed, the addition of only 0.5 mol% *N,N*-dimethyl-*p*-toluidine ($k_q = 3.9 \times 10^8 \text{ M}^{-1}\text{s}^{-1}$) increases the quenching efficiency,

which is reflected in an increase in the rate of product formation by an order of magnitude (Figure 1-3).

Figure 1-3. Comparison of rates of the alkylation reaction in the presence and absence of *N,N*-dimethyl-*p*-toluidine



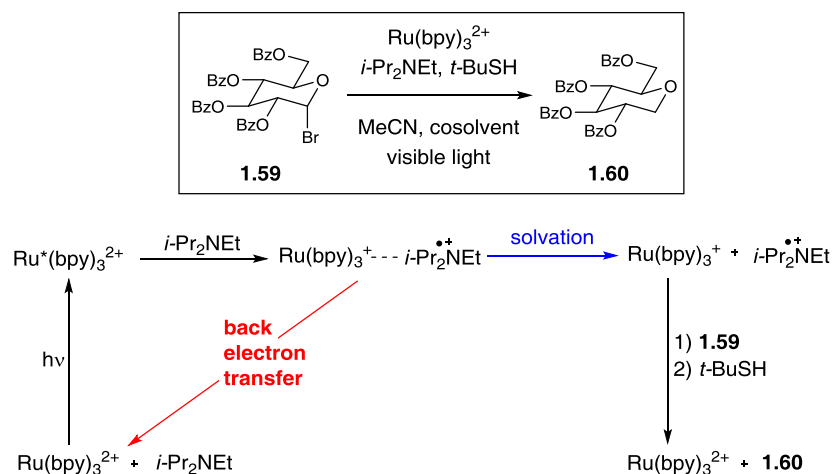
The results of this study demonstrate that the determination of a quenching fraction can be used to identify when the inefficiency of a photocatalytic reaction is due to a slow initiation step. With a better understanding of the mechanism, the authors were able to dramatically increase reactivity.

1.3 Non-Quenching Photocatalyst Studies

While the majority of photocatalyst studies have centered on the mechanisms of quenching, there has also been interest in studying what other processes occur to the photocatalyst aside. One important factor that can decrease reaction efficiency is the phenomenon of back electron transfer (BET), which is essentially the reverse of electron transfer. In BET, the reduced (or oxidized) photocatalyst and the oxidized (or reduced, respectively) quencher are unable to escape the solvent cage and recombine to regenerate the ground state of the photocatalyst. This phenomenon has been extensively investigated in the inorganic literature² but its role in organic synthesis remains largely unexplored. In a study by Gagné and coworkers on the

hydrodehalogenation of glucosides,³⁶ an interesting water effect was discovered. The addition of water as a co-solvent increased reactivity noticeably in the debromination of **1.59** in the presence of $\text{Ru}(\text{bpy})_3\text{Cl}_2$ and *i*- Pr_2NEt (Scheme 1-11).

Scheme 1-11. Hydrodebromination of glucosides and the proposed mechanism

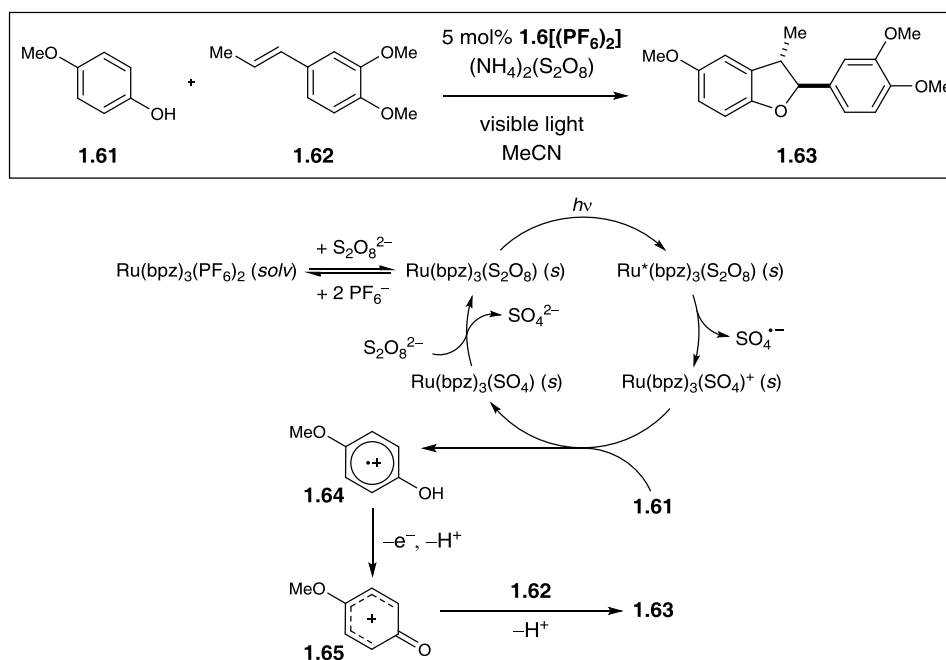


The authors proposed that the water helps by increasing the solvation and separation (in blue) of the $\text{Ru}(\text{bpy})_3^{+ \bullet} - i\text{-Pr}_2\text{NEt}^{\bullet +}$ pair formed immediately after quenching of the photocatalyst, thereby reducing the amount of unproductive back electron transfer (in red). To amplify this effect, the authors also used a more hydrophobic photocatalyst, $\text{Ru}(\text{dmb})_3^{2+}$ (dmb = 4,4'-dimethyl-2,2'-bipyridine), which should resolvate faster after quenching in the presence of water.³⁷ Indeed, $\text{Ru}(\text{dmb})_3^{2+}$ was a more efficient photocatalyst than $\text{Ru}(\text{bpy})_3^{2+}$, although the authors noted that the rate increase could also be attributed to a more negative reduction potential of $\text{Ru}(\text{dmb})_3^{2+}$ (0.12 V vs. SCE more negative than $\text{Ru}(\text{bpy})_3^{2+}$). As demonstrated, back electron transfer can have a noticeable effect on the efficiency of the reaction, and further study of this effect in organic synthesis is important.

Another important mechanistic aspect of these photoredox reactions is change of the photocatalyst under the reaction conditions, either in formation of the active photocatalyst from a

precatalyst or the deactivation of the catalyst. For example, while examining the oxidative cyclization of dihydrobenzofurans (Scheme 1-12),^{15a} Yoon and coworkers noticed an induction period and concurrent formation of an orange precipitate in the reaction. To study this feature further, the authors filtered the reaction and discovered that the supernatant was not catalytically active, but the precipitate was both active and did not exhibit an induction period. The authors proposed that the soluble $\text{Ru}(\text{bpz})_3(\text{PF}_6)_2$ was a precatalyst, and that the active photocatalyst was $\text{Ru}(\text{bpz})_3(\text{S}_2\text{O}_8)$, formed *in situ* upon metathesis with $(\text{NH}_4)_2(\text{S}_2\text{O}_8)$, the terminal oxidant in this reaction. As further evidence for this hypothesis, independently synthesized $\text{Ru}(\text{bpz})_3(\text{S}_2\text{O}_8)$ was shown to be a competent catalyst for the reaction.

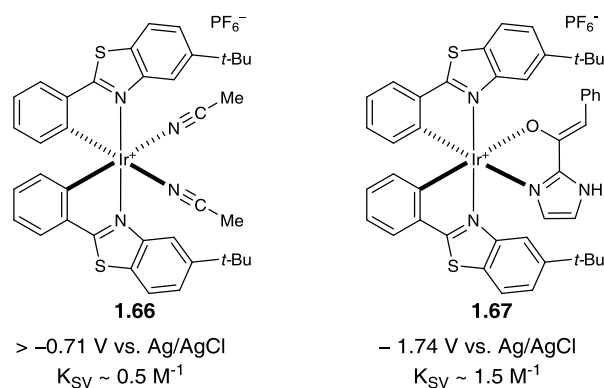
Scheme 1-12. Proposed mechanism of phenol oxidation and cyclization with styrenes



In another example, Meggers and coworkers reported the alkylation of ketones using a photocatalyst proposed to be formed *in situ* (Figure 1-4).³⁸ The proposed catalyst also acts as a Lewis acid and forms an intermediate enolate complex of the ketone that then interacts with a photoredox generated radical species. The authors used a combination of electrochemical and

Stern–Volmer data as evidence for **1.67** as the competent photocatalyst over the precatalyst **1.66**. The reduction potential of **1.67** is more negative than precatalyst **1.66**, and in the case of the Stern–Volmer, **1.67** has a larger K_{SV} value than **1.66**.³⁹ While these data did not rule out the possibility of **1.66** acting as the photocatalyst, they indicated that **1.67** is a more efficient photocatalyst in the system.

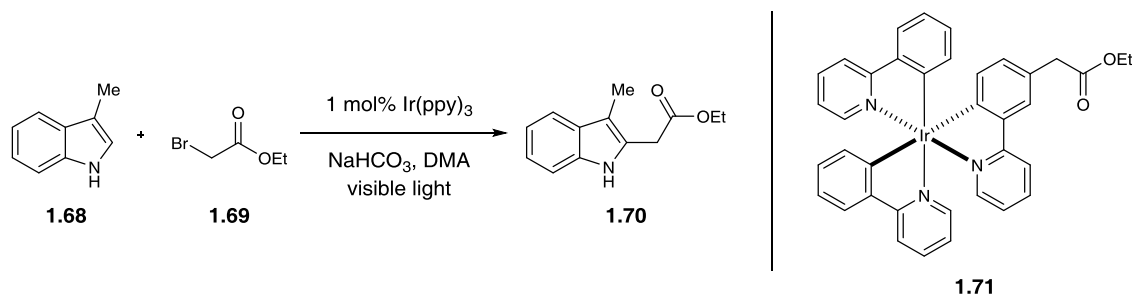
Figure 1-4. Comparison of the precatalyst **1.66** and the proposed photocatalyst **1.67**



Stephenson and Flowers reported the decomposition studies of Ir(ppy)_3 in the alkylation of indoles (Scheme 1-13).^{17e} In the process of studying the alkylation reaction, the authors observed the rate of the reaction slowed over time but still proceeded to completion; they attributed this to catalyst deactivation. During irradiation of Ir(ppy)_3 under reaction conditions excluding the indole, the initial photocatalyst disappeared and was replaced with an intractable mixture of products. Using mass spectrometric analysis, the authors discovered that this mixture contained masses corresponding to mono-, di-, tri-, tetra-, and pentaalkylations of Ir(ppy)_3 and they proposed that this decomposition of the original photocatalyst was the reason for the rate decrease. Additionally, the authors synthesized **1.71**, a mono-alkylated version of the photocatalyst but noted that its reactivity was similar to the original photocatalyst and produced the same mixture of alkylated complexes during irradiation. While the authors did not discover

the exact decomposition product that was responsible for the rate decrease, this study demonstrates the relevance of catalyst deactivation under reaction conditions.

Scheme 1-13. Alkylation of indoles



These photocatalyst studies underscore the important point that the optimization and discovery of new reactivity depends on more factors than just efficient quenching of the excited state. Back electron transfer can have a dramatic effect on the catalytic cycle even if efficient quenching of the photocatalyst occurs. Formation of an active catalyst *in situ* and photocatalyst decomposition can also affect the development of new reactions.

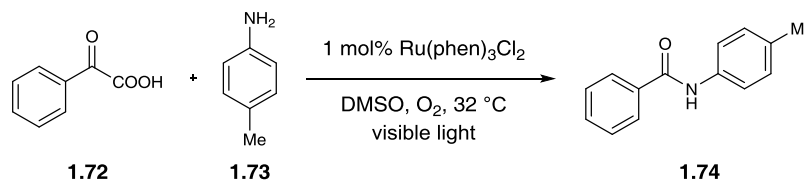
1.4 Intermediate Studies

1.4.1 Characterization of reactive intermediates

As with any mechanistic study, the identification of intermediates can be informative to the mechanistic proposal. NMR and FT-IR are common techniques used for *in situ* characterization of the intermediates in non-photochemical reactions, and photochemical systems have been studied in a similar way.^{22a,22c,27,40,41} However, photoinduced electron transfer generates odd-electron open shell species (radicals, radical anions, radical cations). In some cases, these radical species have been characterized *via* electron paramagnetic resonance spectroscopy (EPR).^{16e,42,43} For example, Lei and coworkers characterized the decarboxylation and amidation of keto acid

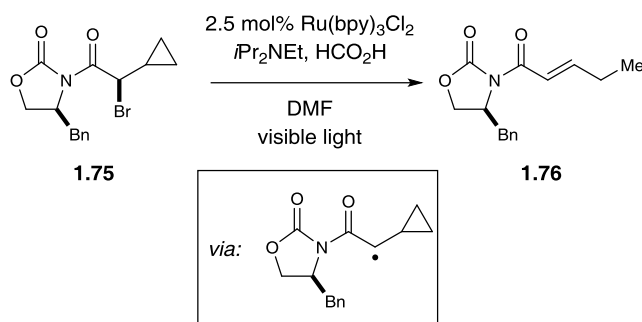
1.72 with toluidine **1.73** using EPR (Scheme 1-14).⁴² The authors irradiated a mixture of the photocatalyst ($\text{Ru}(\text{phen})_3\text{Cl}_2$) and **1.73** and observed an EPR signal, confirming that a radical species was present and moreover, that toluidine quenched the photocatalyst excited state. Furthermore, with the addition of keto acid **1.72** to the mixture, the finer peaks in the EPR signal disappeared, leaving a broader peak consistent with the known EPR signal of $\text{Ru}(\text{bpy})_3^+$. The authors rationalize that the organic radical seen in the former EPR experiment was consumed in the latter and this indicated an interaction between the amino radical species and the keto acid.

Scheme 1-14. Amidation of keto acid **1.63**



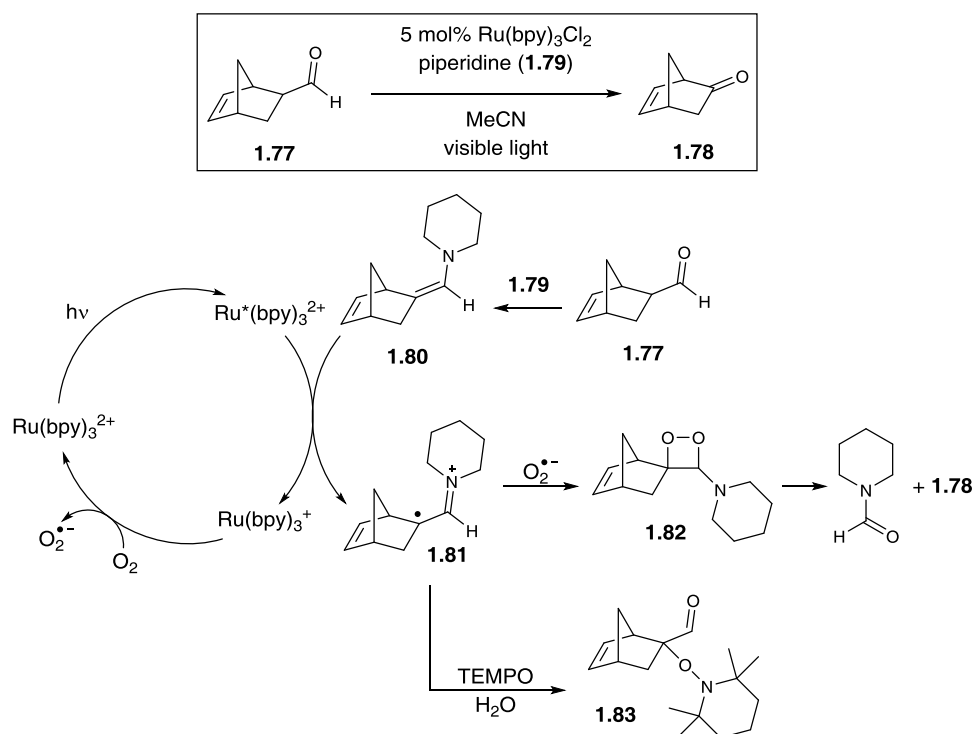
Other common techniques to probe the intermediate identity in photoredox include the addition of a radical trap or the use of a radical clock experiment. The cyclopropyl radical clock experiment,⁴⁴ in which a substrate that is proposed to undergo SET is designed to have a cyclopropyl group adjacent to the radical, is the most common radical clock experiment used in photoredox catalysis.^{16a,17c,43a,45,46} When there is a long-lived radical next to the cyclopropyl moiety, the three membered ring opens and usually rearranges to form a corresponding alkene. In some cases, the cyclopropyl ring can open and close, which can be noted through a scrambling of stereochemistry. As an example, Stephenson reported the use of a cyclopropyl radical clock experiment in the dehalogenation of activated bromides and chlorides. Under standard conditions, substrate **1.75** undergoes ring opening and rearrangement to **1.76**, evidence used to indicate a radical intermediate was a part of the mechanism (Scheme 1-15).

Scheme 1-15. Radical clock experiment



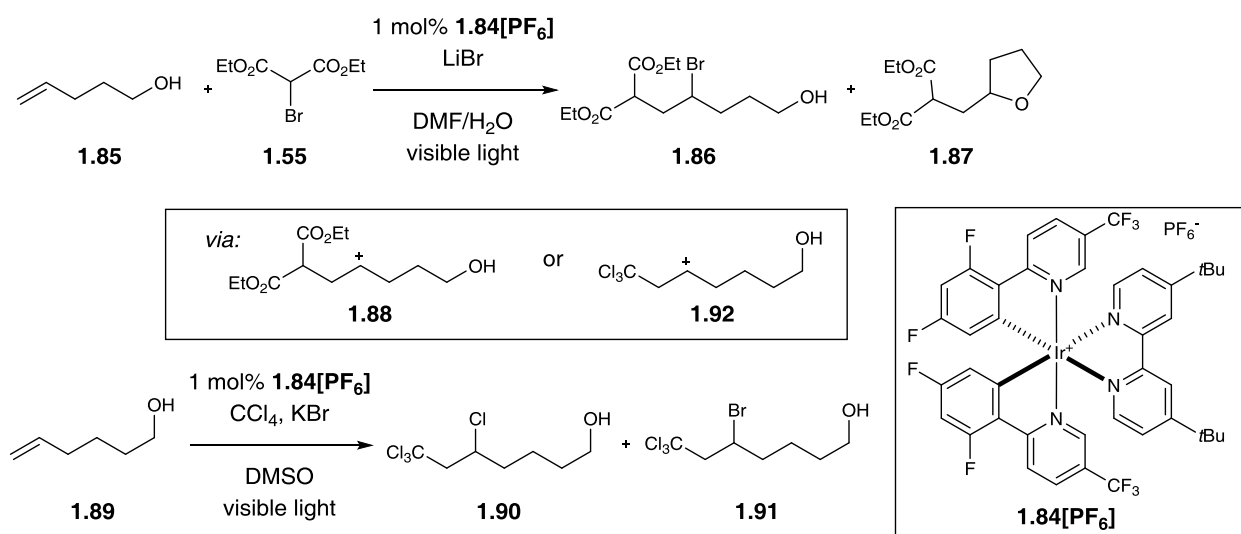
A variety of radical scavengers have also been employed, most commonly 2,2,6,6-tetramethylpiperidine-1-oxyl (TEMPO).^{22b,23,24a,42,46c,47,48} These experiments are conducted by adding the scavenger to the standard reactions conditions and measuring a diminished or arrested reaction rate. Furthermore, TEMPO-trapped derivatives of intermediates have been characterized and used to discover where the radical species is generated. For example, Xia and coworkers were able to isolate and characterized the TEMPO-trapped **1.83** in a radical scavenger experiment of their reported aldehyde cleavage reaction (Scheme 1-16).⁴⁷ The authors used these data as evidence for the formation of a radical based intermediate generated at the α -carbonyl position (**1.81**). Other radical scavengers used include isopentyl nitrite,^{14a} galvinoxyl,^{48a} hydroquinone,^{48t} dinitrobenzene,^{48t,10} and methyl vinyl ketone.⁴⁹ It is important to note, however, that the addition of radical scavengers can significantly perturb the mechanism of a photocatalytic process, and thus any conclusions should be made with caution.

Scheme 1-16. Aldehyde cleavage TEMPO trapping experiment and proposed mechanism

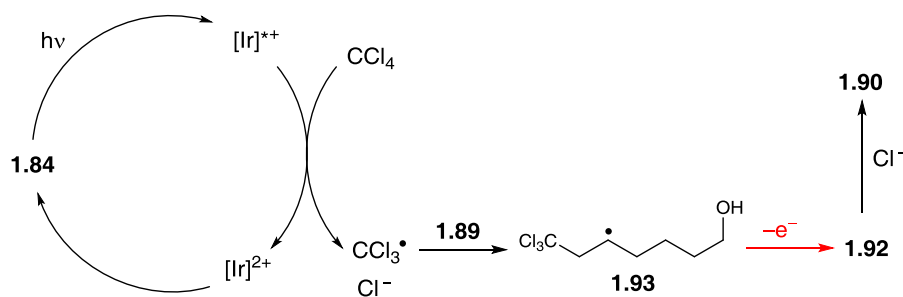


In a similar method, carbocation intermediates generated in photoredox catalyzed reactions have also been trapped and subsequently characterized with a variety of nucleophiles.^{48e,48i,48u,48v,50,51} During a study on the mechanism of atom transfer radical addition (ATRA) reactions catalyzed by photoredox catalysis, Stephenson probed the possibility of carbocation intermediates through the use of a tethered alcohol group on substrate **1.85** and exogenous KBr in the reaction of **1.89** and CCl_4 (Scheme 1-17).^{50b} In both cases, the expected product formed (**1.86** and **1.90**) along with furan **1.87** (*via* intramolecular trapping of **1.88**) and bromide **1.91** (*via* intermolecular trapping of **1.92**). The authors used these data as evidence that a carbocation was formed under the reaction conditions, and thus the reaction underwent a radical-polar crossover mechanism (shown in red).⁵²

Scheme 1-17. Evidence for a carbocation and radical-polar crossover mechanism in the ATRA reaction



radical-polar crossover mechanism:



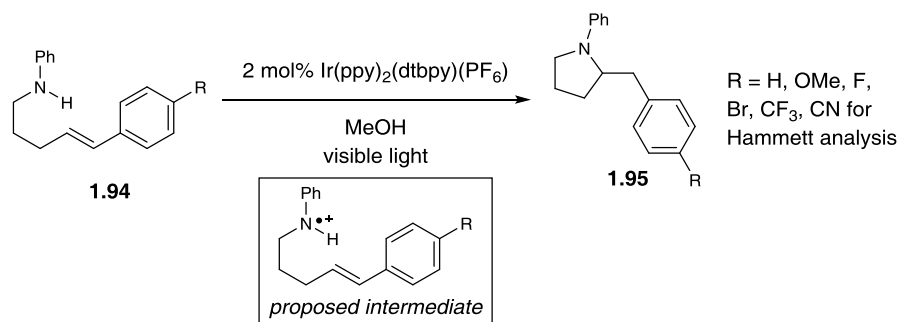
Finally, as Ru(bpy)₃²⁺ and many of its derivatives are able to generate singlet oxygen, many researchers have used appropriate sensitizers and quenchers to probe the mechanistic role of singlet oxygen in a number of transformations.^{22d,26,10c,34,53} Tetraphenylporphyrin and Rose Bengal are commonly used singlet oxygen sensitizers, and as such have been used as a replacement for the original photocatalyst to provide evidence either for or against ¹O₂ generation. If alternative sources of singlet oxygen do not promote product formation, singlet oxygen is generally not considered an essential intermediate in the reaction mechanism. Conversely, other compounds and solvents known to quench or trap singlet oxygen (DMSO, DMF, water, chlorobenzene, DABCO, alkenes) have been added to the reaction mixture to test

for the presence of $^1\text{O}_2$. However, caution should be taken with these results, as changing the reaction conditions may effect more than just singlet oxygen generation.

1.4.2 Transition state studies

Rate and selectivity data can also give information as to what intermediates are forming in the reaction. Use of competition studies,^{19,48e} site selectivity,⁵⁴ and Hammett analyses¹⁹ have been used to understand the mechanism of photoredox reactions. In the course of a study of the photocatalytic hydroamination of styrenes, Knowles performed a Hammett analysis of the reaction, varying the *para*-substitution of styrenyl moiety.¹⁹ This experiment resulted in a linear correlation with σ_p ($R^2 = 0.96$) and a ρ value of -0.56 of which the authors state is consistent with an electrophilic aminium radical intermediate, likely protonated during the addition to the olefin (Scheme 1-18).

Scheme 1-18. Hydroamination of styrenes and the proposed intermediate



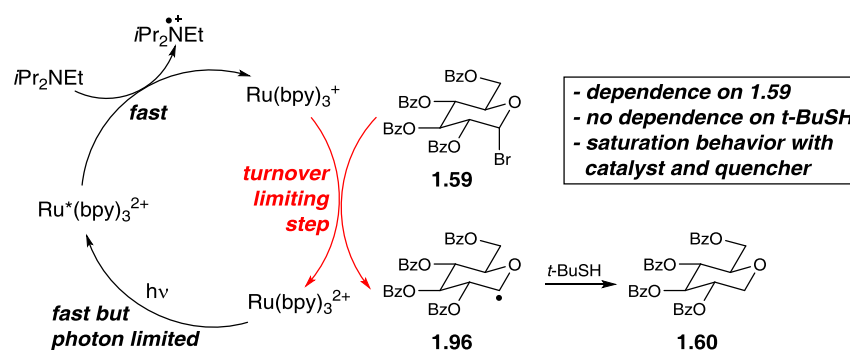
While these experiments do not attempt to characterize the intermediate, the general reactivity observed is consistent with the proposed intermediates and can be evidence for the reaction mechanism.

1.5 Rate Data and Isotope Effects Studies

1.5.1 Rate data and kinetic isotope effects

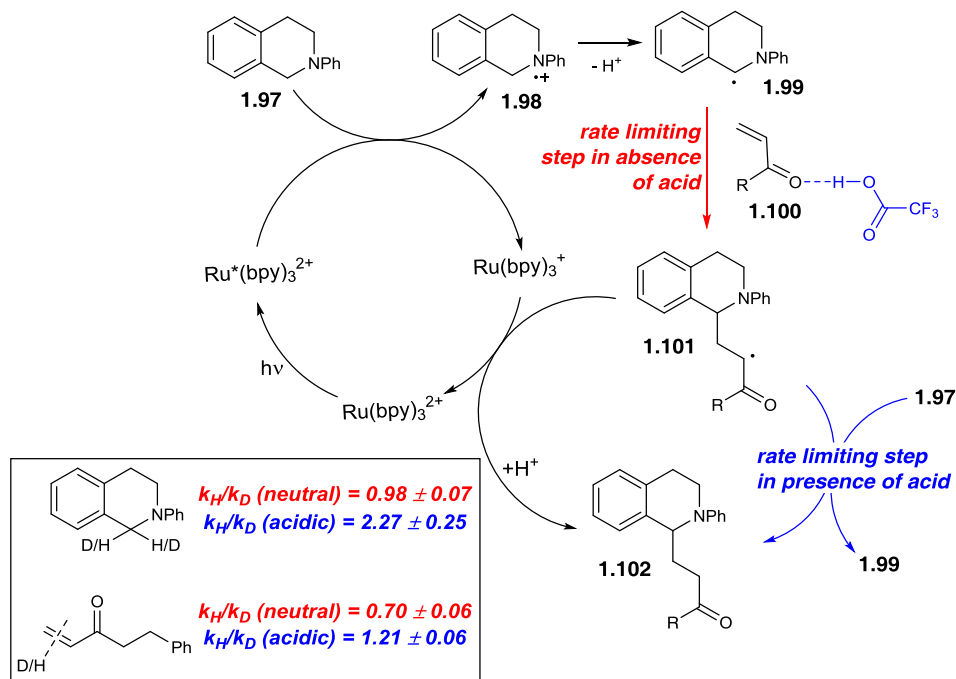
Rate data have been investigated using traditional physical organic experiments in order to understand the mechanism of photoredox reactions. Gagné and coworkers determined that for their reported hydrodebromination of glucosides (Scheme 1-11)³⁶ the rate showed a dependence on the concentration of glucoside **1.59**, no dependence on the concentration of the H-atom donor *t*-BuSH, and a saturation behavior seen with both the catalyst $\text{Ru}(\text{bpy})_3^{2+}$ and amine quencher *i*-Pr₂NEt. These data are consistent with a turnover limiting step of reduction of the glucoside by $\text{Ru}(\text{bpy})_3^+$ (shown in red) and that both quenching of the excited state of the photocatalyst and H-atom transfer are fast (Scheme 1-19). Additionally, the authors noted that the rate plateaus with increasing concentration (> 4 mM) of the photocatalyst and attributed this behavior to a photon-limited regime. In a photon-limited reaction, the absorptivity of the catalyst is sufficiently high that all the photons entering the reaction vessel are absorbed and a maximum concentration of photoexcited catalyst has been reached. The rate of a photon-limited system can be improved by increasing the flux of photons absorbed, either by utilizing more intense light sources (*e.g.* LEDs instead of CFL)⁵⁵ or by using reaction vessels that increase the surface area available for irradiation relative to the volume of the reaction (*e.g.* NMR tube instead of round bottom flask).

Scheme 1-19. Proposed mechanism for hydrodebromination of glucosides



In addition, kinetic isotope effects (KIE) have been used to identify the rate-limiting step in a mechanism. The Yoon group reported an α -amino radical addition procedure that was greatly enhanced, both in rate and selectivity, in the presence of a co-catalytic amount of trifluoroacetic acid (TFA).⁵⁶ To understand the effect of the Brønsted acid, the authors undertook KIE experiments, in both the α -amino precursor **1.97** and the addition partner **1.100** (Scheme 1-20). Without the presence of acid, there was no KIE observed with respect to the amine substrate and an inverse secondary KIE with respect to the enone. This is consistent with the rate limiting step being the addition of the α -amino radical into the enone (shown in red). In the presence of the acid, the authors noted a dramatic change in the KIE. They observed a primary KIE with respect to the amine substrate and a normal secondary KIE with respect to the enone, consistent with a chain propagation step being rate-limiting (shown in blue).

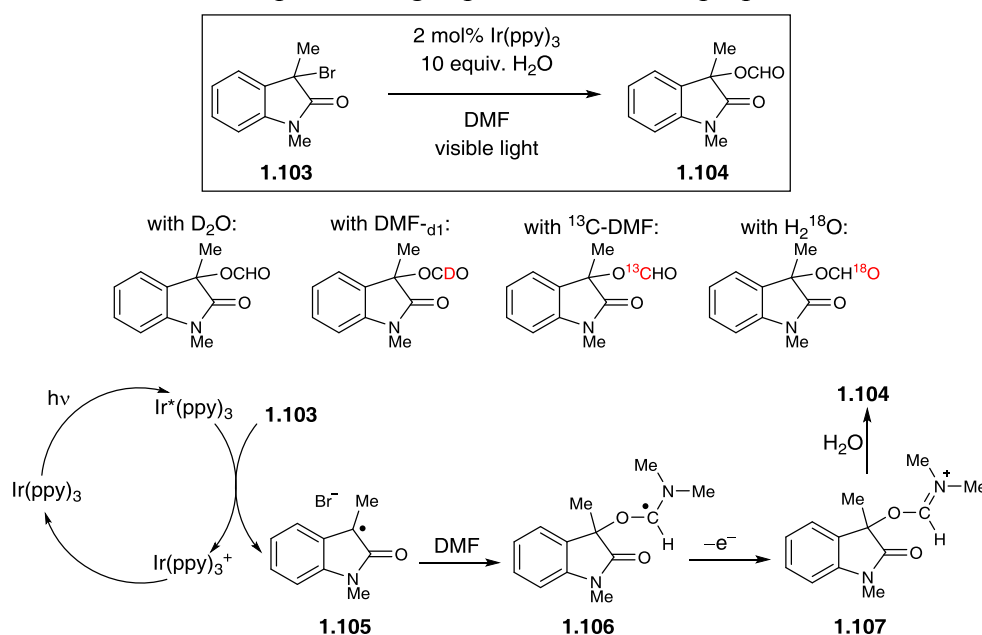
Scheme 1-20. Proposed mechanism of the α -amino radical addition



1.5.2 Isotopic labeling studies

Isotopically labeled reagents have been used to determine the origin of the atoms in the final product.^{11a,14b,17c,21f,22b,24c,41,45,46a,48r,48s,53b,53c, 57} For example, Xiao and coworkers performed a series of D, ¹³C, and ¹⁸O isotopic studies to understand where all new elements came from in their reported formyloxylation of oxindoles (Scheme 1-21).^{22a} Deuterium labeled DMF-*d*₁ and D₂O were used in the reaction and only deuterium incorporation was seen with the DMF-*d*₁. When the DMF was ¹³C labeled, the isotope was seen in the added formyl group. Finally, ¹⁸O labeling of water indicated by mass spectrometry (MS) that there was incorporation of one ¹⁸O. In order to determine which of the two new oxygens arose from water, the formyloxy group was hydrolyzed and the resulting oxindole did not have any ¹⁸O isotopes, indicating that the formyl oxygen came from water. With these data,⁵⁸ the authors proposed the following mechanism: 1) quenching of the photocatalyst excited state by **1.103**; 2) addition of radical species **1.105** into DMF; 3) oxidation to the iminium **1.106**; and 4) hydrolysis to deliver the final product **1.104**.

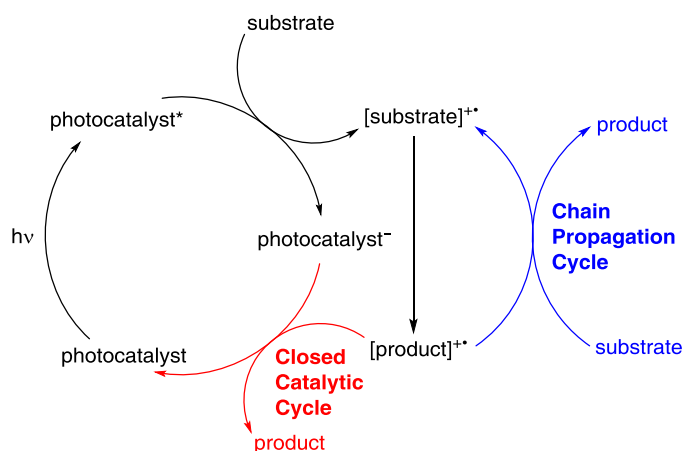
Scheme 1.21. Isotopic labeling experiments and the proposed mechanism



1.6 Chain Propagation Studies

Due to the radical nature of most photoredox reactions, several researchers have proposed that chain mechanisms are probable. Chain propagation (Scheme 1-22) occurs when the radical intermediate in a system reacts with another equivalent of substrate (shown in blue) instead of terminating through interaction with the photocatalyst or other radical species (shown in red). Most, if not all, photoredox reactions proceed through the closed catalytic cycle to some extent. More importantly, a chain propagation mechanism can operate alongside the closed catalytic cycle and in some cases has been demonstrated to be the dominant mechanism. Much research has been devoted to studying whether a mechanism is exclusively a closed catalytic cycle or if the mechanism also contains chain propagation. This distinction is important as it can have dramatic effects on the optimization of new reactions.

Scheme 1-22. Generic reaction scheme involving both chain propagation and closed cycle

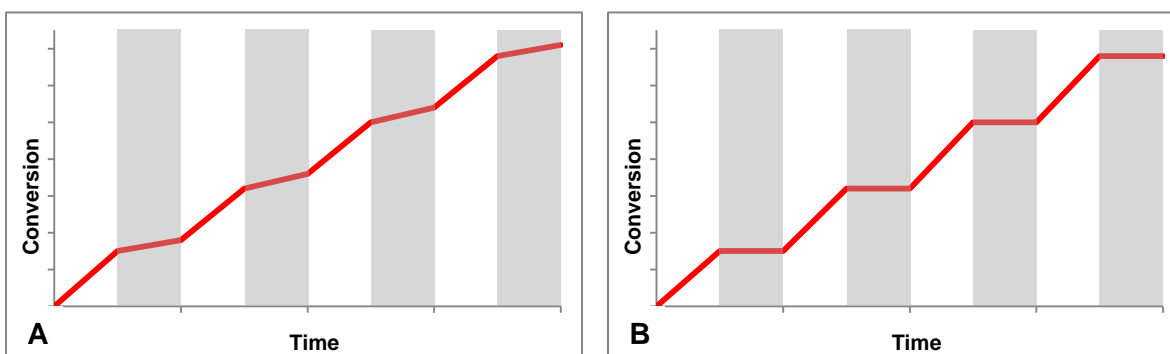


1.6.1 Light dependence studies

There are many different ways that chain propagation and its extent in the reaction have been probed. One of the more commonly used experiments to determine the presence of chain propagation is the “light/dark” experiment.⁵⁹ A light/dark experiment is performed by running

the photoredox catalyzed reaction under alternating periods of irradiation and darkness and the consumption of starting material or appearance of product is recorded and plotted over time (Figure 1-5). A positive test is observed when product formation continues to grow in during periods of darkness, indicating that the reaction can continue without the intermediacy of the photocatalyst. A negative test, in which product formation halts during periods of darkness, is often interpreted as disproving chain propagation since the system requires light to enable catalyst turnover. While this test has been performed frequently,^{60,61} it should be used with great caution. Radical chain lifetimes are commonly on the order of seconds to subseconds,⁶² and would end before conversion was measured,⁶³ thus yielding a false negative result. Indeed, in reactions that have provided stronger evidence for chain propagation (*vide infra*),⁶⁴ a negative result light/dark experiment has also been reported.

Figure 1-5. General example of a positive (A) and negative (B) light/dark experiment



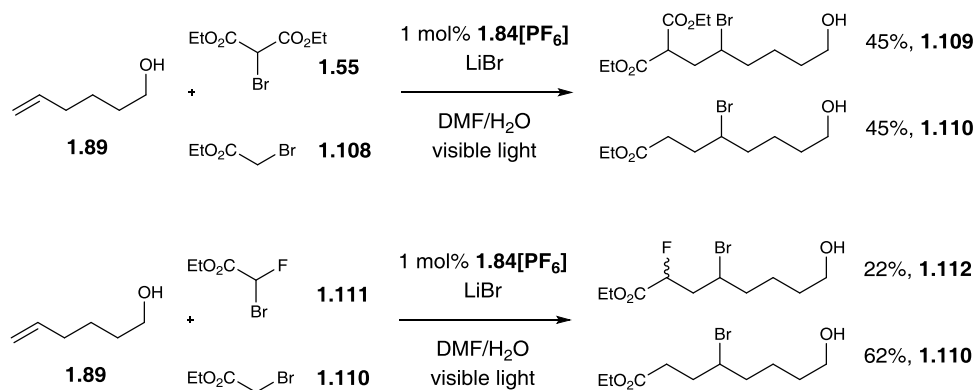
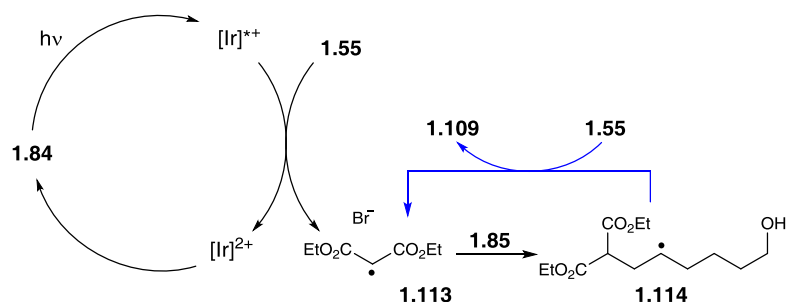
1.6.2 Additive effect studies

Many reactions that can be conducted under photoredox conditions also have non-photochemical versions that have been reported to be chains, such as the ATRA reaction⁶⁵ studied by Stephenson⁵⁰ and radical cation Diels–Alder of anethole and isoprene⁶⁶ reported by Yoon.³⁴ As such, the use of radical initiators in place of the photocatalyst has been used as evidence for

chain propagation. Both Kellogg¹⁰ and Okada and Oda⁶⁷ reported photochemical reactions that also proceed through the use of azobis(isobutylnitrile) (AIBN) as the radical initiator and heat, which corroborates the chain nature in their reactions. Conversely, Nishibayashi reported that his reported α -amino radical addition reactions could not be initiated with AIBN, BET_3 , or $(t\text{-BuO})_2$. While this evidence was interpreted to suggest that there is no chain propagation,^{46a} such negative results cannot be considered conclusive.

1.6.3 Crossover studies and kinetic isotope effects

In studying the photoredox ATRA reactions,^{50b} Stephenson discussed the potential of both radical chain propagation and (closed catalytic) radical-polar crossover mechanisms.⁶⁸ As evidence for formation of a carbocation and the radical-polar mechanism, Stephenson performed crossover experiments (Scheme 1-17) in which the carbocation was trapped with either a bromide ion or a tethered hydroxyl group (*vide supra*). Stephenson and coworkers also performed crossover experiments as evidence for chain propagation as well. The authors noted that while ethyl bromoacetate **1.108** cannot undergo ATRA because its reduction potential is higher than the potential for the catalyst, the addition of ethyl bromoacetate to a reaction involving the reducible diethyl bromomalonate **1.55**, both the ATRA products **1.109** and **1.110** are observed (Scheme 1-23). This result is consistent with the malonyl radical being able to reduce **1.108** through a chain propagation reaction (shown in blue). The authors conducted the same experiment with **1.111** and discovered that the ratio between the products **1.112** and **1.110** is different than the other experiment, indicating that the extent of chain propagation in the reaction is dependent upon the reaction components. This experiment is important because it shows that the extent of chain propagation is likely very sensitive to changes in the reaction conditions.

Figure 1-23. Evidence for chain propagation and proposed mechanism*chain propagation mechanism:*

As mentioned earlier, Yoon and coworkers used KIE data as evidence for chain propagation in the mechanism of α -amino radical addition into enones (Scheme 1-20).⁵⁶ In the co-catalytic Brønsted acid version of the reaction, they observed a primary KIE with respect to the tetrahydroisoquinone **1.97** and a secondary KIE with respect to the enone **1.100**, indicating that the rate limiting step of the mechanism must involve both species **1.97** and **1.100**. These data are consistent with chain propagation being the rate limiting step as the C–H/D bond in **1.97** is oxidized while the enone portion of **1.111** is being reduced during the propagation step. No other step of the catalytic cycle is consistent with these data. While these data are convincing evidence for chain propagation, chain processes are not always involved in the rate-limiting step and as such these experiments are not broadly applicable to other systems. An experiment that uses the

inherent photophysical properties, such as quantum yields, would be a more generalizable method.

1.6.4 Quantum yield measurements and chain length calculations

Quantum yields (Φ) have long been used to measure the effectiveness of photophysical and photochemical reactions. The quantum yield of a reaction is the efficiency of product formation relative to the amount of light absorbed (eq 1-6). To have a quantum yield of $\Phi = 1$, for every photon of light absorbed in a reaction, one molecule of product is generated. In an exclusive closed catalytic mechanism, the maximum quantum yield value is unity, whereas mechanisms involving chain propagation can have any quantum yield value greater than zero. Therefore, quantum yield values greater than unity have been used as evidence for a mechanism including chain propagation.^{12b,15b,10e,48v,57a,67,69}

$$\Phi = \frac{\text{moles of product formed}}{\text{moles of photons absorbed}} \quad \text{eq 1 - 6}$$

During the characterization of chain propagation by the Yoon group on a few typical photoredox reactions,^{15b} the authors measured the quantum yield for each reaction (Scheme 1-24). In all three cases studied the quantum yield value was large (44, 77, and 18 for eq 1-3, 1-4, 1-5 respectively), indicating that chain propagation was not only present but also a dominant part of the mechanism.

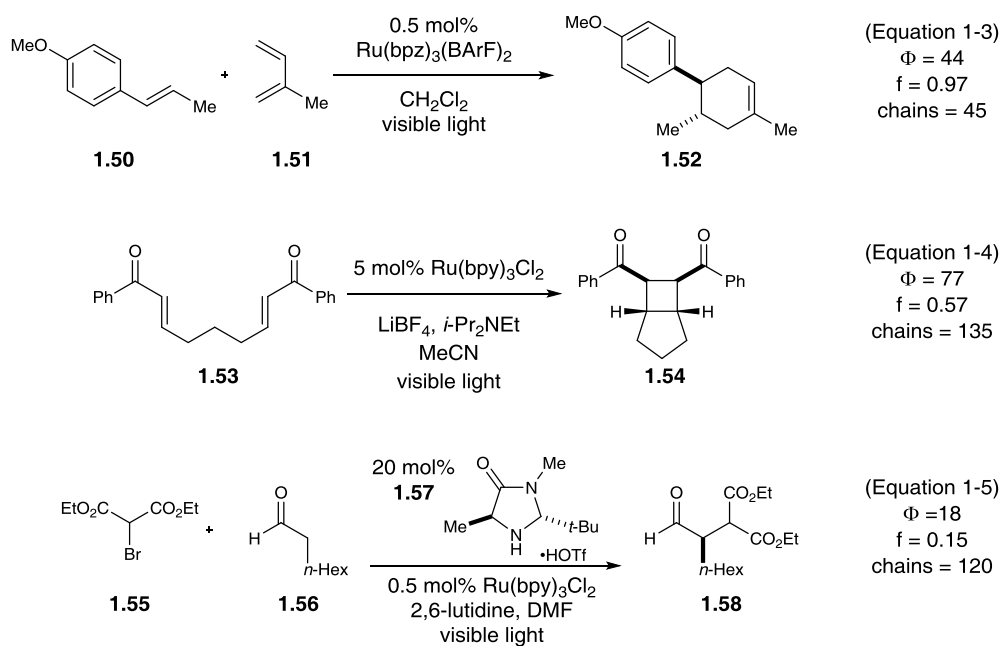
Reactions with a quantum yield less than unity have also been reported,^{11b,12b,13,14,20,30,40,60h,70} and in some cases have been used as evidence against chain propagation. While low quantum yields may indicate that a closed catalytic cycle mechanism is dominant, it cannot solely rule out the presence of chains. Quantum yield measurements relate product yield to photons absorbed,

but do not account for the loss of photons through non-productive pathways (e.g. phosphorescence, back electron transfer). One way to account for the photon waste and to calculate a low estimate of chain length is to divide the quantum yield by the quenching fraction. eq 1-7 takes into account the loss of photons due to phosphorescence, internal conversion, and non-productive electron and energy transfer, yet it does not account for back electron transfer.

$$\text{chain length} = \frac{\Phi}{f} \quad \text{eq 1 - 7}$$

The quenching fraction, f , is of the product-forming quencher in the system and is calculated using eq 1-2.

In the previous example by Yoon and coworkers, the chain lengths for the three reactions were calculated to be 45, 135, and 120 (Scheme 1-24).^{15b} Since the chain lengths were much greater than one, the authors again claimed that chain propagation was not only present in these mechanisms but also the main pathway. As each of the three reactions examined had a different intermediate (radical cation in 1-3, radical anion in 1-4, and radical in 1-5), this shows that chain propagation can be a dominant mechanism in a variety of photoredox reactions. The calculated chain lengths also demonstrate the importance of considering quenching efficiency when discussing the quantum yield measurement, and eqs 1-4 and 1-5 both show that the chain lengths are much longer than the quantum yields might suggest.

Scheme 1-24. Quantum yield and chain length for eqs 1-3, 1-4, and 1-5

1.7 Conclusion

As the interest in designing new transition metal based photoredox reactions has increased, there has been a desire to understand the mechanism of these reactions. The photochemical nature of these reactions enables a variety of spectroscopic techniques to probe the efficiency of quenching the excited state and explore further reactivity. Additionally, traditional physical organic experiments have also been used to investigate the mechanism. In some cases, a combination of multiple experiments (such as electrochemical and luminescence quenching data) is necessary to better understand of the mechanism. Some techniques (additive studies, and light/dark experiments) should be used with caution when drawing conclusions. With all these experiments available, researchers can begin to understand the mechanisms of these photoredox processes and design more efficient and new reactions.

1.8 References

1. Ciamician, G. "The photochemistry of the future" *Science* **1912**, *36*, 385–394.
2. (a) Kalyanasundaram, K. "Photophysics, photochemistry and solar energy conversion with tris(bipyridyl)ruthenium(II) and its analogues" *Coord. Chem. Rev.* **1982**, *46*, 159–244. (b) Juris, A.; Balzani, V.; Barigelletti, F.; Campagna, S.; Belser, P.; Von Zelewsky, A. "Ru(II) polypyridine complexes: photophysics, photochemistry, electrochemistry, and chemiluminescence" *Coord. Chem. Rev.* **1988**, *84*, 85–277.
3. Tucker, J. W.; Stephenson, C. R. J. "Shining Light on Photoredox Catalysis: Theory and Synthetic Applications" *J. Org. Chem.* **2012**, *77*, 1617–1622.
4. Prier, C. K.; Rankic, D. A.; MacMillan, D. W. C. "Visible Light Photoredox Catalysis with Transition Metal Complexes: Application in Organic Synthesis" *Chem. Rev.* **2013**, *113*, 5322–5663.
5. Ischay, M. A.; Ament, M. S.; Yoon, T. P. "Crossed intermolecular [2+2] cycloaddition of styrenes by visible light photocatalysis" *Chem. Sci.* **2012**, *3*, 2807–2811.
6. Tyson, E. L.; Niemeyer, Z. L.; Yoon, T. P. "Redox Mediators in Visible Light Photocatalysis: Photocatalytic Radical Thiol–ene Additions" *J. Org. Chem.* **2014**, *79*, 1427–1436.
7. (a) Tarantino, K. T.; Liu, P.; Knowles, R. R. "Catalytic Ketyl-Olefin Cyclization Enabled by Proton-Coupled Electron Transfer" *J. Am. Chem. Soc.* **2013**, *135*, 10022–10025. (b) Rono, L. J.; Yayla, H. G.; Wang, D. Y.; Armstrong, M. F.; Knowles, R. R. "Enantioselective Photoredox Catalysis Enabled by Proton-Coupled Electron Transfer: Development of an Asymmetric Aza-Pinacol Cyclization" *J. Am. Chem. Soc.* **2013**, *135*, 17735–17738. (c) Choi, G. J.; Knowles, R. B. "Catalytic Alkene Carboaminations Enabled by Oxidative Proton-Coupled Electron Transfer" *J. Am. Chem. Soc.* DOI: 10.1021/jacs.5b05377
8. (a) Qvortrup, K.; Rankic, D. A.; MacMillan, D. W. C. "A General Strategy for Organocatalytic Activation of C–H Bonds via Photoredox Catalysis: Direct Arylation of Benzylic Ethers" *J. Am. Chem. Soc.* **2014**, *136*, 626–629. (b) Hager, D.; MacMillan, D. W. C. "Activation of C–H Bonds via the Merger of Photoredox and Organocatalysis: A Coupling of Benzylic Ethers with Schiff Bases" *J. Am. Chem. Soc.* **2014**, *136*, 16986–16989.
9. Electrochemical potentials were used as evidence for the quenching of the photocatalyst.
10. van Bergen, T. J.; Hedstrand, D. M.; Kruizinga, W. H.; Kellogg, R. M. "Hydride Transfer from 1,4-Dihydropyridines to sp³-Hybridized Carbon in Sulfonium Salts and Activated Halides. Studies with NAD(P)H Models" *J. Org. Chem.* **1979**, *44*, 4953–4962.

-
11. (a) Pac, C.; Ihama, M.; Yasuda, M.; Miyauchi, Y.; Sakurai, H. "Ru(bpy)₃²⁺-Mediated Photoreduction of Olefins with 1-Benzyl-1,4-dihydronicotinamide: A Mechanistic Probe for Electron-Transfer Reactions of NAD(P)H-Model Compounds" *J. Am. Chem. Soc.* **1981**, *103*, 6495–6497. (b) Pac, C.; Miyauchi, Y.; Ishitani, O.; Ihama, M.; Yasuda, M.; Sakurai, H. "Redox-Photosensitized Reactions. 11. Ru(bpy)₃²⁺-Photosensitized Reactions of 1-Benzyl-1,4-dihydronicotinamide with Aryl-Substituted Enones, Derivatives of Methyl Cinnamate, and Substituted Cinnamitriles: Electron-Transfer Mechanism and Structure-Reactivity Relationships" *J. Org. Chem.* **1984**, *49*, 26–34.
12. (a) Maidan, R.; Goren, Z.; Becker, J. Y.; Willner, I. "Application of Multielectron Charge Relays in Chemical and Photochemical Debromination Processes. The Role of Induced Disproportionation of *N,N*-Dioctyl-4,4'-bipyridium Radical Cation in Two-Phase Systems" *J. Am. Chem. Soc.* **1984**, *106*, 6217–6222. (b) Willner, I.; Tsfania, T.; Eichen, Y. "Photocatalyzed and Electrocatalyzed Reduction of *vic*-Dibromides and Activated Ketones Using Ruthenium(I) Tris(bipyridine) as Electron-Transfer Mediator" *J. Org. Chem.* **1990**, *55*, 2656–2662.
13. (a) Cano-Yelo, H.; Deronzier, A. "Photocatalysis of the Pschorr Reaction by Tris-(2,2'-bipyridyl)ruthenium(II) in the Phenanthrene Series" *J. Chem. Soc. Perkin Trans. II* **1984**, 1093–1098. (b) Cano-Yelo, H.; Deronzier, A.; "Photo-oxidation of some carbinols by the Ru(II) polypyridyl complex-aryl diazonium salt system" *Tetrahedron Lett.* **1984**, *25*, 5517–5520.
14. (a) Hironaka, K.; Fukuzumi, S.; Tanaka, T. "Tris(bipyridyl)ruthenium(II)-photosensitized Reaction of 1-Benzyl-1,4-dihydronicotinamide with Benzyl Bromide" *J. Chem. Soc. Perkin Trans. II* **1984**, 1705–1709. (b) Fukuzumi, S.; Mochizuki, S.; Tanaka, T.; "Photocatalytic Reduction of Phenacyl Halides by 9,10-Dihydro-10-methylacridine. Control between the Reductive and Oxidative Quenching Pathways of Tris(bipyridine)ruthenium Complex Utilizing an Acid Catalysis" *J. Phys. Chem.* **1990**, *94*, 722–726.
15. (a) Blum, T. R.; Zhu, Y.; Nordeen, S. A.; Yoon, T. P. "Photocatalytic Synthesis of Dihydrobenzofurans by Oxidative [3+2] Cycloaddition of Phenols" *Angew. Chem Int. Ed.* **2014**, *53*, 11056–11059. (b) Cismesia, M. A.; Yoon, T. P. "Characterizing chain processes in visible light photoredox catalysis" *Chem. Sci.* **2015** DOI: 10.1039/c5sc02185e
16. (a) Nicewicz, D. A.; MacMillan, D. W. C. "Merging Photoredox Catalysis with Organocatalysis: The Direct Asymmetric Alkylation of Aldehydes" *Science* **2008**, *322*, 77–80. (b) Nagib, D. A.; Scott, M. E.; MacMillan, D. W. C. "Enantioselective α -Trifluoromethylation of Aldehydes via Photoredox Organocatalysis" *J. Am. Chem. Soc.* **2009**, *131*, 10875–10877. (c) Shih, H.-W.; Vander Wal, M. N.; Grange, R. L.; MacMillan, D. W. C. "Enantioselective α -Benzylation of Aldehydes via Photoredox Organocatalysis" *J. Am. Chem. Soc.* **2010**, *132*, 13600–13603. (d) McNally, A.; Prier, C. K.; MacMillan, D. W. C. "Discovery of an α -Amino C–H Arylation Reaction Using the Strategy of Accelerated Serendipity" *Science* **2011**, *334*, 1114–1117. (e) Terrett, J. A.; Clift, M. D.; MacMillan, D. W. C. "Direct β -Alkylation of Aldehydes via Photoredox Organocatalysis" *J. Am. Chem.*

- Soc.* **2014**, *136*, 6858–6861. (f) Petronijević, F. R.; Nappi, M.; MacMillan, D. W. C. “Direct β -Functionalization of Cyclic Ketones with Aryl Ketones via the Merger of Photoredox and Organocatalysis” *J. Am. Chem. Soc.* **2013**, *135*, 18323–18326. (g) Prier, C. K.; MacMillan, D. W. C. “Amine α -heteroarylation via photoredox catalysis: a homolytic aromatic substitution pathway” *Chem. Sci.* **2014**, *5*, 4173–4178. (h) Ventre, S.; Petronijević, F. R.; MacMillan, D. W. C. “Decarboxylative Fluorination of Aliphatic Carboxylic Acids via Photoredox Catalysis” *J. Am. Chem. Soc.* **2015**, *137*, 5654–5657. (i) Jeffrey, J. L.; Petronijević, F. R.; MacMillan, D. W. C. “Selective Radical–Radical Cross-Couplings: Design of a Formal β -Mannich Reaction” *J. Am. Chem. Soc.* **2015**, *137*, 8404–8407.
17. (a) Condie, A. G.; González-Gómez, J. C.; Stephenson, C. R. J. “Visible-Light Photoredox Catalysis: Aza-Henry Reactions via C–H Functionalization” *J. Am. Chem. Soc.* **2010**, *132*, 1464–1465. (b) Furst, L.; Matsuura, B. S.; Narayanam, J. M. R.; Tucker, J. W.; Stephenson, C. R. J. “Visible Light-Mediated Intermolecular C–H Functionalization of Electron-Rich Heterocycles with Malonates” *Org. Lett.* **2010**, *12*, 3104–3107. (c) Dai, C.; Narayanam, J. M. R.; Stephenson, C. R. J. “Visible-light-mediated conversion of alcohols to halides” *Nature Chem.* **2011**, *3*, 140–145. (d) Douglas, J. J.; Cole, K. P.; Stephenson, C. R. J. “Photoredox Catalysis in a Complex Pharmaceutical Setting: Toward the Preparation of JAK2 Inhibitor LY2784544” *J. Org. Chem.* **2014**, *79*, 11631–11643. (e) Devery, J. J.; Douglas, J. J.; Nguyen, J. D.; Cole, K. P.; Flowers, R. A.; Stephenson, C. R. J. “Ligand functionalization as a deactivation pathway in a *fac*-Ir(ppy)₃-mediated radical addition” *Chem. Sci.* **2015**, *6*, 537–541.
18. Pitre, S. P.; McTiernan, C. D.; Ismaili, H.; Scaiano, J. C. “Mechanistic Insights and Kinetic Analysis for the Oxidative Hydroxylation of Arylboronic Acids by Visible Light Photoredox Catalysis: A Metal-Free Alternative” *J. Am. Chem. Soc.* **2013**, *135*, 13286–13289.
19. Musacchio, A. J.; Nguyen, L. Q.; Beard, G. H.; Knowles, R. R. “Catalytic Olefin Hydroamination with Aminium Radical Cations: A Photoredox Method for Direct C–N Bond Formation” *J. Am. Chem. Soc.* **2014**, *136*, 12217–12220.
20. Miyake, Y.; Nakajima, K.; Nishibayashi, Y. “Visible light-mediated oxidative decarboxylation of arylacetic acids into benzyl radicals: addition to electron-deficient alkenes by using photoredox catalysts” *Chem. Commun.* **2013**, *49*, 7854–7856.
21. (a) Koike, T.; Yasu, Y.; Akita, M. “Visible-light-driven Oxidation of 1,3-Dicarbonyl Compounds via Catalytic Disproportionation of TEMPO by Photoredox Catalysis” *Chem. Lett.* **2012**, *41*, 999–1001. (b) Yasu, Y.; Koike, T.; Akita, M. “Three-component Oxytrifluoromethylation of Alkenes: Highly Efficient and Regioselective Difunctionalization of C=C Bonds Mediated by Photoredox Catalysis” *Angew. Chem. Int. Ed.* **2012**, *51*, 9567–9571. (c) Miyazawa, K.; Yasu, Y.; Koike, T.; Akita, M. “Visible-light-induced hydroalkoxymethylation of electron-deficient alkenes by photoredox catalysis” *Chem. Commun.* **2013**, *49*, 7249–7251. (d) Yasu, Y.; Arai, Y.; Tomita, R.; Koike, T.; Akita, M. “Highly Regio- and Diastereoselective Synthesis of CF₃-Substituted Lactones via Photoredox-Catalyzed Carbolactonization of Alkenoic Acids” *Org. Lett.* **2014**, *16*, 780–783.

- (e) Miyazawa, K.; Koike, T.; Akita, M. "Hydroaminomethylation of Olefins with Aminomethyltrifluoroborate by Photoredox Catalysis" *Adv. Synth. Catal.* **2014**, *356*, 2749–2755. (f) Li, Y.; Miyazawa, K.; Koike, T.; Akita, M. "Alkyl- and aryl-thioalkylation of olefins with organotrifluoroborates by photoredox catalysis" *Org. Chem. Front.* **2015**, *2*, 319–323.
22. (a) Zou, Y.-Q.; Guo, W.; Liu, F.-L.; Lu, L.-Q.; Chen, J.-R.; Xiao, W.-J. "Visible-light-induced photocatalytic formyloxylations of 3-bromooxindoles with water and DMF: the scope and mechanism" *Green Chem.* **2014**, *16*, 3787–3795. (b) Hu, X.-Q.; Chen, J.-R.; Wei, Q.; Liu, F.-L.; Deng, Q.-H.; Beauchemin, A. M.; Xiao, W.-J. "Photocatalytic Generation of N-Centered Hydrazone Radicals: A Strategy for Hydroamination of β,γ -Unsaturated Hydrazones" *Angew. Chem. Int. Ed.* **2014**, *53*, 12163–12167. (c) Ding, W.; Zhou, Q.-Q.; Xuan, J.; Li, T.-R.; Lu, L.-Q.; Xiao, W.-J. "Photocatalytic aerobic oxidation/semipinacol rearrangement sequence: a concise route to the core of pseudooxindole alkaloids" *Tetrahedron Lett.* **2014**, *55*, 4648–4652. (d) Xia, X.-D.; Ren, Y.-L.; Chen, J.-R.; Yu, X.-L.; Lu, L.-Q.; Zou, Y.-Q.; Wan, J.; Xiao, W.-J. "Phototandem Catalysis: Efficient Synthesis of 3-Ester-3-hydroxy-2-oxindoles by a Visible Light-Induced Cyclization of Diazoamides through an Aerobic Oxidation Sequence" *Chem. Asian J.* **2015**, *10*, 124–128.
23. Brachet, E.; Ghosh, T.; Ghosh, I.; König, B. "Visible light C–H amidation of heteroarenes with benzoyl azides" *Chem. Sci.* **2015**, *6*, 987–992.
24. (a) Liu, Q.; Yi, H.; Liu, J.; Yang, Y.; Zhang, X.; Zeng, Z.; Lei, A. "Visible-Light Photocatalytic Radical Alkenylation of α -Carbonyl Alkyl Bromides and Benzyl Bromides" *Chem. Eur. J.* **2013**, *19*, 5120–5126. (b) Yi, H.; Zhang, X.; Qin, C.; Liao, Z.; Liu, J.; Lei, A. "Visible Light-Induced γ -Alkoxy nitrile Synthesis via Three-Component Alkoxy cyanomethylation of Alkenes" *Adv. Synth. Catal.* **2014**, *356*, 2873–2877. (c) Wei, X.-J.; Yang, D.-T.; Wang, L.; Song, T.; Wu, L.-Z.; Liu, Q. "A Novel Intermolecular Synthesis of γ -Lactones via Visible-Light Photoredox Catalysis" *Org. Lett.* **2013**, *15*, 6054–6057. (d) Wang, L.; Wei, X.-J.; Jia, W.-L.; Zhong, J.; Wu, L.-Z.; Liu, Q. "Visible-Light-Driven Difluoroacetamidation of Unactive Arenes and Heteroarenes by Direct C–H Functionalization at Room Temperature" *Org. Lett.* **2014**, *16*, 5842–5845.
25. Singh, A.; Arora, A.; Weaver, J. D. "Photoredox-Mediated C–H Functionalization and Coupling of Tertiary Aliphatic Amines with 2-Chloroazoles" *Org. Lett.* **2013**, *15*, 5390–5393.
26. Yoo, W.-J.; Tsukamoto, T.; Kobayashi, S. "Visible-Light-Mediated Chan–Lam Coupling Reactions of Aryl Boronic Acids and Aniline Derivatives" *Angew. Chem. Int. Ed.* **2015**, *54*, 6587–6590.
27. Lu, P.; Hou, T.; Gu, X.; Li, P. "Visible-Light-Promoted Conversion of Alkyl Benzyl Ether to Alkyl Ester of Alcohol via O- α -sp³ C–H Cleavage" *Org. Lett.* **2015**, *17*, 1954–1957.

-
28. (a) Herance, J. R.; Ferrer, B.; Bourdelande, J. L.; Marquet, J.; Garcia, H. "A Photocatalytic Acid- and Base-Free Meerwein-Ponndorf-Verley-Type Reduction Using a $[\text{Ru}(\text{bpy})_3]^{2+}$ /Viologen Couple" *Chem. Eur. J.* **2006**, *12*, 3890–3895. (b) Yu, C.; Lee, K.; You, Y.; Cho, E. J. "Synthesis of 2-Substituted Benzothiazoles by Visible Light-Driven Photoredox Catalysis" *Adv. Synth. Catal.* **2013**, *355*, 1471–1476. (c) Iqbal, N.; Choi, S.; You, Y.; Cho, E. J. "Aerobic oxidation of aldehydes by visible light photocatalysis" *Tetrahedron Lett.* **2013**, *54*, 6222–6225. (d) Jung, J.; Kim, E.; You, Y.; Cho, E. J. "Visible Light-Induced Aromatic Difluoroalkylation" *Adv. Synth. Catal.* **2014**, *356*, 2741–2748. (e) Choi, W. J.; Choi, S.; Ohkubo, K.; Fukuzumi, S.; Cho, E. J.; You, Y. "Mechanisms and applications of cyclometalated Pt(II) complexes in photoredox catalytic trifluoromethylation" *Chem. Sci.* **2015**, *6*, 1454–1464.
29. In some cases the line will curve upwards at higher concentrations of quencher due to transient effects or static quenching.
30. Miyake, Y.; Nakajima, K.; Nishibayashi, Y. "Direct sp^3 C–H Amination of Nitrogen-Containing Benzoheterocycles Mediated by Visible-Light-Photoredox Catalysts" *Chem. Eur. J.* **2012**, *18*, 16473–16477.
31. Rueda-Becerril, M.; Mahé, O.; Drouin, M.; Majewski, M. B.; West, J. G.; Wolf, M. O.; Sammis, G. M.; Paquin, J.-F. "Direct C–F Bond Formation Using Photoredox Catalysis" *J. Am. Chem. Soc.* **2014**, *136*, 2637–2641.
32. A difference spectrum is the excited state absorption spectrum minus the ground state absorption spectrum. The band *ca.* 370 nm corresponds to $\text{Ru}(\text{bpy})_3^{2+*}$ and decreases over time as it relaxes back to the ground state while the band *ca.* 450 nm corresponds to $\text{Ru}(\text{bpy})_3^{2+}$ and increases over time as the ground state is regenerated. A flat line indicates all ruthenium species are $\text{Ru}(\text{bpy})_3^{2+}$.
33. A discussion of quantum yields is given in section 1.6.
34. Lin, S.; Ischay, M. A.; Fry, C. G.; Yoon, T. P. "Radical Cation–Diels Alder Cycloadditions by Visible Light Photocatalysis" *J. Am. Chem. Soc.* **2011**, *133*, 19350–19353.
35. Ischay, M. A.; Anzovino, M. E.; Du, J.; Yoon, T. P. "Efficient Visible Light Photocatalysis of [2+2] Enone Cycloadditions" *J. Am. Chem. Soc.* **2008**, *130*, 12886–12887.
36. Andrews, R. S.; Becker, J. J.; Gagné, M. R. "Investigating the Rate of Photoreductive Glucosyl Radical Generation" *Org. Lett.* **2011**, *13*, 2406–2409.
37. (a) DeLaive, P. J.; Lee, J. T.; Sprintschnik, H. W.; Abruña, H.; Meyer, T. J.; Whitten, D. G. "Photoinduced Redox Reactions of Hydrophobic Ruthenium(II) Complexes" *J. Am. Chem. Soc.* **1977**, *99*, 7094–7097. (b) DeLaive, P. J.; Foreman, T. K.; Giannotti, C.; Whitten, D. G. "Photoduced Electron Transfer Reactions of Transition-Metal Complexes with Amines."

-
- Mechanistic Studies of Alternate Pathways to Back Electron Transfer” *J. Am. Chem. Soc.* **1980**, *102*, 5627–5631.
38. Huo, H.; Shen, X.; Wang, C.; Röse P.; Chen, L.-A.; Harms, K.; Marsch, M.; Hilt, G.; Meggers, E. “Asymmetric photoredox transition-metal catalysis activated by visible light” *Nature* **2014**, *515*, 100–103.
39. It should be noted that the authors compare the slopes in the luminescence quenching experiments but as the slope is dependent on both the photocatalyst lifetime and rate of quenching, the comparison of only the slopes is inconclusive. A comparison of the rate of quenching would be more informative.
40. Ohzu, S.; Ishizuka, T.; Hirai, Y.; Fukuzumi, S.; Kojima, T. “Photocatalytic Oxidation of Organic Compounds in Water Using Ruthenium(II)-Pyridylamine Complexes as Catalysts with High Efficiency and Selectivity” *Chem. Eur. J.* **2013**, *19*, 1563–1567.
41. Shu, X.-Z.; Zhang, M.; He, Y.; Frei, H.; Toste, F. D. “Dual Visible Light Photoredox and Gold-Catalyzed Arylative Ring Expansion” *J. Am. Chem. Soc.* **2014**, *136*, 5844–5847.
42. Liu, J.; Liu, Q.; Yi, H.; Qin, C.; Bai, R.; Qi, X.; Lan, Y.; Lei, A. “Visible-Light-Mediated Decarboxylation/Oxidative Amidation of α -Keto Acids with Amines under Mild Reaction Conditions Using O_2 ” *Angew. Chem. Int. Ed.* **2014**, *53*, 502–506.
43. (a) Andrews, R. S.; Becker, J. J.; Gagné, M. R. “Intermolecular Addition of Glycosyl Halides to Alkenes Mediated by Visible Light” *Angew. Chem. Int. Ed.* **2010**, *49*, 7274–7276. (b) Wang, L.; Wei, X.-J.; Jia, W.-L.; Zhong, J.-J.; Wu, L.-Z.; Liu, Q. “Visible-Light-Driven Difluoroacetamidation of Unactive Arenes and Heteroarenes by Direct C–H Functionalization at Room Temperature” *Org. Lett.* **2014**, *16*, 5842–5845.
44. Cyclopropyl rings are just one example of radical clocks, typically used to determine the lifetime of the radical. As such, a negative result does not necessarily indicate a lack of radical species but can rather indicate a short-lived species. See: (a) Griller, D.; Ingold, K. U. “Free-Radical Clocks” *Acc. Chem. Res.* **1980**, *13*, 317–323. (b) Newcomb, M. “Competition Methods and Scales for Alkyl Radical Reaction Kinetics” *Tetrahedron* **1993**, *49*, 1151–1176.
45. Narayanam, J. M. R.; Tucker, J. W.; Stephenson, C. R. J. “Electron-Transfer Photoredox Catalysis: Development of a Tin-Free Reductive Dehalogenation Reaction” *J. Am. Chem. Soc.* **2009**, *131*, 8756–8757.
46. (a) Miyake, Y.; Nakajima, K.; Nishibayashi, Y. “Visible-Light-Mediated Utilization of α -Aminoalkyl Radicals: Addition to Electron-Deficient Alkenes Using Photoredox Catalysts” *J. Am. Chem. Soc.* **2012**, *134*, 3338–3341. (b) Zlotorzynska, M.; Sammis, G. M. “Photoinduced Electron-Transfer-Promoted Redox Fragmentation of *N*-Alkoxyphthalimides” *Org. Lett.* **2011**, *13*, 6264–6267. (c) Qin, Q.; Yu, S. “Visible-Light-

- Promoted Remote C(sp³)-H Amidation and Chlorination” *Org. Lett.* **2015**, *17*, 1894–1897. (d) Zhou, Q.-Q.; Guo, W.; Ding, W.; Wu, X.; Chem, X.; Lu, L.-Q.; Xiao, W.-J. “Decarboxylative Alkynylation and Carbonylative Alkynylation of Carboxylic Acids Enabled by Visible-Light Photoredox Catalysis” *Angew. Chem. Int. Ed.* DOI: 10.1002/anie.201504559
47. Sun, H.; Yang, C.; Gao, F.; Li, Z.; Xia, W. “Oxidative C–C Bond Cleavage of Aldehydes via Visible-Light Photoredox Catalysis” *Org. Lett.* **2013**, *15*, 624–627.
48. (a) Neufeldt, S. R.; Sanford, M. S. “Combining Transition Metal Catalysis with Radical Chemistry: Dramatic Acceleration of Palladium-Catalyzed C–H Arylation with Diaryliodonium Salts” *Adv. Synth. Catal.* **2012**, *354*, 3517–3522. (b) Courant, T.; Masson, G. “Photoredox-Initiated α -Alkylation of Imine through a Three-Component Radical/Cationic Reaction” *Chem. Eur. J.* **2012**, *18*, 423–427. (c) Jiang, H.; Huang, C.; Guo, J.; Zeng, C.; Zhang, Y.; Yu, S. “Direct C–H Functionalization of Enamides and Enecarbamates by Using Visible-Light Photoredox Catalysis” *Chem. Eur. J.* **2012**, *18*, 15158–15166. (d) Paria, S.; Pirtsch, M.; Kais, V.; Reiser, O. “Visible-Light-Induced Intermolecular Atom-Transfer Radical Addition of Benzyl Halides to Olefins: Facile Synthesis of Tetrahydroquinolines” *Synthesis* **2013**, *45*, 2689–2698. (e) Guo, L.; Yang, C.; Zheng, L.; Xia, W. “Visible light-mediated oxidative quenching reaction to electron rich epoxides: highly regioselective synthesis of α -bromo (di)ketones and mechanism study” *Org. Biomol. Chem.* **2013**, *11*, 5787–5792. (f) Liu, Y.-X.; Xue, D.; Wang, J.-D.; Zhao, C.-J.; Zou, Q.-Z.; Wang, C.; Xiao, J. “Room-Temperature Arylation of Arenes and Heteroarenes with Diaryliodonium Salts by Photoredox Catalysis” *Synlett* **2013**, *24*, 507–513. (g) Jiang, H.; Cheng, Y.; Wang, R.; Zheng, M.; Zhang, Y.; Yu, S. “Synthesis of 6-Alkylated Phenanthridine Derivatives Using Photoredox Neutral Somophilic Isocyanide Insertion” *Angew. Chem. Int. Ed.* **2013**, *52*, 13289–13292. (h) Jiang, H.; Cheng, Y.; Zhang, Y.; Yu, S. “Sulfonation and Trifluoromethylation of Enol Acetates with Sulfonyl Chlorides Using Visible-Light Photoredox Catalysis” *Eur. J. Org. Chem.* **2013**, 5485–5492. (i) Hari, D. P.; Hering, T.; König, B. “The Photoredox-Catalyzed Meerwein Addition Reaction; Intermolecular Amino-Arylation of Alkenes” *Angew. Chem. Int. Ed.* **2014**, *53*, 725–728. (j) Paria, S.; Kais, V.; Reiser, O. “Visible Light-Mediated Coupling of α -Bromo chalcones with Alkenes” *Adv. Synth. Catal.* **2014**, *356*, 2853–2858. (k) Cheng, Y.; Yuan, X.; Jiang, H.; Wang, R.; Ma, J.; Zhang, Y.; Yu, S. “Regiospecific Synthesis of 1-Trifluoromethylisoquinolines Enabled by Photoredox Somophilic Vinyl Isocyanide Insertion” *Adv. Synth. Catal.* **2014**, *356*, 2859–2866. (l) Qin, Q.; Yu, S. “Visible-Light-Promoted Redox Neutral C–H Amidation of Heteroarenes with Hydroxylamine Derivatives” *Org. Lett.* **2014**, *16*, 3504–3507. (m) Dagousset, G.; Carboni, A.; Magnier, E.; Masson, G. “Photoredox-Induced Three-Component Azido- and Aminotrifluoromethylation of Alkenes” *Org. Lett.* **2014**, *16*, 4340–4343. (n) Xu, P.; Abdulkader, A.; Hu, K.; Cheng, Y.; Zhu, C. “Room temperature decarboxylative trifluoromethylation of α,β -unsaturated carboxylic acids by photoredox catalysis” *Chem. Commun.* **2014**, *50*, 2038–2310. (o) Nakajima, M.; Lefebvre, Q.; Rueping, M. “Visible light photoredox-catalysed intermolecular radical addition of α -halo amides to olefins” *Chem. Commun.* **2014**, *50*, 3619–3622. (p) Jiang, H.; Cheng, Y.; Wang, R.; Zhang, Y.; Yu, S. “Synthesis of isoquinolines via visible light-

- promoted insertion of vinyl isocyanides with diaryliodonium salts” *Chem. Commun.* **2014**, 50, 6164–6167. (q) Carboni, A.; Dagousset, G.; Magnier, E.; Masson, G. “One pot and selective intermolecular aryl- and heteroaryl-trifluoromethylation of alkenes by photoredox catalysis” *Chem. Commun.* **2014**, 50, 14197–14200. (r) Senaweera, S. M.; Singh, A.; Weaver, J. D. “Photocatalytic Hydrodefluorination: Facile Access to Partially Fluorinated Aromatics” *J. Am. Chem. Soc.* **2014**, 136, 3002–3005. (s) Yao, C.-J.; Sun, Q.; Rastogi, N.; König, B. “Intermolecular Formyloxylation of Alkenes by Photoredox Meerwein Reaction” *ACS Catal.* **2015**, 5, 2935–2938. (t) Xie, J.; Shi, S.; Zhang, T.; Mehrkens, N.; Rudolph, M.; Hashmi, A. S. K. “A Highly Efficient Gold-Catalyzed Photoredox α -C(sp³)-H Alkynylation of Tertiary Aliphatic Amines with Sunlight” *Angew. Chem. Int. Ed.* **2015**, 54, 6046–6050. (u) Lin, R.; Sun, H.; Yang, C.; Shen, W.; Xia, W. “Visible light-induced difunctionalization of electron-enriched styrenes: synthesis of tetrahydrofurans and tetrahydropyrans” *Chem. Commun.* **2015**, 51, 399–401. (v) Sahoo, B.; Li, J.-L.; Glorius, F. “Visible-Light Photoredox-Catalyzed Semipinacol-Type Rearrangement: Trifluoromethylation/Ring Expansion via a Radical-Polar Mechanism” *Angew. Chem. Int. Ed.* DOI: 10.1002/anie.201503210 (w) Fumagalli, G.; Rabet, P. T. G.; Boyd, S.; Greaney, M. F. “Three-Component Azidation of Styrene-Type Double Bonds: Light-Switchable Behavior of a Copper Photoredox Catalyst” *Angew. Chem. Int. Ed.* DOI: 10.1002/anie.201502980
49. Sun, H.; Yang, C.; Lin, R.; Xia, W. “Regioselective Ring-Opening Nucleophilic Addition of Aziridines through Photoredox Catalyst” *Adv. Synth. Catal.* **2014**, 356, 2775–2780.
50. (a) Nguyen, J. D.; Tucker, J. W.; Konieczynska, M. D.; Stephenson, C. R. J. “Intermolecular Atom Transfer Radical Addition to Olefins Mediated by Oxidative Quenching of Photoredox Catalysts” *J. Am. Chem. Soc.* **2011**, 133, 4160–4163. (b) Wallentin, C.-J.; Nguyen, J. D.; Finkbeiner, P.; Stephenson, C. R. J. “Visible Light-Mediated Atom Transfer Radical Addition via Oxidative and Reductive Quenching of Photocatalysts” *J. Am. Chem. Soc.* **2012**, 134, 8875–8884.
51. a) Gu, X.; Li, X.; Qu, Y.; Yang, Q.; Li, P.; Yao, Y. “Intermolecular Visible-Light Photoredox Atom-Transfer Radical [3+2]-Cyclization of 2-(Iodomethyl)cyclopropane-1,1-dicarboxylate with Alkenes and Alkynes” *Chem. Eur. J.* **2013**, 19, 11878–11882. b) Zhao, G.; Yang, C.; Guo, L.; Chen, C.; Xia, W. “Visible light-induced oxidative coupling reaction: easy access to Mannich-type products” *Chem. Commun.* **2012**, 48, 2337–2339.
52. The ATRA mechanism is further discussed in section 1.6.
53. (a) Parrish, J. D.; Ischay, M. A.; Lu, Z.; Guo, S.; Peters, N.; Yoon, T. P. “Endoperoxide Synthesis by Photocatalytic Aerobic [2+2+2] Cycloadditions” *Org. Lett.* **2012**, 14, 1640–1643. (b) Xhu, S.; Das, A.; Bui, L.; Zhou, H.; Curran, D. P.; Rueping, M. “Oxygen Switch in Visible-Light Photoredox Catalysis: Radical Additions and Cyclizations and Unexpected C–C-Bond Cleavage Reactions” *J. Am. Chem. Soc.* **2013**, 135, 1823–1829. (c) Fabry, D. C.; Zoller, J.; Raja, S.; Rueping, M. “Combining Rhodium and Photoredox Catalysis for the C–H Functionalizations of Arenes: Oxidative Heck Reactions with Visible Light” *Angew. Chem. Int. Ed.* **2014**, 53, 10228–10231.

-
54. Allen, L. J.; Cabrera, P. J.; Lee, M.; Sanford, M. S. “*N*-Acyloxyphthalimides as Nitrogen Radical Precursors in the Visible Light Photocatalyzed Room Temperature C–H Amination of Arenes and Heteroarenes” *J. Am. Chem. Soc.* **2014**, *136*, 5607–5610.
55. LEDs are not always more intense than CFL, but in Ru(bpy)₃²⁺ catalyzed reactions blue LEDs are more intense than a CFL in the region that the photocatalyst absorbs.
56. Ruiz Espelt, L.; Wiensch, E. M.; Yoon, T. P. “Brønsted Acid Cocatalysts in Photocatalytic Radical Addition of α -Amino C–H Bonds across Michael Acceptors” *J. Org. Chem.* **2013**, *78*, 4107–4114.
57. (a) Okada, K.; Okamoto, K.; Morita, N.; Okubo, K.; Oda, M. “Photosensitized Decarboxylative Michael Addition through *N*-(Acyloxy)phthalimides via an Electron-Transfer Mechanism” *J. Am. Chem. Soc.* **1991**, *113*, 9401–9402. (b) Du, J.; Ruiz Espelt, R.; Guzei, I. A.; Yoon, T. P. “Photocatalytic reductive cyclizations of enones: Divergent reactivity of photogenerated radical and radical anion intermediates” *Chem. Sci.* **2011**, *2*, 2115–2119. (c) Zou, Y.-Q.; Chen, J.-R.; Liu, X.-P.; Lu, L.-Q.; Davis, R. L.; Jørgenson, K. A.; Xiao, W.-J. “Highly Efficient Aerobic Oxidative Hydroxylation of Arylboronic Acids: Photoredox Catalysis Using Visible Light” *Angew. Chem. Int. Ed.* **2012**, *51*, 784–788. (d) Sahoo, B.; Hopkinson, M. N.; Glorius, F. “Combining Gold and Photoredox Catalysis: Light-Mediated Oxy- and Aminoarylation of Alkenes” *J. Am. Chem. Soc.* **2013**, *135*, 5505–5508. (e) Guo, W.; Cheng, H.-G.; Chen, L.-Y.; Xuan, J.; Feng, Z.-J.; Chen, J.-R.; Lu, L.-Q.; Xiao, W.-J. “*De Novo* Synthesis of γ,γ -Disubstituted Butyrolactones through a Visible Light Photocatalytic Arylation–Lactonization Sequence” *Adv. Synth. Catal.* **2014**, *356*, 2787–2793. (f) Hollister, K. A.; Conner, E. S.; Spell, M. L.; Deveaux, K.; Maneval, L.; Beal, M. W.; Ragains, J. R. “Remote Hydroxylation through Radical Translocation and Polar Crossover” *Angew. Chem. Int. Ed.* **2015**, *54*, 7837–7841. (g) Lackner, G. L.; Quasdorf, K. W.; Pratsch, G.; Overman, L. E. “Fragment Coupling and the Construction of Quaternary Carbons Using Tertiary Radicals Generated From *tert*-Alkyl *N*-Phthalimidoyl Oxalates By Visible-Light Photocatalysis” *J. Org. Chem.* **2015**, *80*, 6012–6024. (h) Pratsch, G.; Lackner, G. L.; Overman, L. E. “Constructing Quaternary Carbons from *N*-(Acyloxy)phthalimide Precursors of Tertiary Radicals Using Visible-Light Photocatalysis” *J. Org. Chem.* **2015**, *80*, 6025–6036.
58. The authors also used luminescence quenching, NMR and IR data as evidence for their proposed mechanism.
59. The “light/dark” experiment is also referred to as “on/off” and light dependence experiments.
60. These references exhibit a negative light/dark plot (a) see ref. 6, 15, 17d, 17e, 21b, 21f, 22a, 22b, 24, 46a, 46b, 48b, 48c, 48g, 48h, 48m, 48p, 48q, 48t, 50, 51a, 53b, 54, 56, 57d (b) Shimizu, H.; Onitsuka, S.; Egami, H.; Katsuki, T. “Ruthenium(salen)-Catalyzed Aerobic Oxidative Desymmetrization of *meso*-Diols and Its Kinetics” *J. Am. Chem. Soc.* **2005**, *127*,

5396–5413. (c) Yasu, Y.; Koike, T.; Akita, M. “Visible Light-Induced Selective Generation of Radicals from Organoborates by Photoredox Catalysis” *Adv. Synth. Catal.* **2012**, *354*, 3414–3420. (d) Gu, X.; Lu, P.; Fan, W.; Li, P.; Yao, Y. “Visible light photoredox atom transfer Ueno-Stork reaction” *Org. Biomol. Chem.* **2013**, *11*, 7088–7091. (e) Wever, W. J.; Cinelli, M. A.; Bowers, A. A. “Visible Light Mediated Activation and *O*-Glycosylation of Thioglycosides” *Org. Lett.* **2013**, *15*, 30–33. (f) Mizuta, S.; Engle, K. M.; Verhoog, S.; Galicia-López, O.; O’Duill, M.; Médebielle, M.; Wheelhouse, K.; Rassias, G.; Thompson, A. L.; Gouveneur, V. “Trifluoromethylation of Allylsilanes under Photoredox Catalysis” *Org. Lett.* **2013**, *15*, 1250–1253. (g) Zhou, H.; Lu, P.; Gu, X.; Li, P. “Visible-Light-Mediated Nucleophilic Addition of an α -Aminoalkyl Radical to Isocyanate or Isothiocyanate” *Org. Lett.* **2013**, *15*, 5646–5649. (h) Oh, S. H.; Malpani, Y. R.; Ha, N.; Jung, Y.-S.; Han, S. B. “Vicinal Difunctionalization of Alkenes: Chlorotrifluoromethylation with $\text{CF}_3\text{SO}_2\text{Cl}$ by Photoredox Catalysis” *Org. Lett.* **2014**, *16*, 1310–1313. (i) Tomita, R.; Yasu, Y.; Koike, T.; Akita, M. “Direct C–H trifluoromethylation of di- and trisubstituted alkenes by photoredox catalysis” *Beilstein J. Org. Chem.* **2014**, *10*, 1099–1106. (j) Stevenson, S. M.; Shores, M. P.; Ferreira, E. M. “Photooxidizing Chromium Catalysts for Promoting Radical Cation Cycloadditions” *Angew. Chem. Int. Ed.* **2015**, *54*, 6506–6510. (k) Deng, Q.-H.; Chen, J.-R.; Wei, Q.; Zhao, Q.-Q.; Lu, L.-Q.; Xiao, W.-J. “Visible-light-induced photocatalytic oxytrifluoromethylation of *N*-allylamides for the synthesis of CF_3 -containing oxazolines and benzoxazines” *Chem. Commun.* **2015**, *51*, 3537–3540.

61. These references exhibit a positive light/dark plot: see ref. 27, 28e
62. (a) Burnett, G. M.; Melville, H. W. “Determination of the Concentration of Intermediaries and of Rate Constants in Radical Reactions.” *Chem. Rev.* **1954**, *54*, 225–288. b) McIntosh, R. G.; Eager, R. L.; Spinks, J. W. T. “Mean Lifetime of Free Radical Chains Determined by a Flow Technique” *Science* **1960**, *131*, 992. c) McIntosh, R. G.; Eager, R. L.; Spinks, J. W. T. “Mean Lifetime of Free Radical Chains in ^{60}Co γ -Irradiated Chloral Hydrate and Bromal Hydrate Solutions” *Can. J. Chem.* **1965**, *43*, 3490–3495.
63. Many of these experiments are analyzed by techniques (*e.g.* NMR, MS) that take anywhere from seconds to minutes to measure conversion.
64. References 15b, 50b, 56 have evidence for chain propagation but also observe a negative result for the light/dark experiment. The evidence for chain propagation in these systems is discussed.
65. Yorimitsu, H.; Shinokubo, H.; Matsubara, S.; Oshima, K. “Triethylborane-Induced Bromine Atom-Transfer Radical Addition in Aqueous Media: Study of the Solvent Effect on Radical Addition Reactions” *J. Org. Chem.* **2001**, *66*, 7776–7785.
66. Lorenz, K. T.; Bauld, N. L. “Kinetics and Mechanism of Aminium Salt Initiated Cycloadditions” *J. Am. Chem. Soc.* **1987**, *109*, 1157–1160.

-
67. Okada, K.; Okubo, K.; Morita, N.; Oda, M. “Redox-Mediated Decarboxylative Photo-Phenylselenylation of N-Acyloxyphthalimides” *Chem. Lett.* **1993**, 2021–2024.
68. There is also the possibility of a radical-polar crossover step that involves chain propagation, but the authors do not discuss this possible mechanism.
69. (a) Okada, K.; Okubo, K.; Morita, N.; Oda, M. “Reductive decarboxylation of N-(acyloxy)phthalimides via redox-initiated radical chain mechanism” *Tetrahedron Lett.* **1992**, 33, 7377–7380. (b) Majek, M.; Filace, F.; Jacobi von Wangelin, A. “Visible Light Driven Hydro-/Deuterodefunctionalization of Anilines” *Chem. Eur. J.* **2015**, 21, 4518–4522.
70. (a) Ishitani, O.; Yanagida, S.; Takamuku, S.; Pac, C. “Redox-Photosensitized Reactions. 13. Ru(bpy)₃²⁺-Photosensitized reactions of an NADH Model, 1-Benzyl-1,4-dihydronicotinamide, with Aromatic Carbonyl Compounds and Comparison with Thermal Reactions” *J. Org. Chem.* **1987**, 52, 2790–2796. (b) Megerle, U.; Lechner, R.; König, B.; Riedle, E. “Laboratory apparatus for the accurate, facile and rapid determination of visible light photoreaction quantum yields” *Photochem. Photobiol. Sci.* **2010**, 9, 1400–1406. (c) Miyake, Y.; Ashida, Y.; Nakajima, K.; Nishibayashi, Y. “Visible-light-mediated addition of α -aminoalkyl radicals generated from α -silylamines to α,β -unsaturated carbonyl compounds” *Chem. Commun.* **2012**, 48, 6966–6968. (d) An, J.; Zou, Y.-Q.; Yanf, Q.-Q.; Wang, Q.; Xiao, W.-J. “Visible Light-Induced Aerobic Oxyamidation of Indoles: A Photocatalytic Strategy for the Preparation of Tetrahydro-5H-indolo[2,3-b]quinolinols” *Adv. Synth. Catal.* **2013**, 355, 1483–1489. (e) Nakajima, K.; Kitagawa, M.; Ashida, Y.; Miyake, Y.; Nishibayashi, Y. “Synthesis of nitrogen heterocycles via α -aminoradicals generated from α -silyl secondary amines under visible light irradiation” *Chem. Commun.* **2014**, 50, 8900–8903. (f) Nakajima, K.; Ashida, Y.; Nojima, S.; Nishibayashi, Y. “Radical Addition to Corannulene Mediated by Visible-Light-Photoredox Catalysts” *Chem. Lett.* **2015**, 44, 545–547. (g) Bagal, D. B.; Kachkovskiy, G.; Knorn, M.; Rawner, T.; Bhanage, B. M.; Reiser, O. “Trifluoromethylchlorosulfonylation of Alkenes: Evidence for an Inner-Sphere Mechanism by a Copper Phenanthroline Photoredox Catalyst” *Angew. Chem. Int. Ed.* **2015**, 54, 6999–7002.

Chapter 2. Visible Light Photocatalysis of Radical Anion Hetero-Diels–Alder Cycloadditions

Portions of this work have been previously published:

Hurtley, A. E.; Cismesia, M. A.; Ischay, M. A.; Yoon, T. P. "Visible Light Photocatalysis of Radical Anion Hetero-Diels–Alder Cycloadditions" *Tetrahedron* **2011**, *67*, 4442–4448.

2.1 Introduction

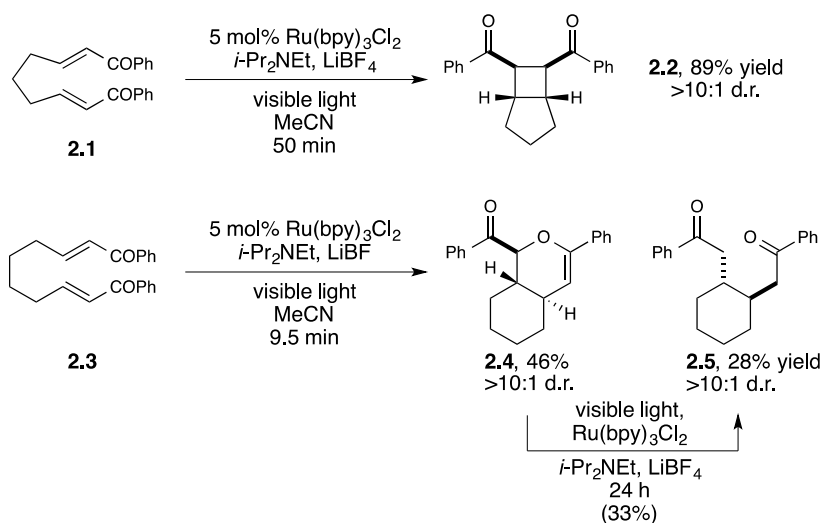
Tetrahydropyrans and related six-membered heterocycles are ubiquitous substructures found in a variety of carbohydrates, polyketide natural products, and other bioactive compounds. Among the most powerful methods for the rapid construction of densely functionalized six-membered oxaheterocycles are formal hetero-Diels–Alder cycloadditions. These methods have been the subject of numerous reviews¹ and have been extensively utilized as key steps in the synthesis of many complex organic structures.² Nevertheless, hetero-Diels–Alder cycloadditions proceed efficiently under mild conditions only when the components are electronically well matched, which involves the reaction of either electron-rich dienes with electron-deficient carbonyl compounds or electron-poor heterodienes with electron-rich olefins. Electronically mismatched hetero-Diels–Alder cycloadditions between two electron-deficient components typically require forcing conditions that limit their utility in synthesis.³

We,⁴ along with several other research groups,⁵ have recently begun to explore the ability of metal polypyridyl photocatalysts to promote a variety of synthetically useful transformations upon irradiation with visible light.⁶ In particular, our lab has become interested in exploiting the ability of $\text{Ru}(\text{bpy})_3^{2+}$ and related photoredox catalysts to initiate one-electron transfer processes without the need for strong stoichiometric reductants or oxidants. The facility with which radical cations and radical anions can be generated under photocatalytic conditions has enabled us to explore the chemistry of these reactive intermediates, whose utility in synthesis has been underdeveloped in comparison to that of neutral radicals. In this chapter, we describe high-yielding and highly diastereoselective radical anion hetero-Diels–Alder cycloadditions between electronically mismatched enones can be conducted using our group's strategy for visible light photocatalysis.

2.2 Results and Discussion

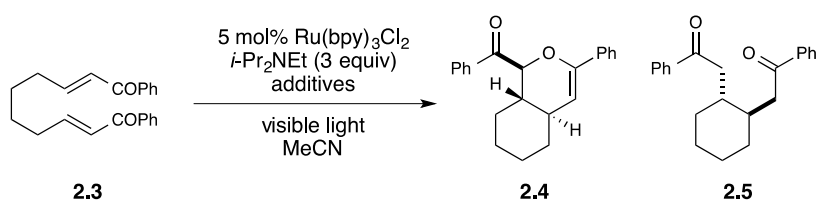
Our interest in the hetero-Diels–Alder cycloaddition arose during an exploration of the scope of the photocatalytic intramolecular [2+2] enone cycloaddition developed in our labs. We observed that the length of the aliphatic tethering group had a dramatic influence on the intrinsic reactivity of the system (Scheme 2-1). Bis(enone) **2.1** bearing a three-carbon tether undergoes efficient [2+2] cycloaddition upon irradiation with visible light in the presence of $\text{Ru}(\text{bpy})_3^{2+}$ with LiBF_4 and *i*-Pr₂NEt as additives.^{4a} However, when bis(enone) **2.3**, in which the tether length was increased by one methylene unit, was subjected to the same conditions, the expected [2+2] cycloadduct was not formed. Instead, the major products are the hetero-Diels–Alder cycloadduct **2.4** and the product of reductive monocyclization (**2.5**). Both products are formed with high diastereoselectivity. While analogous compounds were reported to be side products in the electrochemically induced [2+2] cycloadditions of **2.1** reported by Bauld and Krische,⁷ we did not observe their formation in our studies of the photocatalytic cycloaddition of **2.1**. Intrigued by this unexpected reactivity, we elected to initiate an examination of this hetero-Diels–Alder process by developing conditions that allow selective access to [4+2] cycloadduct **2.4**.

Scheme 2-1. Photocatalytic [2+2] and [4+2] cycloadditions.



We noted that under our initial conditions the selectivity for formation of **2.4** over the undesired reductive cyclization product **2.5** was high at relatively low conversions but steadily decreased over the course of the reaction. We hypothesized, therefore, that **2.5** might be a decomposition product arising from over-reduction and reductive cleavage of **2.4**. Indeed, when **2.4** was isolated and resubjected to the reaction conditions for 24 h, we observed formation of **2.5** in 33% yield, which suggested that the long reaction times were in part responsible for the formation of **2.5**. We therefore sought conditions that would accelerate the overall rate of conversion and limit the formation of this undesired side product.

Table 2-1. Optimization of [4+2] cycloaddition of **2.3**.^a



Entry	Additives	Time	% Yield (2.4 / 2.5) ^{b,c}
1	LiBF ₄ (2 equiv)	9.5 h	28/41
2	LiBF₄ (2 equiv), H₂O (10 equiv)	1 h	86^d/<5
3	LiBF ₄ (2 equiv), MeOH (10 equiv)	1 h	25/19 ^e
4	LiBF ₄ (2 equiv), CF ₃ CH ₂ OH (10 equiv)	1 h	61/25
5	H ₂ O (10 equiv)	1 h	0/0
6	Bu ₄ N ⁺ BF ₄ ⁻ (2 equiv), H ₂ O (10 equiv)	1 h	0/0

^a Reactions conducted in degassed MeCN (0.1 M) under irradiation with a 200 W tungsten filament light bulb at a distance of 30 cm.

^b Yield determined by ¹H NMR spectroscopy against an internal standard unless otherwise noted.

^c The products were formed in >10:1 d.r. unless otherwise noted.

^d Isolated yield.

^e **2.5** was formed as a 2:1 mixture of diastereomers in this experiment.

In an initial screen of solvents, we found that the presence of water had a profound influence on the rate of the reaction. Upon addition of 10 equiv of water, the reaction time decreased dramatically from 9.5 h to 1 h (Table 2-1, entries 1 and 2). Importantly, very little of the undesired over-reduction product **2.5** was formed, and the hetero-Diels–Alder cycloadduct

could be isolated in 86% yield. Water proved to be a uniquely effective protic additive;⁸ while both methanol and trifluoroethanol also afforded an increase in the rate of the reaction, neither provided good yields of the desired [4+2] cycloadduct. Control studies indicated that LiBF₄ was an essential additive. No consumption of the starting bis(enone) occurred when LiBF₄ was either omitted from the reaction or was replaced by Bu₄N⁺BF₄⁻. This indicates that the Lewis acidity of the lithium cation is crucial for successful cycloaddition,⁹ as it is in the analogous [2+2] cycloaddition reactions reported by our group.^{4a}

We next conducted a survey of the scope of the hetero-Diels–Alder cycloaddition, and the results are summarized in Table 2-2. A number of symmetrical aryl bis(enones) were found to be excellent substrates for this reaction. Both electron-deficient (entries 2–3) and electron-rich (entry 4) aryl enones react in high yield and diastereoselectivity, as do polyaromatic (entry 5) and heteroaryl enones (entry 6). Fluoride substitution at the *ortho* position is well tolerated (entry 7), although larger groups at this position significantly hinder reactivity (entry 8). In all cases, the desired [4+2] cycloadduct was formed with excellent diastereoselectivity.

We also became interested in exploring the cycloadditions of unsymmetrical bis(enones) in which two possible constitutional isomers could reasonably be formed. We examined the reactions of a number of substrates bearing one aryl enone and one aliphatic enone under our optimized reaction conditions. An α -benzyloxy enone underwent efficient cycloaddition to afford a single regioisomer of the hetero-Diels–Alder product (entry 9). Other substrates were less successful. A methyl enone required significantly longer reaction times and consequently afforded lower yields of the desired cycloadduct, although the regioselectivity of this process was also excellent (entry 10). Upon careful optimization, we were able to increase the efficiency of this reaction to 73% by removing water and replacing the LiBF₄ additive with Mg(ClO₄)₂

(entry 11). Other aliphatic enones also underwent cycloaddition under these conditions, although the yields of these reactions decreased with increasing steric demand (entries 12–14). Reactions involving enoates and α,β -unsaturated thioesters were unsuccessful under both sets of conditions.

Table 2-2. Scope of the photocatalytic [4+2] cycloaddition.^a

Entry	Method ^b	Substrate	Product	Time	% Yield ^c
1	A	Ar = Ph (2.4)		1 h	86
2	A	Ar = 4-Cl-C ₆ H ₄ (2.6)		30 min	70
3	A	Ar = 4-CF ₃ -C ₆ H ₄ (2.7)		30 min	83 ^d
4	A	Ar = 4-AcO-C ₆ H ₄ (2.8)		1 h	76
5	A	Ar = 2-naphthyl (2.9)		1.5 h	77
6	A	Ar = 2-furyl (2.10)		30 min	77
7	A	Ar = 2-F-C ₆ H ₄ (2.11)		30 min	84
8	A	Ar = 2-Me-C ₆ H ₄ (2.12)		6 h	5 ^e
9	A	R = CH ₂ OBn (2.13)		20 min	76
10	A	R = Me (2.14)		2 h	39
11	B	R = Me (2.14)		10 min	73
12	B	R = <i>i</i> -Pr (2.15)		1.5 h	58
13	B	R = <i>t</i> -Bu (2.16)		6 h	12 ^e
14	B			5 h	17 ^e

^a All reactions were irradiated with a 200 W tungsten filament light bulb at a distance of 30 cm.

^b Method A: Bis(enone) substrate (1 equiv), Ru(bpy)₃Cl₂ (0.05 equiv), LiBF₄ (2 equiv), *i*-Pr₂NEt (3 equiv), and H₂O (10 equiv) in degassed MeCN (0.1 M). Method B: Bis(enone) substrate (1 equiv), Ru(bpy)₃Cl₂ (0.05 equiv), Mg(ClO₄)₂ (2 equiv), and *i*-Pr₂NEt (5 equiv) in degassed MeCN (0.025 M).

^c Data represent the average isolated yields from two reproducible experiments, unless otherwise noted.

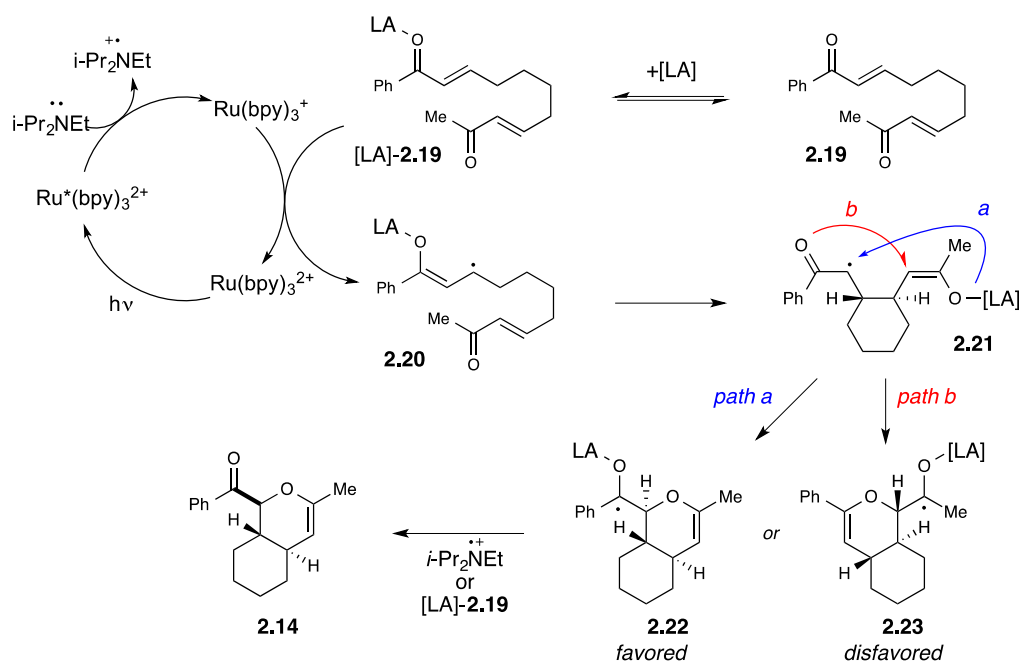
^d Isolated yield of a single experiment.

^e Yield of a single experiment, determined by ¹H NMR spectroscopy against an internal standard.

The high level of regioselectivity observed in the cycloaddition of unsymmetrical bis(enones) (e.g., **2.19**) can be rationalized by the mechanism outlined in Scheme 2-2, which is based upon Krische and Bauld's proposal that radical anion cycloadditions proceed in a step-

wise fashion.⁷ Photoexcitation of $\text{Ru}(\text{bpy})_3^{2+}$ with visible light affords an excited state that can undergo efficient reductive quenching by $i\text{-Pr}_2\text{NEt}$. The Lewis acid-activated enone complex ([LA]-**2.19**) can then accept an electron from the resulting $\text{Ru}(\text{bpy})_3^+$ reductant to afford an activated radical anion intermediate (**2.20**) that should undergo $\beta\text{-}\beta$ coupling to afford a monocyclized distonic radical anion intermediate (**2.21**). Formation of the carbon-oxygen bond could proceed to form two possible isomeric ketyl radicals (**2.22** and **2.23**). We speculate that the greater stabilization of the aryl ketyl radical may then serve as a driving force for selective formation of **2.22**. Finally, the neutral hetero-Diels–Alder cycloadduct is produced upon loss of one electron, either to another equivalent of enone in a chain propagation step or to the photogenerated amine radical cation in a chain termination step.

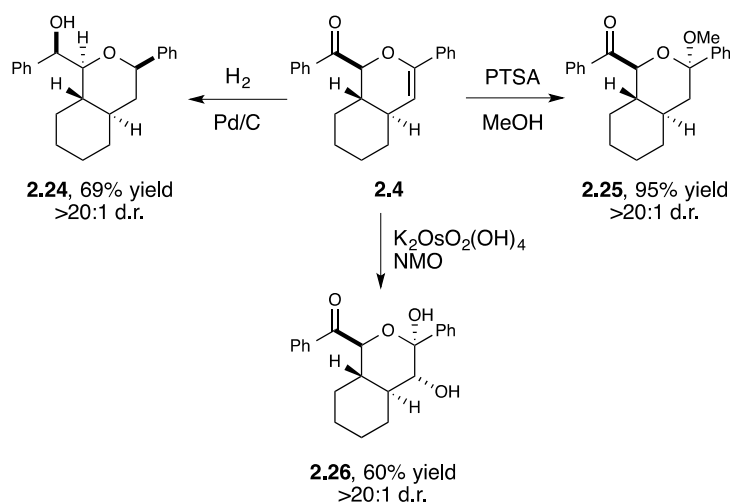
Scheme 2-2. Proposed mechanism for regioselective hetero-Diels–Alder cycloaddition of unsymmetrical bis(enone) **2.19**.



The dihydropyrans formed in this study can be synthetically elaborated in a number of ways (Scheme 2-3). The enol ether functionality of **2.4** can be converted to an acetal (**2.25**) upon

treatment with methanol and catalytic PTSA in excellent yield and diastereoselectivity. Dihydroxylation of the olefin under Upjohn conditions¹⁰ similarly provides the corresponding diol (**2.26**) with high stereochemical purity. Finally, catalytic hydrogenation of **2.4** reduces both the enol ether and the aryl ketone, introducing two new stereocenters with very high diastereoselectivity in the doubly reduced product (**2.24**).

Scheme 2-3. Diastereoselective functionalization of **2.4**.



The origins of the chemoselectivity for [2+2] vs [4+2] pathways in these radical anion processes are not clear at this time, but the length of the aliphatic tether appears to be critical. Subjecting the three-carbon tethered bis(enone) **2.1** to the optimized conditions in Table 2 produced only [2+2] cycloadduct and none of the hetero-Diels–Alder product. Five- and six-carbon tethers that would afford medium-sized rings produced neither cycloadduct. We speculate that the initial bond-forming event in the stepwise cycloaddition of **2.1** has a kinetic preference for formation of the *cis* cyclopentane isomer. Subsequent coupling of the α,α carbons would afford the [3.2.0] bicycloheptane ring structure observed in the intramolecular cyclobutane.^{4a} On the other hand, we speculate that the initial carbon-carbon bond formation in the cycloaddition of **2.3** produces a *trans*-substituted cyclohexane intermediate. Coupling of

the α positions would afford a *trans* [4.2.0] ring system that we would expect to be prohibitively strained, while formation of a new C–O bond would produce a conformationally reasonable *trans* oxadecalin bicycle.

2.3 Conclusions

Our group's investigations of visible light photocatalysis have led to the discovery of an interesting intramolecular hetero-Diels–Alder cycloaddition. This reactivity is notable for a number of reasons. First, the intermediacy of an enone radical anion facilitates the efficient coupling of a dienophile and heterodiene that are both electron-deficient, which enables the construction of a cycloadduct that is difficult to access upon thermal activation. Second, the diastereoselectivity of the process is high, and the products are amenable to a variety of further synthetic manipulations. Finally, one of the most intriguing unanswered questions is how the effect of the tether length controls the chemoselectivity for [4+2] vs. [2+2] cycloaddition. Studies to elucidate the origins of this divergent reactivity are underway in our laboratory, and these investigations provide a promising framework for further studies of the chemistry of photogenerated radical anions.

2.4 Contributions

Anna Hurlley optimized conditions for the [4+2] hetero-Diels–Alder cycloaddition and explored the scope of the reaction.

2.5 Experimental

2.5.1 General experimental information

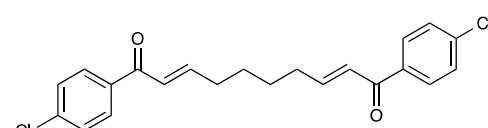
Acetonitrile, dichloromethane and tetrahydrofuran were purified by elution through alumina on a glass contour solvent system as described by Grubbs.¹¹ Diisopropylethylamine was purified by distillation from CaH₂ immediately prior to use. Ru(bpy)₃Cl₂•6H₂O was purchased from Strem and used without purification. LiBF₄ and Mg(ClO₄)₂ were purchased from Sigma-Aldrich and Strem, respectively, and stored in a glove box under an atmosphere of nitrogen. Millipore water was used in all photochemical reactions depicted in tables 2-2 and 2-3, and prepared as a stock solution in acetonitrile. Diastereomeric ratios for all products were determined by ¹H NMR spectroscopic analysis of the isolated products after flash column chromatography. Flash column chromatography was performed with Silicycle 40–63Å silica (230–400 mesh).¹² All glassware was oven-dried prior to use. ¹H and ¹³C NMR data for all previously uncharacterized compounds were obtained using Varian Unity-500 spectrometers and are referenced to TMS (0.0 ppm) and CDCl₃ (77.0 ppm), respectively. Mass spectrometry was performed with a Waters (Micromass) AutoSpec®. These facilities are funded by the NSF (CHE-9974839, CHE-9304546) and the University of Wisconsin.

2.5.2 Preparation of bis(enone) substrates

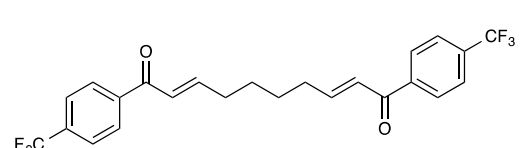
General procedure: A dry 3-neck round-bottomed flask was charged with cyclohexene (1 equiv) and CH₂Cl₂ (0.3–0.4 M) and cooled to –78 °C. The reaction mixture was stirred while a stream of ozone was passed through the solution until a blue color persisted. The excess ozone was removed by a flow of oxygen and the ozonide was quenched with dimethyl sulfide (3

equiv). The ylide (2.5 equiv) was added in a solution of CH_2Cl_2 and the reaction mixture was then allowed to warm slowly to room temperature and stirred under N_2 for 24–48 hours. The reaction mixture was concentrated *in vacuo* and purified by flash column chromatography on silica gel.

(2E,8E)-1,10-bis(4-chlorophenyl)deca-2,8-diene-1,10-dione (2.27): Prepared according to the

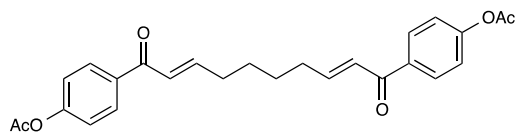

 general procedure with 1.2 mL cyclohexene (12.2 mmol), 30 mL CH_2Cl_2 , 2.7 mL DMS (36.6 mmol), and 12.7 g 1-(4-chloro-phenyl)-2-(triphenylphosphoranylidene)-ethanone¹³ (30.5 mmol). Following ozonolysis, the Wittig reaction was allowed to stir for 36 hours at room temperature and then concentrated *in vacuo*. The residue was purified by flash column chromatography on silica gel (6:1 hexanes:ethyl acetate) and recrystallization in ethyl acetate/hexanes to afford the product (0.828 g, 2.14 mmol, 18%) as a white, crystalline solid. ¹H NMR: (500 MHz, CDCl_3) δ 7.87 (dt, J = 8.6, 1.9 Hz, 4H), 7.44 (dt, J = 8.6, 1.9 Hz, 4H), 7.07 (dt, J = 15.3, 7.0 Hz, 2H), 6.86 (dt, J = 15.3, 1.5 Hz, 2H), 2.37 (tdd, J = 6.7, 6.3, 1.2 Hz, 4H), 1.61 (m, 4H); ¹³C NMR: (125 MHz, CDCl_3) δ 189.3, 149.7, 139.1, 136.2, 129.9, 128.9, 125.7, 32.6, 27.7. HRMS (EI) calculated for $[\text{C}_{22}\text{H}_{20}\text{Cl}_2\text{O}_2]^+$ requires *m/z* 386.0835, found 386.0821.

(2E,8E)-1,10-bis(4-(trifluoromethyl)phenyl)deca-2,8-diene-1,10-dione (2.28): Prepared


 according to the general procedure with 0.140 mL cyclohexene (1.34 mmol), 3.5 mL CH_2Cl_2 , 0.3 mL DMS (4.00 mmol), and 1.5 g 1-(4-(trifluoromethyl)phenyl)-2-(triphenylphosphoranylidene)-ethanone¹³ in a solution of 2 mL

CH₂Cl₂. Following ozonolysis, the Wittig reaction was allowed to stir for 48 hours at room temperature and then concentrated *in vacuo*. The residue was purified by flash column chromatography on silica gel (6:1 hexanes:ethyl acetate) to afford the product (90.5 mg, 0.200 mmol, 30%) as a white solid. ¹H NMR: (500 MHz, CDCl₃) δ 8.01 (d, J = 8.2 Hz, 4H), 7.74 (d, J = 8.2 Hz, 4H), 7.09 (dt, J = 15.2, 7.0 Hz, 2H), 6.87 (dt, J = 15.2, 1.3 Hz, 2H), 2.39 (tdd, J = 6.8, 6.8, 1.3 Hz, 4H), 1.63 (m, 4H); ¹³C NMR: (125 MHz, CDCl₃) δ 192.5, 153.3, 143.4, 136.7 (q, ²J_{CF} = 33 Hz), 131.5, 128.6, 128.3 (q, ³J_{CF} = 3.5 Hz), 126.3 (q, ¹J_{CF} = 273 Hz), 35.3, 30.3. HRMS (EI) calculated for [C₂₄H₂₀F₆O₂]⁺ requires 454.1362, found 454.1367.

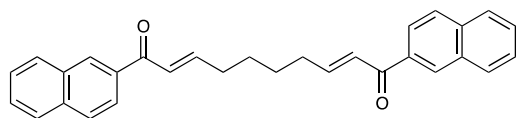
((2E,8E)-deca-2,8-dienedioyl)bis(4,1-phenylene)diacetate (2.29): Prepared according to the



general procedure with 0.3 mL (3.01 mmol) cyclohexene, 10 mL CH₂Cl₂, 0.7 mL DMS (9 mmol), and 3.3 g 1-(4-acetoxy-phenyl)-2-

(triphenylphosphoranylidene)-ethanone¹⁴ (2.7 mmol) in a solution of 5 mL CH₂Cl₂. Following ozonolysis, the Wittig reaction was allowed to stir for 48 hours at room temperature and then concentrated *in vacuo*. The residue was purified by flash column chromatography (3:1 hexanes:acetone) and recrystallization in EtOAc/hexanes to afford the product (0.435 g, 1.00 mmol, 33%) as a white crystalline solid. ¹H NMR: (500 MHz, CDCl₃) δ 7.97 (dt, J = 8.6, 1.8 Hz, 2H), 7.20 (dt, J = 8.6, 1.8 Hz, 2H), 7.07 (dt, J = 15.3, 6.8 Hz, 2H), 6.88 (dt, J = 15.3, 1.3 Hz, 2H), 2.36 (m, 4H), 2.33 (s, 6H), 1.61 (m, 4H); ¹³C NMR: (125 MHz, CDCl₃) δ 189.5, 168.9, 154.1, 149.4, 135.5, 130.1, 125.9, 121.7, 32.5, 27.7, 21.1. HRMS (EI) calculated for [C₂₆H₂₆O₆]⁺ requires *m/z* 434.1724, found 434.1725.

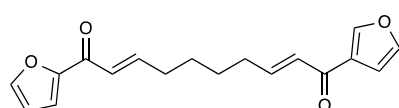
(2E,8E)-1,10-di(naphthalen-2-yl)deca-2,8-diene-1,10-dione (2.30): Prepared according to the



general procedure with 0.86 mL cyclohexene (8.5 mmol), 21 mL CH₂Cl₂, 2 mL DMS (25.5 mmol), and

9.17 g 1-(2-naphthalenyl)-2-(triphenylphosphoranylidene)-ethanone¹⁵ (21.3 mmol) in a solution of 20 mL CH₂Cl₂. Following ozonolysis, the Wittig reaction was allowed to stir for 36 hours at room temperature and then concentrated *in vacuo*. The residue was purified by flash column chromatography (8:1 hexanes:acetone) to afford the product (0.720 g, 1.72 mmol, 20%) as a pale yellow solid. ¹H NMR: (500 MHz, CDCl₃) δ 8.45 (bs, 2H), 8.03 (dd, J = 8.7, 1.7 Hz, 2H), 7.95 (d, J = 8.1 Hz, 2H), 7.90 (d, J = 8.7 Hz, 2H), 7.86 (d, J = 8.1 Hz, 2H), 7.59 (dt, J = 7.0, 1.2 Hz, 2H), 7.54 (dt, J = 7.0, 1.2 Hz, 2H), 7.15 (dt, J = 15.3, 6.7 Hz, 2H), 7.08 (d, J = 15.3 Hz, 2H), 2.43 (td, J = 6.3, 6.1 Hz, 4H), 1.67 (m, 4H); ¹³C NMR: (125 MHz, CDCl₃) δ 190.5, 149.1, 135.4, 135.2, 132.5, 130.0, 129.5, 128.5, 128.3, 127.8, 126.7, 126.1, 124.5, 32.6, 27.9. HRMS (EI) calculated for [C₃₀H₂₆O₂]⁺ requires *m/z* 418.1928, found 418.1925.

(2E,8E)-1-(furan-2-yl)-10-(furan-3-yl)deca-2,8-diene-1,10-dione (2.31): Prepared according

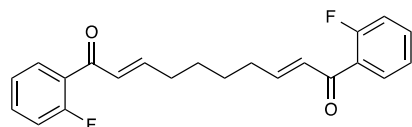


to the general procedure with 0.41 mL cyclohexene (4.05 mmol), 10 mL CH₂Cl₂, 1.47 mL DMS (2.00 mmol), and 3.7 g

1-furan-2-yl-2-(triphenylphosphoranylidene)-ethanone¹⁶ in a solution of 25 mL CH₂Cl₂. Following ozonolysis, the Wittig reaction was allowed to stir for 48 hours at room temperature and then concentrated *in vacuo*. The residue was purified by flash column chromatography on silica gel (2:1 hexanes:ethyl acetate) to afford the product (0.290 g, 0.972 mmol, 24%) as a white solid. ¹H NMR: (500 MHz, CDCl₃) δ 7.62 (dd, J = 1.5, 0.6 Hz, 2H), 7.25 (dd, J = 3.7, 0.6 Hz, 2H), 7.15 (dt, J = 15.5, 7.0 Hz, 2H), 6.82 (dt, J = 15.5, 1.5 Hz, 2H), 6.56 (dd, J = 3.7, 1.5 Hz,

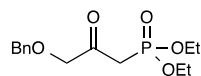
2H), 2.35 (tdd, $J = 6.1, 6.1, 1.3$ Hz, 4H), 1.60 (m, 4H); ^{13}C NMR: (125 MHz, CDCl_3) δ 178.1, 153.3, 148.5, 146.5, 125.2, 117.6, 112.4, 32.4, 27.6. HRMS (EI) calculated for $[\text{C}_{18}\text{H}_{18}\text{O}_4]^+$ requires m/z 298.1200, found 298.1211.

(2E,8E)-1,10-bis(2-fluorophenyl)deca-2,8-diene-1,10-dione (2.32): Prepared according to the



general procedure with 0.6 mL cyclohexene (5.9 mmol), 20 mL CH_2Cl_2 , 1.6 mL DMS (17.7 mmol), and 1-(2-fluorophenyl)-2-(triphenylphosphoranylidene)-ethanone in a solution of 15 mL CH_2Cl_2 . Following ozonolysis, the Wittig reaction was allowed to stir for 48 hours at room temperature and then concentrated in vacuo. The residue was purified by flash column chromatography (4:1 hexanes:acetone) to afford the product (0.235 g, 0.663 mmol, 11%) as a white solid. ^1H NMR: (500 MHz, CDCl_3) δ 7.71 (td, $J = 7.6, 1.8$ Hz, 2H), 7.49 (m, 2H), 7.23 (td, $J = 7.6, 0.8$ Hz, 2H), 7.12 (ddd, $J = 10.6, 8.2, 0.7$ Hz, 2H), 6.97 (dtd, $J = 15.5, 7.0, 1.8$ Hz, 2H), 6.73 (ddt, $J = 15.5, 2.8, 1.5$ Hz, 2H), 2.33 (m, 4H), 1.58 (m, 4H); ^{13}C NMR: (125 MHz, CDCl_3) δ 189.6 (d, $J = 2.1$ Hz), 161.0 (d, $J = 253.6$ Hz), 149.7, 133.7 (d, $J = 8.6$ Hz), 130.8 (d, $J = 2.5$ Hz), 129.8 (d, $J = 5.9$ Hz), 127.0 (d, $J = 13.6$ Hz), 124.4 (d, $J = 3.1$ Hz), 116.4 (d, $J = 23.1$ Hz), 32.3, 27.5. HRMS (EI) calculated for $[\text{C}_{22}\text{H}_{20}\text{F}_2\text{O}_2]^+$ requires m/z 354.1426, found 354.1409.

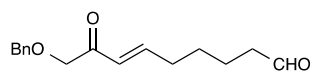
Diethyl (3-(benzyloxy)-2-oxopropyl)phosphonate (2.33): A dry 3-neck round-bottomed flask



was charged with *n*-BuLi (1.6 M solution in hexanes, 7.05 mL, 11.28 mmol) and dry THF (12 mL) under N_2 and cooled to -78 °C. Diethyl methylphosphonate (1.5 mL, 10.25 mmol) in dry THF (1 mL) was added dropwise to the reaction mixture and allowed to stir for 30 min. CuBr (1.62 g, 11.28 mmol) was then added as a

solid and the reaction mixture was warmed to $-50\text{ }^{\circ}\text{C}$. After stirring for 1.5 hours at that temperature, benzyloxyacetyl chloride (1.6 mL, 10.25 mmol) in dry Et_2O (4.5 mL) was added dropwise and the reaction mixture warmed to $-40\text{ }^{\circ}\text{C}$ and allowed to stir at that temperature overnight. The reaction was then quenched with approximately 3 mL H_2O and passed across a plug of silica gel with EtOAc . The eluent was concentrated *in vacuo* and the residue purified by flash column chromatography on silica gel (1.5:1 hexanes:acetone) to afford the product (1.89 g, 6.29 mmol, 61%) as a clear liquid. ^1H NMR: (500 MHz, CDCl_3) δ 7.4-7.29 (m, 5H), 4.61 (s, 2H), 4.21 (s, 2H), 4.18-4.10 (m, 4H), 3.16 (d, $J = 22.7\text{ Hz}$, 2H), 1.32 (t, $J = 7.1\text{ Hz}$, 6H); ^{13}C NMR: (125 MHz, CDCl_3) δ 200.0 (d, $^3J_{\text{C-P}} = 7.5\text{ Hz}$), 137.1, 128.5, 128.1, 128.0, 75.1, 73.4, 62.7 (d, $^2J_{\text{C-P}} = 6.1\text{ Hz}$), 38.5 (d, $^1J_{\text{C-P}} = 129.7\text{ Hz}$), 16.2 (d, $^3J_{\text{C-P}} = 6.1\text{ Hz}$). HRMS (EI) calculated for $[\text{C}_{14}\text{H}_{21}\text{O}_5\text{P} + \text{H}]^+$ requires m/z 301.1200, found 301.1208.

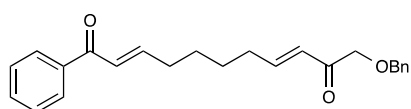
(E)-9-(benzyloxy)-8-oxonon-6-enal: A dry 100 mL 3-neck round-bottomed flask was charged



with NaH (240 mg, 5.99 mmol) and dry THF (23 mL) under N_2 and cooled to $0\text{ }^{\circ}\text{C}$. Diethyl (3-(benzyloxy)-2-oxopropyl)phosphonate (1.8 g, 5.99 mmol) in dry THF (2 mL) was added dropwise to the reaction mixture and allowed to stir for 25 minutes. 6,6-dimethoxyhexanal¹⁷ (0.8 g, 4.99 mmol) in dry THF (2 mL) was added dropwise and the reaction mixture was stirred at $0\text{ }^{\circ}\text{C}$ for 3 hours. The reaction mixture was then diluted in CH_2Cl_2 and quenched with H_2O . The phases were separated and the aqueous phase was washed an additional 2 times with CH_2Cl_2 . The combined organic phases were dried over Na_2SO_4 , concentrated *in vacuo*, and the resulting residue was purified by flash column chromatography on silica gel (3:1 hexanes:acetone) to afford the desired acetal as an impure mixture. The crude material was then transferred to a 50 mL round-bottomed flask and stirred in

a mixture of THF (7 mL) and 1 M HCl (7 mL) for 30 minutes at room temperature at which point it was diluted with CH₂Cl₂ and H₂O. The phases were separated and the aqueous layer washed an additional 2 times with CH₂Cl₂. The combined organic phases were dried over Na₂SO₄, concentrated *in vacuo*, and the resulting residue was purified by flash column chromatography on silica gel (3:1 hexanes:acetone) to afford the desired aldehyde (0.606 g, 2.33 mmol, 47% over 2 steps) as a clear oil, which was carried on immediately in the synthesis of (2E,8E)-11-(benzyloxy)-1-phenylundeca-2,8-diene-1,10-dione.

(2E,8E)-11-(benzyloxy)-1-phenylundeca-2,8-diene-1,10-dione (2.34): A dry 25 mL round-

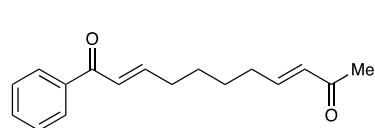


bottomed flask was charged with (E)-9-(benzyloxy)-8-oxonon-6-enal (606 mg, 2.33 mmol),

(benzoylmethylene)triphenylphosphorane (1.77 g, 4.66 mmol), and CH₂Cl₂ (6 mL). The reaction mixture was stirred at room temperature under N₂ for 36 hours at which point an additional portion of (benzoylmethylene)triphenylphosphorane (0.300 g, 0.790 mmol) was added. The reaction mixture was allowed to stir for an additional 12 hours and then concentrated *in vacuo*. The residue was purified by flash column chromatography on silica gel (3:1 hexanes:ethyl acetate) to afford the product (0.609 g, 1.68 mmol, 72%) as a pale yellow oil. ¹H NMR: (500 MHz, CDCl₃) δ7.92 (dt, J = 7.5, 1.5 Hz, 2H), 7.56 (tt, J = 7.5, 1.5 Hz, 1H), 7.47 (tt, J = 7.5, 1.5 Hz, 2H), 7.38-7.28 (m, 5H), 7.03 (dt, J = 15.5, 6.7 Hz, 1H), 6.96 (dt, J = 15.8, 6.8 Hz, 1H), 6.88 (dt, J = 15.5, 1.5 Hz, 1H), 6.31 (dt, J = 15.8, 1.5 Hz, 1H), 4.61 (s, J = Hz, 2H), 4.21 (s, J = Hz, 2H), 2.33 (td, J = 6.6, 6.6 Hz, 2H), 2.26 (td, J = 6.6, 6.6 Hz, 2H), 1.55 (m, 4H); ¹³C NMR: (125 MHz, CDCl₃) δ199.6, 193.4, 151.8, 150.8, 140.6, 139.9, 135.3, 131.2, 131.2, 130.7, 130.6,

128.9, 128.9, 76.8, 76.0, 35.2, 35.0, 30.4, 30.2. HRMS (EI) calculated for $[C_{24}H_{26}O_3]^+$ requires m/z 362.1877, found 362.1868.

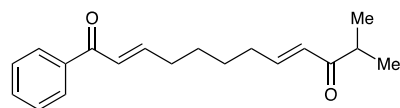
(*E,E*)-8-acetyl-1-benzoyl-1,7-octadiene (2.19): A dry 50 mL round-bottomed flask was charged



with 7-benzoyl-6-heptenal¹⁸ (1.18 g, 5.4 mmol), 1-(triphenylphosphoranylidene)-2-propanone (5.2 g, 16.3 mmol), and CH_2Cl_2 (13.5 mL). The reaction mixture was stirred under N_2 for 48 hours and then concentrated *in vacuo*. The residue was purified by flash column chromatography on silica gel

(4:1 hexanes:ethyl acetate) to afford the product (1.00 g, 3.9 mmol, 73%) as a clear oil. 1H NMR: (500 MHz, $CDCl_3$) δ 7.93 (dt, $J = 7.6, 1.3$ Hz, 2H), 7.56 (tt, $J = 7.6, 1.3$ Hz, 1H), 7.47 (tt, $J = 7.6, 1.3$ Hz, 2H), 7.05 (dt, $J = 15.3, 6.9$ Hz, 1H), 6.89 (dt, $J = 15.3, 1.4$ Hz, 1H), 6.79 (dt, $J = 16.0, 6.8$ Hz, 1H), 6.09 (dt, $J = 16.0, 1.4$ Hz, 1H), 2.35 (tdd, $J = 7.0, 7.0, 1.4$ Hz, 2H), 2.27 (dtd, $J = 7.1, 6.8, 1.4$ Hz, 2H), 2.24 (s, 3H); ^{13}C NMR: (125 MHz, $CDCl_3$) δ 198.6, 190.7, 149.1, 147.7, 137.9, 132.7, 131.5, 128.5, 128.5, 126.2, 32.5, 32.2, 27.7, 27.7, 26.9. HRMS (EI) calculated for $[C_{17}H_{20}O_2]^+$ requires m/z 256.1458, found 256.1451.

(*E,E*)-8-isopropanoyl-1-benzoyl-1,7-octadiene (2.35): A dry 50 ml round-bottomed flask was



charged with 7-benzoyl-6-heptenal (0.863 g, 3.97 mmol), 1-(triphenylphosphoranylidene)-3-methyl-2-butanone (2.03 g, 5.87 mmol), and benzene (10 mL). The reaction flask was fitted to a cold water condenser and allowed to reflux with stirring under N_2 for 18 hours. The reaction mixture was then cooled to room temperature and passed across a plug of silica gel (2:1 hexanes:acetone). The eluent was concentrated *in vacuo* and the resulting residue purified by flash column chromatography on

silica gel (5:1 hexanes:acetone) to afford the product (588 mg, 2.07 mmol, 52%) as a white solid. ^1H NMR: (500 MHz, CDCl_3) δ 7.93 (dt, $J = 7.6, 1.2$ Hz, 2H), 7.56 (tt, $J = 7.6, 1.2$ Hz, 1H), 7.47 (t, $J = 7.6$ Hz, 2H), 7.05 (dt, $J = 15.5, 6.9$ Hz, 1H), 6.89 (d, $J = 15.5$ Hz, 1H), 6.87 (dt, $J = 15.7, 7.1$ Hz, 1H), 6.18 (d, $J = 15.7$ Hz, 1H), 2.82 (sept, $J = 7.0$ Hz, 1H), 2.35 (td, $J = 6.7, 6.3$ Hz, 2H), 2.26 (td, $J = 7.1, 6.7$ Hz, 2H), 1.56 (m, 4H), 1.10 (d, $J = 7.0$ Hz, 6H); ^{13}C NMR: (125 MHz, CDCl_3) δ 204.0, 190.8, 149.2, 146.5, 137.9, 132.7, 128.6, 128.5, 128.5, 126.2, 38.5, 32.5, 32.2, 27.7, 18.4. HRMS (EI) calculated for $[\text{C}_{19}\text{H}_{24}\text{O}_2]^+$ requires m/z 284.1771, found 284.1766.

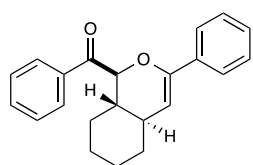
2.5.3 Experimental details for the hetero Diels–Alder cyclization of bis(enone) substrates

General procedure A: To an oven-dried 25 mL Schlenk tube equipped with a magnetic stir bar was added bis(enone) (1 equiv), $\text{Ru}(\text{bpy})_3\text{Cl}_2\cdot\text{H}_2\text{O}$ (0.05 equiv), LiBF_4 (2 equiv), MeCN (0.1 M), H_2O (10 equiv) as a stock solution in MeCN, and *i*- Pr_2NEt (3 equiv). The tube was sealed and degassed by 3 freeze-pump-thaw cycles under nitrogen in the absence of light. The reaction mixture was then stirred in a water bath at room temperature and irradiated with a 200 W light bulb at a distance of 30 cm. Upon consumption of the bis(enone), the reaction mixture was passed across a short plug of silica with a mixture of either hexanes:EtOAc or hexanes:Et₂O, concentrated *in vacuo* to approximately 4 mL and then purified immediately by flash column chromatography on silica gel.

General procedure B: To an oven-dried 50 mL Schlenk tube equipped with a magnetic stir bar was added $\text{Ru}(\text{bpy})_3\text{Cl}_2\cdot\text{H}_2\text{O}$ (0.05 equiv), $\text{Mg}(\text{ClO}_4)$ (2 equiv), and MeCN (0.025 M). The mixture was stirred until homogenous and then charged with the bis(enone) (1 equiv) and *i*- Pr_2NEt (3 equiv). The tube was sealed and degassed by 3 freeze-pump-thaw cycles under

nitrogen in the absence of light. The reaction mixture was then stirred in a water bath at room temperature and irradiated with a 200 W light bulb at a distance of 30 cm. Upon consumption of the bis(enone), the reaction mixture was passed across a 6 inch plug of silica with a mixture of hexanes:Et₂O. The reaction mixture was then concentrated in vacuo to approximately 4 mL and purified immediately by silica gel flash column chromatography.

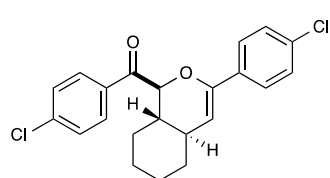
(Table 2-2, entry 1, 2.4): Experiment 1: Prepared according to general procedure A with 100.1



mg (0.314 mmol) bis(enone), 11.9 mg (0.016 mmol) Ru(bpy)₃Cl₂·6H₂O, 59.8 mg (0.638 mmol) LiBF₄, 57 μL (3.14 mmol) H₂O, 164 μL (0.942 mmol) *i*-Pr₂NEt, and 3.14 mL MeCN and an irradiation time of 60 min.

Purification by flash column chromatography (20:1 hexanes:EtOAc) afforded 85 mg cycloadduct (0.267 mmol, 85%). Experiment 2: 100.2 mg (0.315 mmol) bis(enone), 12.2 mg (0.163 mmol) Ru(bpy)₃Cl₂·6H₂O, 59.2 mg (0.631 mmol) LiBF₄, 57 μL (3.14 mmol) H₂O, 164 μL *i*-Pr₂NEt, and 3.14 mL MeCN. Isolated 86 mg cycloadduct (0.270 mmol, 86%) as a white solid. ¹H NMR: (500 MHz, CDCl₃) δ8.13 (ddd, J = 8.1, 1.3, 1.3 Hz, 2H), 7.59 (tt, J = 7.4, 1.3 Hz, 1H), 7.54 (ddd, J = 7.8, 1.3, 1.3 Hz, 2H), 7.31-7.23 (m, 3H), 5.31 (d, J = 1.7 Hz, 1H), 4.93 (d, J = 10.4 Hz, 1H), 2.17 (dddd, J = 10.5, 10.5, 2.2, 2.2 Hz, 1H), 1.95-1.74 (m, 4H), 1.56 (dddd, J = 11.9, 2.2, 2.2, 2.2 Hz, 1H), 1.39 (qt, J = 12.8, 3.3 Hz, 1H), 1.29 (qt, J = 12.8, 3.3 Hz, 1H), 1.21 (qd, J = 12.8, 3.3 Hz, 1H), 1.07 (qd, J = 12.6, 3.5 Hz, 1H); ¹³C NMR: (125 MHz, CDCl₃) δ196.9, 149.6, 135.7, 135.1, 133.5, 129.4, 128.6, 128.1, 128.0, 124.4, 102.5, 83.1, 41.3, 38.4, 32.7, 27.7, 26.0, 25.9. HRMS (EI) calculated for [C₂₂H₂₂O₂]⁺ *m/z* requires 318.1615, found 318.1599.

(Table 2-2, entry 2, 2.6): Experiment 1: Prepared according to general procedure A with 99.3



mg (0.256 mmol) bis(enone), 10.0 mg (0.0134 mmol) Ru(bpy)₃Cl₂·6H₂O, 49.3 mg (0.526 mmol) LiBF₄, 46 μL (2.58 mmol) H₂O, 135 μL (0.774 mmol) *i*-Pr₂NEt, and 2.6 mL MeCN and an

irradiation time of 30 min. Purification by flash column chromatography (20:1 hexanes:EtOAc)

afforded 69 mg cycloadduct (0.178 mmol, 69%) as a white crystalline solid. Experiment 2: 100

mg (0.258 mmol) bis(enone), 9.7 mg (0.0129 mmol) Ru(bpy)₃Cl₂·6H₂O, 48.4 mg (0.516 mmol)

LiBF₄, 46 μL (2.58 mmol) H₂O, 135 μL (0.774 mmol) *i*-Pr₂NEt, and 2.6 mL MeCN. Isolated 71

mg cycloadduct (0.183 mmol, 71%). ¹H NMR: (500 MHz, CDCl₃) δ8.05 (dt, J = 8.7, 2.0 Hz,

2H), 7.44 (dt, J = 8.7, 2.0 Hz, 4H), 7.25 (dt, J = 8.7, 2.0 Hz, 2H), 5.30 (d, J = 1.8 Hz, 1H), 4.86

(d, J = 10.5 Hz, 1H), 2.15 (dddd, J = Hz, 10.8, 10.8, 2.3, 2.3H), 1.90 (dddd, J = 13.0, 2.5, 2.5,

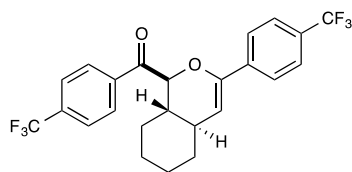
2.5 Hz, 1H), 1.85-1.75 (m, 3H), 1.54 (dddd, J = 13.0, 2.5, 2.5, 2.5 Hz, 1H), 1.44-1.15 (m, 3H),

1.065 (dddd, J = 12.7, 12.7, 12.7, 3.8 Hz, 1H); ¹³C NMR: (125 MHz, CDCl₃) δ195.5, 148.5,

140.1, 133.8, 133.4, 130.8, 129.0, 128.3, 125.7, 103.0, 83.3, 41.2, 38.4, 32.6, 27.6, 26.0, 25.8.

HRMS (EI) calculated for *m/z* [C₂₂H₂₀Cl₂O₂]⁺ requires 386.0835, found 386.0848.

(Table 2-2, entry 3, 2.7): Experiment 1: Prepared according to general procedure A with 81.4



mg (0.179 mmol) bis(enone), 7.7 mg (1.01 mmol) Ru(bpy)₃Cl₂·6H₂O, 36.7 mg (0.391 mmol) LiBF₄, 32 μL (1.76 mmol) H₂O, 92 μL (0.528 mmol) *i*-Pr₂NEt, and 1.76 mL MeCN

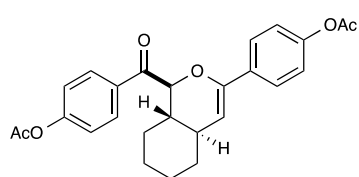
and an irradiation time of 30 min. Purification by flash column chromatography (30:1

hexanes:EtOAc) afforded 68 mg cycloadduct (0.150 mmol, 83%) as a white solid. ¹H NMR:

(500 MHz, CDCl₃) δ8.22 (d, J = 8.3 Hz, 2H), 7.75 (d, J = 8.3 Hz, 2H), 7.62 (d, J = 8.3 Hz, 2H),

7.54 (d, $J = 8.3$ Hz, 2H), 5.44 (d, $J = 1.7$ Hz, 1H), 4.93 (d, $J = 10.4$ Hz, 1H), 2.20 (dddd, $J = 10.4, 10.4, 2.3, 2.3$ Hz, 1H), 1.94 (dd, $J = 12.5, 2.4$ Hz, 1H), 1.87-1.77 (m, $J =$ Hz, 3H), 1.56 (dq, $J = 10.1, 2.7$ Hz, 1H), 1.47-1.18 (m, 3H), 1.10 (qd, $J = 12.4, 3.7$ Hz, 1H). HRMS (EI) calculated for m/z $[\text{C}_{24}\text{H}_{20}\text{F}_6\text{O}_2]^+$ requires 454.1362, found 454.1352.

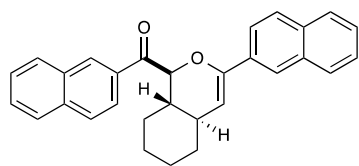
(Table 2-2, entry 4, 2.8): Experiment 1: Prepared according to general procedure A with 101.0



mg (0.232 mmol) bis(enone), 9.1 mg (0.0122 mmol) $\text{Ru}(\text{bpy})_3\text{Cl}_2 \cdot 6\text{H}_2\text{O}$, 42.1 mg (0.449 mmol) LiBF_4 , 41 μL (2.30 mmol) H_2O , 121 μL (0.690 mmol) $i\text{-Pr}_2\text{NEt}$, and 2.3 mL MeCN

and an irradiation time of 30 min. Purification by flash column chromatography (5:1 hexanes:acetone) afforded 77 mg cycloadduct (0.177 mmol, 76%) as a white solid. Experiment 2: 92.0 mg (0.212 mmol) bis(enone), 8.2 mg (0.0109 mmol) $\text{Ru}(\text{bpy})_3\text{Cl}_2 \cdot 6\text{H}_2\text{O}$, 41.0 mg (0.437 mmol) LiBF_4 , 39 μL (2.19 mmol) H_2O , 114 μL (0.651 mmol) $i\text{-Pr}_2\text{NEt}$, and 2.19 mL MeCN. Isolated 70 mg cycloadduct (0.161 mmol, 76%). ^1H NMR: (500 MHz, CDCl_3) δ 8.17 (dt, $J = 8.8, 1.9$ Hz, 2H), 7.54 (dt, $J = 8.8, 1.9$ Hz, 2H), 7.20 (dt, $J = 8.8, 1.9$ Hz, 2H), 7.01 (dt, $J = 8.8, 1.9$ Hz, 2H), 5.28 (d, $J = 1.9$ Hz, 1H), 4.86 (d, $J = 10.4$ Hz, 1H), 2.33 (s, 3H), 2.28 (s, 3H), 2.15 (dddd, $J = 10.6, 10.6, 2.5, 2.5$ Hz, 1H), 1.90 (dddd, $J = 12.7, 2.3, 2.3, 2.3$ Hz, 1H), 1.86-1.75 (m, 3H), 1.54 (dddd, $J = 12.7, 2.3, 2.3, 2.3$ Hz, 1H), 1.45-1.15 (m, 3H), 1.07 (qd, $J = 12.7, 3.9$ Hz, 1H); ^{13}C NMR: (125 MHz, CDCl_3) δ 195.5, 169.4, 168.8, 154.6, 150.5, 148.8, 133.1, 132.8, 131.2, 125.6, 121.8, 121.3, 102.7, 83.6, 41.2, 38.4, 32.6, 27.6, 26.0, 25.8, 21.1, 21.1. HRMS (EI) calculated for $[\text{C}_{26}\text{H}_{26}\text{O}_6]^+$ requires m/z 434.1724, found 434.1714.

(Table 2-2, entry 5, 2.9): Experiment 1: Prepared according to general procedure A with 100.6



mg (0.240 mmol) bis(enone), 9.3 mg (0.0124 mmol) Ru(bpy)₃Cl₂·6H₂O, 43.9 mg (0.468 mmol) LiBF₄, 43 μL (2.39 mmol) H₂O, 125 μL (0.717 mmol) *i*-Pr₂NEt, and 2.39 mL MeCN

and an irradiation time of 1.5 hours. Purification by flash column chromatography (20:1

hexanes:Et₂O) afforded 75 mg cycloadduct (0.177 mmol, 75%). Experiment 2: 99.7 mg (0.238

mmol) bis(enone), 9.3 mg (0.0124 mmol) Ru(bpy)₃Cl₂·6H₂O, 44.5 mg (0.475 mmol) LiBF₄, 43

μL (2.39 mmol) H₂O, 125 μL (0.717 mmol) *i*-Pr₂NEt, and 2.39 mL MeCN. Isolated 79 mg

cycloadduct (0.189 mmol, 79%) as a colorless oil. ¹H NMR: (500 MHz, CDCl₃) δ8.75 (s, 1H),

8.19 (dd, J = 8.8, 1.7 Hz, 1H), 8.03 (s, 1H), 7.93 (t, J = 7.9 Hz, 2H), 7.89 (d, J = 8.1 Hz, 1H),

7.80-7.67 (m 4H), 7.61 (td, J = 7.9, 0.9 Hz, 1H), 7.52 (td, J = 7.9, 0.9 Hz, 1H), 7.43-7.37 (m,

2H), 5.49 (d, J = 1.7 Hz, 1H), 5.16 (d, J = 10.4 Hz, 1H), 2.27 (dddd, J = 10.4, 10.4, 1.5, 1.5 Hz,

1H), 1.96 (qd, J = 10.5, 3.1 Hz, 2H), 1.82 (dt, J = 12.4, 2.4 Hz, 1H), 1.77 (dt, J = 12.4, 2.4 Hz,

1H), 1.61 (dd, J = 12.2, 2.4 Hz, 1H), 1.49-1.22 (m, 3H), 1.12 (qd, J = 13.0, 3.7 Hz, 1H); ¹³C

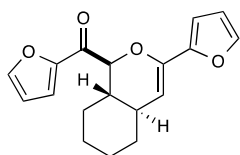
NMR: (125 MHz, CDCl₃) δ196.9, 149.7, 135.8, 133.2, 133.2, 133.1, 132.5, 132.4, 131.5, 129.9,

128.8, 128.5, 128.4, 127.8, 127.7, 127.5, 126.8, 126.1, 125.9, 124.8, 123.4, 122.6, 103.4, 83.1,

41.6, 38.7, 32.7, 27.8, 26.1, 25.9. HRMS (EI) calculated for [C₃₀H₂₆O₂]⁺ requires *m/z* 418.1928,

found 418.1936.

(Table 2-2, entry 6, 2.10): Experiment 1: Prepared according to general procedure A with 102.0



mg (0.342 mmol) bis(enone), 13.4 mg (0.0179 mmol) Ru(bpy)₃Cl₂·6H₂O, 61.5 mg (0.656 mmol) LiBF₄, 60 μL (3.35 mmol) H₂O, 175 μL (1.01 mmol) *i*-Pr₂NEt, and 3.35 mL MeCN and an irradiation time of 30 min.

Purification by flash column chromatography (15:1 hexanes:EtOAc) afforded 79 mg cycloadduct

(0.258 mmol, 77%) as a colorless oil. Experiment 2: 101.5 mg (0.340 mmol) bis(enone), 12.5 mg

(0.0167 mmol) Ru(bpy)₃Cl₂·6H₂O, 62.3 mg (0.665 mmol) LiBF₄, 60 μL (3.35 mmol) H₂O, 175

μL (1.01 mmol) *i*-Pr₂NEt, and 3.35 mL MeCN. Isolated 77 mg cycloadduct (0.258, 76%). ¹H

NMR: (500 MHz, CDCl₃) δ7.67 (dd, J = 1.6, 0.6 Hz, 1H), 7.40 (dd, J = 3.7, 0.6 Hz, 1H), 7.36

(dd, J = 1.4, 1.4 Hz, 1H), 6.55 (dd, J = 3.7, 1.6 Hz, 1H), 6.39-6.36 (m, 2H), 5.29 (d, J = 1.8 Hz,

1H), 4.86 (d, J = 10.6 Hz, 1H), 2.14 (dddd, J = 10.6, 10.6, 2.2, 2.2 Hz, 1H), 1.90 (dddd, J = 13.0,

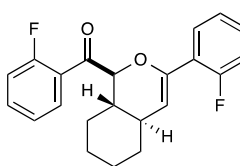
1.3, 1.3, 1.3 Hz, 1H), 1.79 (dddd, J = 12.4, 2.2, 2.2, 2.2 Hz, 1H), 1.69 (dddd, J = 10.5, 10.5, 10.5,

3.0 Hz, 1H), 1.60-1.53 (m, 1H), 1.44-1.08 (m, 4H); ¹³C NMR: (125 MHz, CDCl₃) δ185.6, 150.8,

149.5, 147.4, 142.7, 142.0, 120.4, 112.3, 111.1, 105.9, 101.7, 83.3, 42.1, 38.0, 32.5, 27.2, 25.9,

25.8. HRMS (EI) calculated for *m/z* [C₁₈H₁₈O₄]⁺ requires 298.1200, found 298.1187.

(Table 2-2, entry 7, 2.11): Experiment 1: Prepared according to general procedure A with 99.7



mg (0.281 mmol) bis(enone), 10.5 mg (0.0140 mmol) Ru(bpy)₃Cl₂·6H₂O,

52.1 mg (0.556 mmol) LiBF₄, 51 μL (2.82 mmol) H₂O, 148 μL (0.847

mmol) *i*-Pr₂NEt, and 2.8 mL MeCN and an irradiation time of 30 min.

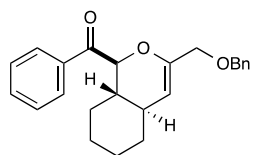
Purification by flash column chromatography (20:1 hexanes:Et₂O) afforded 84 mg cycloadduct

(0.237 mmol, 84%) as a white solid. Experiment 2: 99.8 mg (0.282 mmol) bis(enone), 11.2 mg

(0.0150 mmol) Ru(bpy)₃Cl₂·6H₂O, 51.9 mg (0.554 mmol) LiBF₄, 51 μL (2.82 mmol) H₂O, 148

μL (0.847 mmol) *i*-Pr₂NEt, and 2.8 mL MeCN. Isolated 84 mg cycloadduct (0.237 mmol, 84%).
¹H NMR: (500 MHz, CDCl₃) δ 7.86 (td, *J* = 7.6, 1.7 Hz, 1H), 7.54 (m, 1H), 7.45 (td, *J* = 7.9, 1.7 Hz, 1H), 7.25 (td, *J* = 7.8, 1.1 Hz, 1H), 7.21-7.12 (m, 2H), 7.04-6.98 (m, 2H), 5.39 (bs, 1H), 5.01 (d, *J* = 10.4 Hz, 1H), 2.19 (dddd, *J* = 11.0, 11.0, Hz, 1H), 1.91-1.75 (m, 4H), 1.70 (dddd, *J* = 12.6, 2.7, 2 Hz, 1H), 1.45-1.08 (m, 4H); ¹³C NMR: (125 MHz, CDCl₃) δ 196.9 (d, *J* = 3.2), 161.4 (d, *J* = 254.0), 159.8 (d, *J* = 251.2), 144.7 (d, *J* = 3.5), 134.6 (d, *J* = 9.8), 130.9 (d, *J* = 2.3), 128.9 (d, *J* = 8.6), 128.1 (d, *J* = 2.2), 125.8 (d, *J* = 13.1), 124.5 (d, *J* = 3.2), 123.8 (d, *J* = 3.6), 123.3 (d, *J* = 10.8), 116.7 (d, *J* = 23.2), 115.8 (d, *J* = 23.2), 107.9 (d, *J* = 12.1), 83.4 (d, *J* = 5.0), 40.9, 38.5, 27.4, 26.1, 25.9, 32.6. HRMS (EI) calculated for [C₂₂H₂₀F₂O₂]⁺ *m/z* requires 354.1426, found 354.1423.

(Table 2-2, entry 9, 2.13): Experiment 1: Prepared according to general procedure A with 99.7

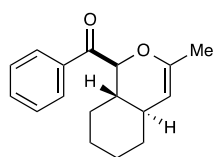


mg (0.275 mmol) bis(enone), 10.8 mg (0.0144 mmol) Ru(bpy)₃Cl₂·6H₂O, 52 mg (0.555 mmol) LiBF₄, 50 μL (2.76 mmol) H₂O, 144 μL (0.828 mmol) *i*-Pr₂NEt, and 2.76 mL MeCN and an irradiation time of 20 min.

Purification by flash column chromatography (10:1 hexanes:Et₂O) afforded 75 mg cycloadduct (0.207 mmol, 75%) as a colorless oil. Experiment 2: 100.2 mg (0.276 mmol) bis(enone), 10.3 mg (0.0138 mmol) Ru(bpy)₃Cl₂·6H₂O, 52 mg (0.555 mmol) LiBF₄, 50 μL (2.76 mmol) H₂O, 144 μL (0.828 mmol) *i*-Pr₂NEt, and 2.76 mL MeCN. Isolated 76 mg cycloadduct (0.210 mmol, 76%). ¹H NMR: (500 MHz, CDCl₃) δ 8.07 (dt, *J* = 7.5, 1.2 Hz, 2H), 7.57 (tt, *J* = 7.5, 1.2 Hz, 1H), 7.43 (td, *J* = 7.5, 1.2 Hz, 2H), 7.36-7.25 (m, 5H), 4.84 (d, *J* = 10.4 Hz, 1H), 4.80 (s, 1H), 4.57 (s, 2H), 3.96 (ABq, *J* = 12.0 Hz, 2H), 2.03 (dddd, *J* = 11.0, 11.0, 1.4, 1.4 Hz, 1H), 1.84-1.69 (m, 4H), 1.49 (ddd, *J* = 12.8, 2.3, 2.3 Hz, 1H), 1.39-1.19 (m, 2H), 1.12 (dddd, *J* = 12.8, 12.8, 12.8, 3.2 Hz, 1H),

1.00 (dddd, $J = 12.8, 12.8, 12.8, 3.7$ Hz, 1H); ^{13}C NMR: (125 MHz, CDCl_3) δ 197.0, 149.0, 138.2, 135.8, 133.4, 129.3, 128.5, 128.3, 127.8, 127.6, 104.9, 82.6, 72.3, 69.9, 41.4, 37.8, 32.4, 27.7, 26.0, 25.9. HRMS (EI) calculated for $[\text{C}_{24}\text{H}_{26}\text{O}_3]^+$ requires m/z 362.1877, found 362.1869.

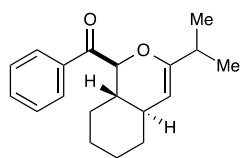
(Table 2-2, entry 10, 2.14): Experiment 1: Prepared according to general procedure B with



101.0 mg (0.394 mmol) bis(enone), 14.4 mg (0.0192 mmol) $\text{Ru}(\text{bpy})_3\text{Cl}_2 \cdot 6\text{H}_2\text{O}$, 173.9 mg (0.779 mmol) $\text{Mg}(\text{ClO}_4)_2$, 340 μL (1.95 mmol) $i\text{-Pr}_2\text{NEt}$, and 15.6 mL MeCN and an irradiation time of 10 min. Purification

by flash column chromatography (20:1 hexanes:EtOAc) afforded 75 mg cycloadduct (0.293 mmol, 74%) as a colorless oil. Experiment 2: 98.9 mg (0.386 mmol) bis(enone), 14.4 mg (0.0192 mmol) $\text{Ru}(\text{bpy})_3\text{Cl}_2 \cdot 6\text{H}_2\text{O}$, 172.9 mg (0.775 mmol) $\text{Mg}(\text{ClO}_4)_2$, 340 μL (1.95 mmol) $i\text{-Pr}_2\text{NEt}$, and 15.6 mL MeCN. Isolated 72 mg cycloadduct (0.281, 72%). ^1H NMR: (500 MHz, CDCl_3) δ 8.05 (dt, $J = 7.7, 1.3$ Hz, 2H), 7.58 (tt, $J = 7.7, 1.3$ Hz, 1H), 7.47 (tt, $J = 7.7, 1.3$ Hz, 2H), 4.82 (d, $J = 10.3$ Hz, 1H), 4.43 (s, 1H), 1.95 (dddd, $J = 11.3, 11.3, 1.8, 1.8$ Hz, 1H), 1.79 (dd, $J = 2.0, 0.8$ Hz, 3H), 1.77-1.64 (m, 4H), 1.44 (dddd, $J = 12.4, 2.7, 2.7, 2.7$ Hz, 1H), 1.37-1.18 (m, 2H), 1.07 (dddd, $J = 12.4, 12.4, 12.4, 2.7$ Hz, 1H), 0.97 (dddd, $J = 12.6, 12.6, 12.6, 3.6$ Hz, 1H); ^{13}C NMR: (125 MHz, CDCl_3) δ 197.5, 149.2, 136.0, 133.4, 129.2, 128.5, 128.5, 101.5, 82.3, 41.7, 38.1, 32.7, 27.7, 25.9, 25.9, 19.7. HRMS (EI) calculated for $[\text{C}_{17}\text{H}_{20}\text{O}_2]^+$ requires m/z 256.1458, found 256.1455.

(Table 2-2, entry 12, 2.15): Experiment 1: Prepared according to general procedure B with

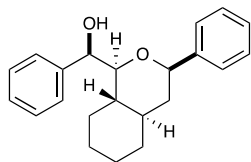


100.2 mg (0.353 mmol) bis(enone), 13.6 mg (0.0182 mmol) $\text{Ru}(\text{bpy})_3\text{Cl}_2 \cdot 6\text{H}_2\text{O}$, 158.5 mg (0.710 mmol) $\text{Mg}(\text{ClO}_4)_2$, 307 μL (1.76 mmol) *i*- Pr_2NEt , and 14.1 mL MeCN and an irradiation time of 1.5 hours.

Purification by flash column chromatography (20:1 hexanes: Et_2O) afforded 58 mg cycloadduct (0.204 mmol, 58%) as a colorless oil. Experiment 2: 100.6 mg (0.354 mmol) bis(enone), 13.7 mg (0.0183 mmol) $\text{Ru}(\text{bpy})_3\text{Cl}_2 \cdot 6\text{H}_2\text{O}$, 158.0 mg (0.708 mmol) $\text{Mg}(\text{ClO}_4)_2$, 307 μL (1.76 mmol) *i*- Pr_2NEt , and 14.1 mL MeCN. Isolated 58 mg cycloadduct (0.204 mmol, 58%). ^1H NMR: (500 MHz, CDCl_3) δ 8.07 (ddd, $J = 7.8, 1.2, 1.0$ Hz, 2H), 7.57 (tt, $J = 7.8, 1.2, 1.0$ Hz, 1H), 7.46 (ddd, $J = 7.8, 7.8, 1.0$ Hz, 2H), 4.70 (d, $J = 10.4$ Hz, 1H), 4.42 (s, $J = 10.4$ Hz, 1H), 2.27 (sept, $J = 6.8$ Hz, 1H), 1.95 (dddd, $J = 10.5, 10.5, 6.8, 6.8$ Hz, 1H), 1.80-1.59 (m, 4H), 1.47 (dddd, $J = 13.0, 3.0, 3.0, 3.0$ Hz, 1H), 1.38-1.16 (m, 2H), 1.24-0.92 (m, 8H); ^{13}C NMR: (125 MHz, CDCl_3) δ 197.5, 157.6, 135.7, 133.3, 129.4, 128.4, 98.4, 83.2, 41.7, 37.9, 32.9, 32.0, 27.6, 26.0, 26.0, 20.5. HRMS (EI) calculated for $[\text{C}_{19}\text{H}_{24}\text{O}_2]^+$ requires m/z 284.1771, found 284.1780.

2.5.4 Experimental details for the functionalization of cycloadduct 2.4

(Scheme 2-3, 2.24): To an oven-dried 500 ml pressure flask equipped with a magnetic stir bar

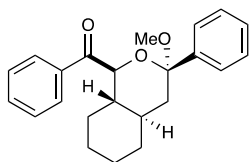


was added 10% Pd/C (62 mg) followed by cycloadduct **2.4** (100 mg, 0.314 mmol) in dichloromethane (8.0 mL) under an atmosphere of nitrogen. The flask was fitted with a regulator and filled with H_2 and evacuated twice,

then filled with 20 psi of H_2 . The reaction was allowed to stir at room temperature for 3 hours and then the excess H_2 was vented. The reaction was filtered over wet Celite and concentrated *in vacuo*. The residue was purified by flash column chromatography on silica gel (8:1

hexanes:ethyl acetate) to afford the product (70 mg, 0.217 mmol, 69%) as a clear oil. IR(thin film): 3553, 3432, 2926, 2852 cm^{-1} . ^1H NMR: (500 MHz, CDCl_3) δ 7.46 (dt, $J = 7.0, 1.5$ Hz, 2H), 7.39-7.26 (m, 8H), 4.80 (dd, $J = 9.4, 3.2$ Hz, 1H), 4.49 (dd, $J = 11.3, 2.2$ Hz, 1H), 3.70 (dd, $J = 10.1, 3.3$ Hz, 1H), 3.40 (d, $J = 9.6$ Hz, 1H, (OH)), 1.80 (dddd, $J = 12.4, 2.8, 2.8, 2.8$ Hz, 1H), 1.73 (m, 1H), 1.67 (tt, $J = 12.4, 2.8$ Hz, 2H), 1.56 (dddd, $J = 12.9, 2.8, 2.8, 2.8$ Hz, 1H), 1.40 (tt, $J = 11.7, 3.3$ Hz, 1H), 1.27 (qt, $J = 13.0, 3.7$ Hz, 1H), 1.16 (q, $J = 12.3$ Hz, 1H), 1.12 (qt, $J = 13.0, 3.7$ Hz, 1H), 1.00 (qd, $J = 12.1, 3.3$ Hz, 1H), 0.89 (qd, $J = 12.8, 3.7$ Hz, 1H), 0.76 (qd, $J = 10.2, 3.2$ Hz, 1H); ^{13}C NMR: (125 MHz, CDCl_3) δ 143.2, 140.62, 128.3, 128.0, 127.9, 127.5, 127.3, 125.8, 84.5, 80.1, 73.8, 42.4, 41.7, 41.1, 32.7, 27.2, 25.9, 25.6. HRMS (EI) calculated for $[\text{C}_{22}\text{H}_{26}\text{O}_2 + \text{Na}]^+$ requires m/z 345.1825, found 345.1835.

(Scheme 2-3, 2.25): To an oven-dried 10 mL round bottom flask equipped with a magnetic stir

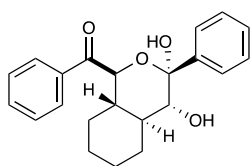


bar was added cycloadduct **2.4** (100 mg, 0.314 mmol), *p*-toluenesulfonic acid monohydrate (6 mg, 0.032 mmol), and methanol (3.2 mL). The reaction was allowed to stir at room temperature for 3.5 hours and then

concentrated *in vacuo*. The residue was purified by flash column chromatography on silica gel (8:1 hexanes:ethyl acetate) to afford the product (104 mg, 0.297 mmol, 95%) as a white solid. IR(thin film): 3059, 2924, 2854, 1679 cm^{-1} . ^1H NMR: (500 MHz, CDCl_3) δ 8.21 (ddd, $J = 7.5, 1.0, 1.0$ Hz, 2H), 7.61 (tt, $J = 7.5, 1.0$ Hz, 1H), 7.51 (t, $J = 7.8$ Hz, 2H), 7.49 (d, $J = 7.3$ Hz, 2H), 7.34 (td, $J = 7.4, 1.0$ Hz, 2H), 7.28 (tt, $J = 7.3, 1.0$ Hz, 1H), 4.73 (d, $J = 10.6$ Hz, 1H), 3.05 (s, 3H), 2.09 (dd, $J = 13.6, 3.6$ Hz, 1H), 1.94 (qt, $J = 11.8, 3.5$ Hz, 1H), 1.70 (m, 4H), 1.51 (t, $J = 13.0$ Hz, 1H), 1.44 (dt, $J = 12.8, 2.2$ Hz, 1H), 1.35 (qt, $J = 12.7, 3.5$ Hz, 1H), 1.23 (qt, $J = 12.8, 3.5$ Hz, 1H), 1.07 (qd, $J = 12.2, 3.5$ Hz, 1H), 1.00 (qd, $J = 12.2, 3.5$ Hz, 1H); ^{13}C NMR: (125

MHz, CDCl₃) δ 197.8, 142.0, 136.2, 133.3, 129.4, 128.5, 128.2, 127.8, 125.9, 100.8, 78.5, 49.5, 44.8, 43.2, 36.0, 32.8, 27.4, 25.9, 25.7;. HRMS (EI) calculated for [C₂₃H₂₆O₃ -MeO]⁺ requires m/z 319.1693, found 319.1689.

(Scheme 2-3, 2.26): A 1.5 dram vial was charged with potassium osmate (VI) dihydrate (2 mg,



0.005 mmol) and sealed with a teflon cap. To the vial was added cycloadduct **2.4** (100 mg, 0.314 mmol), *N*-methylmorpholine *N*-oxide (54 mg, 0.461 mmol), citric acid (60 mg, 0.312 mmol) and a magnetic stir bar,

followed by *tert*-butanol (0.93 mL) and distilled water (0.31 mL). The reaction was then resealed and allowed to stir at room temperature for 23 hours. Sodium sulfite (40 mg, 0.317 mmol) was then added and the reaction was stirred another 30 minutes. The reaction was diluted with water and extracted twice with ethyl acetate. The combined organic extracts were dried over sodium sulfate, filtered and concentrated *in vacuo* to a white solid. The solid was purified by flash column chromatography on silica gel (10:1 toluene:acetone) then recrystallized in hexanes and ethyl acetate to afford the product (65 mg, 0.184 mmol, 60%) as a white crystalline solid. IR(thin film): 3447, 2931, 2856, 1684 cm⁻¹. ¹H NMR: (500 MHz, Acetone-*d*₆) δ 8.14 (dt, *J* = 8.5, 1.5 Hz, 2H), 7.61 (dd, *J* = 8.5, 1.5 Hz, 1H), 7.60 (qt, *J* = 6.7, 1.3 Hz, 2H), 7.48 (tt, *J* = 7.8, 1.5 Hz, 2H), 7.29-7.21 (m, 3H), 5.63 (s, 1H, (OH)), 5.13 (d, *J* = 10.4 Hz, 1H), 3.40 (d, *J* = 9.3 Hz, 1H, (OH)), 3.29 (t, *J* = 9.3 Hz, 1H), 2.24 (m, 1H), 1.98 (qd, *J* = 11.0, 3.2 Hz, 1H), 1.86 (qd, *J* = 11.0, 3.2 Hz, 1H), 1.81 (m, 1H), 1.72 (m, 1H), 1.57 (m, 1H), 1.38-1.24 (m, 2H), 1.13-0.94 (m, 2H); ¹³C NMR: (125 MHz, Acetone-*d*₆) δ 196.1, 143.8, 136.4, 133.1, 129.2, 128.5, 127.5, 127.2, 126.6, 98.7, 76.7, 74.8, 42.7, 41.7, 28.4, 27.2, 25.7, 25.2. HRMS (EI) calculated for [C₂₂H₂₄O₄ + Na]⁺ requires m/z 375.1567, found 375.1583.

2.5.5 Stereochemical determinations

NOE correlations were used to verify the relative stereochemistry of acetal **2.25** and dihydroxylation product **2.26**, as well as the regiochemistry of cycloadduct **2.14**. X-ray crystallography was used to verify the relative stereochemistry in cycloadduct **2.4** and hydrogenation product **2.24** (refer to Appendix D for the experimental details). Subsequent assignments were made by analogy.

2.6 References

- For recent reviews, see: (a) Tietze, L. F.; Kettschau, G. "Hetero Diels–Alder reactions in organic chemistry" *Top. Curr. Chem.* **1997**, *189*, 1–120. (b) Tietze, L. F.; Kettschau, G.; Gewert, J. A.; Schuffenhauer, A. "Hetero-Diels–Alder reactions of 1-oxa-1,3-butadienes" *Curr. Org. Chem.* **1998**, *2*, 19–62. (c) Boger, D. L.; Weinreb, S. M. *Hetero-Diels–Alder Methodology in Organic Synthesis*; Wasserman, H. H., Ed.; Academic Press: San Diego, 1987. (d) Jørgensen, K. A. "Hetero-Diels–Alder reaction of ketones – a challenge for chemists" *Eur. J. Org. Chem.* **2004**, 2093–2102. (e) Pellissier, H. "Asymmetric hetero-Diels–Alder of carbonyl compounds" *Tetrahedron* **2009**, *65*, 2839–2877.
- For seminal examples, see: (a) Thompson, C. F.; Jamison, T. F.; Jacobsen, E. N. "Total Synthesis of FR901464. Convergent Assembly of Chiral Components Prepared by Asymmetric Catalysis" *J. Am. Chem. Soc.* **2000**, *122* 10482–10483. (b) Liu, P.; Jacobsen, E. N. "Total Synthesis of (+)-Ambruticin" *J. Am. Chem. Soc.* **2001**, *123*, 10772–10773. (c) Chavez, D. E.; Jacobsen, E. N. "Total Synthesis of Fostriecin (CI-920)" *Angew. Chem., Int. Ed.* **2001**, *40*, 3667–3670. (d) Paterson, I.; De Savi, C.; Tudge, M. "Total Synthesis of the Microtubule-Stabilising Agent (–)-Laulimalide" *Org. Lett.* **2001**, *3*, 3149–3152. (e) Evans, D. A.; Starr, J. T. "A Cascade Cycloaddition Strategy Leading to the Total Synthesis of (–)-FR182877" *Angew. Chem., Int. Ed.* **2002**, *41* 1787–1790. (f) Paterson, I.; Tudge, M. "Stereocontrolled Total Synthesis of (+)-Leucascandrolide A" *Angew. Chem., Int. Ed.* **2003**, *42*, 343–347. (g) Voight, E. A.; Seradj, H.; Roethle, P. A.; Burke, S. D. "Synthesis of the Bryostatin 1 Northern Hemisphere (C1–C16) via Desymmetrization by Ketalization. Ring-Closing Metathesis" *Org. Lett.* **2004**, *6*, 4045–4048. (h) Tietze, L. F.; Rackelmann, N.; Müller, I. "Enantioselective Total Syntheses of the *Ipecacuanha* Alkaloid Emetine, the *Alangium* Alkaloid Tubulosine and a Novel Benzoquinolizidine Alkaloid by Using a Domino Process" *Chem. Eur. J.* **2004**, *10*, 2722–2731. (i) Lucas, B. S.; Luther, L. M.; Burke, S. D. "A Catalytic Enantioselective Hetero Diels–Alder Approach to the C20–C32 Segment of the Phorboxazoles" *J. Org. Chem.* **2005**, *70*, 3757–3760. (j) Majumder, U.; Cox, J. M.; Johnson, H. W. B.; Rainier, J. D. "Total Synthesis of Gambierol: The Generation of the A–C and F–H Subunits by Using a C-Glycoside Centered Strategy" *Chem. Eur. J.* **2006**, *12* 1736–1746. (k) Louis, I.; Hungerford, N. L.; Humphries, E. J.; McLeod, M. D. "Enantioselective Total

- Synthesis of (-)-Dactylolide” *Org. Lett.* **2006**, *8*, 1117–1120. (l) Lucas, B. S.; Gopalsamuthiram, V.; Burke, S. D. “Total Synthesis of Phorboxazole B” *Angew. Chem., Int. Ed.* **2007**, *46*, 769–772. (m) Ghosh, A. K.; Gong, G. “Enantioselective Total Synthesis of Macrolide Antitumor Agent (-)-Lasonolide A” *Org. Lett.* **2007**, *9*, 1437–1440. (n) Bonazzi, S.; Güttinger, S.; Zemp, I.; Kutay, U.; Gademann, K. “Total Synthesis, Configuration, and Biological Evaluation of Anguinomycin C” *Angew. Chem., Int. Ed.* **2007**, *46*, 8707–8710. (o) Dilger, A. K.; Gopalsamuthiram, V.; Burke, S. D. “A Two-Directional Approach to a (-)-Dictyostatin C11–C23 Segment: Development of a Highly Diastereoselective, Kinetically-Controlled Meerwein–Ponndorf–Verley Reduction” *J. Am. Chem. Soc.* **2007**, *129*, 16273–16277.
3. (a) Desimoni, G.; Tacconi, G. “Heterodiene Syntheses with α,β -Unsaturated Carbonyl Compounds” *Chem. Rev.* **1975**, *75*, 651–692. (b) Schmidt, J. A.; Jorgensen, W. L. “Computer-assisted mechanistic evaluation of organic reactions. 7. Six electron cycloadditions” *J. Org. Chem.* **1983**, *48*, 3923–3941. (c) Jun, J.-G.; Shin, D. G.; Lee, C. K.; Sin, K. S. “Selective reduction of methyl vinyl ketone dimer” *Bull. Korean Chem. Soc.* **1990**, *11*, 307–309.
4. For our leading contributions, see: (a) Ischay, M. A.; Anzovino, M. E.; Du, J.; Yoon, T. P. “Efficient Visible Light Photocatalysis of [2+2] Enone Cycloadditions” *J. Am. Chem. Soc.* **2008**, *130*, 12886–12887. (b) Du, J.; Yoon, T. P. “Crossed Intermolecular [2+2] Cycloadditions of Acyclic Enones vis Visible Light Photocatalysis” *J. Am. Chem. Soc.* **2009**, *131*, 14604–14605. (c) Ischay, M. A.; Lu, Z.; Yoon, T. P. “[2+2] Cycloadditions by Oxidative Visible Light Photocatalysis” *J. Am. Chem. Soc.* **2010**, *132*, 8572–8574. (d) Lu, Z.; Shen, M.; Yoon, T. P. “[3+2] Cycloadditions of Aryl Cyclopropyl Ketones by Visible Light Photocatalysis” *J. Am. Chem. Soc.* **2011**, *133*, 1162–1164. (e) Lin, S.; Ischay, M. A.; Fry, C. G.; Yoon, T. P. “Radical Cation Diels–Alder Cycloadditions by Visible Light Photocatalysis” *J. Am. Chem. Soc.* **2011**, *133*, 19350–19353.
5. For leading contributions, see: (a) Nicewicz, D.; MacMillan, D. W. C. “Merging Photoredox Catalysis with Organocatalysis: The Direct Asymmetric Alkylation of Aldehydes” *Science* **2008**, *322*, 70–80. (b) Narayanam, J. M. R.; Tucker, J. W.; Stephenson, C. R. J. “Electron-Transfer Photoredox Catalysis: Development of a Tin-Free Reductive Dehalogenation Reaction” *J. Am. Chem. Soc.* **2009**, *131*, 8756–8757.
6. For reviews on recent developments in transition metal photoredox catalysis in organic synthesis, see: (a) Zeitler, K. “Photoredox Catalysis with Visible Light” *Angew. Chem. Int. Ed.* **2009**, *48*, 9785–9789. (b) Yoon, T. P.; Ischay, M. A.; Du, J. “Visible light photocatalysis as a greener approach to photochemical synthesis” *Nature Chem.* **2010**, *2*, 527–532. (c) Narayanam, J. M. R.; Stephenson, C. R. J. “Visible light photoredox catalysis: application in organic synthesis” *Chem. Soc. Rev.* **2011**, *40*, 102–113. (d) Prier, C. K.; Rankic, D. A.; MacMillan, D. W. C. “Visible Light Photoredox Catalysis with Transition Metal Complexes: Applications in Organic Synthesis” *Chem. Rev.* **2013**, *113*, 5322–5363. (e) Yoon, T. P. *ACS Catal.* **2013**, *3*, 895–902. (f) Schultz, D. M.; Yoon, T. P. “Solar Synthesis: Prospects in Visible Light Photocatalysis” *Science* **2014**, *343*, 1239176.

-
7. (a) Roh, Y.; Jang, H. Y.; Lynch, V.; Bauld, N. L.; Krische, M. J. "Anion Radical Chain Cycloaddition of Tethered Enones: Intramolecular Cyclobutanation and Diels–Alder Cycloaddition" *Org. Lett.* **2002**, *4*, 611–613. (b) Yang, J.; Felton, G. A. N.; Bauld, N. L.; Krische, M. J. "Chemically Induced Anion Radical Cycloadditions: Intramolecular Cyclobutanation of Bis(enones) via Homogeneous Electron Transfer" *J. Am. Chem. Soc.* **2004**, *126*, 1634–1635. (c) Felton, G. A. N.; Bauld, N. L. "Dramatic effects of the electrolyte cation on the selectivity of electroreductive cycloaddition reactions of bis(enones)" *Tetrahedron Lett.* **2004**, *45*, 8465–8469. (d) Felton, G. A. N.; Bauld, N. L. "Efficient electrocatalytic intramolecular anion radical cyclobutanation reactions" *Tetrahedron* **2004**, *60*, 10999–11010.
 8. The origin of this effect is not clear at this time, but given the polar nature of the intermediates and the step-wise mechanism proposed for radical anion cycloadditions, the hydrophobic effect proposed by Breslow for the rate acceleration of thermal Diels–Alder reactions in water is most likely not operational: Breslow, R. "Hydrophobic effects on simple organic reactions in water" *Acc. Chem. Res.* **1991**, *24*, 159–164.
 9. Fournier, F.; Fournier, M. "Transition metal assisted electron transfer: influence of the nature of the metallic cation on the reduction of carbonyl compounds in an aprotic medium" *Can. J. Chem.* **1986**, *64*, 881–890.
 10. VanRheenen, V.; Kelly, R. C.; Cha, D. Y. "An improved catalytic OsO₄ oxidation of olefins to *cis*-1,2-glycols using tertiary amine oxides as the oxidant" *Tetrahedron Lett.* **1976**, *17*, 1973–1976.
 11. Pangborn, A. B.; Giardello, M. A.; Grubbs, R. H.; Rosen, R. K.; Timmers, F. T. "Safe and Convenient Procedure for Solvent Purification" *Organometallics* **1996**, *15*, 1518–1520.
 12. Still, W. C.; Kahn, M.; Hong, P. C.; Lu, L. "Rapid chromatographic technique for preparative separations with moderate resolution" *J. Org. Chem.* **1978**, *43*, 2923–2925.
 13. Blank, B.; DiTullio, N. W.; Deviney, L.; Roberts, J. T.; Saunders, H. L. "Synthesis and hypoglycemic activity of phenacyltriphenylphosphoranes and phosphonium salts" *J. Med. Chem.* **1975**, *18*, 952–954.
 14. Bravo, P.; Ticozzi, C.; Cezza, A. "Reaction of carbonyl-stabilized phosphonium and arsonium ylids with *o*-hydroxybenzaldehydes. Synthesis of *o*-hydroxychalcones" *Gazzetta Chimica Italiana.* **1975**, *105*, 109–115.
 15. Marques-Lopez, E.; Herrera, R. P.; Marks, T.; Jacobs, W. C.; Konning, D.; de Figueiredo, R. M.; Christmann, M. "Crossed Intramolecular Rauhut–Currier-Type Reactions via Dienamine Activation: *Org. Lett.* **2009**, *11*, 4116–4119.

-
16. Hayashi, Y.; Gotoh, H.; Tamura, T.; Yamaguchi, H.; Masui, R.; Shoji, M. "Cysteine-Derived Organocatalyst in a Highly Enantioselective Intramolecular Michael Reaction" *J. Am. Chem. Soc.* **2005**, *127*, 16028–16029.
 17. Nakamura, H.; Aoyagi, K.; Shim, J-G.; Yamamoto, Y. "Catalytic Amphiphilic Allylation via Bis- π -allylpalladium Complexes and Its Application to the Synthesis of Medium-Sized Carbocycles" *J. Am. Chem. Soc.* **2001**, *123*, 372–377.
 18. Claus, R. E.; Schreiber, S. L. "Ozonolytic cleavage of cyclohexene to terminally differentiated products: Methyl 6-oxohexanoate, 6,6-dimethoxyhexanal, methyl 6,6-dimethoxyhexanoate" *Org. Synth.* **1968**, *64*, 150–156.

Chapter 3. Reductive Cyclizations of Nitroarenes to Hydroxamic Acids by Visible Light Photoredox Catalysis

Portions of this work have been previously published:

Cismesia, M. A.; Ischay, M. A.; Yoon, T. P. "Reductive Cyclizations of Nitroarenes to Hydroxamic Acids by Visible Light Photoredox Catalysis" *Synthesis* **2013**, *45*, 2699–2705.

3.1 Introduction

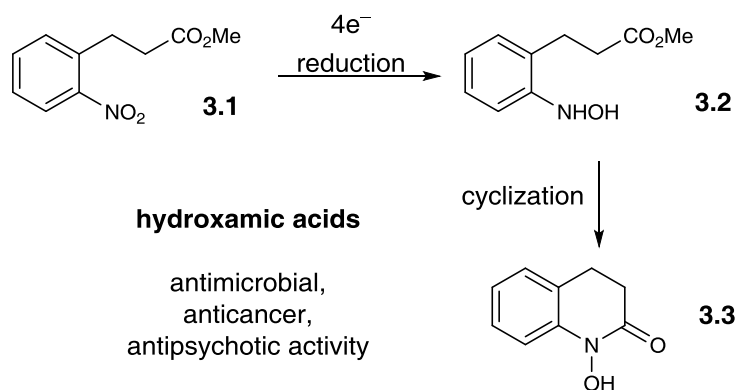
Hydroxamic acids are high-affinity chelating ligands for a wide range of metal cations.¹ Many hydroxamic acid containing secondary metabolites are produced naturally, and they have important biological roles in a variety of contexts including microbial iron metabolism and endogenous chemical defense in plants.² In medicinal chemistry, cyclic hydroxamic acids have been reported to possess antimicrobial and antifungal activity and have also been investigated as potential treatments for conditions ranging from cancer to schizophrenia.³

The most common strategies for the synthesis of cyclic hydroxamic acids involve reduction of nitroarenes to the corresponding hydroxylamines followed by intramolecular cyclization with a tethered acyl moiety (Scheme 3-1). A variety of methods to achieve this transformation have been reported, including those using stoichiometric zinc or tin⁴ as well as palladium⁵ or platinum⁶ catalyzed partial reduction. Many of these methods can be somewhat problematic. First, the stoichiometric processes can generate metal-containing byproducts that complicate the isolation and purification of these strong chelators. Second, the strongly reducing conditions used in many of these reactions can be incompatible with sensitive, easily reduced functional groups such as aryl halides. Finally, a significant challenge in this approach to the synthesis of hydroxamic acids is to achieve selective four-electron reduction of the nitroarene to the desired hydroxamic acid without competitive six-electron reduction to the fully reduced quinolinone.

Over the last several years, our laboratory, along with several others, has been investigating the design of synthetically useful new reactions that exploit the photochemical properties of $\text{Ru}(\text{bpy})_3^{2+}$ and related transition metal chromophores in the visible light regime.⁷ Our efforts have led to a wide range of cycloaddition reactions that are initiated by photocatalytic oxidation or reduction of alkenes;⁸ related efforts in other groups investigating photocatalytic redox

reactions of amines, arenes, and alkyl halides have resulted in the development of a remarkable diversity of synthetically useful transformations.⁹ As part of our ongoing efforts to broaden the scope of reactions amenable to visible light photocatalysis, we became interested in designing a selective photocatalytic four-electron reduction of nitroarenes to afford hydroxamic acids.

Scheme 3-1. Preparation of hydroxamic acids by reduction and cyclization of nitroarenes.



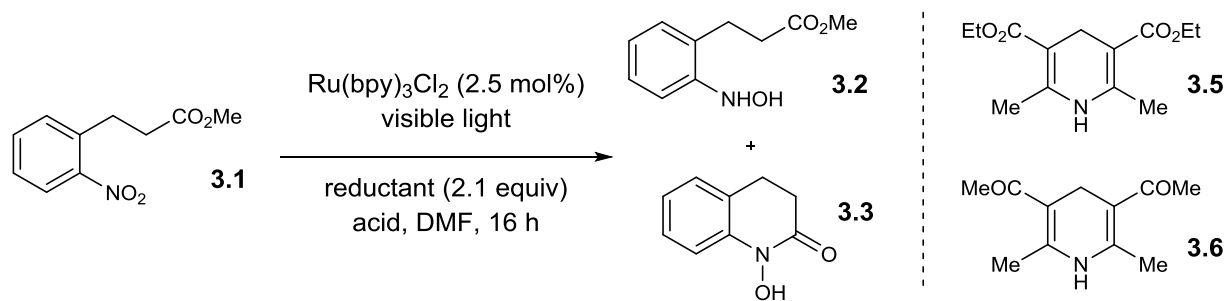
3.2 Results and Discussion

The use of $\text{Ru}(\text{bpy})_3^{2+}$ as a photocatalyst for the exhaustive six-electron reduction of nitrobenzene to aniline has been previously reported using hydrazine as the terminal reductant.¹⁰ Similarly, the photocatalytic four-electron reduction of nitroalkenes to oximes has been accomplished using EDTA as the terminal reductant.¹¹ To the best of our knowledge, the photocatalytic four-electron reduction of nitrobenzene to a hydroxylamine or hydroxamic acid has not been previously been described. Since we reported this method, other nitro group reductions by $\text{Ru}(\text{bpy})_3\text{Cl}_2$ have been published.¹²

Table 3-1 summarizes optimization and control experiments for the photocatalytic reductive cyclization of nitroarene **3.1** to hydroxamic acid **3.3**. We began by applying conditions reported by Stephenson for reductive dehalogenation reactions^{9b} to this reduction. However, when **3.1** was irradiated in the presence of formic acid, *i*-Pr₂NEt, and 2.5 mol% $\text{Ru}(\text{bpy})_3^{2+}$, we observed

none of the expected hydroxamic acid **3.3** and only a trace of the intermediate hydroxylamine **3.2** (entry 1). In a screen of alternate terminal reductants, we observed that while Hantzsch ester **3.4** provided only a trace of reduction products (entry 2), the related diketone **3.5** resulted in good conversion of **3.1** to a mixture of hydroxylamine and hydroxamic acid (entry 3). We speculated that the Brønsted acid could be responsible for the cyclization of **3.2** to **3.3**; indeed, in the absence of an exogenous Brønsted acid additive, we observed exclusive formation of **3.2** without any obvious change in the rate of the photoreduction process (entry 4). The use of stronger acids, on the other hand, increased the yield of **3.3** (Entries 5–7). Optimal results were obtained using camphorsulfonic acid (CSA), and we found that the stoichiometry of this acid could be lowered to 0.1 equiv without affecting the yield of the reaction (entry 8). Finally, control experiments verified the photocatalytic nature of this reaction; in the absence of either $\text{Ru}(\text{bpy})_3^{2+}$ or light, we observed no significant formation of **3.3** (entries 9–10).

Table 3-1. Optimization studies for photocatalytic hydroxamic acid synthesis.



Entry	Reductant	Acid (equiv)	Yield 3.2 (%) ^a	Yield 3.3 (%) ^a
1	<i>i</i> -Pr ₂ NEt	HCO ₂ H (1)	<5	0
2	4	HCO ₂ H (1)	0	<5
3	5	HCO ₂ H (1)	50	20
4	5	none	71	0
5	5	AcOH (1)	52	25
6	5	TFA (1)	0	84
7	5	CSA (1)	0	89
8	5	CSA (0.1)	0	88
9 ^b	5	CSA (0.1)	0	<5
10 ^c	5	CSA (0.1)	0	0

^a Yield determined by ¹H NMR analysis.

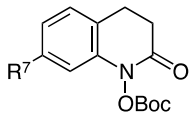
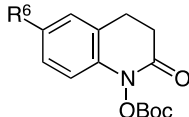
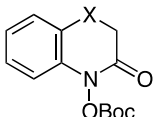
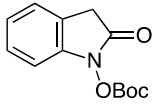
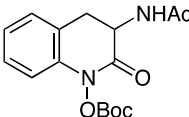
^b Reaction conducted in the absence of Ru(bpy)₃Cl₂.

^c Reaction conducted in the dark.

On larger scales, isolation of pure hydroxamic acid **3.3** could easily be accomplished in good yields by recrystallization. Chromatographic isolation of this material, however, proved to be more challenging; the mass recovery was low, and the eluted product was deeply colored, which we attributed to the ability of this strongly chelating compound to leach metallic impurities from the silica gel. However, treatment of the unpurified reaction mixture with Boc₂O and Et₃N resulted in the formation of a protected hydroxamic acid that could be easily be purified by standard chromatographic methods.^{4c}

Using these optimized conditions for production and protection of hydroxamic acids, we conducted an exploration of the scope of this process (Table 3-2). The reaction proved to be relatively insensitive to electronic perturbation at C7; both electron-donating and electron-withdrawing substituents at this position provide similarly good yields of hydroxamic acids (entries 1–6). Importantly, we observed no reduction of potentially reducible functional groups such as aryl bromides or nitriles (entries 5 and 6). The identity of the C6 substituent had a more dramatic effect. While electron-withdrawing groups at this position had little impact (entry 7), the methoxy-substituted substrate cleanly underwent overreduction to the quinolinone. A similar effect of electron-donating substituents was reported by McAllister,^{4c} who proposed that the accessibility of an iminoquinone intermediate could be responsible for the ease of subsequent overreduction (Scheme 3-2). Changes to the tethering moiety were also tolerated (entries 9–11), although either introducing a tosyl-protected nitrogen (entry 10) or reducing the length of the tether by one carbon (entry 11) resulted in slower cyclizations that necessitated stoichiometric acid. Finally, these conditions tolerated an α -acetamido substituent (entry 12), which provided access to a privileged scaffold reported to possess a range of biological properties.¹³

Table 3-2. Scope studies for hydroxamic acid synthesis.

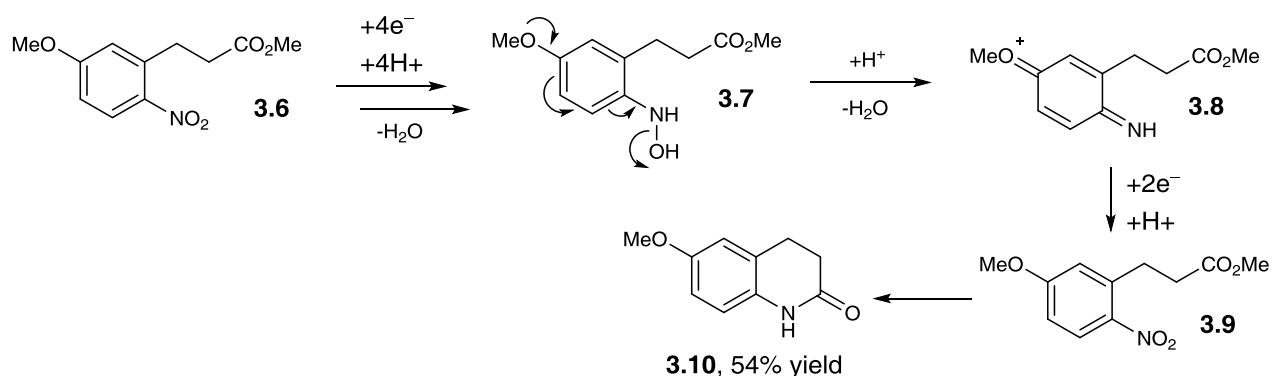
Entry ^a	Product		Yield (%) ^b
1		R ⁷ = H	83
2		R ⁷ = OMe	77
3		R ⁷ = Me	85
4		R ⁷ = CF ₃	81
5		R ⁷ = CN	72
6		R ⁷ = Br	76
7		R ⁶ = F	79
8		R ⁶ = OMe	0 ^c
9		X = O	78
10 ^d		X = NTs	53
11 ^d			64
12 ^d			58

^a Reactions conducted using 2.5 mol% Ru(bpy)₃Cl₂, 2.1 equiv **3.5**, and 0.1 equiv CSA unless otherwise noted.

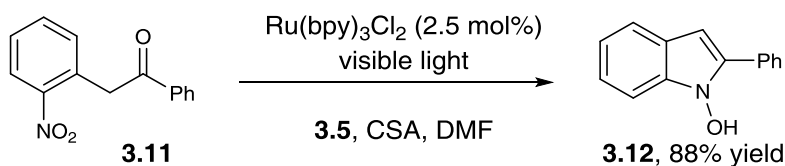
^b Values represent the averaged isolated yields from two reproducible experiments.

^c Quinolinone **3.10** was isolated in 54% yield (Scheme 2).

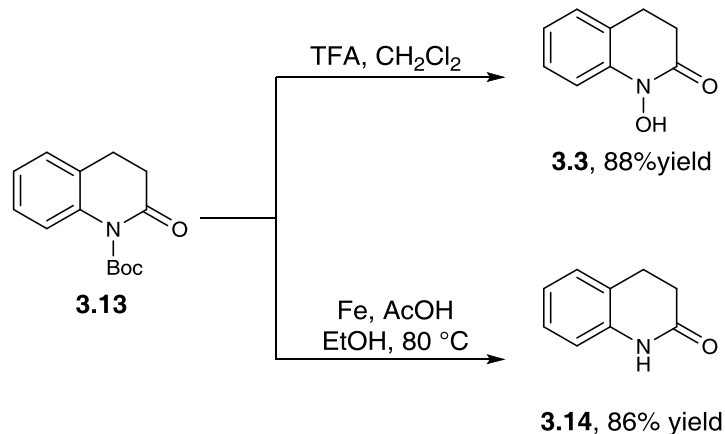
^d Reaction conducted using 3 equiv of **3.5** and 1 equiv of CSA.

Scheme 3-2. Origin of overreduction of **3.6**.

N-Hydroxyindoles have also received considerable attention as potential pharmacophores, and the methods for their synthesis have been similar to those used for the preparation of hydroxamic acids.¹⁴ Thus, we examined the photocatalytic reduction of **3.11** under conditions identical to those optimized for reduction of **3.1**. Indeed, hydroxyindole **3.12** could be isolated in 88% yield without *O*-protection (eq 3-1).

Equation 3-1. Preparation of *N*-hydroxyindoles.

Finally, the Boc protecting group can be cleaved in good yield using previously reported conditions (Scheme 3-3).¹⁵ Treatment of **3.13** with TFA in CH_2Cl_2 reveals the unprotected hydroxamic acid **3.3** in 83% yield. Alternatively, the N–O bond of **3.13** can be cleaved with Fe powder to afford quinolinone **3.14** in 86% yield. Thus, the easily handled *O*-Boc hydroxamic acid can be converted to these useful scaffolds with good efficiency.

Scheme 3-3. Manipulation of *N*-Boc hydroxamic acids.

3.3 Conclusions

We have developed a mild photocatalytic method for the reduction and cyclization of nitroarenes to hydroxamic acids. This method provides access to a class of biologically relevant scaffolds that should possess utility in drug discovery efforts. In the context of our ongoing studies of visible light-induced organic reactions, this study is significant because it shows that synthetically useful transformations can be initiated by photoreduction of nitroarenes. These results raise intriguing questions concerning the precise mechanism of this process, including the effect of the terminal reductant both of the effectiveness of the reduction and the selectivity between four-electron and six-electron reduction. Studies to further interrogate this reaction and design new transformations initiated by reduction of nitro organics are subjects of continuing interest in our laboratory.

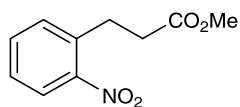
3.4 Experimental

3.4.1 General experimental information

N,N-Dimethylformamide (DMF), triethylamine, and diisopropylethylamine were purified by distillation from CaH₂ prior to use. Dihydropyridines **3.4** and **3.5** were prepared using known methods.¹⁶ The syntheses of the nitroarene substrates are described below. All other reagents were purchased from commercial sources and used without further purification. Chromatography was performed with Purasil 60Å silica gel (230–400 mesh). ¹H and ¹³C NMR data for all previously uncharacterized compounds were obtained using Varian Inova-500 spectrometers and are referenced to TMS (0.00 ppm) and CDCl₃ (77 ppm), respectively. IR spectral data were obtained using a Bruker Vector 22 spectrometer (thin film, NaCl). Melting points were obtained using a Mel-Temp II (Laboratory Devices, Inc., USA) melting point apparatus. Mass spectrometry was performed with a Micromass LCT (electrospray ionization, time-of-flight analyzer).

3.4.2 Preparation of nitroarene substrates

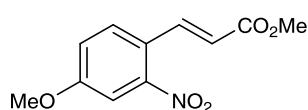
Methyl 2-(2-nitrophenyl)acetate (**3.15**)¹⁷ and 2-(2-nitrophenyl)-1-phenylethanone (**3.11**)¹⁸ were prepared from known procedures.



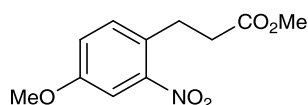
Methyl 3-(2-nitrophenyl)propanoate (3.1): Prepared using a modification of a procedure reported by Zhu.¹⁹ To an oven-dried 150 mL glass pressure

vessel containing a magnetic stirbar was added 945 mg (4.56 mmol) methyl 2-nitrocinnamate²⁰ and 30 mL degassed 1:1 mixture of THF and *t*-BuOH. H₂ gas was bubbled through the solution and the vessel was charged with 419 mg (0.453 mmol) Wilkinson's catalyst. The vessel was fitted with a regulator and pressurized to 30 psi with H₂ gas. The reaction was allowed to stir for

2 days before being passed through a silica plug. Purification by column chromatography (20:1 hexanes:ethyl acetate) yielded 758 mg (3.62 mmol, 79%) of a yellow oil. All spectra data were consistent with reported values.¹⁸

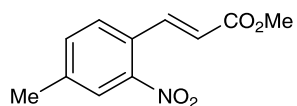


(E)-Methyl 3-(4-methoxy-2-nitrophenyl)acrylate (3.16): An oven-dried Schlenk flask with magnetic stirbar was charged with 252 mg (1.08 mmol) 4-bromo-3-nitroanisole, 0.20 mL (2.2 mmol) methyl acrylate, 5.3 mg (0.024 mmol) Pd(OAc)₂, 11.2 mg (0.0427 mmol) triphenylphosphine, and 0.40 mL (2.9 mmol) triethylamine. The reaction was sealed under N₂ and heated gradually to 125 °C for 5 h. An additional portion of Pd(OAc)₂ was added and the reaction was heated to 125 °C for an additional 1 h before being cooled to room temperature and passed through a silica plug. Purification by column chromatography (5:1 hexanes:ethyl acetate) yielded 189 mg (0.80 mmol, 73%) of a yellow solid. All spectra data were consistent with reported values.²¹

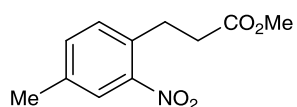


Methyl 3-(4-methoxy-2-nitrophenyl)propanoate (3.17): An oven-dried 150 mL glass pressure vessel containing a magnetic stirbar was charged with 500 mg (2.11 mmol) **3.16** and 15 mL degassed 1:1 mixture of THF and *t*-BuOH. H₂ gas was bubbled through the solution and the vessel was charged with 154 mg (0.166 mmol) Wilkinson's catalyst. The vessel was fitted with a regulator and pressurized to 30 psi with H₂ gas. The reaction was allowed to stir for 6 days before being passed through a silica plug. Purification by column chromatography (8:1 hexanes:ethyl acetate) yielded 490 mg (2.05 mmol, 97%) of a brown oil. IR (thin film, NaCl): 2952, 2842, 1735, 1531 cm⁻¹. ¹H NMR (500 MHz, CDCl₃) δ 7.46 (d, J = 2.8 Hz, 1H), 7.30 (d, J = 8.5 Hz, 1H), 7.09 (dd, J = 8.5, 2.8 Hz, 1H), 3.85 (s, 3H), 3.67 (s, 3H), 3.15 (t, J = 7.5 Hz, 2H), 2.69 (t, J = 7.5 Hz, 2H). ¹³C NMR (126 MHz,

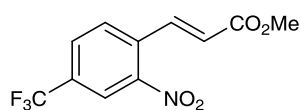
CDCl_3) δ 172.9, 158.5, 149.5, 133.0, 127.5, 120.0, 109.4, 55.8, 51.7, 34.8, 27.8. HRMS (ESI) calc'd for $[\text{C}_{11}\text{H}_{13}\text{NO}_5+\text{NH}_4]^+$ requires m/z 257.1132, found m/z 257.1125.



(E)-Methyl 3-(4-methyl-2-nitrophenyl)acrylate (3.18): An oven-dried Schlenk flask with magnetic stirbar was charged with 496 mg (2.06 mmol) 4-bromo-3-nitrotoluene (90%), 0.40 mL (4.4 mmol) methyl acrylate, 10.8 mg (0.0481 mmol) $\text{Pd}(\text{OAc})_2$, 23.3 mg (0.0888 mmol) triphenylphosphine, and 1.0 mL (7.2 mmol) triethylamine. The reaction was sealed under N_2 and heated gradually to 125 °C for 6 h before cooled to room temperature and passed through a silica plug. Purification by column chromatography (9:1 hexanes:ethyl acetate) yielded 308 mg (1.4 mmol, 68%) of a yellow solid. All spectra data were consistent with reported values.²⁰

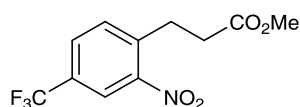


Methyl 3-(4-methyl-2-nitrophenyl)propanoate (3.19): To an oven-dried 150 mL glass pressure vessel containing a magnetic stirbar was added 327 mg (1.48 mmol) **3.18** and 10 mL degassed 1:1 mixture of THF and *t*-BuOH. H_2 gas was bubbled through the solution and the vessel was charged with 114 mg (0.123 mmol) Wilkinson's catalyst. The vessel was fitted with a regulator and pressurized to 30 psi with H_2 gas. The reaction was allowed to stir for 2 days before being passed through a silica plug. Purification by column chromatography (8:1 hexanes:ethyl acetate) yielded 251 mg (1.13 mmol, 76%) of a brown oil. IR (thin film, NaCl): 2953, 1739, 1529 cm^{-1} . ^1H NMR (500 MHz, CDCl_3) δ 7.75 (d, J = 1.4 Hz, 1H), 7.34 (dd, J = 7.8, 1.4 Hz, 1H), 7.28 (d, J = 7.5 Hz, 1H), 3.67 (s, 3H), 3.18 (t, J = 7.5 Hz, 2H), 2.71 (t, J = 7.5 Hz, 2H), 2.40 (s, 3H). ^{13}C NMR (126 MHz, CDCl_3) δ 173.1, 149.2, 138.2, 134.3, 132.8, 132.2, 125.4, 51.9, 35.0, 28.3, 21.0. HRMS (ESI) calc'd for $[\text{C}_{11}\text{H}_{13}\text{NO}_4+\text{Na}]^+$ requires m/z 246.0737, found m/z 246.0741.



(E)-Methyl 3-(2-nitro-4-(trifluoromethyl)phenyl)acrylate (3.20): An

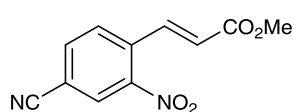
oven-dried Schlenk flask with magnetic stirbar was charged with 0.33 mL (2.2 mmol) 4-bromo-3-nitrobenzotrifluoride, 0.40 mL (4.4 mmol) methyl acrylate, 10.1 mg (0.0450 mmol) Pd(OAc)₂, 23.8 mg (0.0907 mmol) triphenylphosphine, and 0.40 mL (2.9 mmol) triethylamine. The reaction was sealed under N₂ and heated gradually to 125 °C for 21 h before being cooled to room temperature and passed through a silica plug. Purification by column chromatography (20:1 hexanes:ethyl acetate) yielded 346 mg (1.3 mmol, >10:1 E:Z, 58%) of a yellow solid. mp = 77.6–79.3 °C. IR (thin film, NaCl): 3096, 2956, 1718, 1540, 1324 cm⁻¹. ¹H NMR (500 MHz, CDCl₃) δ 8.33 (d, *J* = 1.7 Hz, 1H), 8.13 (d, *J* = 15.9 Hz, 1H), 7.92 (dd, *J* = 8.4, 1.6 Hz, 1H), 7.78 (d, *J* = 8.1 Hz, 1H), 6.43 (d, *J* = 15.9 Hz, 1H), 3.86 (s, 3H). ¹³C NMR (126 MHz, CDCl₃) δ 165.6, 148.1, 138.7, 134.1, 132.6 (q, *J* = 35.3 Hz), 130.2, 130.0 (q, *J* = 3.8 Hz), 124.9, 122.5 (q, *J* = 273.4 Hz), 122.4 (q, *J* = 3.8 Hz), 52.2. HRMS (ESI) calc'd for [C₁₁H₈F₃NO₄+NH₄]⁺ requires *m/z* 293.0744, found *m/z* 293.0735.



Methyl 3-(2-nitro-4-(trifluoromethyl)phenyl)propanoate (3.21): To

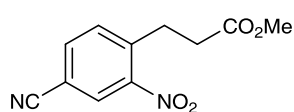
an oven-dried 150 mL glass pressure vessel containing a magnetic stirbar was added 307 mg (1.11 mmol) **3.20** and 8 mL degassed 1:1 mixture of THF and *t*-BuOH. H₂ gas was bubbled through the solution and the vessel was charged with 86.6 mg (0.0936 mmol) Wilkinson's catalyst. The vessel was fitted with a regulator and pressurized to 30 psi with H₂ gas. The reaction was allowed to stir for 24 h before another portion of catalyst was added. The reaction was pressurized to 30 psi of H₂ and allowed to stir for another 24 h before being passed through a silica plug. Purification by column chromatography (20:1 hexanes:ethyl acetate) yielded 238 mg (0.859 mmol, 77%) of a yellow oil. IR (thin film, NaCl): 2956, 1735,

1540, 1327 cm^{-1} . ^1H NMR (500 MHz, CDCl_3) δ 8.23 (d, $J = 1.0$ Hz 1H), 7.80 (dd, $J = 8.1$, 1.3 Hz 1H), 7.61 (d, $J = 8.1$ Hz, 1H), 3.68 (s, 3H), 3.30 (t, $J = 7.4$ Hz, 2H), 2.76 (t, $J = 7.4$ Hz, 2H). ^{13}C NMR (126 MHz, CDCl_3) δ 172.3, 149.2, 139.6, 133.3, 130.4 (q, $J = 34.0$ Hz), 129.5 (q, $J = 3.8$ Hz), 122.8 (q, $J = 273.4$ Hz), 122.3 (q, $J = 3.8$ Hz), 51.9, 34.2, 28.2. HRMS (ESI) calc'd for $[\text{C}_{11}\text{H}_{10}\text{F}_3\text{NO}_4+\text{Na}]^+$ requires m/z 300.0455, found m/z 300.0454.



(E)-Methyl 3-(4-cyano-2-nitrophenyl)acrylate (3.22): An oven-dried

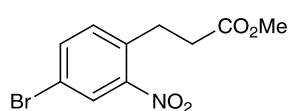
Schlenk flask with magnetic stirbar was charged with 502 mg (2.21 mmol) 4-bromo-3-nitrobenzonitrile, 0.40 mL (4.4 mmol) methyl acrylate, 9.2 mg (0.041 mmol) $\text{Pd}(\text{OAc})_2$, 22.7 mg (0.0865 mmol) triphenylphosphine, and 0.40 mL (2.9 mmol) triethylamine. The reaction was sealed under N_2 and heated gradually to 125 $^\circ\text{C}$ for 21 h before being cooled to room temperature and passed through a silica plug. Purification by column chromatography (20:1 hexanes:ethyl acetate) yielded 289 mg (1.3 mmol, 8:1 E:Z, 56%) of a tan solid. mp = 43.4–45.6 $^\circ\text{C}$. IR (thin film, NaCl): 3061, 2959, 2243, 1718, 1532 cm^{-1} . ^1H NMR (500 MHz, CDCl_3) δ 8.35 (d, $J = 1.7$ Hz, 1H), 8.10 (d, $J = 15.9$ Hz, 1H), 7.93 (dd, $J = 8.0$, 1.7 Hz, 1H), 7.78 (d, $J = 8.1$ Hz, 1H), 6.45 (d, $J = 15.9$ Hz, 1H), 3.86 (s, 3H). ^{13}C NMR (126 MHz, CDCl_3) δ 165.4, 148.1, 138.1, 136.2, 134.8, 130.3, 128.6, 125.6, 116.1, 114.3, 52.3. HRMS (ESI) calc'd for $[\text{C}_{11}\text{H}_8\text{N}_2\text{O}_4+\text{NH}_4]^+$ requires m/z 250.0823, found m/z 250.0822.



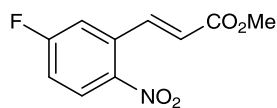
Methyl 3-(4-cyano-2-nitrophenyl)propanoate (3.23): To an oven-

dried 150 mL glass pressure vessel containing a magnetic stirbar was added 313 mg (1.35 mmol) **3.22** and 10 mL degassed 1:1 mixture of THF and *t*-BuOH. H_2 gas was bubbled through the solution and the vessel was charged with 295 mg (0.319 mmol)

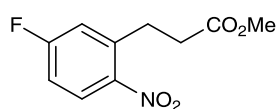
Wilkinson's catalyst. The vessel was fitted with a regulator and pressurized to 40 psi with H₂ gas. The reaction was allowed to stir for 3 days before being passed through a silica plug. Purification by column chromatography (4:1 hexanes:ethyl acetate) yielded 167 mg (0.713 mmol, 53%) of a yellow solid. mp = 137.3–138.6 °C. IR (thin film, NaCl): 2955, 2237, 1735, 1535 cm⁻¹. ¹H NMR (500 MHz, CDCl₃) δ 8.25 (d, *J* = 1.7 Hz, 1H), 7.82 (dd, *J* = 8.0, 1.7 Hz, 1H), 7.62 (d, *J* = 8.0 Hz, 1H), 3.68 (s, 3H), 3.30 (t, *J* = 7.3 Hz, 2H), 2.76 (t, *J* = 7.3 Hz, 2H). ¹³C NMR (126 MHz, CDCl₃) δ 172.1, 149.3, 140.8, 135.8, 133.6, 128.5, 116.4, 112.1, 51.9, 33.9, 28.3. HRMS (ESI) calc'd for [C₁₁H₁₀N₂O₄+NH₄]⁺ requires *m/z* 252.0979, found *m/z* 252.0981.



Methyl 3-(4-bromo-2-nitrophenyl)propanoate (3.24): In a round-bottom flask with magnetic stirbar was dissolved 528 mg (2.52 mmol) methyl 3-(2-nitrophenyl)propanoate and 500 mg (2.81 mmol) *N*-bromosuccinimide in 1.3 mL sulfuric acid and 12.6 mL trifluoroacetic acid. The reaction was stirred for 2 days, and then diluted with ethyl acetate and washed with 50 mL water, 50 mL saturated NaHCO₃, and 50 mL brine. The organic layer was dried with MgSO₄, filtered, and concentrated *in vacuo*. Purification by column chromatography (50:1 hexanes:ethyl acetate) yielded 176 mg (0.611 mmol, 24%) of a yellow solid. mp = 47.8–49.1 °C. IR (thin film, NaCl): 2952, 2850, 1734, 1528 cm⁻¹. ¹H NMR (500 MHz, CDCl₃) δ 8.09 (d, *J* = 2.1 Hz, 1H), 7.66 (dd, *J* = 8.3, 2.1 Hz, 1H), 7.31 (d, *J* = 8.3 Hz, 1H), 3.67 (s, 3H), 3.18 (t, *J* = 7.4 Hz, 2H), 2.71 (t, *J* = 7.4 Hz, 2H). ¹³C NMR (126 MHz, CDCl₃) δ 172.5, 149.6, 136.2, 134.5, 133.6, 127.8, 120.6, 51.8, 34.3, 27.9. HRMS (ESI) calc'd for [C₁₀H₁₀BrNO₄+NH₄]⁺ requires *m/z* 305.0132, found *m/z* 305.0136.

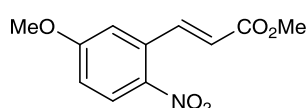


(E)-Methyl 3-(5-fluoro-2-nitrophenyl)acrylate (3.25): An oven-dried Schlenk flask with magnetic stirbar was charged with 155 mg (0.705 mmol) 2-bromo-4-fluoro-1-nitrobenzene,²² 0.13 mL (1.4 mmol) methyl acrylate, 3.2 mg (0.014 mmol) Pd(OAc)₂, 7.8 mg (0.030 mmol) triphenylphosphine, and 0.12 mL (0.86 mmol) triethylamine. The reaction was sealed under N₂ and heated gradually to 125 °C for 2 days before being cooled to room temperature and passed through a silica plug. Purification by column chromatography (9:1 hexanes:ethyl acetate) yielded 89.5 mg (0.40 mmol, 10:1 E:Z, 56%) of a yellow solid. mp = 76.7–77.8 °C. IR (thin film, NaCl): 3081, 2961, 1717, 1525 cm⁻¹. ¹H NMR (500 MHz, CDCl₃) δ 8.15 (dd, *J* = 8.9, 5.0 Hz, 1H), 8.13 (d, *J* = 15.8 Hz, 1H), 7.30 (dd, *J* = 8.8, 2.7 Hz, 1H), 7.23 (ddd, *J* = 9.6, 7.1, 2.8 Hz, 1H), 6.35 (d, *J* = 15.8 Hz, 1H), 3.84 (s, 3H). ¹³C NMR (126 MHz, CDCl₃) δ 165.8, 164.8 (d, *J* = 258.3 Hz), 144.3, 139.3, 133.9 (d, *J* = 8.8 Hz), 127.9 (d, *J* = 8.8 Hz), 123.9, 117.2 (d, *J* = 22.7 Hz), 116.0 (d, *J* = 23.9 Hz), 52.1. HRMS (ESI) calc'd for [C₁₀H₈FNO₄+NH₄]⁺ requires *m/z* 243.0776, found *m/z* 243.0775.

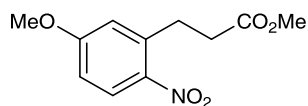


Methyl 3-(5-fluoro-2-nitrophenyl)propanoate (3.26): To an oven-dried 150 mL glass pressure vessel containing a magnetic stirbar was added 146 mg (0.646 mmol) **3.25** and 4.5 mL degassed 1:1 mixture of THF and *t*-BuOH. H₂ gas was bubbled through the solution and the vessel was charged with 123 mg (0.133 mmol) Wilkinson's catalyst. The vessel was fitted with a regulator and pressurized to 40 psi with H₂ gas. The reaction was allowed to stir for 2 days before being passed through a silica plug. Purification by column chromatography (9:1 hexanes:ethyl acetate) yielded 87.1 mg (0.383 mmol, 59%) of a yellow oil. IR (thin film, NaCl): 2953, 2850, 1737, 1527 cm⁻¹. ¹H NMR (500 MHz, CDCl₃) δ 8.05 (dd, *J* = 9.1, 5.2 Hz, 1H), 7.12 (dd, *J* = 9.0, 2.8 Hz, 1H), 7.07 (ddd, *J* = 8.8, 7.1, 2.8 Hz, 1H),

3.69 (s, 3H), 3.25 (t, $J = 7.4$ Hz, 2H), 2.74 (t, $J = 7.4$ Hz, 2H). ^{13}C NMR (126 MHz, CDCl_3) δ 172.5, 164.6 (d, $J = 256.9$ Hz), 145.2, 139.4 (d, $J = 9.0$ Hz), 127.9 (d, $J = 10.0$ Hz), 118.9 (d, $J = 23.4$ Hz), 114.7 (d, $J = 23.1$ Hz), 51.8, 34.2, 28.6. HRMS (ESI) calc'd for $[\text{C}_{10}\text{H}_{10}\text{FNO}_4+\text{Na}]^+$ requires m/z 250.0487, found m/z 250.0487.

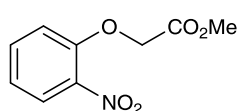


(E)-Methyl 3-(5-methoxy-2-nitrophenyl)acrylate (3.27): An oven-dried Schlenk flask with magnetic stirbar was charged with 780 mg (3.36 mmol) 3-bromo-4-nitroanisole,²³ 0.61 mL (6.8 mmol) methyl acrylate, 15.6 mg (0.0695 mmol) $\text{Pd}(\text{OAc})_2$, 36.4 mg (0.139 mmol) triphenylphosphine, and 1.2 mL (8.6 mmol) triethylamine. The reaction was sealed under N_2 and heated gradually to 125 °C for 3 h. An additional 0.30 mL of methyl acrylate was added and the reaction was heated to 125 °C for an additional 3 h before being cooled to room temperature and passed through a silica plug. Purification by column chromatography (8:1 hexanes:ethyl acetate) yielded 659 mg (2.8 mmol, >10:1 E:Z, 83%) of a yellow solid. mp = 43.1–43.9 °C. IR (thin film, NaCl): 3017, 2953, 1719, 1585 cm^{-1} . ^1H NMR (500 MHz, CDCl_3) δ 8.21 (d, $J = 15.8$ Hz, 1H), 8.14 (d, $J = 8.8$ Hz, 1H), 7.04 – 6.93 (m, 2H), 6.30 (d, $J = 15.8$ Hz, 1H), 3.93 (s, 3H), 3.83 (s, 3H). ^{13}C NMR (126 MHz, CDCl_3) δ 194.7, 166.2, 163.4, 141.5, 133.7, 127.7, 122.7, 114.9, 114.2, 56.1, 52.0. HRMS (ESI) calc'd for $[\text{C}_{11}\text{H}_{11}\text{NO}_5+\text{NH}_4]^+$ requires m/z 255.0976, found m/z 255.0988.



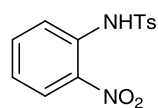
Methyl 3-(5-methoxy-2-nitrophenyl)propanoate (3.28): To an oven-dried 150 mL glass pressure vessel containing a magnetic stirbar was added 415 mg (1.75 mmol) **3.27** and 11 mL degassed 1:1 mixture of THF and *t*-BuOH. H_2 gas was bubbled through the solution and the vessel was charged with 131 mg (0.142 mmol)

Wilkinson's catalyst. The vessel was fitted with a regulator and pressurized to 30 psi with H₂ gas. The reaction was allowed to stir for 2 days before being passed through a silica plug. Purification by column chromatography (5:1 hexanes:ethyl acetate) yielded 365 mg (1.53 mmol, 87%) of a yellow solid. mp = 117.2–118.2 °C. IR (thin film, NaCl): 2952, 2845, 1735, 1516 cm⁻¹. ¹H NMR (500 MHz, CDCl₃) δ 8.08 (d, *J* = 8.7 Hz, 1H), 6.89 – 6.78 (m, 2H), 3.88 (s, 3H), 3.68 (s, 3H), 3.27 (t, *J* = 7.5 Hz, 2H), 2.73 (t, *J* = 7.6 Hz, 2H). ¹³C NMR (126 MHz, CDCl₃) δ 172.9, 163.2, 142.0, 139.0, 127.9, 117.0, 112.5, 55.8, 51.7, 34.5, 29.4. HRMS (ESI) calc'd for [C₁₁H₁₃NO₅+NH₄]⁺ requires *m/z* 257.1132, found *m/z* 257.1137.

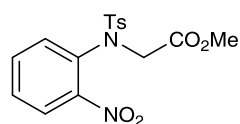


Methyl 2-(2-nitrophenoxy)acetate (3.29): To a suspension of 409 mg (7.28 mmol) KOH in 74 mL ethanol was added 1.00 g (7.20 mmol) 2-nitrophenol.

The reaction was allowed to stir 30 min before the solvent was removed *in vacuo*. 50 mL of DMF and 0.82 mL (8.7 mmol) of bromomethyl acetate were added and the reaction was allowed to stir overnight before being diluted with ethyl acetate and washed with three 100 mL portions of water and one 100 mL portion of brine. The organic layer was dried with MgSO₄, filtered, and concentrated *in vacuo*. Purification by column chromatography (5:1 hexanes:ethyl acetate) yielded 768 mg (3.6 mmol, 51%) of a yellow solid. mp = 54.2–54.7 °C. IR (thin film, NaCl): 2954, 2922, 1743, 1507 cm⁻¹. ¹H NMR (500 MHz, CDCl₃) δ 7.86 (dd, *J* = 8.1, 1.7 Hz, 1H), 7.53 (ddd, *J* = 8.4, 7.4, 1.7 Hz, 1H), 7.11 (ddd, *J* = 8.3, 7.5, 1.1 Hz, 1H), 7.00 (dd, *J* = 8.4, 1.2 Hz, 1H), 4.80 (s, 2H), 3.80 (s, 3H). ¹³C NMR (126 MHz, CDCl₃) δ 168.2, 151.1, 140.3, 134.0, 125.8, 121.7, 115.1, 66.4, 52.4. HRMS (ESI) calc'd for [C₉H₉NO₅+NH₄]⁺ requires *m/z* 229.0819, found *m/z* 229.0809.

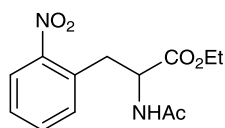


4-Methyl-N-(2-nitrophenyl)benzenesulfonamide (3.30): To a round-bottom flask with magnetic stirbar was added 500 mg (3.62 mmol) 2-nitroaniline, 1.03 g (5.41 mmol) *p*-toluenesulfonylchloride, 0.44 mL (5.4 mmol) pyridine, and 9 mL dichloromethane. The reaction was stirred overnight. The next day, the reaction was poured onto water, and the organic layer was washed with twice with 50 mL water and once with 50 mL brine. The organic layer was dried over MgSO₄, filtered, and concentrated *in vacuo*. Purification by column chromatography (10:1 hexanes:ethyl acetate) and recrystallization (hexanes and ethyl acetate) yielded 605 mg (2.1 mmol, 57%) of a yellow solid. mp = 114.7–115.5 °C. IR (thin film, NaCl): 3285, 3057, 1529, 1348, 1170 cm⁻¹. ¹H NMR (500 MHz, CDCl₃) δ 9.86 (s, 1H), 8.11 (dd, *J* = 8.4, 1.6 Hz, 1H), 7.84 (dd, *J* = 8.4, 1.3 Hz, 1H), 7.73 (d, *J* = 8.4 Hz, 2H), 7.58 (ddd, *J* = 8.7, 7.3, 1.6 Hz, 1H), 7.26 (d, *J* = 8.1 Hz, 2H), 7.15 (ddd, *J* = 8.5, 7.3, 1.3 Hz, 1H), 2.39 (s, 3H). ¹³C NMR (126 MHz, CDCl₃) δ 144.8, 136.9, 135.8, 135.6, 133.9, 130.0, 127.2, 126.1, 123.7, 121.0, 21.6. HRMS (ESI) calc'd for [C₁₃H₁₂N₂O₄S+NH₄]⁺ requires *m/z* 310.0857, found *m/z* 310.0842.



Methyl 2-(4-methyl-N-(2-nitrophenyl)phenylsulfonamido)acetate (3.31): In a round-bottom flask with magnetic stirbar was placed 1.00 g (3.44 mmol) **3.30** and 205 mg (5.13 mmol) NaH (60% dispersion) in 8 mL DMF. The reaction was stirred 15 min before 0.49 mL (5.2 mmol) of bromomethyl acetate was added and the flask was heated to 80 °C overnight. After cooling to room temperature, the reaction was diluted with ethyl acetate and the organic layer was washed with twice with 50 mL water and once with 50 mL brine. The organic layer was dried over MgSO₄, filtered, and concentrated *in vacuo*. Purification by column chromatography (4:1 hexanes:ethyl acetate) yielded 1.06 g (2.9 mmol, 84%) of a yellow solid. mp = 104.0–105.1 °C. IR (thin film, NaCl): 2954, 1754, 1533, 1352,

1161 cm^{-1} . ^1H NMR (500 MHz, CDCl_3) δ 7.85 (dd, $J = 7.9, 1.7$ Hz, 1H), 7.73 (dd, $J = 7.8, 1.6$ Hz, 1H), 7.57 (td, $J = 7.7, 1.7$ Hz, 1H), 7.52 (td, $J = 7.7, 1.7$ Hz, 1H), 7.50 (d, $J = 7.9$ Hz, 2H), 7.23 (d, $J = 7.9$ Hz, 2H), 4.62 (apparent s, 1H), 3.74 (s, 3H), 2.42 (s, 3H). ^{13}C NMR (126 MHz, CDCl_3) δ 169.9, 149.0, 144.2, 136.0, 135.1, 133.5, 132.1, 130.1, 129.5, 127.7, 125.3, 53.1, 52.3, 21.6. HRMS (ESI) calc'd for $[\text{C}_{16}\text{H}_{16}\text{N}_2\text{O}_6\text{S}+\text{Na}]^+$ requires m/z 387.0622, found m/z 387.0634.

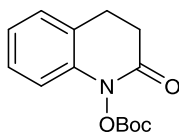


Ethyl 2-acetamido-3-(2-nitrophenyl)propanoate (3.32): In a round-bottom

flask with magnetic stirbar was placed 161 mg (2.87 mmol) KOH in 3 mL of ethanol. 997 mg (2.83 mmol) diethyl 2-acetamido-2-(2-nitrobenzyl)malonate²⁴ was added and stirred for 1 h. The reaction was acidified with concentrated HCl and solvent was removed *in vacuo*. 6 mL of dioxane was added and the reaction was heated to reflux for 1 h before cooling to room temperature. The reaction was diluted with ethyl acetate and washed twice with saturated NaHCO_3 and once with brine. The organic layer was dried over MgSO_4 , filtered, and concentrated *in vacuo*. Purification by column chromatography (2:1 hexanes:ethyl acetate) yielded 488 mg (1.74 mmol, 61%) of a yellow solid. mp = 74.6–75.1 $^\circ\text{C}$. IR (thin film, NaCl): 3276, 2985, 1740, 1654, 1577 cm^{-1} . ^1H NMR (500 MHz, CDCl_3) δ 7.92 (dd, $J = 8.5, 1.4$ Hz, 1H), 7.56 (td, $J = 7.7, 1.4$ Hz, 1H), 7.46 – 7.38 (m, 2H), 6.27 (s, 1H), 4.91 (X of ABX, $J = 8.1, 6.1$ Hz, 1H), 4.19 4.14 (AB of ABX₃, $J = 10.7, 7.2$ Hz, 2H), 3.50 3.34 (AB of ABX, $J = 13.8, 8.1, 6.1$ Hz, 2H), 1.94 (s, 3H), 1.23 (X₃ of ABX₃, $J = 7.2$ Hz, 3H). ^{13}C NMR (126 MHz, CDCl_3) δ 171.2, 169.8, 149.8, 133.0, 132.7, 131.5, 128.2, 124.8, 61.9, 53.0, 34.7, 23.0, 14.0. HRMS (ESI) calc'd for $[\text{C}_{13}\text{H}_{16}\text{N}_2\text{O}_5+\text{H}]^+$ requires m/z 281.1132, found m/z 281.1127.

3.4.3 Experimental details for the reductive cyclization of nitroarenes

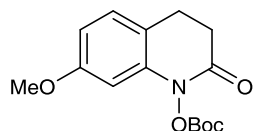
General Procedure for Photochemical Reactions: A solution of the appropriate nitroarene (1 equiv), Ru(bpy)₃Cl₂•6H₂O (0.025 equiv), CSA (0.10 or 1.0 equiv), and dihydropyridine **3.5** (2.1, 3.0, or 4.0 equiv) in DMF (0.1 M) was placed in a sealed 25 mL Schlenk flask. The solution was degassed using three freeze-pump-thaw cycles and then irradiated using a household 20 W compact fluorescent light bulb. After 16 h, the reaction was diluted with ethyl acetate, then washed twice with 1 M HCl. The aqueous phases were extracted with ethyl acetate, and the organic phases were combined and washed once with brine, dried over MgSO₄, and concentrated *in vacuo*. A solution of Boc₂O (1.1 or 2.2 equiv), Et₃N (5.0 equiv), and THF (0.05 M) was added. After 2–24 h, the reaction mixture was concentrated *in vacuo* and purified by column chromatography.



tert-Butyl (2-oxo-3,4-dihydroquinolin-1(2H)-yl) carbonate (Table 3-2,

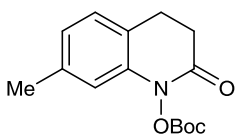
Entry 1, 3.13): Experiment 1: 105 mg (0.500 mmol) of methyl 3-(2-nitrophenyl)propanoate, 9.3 mg (0.012 mmol) Ru(bpy)₃Cl₂•6H₂O, 204 mg (1.05 mmol) **3.5**, 11.3 mg (0.0486 mmol) CSA, 5 mL (0.1 M) DMF, 123 mg (0.562 mmol) Boc₂O, 0.35 mL (2.5 mmol) triethylamine, and 10 mL (0.05 M) THF. Purification by column chromatography (8:1 hexanes:ethyl acetate) yielded 111 mg (0.42 mmol, 84%) of a white solid. Experiment 2: 105 mg (0.500 mmol) of methyl 3-(2-nitrophenyl)propanoate, 9.5 mg (0.013 mmol) Ru(bpy)₃Cl₂•6H₂O, 203 mg (1.05 mmol) **3.5**, 11.8 mg (0.0508 mmol) CSA, 5 mL (0.1 M) DMF, 122 mg (0.559 mmol) Boc₂O, 0.35 mL (2.5 mmol) triethylamine, and 10 mL (0.05 M) THF yielded 106 mg (0.40 mmol, 81%). mp = 112.6–116.4 °C. IR (thin film, NaCl): 2983, 1792, 1701, 1247 cm⁻¹. ¹H NMR (500 MHz, CDCl₃) δ 7.28 – 7.22 (m, 1H), 7.18 (dd, *J* = 7.5, 1.1 Hz,

1H), 7.05 (td, $J = 7.5, 1.2$ Hz, 1H), 6.99 (dd, $J = 8.0, 1.1$ Hz, 1H), 3.02 – 2.98 (m, 2H), 2.80 (t, $J = 7.4$ Hz, 2H), 1.57 (s, 9H). ^{13}C NMR (126 MHz, CDCl_3) δ 164.6, 150.7, 138.3, 127.7, 127.7, 123.9, 123.9, 111.7, 86.4, 31.4, 27.5, 24.8. HRMS (ESI) calc'd for $[\text{C}_{14}\text{H}_{17}\text{NO}_4+\text{Na}]^+$ requires m/z 288.1050, found m/z 288.1050.



tert-Butyl (7-methoxy-2-oxo-3,4-dihydroquinolin-1(2H)-yl) carbonate

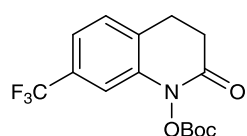
(Table 3-2, Entry 2, 3.33): Experiment 1: 117 mg (0.490 mmol) of methyl 3-(4-methoxy-2-nitrophenyl)propanoate, 9.1 mg (0.012 mmol) $\text{Ru}(\text{bpy})_3\text{Cl}_2 \cdot 6\text{H}_2\text{O}$, 203 mg (1.05 mmol) **3.5**, 11.8 mg (0.0508 mmol) CSA, 5 mL (0.1 M) DMF, 124 mg (0.569 mmol) Boc_2O , 0.35 mL (2.5 mmol) triethylamine, and 10 mL (0.05 M) THF. Purification by column chromatography (5:1 hexanes:ethyl acetate) yielded 109 mg (0.37 mmol, 74%) of a white solid. Experiment 2: 120 mg (0.500 mmol) of methyl 3-(4-methoxy-2-nitrophenyl)propanoate, 9.3 mg (0.012 mmol) $\text{Ru}(\text{bpy})_3\text{Cl}_2 \cdot 6\text{H}_2\text{O}$, 202 mg (1.05 mmol) **3.5**, 11.7 mg (0.0504 mmol) CSA, 5 mL (0.1 M) DMF, 123 mg (0.564 mmol) Boc_2O , 0.35 mL (2.5 mmol) triethylamine, and 10 mL (0.05 M) THF yielded 117 mg (0.40 mmol, 80%). mp = 73.4–74.5 °C. IR (thin film, NaCl): 2983, 1793, 1713, 1248 cm^{-1} . ^1H NMR (500 MHz, CDCl_3) δ 7.08 (d, $J = 8.0$ Hz, 1H), 6.61 – 6.50 (m, 2H), 3.78 (s, 3H), 2.97 – 2.85 (m, 2H), 2.76 (t, $J = 7.3$ Hz, 2H), 1.57 (s, 9H). ^{13}C NMR (126 MHz, CDCl_3) δ 164.7, 159.3, 150.5, 139.1, 128.5, 115.9, 108.2, 98.8, 86.4, 55.4, 31.6, 27.5, 23.9. HRMS (ESI) calc'd for $[\text{C}_{15}\text{H}_{19}\text{NO}_5+\text{Na}]^+$ requires m/z 316.1156, found m/z 316.1151.



tert-Butyl (7-methyl-2-oxo-3,4-dihydroquinolin-1(2H)-yl) carbonate

(Table 3-2, Entry 3, 3.34): Experiment 1: 108 mg (0.485 mmol) of methyl 3-(4-methyl-2-nitrophenyl)propanoate, 9.1 mg (0.012 mmol) $\text{Ru}(\text{bpy})_3\text{Cl}_2 \cdot 6\text{H}_2\text{O}$, 203 mg

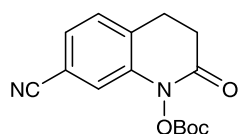
(1.05 mmol) **3.5**, 11.8 mg (0.0508 mmol) CSA, 5 mL (0.1 M) DMF, 124 mg (0.569 mmol) Boc₂O, 0.35 mL (2.5 mmol) triethylamine, and 10 mL (0.05 M) THF. Purification by column chromatography (5:1 hexanes:ethyl acetate) yielded 118 mg (0.42 mmol, 87%) of a white solid. Experiment 2: 111 mg (0.499 mmol) of methyl 3-(4-methyl-2-nitrophenyl)propanoate, 9.7 mg (0.013 mmol) Ru(bpy)₃Cl₂•6H₂O, 203 mg (1.05 mmol) **3.5**, 11.6 mg (0.0499 mmol) CSA, 5 mL (0.1 M) DMF, 123 mg (0.564 mmol) Boc₂O, 0.35 mL (2.5 mmol) triethylamine, and 10 mL (0.05 M) THF yielded 115 mg (0.42 mmol, 83%). mp = 96.4–97.0 °C. IR (thin film, NaCl): 3092, 2959, 1733, 1204 cm⁻¹. ¹H NMR (500 MHz, CDCl₃) δ 7.05 (d, *J* = 7.5 Hz, 1H), 6.84 (d, *J* = 7.5 Hz, 1H), 6.79 (s, 1H), 3.01 – 2.86 (m, 2H), 2.75 (t, *J* = 7.3 Hz, 2H), 2.33 (s, 3H), 1.57 (s, 9H). ¹³C NMR (126 MHz, CDCl₃) δ 164.6, 150.6, 138.0, 137.5, 127.5, 124.4, 120.8, 112.3, 86.3, 31.5, 27.4, 24.3, 21.3. HRMS (ESI) calc'd for [C₁₅H₁₉NO₄+NH₄]⁺ requires *m/z* 295.1653, found *m/z* 295.1664.



tert-Butyl (2-oxo-7-(trifluoromethyl)-3,4-dihydroquinolin-1(2H)-yl) carbonate (Table 3-2, Entry 4, 3.35): Experiment 1: 141 mg (0.507 mmol)

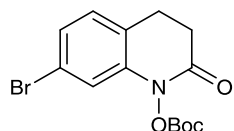
of methyl 3-(2-nitro-4-(trifluoromethyl)phenyl)propanoate, 9.7 mg (0.013 mmol) Ru(bpy)₃Cl₂•6H₂O, 204 mg (1.06 mmol) **3.5**, 11.8 mg (0.0508 mmol) CSA, 5 mL (0.1 M) DMF, 120 mg (0.550 mmol) Boc₂O, 0.35 mL (2.5 mmol) triethylamine, and 10 mL (0.05 M) THF. Purification by column chromatography (5:1 hexanes:ethyl acetate) yielded 139 mg (0.42 mmol, 82%) of a white solid. Experiment 2: 139 mg (0.501 mmol) of methyl 3-(2-nitro-4-(trifluoromethyl)phenyl)propanoate, 9.4 mg (0.013 mmol) Ru(bpy)₃Cl₂•6H₂O, 204.2 mg (1.06 mmol) **3.5**, 11.6 mg (0.0499 mmol) CSA, 5 mL (0.1 M) DMF, 122 mg (0.559 mmol) Boc₂O, 0.35 mL (2.5 mmol) triethylamine, and 10 mL (0.05 M) THF yielded 132 mg (0.40 mmol, 79%).

mp = 70.0–73.8 °C. IR (thin film, NaCl): 2986, 1794, 1716, 1335, 1248 cm^{-1} . ^1H NMR (500 MHz, CDCl_3) δ 7.35 – 7.29 (m, 2H), 7.23 – 7.18 (m, 1H), 3.12 – 3.03 (m, 2H), 2.83 (t, $J = 7.4$ Hz, 2H), 1.58 (s, 9H). ^{13}C NMR (126 MHz, CDCl_3) δ 164.3, 150.3, 138.8, 130.3 (q, $J = 32.9$ Hz), 128.2, 127.6, 123.8 (q, $J = 272.2$ Hz), 120.6 (q, $J = 3.8$ Hz), 108.7 (q, $J = 3.9$ Hz), 87.1, 30.8, 27.4, 24.7. HRMS (ESI) calc'd for $[\text{C}_{15}\text{H}_{16}\text{F}_3\text{NO}_4+\text{Na}]^+$ requires m/z 354.0924, found m/z 354.0932.



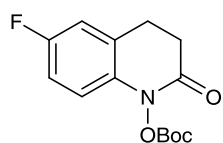
tert-Butyl (7-cyano-2-oxo-3,4-dihydroquinolin-1(2H)-yl) carbonate

(Table 3-2, Entry 5, 3.36): Experiment 1: 118 mg (0.503 mmol) of methyl 3-(4-cyano-2-nitrophenyl)propanoate, 9.6 mg (0.013 mmol) $\text{Ru}(\text{bpy})_3\text{Cl}_2\cdot 6\text{H}_2\text{O}$, 204 mg (1.06 mmol) **3.5**, 11.6 mg (0.0499 mmol) CSA, 5 mL (0.1 M) DMF, 121 mg (0.554 mmol) Boc_2O , 0.35 mL (2.5 mmol) triethylamine, and 10 mL (0.05 M) THF. Purification by column chromatography (2:1 hexanes:ethyl acetate) yielded 102 mg (0.35 mmol, 70%) of a white solid. Experiment 2: 117 mg (0.501 mmol) of methyl 3-(4-cyano-2-nitrophenyl)propanoate, 9.7 mg (0.013 mmol) $\text{Ru}(\text{bpy})_3\text{Cl}_2\cdot 6\text{H}_2\text{O}$, 204 mg (1.06 mmol) **3.5**, 11.9 mg (0.0512 mmol) CSA, 5 mL (0.1 M) DMF, 123 mg (0.565 mmol) Boc_2O , 0.35 mL (2.5 mmol) triethylamine, and 10 mL (0.05 M) THF yielded 105 mg (0.36 mmol, 73%). mp = 199.4–200.2 °C. IR (thin film, NaCl): 2984, 2231, 1794, 1717, 1249 cm^{-1} . ^1H NMR (500 MHz, CDCl_3) δ 7.36 (dd, $J = 7.7, 1.4$ Hz, 1H), 7.31 (dd, $J = 7.7, 1.0$ Hz, 1H), 7.24 (d, $J = 1.3$ Hz, 1H), 3.14 – 3.02 (m, 2H), 2.83 (t, $J = 7.4$ Hz, 2H), 1.59 (s, 9H). ^{13}C NMR (126 MHz, CDCl_3) δ 163.9, 150.3, 139.2, 129.1, 128.7, 127.6, 118.2, 114.7, 111.8, 87.4, 30.5, 27.5, 25.0. HRMS (ESI) calc'd for $[\text{C}_{15}\text{H}_{16}\text{N}_2\text{O}_4+\text{NH}_4]^+$ requires m/z 306.1449, found m/z 306.1447.



tert-Butyl (7-bromo-2-oxo-3,4-dihydroquinolin-1(2H)-yl) carbonate

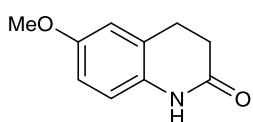
(Table 3-2, Entry 6, 3.37): Experiment 1: 145 mg (0.503 mmol) of methyl 3-(4-bromo-2-nitrophenyl)propanoate, 9.7 mg (0.013 mmol) Ru(bpy)₃Cl₂•6H₂O, 205 mg (1.06 mmol) **3.5**, 12.2 mg (0.0525 mmol) CSA, 5 mL (0.1 M) DMF, 121 mg (0.554 mmol) Boc₂O, 0.35 mL (2.5 mmol) triethylamine, and 10 mL (0.05 M) THF. Purification by column chromatography (6:1 hexanes:ethyl acetate) yielded 125 mg (0.36 mmol, 72%) of a white solid. Experiment 2: 145 mg (0.504 mmol) of methyl 3-(4-bromo-2-nitrophenyl)propanoate, 9.5 mg (0.013 mmol) Ru(bpy)₃Cl₂•6H₂O, 204 mg (1.06 mmol) **3.5**, 12.5 mg (0.0538 mmol) CSA, 5 mL (0.1 M) DMF, 122 mg (0.560 mmol) Boc₂O, 0.35 mL (2.5 mmol) triethylamine, and 10 mL (0.05 M) THF yielded 137 mg (0.40 mmol, 79%). mp = 108.2–109.7 °C. IR (thin film, NaCl): 2982, 1793, 1716, 1247 cm⁻¹. ¹H NMR (500 MHz, CDCl₃) δ 7.18 (dd, *J* = 7.9, 1.9 Hz, 1H), 7.14 (d, *J* = 1.9 Hz, 1H), 7.05 (d, *J* = 7.9 Hz, 1H), 3.03 – 2.89 (m, 2H), 2.78 (t, *J* = 6.8 Hz, 2H), 1.58 (s, 9H). ¹³C NMR (126 MHz, CDCl₃) δ 164.4, 150.4, 139.4, 129.1, 126.7, 122.8, 121.1, 115.0, 86.9, 31.1, 27.5, 24.4. HRMS (ESI) calc'd for [C₁₄H₁₆BrNO₄+NH₄]⁺ requires *m/z* 359.0601, found *m/z* 359.0597.



tert-Butyl (6-fluoro-2-oxo-3,4-dihydroquinolin-1(2H)-yl) carbonate

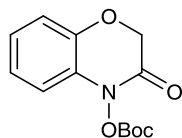
(Table 3-2, Entry 7, 3.38): Experiment 1: 114 mg (0.500 mmol) of methyl 3-(5-fluoro-2-nitrophenyl)propanoate, 9.5 mg (0.013 mmol) Ru(bpy)₃Cl₂•6H₂O, 204 mg (1.06 mmol) **5**, 11.7 mg (0.0504 mmol) CSA, 5 mL (0.1 M) DMF, 124 mg (0.566 mmol) Boc₂O, 0.35 mL (2.5 mmol) triethylamine, and 10 mL (0.05 M) THF. Purification by column chromatography (6:1 hexanes:ethyl acetate) yielded 109 mg (0.39 mmol, 78%) of a white solid. Experiment 2: 114 mg (0.502 mmol) of methyl 3-(5-fluoro-2-nitrophenyl)propanoate, 9.4 mg

(0.013 mmol) Ru(bpy)₃Cl₂•6H₂O, 205 mg (1.06 mmol) **5**, 12.2 mg (0.0525 mmol) CSA, 5 mL (0.1 M) DMF, 121 mg (0.554 mmol) Boc₂O, 0.35 mL (2.5 mmol) triethylamine, and 10 mL (0.05 M) THF yielded 112 mg (0.40 mmol, 79%). mp = 94.6–95.4 °C. IR (thin film, NaCl): 2984, 1793, 1707, 1248 cm⁻¹. ¹H NMR (500 MHz, CDCl₃) δ 6.98 – 6.89 (m, 3H), 3.08 – 2.90 (m, 2H), 2.79 (t, *J* = 7.4 Hz, 2H), 1.57 (s, 9H). ¹³C NMR (126 MHz, CDCl₃) δ 164.2, 159.1 (d, *J* = 243.6 Hz), 150.6, 134.6 (d, *J* = 2.6 Hz), 126.1 (d, *J* = 7.8 Hz), 114.9 (d, *J* = 23.6 Hz), 114.1 (d, *J* = 23.0 Hz), 113.2 (d, *J* = 8.3 Hz), 86.6, 31.2, 27.5, 24.9 (d, *J* = 1.2 Hz). HRMS (ESI) calc'd for [C₁₄H₁₆FNO₄+NH₄]⁺ requires *m/z* 299.1402, found *m/z* 299.1415.



6-methoxy-2-oxo-3,4-dihydroquinolin-1(2H)-yl (Table 3-2, Entry 8,

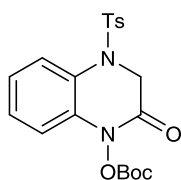
3.10): Following general procedure but without protection after aqueous workup. 121 mg (0.506 mmol) of methyl 3-(5-methoxy-2-nitrophenyl)propanoate, 9.7 mg (0.013 mmol) Ru(bpy)₃Cl₂•6H₂O, 388 mg (1.96 mmol) **3.5**, 113 mg (0.486 mmol) CSA, 5 mL (0.1 M) DMF. Purification by column chromatography (1:1 hexanes:ethyl acetate, 0.5% triethylamine) yielded 60.2 mg (0.27 mmol, 54%) of a white solid. All spectra data were consistent with reported values.²⁵



tert-Butyl (3-oxo-2H-benzo[b][1,4]oxazin-4(3H)-yl) carbonate (Table 3-2,

Entry 9, 3.39): Experiment 1: 106 mg (0.502 mmol) of methyl 2-(2-nitrophenoxy)acetate, 9.5 mg (0.013 mmol) Ru(bpy)₃Cl₂•6H₂O, 203 mg (1.05 mmol) **3.5**, 11.3 mg (0.0486 mmol) CSA, 5 mL (0.1 M) DMF, 122 mg (0.559 mmol) Boc₂O, 0.35 mL (2.5 mmol) triethylamine, and 10 mL (0.05 M) THF. Purification by column chromatography (5:1 hexanes:ethyl acetate) yielded 98.0 mg (0.37 mmol, 74%) of a white solid. Experiment 2: 106

mg (0.501 mmol) of methyl 2-(2-nitrophenoxy)acetate, 9.3 mg (0.012 mmol) Ru(bpy)₃Cl₂•6H₂O, 203 mg (1.05 mmol) **3.5**, 11.9 mg (0.0512 mmol) CSA, 5 mL (0.1 M) DMF, 122 mg (0.559 mmol) Boc₂O, 0.35 mL (2.5 mmol) triethylamine, and 10 mL (0.05 M) THF yielded 107 mg (0.41 mmol, 81%). mp = 89.1–90.5 °C. IR (thin film, NaCl): 2979, 1700, 1685, 1244 cm⁻¹. ¹H NMR (500 MHz, CDCl₃) δ 7.14 – 6.85 (m, 4H), 4.76 (s, 2H), 1.58 (s, 9H). ¹³C NMR (126 MHz, CDCl₃) δ 159.4, 149.9, 143.5, 127.8, 124.8, 122.9, 116.9, 112.1, 87.2, 68.2, 27.4. HRMS (ESI) calc'd for [C₁₃H₁₅NO₅+Na]⁺ requires *m/z* 288.0843, found *m/z* 288.0842.

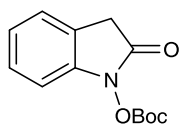


***tert*-Butyl (2-oxo-4-tosyl-3,4-dihydroquinoxalin-1(2*H*)-yl) carbonate (Table**

3-2, Entry 10, 3.40): Experiment 1: Following general procedure without aqueous workup before protection. After protection is complete, the reaction

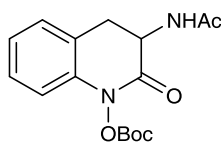
mixture is diluted with ethyl acetate and washed twice with water and once with brine. 182 mg (0.499 mmol) of methyl 2-(4-methyl-*N*-(2-nitrophenyl)phenylsulfonamido)acetate, 9.4 mg (0.013 mmol) Ru(bpy)₃Cl₂•6H₂O, 290 mg (1.50 mmol) **3.5**, 116 mg (0.498 mmol) CSA, 5 mL (0.1 M) DMF, 242 mg (1.11 mmol) Boc₂O, 0.35 mL (2.5 mmol) triethylamine, and 10 mL (0.05 M) THF. Purification by column chromatography (9:1 hexanes:ethyl acetate) yielded 109 mg (0.26 mmol, 52%) of a white solid. Experiment 2: 182 mg (0.500 mmol) of methyl 2-(4-methyl-*N*-(2-nitrophenyl)phenylsulfonamido)acetate, 9.4 mg (0.013 mmol) Ru(bpy)₃Cl₂•6H₂O, 289 mg (1.50 mmol) **3.5**, 116 mg (0.500 mmol) CSA, 5 mL (0.1 M) DMF, 237 mg (1.09 mmol) Boc₂O, 0.35 mL (2.5 mmol) triethylamine, and 10 mL (0.05 M) THF yielded 112 mg (0.27 mmol, 53%). mp = 117.2–117.8 °C. IR (thin film, NaCl): 2983, 1798, 1721, 1361, 1248 cm⁻¹. ¹H NMR (500 MHz, CDCl₃) δ 7.78 (dd, *J* = 8.0, 1.4 Hz, 1H), 7.35 (d, *J* = 8.3 Hz, 2H), 7.29 (td, *J* = 7.8, 1.4 Hz, 1H), 7.20 (td, *J* = 7.8, 1.4 Hz, 1H), 7.16 (d, *J* = 8.4 Hz, 2H), 6.76 (dd, *J* = 8.1, 1.4 Hz, 1H), 4.56

(apparent s, 1H), 2.36 (s, 3H), 1.51 (s, 9H). ^{13}C NMR (126 MHz, CDCl_3) δ 160.1, 149.6, 144.7, 133.8, 132.8, 129.8, 128.1, 127.6, 126.9, 124.4, 124.0, 112.0, 87.1, 49.6, 27.4, 21.6. HRMS (ESI) calc'd for $[\text{C}_{20}\text{H}_{22}\text{N}_2\text{O}_6\text{S}+\text{NH}_4]^+$ requires m/z 436.1537, found m/z 437.1555.



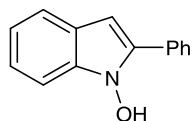
***tert*-Butyl (2-oxoindolin-1-yl) carbonate (Table 3-2, Entry 11, 3.41):**

Experiment 1: Following general procedure without aqueous workup before protection. After protection is complete, the reaction mixture is diluted with ethyl acetate and washed twice with water and once with brine. 97.3 mg (0.499 mmol) of methyl 2-(2-nitrophenyl)acetate, 9.3 mg (0.012 mmol) $\text{Ru}(\text{bpy})_3\text{Cl}_2\cdot 6\text{H}_2\text{O}$, 291 mg (1.50 mmol) **3.5**, 117 mg (0.503 mmol) CSA, 5 mL (0.1 M) DMF, 241 mg (1.11 mmol) Boc_2O , 0.35 mL (2.5 mmol) triethylamine, and 10 mL (0.05 M) THF. Purification by column chromatography (4:1 hexanes:ethyl acetate) yielded 76.9 mg (0.31 mmol, 62%) of a white solid. Experiment 2: 97.0 mg (0.497 mmol) of methyl 2-(2-nitrophenyl)acetate, 9.7 mg (0.013 mmol) $\text{Ru}(\text{bpy})_3\text{Cl}_2\cdot 6\text{H}_2\text{O}$, 290 mg (1.50 mmol) **3.5**, 116 mg (0.500 mmol) CSA, 5 mL (0.1 M) DMF, 240 mg (1.10 mmol) Boc_2O , 0.35 mL (2.5 mmol) triethylamine, and 10 mL (0.05 M) THF yielded 81.9 mg (0.33 mmol, 66%). mp = 88.1–89.4 °C. IR (thin film, NaCl): 2984, 1796, 1743, 1247 cm^{-1} . ^1H NMR (500 MHz, CDCl_3) δ 7.29 (td, $J = 7.7, 1.0$ Hz, 1H), 7.25 (d, $J = 7.6$ Hz, 1H), 7.08 (td, $J = 7.6, 1.0$ Hz, 1H), 6.85 (d, $J = 7.8$ Hz, 1H), 3.60 (s, 2H), 1.57 (s, 9H). ^{13}C NMR (126 MHz, CDCl_3) δ 169.1, 150.2, 141.2, 128.1, 124.9, 123.3, 120.1, 107.2, 87.1, 33.6, 27.4. HRMS (ESI) calc'd for $[\text{C}_{13}\text{H}_{19}\text{NO}_4+\text{Na}]^+$ requires m/z 229.0819, found m/z 229.0809.



***tert*-Butyl 3-acetamido-2-oxo-3,4-dihydroquinolin-1(2H)-yl carbonate (Table 3-2, Entry 12, 3.42):** Experiment 1: Following general procedure

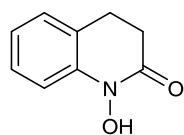
without aqueous workup before protection. After protection is complete, the reaction mixture is diluted with ethyl acetate and washed twice with water and once with brine. 140 mg (0.500 mmol) of ethyl 2-acetamido-3-(2-nitrophenyl)propanoate, 9.7 mg (0.013 mmol) Ru(bpy)₃Cl₂•6H₂O, 290 mg (1.50 mmol) **3.5**, 116 mg (0.501 mmol) CSA, 5 mL (0.1 M) DMF, 240 mg (1.10 mmol) Boc₂O, 0.35 mL (2.5 mmol) triethylamine, and 10 mL (0.05 M) THF. Purification by column chromatography (3:1 to 0:1 hexanes:ethyl acetate) yielded 92.2 mg (0.29 mmol, 58%) of a white solid. Experiment 2: 141 mg (0.503 mmol) of ethyl 2-acetamido-3-(2-nitrophenyl)propanoate, 9.9 mg (0.013 mmol) Ru(bpy)₃Cl₂•6H₂O, 290 mg (1.50 mmol) **3.5**, 117 mg (0.502 mmol) CSA, 5 mL (0.1 M) DMF, 246 mg (1.12 mmol) Boc₂O, 0.35 mL (2.5 mmol) triethylamine, and 10 mL (0.05 M) THF yielded 94.8 mg (0.29 mmol, 58%). mp = 112.6–113.9 °C. IR (thin film, NaCl): 3308, 2984, 1795, 1715, 1246 cm⁻¹. ¹H NMR (500 MHz, CDCl₃) δ 7.29 (t, *J* = 7.8 Hz, 1H), 7.24 (d, *J* = 7.5 Hz, 1H), 7.11 (td, *J* = 7.5, 1.1 Hz, 1H), 7.10–6.82 (m, 1H), 6.61 (d, *J* = 5.5 Hz, 1H), 4.78 (dt, *J* = 14.1, 5.8 Hz, 1H), 3.51 (dd, *J* = 15.1, 6.0 Hz, 1H), 3.01 – 2.85 (m, 1H), 2.08 (s, 3H), 1.56 (s, 9H). ¹³C NMR (126 MHz, CDCl₃) δ 170.3, 163.9, 150.3, 128.5, 128.1, 124.8, 112.7, 86.9, 65.8, 49.5, 31.7, 27.4, 23.1, 15.2. HRMS (ESI) calc'd for [C₁₆H₂₀N₂O₅+NH₄]⁺ requires *m/z* 338.1711, found *m/z* 338.1718.



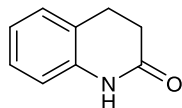
2-Phenyl-1H-indol-1-ol (3.12): Experiment 1: Following general procedure but without protection after aqueous workup. 121 mg (0.500 mmol) of 2-(2-nitrophenyl)-1-phenylethanone **3.11**, 10.0 mg (0.013 mmol) Ru(bpy)₃Cl₂•6H₂O, 205 mg (1.06 mmol) **3.5**, 11.6 mg (0.0499 mmol) CSA, 5 mL (0.1 M) DMF. Purification by column chromatography (20:1 hexanes:ethyl acetate) yielded 94.3 mg (0.45 mmol, 90%) of a white solid. Experiment 2: 122 mg (0.505 mmol) of 2-(2-nitrophenyl)-1-phenylethanone **3.11**, 9.2 mg

(0.012 mmol) Ru(bpy)₃Cl₂•6H₂O, 205 mg (1.06 mmol) **3.5**, 11.7 mg (0.0504 mmol) CSA, 5 mL (0.1 M) DMF yielded 90.2 mg (0.43 mmol, 85%). mp = 149.1–150.3 °C. IR (thin film, NaCl): 3277, 3053, 2923, 2520, 1532 cm⁻¹. ¹H NMR (500 MHz, DMSO-*d*₆) δ 11.17 (s, 1H), 7.88 (d, *J* = 7.3 Hz, 2H), 7.54 (d, *J* = 7.9 Hz, 1H), 7.49 (t, *J* = 7.7 Hz, 2H), 7.44 (d, *J* = 8.1 Hz, 1H), 7.38 (t, *J* = 7.4 Hz, 1H), 7.18 (t, *J* = 7.5 Hz, 1H), 7.05 (t, *J* = 7.4 Hz, 1H), 6.63 (s, 1H). ¹³C NMR (126 MHz, DMSO-*d*₆) δ 136.9, 135.5, 130.9, 128.6, 127.7, 123.0, 121.8, 120.2, 119.7, 108.8, 96.2. HRMS (ESI) calc'd for [C₁₄H₁₁NO+H]⁺ requires *m/z* 210.0914, found *m/z* 210.0919.

3.4.4 Experimental details for the cleavage of C–O and N–O bonds



1-Hydroxy-3,4-dihydroquinolin-2(1H)-one (3.3): A round-bottom flask was charged with 100 mg (0.380 mmol) **3.13**, 7.5 mL (0.05 M) CH₂Cl₂, and 7.5 mL (0.05M) trifluoroacetic acid. The reaction was stirred for 1 hour before diluting with 50 mL CH₂Cl₂ and pouring onto 50 mL water. The reaction was washed twice with 50 mL CH₂Cl₂. The organic layers were combined, dried over MgSO₄, and concentrated *in vacuo*. Purification by recrystallization in ether yielded 51.7 mg (0.317 mmol, 83%) of a tan solid. All spectra data were consistent with reported values.²⁶



3,4-Dihydroquinolin-2(1H)-one (3.14): A 2 dram vial was charged with 100 mg (0.380 mmol) **3.13**, 41.9 mg (0.776 mmol) iron metal, 1.0 mL (0.4 M) ethanol, and 1.0 mL (0.4 M) acetic acid. The reaction was heated to 80 °C for 1.5 h before cooling to room temperature. A saturated solution of Na₂CO₃ was added, and the reaction was extracted with three 50 mL portions of ether. The organic layers were combined, dried over

MgSO₄, and concentrated *in vacuo*. Purification by recrystallization in ether yielded 48.0 mg (0.326 mmol, 86%) of a white solid. All spectra data were consistent with reported values.²⁷

3.5 References

1. Kurzak, B.; Kozłowski, H.; Farkas, E. "Hydroxamic and aminohydroxamic acids and their complexes with metal ions" *Coord. Chem. Rev.* **1992**, *114*, 169–200.
2. (a) Weisburger, J. H.; Weisburger, E. K. "Biochemical Formation and Pharmacological, Toxicological, and Pathological Properties of Hydroxylamines and Hydroxamic Acids" *Pharmacol. Rev.* **1973**, *25*, 1–66. (b) Hider, R. C.; Kong, X. "Chemistry and biology of siderophores" *Nat. Prod. Rep.* **2010**, *27*, 637–657.
3. (a) Miller, M. J. "Syntheses and therapeutic potential of hydroxamic acid based siderophores and analogues" *Chem. Rev.* **1989**, *89*, 1563–1579. (b) Muri, E. M. F.; Nieto, M. J.; Sindelar, R. D.; Williamson, J. S. "Hydroxamic Acids as Pharmacological Agents" *Curr. Med. Chem.* **2002**, *9*, 1631–1653.
4. (a) Wright, W. B.; Collins, K. H. "Cyclic Hydroxamic Acids Derived from Indole" *J. Am. Chem. Soc.* **1956**, *78*, 221–224. (b) Sicker, D.; Prätorius, B.; Mann, G.; Meyer, L. "A Convenient Synthesis of 2,4-Dihydroxy-2*H*-1,4-benzoxazin-3(4*H*)-one" *Synthesis* **1989**, 211–212. (c) McAllister, L. A.; Bechle, B. M.; Dounay, A. B.; Evrard, E.; Gan, X.; Ghosh, S.; Kim, J.-Y.; Parikh, V. D.; Tuttle, J. B.; Verhoest, P. R. "A General Strategy for the Synthesis of Cyclic *N*-Aryl Hydroxamic Acids via Partial Nitro Group Reduction" *J. Org. Chem.* **2011**, *76*, 3484–3497.
5. Coutts, R. T.; Wibberley, D. G. "Reductive Cyclisations by Means of Sodium Borohydride and Palladium–Charcoal" *J. Chem. Soc.* **1963**, 4610–4621.
6. Davis, A. L.; Choun, O. H. P.; Cook, D. E.; McCord, T. J. "Synthesis and Microbiological Properties of 3-Amino-3,4-dihydro-1-hydroxycarbostyryl" *J. Med. Chem.* **1964**, *7*, 632–634.
7. For reviews, see: (a) Zeitler, K. "Photoredox Catalysis with Visible Light" *Angew. Chem. Int. Ed.* **2009**, *48*, 9785–9789. (b) Yoon, T. P.; Ischay, M. A.; Du, J. "Visible light photocatalysis as a greener approach to photochemical synthesis" *Nature Chem.* **2010**, *2*, 527–532. (c) Narayanam, J. M. R.; Stephenson, C. R. J. "Visible light photoredox catalysis: applications in organic synthesis" *Chem. Soc. Rev.* **2011**, *40*, 102–113. (d) Telpý, F. "Photoredox catalysis by [Ru(bpy)₃]²⁺ to trigger transformations of organic molecules. Organic synthesis using visible-light photocatalysis and its 20th century roots" *Collect. Czech. Chem. Commun.* **2011**, *76*, 859–917. (e) Tucker, J. W.; Stephenson, C. R. J. "Shining Light on Photoredox Catalysis: Theory and Synthetic Applications" *J. Org. Chem.*

-
- 2012**, *77*, 1617–1622. (f) Xuan, J.; Xiao, W.-J. “Visible-Light Photoredox Catalysis” *Angew. Chem. Int. Ed.* **2012**, *51*, 6828–6838.
8. (a) Ischay, M. A.; Anzovino, M. E.; Du, J.; Yoon, T. P. “Efficient Visible Light Photocatalysis of [2+2] Enone Cycloadditions” *J. Am. Chem. Soc.* **2008**, *130*, 12886–12887. (b) Du, J.; Yoon, T. P. “Crossed Intermolecular [2+2] Cycloadditions of Acyclic Enones via Visible Light Photocatalysis” *J. Am. Chem. Soc.* **2009**, *131*, 14604–14605. (c) Ischay, M. A.; Lu, Z.; Yoon, T. P. “[2+2] Cycloadditions by Oxidative Visible Light Photocatalysis” *J. Am. Chem. Soc.* **2010**, *132*, 8572–8574. (d) Du, J.; Ruiz Espelt, L.; Guzei, I. A.; Yoon, T. P. “Photocatalytic reductive cyclizations of enones: Divergent reactivity of photogenerated radical and radical anion intermediates” *Chem. Sci.* **2011**, *2*, 2115–2119. (e) Ischay, M. A.; Ament, M. S.; Yoon, T.P. “Crossed intermolecular [2+2] cycloaddition of styrenes by visible light photocatalysis” *Chem. Sci.* **2012**, *3*, 2807–2811.
9. For leading examples from other groups, see: (a) Nicewicz, D. A.; MacMillan, D. W. C. “Merging Photoredox Catalysis with Organocatalysis: The Direct Asymmetric Alkylation of Aldehydes” *Science* **2008**, *322*, 77–80. (b) Narayanam, J. M. R.; Tucker, J. W.; Stephenson, C. R. J. “Electron-Transfer Photoredox Catalysis: Development of a Tin-Free Reductive Dehalogenation Reaction” *J. Am. Chem. Soc.* **2009**, *131*, 8756–8757. (c) McNally, A.; Prier, C. K.; MacMillan, D. W. C. “Discovery of an α -Amino C–H Arylation Reaction Using the Strategy of Accelerated Serendipity” *Science* **2011**, *334*, 1114–1117. (d) Kalyani, D.; McMurtrey, K. B.; Neufeldt, S. R.; Sanford, M. S. “Room-Temperature C–H Arylation: Merger of Pd-Catalyzed C–H Functionalization and Visible-Light Photocatalysis” *J. Am. Chem. Soc.* **2011**, *133*, 18566–18569. (e) Freeman, D. B.; Furst, L.; Condie, A. G.; Stephenson, C. R. J. “Functionally Diverse Nucleophilic Trapping of Iminium Intermediates Generated Utilizing Visible Light” *Org. Lett.* **2012**, *14*, 94–97. (f) Maity, S.; Zhu, M.; Shinabery, R. S.; Zheng, N. “Intermolecular [3+2] Cycloaddition of Cyclopropylamines with Olefins by Visible-Light Photocatalysis” *Angew. Chem. Int. Ed.* **2012**, *51*, 222–226. (g) Leung, J. C. T.; Chatalova-Sazepin, C.; West, J. G.; Rueda-Becerril, M.; Paquin, J.-F.; Sammis, G. M. “Photo-fluorodecarboxylation of 2-Aryloxy and 2-Aryl Carboxylic Acids” *Angew. Chem. Int. Ed.* **2012**, *51*, 10804–10807.
10. Hirao, T.; Shiori, J.; Okahata, N. “Ruthenium–Bipyridine Complex-Catalyzed Photo-Induced Reduction of Nitrobenzenes with Hydrazine” *Bull. Chem. Soc. Jpn.* **2004**, *77*, 1763–1764.
11. Tomioka, H.; Ueda, K.; Ohi, H.; Izawa, Y. “Photochemical and Chemical Reduction of Nitroalkenes Using Viologens as an Electron Phase-Transfer Catalyst” *Chem. Lett.* **1986**, *15*, 1359–1362.
12. (a) Cai, S.; Zhang, S.; Zhao, Y.; Wang, D. Z. “New Approach to Oximes through Reduction of Nitro Compounds Enabled by Visible Light Photoredox Catalysis” *Org. Lett.* **2013**, *15*, 2660–2663. (b) Lin, W.-C.; Yang, D.-Y. “Visible Light Photoredox Catalysis: Synthesis of Indazolo[2,3-*a*]quinolines from 2-(2-Nitrophenyl)-1,2,3,4-tetrahydroquinolines” *Org. Lett.* **2013**, *15*, 4862–4865. (c) Lin, C.-W.; Hong, B.-C.;

-
- Chang, W.-C.; Lee, G.-H. "A New Approach to Nitrones through Cascade Reaction of Nitro Compounds by Visible Light Photoredox Catalysis" *Org. Lett.* **2015**, *17*, 2314–2317.
13. (a) Davis, A. L.; Chambers, W. H.; Kelley, D. H.; Fell, D. A.; Haynes, J. R.; Hulme, K. L.; Gage, L. D.; McCord, T. J. "Synthesis and antibacterial activities of some chloro analogs of 3-amino-3,4-dihydro-1-hydroxycarbostyryl" *J. Med. Chem.* **1975**, *18*, 752–755. (b) Erhardt, S.; Olsson, S. K.; Engberg, G. "Pharmacological Manipulation of Kynurenic Acid" *CNS Drugs* **2009**, *23*, 91–101.
 14. (a) Dong, W.; Jimenez, L. S. "Synthesis of a Fully Functionalized 7-Methoxyaziridinomitosene" *J. Org. Chem.* **1999**, *64*, 2520–2523. (b) Wong, A.; Kuethe, J. T.; Davies, I. W. "A General Synthesis of *N*-Hydroxyindoles" *J. Org. Chem.* **2003**, *68*, 9865–9866. (c) Wong, A.; Kuethe, J. T.; Davies, I. W.; Hughes, D. L. "Synthesis of Novel KDR Kinase Inhibitors through Catalytic Reductive Cyclization of *o*-Nitrobenzylcarbonyl Compounds" *J. Org. Chem.* **2004**, *69*, 7761–7764. (d) Nicolaou, K. C.; Lee, S. H.; Estrada, A. A.; Zak, M. "Construction of Substituted *N*-Hydroxyindoles: Synthesis of a Nocathiacin I Model System" *Angew. Chem. Int. Ed.* **2005**, *44*, 3736–3740.
 15. Claffey, M. M.; Dounay, A. B.; Gan, X.; Hayward, M. M.; Rong, S.; Tuttle, J. B.; Verhoest, P. R. "Bicyclic and Tricyclic Compounds as KAT II Inhibitors" PCT In. Appl. WO2010/146488, December 23, 2010.
 16. Wang, G.-W.; Xia, J.-J.; Miao, C.-B.; Wu, X.-L. "Environmentally Friendly and Efficient Synthesis of Various 1,4-Dihydropyridines in Pure Water" *Bull. Chem. Soc. Jpn.* **2006**, *79*, 454–459.
 17. Motoyama, Y.; Kamo, K.; Nagashima, H. "Catalysis in Polysiloxane Gels: Platinum-Catalyzed Hydrosilation of Polymethylhydrosiloxane Leading to Reusable Catalysts for Reduction of Nitroarenes" *Org. Lett.* **2009**, *11*, 1345–1348.
 18. Daniela, B.; Polackkova, W. "Synthesis of nitro derivatives of 1,2,3-triphenylbenzene" *Rocz. Chem.* **1965**, *39*, 545–555.
 19. Jourdan, A.; González-Zamora, E.; Zhu, J. "Wilkinson's Catalyst Catalyzed Selective Hydrogenation of Olefin in the Presence of an Aromatic Nitro Function: A Remarkable Solvent Effect" *J. Org. Chem.* **2002**, *67*, 3163–3164.
 20. Park, S. J.; Park, S. J.; Lee, M. J.; Rhim, H.; Kim, Y.; Lee, J.-H.; Chung, B. Y.; Lee, J. Y. "Synthesis and SAR studies of a novel series of T-type calcium channel blockers" *Bioorg. Med. Chem.* **2006**, *14*, 3502–3511.
 21. Le Callonnec, F.; Fouquet, E.; Felpin, F.-X. "Unprecedented Substoichiometric Use of Hazardous Aryl Diazonium Salts in the Heck-Matsuda Reaction via a Double Catalytic Cycle" *Org. Lett.* **2011**, *13*, 2646–2649.

-
22. Schlosser, M.; Ginanneschi, A.; Leroux, F. "In Search of Simplicity and Flexibility: A Rational Access to Twelve Fluoroindolecarboxylic Acids" *Eur. J. Org. Chem.* **2006**, 2956–2969.
 23. Zhang, Y. J.; Wei, H.; Zhang, W. "Synthesis of atropisomeric 5,5'-linked biphenyl bisaminophosphine ligands and their application in asymmetric catalysis" *Tetrahedron* **2009**, *65*, 1281–1286.
 24. Varnavas, A.; Lassiani, L.; Valenta, V.; Mennuni, L.; Makovec, F.; Hadjipavlou-Litina, D. "Abthranilic acid based CCK₁ receptor antagonists: preliminary investigation on their second 'touch point'" *Eur. J. Med. Chem.* **2005**, *40*, 563–581.
 25. Zhou, W.; Zhang, L.; Jiao, N. "The tandem reaction combining radical and ionic processes: an efficient approach to substituted 3,4-dihydroquinolin-2-ones" *Tetrahedron* **2009**, *65*, 1982–1987.
 26. Murahashi, S.-I.; Oda, T.; Sugahara, T.; Masui, Y. "Tungstate-catalyzed oxidation of tetrahydroquinolines with hydrogen peroxide: A novel method for the synthesis of cyclic hydroxamic acids" *J. Org. Chem.* **1990**, *55*, 1744–1749.
 27. Liu, B.; Hu, L. "5'-(2-Nitrophenylalkanoyl)-2'-deoxy-5-fluorouridines as potential prodrugs of FUDR for reductive activation" *Bioorg. Med. Chem.* **2003**, *11*, 3889–3899.

Chapter 4. Characterizing Chain Processes in Visible Light Photoredox Catalysis

Portions of this work have been previously published:

Cismesia, M. A.; Yoon, T. P. "Characterizing chain processes in visible light photoredox catalysis" *Chem. Sci.* DOI: 10.1039/c5sc02185e

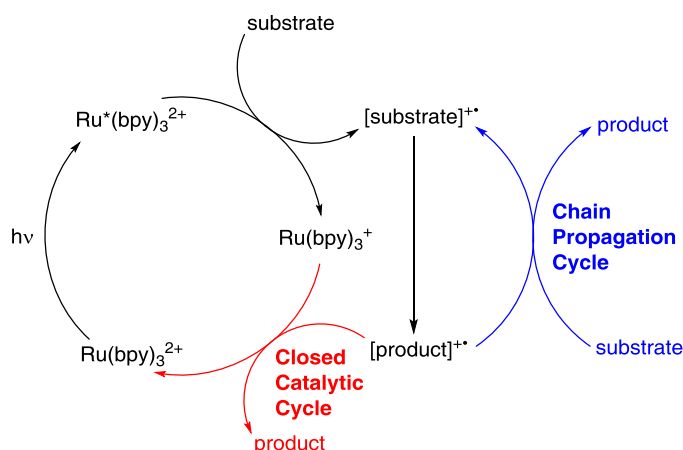
4.1 Introduction

Over the past several years, a growing number of researchers have become interested in reactions that utilize $\text{Ru}(\text{bpy})_3^{2+}$ and similar visible light-activated transition metal chromophores in synthetically useful photoredox reactions. Numerous recent studies have resulted in the development of an impressively diverse range of photocatalytic transformations;¹ the applications of these reactions have ranged from natural product synthesis² to late-stage pharmaceutical functionalization³ and polymer synthesis.⁴ Notably, the burst of renewed activity in visible light enabled photochemical synthesis has been accompanied by relatively little detailed mechanistic investigation to date.⁵ While the photophysical properties of $\text{Ru}(\text{bpy})_3^{2+}$ and its analogues have been extensively studied and are well understood,⁶ only a handful of published reports have focused upon the equally important non-photochemical steps in photoredox transformations.⁷ Consequently, many of the salient mechanistic features of these reactions remain unclear.

One area of significant disagreement has concerned the degree to which photoredox reactions involve chain processes. As a framework for this discussion, consider the generic mechanism for an oxidatively induced photoredox transformation depicted in Scheme 4-1. The essential details of the initial photochemical activation steps are not controversial: photoexcitation of $\text{Ru}(\text{bpy})_3^{2+}$ produces a long-lived redox-active triplet state ($\text{Ru}^*(\text{bpy})_3^{2+}$) that can be reductively quenched by a wide range of organic substrates. The resulting radical cations ($[\text{substrate}]^{+\bullet}$) are able to participate in a number of possible reaction manifolds, resulting in the formation of an open-shelled odd-electron product ($[\text{product}]^{+\bullet}$). Many of the recent reports of photoredox transformations have posited that the generation of the final neutral product proceeds only via a closed catalytic loop (shown in red) involving reduction of this first-formed product

by the reduced form of the photocatalyst ($\text{Ru}(\text{bpy})_3^+$), which regenerates the photochemically active $\text{Ru}(\text{II})$ state. Other researchers, however, have proposed that this class of reactions, like most other reactions of open-shell odd-electron reactive intermediates,⁸ are likely to involve chain mechanisms that operates in addition to the closed catalytic cycle. In this scenario, product formation would occur primarily via a chain propagation step (shown in blue) in which oxidized product radical cation interacts with another equivalent of neutral substrate, thereby generating the neutral product and another substrate radical cation by a single electron transfer process.⁹

Scheme 4-1. Generalized mechanism for oxidative photoredox reactions.



The distinction between chain and non-chain mechanisms is an important one because the strategies appropriate for optimizing these two classes of reactions differ significantly. For instance, if product is only formed by a closed catalytic loop, then optimization of the structural and electrochemical properties of the photocatalyst might be expected to strongly impact the efficiency of catalyst turnover. On the other hand, if chain reactions dominate product formation, then reaction variables that increase the rate of chain propagation or decrease the rate of chain termination should have a large effect even if they do not impact the activity of the catalyst itself.

Many recent publications describing photoredox reactions have dismissed the relevance of chain propagation steps. The evidence most commonly used for this purpose involves “light/dark” experiments, which examine the progress of a reaction in alternating periods of irradiation and darkness.¹¹ The observation that productive reaction requires constant irradiation is commonly construed to mean that chain processes are either not occurring or are quite short. We disagree with this interpretation. The fact that conversion ceases during dark periods could also be consistent with chain processes that terminate faster than the timescale of the analytical measurement used, which may be several seconds or even minutes when an *ex situ* measurement is used.¹²

Moreover, in a closed system, the concentration of [product]⁺⁺ must be the same as that of the reduced photocatalyst (Ru(bpy)₃⁺), which in turn can be no higher than the total initial concentration of photocatalyst. A non-chain catalytic cycle thus requires the encounter of two low-concentration reactive intermediates, which seems unlikely to produce the fast reaction times and low catalyst loadings reported in many of the most efficient photoredox methods. In addition, non-photochemical versions of many of these transformations are known and are widely accepted to involve chain processes.¹³ It therefore seems reasonable to consider the possibility that chain processes might be operative in a much wider range of photoredox reactions than is generally appreciated.

Quantum yield measurements provide a useful tool for identifying photochemical reactions that involve radical chains.¹⁴ The closed photoredox loop lacking chain propagation shown in Scheme 4-1 could exhibit a maximum theoretical quantum yield (Φ) of 1, which would indicate that every photon absorbed by the photocatalyst was producing one product molecule. This is the maximum value for this scenario: the occurrence of any non-productive photochemical processes

such as phosphorescence, internal conversion, or back electron transfer would only decrease the observed quantum yield. Chain processes, on the other hand, could potentially provide multiple equivalents of product from each photon-induced initiation step. A reaction with $\Phi \gg 1$, therefore, could only be consistent with a chain mechanism.¹⁵

In this chapter, we demonstrate that a combination of quantum yield and luminescence quenching measurements can provide a powerful method to study chain processes in synthetic photoredox reactions. We provide evidence that supports the involvement of chain propagation steps in three mechanistically diverse reactions involving radical cations, radical anions, and neutral radical intermediates. We further show that several important mechanistic features of these reactions are revealed using this analysis. Finally, we demonstrate that even reactions that unambiguously involve chain propagation steps can nevertheless require constant irradiation for product formation, and thus that “light/dark” experiments do not provide reliable information about the participation of chain processes.

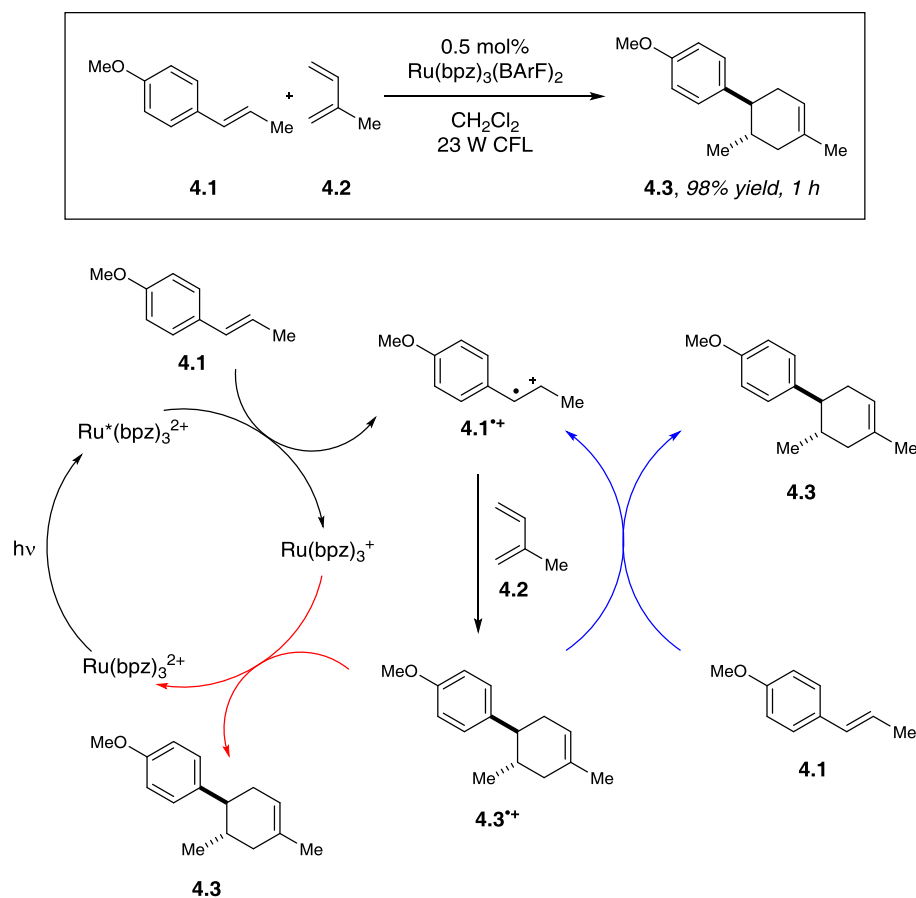
4.2 Results and Discussion

4.2.1 Photoinitiated radical cation reaction

We began our studies by investigating a photocatalytic radical cation Diels–Alder cycloaddition recently reported by our laboratory.¹⁶ This reaction was an attractive initial target for interrogation because a great deal is already known about the mechanisms of radical cation cycloaddition reactions, largely due to detailed investigations performed by Bauld¹⁷ and Ledwith.¹⁸ In particular, radical cation mediated [4+2] cycloaddition reactions can be conducted using sub-stoichiometric one-electron oxidants such as aminium radicals,¹⁹ and it is well accepted that these chemically initiated cycloadditions are chain processes. It stands to reason,

therefore, that photoinitiated versions of these reactions would likely also proceed through a chain mechanism.²⁰

Scheme 4-2. Chain and closed catalytic mechanisms for a photoredox radical cation Diels–Alder cycloaddition.



Our working model for the mechanism of the photoredox process is depicted in Scheme 4-2. The reaction is initiated upon reductive quenching of photoexcited $\text{Ru}^*(\text{bpz})_3^{2+}$ by anethole (4.1), which affords the alkene radical cation $4.1^{\bullet+}$ along with an equivalent quantity of the reduced catalyst $\text{Ru}(\text{bpz})_3^+$. The alkene radical cation is activated towards [4+2] cycloaddition with a diene (4.2) to produce radical cation $4.3^{\bullet+}$ as the first-formed, open-shelled product of this reaction. In order to generate the neutral cycloadduct 4.3, the product radical cation must be reduced by one electron. This can either occur via chain-terminating electron transfer from the

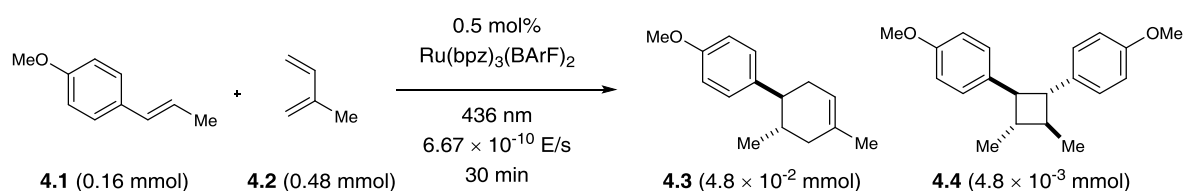
reduced photocatalyst $\text{Ru}(\text{bpz})_3^+$ (as shown in red), or via chain-propagating electron transfer from another equivalent of electron-rich alkene substrate **4.1** (blue).

To begin our investigations of chain propagation in the radical cation [4+2] cycloaddition, we calibrated its quantum yield against the photodecomposition of potassium ferrioxalate, a well-established chemical actinometer with known quantum efficiencies at multiple wavelengths.²¹ We selected 436 nm light for our experiments, a wavelength at which the $\text{Ru}(\text{bpz})_3^{2+}$ photocatalyst absorbs strongly²² and for which the quantum efficiency of ferrioxalate decomposition has been established ($\Phi = 1.01$). We conducted the quantum yield measurements in a 1 cm quartz cuvette placed in a standard fluorescence spectrophotometer capable of variable wavelength emission. First, in order to determine the intensity of the fluorometer at $\lambda = 436$ nm, we irradiated a solution containing a known concentration of ferrioxalate and quantified the appearance of Fe(II) by UV-vis absorbance spectroscopy. From these data and the reported quantum yield of Fe(III) reduction, we calculated a photon flux of 6.67×10^{-10} E/s from the fluorometer source.

Next, we conducted a radical cation Diels–Alder cycloaddition in the fluorometer with 0.16 mmol anethole (**4.1**) and 0.48 mmol isoprene (**4.2**) in the presence of 0.5 mol% $\text{Ru}(\text{bpz})_3^{2+}$ (Scheme 4-3). Importantly, despite the relatively low concentration of the photocatalyst (4.0×10^{-4} M), the optical transmittance at 436 nm was negligible (Figure 4-1). Each of the organic coupling partners, on the other hand, was transparent at 436 nm, so we could make the limiting assumption that the incident photon flux is completely absorbed by the photocatalyst. After 30 min of irradiation in the fluorometer, we obtained 30% yield of Diels–Alder cycloadduct **4.3** (4.8×10^{-2} mmol). In addition, [2+2] homodimer **4.4**, a byproduct also arising from reaction of alkene radical cation $\mathbf{4.1}^{+\bullet}$,²³ was formed in 3% yield (4.8×10^{-3} mmol). Thus, the overall

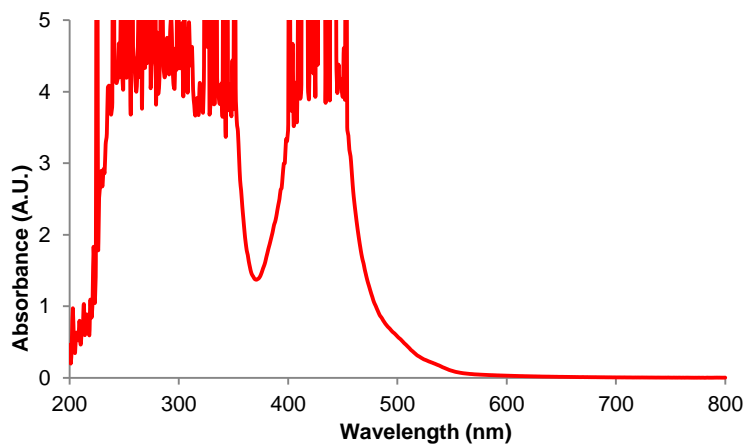
quantum yield for formation of all radical cation cycloaddition products can be calculated by dividing the combined moles of **4.3** and **4.4** formed by the einsteins of photons consumed (eq 4-1); from these data, we calculate a quantum yield value of $\Phi = 44$. In other words, 44 equivalents of product are formed for every photon absorbed by the photocatalyst, which is a result that could only be consistent with a chain mechanism.

Scheme 4-3. Calculating quantum yield for photocatalytic radical cation Diels–Alder cycloaddition.



$$\begin{aligned} \Phi &= \frac{\text{moles of product formed}}{\text{einstein of light absorbed}} && \text{(eq 4-1)} \\ &= \frac{5.28 \times 10^{-5} \text{ mol}}{6.67 \times 10^{-10} \text{ mol/s} \cdot 1800 \text{ s}} \\ &= 44 \end{aligned}$$

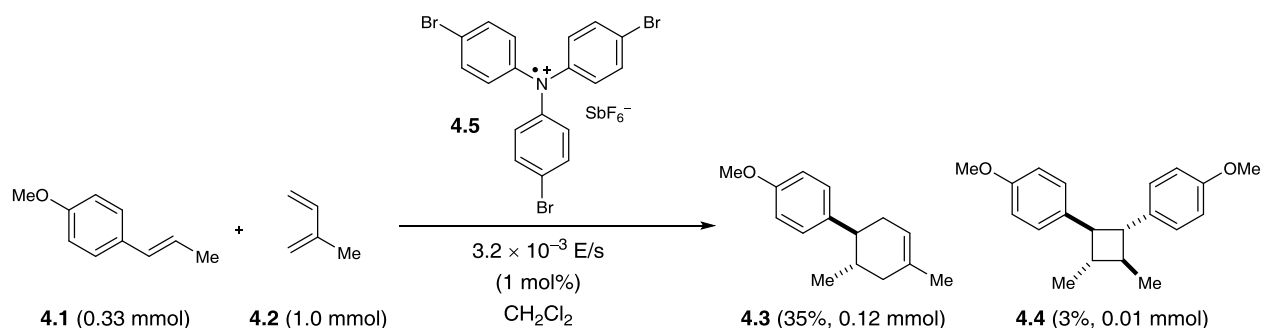
Figure 4-1. UV-vis absorption spectrum for $\text{Ru}(\text{bpz})_3(\text{BArF})_2$ at 4×10^{-4} M in CH_2Cl_2 .



It is important to note that this calculation does not take into account the participation of any other photoinitiated processes that do not lead to product. For example, the photoexcited $\text{Ru}^*(\text{bpz})_3^{2+}$ catalyst could relax to the ground state via either radiative or vibrational pathways without undergoing electron-transfer processes; the reduced photocatalyst $\text{Ru}(\text{bpz})_3^+$ and the oxidized alkene $\mathbf{4.1}^+$ could also recombine to regenerate $\text{Ru}(\text{bpz})_3^{2+}$ and neutral $\mathbf{4.1}$ via back electron transfer. Crucially, any such non-productive processes would reduce the numerator of eq 4-1 without affecting the denominator. Thus, although the observation of a quantum yield much greater than unity provides confirmation of the chain nature of this reaction, the actual length of the chains could be substantially higher than the quantum yield.

We were, however, intrigued by the observation that the quantum yield that we calculated is of the same order of magnitude as the chain lengths reported by Bauld for mechanistically similar [2+2] styrene radical cation cycloaddition reactions (ca. 20).²⁴ This led us to wonder whether the quantum yield might indeed be a reasonable estimate for the length of the radical cation chains in the Diels–Alder cycloaddition. To enable a reasonable comparison, we chemically initiated a radical cation [4+2] cycloaddition of 0.33 mmol $\mathbf{4.1}$ and 1.0 mmol $\mathbf{4.2}$ using a catalytic quantity of triarylaminium cation $\mathbf{4.5}$ (3.2×10^{-3} mmol). In this experiment, we observed the formation of 38% combined yield of $\mathbf{4.3}$ and $\mathbf{4.4}$ (0.13 mmol total). This corresponds to an average chain length of 41 (eq 4-2), a value within experimental error of the quantum yield that we calculated using eq 4-1. Thus, in addition to providing compelling evidence that the photocatalytic radical cation Diels–Alder cycloaddition is a chain process, this study also suggested to us that quantum yield measurements might provide a convenient method to quickly estimate the average chain length involved in photocatalytic reactions. This conjecture is further interrogated in the next section.

Scheme 4-4. Calculating chain length for chemically induced radical cation Diels–Alder cycloaddition.



$$\begin{aligned} \text{chain length} &= \frac{\text{moles of product formed}}{\text{moles of initiator}} && \text{(eq 4-2)} \\ &= \frac{1.3 \times 10^{-4} \text{ mol}}{3.2 \times 10^{-6} \text{ mol}} \\ &= 41 \end{aligned}$$

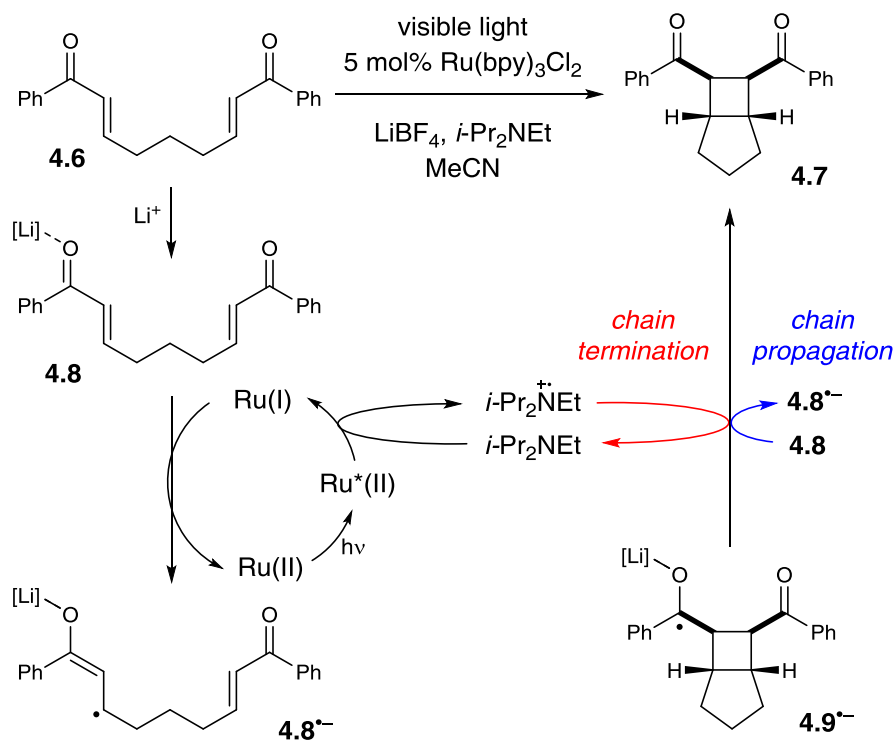
4.2.2 Photoinitiated radical anion reaction

Much of the recent research in photoredox catalysis has been motivated by the fact that both oxidative and reductive one-electron transfer processes are readily accessible. The versatile redox properties of Ru(bpy)₃²⁺ and similar photoredox catalysts provide uniquely direct access to a wide range of odd-electron reactive intermediates with diverse chemical behavior.²⁵ In order to probe our hypothesis that chain mechanisms are a general feature of photoredox reactions, we next elected to study the photocatalytic [2+2] cycloaddition of enones reported by our group several years ago.²⁶ We selected this reaction as an example of a *photoreductively* initiated process that would contrast with the *photooxidative* radical cation Diels–Alder reaction described in the previous section. We hoped that evidence that both of these classes of reactions possess

quantum yields greater than unity would provide further evidence supporting our contention that chain mechanisms are more common in photoredox chemistry than is generally appreciated.

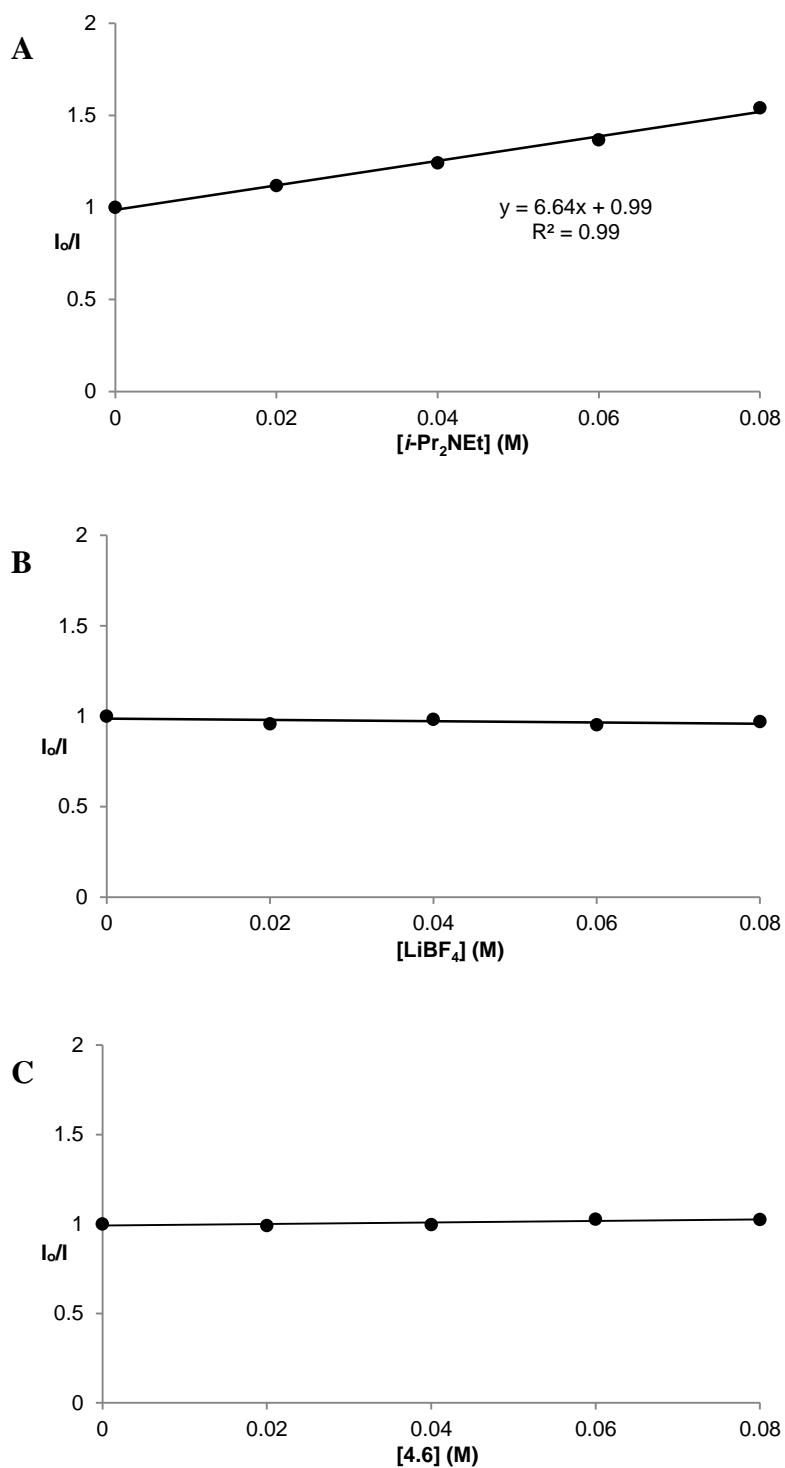
Scheme 4-5 depicts a working model for the mechanism of this transformation. We have proposed that the initiating step involves reductive quenching of photoexcited $\text{Ru}^*(\text{bpy})_3^{2+}$ by $i\text{-Pr}_2\text{NEt}$. This step produces $\text{Ru}(\text{bpy})_3^+$, which reacts with Lewis acid-activated enone **4.8** in a one-electron reduction process to generate the key radical anion **4.8^{•-}**. The enone radical anion then undergoes [2+2] cycloaddition to afford the cyclobutyl radical anion **4.9^{•-}**, which must lose an electron in order to generate the neutral product **4.7**. This final product-forming electron-transfer step could either be chain-terminating reduction of photogenerated amine radical cation $i\text{-Pr}_2\text{NEt}^{\bullet+}$, or chain-propagating reduction of another equivalent of Li-activated enone **4.8**.

Scheme 4-5. Mechanistic proposal for the radical anion [2+2] cycloaddition.



Using the same experimental setup described in the previous section, we calculated a quantum yield of $\Phi = 77$, again demonstrating that product formation is dominated by a chain process. However, we suspected that the average chain length might actually be somewhat longer than the quantum yield suggests on its own. In the course of measuring the quantum yield for this reaction, we observed that the reaction sample continued to luminesce visibly throughout the reaction. Thus, some non-negligible proportion of the photons absorbed by $\text{Ru}(\text{bpy})_3^{2+}$ are re-emitted via phosphorescence, and only a fraction of the excited $\text{Ru}^*(\text{bpy})_3^{2+}$ triplets participate in productive electron transfer processes. This contrasts sharply to the radical cation Diels–Alder reaction, which displayed negligible luminescence compared to a blank sample of catalyst.²⁷

The partitioning of excited state $\text{Ru}^*(\text{bpy})_3^{2+}$ between reductive quenching by *i*-Pr₂NEt, which initiates the product-forming radical anion cycle, and non-productive relaxation pathways such as phosphorescence can be expressed as a quenching fraction (Q). The initial value of Q can be calculated using eq 4-3, which expresses the quenching fraction as a ratio of the rate at which the excited photocatalyst is productively quenched by *i*-Pr₂NEt to the sum of the rates of all of the relaxation processes available to the excited state. The intrinsic rate of all unimolecular radiative and non-radiative relaxation reactions of $\text{Ru}^*(\text{bpy})_3^{2+}$ is given by inverse of the lifetime of an excited state (τ_0), a known quantity with a value of 855 ns in MeCN.²⁸ The quenching rates (k_q) for each of the reaction components can be directly measured using standard Stern–Volmer analyses, the results of which are shown in Figure 4-2. Of the various reaction components, only *i*-Pr₂NEt resulted in any measurable Stern–Volmer quenching ($k_{q,HB} = 7.9 \times 10^6 \text{ M}^{-1}\text{s}^{-1}$);²⁹ we observed no change in $\text{Ru}^*(\text{bpy})_3^{2+}$ luminescence upon varying the concentrations of either LiBF₄ or the enone substrate, consistent with the mechanism shown in Scheme 4-5. From these data, we calculated a quenching fraction of $Q = 0.57$.

Figure 4-2. Stern–Volmer quenching studies for (A) *i*-Pr₂NEt, (B) LiBF₄, and (C) enone **4.6**.

I_0 is the phosphorescence intensity without any added quencher. I is the phosphorescence intensity in the presence of a quencher.

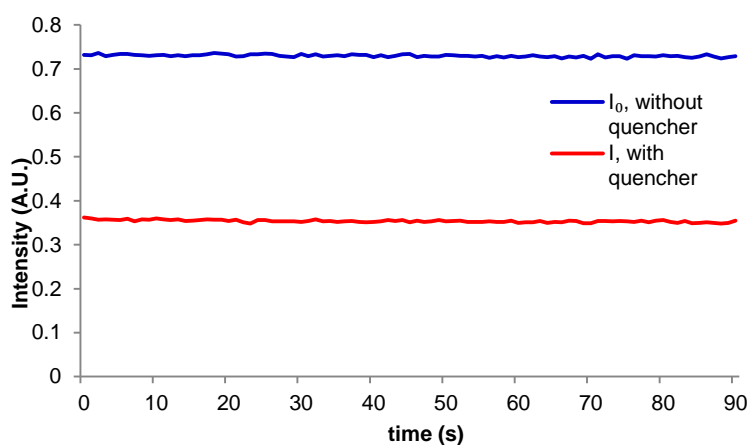
$$\begin{aligned}
 Q &= \frac{k_{q,HB}[i\text{-Pr}_2\text{NEt}]}{\tau_0^{-1} + k_{q,HB}[i\text{-Pr}_2\text{NEt}] + k_{q,Li}[\text{LiBF}_4] + k_{q,4.6}[\mathbf{4.6}]} && \text{(eq 4-3)} \\
 &= \frac{7.9 \times 10^6 \text{ M}^{-1}\text{s}^{-1} \cdot [0.2\text{M}]}{(8.55 \times 10^{-7} \text{ s})^{-1} + 7.9 \times 10^6 \text{ M}^{-1}\text{s}^{-1} \cdot [0.2\text{M}] + 0 + 0} \\
 &= \mathbf{0.57}
 \end{aligned}$$

Thus the product-forming electron-transfer event is relatively inefficient: only 57% of the photons absorbed by the photocatalyst result in product-forming electron transfer, and 43% of the excited metal complexes relax via energy-wasting luminescence or internal conversion processes. The chain length, therefore, is more accurately expressed by dividing the calculated quantum yield by the quenching fraction. This analysis suggests that the average chain length of $\Phi/Q = 135$ for the radical anion mediated intramolecular [2+2] cycloaddition of **4.6**.

The measurement of Stern–Volmer quenching rates is a well-validated but somewhat time-consuming process. For operational simplicity, we wondered if a more rapid estimation of the initial quenching fraction might be available by comparing the phosphorescence of the reaction in progress to a control sample of the photocatalyst alone. This approach is facilitated by the fact that we determined quantum yields using an irradiation source capable of simultaneous luminescence detection. Indeed, the phosphorescence intensity (I) of the catalyst under radical anion [2+2] cycloaddition reaction conditions is 50% that of the catalyst when $i\text{-PrNEt}_2$ is omitted (I_0), which provides an estimated quenching fraction within experimental error of the value calculated from a complete Stern–Volmer analysis (Figure 4-3). The chain length derived from this value is calculated by dividing the measured total quantum yield by the fraction of catalysts whose phosphorescence is quenched ($1 - I/I_0$), which gives a calculated value for average chain length of 154.^{30,31}

While the chain length for radical anion [2+2] cycloadditions of electron-deficient alkenes has not previously been reported, evidence supporting their chain nature is available. Most convincingly, Bauld has measured faradaic efficiencies greater than unity for the cathodic reduction and intramolecular [2+2] cycloadditions of aryl vinyl ketones; the values reported have been as high as 10.6.³² Thus the faradaic efficiency for the electrochemical reaction, like the directly measured quantum efficiency of the photoredox reaction, is substantially lower than the average chain lengths estimated by our calculations. This observation reinforces the important caveat that both quantum yield and faradaic efficiency measurements can be diminished by the occurrence of non-productive processes such as back electron transfer or competitive reaction manifolds. For example, we have previously argued that the products of this [2+2] cycloaddition reaction are subject to slow over-reduction and decomposition processes that consume reducing equivalents without producing cycloadduct.³³ We do not account for the possibility of these non-productive pathways in our calculations, so the true chain length of the radical reactions may be quite a bit larger. Thus the large values calculated using this method should best be considered as lower reasonable limits.

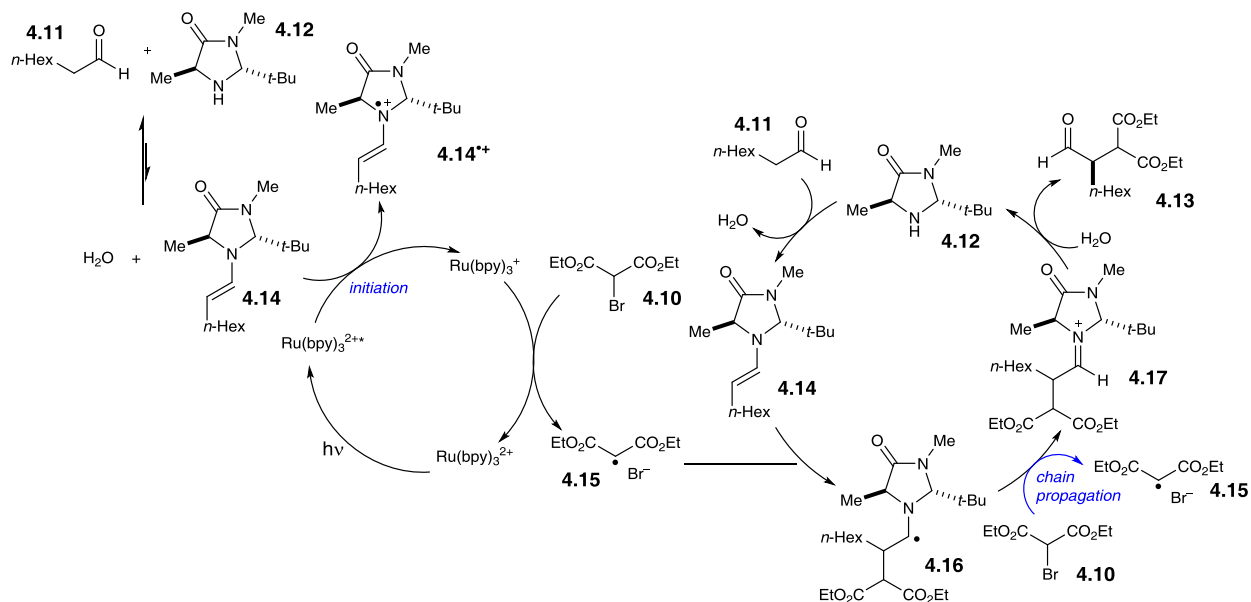
Figure 4-3. Phosphorescence intensity during reaction.



4.2.3 Photoinitiated neutral radical reaction

Photoredox processes result in the formation of radical ion intermediates that can be induced to directly participate in a variety of productive transformations such as those described in the previous two sections. A very common alternative mode of reactivity in photoredox catalysis involves a secondary fragmentation of photogenerated radical ions into discrete radical and ionic species, thereby affording access into the rich chemistry of neutral radical intermediates.

Scheme 4-6. Mechanistic proposal for organocatalytic photoredox α -alkylation of aldehydes.



An important, seminal example of this reaction is the asymmetric α -alkylation reaction reported by MacMillan (Scheme 4-6).³⁴ Mechanistically, this reaction involves two interacting catalytic cycles and is thus somewhat more complicated than the prior two examples. Nevertheless, it shares several similar essential features. First, the reaction is proposed to be initiated by reductive quenching of $\text{Ru}^*(\text{bpy})_3^{2+}$ by a sacrificial quantity of enamine **4.14**, generated by condensation of organocatalyst **4.12** with aldehyde substrate **4.11**. Second, the ultimate, closed-shell product **4.13** arises from one-electron oxidation of **4.16** followed by

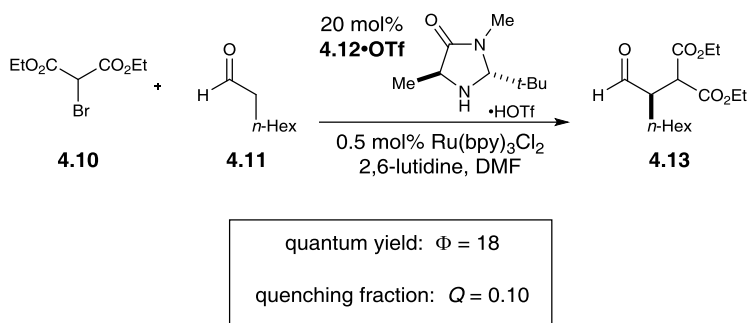
hydrolysis of the resulting iminium. MacMillan has proposed a closed catalytic cycle in which this final oxidation is a chain-terminating electron-transfer to $\text{Ru}^*(\text{bpy})_3^{2+}$. We propose that a more likely product-forming step would be chain-propagating reduction of the bromomalonate **4.10** by α -amino radical **4.16**, which is also a quite exergonic process.

We studied the reaction of **4.10** with **4.11** (Scheme 4-7) and found that this reaction possesses a quantum yield of $\Phi = 18$, again signifying a chain mechanism. Surprisingly, this value is quite a bit larger than that determined by König and Riedle, who reported $\Phi = 0.49$ for the same transformation.³⁵ These two experiments involve experimental setups that differ in several ways that might account for the discrepancy between the two measurements, the most significant of which is the presence of oxygen, which we excluded in our experiments. Triplet dioxygen is a rapid and efficient quencher of $\text{Ru}^*(\text{bpy})_3^{2+}$;³⁶ by sparging the reaction solution with N_2 , we eliminate a major source of inefficiency in the photocatalytic α -alkylation reaction that would otherwise negatively impact the observed quantum yield. Indeed, our attempt to measure Φ under aerobic conditions using our experimental setup were unsuccessful because the low intensity of the spectrophotometer source resulted in only trace conversion after 4 h of irradiation.

This reemphasizes the important point that many non-productive processes, including parasitic quenching by energy or electron transfer as well as unimolecular decay processes, can result in a loss of measured quantum efficiency for a photochemical reaction. Indeed, in determining the quantum yield for the α -alkylation, we observed that the phosphorescence of the catalyst is only diminished by 10% under our experimental conditions. Thus, only a small fraction of the photoexcited $\text{Ru}^*(\text{bpy})_3^{2+}$ complexes productively initiate product-forming chains before they relax to the ground state by non-productive phosphorescence or internal conversion.

This observation indicates that the radical chain lengths are in fact quite long, with a lower limit of 180.

Scheme 4-7. Quantum yield measurement for the organocatalytic photoredox α -aldehyde alkylation.

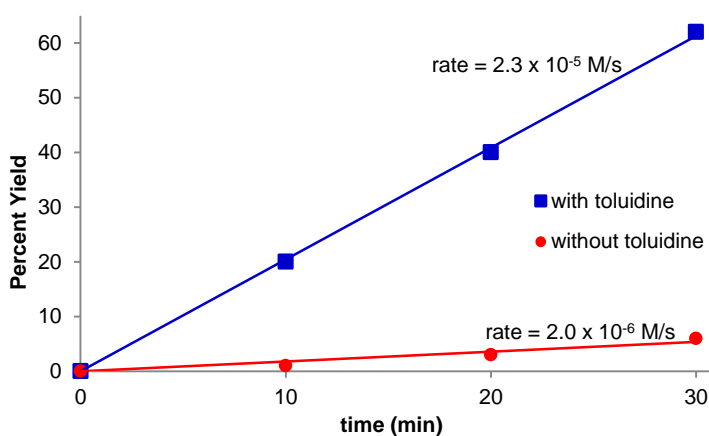
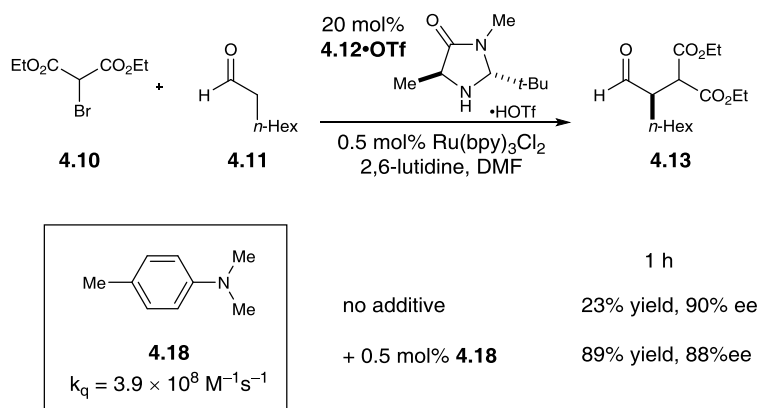


The combination of quantum yield and luminescence quenching measurements, therefore, reveals that the α -alkylation reaction involves long radical chains but a relatively inefficient initiation process. We can rationalize the poor phosphorescence quenching as a consequence of several factors. First, the equilibrium for formation of enamine **4.14** is unfavorable; we measured $K_{\text{eq}} = 8.1 \times 10^{-3}$. Second, organocatalyst **4.12** is used at sub-stoichiometric loadings, resulting in a quite low concentration of initiating enamine. Finally, MacMillan reports a small Stern–Volmer quenching constant of 10 for **4.14**.³⁴ These observations provide a satisfying explanation for the inefficient rate of initiation and for the relatively high reaction concentration required for successful reaction (0.5 M in **4.10**).

These insights suggested to us that a simple, rational modification to the reaction might dramatically improve the rate of this reaction. If our model for the mechanism of this reaction is correct, then the addition of a catalytic quantity of a co-reductant that could reductively quench $\text{Ru}^*(\text{bpy})_3^{2+}$ at faster rates than enamine **4.14** would be expected to increase the overall rate of product formation. To probe this hypothesis, we elected to study the effect of *N,N*-dimethyl-*p*-

toluidine (**4.18**) on this reaction (Figure 4-4). We selected this additive because it is known to quench $\text{Ru}^*(\text{bpy})_3^{2+}$ at near diffusion-controlled rates.³⁷

Indeed, upon addition of only 0.5 mol% **4.18**, we observed that the rate of product formation increased by over an order of magnitude (Figure 4-4). When the reaction was allowed to proceed to a 1 h timepoint, the experiment conducted without **4.18** had progressed to only 23% yield; the reaction conducted with co-catalytic **4.18**, on the other hand, was essentially complete (89% yield), and the product was formed with essentially the same enantioselectivity in both cases. Control experiments conducted in the absence of $\text{Ru}(\text{bpy})_3\text{Cl}_2$ showed that **4.18** had no impact on the rate of the direct photoreaction.³⁸ Thus, we conclude that **4.18** improves the rate of the reaction by accelerating an otherwise inefficient radical chain initiation step, consistent with our guiding hypothesis.

Figure 4-4. Effect of exogenous co-catalytic reductive quencher.

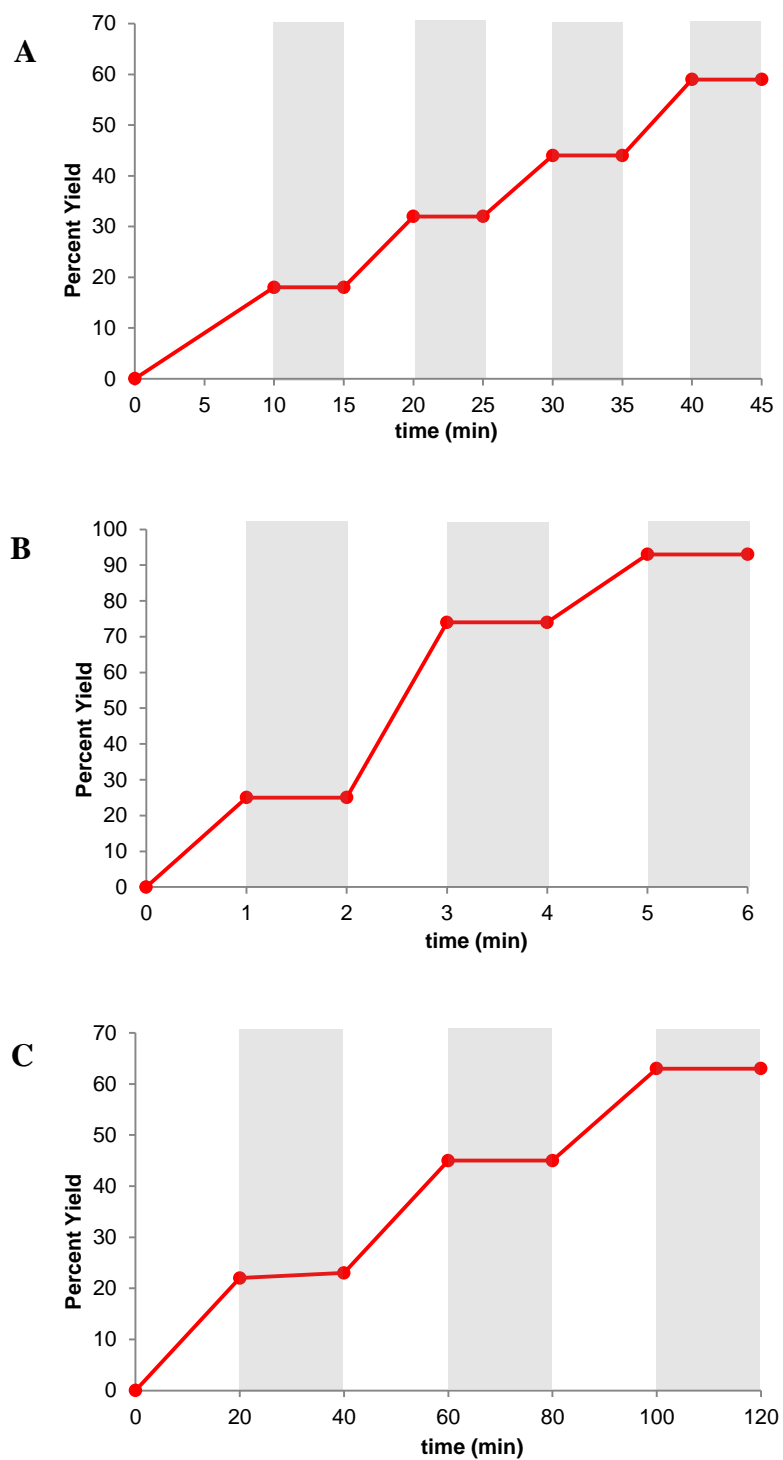
Thus, these experiments are valuable for a variety of reasons. First, the ability to rapidly determine chain lengths in photocatalytic reactions can provide valuable information on whether product formation is dominated by single-turnover catalyst-mediated steps or by catalyst-free chain propagation reactions, a detail that is critical for fully understanding the mechanism of a photocatalytic reaction. Moreover, the ability to easily diagnose whether inefficiencies in a photoredox reaction are a result of short chain lengths or of slow initiation steps can provide valuable insights that can guide the rational optimization of the method. We suggest that this approach to studying the mechanism of photocatalytic reactions should be generally applicable to the growing body of literature involving photoredox catalysis.

4.2.4 Light/Dark experiments

Finally, we wished to interrogate the suggestion that “light/dark” experiments could be used to disprove the occurrence of chain processes in photoredox reactions. As described in the previous sections, we have obtained compelling evidence that the radical cation [4+2], radical anion [2+2], and neutral radical α -alkylation reactions all involve long product-forming chains. Nevertheless, when each of these reactions is conducted using alternating intervals of light and dark, we observe that product formation occurs only during periods of constant irradiation (Figure 5a–c), consistent with the results of other “light/dark” experiments recently reported in the literature.¹¹

There are indeed a number of useful conclusions that can be drawn from “light/dark” experiments such as these. For instance, the observation that product is formed only upon constant irradiation suggests that a photocatalytic reaction might be susceptible to temporal and spatial control, a characteristic that can have important ramifications in materials applications.^{4,39} These experiments, however, clearly cannot be used to rule out the participation of long chain process in the mechanism of a photocatalytic reaction, and we urge caution in drawing conclusions about chain propagation from “light/dark” experiments.

Figure 4-5. “Light/dark” experiments for (A) the radical cation [4+2] cycloaddition, (B) radical anion [2+2] cycloaddition, and (C) photoredox aldehyde alkylation reaction.



4.3 Conclusions

We have demonstrated that chain processes dominate product formation in three representative photoredox transformations. Quantum yields much greater than unity were obtained for this selection of mechanistically distinct reactions involving both photooxidative and photoreductive initiation. Collectively, the studies described in this paper support our contention that radical chain processes should be routinely considered when proposing the mechanisms of photoredox reactions, and that “light/dark” experiments cannot be used to conclusively rule them out. Further, we demonstrated that the combination of quantum yield measurements and luminescence quenching experiments provides a convenient method to rapidly determine a lower limit for chain lengths and to diagnose inefficient initiation steps in photoredox reactions. Our hope is that this simple approach to characterizing chain processes in photoredox reactions will become a routine analytical tool that will help to elucidate the fundamental mechanistic characteristics of this growing class of synthetically powerful transformations.

4.4 Experimental

4.4.1 General experimental information

Dichloromethane (CH_2Cl_2) and acetonitrile (MeCN) were purified through alumina as described by Grubbs.⁴⁰ $\text{Ru}(\text{bpz})_3(\text{BArF})_2$ was synthesized as previously reported.⁴¹ $\text{Ru}(\text{bpy})_3\text{Cl}_2 \cdot 6\text{H}_2\text{O}$ was purchased from Strem and used without further purification. Anethole, octanal, diethyl bromomalonate, and *N,N*-dimethyl-*p*-toluidine were purified *via* silica gel chromatography. Isoprene was distilled prior to use. Diisopropyl ethyl amine (*i*-Pr₂NEt) and 2,6-lutidine were distilled over calcium hydride, and *N,N*-dimethylformamide (DMF) was distilled over magnesium sulfate. Lithium tetrafluoroborate (LiBF_4) was purchased from Sigma–Aldrich and

stored in a glovebox under an atmosphere of nitrogen. (*E,E*)-1,7-Dibenzoyl-1,6-heptadiene was prepared as previously reported (**4.6**)⁴² and purified by flash chromatography immediately prior to use. (*2R,5S*)-2-*t*-Butyl-3,5-dimethylimidazolidine-4-one (**4.12**) was prepared as previously reported.⁴³ All solutions were prepared in the dark. Reactions were conducted in a 1 cm square quartz cuvette and capped with either a PTFE stopper or sealed with a rubber septum unless otherwise noted. A Hitachi F-4500 fluorescence spectrophotometer with a 150 W Xe lamp was used as the light source for the quantum yield measurements and luminescence quenching data. A 20 W compact fluorescent light bulb was used for “light/dark” and time course experiments at a distance of 8–10 cm away from the reaction flask. UV-vis data were measured on a Varian Cary 50 spectrophotometer. NMR data were measured on a Bruker AC 300 MHz or Bruker Avance 400 or 500 MHz spectrometer. The NMR facilities at UW–Madison are supported by the NSF (CHE-1048642, CHE-9208463) and NIH (S10 RR08389-01).

4.4.2 Determination of light intensity

4.4.2.1 Determination of the light intensity at 436 nm

The photon flux of the spectrophotometer was determined by standard ferrioxalate actinometry.^{21,44} A 0.15 M solution of ferrioxalate was prepared by dissolving 2.21 g of potassium ferrioxalate hydrate in 30 mL of 0.05 M H₂SO₄. A buffered solution of phenanthroline was prepared by dissolving 50 mg of phenanthroline and 11.25 g of sodium acetate in 50 mL of 0.5 M H₂SO₄. Both solutions were stored in the dark. To determine the photon flux of the spectrophotometer, 2.0 mL of the ferrioxalate solution was placed in a cuvette and irradiated for 90.0 seconds at $\lambda = 436$ nm with an emission slit width at 10.0 nm. After irradiation, 0.35 mL of the phenanthroline solution was added to the cuvette. The solution was then allowed to rest for

1 h to allow the ferrous ions to completely coordinate to the phenanthroline. The absorbance of the solution was measured at 510 nm. A non-irradiated sample was also prepared and the absorbance at 510 nm measured. Conversion was calculated using eq 4-4 .

$$\text{mol Fe}^{2+} = \frac{V \cdot \Delta A}{l \cdot \epsilon} \quad (\text{eq 4-4})$$

Where V is the total volume (0.00235 L) of the solution after addition of phenanthroline, ΔA is the difference in absorbance at 510 nm between the irradiated and non-irradiated solutions, l is the path length (1.000 cm), and ϵ is the molar absorptivity at 510 nm ($11,100 \text{ L mol}^{-1} \text{ cm}^{-1}$).⁵ The photon flux can be calculated using eq 4-5.

$$\text{photon flux} = \frac{\text{mol Fe}^{2+}}{\Phi \cdot t \cdot f} \quad (\text{eq 4-5})$$

Where Φ is the quantum yield for the ferrioxalate actinometer (1.01 for a 0.15 M solution at $\lambda = 436 \text{ nm}$),⁵ t is the time (90.0 s), and f is the fraction of light absorbed at $\lambda = 436 \text{ nm}$ (0.99833, *vide infra*). The photon flux was calculated (average of three experiments) to be $6.67 \times 10^{-10} \text{ einstein s}^{-1}$.

Sample calculation:

$$\text{mol Fe}^{2+} = \frac{0.00235 \text{ L} \cdot 0.2868196}{1.000 \text{ cm} \cdot 11,100 \text{ L mol}^{-1} \text{ cm}^{-1}} = 6.07 \times 10^{-8} \text{ mol}$$

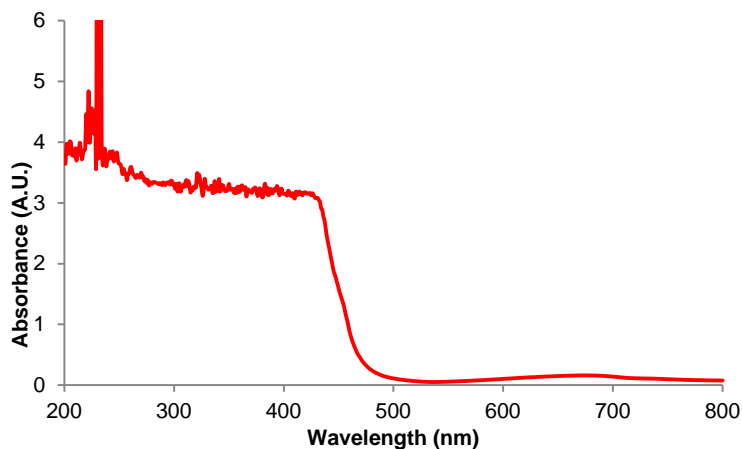
$$\text{photon flux} = \frac{6.07 \times 10^{-8} \text{ mol}}{1.01 \cdot 90.0 \text{ s} \cdot 0.99833} = 6.69 \times 10^{-10} \text{ einstein s}^{-1}$$

4.4.2.2 Determination of fraction of light absorbed at 436 nm for the ferrioxalate solution

The absorbance of the above ferrioxalate solution at 436 nm was measured to be 2.777683. The fraction of light absorbed (f) by this solution was calculated using eq 4-6, where A is the measured absorbance at 436 nm.

$$f = 1 - 10^{-A} \quad (\text{eq 4-6})$$

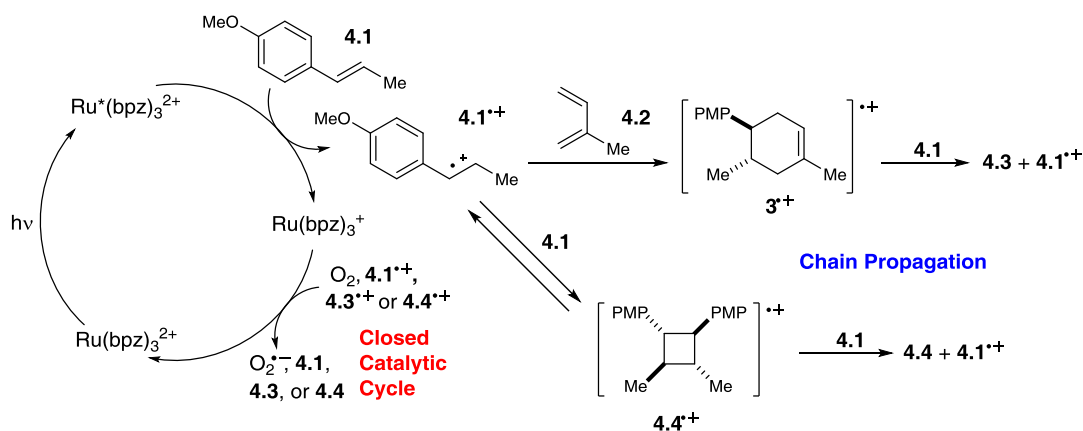
Figure 4-6. Absorbance of the ferrioxalate actinometer solution.



4.4.3 Analysis of [4+2] Diels–Alder reaction

4.4.3.1 Proposed mechanism

Scheme 4-8: Proposed mechanism of the [4+2] radical cation Diels–Alder reaction between anethole (**4.1**) and isoprene (**4.2**).

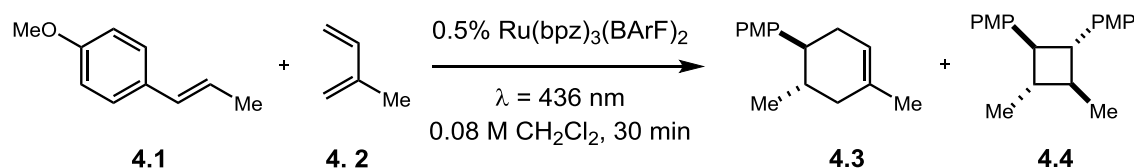


The reaction begins with $\text{Ru}(\text{bpz})_3^{2+}$ absorbing a photon and generating the excited state. $\text{Ru}^*(\text{bpz})_3^{2+}$ is quenched by **4.1**, forming both $\text{Ru}(\text{bpz})_3^+$ and the radical cation **4.1**^{•+}. The reactivity of **4.1**^{•+} can follow multiple pathways: (1) productive [4+2] formation with isoprene **4.2** to form **4.3**^{•+}, (2) reversible [2+2] cycloaddition with another molecule of **4.1** to generate **4.4**^{•+}, and (3) back electron transfer with $\text{Ru}(\text{bpz})_3^+$ to regenerate **4.1** and the photocatalyst. In a

closed catalytic cycle, **4.3**⁺ and **4.4**⁺ reoxidize Ru(bpz)₃⁺ to regenerate the photocatalyst and form the neutral products. In a chain process, **4.3**⁺ and **4.4**⁺ oxidize a molecule of **4.1** to generate another equivalent of **1**⁺ and furnish the products.

4.4.3.2 Determination of quantum yield

Scheme 4-9: [4+2] Reaction between anethole and isoprene.



A cuvette was charged with anethole (0.16 mmol, 1 equiv), isoprene (0.48 mmol, 3 equiv), Ru(bpz)₃(BArF)₂ (0.00080 mmol, 0.5 mol%), and 2.0 mL CH₂Cl₂ (0.08 M). The cuvette was then capped with a PTFE stopper. The sample was stirred and irradiated (λ = 436 nm, slit width = 10.0 nm) for 1800 s (30 min). After irradiation, the solution was passed through a silica plug. The yield of product formed was determined by ¹H NMR based on a dibromomethane standard. The quantum yield was determined using eq 4-7. Essentially all incident light (f > 0.999, *vide infra*) is absorbed by the Ru(bpz)₃(BArF)₂ at the reaction conditions described above.

$$\Phi = \frac{\text{mol product}}{\text{flux} \cdot t \cdot f} \quad (\text{eq 4-7})$$

Experiment 1: 23.7 mg (0.16 mmol) anethole, 48 μL (0.48 mmol) isoprene, 1.8 mg (0.00078 mmol) Ru(bpz)₃(BArF)₂, 2.0 mL (0.08 M) CH₂Cl₂ after 1800 s yielded 30% of **4.3** and 3% of **4.4**. Φ(33%) = 44.

Sample quantum yield calculation:

$$\Phi = \frac{5.28 \times 10^{-5} \text{ mol}}{6.67 \times 10^{-10} \text{ einstein s}^{-1} \cdot 1800 \text{ s} \cdot 1.00} = 44$$

Experiment 2: 23.6 mg (0.16 mmol) anethole, 48 μL (0.48 mmol) isoprene, 1.8 mg (0.00078 mmol) $\text{Ru}(\text{bpz})_3(\text{BARF})_2$, 2.0 mL (0.08 M) CH_2Cl_2 after 1800 s yielded 31% of **4.3** and 2.5% of **4.4**. $\Phi(33.5\%) = 44$.

4.4.3.3 Absorbance of catalyst

The absorbance of $\text{Ru}(\text{bpz})_3(\text{BARF})_2$ in CH_2Cl_2 was measured at the reaction concentration of 4.0×10^{-4} M and at a substantially more dilute concentration of 4.0×10^{-6} M. The absorbance at 436 nm for a 4.0×10^{-4} M solution is >3 indicating the fraction of light absorbed is >0.999 .

Figure 4-7. Absorbance of a 4.0×10^{-4} M solution of $\text{Ru}(\text{bpz})_3(\text{BARF})_2$ in CH_2Cl_2 .

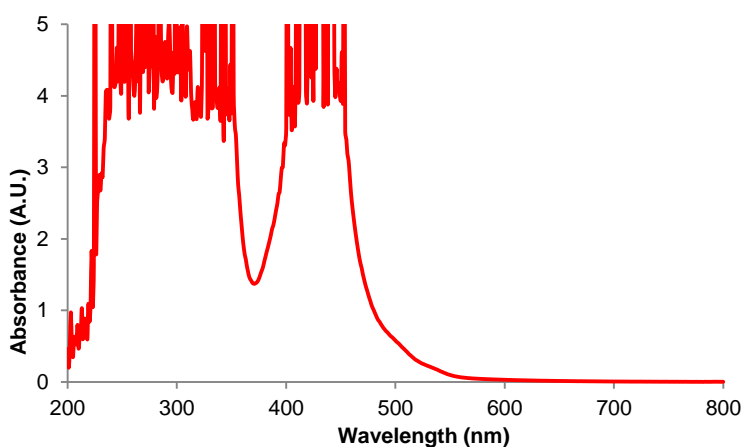
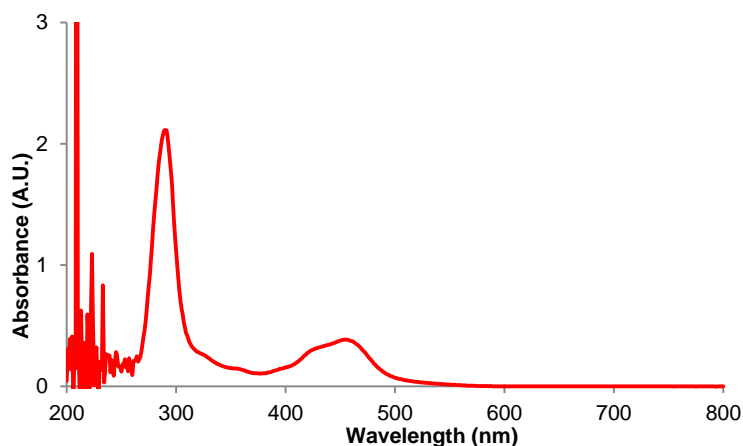


Figure 4-8. Absorbance of a 4.0×10^{-6} M solution of $\text{Ru}(\text{bpz})_3(\text{BARF})_2$ in CH_2Cl_2 .



4.4.3.4 Lifetime measurement

The excited state lifetime of Ru(bpz)₃(BArF)₂ in CH₂Cl₂ (395 ns, 3.9 × 10⁻⁵ M) was measured by the frequency-domain method with an ISS K2 spectrofluorometer. The excitation source was intensity modulated through varying MHz frequencies at the sample's absorption maximum, producing shifts in the intensity and phase of fluorescence emission. Comparison to a standard (in this case fluorescein and glycogen) allows lifetime determination. Data was analyzed in Vinci (ISS).

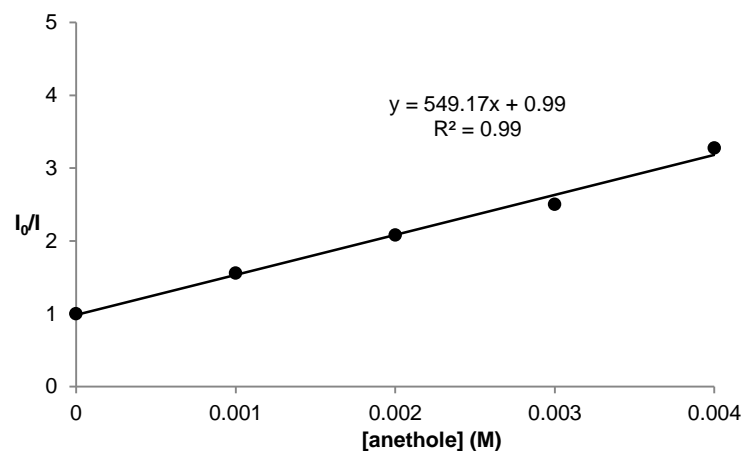
4.4.3.5 Stern–Volmer quenching rate data

Rates of quenching (k_q) were determined using Stern–Volmer kinetics (eq 4-8).

$$\frac{I_0}{I} = k_q \tau_0 [\text{quencher}] \quad (\text{eq 4 - 8})$$

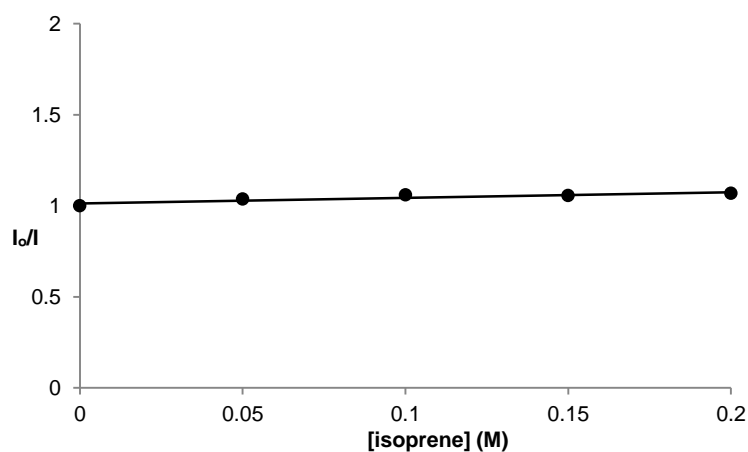
Where I_0 is the luminescence intensity without the quencher, I is the intensity with the quencher, and τ_0 is the lifetime of the photocatalyst. For anethole and Ru(bpz)₃(BArF)₂, samples were prepared by adding solutions of photocatalyst, quencher, and CH₂Cl₂ to obtain a total volume of 2.0 mL. A glass cuvette with a 14/20 joint and screw cap was used. The cuvette was degassed by three freeze-pump-thaw cycles and then backfilled with N₂. The concentration of Ru(bpz)₃(BArF)₂ was 3.9 × 10⁻⁵ M. Samples were irradiated at 436 nm, and emission was detected at 558 nm.

Figure 4-9. Stern–Volmer quenching experiment of $\text{Ru}(\text{bpz})_3(\text{BArF})_2$ and anethole. For anethole, $k_q = 1.4 \times 10^9 \text{ M}^{-1} \text{ s}^{-1}$.



For isoprene and $\text{Ru}(\text{bpz})_3(\text{BArF})_2$, a cuvette containing a solution of catalyst in CH_2Cl_2 was degassed by three freeze-pump-thaw cycles and then backfilled with N_2 . Samples were prepared by adding the solution of photocatalyst and isoprene (sparged) to a cuvette with a rubber septum under N_2 . The concentration of $\text{Ru}(\text{bpz})_3(\text{BArF})_2$ was $3.9 \times 10^{-5} \text{ M}$. The samples were irradiated at 436 nm, and emission was detected at 558 nm.

Figure 4-10. Stern–Volmer quenching experiment of $\text{Ru}(\text{bpz})_3(\text{BArF})_2$ and isoprene. No quenching observed.



For oxygen and Ru(bpz)₃(BArF)₂, values for k_q in MeCN have previously been reported.⁴⁵ The concentration of oxygen was calculated using Henry's Law.⁴⁶

The quenching fraction, Q, was calculated using eq 4-9, where other processes include quenching through non-productive pathways (*e.g.* quenching by oxygen).

$$Q = \frac{k_q[\text{quencher}]}{\tau_0^{-1} + k_q[\text{quencher}] + \text{other processes}} \quad (\text{eq 4 - 9})$$

Quenching fraction calculation:

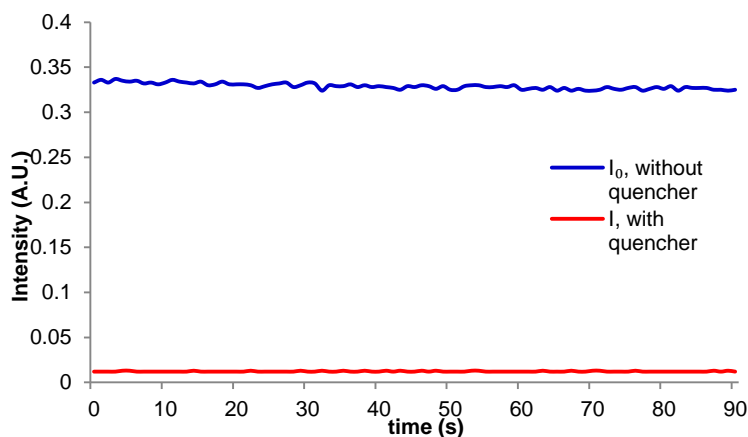
$$\begin{aligned} Q &= \frac{k_{q,\text{anethole}}[\text{anethole}]}{\tau_0^{-1} + k_{q,\text{anethole}}[\text{anethole}] + k_{q,\text{O}_2}[\text{O}_2]} \\ &= \frac{1.4 \times 10^9 \text{ M}^{-1}\text{s}^{-1}[0.080 \text{ M}]}{\frac{1}{3.95 \times 10^{-7} \text{ s}} + 1.4 \times 10^9 \text{ M}^{-1}\text{s}^{-1}[0.080 \text{ M}] + 2.6 \times 10^8 \text{ M}^{-1}\text{s}^{-1}[0.0019 \text{ M}]} \\ &= 0.97 \end{aligned}$$

4.4.3.6 Simple quenching experiment

The luminescence intensity under the reaction conditions (I) was recorded ($\lambda = 558 \text{ nm}$) while being irradiated in the fluorometer for the quantum yield measurement. Luminescence intensity without quencher (I₀) was also recorded for each reaction under the standard reaction conditions but excluding anethole. The quenching fraction, Q, was determined by eq 4-10 and averaged over the first 90 s of the reaction.

$$Q = \frac{I_0 - I}{I_0} \quad (\text{eq 4 - 10})$$

Figure 4-11. Phosphorescence intensity of the reaction over 90 s with (red line) and without (blue line) anethole. For this reaction, $Q = 0.96$.



4.4.3.7 Chain length calculation

Chain length values calculated in this paper are a lower limit approximation of the actual chain lengths and were calculated using eq 4-11, where Q was calculated either through the Stern–Volmer analysis or the simple quenching experiment.

$$\text{chain length} = \frac{\Phi}{Q} \quad (\text{eq 4 – 11})$$

Sample chain length calculation:

$$\text{chain length} = \frac{44}{0.97} = 45$$

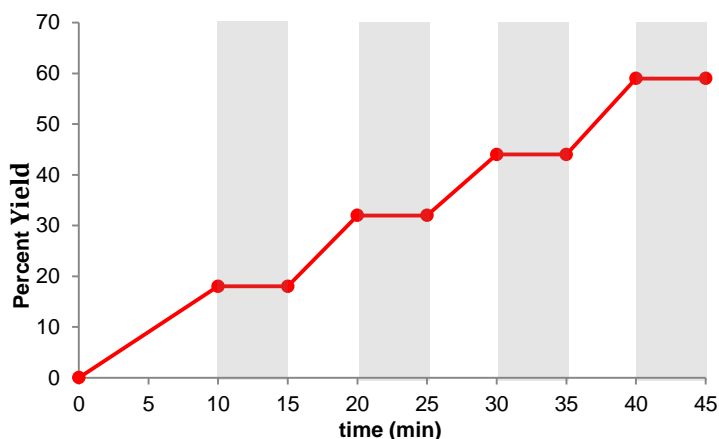
For the Stern–Volmer analysis, the chain length was calculated to be 45; for the simple quenching experiment, the chain length was 46.

4.4.3.8 Light/dark experiment

A vial was equipped with a stir bar and charged with 23.5 mg (0.16 mmol) anethole, 48 μL (0.48 mmol) isoprene, 1.7 mg (0.00074 mmol) $\text{Ru}(\text{bpz})_3(\text{BArF})_2$, 10.0 μL (0.058 mmol) trimethyl(phenyl)silane, and 2.0 mL (0.08 M) CD_2Cl_2 . The reaction was stirred under ambient atmosphere. The reaction was alternatively irradiated with a 20 W CFL bulb and kept in the dark

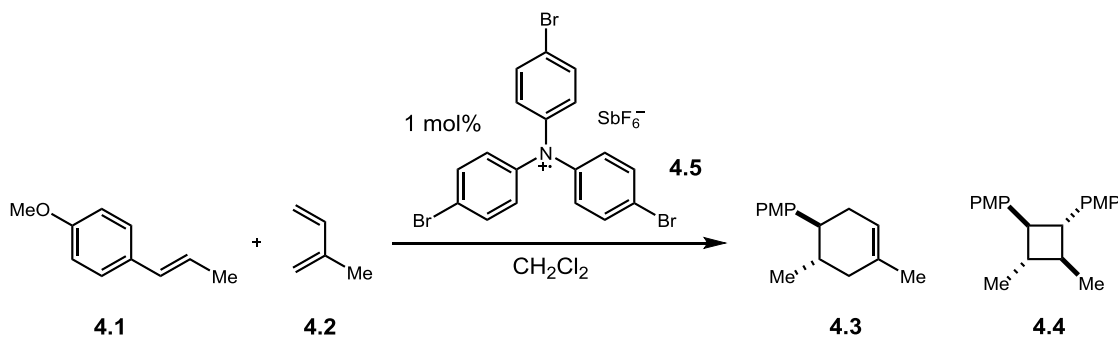
in five minute intervals. Aliquots were removed at the start and after each interval, passed through a silica plug, and diluted with CDCl_3 . Yields of the **4.3** and **4.4** were determined by ^1H NMR and based on trimethyl(phenyl)silane as an internal standard.

Figure 4-12. Light/dark experiment.



4.4.3.9 Non-photochemical [4+2] reaction

Scheme 4-10. Aminium initiated [4+2] reaction between anethole and isoprene.



A vial was equipped with a stir bar and charged with 49.5 mg (0.33 mmol) anethole, 100 μL (1.0 mmol) isoprene, 2.6 mg (0.0032 mmol) tris(4-bromophenyl)ammoniumyl hexachloroantimonate (**4.5**), and 4.2 mL (0.08 M) CH_2Cl_2 . The reaction was stirred for 1 h and then passed through a silica plug. The yield of product formed was determined by ^1H NMR based on trimethyl(phenyl)silane as an internal standard. The chain length was calculated by eq 4-12.

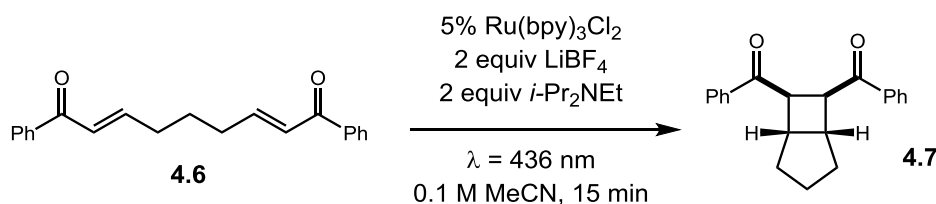
$$\text{chain length} = \frac{\text{mol } \mathbf{4.3} + \text{mol } \mathbf{4.4}}{\text{mol initiator}} \quad (\text{eq } 4 - 12)$$

The above reaction yielded 0.12 mmol of **4.3** and 0.010 mmol of **4.4**. The chain length was calculated to be 41.

4.4.4 Analysis of [2+2] cycloaddition reaction

4.4.4.1 Determination of quantum yield

Scheme 4-11. [2+2] Cycloaddition of bis(enone) **4.6**.



A cuvette was charged with bis(enone) **4.6** (0.20 mmol, 1 equiv), *i*-Pr₂NEt (0.40 mmol, 2 equiv), LiBF₄ (0.40 mmol, 2 equiv), Ru(bpy)₃Cl₂•6H₂O (0.010 mmol, 5 mol%), and 2.0 mL MeCN (0.1 M). The cuvette was sealed with a rubber septum and parafilm, then degassed by sparging with N₂ for 15 min. The reaction was stirred and irradiated (λ = 436 nm, slit width = 10.0 nm) for 900 s (15 min). After irradiation, the solution was passed through a silica plug. The yield of product formed was determined by ¹H NMR based on a dibromomethane standard. The quantum yield was determined using eq 4-7. Essentially all incident light (*f* > 0.999, *vide infra*) is absorbed by the Ru(bpy)₃Cl₂ at the reaction conditions described above.

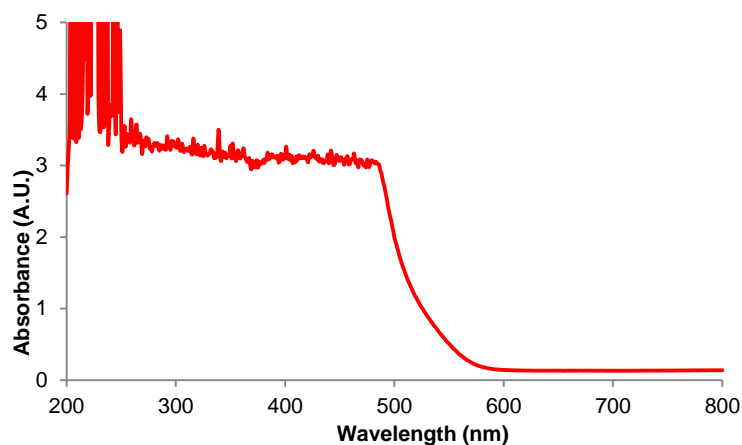
Experiment 1: 60.8 mg (0.20 mmol) of **4.6**, 70 μL (0.40 mmol) *i*-Pr₂NEt, 37.5 mg (0.40 mmol) LiBF₄, 7.5 mg Ru(bpy)₃Cl₂•6H₂O (0.010 mmol), 2.0 mL MeCN after 900 s yielded 23% of **4.7**. Φ(23%) = 77.

Experiment 2: 60.7 mg (0.20 mmol) of **4.6**, 70 μL (0.40 mmol) *i*-Pr₂NEt, 37.5 mg (0.40 mmol) LiBF₄, 7.5 mg Ru(bpy)₃Cl₂•6H₂O (0.010 mmol), 2.0 mL MeCN after 900 s yielded 23% of **4.7**. $\Phi(23\%) = 76$.

4.4.4.2 Absorbance of catalyst

The absorbance of Ru(bpy)₃Cl₂ in MeCN at a concentration of 1.0×10^{-3} M (20% the reaction conditions above) was measured. Absorbance at 436 nm is >3 indicating the fraction of light absorbed is >0.999.

Figure 4-13. Absorbance of a 1.0×10^{-3} M solution of Ru(bpy)₃Cl₂ in MeCN.



4.4.4.3 Stern–Volmer quenching rate data

Samples were prepared by adding solutions of photocatalyst, quencher, and MeCN to obtain a total volume of 2.0 mL. The cuvette was sealed with a septum and parafilm, and then sparged for 15 min with N₂. The concentration of Ru(bpy)₃Cl₂ was 5.0×10^{-5} M. Samples were irradiated at 451 nm, and emission was detected at 600 nm. The lifetime measurement for Ru(bpy)₃Cl₂ in MeCN (855 ns) was previously reported.²⁸

Figure 4-14. Stern–Volmer quenching of $\text{Ru}(\text{bpy})_3\text{Cl}_2$ and $i\text{-Pr}_2\text{NEt}$. For the amine, $k_q = 7.8 \times 10^6 \text{ M}^{-1} \text{ s}^{-1}$.

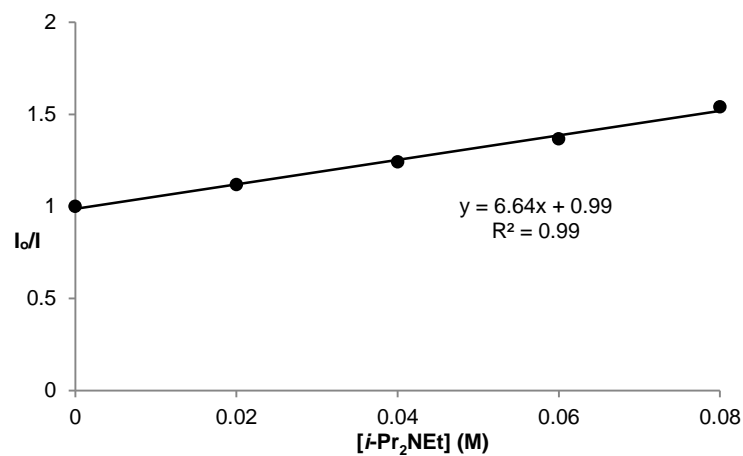


Figure 4-15. Stern–Volmer quenching of $\text{Ru}(\text{bpy})_3\text{Cl}_2$ and LiBF_4 . No quenching observed.

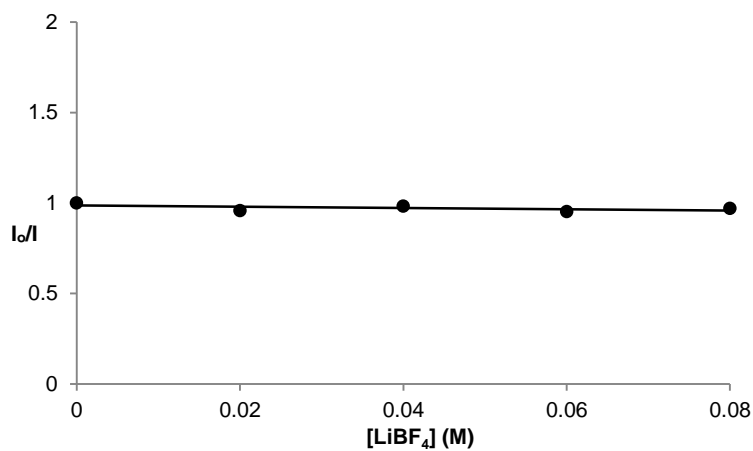
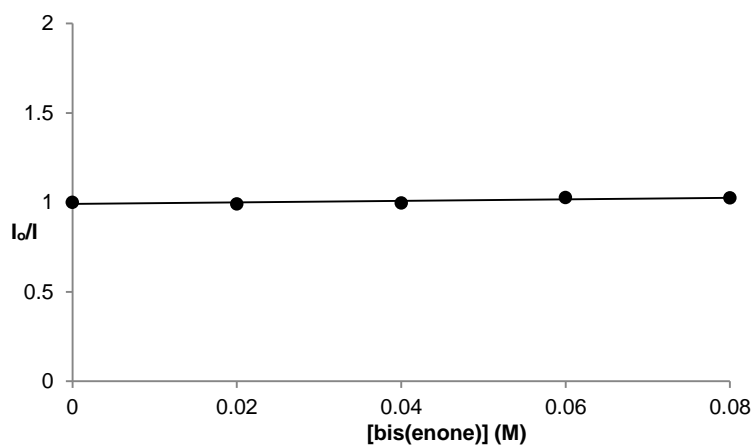


Figure 4-16. Stern–Volmer quenching of $\text{Ru}(\text{bpy})_3\text{Cl}_2$ and the bis(enone) **4.6** starting material. No quenching observed.



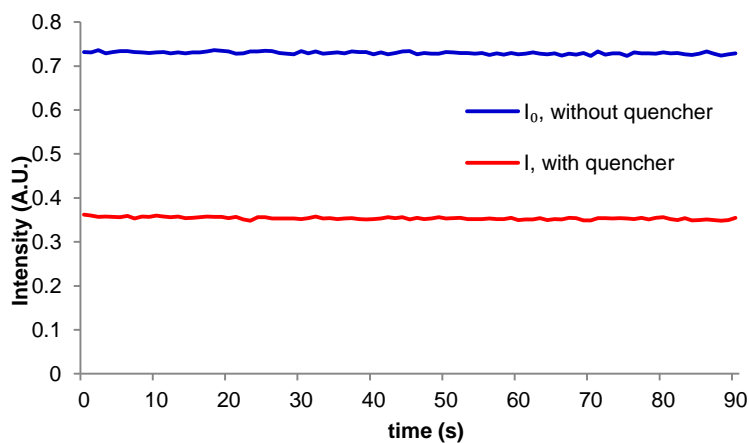
Quenching fraction calculation:

$$\begin{aligned}
 Q &= \frac{k_{q,i\text{-Pr}_2\text{NEt}}[i\text{-Pr}_2\text{NEt}]}{\tau_0^{-1} + k_{q,i\text{-Pr}_2\text{NEt}}[i\text{-Pr}_2\text{NEt}]} \\
 &= \frac{7.8 \times 10^6 \text{ M}^{-1}\text{s}^{-1}[0.20 \text{ M}]}{\frac{1}{8.55 \times 10^{-7} \text{ s}} + 7.8 \times 10^6 \text{ M}^{-1}\text{s}^{-1}[0.20 \text{ M}]} \\
 &= 0.57
 \end{aligned}$$

4.4.4.4 Simple quenching experiment

The luminescence intensity under the reaction conditions (I) was recorded ($\lambda = 600 \text{ nm}$) while being irradiated in the fluorometer for the quantum yield measurement. Luminescence intensity without quencher (I_0) was also recorded for each reaction under the standard reaction conditions but excluding $i\text{-Pr}_2\text{NEt}$. The quenching fraction was determined by eq 4-10 and averaged over the first 90 s of the reaction.

Figure 4-17. Phosphorescence intensity of the reaction over 90 s with (red line) and without (blue line) $i\text{-Pr}_2\text{NEt}$. For this reaction, $Q = 0.50$.



4.4.4.5 Chain length calculation

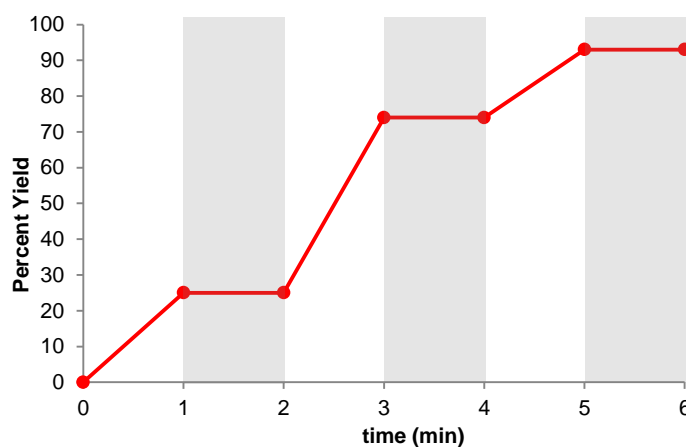
Chain length values calculated in this paper are a lower limit approximation of the actual chain lengths and were calculated using eq 4-11, where Q was calculated either through the Stern–Volmer analysis or the simple quenching experiment.

For the Stern–Volmer analysis, the chain length was calculated to be 135; for the simple quenching experiment, the chain length was 154.

4.4.4.6 Light/dark experiment

A J. Young NMR tube was charged with 30.6 mg (0.10 mmol) **4.6**, 35 μL (0.20 mmol) *i*-Pr₂NEt, 18.8 mg (0.20 mmol) LiBF₄, 3.6 mg (0.048 mmol) Ru(bpy)₃Cl₂•6H₂O, 10.0 μL (0.058 mmol) trimethyl(phenyl)silane, and 1.0 mL (0.1 M) CD₃CN. The vessel was degassed by three freeze-pump-thaw cycles and backfilled with N₂. The reaction was alternatively irradiated with a 20 W CFL bulb and kept in the dark in one minute intervals until the reaction had reached completion. Yields of **4.7** at time points at the start and after each interval were determined by ¹H NMR and based on trimethyl(phenyl)silane as an internal standard.

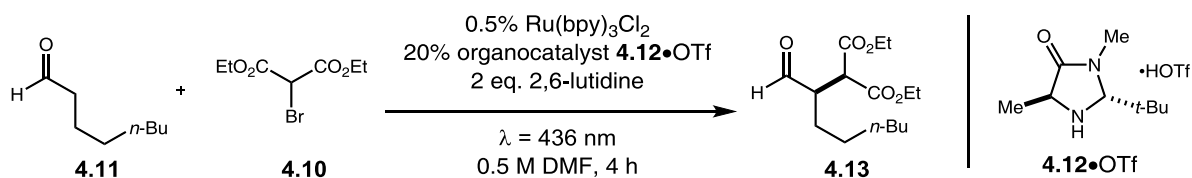
Figure 4-18. Light/dark experiment.



4.4.5 Analysis of α -alkylation of aldehydes reaction

4.4.5.1 Determination of quantum yield

Scheme 4-12. Asymmetric α -alkylation of octanal by diethyl bromomalonate.



A cuvette was charged with octanal (1.3 mmol, 2 equiv), diethyl bromomalonate (0.65 mmol, 1 equiv), $\text{Ru}(\text{bpy})_3\text{Cl}_2 \cdot 6\text{H}_2\text{O}$ (0.0032 mmol, 0.5 mol%), the organocatalyst **4.12**•OTf (0.13 mmol, 20 mol%), 2,6-lutidine (1.3 mmol, 2 equiv) and 1.3 mL DMF (0.5 M). The cuvette was sealed with a rubber septum and parafilm. The cuvette was degassed by sparging with N_2 for 15 min. The reaction was stirred and irradiated ($\lambda = 436 \text{ nm}$, slit width = 10.0 nm) for 14400 s (4 h). After irradiation, the solution was passed through a silica column. The yield of product formed was determined by ^1H NMR based on a trimethyl(phenyl)silane standard. The quantum yield was determined using eq 4-7. Essentially all incident light ($f > 0.999$, *vide infra*) is absorbed by the $\text{Ru}(\text{bpy})_3\text{Cl}_2$ at the reaction conditions described above.

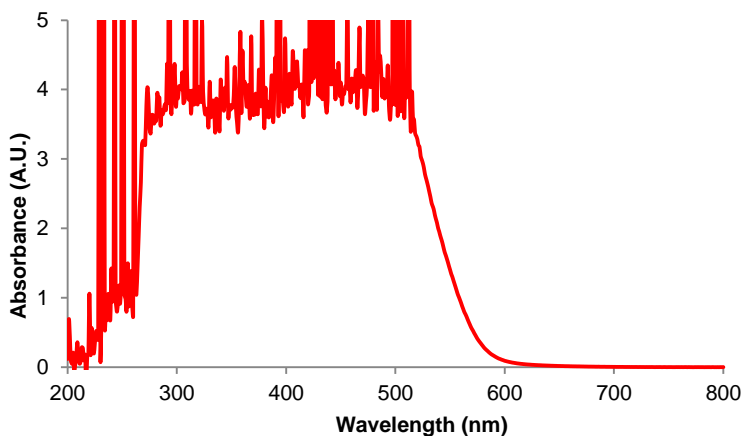
Experiment 1: 200 μL octanal (1.3 mmol), 110 μL diethyl bromomalonate (0.65 mmol), 2.4 mg $\text{Ru}(\text{bpy})_3\text{Cl}_2 \cdot 6\text{H}_2\text{O}$ (0.0032 mmol), 41.3 mg of **4.12**•OTf (0.13 mmol), 150 μL 2,6-lutidine (1.3 mmol) and 1.3 mL DMF after 14400 s yielded 27% of **4.13**. $\Phi(27\%) = 18$.

Experiment 2: 200 μL octanal (1.3 mmol), 110 μL diethyl bromomalonate (0.65 mmol), 2.4 mg $\text{Ru}(\text{bpy})_3\text{Cl}_2 \cdot 6\text{H}_2\text{O}$ (0.0032 mmol), 41.4 mg of **4.12**•OTf (0.13 mmol), 150 μL 2,6-lutidine (1.3 mmol) and 1.3 mL DMF after 14400 s yielded 27% of **4.13**. $\Phi(27\%) = 18$.

4.4.5.2 Absorbance of catalyst

The absorbance of Ru(bpy)₃Cl₂ in DMF was measured at the reaction concentration of 2.5×10^{-3} M. The absorbance at 436 nm is >3 indicating the fraction of light absorbed is >0.999.

Figure 4-19. Absorbance of a 2.5×10^{-3} M solution of Ru(bpy)₃Cl₂ in DMF.



4.4.5.3 Stern–Volmer quenching rate data

Nicewicz and MacMillan report a Stern–Volmer constant ($K_{SV} = k_q\tau_0$) of 10 M^{-1} for the enamine formed *in situ* and found no quenching of Ru(bpy)₃²⁺ by any of the other reagents.³³ The k_q for the enamine was derived from this Stern–Volmer constant ($k_q = 1.1 \times 10^7 \text{ M}^{-1} \text{ s}^{-1}$). The lifetime measurement for Ru(bpy)₃Cl₂ in DMF (912 ns) was previously reported.⁴⁴

The concentration of the enamine at initial reaction conditions was estimated by ¹H NMR. In an NMR tube were combined 75 μL octanal, 41 μL diethyl bromomalonate, 15.4 mg organocatalyst **4.12**•OTf, 45 μL 2,6-lutidine and 0.50 mL DMF. The ¹H NMR showed a 3.2:1 ratio of organocatalyst (**4.12**) to enamine (**4.14**). This corresponds to a 0.018 M concentration of enamine under the standard reaction conditions (0.031 mmol enamine in a total volume of 1.76 mL).

Quenching fraction calculation:

$$\begin{aligned}
 Q &= \frac{k_{q,4.14}[\mathbf{4.14}]}{\tau_0^{-1} + k_{q,4.14}[\mathbf{4.14}]} \\
 &= \frac{1.1 \times 10^7 \text{ M}^{-1}\text{s}^{-1}[0.018 \text{ M}]}{\frac{1}{9.12 \times 10^{-7} \text{ s}} + 1.1 \times 10^7 \text{ M}^{-1}\text{s}^{-1}[0.018 \text{ M}]} \\
 &= 0.15
 \end{aligned}$$

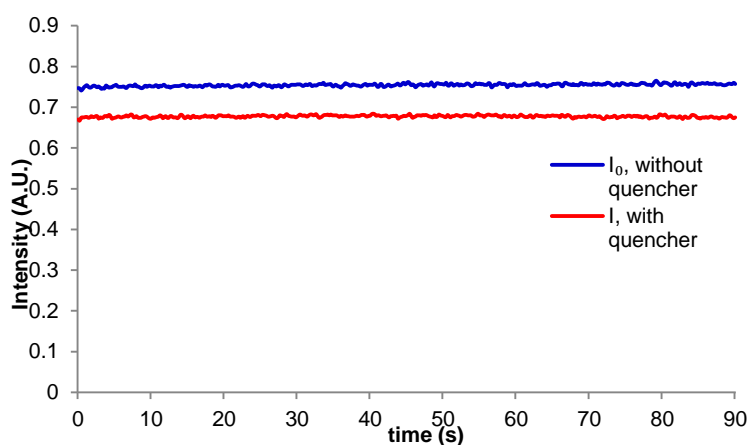
The equilibrium constant, K_{eq} , for enamine formation was calculated using eq 4-13.

$$\begin{aligned}
 K_{\text{eq}} &= \frac{[\mathbf{4.14}][\text{H}_2\text{O}]}{[\mathbf{4.11}][\mathbf{4.12}]} && \text{(eq 4 - 13)} \\
 &= \frac{[0.018 \text{ M}][0.018 \text{ M}]}{[0.71 \text{ M}][0.056 \text{ M}]} \\
 &= 8.1 \times 10^{-3}
 \end{aligned}$$

4.4.5.4 Simple quenching experiment

The quenching fraction was determined by eq 4-10 and averaged over the first 90 s of the reaction. For the α -alkylation, the luminescence intensity (detected at $\lambda = 600 \text{ nm}$) without the organocatalyst quencher **4.12** (I_0) was measured by combining 240 μL (2 equiv) octanal, 230 μL (1 equiv) diethyl bromomalonate, 160 μL (1.8 equiv) 2,6-lutidine, 39.2 mg (0.2 equiv) 2,6-lutidine triflate salt, 2.9 mg (0.5 mol%) $\text{Ru}(\text{bpy})_3\text{Cl}_2 \cdot 6\text{H}_2\text{O}$, and 1.5 mL (0.5 M) DMF in a cuvette. The intensity with the quencher (I) was recorded by combining the above solution with 25.8 mg (0.2 equiv) of **4.12**. The triflic acid is necessary in the I_0 measurement to obtain accurate results.

Figure 4-20. Phosphorescence intensity of the reaction over 90 s with (red line) and without (blue line) organocatalyst **4.12**. For this reaction, $Q = 0.10$.



4.4.5.5 Chain length calculation

Chain length values calculated in this paper are a lower limit approximation of the actual chain lengths and were calculated using eq 4-11, where Q was calculated either through the Stern–Volmer analysis or the simple quenching experiment.

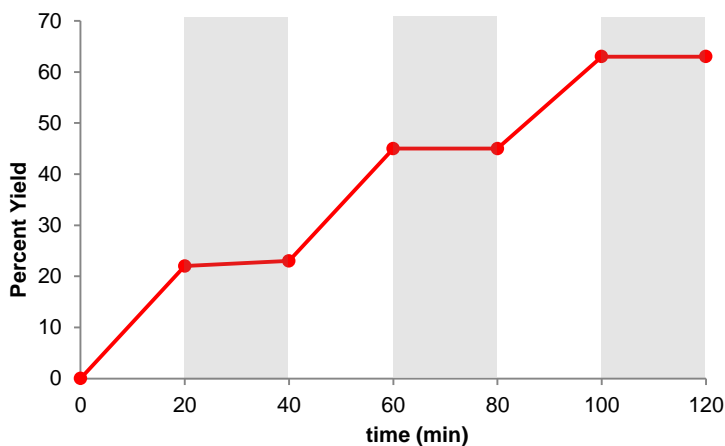
For the Stern–Volmer analysis, the chain length was calculated to be 120; for the simple quenching experiment, the chain length was 180.

4.4.5.6 Light/dark experiment

A Schlenk tube was equipped with a stir bar and charged with 300 μL octanal (1.9 mmol), 165 μL diethyl bromomalonate (0.97 mmol), 3.7 mg $\text{Ru}(\text{bpy})_3\text{Cl}_2 \cdot 6\text{H}_2\text{O}$ (0.0049 mmol), 62.0 mg of **4.12**•OTf (0.19 mmol), 230 μL 2,6-lutidine (2.0 mmol), 40 μL trimethyl(phenyl)silane (0.23 mmol), and 2.0 mL (0.50 M) DMF. The reaction vessel was degassed by three cycles of freeze-pump-thaw and backfilled with N_2 . The reaction was alternatively irradiated with a 20 W CFL bulb and kept in the dark in twenty minute intervals. Aliquots were taken at the start and after

each interval, passed through a silica plug, and diluted with CDCl_3 . Yields of **4.13** were determined by ^1H NMR and based on trimethyl(phenyl)silane as an internal standard.

Figure 4-21. Light/dark experiment.

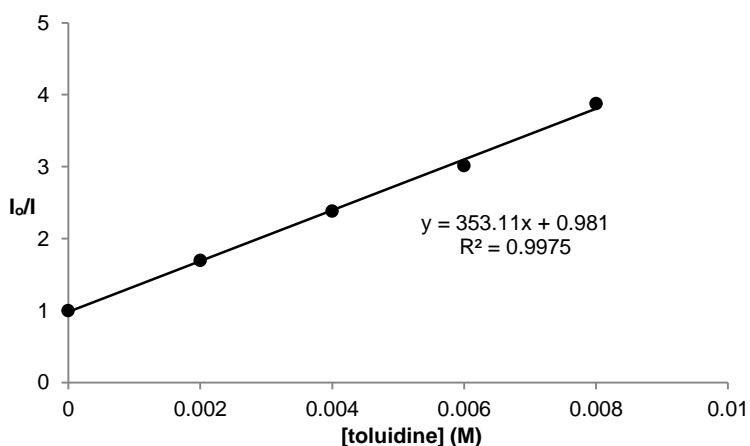


4.4.6 *N,N*-dimethyl-*p*-toluidine studies

4.4.6.1 Stern–Volmer quenching rate data

Samples were prepared by adding solutions of photocatalyst, *N,N*-dimethyl-*p*-toluidine, and DMF to obtain a total volume of 2.0 mL. The cuvette was sealed with a septum and parafilm, and then sparged for 15 min with N_2 . The concentration of $\text{Ru}(\text{bpy})_3\text{Cl}_2$ was 5.0×10^{-5} M. Samples were irradiated at 455 nm, and emission was detected at 600 nm.

Figure 4-22. Stern–Volmer quenching of $\text{Ru}(\text{bpy})_3\text{Cl}_2$ and *N,N*-dimethyl-*p*-toluidine. For the amine, $k_q = 3.9 \times 10^8 \text{ M}^{-1} \text{ s}^{-1}$.

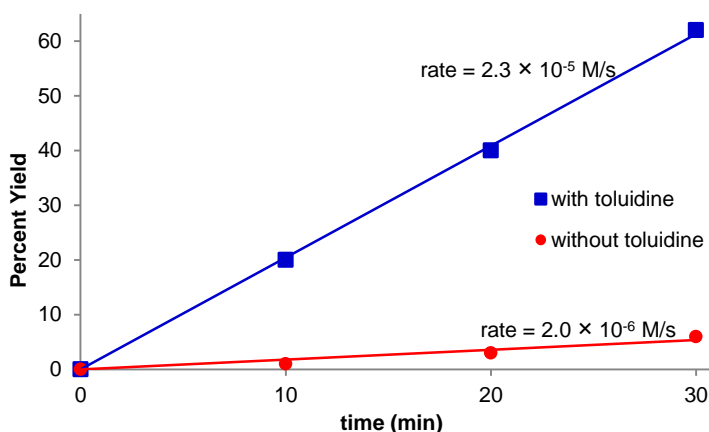


4.4.6.2 Time course experiments

For the standard conditions, a Schlenk tube was equipped with a stir bar and charged with 200 μL octanal (1.3 mmol), 110 μL diethyl bromomalonate (0.65 mmol), 2.4 mg $\text{Ru}(\text{bpy})_3\text{Cl}_2\cdot 6\text{H}_2\text{O}$ (0.0032 mmol), 41.3 mg of **4.12** $\cdot\text{OTf}$ (0.13 mmol), 150 μL 2,6-lutidine (1.3 mmol), 29.5 mg phenanthrene (0.16 mmol), and 1.3 mL (0.50 M) DMF. The reaction vessel was degassed by three cycles of freeze-pump-thaw and backfilled with N_2 . The reaction was alternatively irradiated with a 20 W CFL bulb and kept in the dark in ten minute intervals. Aliquots were taken at the start and after each interval, passed through a silica plug, and concentrated. Yields of **4.13** were determined by ^1H NMR and based on phenanthrene as an internal standard.

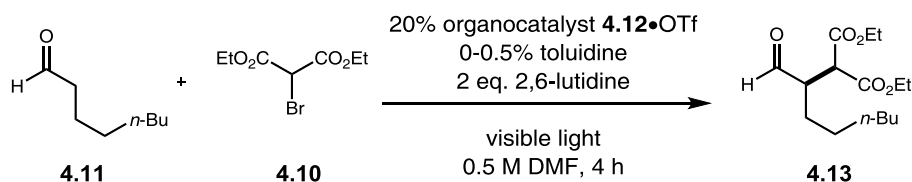
For the addition of exogenous quencher, a Schlenk tube was equipped with a stir bar and charged with 200 μL octanal (1.3 mmol), 110 μL diethyl bromomalonate (0.65 mmol), 2.4 mg $\text{Ru}(\text{bpy})_3\text{Cl}_2\cdot 6\text{H}_2\text{O}$ (0.0032 mmol), 41.4 mg of **4.12** $\cdot\text{OTf}$ (0.13 mmol), 150 μL 2,6-lutidine (1.3 mmol), 0.40 mg *N,N*-dimethyl-*p*-toluidine (0.0030 mmol), 33.6 mg phenanthrene (0.19 mmol), and 1.3 mL (0.50 M) DMF. The reaction vessel was degassed by three cycles of freeze-pump-thaw and backfilled with N_2 . The reaction was alternatively irradiated with a 20 W CFL bulb and kept in the dark in ten minute intervals. Aliquots were taken at the start and after each interval, passed through a silica plug, and concentrated. Yields of **4.13** were determined by ^1H NMR and based on phenanthrene as an internal standard.

Figure 4-23. Time course of the reaction with (blue line) and without (red line) *N,N*-dimethyl-*p*-toluidine.



4.4.6.3 Experiments without Ru(bpy)₃Cl₂

Scheme 4-13. Asymmetric α -alkylation of octanal in the absence of Ru(bpy)₃Cl₂.



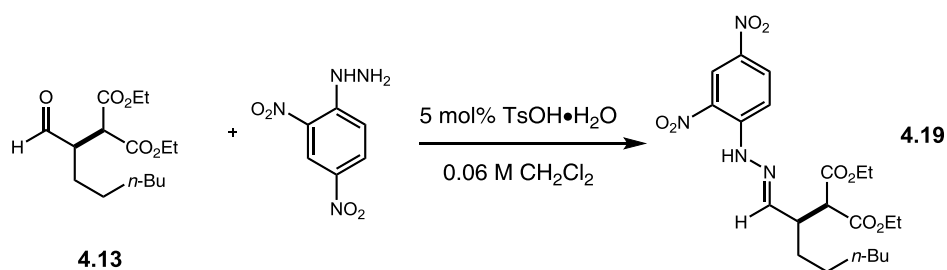
A Schlenk tube was equipped with a stir bar and charged with 200 μ L octanal (1.3 mmol), 110 μ L diethyl bromomalonate (0.65 mmol), 41.3 mg of **4.12**•OTf (0.13 mmol), 150 μ L 2,6-lutidine (1.3 mmol), 26.0 mg phenanthrene (0.15 mmol), and 1.3 mL (0.50 M) DMF. The reaction vessel was degassed by three cycles of freeze-pump-thaw and backfilled with N₂. The reaction was irradiated with a 20 W CFL bulb for 1 h, then passed through a silica plug and concentrated. The reaction yielded 13% of **4.13** as determined by ¹H NMR using phenanthrene as an internal standard.

A Schlenk tube was equipped with a stir bar and charged with 200 μ L octanal (1.3 mmol), 110 μ L diethyl bromomalonate (0.65 mmol), 41.3 mg of **4.12**•OTf (0.13 mmol), 150 μ L 2,6-lutidine (1.3 mmol), 0.40 mg *N,N*-dimethyltoluidine (0.0030 mmol), 30.7 mg phenanthrene (0.17 mmol),

and 1.3 mL (0.50 M) DMF. The reaction vessel was degassed by three cycles of freeze-pump-thaw and backfilled with N₂. The reaction was irradiated with a 20 W CFL bulb for 1 h, then passed through a silica plug and concentrated. The reaction yielded 11% of **4.13** as determined by ¹H NMR using phenanthrene as an internal standard.

4.4.6.4 Determination of enantioselectivity

Scheme 4-14. Conversion of **4.10** into the corresponding hydrazone.



The enantiomeric excess of the product was determined by converting **4.13** into the corresponding hydrazone (**4.19**) using 2,4-dinitrophenylhydrazine. A vial was charged with **4.13** (0.12 mmol, 1 equiv), 2,4-dinitrophenylhydrazine (0.12 mmol, 1 equiv), *p*-toluenesulfonic acid monohydrate (0.0060 mmol, 5 mol%), and 2.0 mL (0.06 M) CH₂Cl₂. The reaction was stirred for 2.5 h and then was purified *via* silica gel chromatography. Enantiomeric excesses were determined by supercritical fluid chromatography (SFC) on a TharSFC investigator instrument equipped with a Waters 2996 photodiode array detector using a Daicel CHIRALCEL[®]OJ-H chiral column, 5-50% MeOH gradient over 15 min, λ = 345 nm, *t*₁ = 4.2 min, *t*₂ = 4.9 min. Racemic **4.13** was synthesized using morpholine in place of **4.12**·OTf.

Figure 4-24. SFC chromatogram of racemic hydrazone **4.19**.

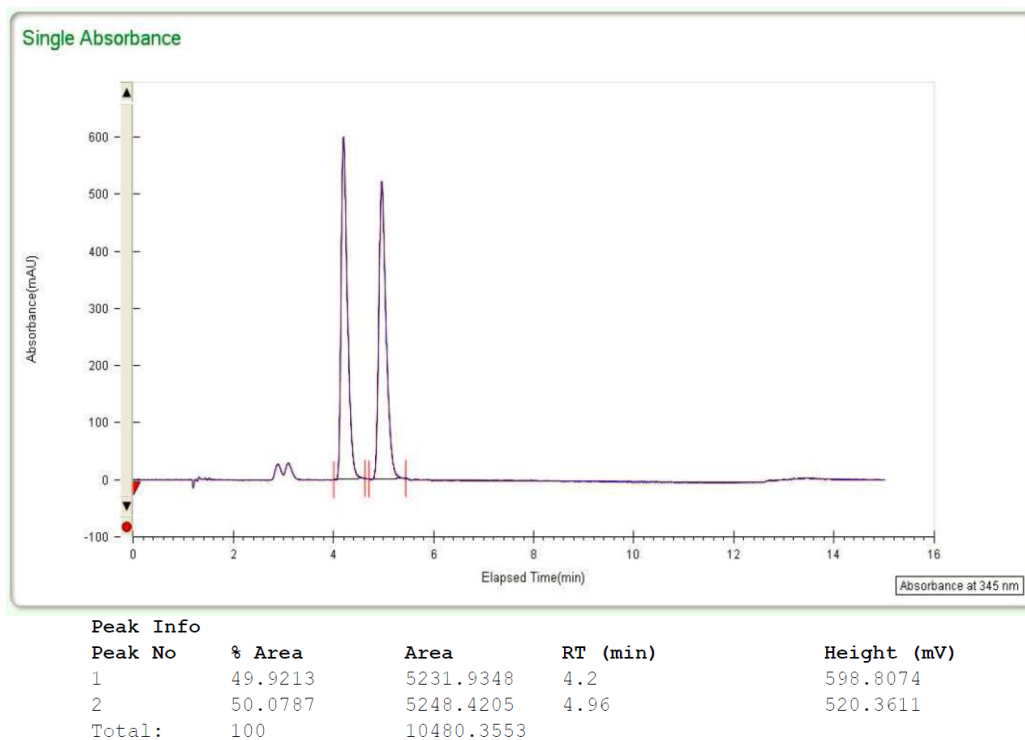


Figure 4-25. SFC chromatogram of **4.19** (90% ee) from **4.13** that was synthesized using the standard conditions reported by MacMillan.³³

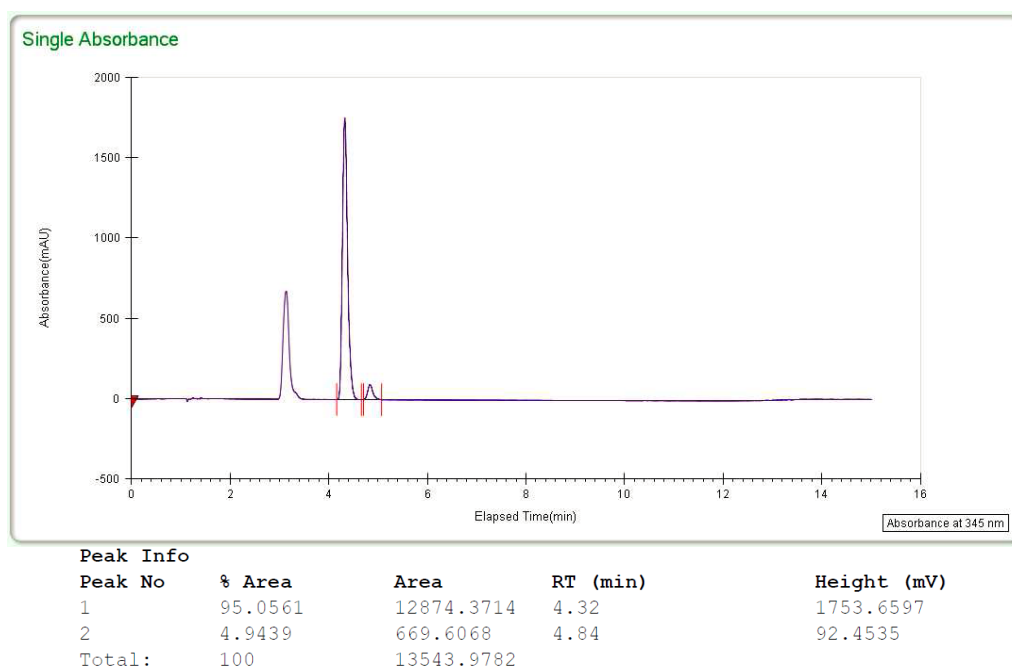
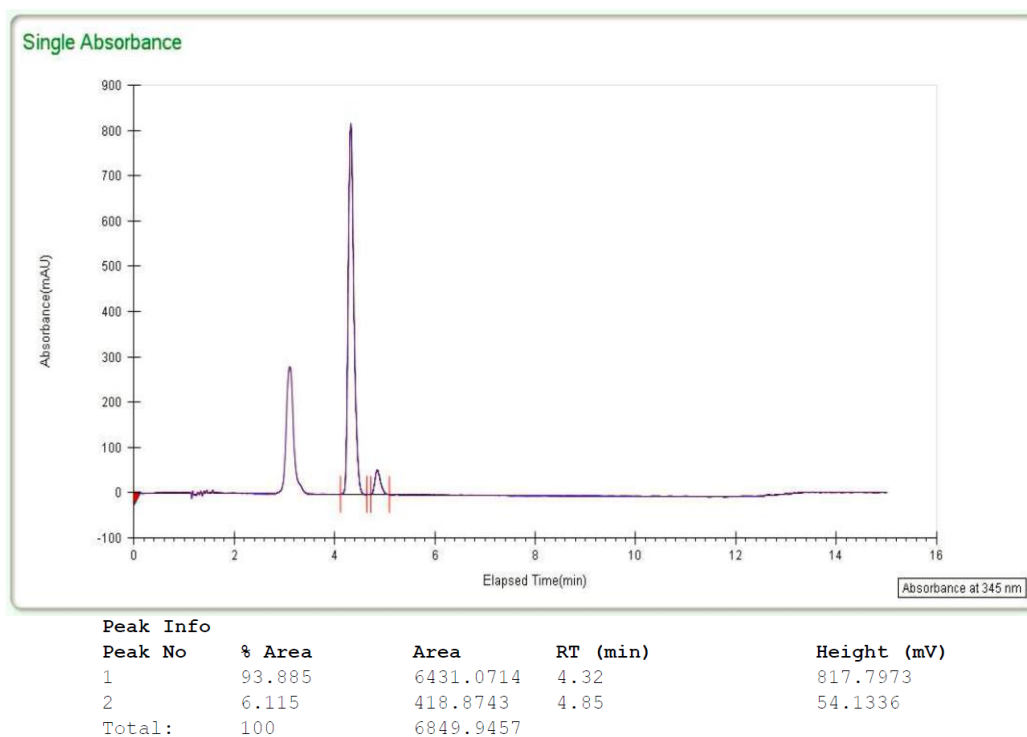


Figure 4-26. SFC chromatogram of **4.19** (88% ee) from **4.13** that was synthesized using the method with *N,N*-dimethyl-*p*-toluidine.



4.5 References

1. Prier, C. K.; Rankic, D. A.; MacMillan, D. W. C. "Visible Light Photoredox Catalysis with Transition Metal Complexes: Applications in Organic Synthesis" *Chem. Rev.* **2013**, *113*, 5322–5363.
2. (a) Furst, L.; Narayanam, J. M. R.; Stephenson, C. R. J. "Total Synthesis of (+)-Gliocladin C Enabled by Visible-Light Photoredox Catalysis" *Angew. Chem. Int. Ed.* **2011**, *50*, 9655–9659; (b) Schnermann, M. J.; Overman, L. E. "A Concise Synthesis of (–)-Aplyviolene Facilitated by a Strategic Tertiary Radical Conjugate Addition" *Angew. Chem. Int. Ed.* **2012**, *51*, 9576–9580; (c) Müller, D. S.; Untiedt, N. L.; Dieskau, A. P.; Lackner, G. L.; Overman, L. E. "Constructing Quaternary Stereogenic Centers Using Tertiary Organocuprates and Tertiary Radicals. Total Synthesis of *trans*-Clerodane Natural Products" *J. Am. Chem. Soc.* **2015**, *137*, 660–663.
3. (a) Nagib, D. A.; MacMillan, D. W. C. "Trifluoromethylation of Arenes and Heteroarenes by Means of Photoredox Catalysis" *Nature* **2011**, *480*, 224–228; (b) DiRocco, D. A.; Dykstra, K.; Krska, S.; Vachal, P.; Conway, D. V.; Tudge, M. "Late-Stage Functionalization of

-
- Biologically Active Heterocycles Through Photoredox Catalysis” *Angew. Chem. Int. Ed.* **2014**, *53*, 4802–4806.
- (a) Fors, B. P.; Hawker, C. J. “Control of a Living Radical Polymerization of Methacrylates by Light” *Angew. Chem. Int. Ed.* **2012**, *51*, 8850–8853; (b) Fors, B. P.; Poelma, J. E.; Menyo, M. S.; Robb, M. J.; Spokoyny, D. M.; Kramer, J. W.; Waite, J. H.; Hawker, C. J. “Fabrication of Unique Chemical Patterns and Concentration Gradients with Visible Light” *J. Am. Chem. Soc.* **2013**, *135*, 14106–14109.
 - (a) Andrews, R. S.; Becker, J. J.; Gagné, M. “Investigating the Rate of Photoreductive Glucosyl Radical Generation” *Org. Lett.* **2011**, *13*, 2406–2409; (b) Tarantino, K. T.; Liu, P.; Knowles, R. R. “Catalytic Ketyl-Olefin Cyclizations Enabled by Proton-Coupled Electron Transfer” *J. Am. Chem. Soc.* **2013**, *135*, 10022–10025; (c) Pitre, S. P.; McTiernan, C. D.; Ismaili, H.; Scaiano, J. C. “Mechanistic Insights and Kinetic Analysis for the Oxidative Hydroxylation of Arylboronic Acids by Visible Light Photoredox Catalysis: A Metal-Free Alternative” *J. Am. Chem. Soc.* **2013**, *135*, 13286–13289; (d) Romero, N.; Nicewicz, D. A. “Mechanistic Insight into the Photoredox Catalysis of Anti-Markovnikov Alkene Hydrofunctionalization Reactions” *J. Am. Chem. Soc.* **2014**, *136*, 17024–17035; (e) Devery, J. J.; Douglas, J. J.; Nguyen, J. D.; Cole, K. P.; Flowers, R. A.; Stephenson, C. R. J. “Ligand functionalization as a deactivation pathway in a *fac*-Ir(ppy)₃-mediated radical addition” *Chem. Sci.* **2015**, *6*, 537–541.
 - (a) Kalyanasundaram, K. “Photophysics, photochemistry and solar energy conversion with tris(bipyridyl)ruthenium(II) and its analogues” *Coord. Chem. Rev.* **1982**, *46*, 159–244; (b) Juris, A.; Balzani, V.; Barigelletti, F.; Campagna, S.; Belser, P.; von Zelewsky, A. “Ru(II) polypyridine complexes: photophysics, photochemistry, electrochemistry, and chemiluminescence” *Coord. Chem. Rev.* **1988**, *84*, 85–277.
 - (a) Ruiz Espelt, L.; Wiensch, E. M.; Yoon, T. P. “Brønsted Acid Cocatalysts in Photocatalytic Radical Addition of α -Amino C–H Bonds across Michael Acceptors” *J. Org. Chem.* **2013**, *78*, 4107–4114; (b) Musacchio, A. J.; Nguyen, L. Q.; Beard, G. H.; Knowles, R. R. “Catalytic Olefin Hydroamination with Aminium Radical Cations: A Photoredox Method for Direct C–N Bond Formation” *J. Am. Chem. Soc.* **2014**, *136*, 12217–12220; (c) McTiernan, C. D.; Pitre, S. P.; Scaiano, J. C. “Photocatalytic Dehalogenation of Vicinal Dibromo Compounds Utilizing Sexithiophene and Visible-Light Irradiation” *ACS Catal.* **2014**, *4*, 4034–4039.
 - (a) Curran, D. P. “The Design and Application of Free Radical Chain Reactions in Organic Synthesis. Part 1” *Synthesis* **1988**, 417–439; (b) Curran, D. P. “The Design and Application of Free Radical Chain Reactions in Organic Synthesis. Part 2” *Synthesis* **1988**, 489–513.
 - An excellent framework for conceptualizing odd-electron chain processes has recently been published: Studer, A.; Curran, D. P. “The electron is a catalyst” *Nature Chem.* **2014**, *6*, 765–773.

-
10. Ruiz Espelt, L.; McPherson, I. S.; Wiensch, E. M.; Yoon, T. P. "Enantioselective Conjugate Additions of α -Amino via Cooperative Photoredox Catalysis" *J. Am. Chem. Soc.* **2015**, *137*, 2452–2455.
11. For a selection of recent studies that report "light/dark" experiments, see: (a) Miyake, Y.; Nakajima, K.; Nishibayashi, Y. "Visible-Light-Mediated Utilization of α -Aminoalkyl Radicals: Addition to Electron-Deficient Alkenes Using Photoredox Catalysis" *J. Am. Chem. Soc.* **2012**, *134*, 3338–3341; (b) Wallentin, C.-J.; Nguyen, J. D.; Finkbeiner, P.; Stephenson, C. R. J. "Visible Light-Mediated Atom Transfer Radical Addition via Oxidative and Reductive Quenching of Photocatalysts" *J. Am. Chem. Soc.* **2012**, *134*, 8875–8884; (c) Jiang, H.; Cheng, Y.; Zhang, Y.; Yu, S. "Sulfonation and Trifluoromethylation of Enol Acetates with Sulfonyl Chlorides Using Visible-Light Photoredox Catalysis" *Eur. J. Org. Chem.* **2013**, 5485–5492; (d) Liu, Q.; Yi, H.; Liu, J.; Yang, Y.; Zhang, X.; Zeng, Z.; Lei, A. "Visible-Light Photocatalytic Radical Alkenylation of α -Carbonyl Alkyl Bromides and Benzyl Bromides" *Chem. Eur. J.* **2013**, *19*, 5120–5126; (e) Liu, X. Y.; Xue, D.; Wang, J. D.; Zhao, C. J.; Zou, Q. Z.; Wang, C.; Xiao, J. L. "Room-Temperature Arylation of Arenes and Heteroarenes with Diaryliodonium Salts by Photoredox Catalysis" *Synlett* **2013**, *24*, 507–513; (f) Sahoo, B.; Hopkinson, M. N.; Glorius, F. "Combining Gold and Photoredox Catalysis: Visible Light-Mediated Oxy- and Aminoarylation of Alkenes" *J. Am. Chem. Soc.* **2013**, *135*, 5505–5508; (g) Mizuta, S.; Engle, K. M.; Verhoog, S.; Galicia-López, O.; O'Duill, M.; Médebielle, M.; Wheelhouse, K.; Rassias, G.; Thompson, A. L.; Gouverneur, V. "Trifluoromethylation of Allylsilanes under Photoredox Catalysis" *Org. Lett.* **2013**, *15*, 1250–1253; (h) Carboni, A.; Dagousset, G.; Magnier, E.; Masson, G. "Photoredox-Induced Three-Component Oxy-, Amino-, and Carbotrifluoromethylation of Enecarbamates" *Org. Lett.* **2014**, *16*, 1240–1243; (i) Dagousset, G.; Carboni, A.; Magnier, E.; Masson, G. "Photoredox-Induced Three-Component Azido- and Aminotrifluoromethylation of Alkenes" *Org. Lett.* **2014**, *16*, 4340–4343; (j) Oh, S. H.; Malpani, Y. R.; Ha, N.; Jung, Y. S.; Han, S. B. "Vicinal Difunctionalization of Alkenes: Chlorotrifluoromethylation with $\text{CF}_3\text{SO}_2\text{Cl}$ by Photoredox Catalysis" *Org. Lett.* **2014**, *16*, 1310–1313.
12. Chain lifetimes on the second or sub-second timescale are common in radical chemistry: (a) Burnett, G. M.; Melville, H. W. "Determination of the Concentration of Intermediaries and of Rate Constants in Radical Reactions" *Chem. Rev.* **1954**, *54*, 225–288; (b) McIntosh, R. G.; Eager, R. L.; Spinks, J. W. T. "Mean Lifetime of Free Radical Chains Determined by a Flow Technique" *Science* **1960**, *131*, 992; (c) McIntosh, R. G.; Eager, R. L.; Spinks, J. W. T. "Mean Lifetime of Free Radical Chains in ^{60}Co γ -Irradiated Chloroform Hydrate and Bromal Hydrate Solutions" *Can. J. Chem.* **1965**, *43*, 3490–3495.
13. For selected reviews, see: (a) Curran, D. P. *Comprehensive Organic Synthesis*, B. M. Trost and I. Fleming, Eds. Pergamon Press 1991, Volume 4, Chapter 4.1, 715–778; (b) Pintauer, T.; Matyjaszewski, K. "Atom transfer radical addition and polymerization reactions catalyzed by ppm amounts of copper complexes" *Chem. Soc. Rev.* **2008**, *37*, 1087–1097; (c) Hoyle, C. E.; Bowman, C. N. "Thiol-Ene Click Chemistry" *Angew. Chem. Int. Ed.* **2010**, *49*, 1540–1573.

-
14. The quantum yield of a photochemical reaction is defined as the ratio of the moles of product formed to the einsteins (mol of photons) absorbed. For a discussion of the concept of quantum yield and its use in studying photochemical reaction mechanisms, see: Julliard, M.; Chanon, M. "Photoelectron-transfer catalysis: its connections with thermal and electrochemical analogs" *Chem. Rev.* **1983**, *83*, 425–506.
 15. An important caveat is that a value of $\Phi < 1$ for the reaction in Scheme 1 could be consistent with either a chain process or a closed catalytic cycle. The observation of small quantum yields, therefore, would be inconclusive.
 16. (a) Lin, S.; Ischay, M. A.; Fry, C. G.; Yoon, T. P. "Radical Cation Diels–Alder Cycloadditions by Visible Light Photocatalysis" *J. Am. Chem. Soc.* **2011**, *133*, 19350–19353; (b) Lin, S.; Padilla, C. E.; Ischay, M. A.; Yoon, T. P. "Visible light photocatalysis of intramolecular radical cation Diels–Alder cycloadditions" *Tetrahedron Lett.* **2012**, *53*, 3073–3076.
 17. (a) Bauld, N. L.; Bellville, D. J.; Harirchian, B.; Lorenz, K. T.; Pabon, R. A.; Reynolds, D. W. Wirth, D. D.; Chiou, H. S.; Marsh, B. K. "Cation radical pericyclic reactions" *Acc. Chem. Res.* **1987**, *20*, 371–378; (b) Bauld, N. L. "Cation radical cycloadditions and related sigmatropic reactions" *Tetrahedron* **1989**, *45*, 5307–5363.
 18. Ledwith, A. "Cation radicals in electron transfer reactions" *Acc. Chem. Res.* **1972**, *5*, 133–139.
 19. (a) Bauld, N. L.; Bellville, D. J.; Pabon, R.; Chelsky, R.; Green, G. "Theory of cation-radical pericyclic reactions" *J. Am. Chem. Soc.* **1983**, *105*, 2378–2382; (b) Bellville, D. J.; Bauld, N. L.; Pabon, R.; Gardner, S. "Theoretical analysis of selectivity in the cation radical Diels–Alder" *A. J. Am. Chem. Soc.* **1983**, *105*, 3584–3588; (c) Pabon, R. A.; Bauld, N. L. "Mechanisms of hole-catalyzed reactions: ab initio theoretical reaction paths for olefin cation radical/olefin cycloaddition" *J. Am. Chem. Soc.* **1984**, *106*, 1145–1146; (d) Lim, H. N.; Parker, K. A. "Total Synthesis of Kingianin A" *Org. Lett.* **2013**, *15*, 398–401; (e) Drew, S. L.; Lawrence, A. L.; Sherburn, M. S. "Total Synthesis of Kingianins A, D, and F" *Angew. Chem. Int. Ed.* **2013**, *52*, 4221–4224.
 20. For instance, see: Crellin, R. A.; Lambert, M. C.; Ledwith, A. "Photochemical 2+2 cycloaddition via a cation-radical chain reaction" *J. Chem. Soc. D: Chem. Commun.* **1970**, 682–693.
 21. Hatchard, C. G.; Parker, C. A. "A New Sensitive Chemical Actinometer. II. Potassium Ferrioxalate as a Standard Chemical Actinometer" *Proc. Roy. Soc. (London)* **1956**, *A235*, 518–536.
 22. The UV-vis spectrum in CH_2Cl_2 can be found in the Experimental section (4.4). For the UV-vis spectrum in MeCN, see: Haga, M.-A.; Dodsworth, E. S.; Eryavec, G.; Seymour, P.;

-
- Lever, A. B. P. "Luminescence quenching of the tris(2,2'-bipyrazine)ruthenium(II) cation and its monoprotonated complex" *Inorg. Chem.* **1985**, *24*, 1901–1906.
23. (a) Bell, F. A.; Crellin, R. A.; Fugii, N.; Ledwith, A. "Cation-radicals: metal-catalyzed cyclodimerisation of aromatic enamines" *J. Chem. Soc., Chem. Commun.* **1969**, 251–252; (b) Carruthers, R. A.; Crellin, R. A.; Ledwith, A. "Cation-radicals: oxygen catalysis in the photosensitized cyclodimerisation of aromatic enamines: *J. Chem. Soc., Chem. Commun.* **1969**, 252–253; (c) Ischay, M. A.; Lu, Z.; Yoon, T. P. "[2+2] Cycloadditions by Oxidative Visible Light Photocatalysis" *J. Am. Chem. Soc.* **2010**, *132*, 8572–8574; (d) Ischay, M. A.; Ament, M. S.; Yoon, T. P. "Crossed intermolecular [2+2] cycloaddition of styrenes by visible light photocatalysis" *Chem. Sci.* **2012**, *3*, 2807–2811.
24. Lorenz, K. T.; Bauld, N. L. "Kinetics and mechanism of aminium salt-initiated cycloadditions: *J. Am. Chem. Soc.* **1987**, *109*, 1157–1160.
25. Schultz, D. A.; Yoon, T. P. "Solar Synthesis: Prospects in Visible Light Photocatalysis" *Science* **2014**, *343*, 1239176.
26. (a) Ischay, M. A.; Anzovino, M. E.; Du, J.; Yoon, T. P. "Efficient Visible Light Photocatalysis of [2+2] Enone Cycloadditions" *J. Am. Chem. Soc.* **2008**, *130*, 12886–12887; (b) Du, J.; Yoon, T. P. "Crossed Intermolecular [2+2] Cycloadditions of Acyclic Enones via Visible Light Photocatalysis" *J. Am. Chem. Soc.* **2009**, *131*, 14604–14605.
27. See the Experimental section (4.4) for complete details.
28. Caspar, J. V.; Meyer, T. J. "Photochemistry of Ru(bpy)₃²⁺. Solvent effects" *J. Am. Chem. Soc.* **1983**, *105*, 5583–5590.
29. This value for the quenching of Ru*(bpy)₃²⁺ by *i*-Pr₂NEt is in good accord with that recently reported by Scaiano. See Ref 5c.
30. Scaiano has proposed that α-aminoradicals derived from photooxidation of *i*-Pr₂NEt might be involved in a conceptually similar reductive coupling of aryl enones under photoredox conditions. We cannot rule out the possibility that α-aminoradicals are initiators of this [2+2] cycloaddition as well, although we have not been able to observe byproducts resulting from oxidation of *i*-Pr₂NEt in the unpurified reaction mixtures arising from cycloaddition of **4.6**. Nevertheless, in the limiting scenario where [*i*-Pr₂NEt^{•+}] is never reduced by **4.9**^{•-} and always results in reduction of **4.8**, the error in the chain length calculation could maximally be a factor of 2. Thus, whether or not Scaiano's proposal is operational in the [2+2] cycloaddition of **6**, the evidence for a chain process remains unambiguous. See: Ismaili, H.; Pitre, S. P.; Scaiano, J. C. "Active participation of amine-derived radicals in photoredox catalysis as exemplified by a reductive cyclization" *Catal. Sci. Technol.* **2013**, *3*, 935–937.
31. A reviewer correctly pointed out that our calculation relies upon the exceptionally high intersystem crossing (ISC) quantum yield of 1 that is characteristic of Ru(bpy)₃²⁺ and its

- analogues; other common photosensitizers often reach their relevant excited states with much lower efficiency, a factor that could even further deflate the macroscopic quantum yield with respect to the true chain length. For a discussion of the ISC quantum yield of $\text{Ru}(\text{bpy})_3^{2+}$, see: Demas, J. N.; Taylor, D. G. "On the 'intersystem crossing' yields in ruthenium(II) and osmium(II) photosensitizers" *Inorg. Chem.* **1979**, *18*, 3177–3179.
32. Felton, G. A. N.; Bauld, N. L. "Efficient electrocatalytic intramolecular anion radical cyclobutanation reactions" *Tetrahedron* **2004**, *60*, 10999–11010.
 33. Yoon, T. P. "Visible Light Photocatalysis: The Development of Photocatalytic Radical Ion Cycloadditions" *ACS Catal.* **2013**, *3*, 895–902.
 34. Nicewicz, D. A.; MacMillan, D. W. C. "Merging Photoredox Catalysis with Organocatalysis: The Direct Asymmetric Alkylation of Aldehydes" *Science* **2008**, *322*, 77–80.
 35. Megerle, U.; Lechner, R.; König, B.; Riedle, E. "Laboratory apparatus for the accurate, facile and rapid determination of visible light photoreaction quantum yields" *Photochem. Photobiol. Sci.* **2010**, *9*, 1400–1406.
 36. Demas, J. N.; Diamente, D.; Harris, W. "Oxygen quenching of charge-transfer excited states of ruthenium(II) complexes. Evidence for singlet oxygen production" *J. Am. Chem. Soc.* **1973**, *95*, 6864–6865.
 37. The value of $k_q = 3.9 \times 10^8 \text{ M}^{-1} \text{ s}^{-1}$ reported in Figure 4-4 was measured in DMF. See the Experimental section (4.4) for details. For the value in MeCN, see: Bock, C. R.; Connor, J. A.; Gutierrez, A. R.; Meyer, T. J.; Whitten, D. G.; Sullivan, B. P.; Nagle, J. K. "Estimation of excited-state redox potentials by electron-transfer quenching. Application of electron-transfer theory to excited-state redox processes" *J. Am. Chem. Soc.* **1979**, *101*, 4815–4824.
 38. We observe a slow rate of product formation promoted by direct, uncatalyzed photoexcitation of enamine **4.14**, consistent with a very recent report by Melchiorre: Silvi, M.; Arceo, E.; Jurberg, I. D.; Cassani, C.; Melchiorre, P. "Enantioselective Organocatalytic Alkylation of Aldehydes and Enals Driven by the Direct Photoexcitation of Enamides" *J. Am. Chem. Soc.* **2015**, *137*, 6120–6123.
 39. Ogawa, K. A.; Goetz, A. E.; Boydston, A. J. "Metal-Free Ring-Opening Metathesis Polymerization" *J. Am. Chem. Soc.* **2015**, *137*, 1400–1403.
 40. Pagnorn, A. B.; Giardello, M. A.; Grubbs, R. H.; Rosen, R. K.; Timmers, F. J. "Safe and Convenient Procedure for Solvent Purification" *Organometallics* **1996**, *15*, 1518–1520.
 41. Schultz, D. M.; Sawicki, J. W.; Yoon, T. P. "An improved procedure for the preparation of $\text{Ru}(\text{bpz})_3(\text{PF}_6)_2$ via a high-yielding synthesis of 2,2'-bipyrazine" *Beilstein J. Org. Chem.* **2015**, *11*, 61–65.

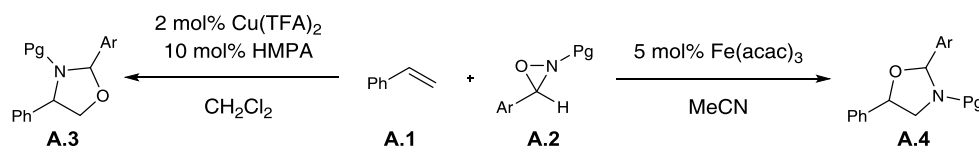
-
42. Wang, L. -C.; Jang, H. -Y.; Roh, Y.; Lynch, V.; Schultz, A. J.; Wang, X.; Krische, M. J. "Diastereoselective Cycloreductions and Cycloadditions Catalyzed by Co(dpm)₂-Silane (dpm = 2,2,6,6-tetramethylheptane-3,5-dionate): Mechanism and Partitioning of Hydrometallative versus Anion Radical Pathways" *J. Am. Chem. Soc.* **2002**, *124*, 9448–9453.
 43. Graham, T. H.; Horning, B. D.; MacMillan, D. W. C. "The preparation of (2*R*,5*S*)-2-*t*-butyl-3,5-dimethylimidazolidin-4-one" *Org. Syn.* **2011**, *88*, 42–54.
 44. For useful references on the actinometry: a) Kuhn, H. J.; Braslavsky, S. E.; Schmidt, R. "Chemical Actinometry" *Pure Appl. Chem.* **2004**, *76*, 2105–2146. b) Monalti, M. *et. al.* Chemical Actinometry. *Handbook of Photochemistry*, 3rd Ed; Taylor & Francis Group, LLC. Boca Raton, FL, **2006**, 601–616.
 45. Barqawi, K. R.; Akasheh, T. S.; Beaumont, P. C.; Parsons, B. J.; Phillips, G. O. J. "The luminescent charge-transfer state of ruthenium-pyrazine complexes" *Phys. Chem.* **1988**, *92*, 291–294.
 46. For a χ for oxygen in CH₂Cl₂, see: Shirono, K.; Morimatsu, T.; Takemura, F. "Gas Solubilities (CO₂, O₂, Ar, N₂, H₂, and He) in Liquid Chlorinated Methanes" *J. Chem. Eng. Data* **2008**, *53*, 1867–1871.

Appendix A. Dihydroxylation and Aminohydroxylation of Alkenes

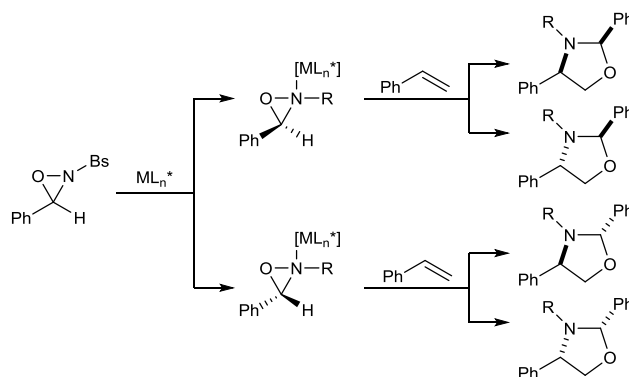
A.1 Introduction

One of the main goals in organic synthesis is to efficiently add complexity to simple compounds. Difunctionalization of alkenes is a powerful route to more complex molecules as it forms two new C–X (X being H, C, or a heteroatom) bonds. In the Yoon group, one of our main areas of research is the use of oxaziridines to functionalize simple organic molecules. More so, we have shown that use of a copper or iron catalyst can activate an oxaziridine towards aminohydroxylation of alkenes with the regioselectivity depending on the catalyst employed (Scheme A-1).¹

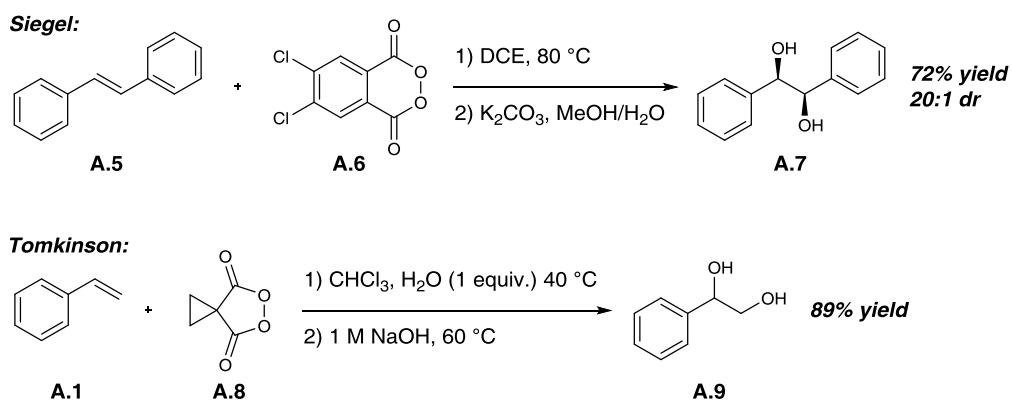
Scheme A-1. Regioselective aminohydroxylation of styrene



As the aminohydroxylation of terminal alkenes, such as styrene, result in the formation of a stereocenter, we have also investigated the enantioselective version of these reactions.² One major problem in the development of enantioselective conditions was that the oxaziridine starting material is chiral, resulting in diastereomers of metal bound oxaziridines. Consequently, the product is formed in one of four stereoisomers (Scheme A-2), two diastereomers and their enantiomers.

Scheme A-2. Possible formation of 4 stereoisomers in the aminohydroxylation of styrene

The use of an achiral reagent would relieve this problem; therefore, we sought to investigate the use of achiral cyclic O–O bond and N–O bond containing oxidants in the enantioselective difunctionalization of alkenes. Our work was inspired by recent publications by both the Siegel³ and Tomkinson⁴ groups on the racemic dihydroxylation of alkenes using cyclic peroxides activated by thermal conditions (Scheme A-3). The peroxides that Siegel and Tomkinson use in their methods are achiral, and as such we were drawn to the phthaloyl and malonyl backbones for possible oxidants to explore.

Scheme A-3. Dihydroxylation of alkenes by cyclic peroxides

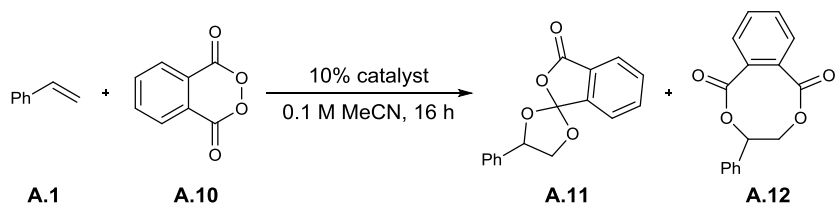
As we have previously developed an enantioselective method to activate the N–O bond of oxaziridines through transition metal-chiral ligand complexes, we hypothesized that we could activate other similar heteroatom–heteroatom bonded compounds in an analogous fashion. We

were interested in the enantioselective method of both aminohydroxylation and dihydroxylation of alkenes; and thus, this appendix summarizes the development of using both achiral peroxides and hydroxylamines oxidants in the presence of an enantioselective catalyst in the enantioselective difunctionalization of alkenes.

A.2 Results and Discussion

A.2.1 Dihydroxylation of alkenes by cyclic peroxides

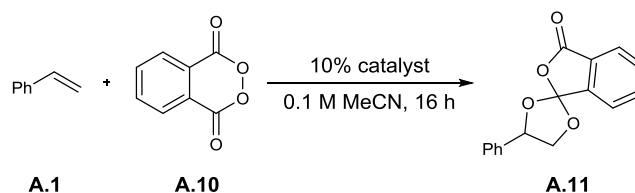
We began our investigations with the dihydroxylation of alkenes by achiral cyclic peroxides. The model system of styrene (**A.1**) as the alkene and phthaloyl peroxide (**A.10**) as the oxidant was chosen for study as **A.10** has been previously synthesized^{3,5} and the subsequent products (**A.11** and **A.12**) been shown to be readily cleaved to the diol.³ A variety of metal catalysts were initially screened for reactivity (Table A-1). In the absence of any catalyst, a minor product **A.12** was formed in low yield. **A.12** was also observed in most reactions in a 1-3% yield. More interestingly, spiro-product **A.11** was formed as one diastereomer in the presence of copper, iron, vanadium, gold and zinc catalysts. As copper gave the highest yields of product and has a rich history in enantioselective catalysis,⁶ it was selected for further study.

Table A-1. Preliminary metal catalyst screen for the dihydroxylation of styrene


Entry	catalyst	A.10 (equiv) ^b	A.11 (%) ^b	A.12 (%) ^b
1	none	1	0	1
2	FeCl ₂	0.8	<1	2
3	FeCl ₃	1	2	3
4	CuCl ₂	0.2	19	2
5	CuI	0	18	2
6	Pd ₂ (dba) ₃	0	0	<2
7	Pd(OAc) ₂	0	0	<2
8	VO(acac) ₂	0	16	3
9	CrCl ₃ ^c	1.1	0	0
10	MnCl ₂ ^c	0.9	5	2
11	CoCl ₂	1.2	0	trace
12	ZnCl ₂	1.5	7	<2
13	IPrAuNTf ₂	1.1	7	1

^a Reaction conducted using 0.17 mmol **A.1**, 0.26 mmol **A.10**, 0.017 mmol catalyst and 1.7 mL MeCN ^b Yields determined by ¹H NMR spectroscopy with respect to TMSPh as standard. ^c Catalyst not fully soluble.

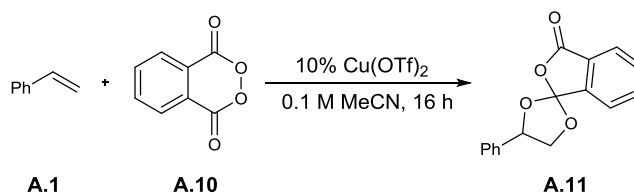
Next, a series of copper catalysts were screened (Table A-2). All copper salts yielded a small amount of product as long as they were soluble in acetonitrile. The best performing catalysts were CuBr₂ (25% yield), Cu(NO₃)₂ (28% yield) and Cu(OTf)₂ (30% yield). Furthermore, the effect of water was probed; addition of 10 equiv of water gave a lower yield while addition of a drying agent (MgSO₄) gave a boost in yield.

Table A-2. Copper screen for the dihydroxylation of styrene

Entry	catalyst	A.10 (equiv) ^b	A.11 (%) ^b
1	CuCl ₂	0.2	19
2	CuCl ^c	0.9	<1
3	CuBr ₂	0.5	25
4	Cu(OH) ₂ ^c	1.3	0
5	CuI	0	18
6	CuSO ₄ ^c	1.3	<1
7	Cu(NO ₃) ₂	trace	28
8	Cu(OAc) ₂	0.8	10
9	Cu(F ₆ acac) ₂	0.1	20
10	Cu(OTf) ₂	trace	30
11	Cu(OTf) ₂ ^d	trace	40
12	Cu(OTf) ₂ ^e	trace	23

^a Reaction conducted using 0.17 mmol **A.1**, 0.26 mmol **A.10**, 0.017 mmol catalyst and 1.7 mL MeCN ^b Yields determined by ¹H NMR spectroscopy with respect to TMSPh as standard. ^c Catalyst not fully soluble. ^d Added MgSO₄. ^e Added 10 equiv. H₂O.

The effect from changing the equivalents of peroxide **A.10** was examined next. In the above reactivity screens, 1.5 equiv of **A.10** were used. Table A-3 shows the yield of product **A.11** with respect to equivalents of peroxide used. At 1 and 1.5 equiv of **A.10**, there is barely any peroxide left, while at 2 and 3 equiv, there is the excess (0.3 and 1.3 equiv, respectively) remaining at the end of the reaction. Additionally, with 1.5 or more equiv of peroxide, styrene is essentially fully consumed. As, the yield halts around 27-29% with 1.5–3 equiv **A.10**, 1.5 equiv of the peroxide was all that is necessary for further screening. Portionwise addition of either the styrene or the peroxide resulted in no change in reactivity.

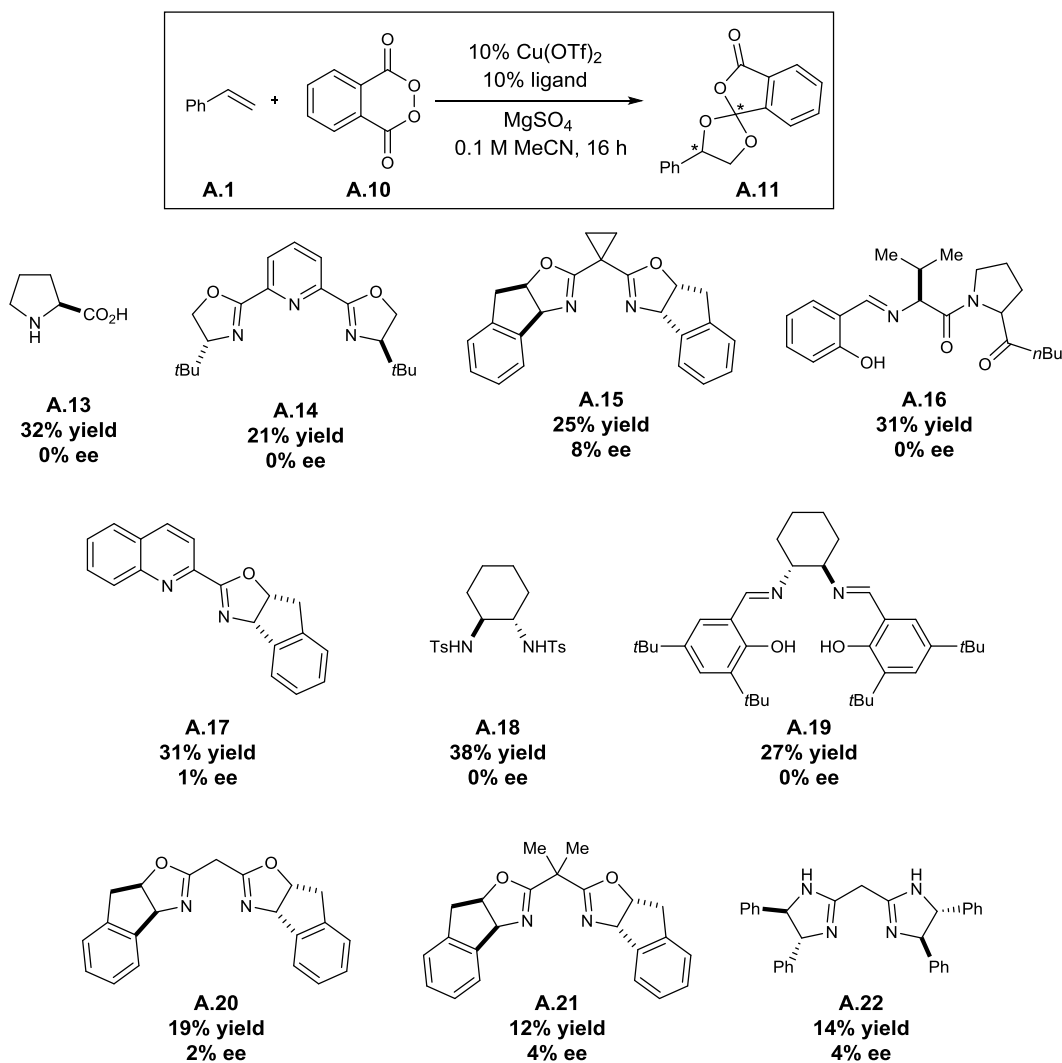
Table A-3. Peroxide equivalent screen

Entry	initial equiv A.10	A.10 (equiv) ^b	A.1 (%) ^c	A.11 (%) ^b
1	1	trace	42	19
2	1.5	trace	5	29
3	2	0.3	1	27
4	3	1.3	trace	29

^a Reaction conducted using 0.17 mmol **A.1**, 0.017 mmol catalyst and 1.7 mL MeCN ^b Yields determined by ¹H NMR spectroscopy with respect to TMSPh as standard. ^c Yields determined by ¹H NMR spectroscopy with respect to decane as standard.

With a modest yield of **A.11** achieved, enantioselective ligands were screened (Figure A-1). A variety of bi- and tridentate ligands were examined with ligands base on a bisoxazoline (Box) and bisimidazoline (Bim) scaffold affording a low enantioselectivity (2-8% ee) albeit at the cost of reactivity. Phosphorous ligands were not screened because **A.10** was shown to oxidize triphenylphosphine readily. Ligand **A.15** gave the highest ee (8%) and a reasonable yield (25%) in comparison to the other ligands screened.

Figure A-1. Enantioselective ligand screen

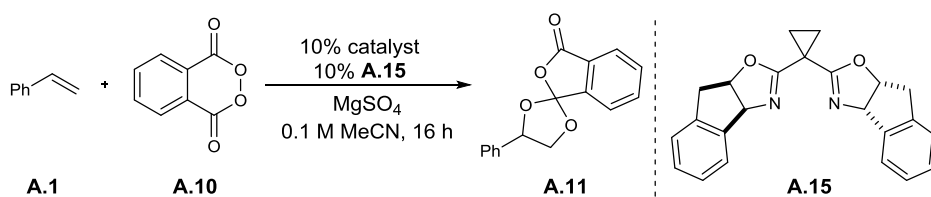


^a Reaction conducted using 0.17 mmol **A.1**, 0.26 mmol **A.10**, 0.017 mmol $\text{Cu}(\text{OTf})_2$, 0.17 mmol ligand, and 1.7 mL MeCN ^b Yields determined by ¹H NMR spectroscopy with respect to TMSPh as standard. Enantiomeric excess determined by SFC.

A solvent screen was performed using many different solvents (*i.e.* dichloromethane, toluene, tetrahydrofuran, ethyl acetate, *N,N*-dimethylformamide, and dimethylsulfoxide) but no reactivity was observed in anything other than in acetonitrile. Additionally, a screen of different metal triflate salts resulted in reactivity worse than $\text{Cu}(\text{OTf})_2$; only salts based on iron, cerium and silver formed product ($\leq 8\%$) and no significant ee ($\leq 2\%$) was observed. However, a rescreen of copper salts in the presence of a ligand (Table A-4), gave some interesting results. Both

CuOTf and CuBr₂ showed a dramatic increase in the enantioselectivity (22% ee) but at a lower product yield (15% and 10%, respectively). On the other hand, Cu(NTf₂)₂ showed an increase in yield (36%) but at expense of the enantioselectivity (2% ee).

Table A-4. Copper metal screen with ligand **A.15**



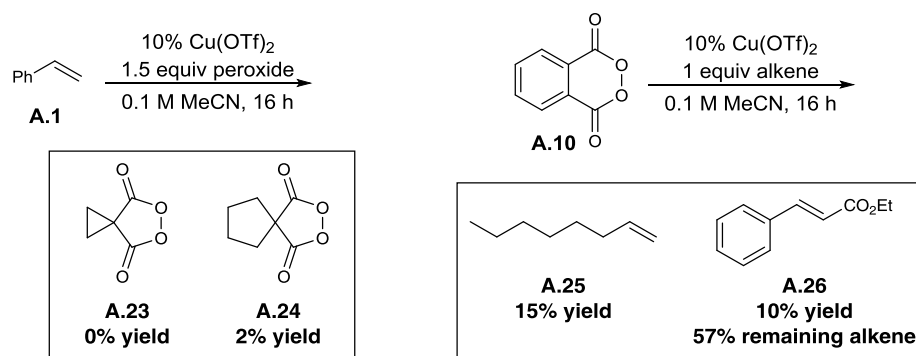
Entry	catalyst	A.10 (equiv) ^b	A.1 (%) ^c	A.11 (% yield/% ee) ^{b,d}
1	CuOTf • 4 MeCN	0	nd	15/22
2	CuF ₂	1.0	nd	<1/nd
3	CuCl	0.5	nd	3/nd
4	CuCl ₂	0.8	62	<3/nd
5	CuBr	0.6	nd	3/nd
6	CuBr ₂	0.2	7	10/22
7	CuI	0.7	nd	<2/nd
8	Cu(NO ₃) ₂	1.1	76	trace/nd
9	Cu(OTf) ₂	trace	0	30/8
10	Cu(OAc) ₂	0.7	62	2/nd
11	Cu(TFA) ₂	1.3	75	trace/nd
12	Cu(benzoate) ₂	0.9	62	<2/nd
13	Cu(F ₆ acac) ₂	0.8	67	2/nd
14	Cu(mesityl)	0.8	68	<3/nd
15	CuPF ₆ • 4 MeCN	1.0	75	<2/nd
16	Cu(NTf ₂) ₂	0	2	36/2

^a Reaction conducted using 0.17 mmol **A.1**, 0.017 mmol catalyst, 0.017 mmol **A.15** and 1.7 mL MeCN ^b Yields determined by ¹H NMR spectroscopy with respect to TMSPh as standard. ^c Yields determined by GC with respect to decane as standard. ^d Enantiomeric excess determined by SFC.

Other alkenes and peroxides were investigated (Figure A-2). Spirocyclic peroxides **A.23** and **A.24**, previously been investigated by Tomkinson or the dihydroxylation of alkenes,^{4a} yielded little to no product with styrene as the alkene. 1-Octene in the presence of peroxide **A.10** yielded 15% of a product (unknown if it is analogous to spiro-product **A.11** or the eight-membered ring product **A.12**). Ethyl cinnamate yielded only 10% of the spiro-product but promisingly had a

better mass balance (more alkene was recovered). Further investigations into the dihydroxylation of ethyl cinnamate resulted in low yields and poor enantioselectivities.

Figure A-2. Different alkenes and peroxides investigated

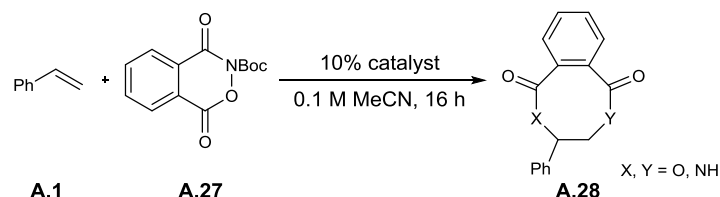


A.2.2 Aminohydroxylation of styrene by cyclic hydroxylamines

The aminohydroxylation of styrene was also investigated using cyclic hydroxylamines. Cyclic hydroxylamine **A.27**, analogous to the phthaloyl peroxide **A.10**, was synthesized in a similar fashion as described by Siegel.³ Table A-5 summarizes the screening efforts of **A.27** (1 equiv) with styrene (5 equiv) in the presence of 10% catalyst in MeCN. Many palladium, nickel, iron and zinc catalysts were investigated but yielded no product. In many cases, **A.27** decomposed under the reaction conditions yielding mostly deprotected material. While most copper salts investigated gave no reactivity, $\text{Cu}(\text{BF}_4)_2$ resulted in 2% yield of an eight-membered ring **A.28** with unknown regioselectivity. $\text{Cu}(\text{NO}_3)_2$ and $\text{Cu}(\text{ClO}_4)_2$ also showed promise with trace amounts of other potential products (as seen by ^1H NMR spectroscopy). A screen of $\text{Cu}(\text{BF}_4)_2$ as the catalyst in a variety of solvents (toluene, diethyl ether, dichloromethane, tetrahydrofuran, *N,N*-dimethylformamide, acetone, ethyl acetate, dimethylsulfoxide, 1,4-dioxane,

isopropylalcohol, water) resulted in no product formation at all but in almost all cases deprotection of **A.27** was observed.

Table A-5. Metal catalyst screen in the aminohydroxylation of styrene



Entry	catalyst	A.27 (%) ^b	A.28 (%) ^b
1	Pd(OAc) ₂ ^c	89 ^d	0
2	PdBr ₂ ^c	74 ^d	0
3	Pd ₂ (dba) ₃ ^c	89	0
4	Pd(PPh ₃) ₄ ^c	66 ^d	0
5	Ni(OTf) ₂	89	0
6	Ni(COD) ₂	89	0
7	Fe(OTf) ₂	18 ^d	0
8	Fe(OTf) ₃	0 ^d	0
9	ZnCl ₂	75 ^d	0
10	Zn(OTf) ₂	83 ^d	0
11	CuOTf	90	0
12	Cu(OTf) ₂	0 ^d	0
13	Cu(ClO ₄) ₂	trace ^d	0 ^e
14	Cu(OAc) ₂	93	0
15	CuBr ₂	93	0
16	Cu(NO ₃) ₂	76	0 ^e
17	CuBr	91	0
18	Cu(BF ₄) ₂	36 ^d	2

^a Reaction conducted using 0.87 mmol **A.1**, 0.17 mmol **A.27**, 0.017 mmol catalyst and 1.7 mL

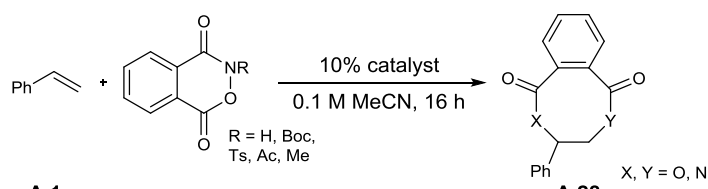
MeCN ^b Yields determined by ¹H NMR spectroscopy with respect to TMSPh as standard.

^c Reaction conducted at 50 °C. ^d Decomposition of **A.27** was observed including deprotection and anhydride formation. ^e Other potential products observed in trace amounts.

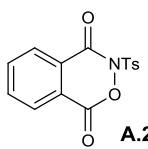
As the product **A.28** has no protecting group on the nitrogen, we wanted to further investigate the role of the protecting group in the aminohydroxylation (Table A-6). The three catalysts that resulted in product formation (Cu(BF₄)₂, Cu(NO₃)₂, and Cu(ClO₄)₂) were screened amongst a few standard protecting groups for nitrogen as well as the unprotected version. Tosyl and methyl protecting groups resulted in no formation of product along with no deprotection of

the starting materials (**A.29** and **A.31**, respectively). Use of the acetyl protecting group (**A.30**) resulted in trace amounts of product formation along with the appearance of deacylated starting material. The unprotected version of the starting material, **A.32**, yielded the same results as the original Boc-protected **A.27**. These data lead us to hypothesize that the starting material first undergoes a deprotection before aminohydroxylation occurs. Oxidant **A.32** was chosen for further investigation.

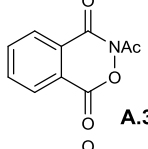
Table A-6. Investigation of the protecting group of the oxidant



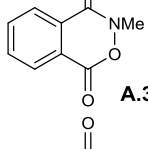
Entry	catalyst	R =	oxidant (%) ^b	A.28 (%) ^b
1	Cu(NO ₃) ₂	Boc	76	0 ^d
2	Cu(BF ₄) ₂	Boc	36 ^c	2
3	Cu(ClO ₄) ₂	Boc	trace ^c	0 ^d
4	Cu(NO ₃) ₂	Ts	93	0
5	Cu(BF ₄) ₂	Ts	93	0
6	Cu(ClO ₄) ₂	Ts	92	0
7	Cu(NO ₃) ₂	Ac	75	trace
8	Cu(BF ₄) ₂	Ac	72 ^c	trace
9	Cu(ClO ₄) ₂	Ac	59 ^c	0
10	Cu(NO ₃) ₂	Me	93	0
11	Cu(BF ₄) ₂	Me	95	0
12	Cu(ClO ₄) ₂	Me	93	0
13	Cu(NO ₃) ₂	H	79	0 ^e
14	Cu(BF ₄) ₂	H	84	2
15	Cu(ClO ₄) ₂	H	80	0



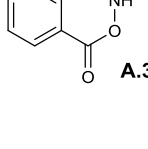
A.29



A.30



A.31



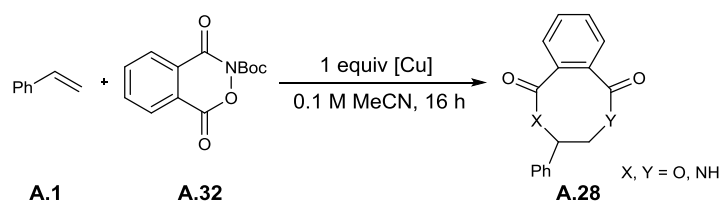
A.32

^a Reaction conducted using 0.87 mmol **A.1**, 0.17 mmol oxidant, 0.017 mmol catalyst and 1.7 mL MeCN ^b Yields determined by ¹H NMR spectroscopy with respect to TMSPh as standard. ^c Deprotection of starting material was observed. ^d Other potential products observed in trace amounts.

We then investigated the use of stoichiometric amounts of copper salts (for Cu(NO₃)₂ and Cu(BF₄)₂) with the unprotected **A.32**. At a full equivalent of copper, the yield increases (up to 12%) for both salts investigated. For Cu(NO₃)₂, an increase in temperature (50 °C and 80 °C)

also lead to an increase in yield (7% and 10-15%, respectively) of product **A.28** but also increases the amount of other products observed in the ^1H NMR. However, with $\text{Cu}(\text{BF}_4)_2$, an increase in temperature does not affect the yield.

Table A-7. Stoichiometric use of copper salts and the effect of temperature



Entry	[Cu]	temp (°C)	A.32 (%) ^b	A.28 (%) ^b
1	$\text{Cu}(\text{NO}_3)_2$	23	62	2 ^c
2	$\text{Cu}(\text{BF}_4)_2$	23	72	12
3	$\text{Cu}(\text{NO}_3)_2$	50	13	7 ^c
4	$\text{Cu}(\text{BF}_4)_2$	50	49	13
5	$\text{Cu}(\text{NO}_3)_2$	80	<12	10-15 ^c
6	$\text{Cu}(\text{BF}_4)_2$	80	38	10

^a Reaction conducted using 0.87 mmol **A.1**, 0.17 mmol **A.32**, 0.017 mmol catalyst and 1.7 mL MeCN ^b Yields determined by ^1H NMR spectroscopy with respect to TMSPh as standard. ^c Other potential products observed in <5% yield. ^d 11% and 14% of other potential products observed.

A.3 Conclusions and Future Directions

We have demonstrated that using copper metal catalysts, the dihydroxylation and aminohydroxylation of styrene can be achieved using achiral oxidants. In the case of dihydroxylation, combination of the copper catalyst with a chiral ligand can impart some amount of stereochemical control. At this point the yields and enantioselectivities are still low, and further optimization is necessary to develop a synthetically useful method.

A.4 Experimental

A.4.1 Synthesis of phthaloyl peroxide A.10

CAUTION: Peroxides are dangerous and should be handled with care.

A 50 mL Erlenmeyer flask with a large magnetic stir bar was charged with 8.5 g urea hydrogen peroxide (90 mmol) and 25 mL of methanesulfonic acid. Phthalic acid (5.0 g, 30 mmol) was added and the reaction was stirred vigorously for 18 h. The reaction mixture was poured onto a mixture of ice and ethyl acetate and the layers were separated. The aqueous layer was extracted twice with ethyl acetate. The combine organic layers were washed twice with saturated aqueous sodium bicarbonate and once with brine, then dried over MgSO₄. Solvent was removed by a rotary evaporator at 23 °C. The crude solid was recrystallized with care in hexanes and ethyl acetate to yield 2.2 g (13 mmol, 45%) of white crystals. All spectra data were consistent with reported values.³

A.4.2 General method for the dihydroxylation of styrene

A 2 dram vial with magnetic stir bar was charged with 1.5 equiv peroxide (0.26 mmol), 10 mol% catalyst (0.017 mmol), and 10 mol% ligand (0.017 mmol). The solids were dissolved in 1.7 mL MeCN, and styrene (0.17 mmol) was added. Reactions were sealed and stirred for 16 h. The reaction mixture was diluted with ethyl acetate, washed with saturated aqueous ammonium chloride and dried over MgSO₄. Solvent was removed *in vacuo*.

A.4.3 Synthesis of aminohydroxylating reagents A.27, A.29-A.32

An Erlenmeyer flask was charged with 1 equiv of the appropriate hydroxylamine (or its HCl salt) and CH₂Cl₂ (0.2 M). Next, 2 equiv triethylamine (3 equiv if using the HCl salt) was added to the mixture and the flask was chilled in an ice bath. Dropwise, 1.2 equiv of phthaloyl chloride was

added while the reaction was cooled. The reaction was stirred over night at room temperature before being washed twice with 1 M aqueous HCl and once with brine. The organic layers were dried over MgSO₄ and the solvent was concentrated *in vacuo*. The resulting solid was purified by either recrystallization in CH₂Cl₂ or column chromatography in hexanes and ethyl acetate. **A.32** was synthesized by stirring **A.27** in 0.4 M CH₂Cl₂ and 0.4 M trifluoroacetic acid for 45 min and purified by recrystallization.

A.4.4 General method for the aminohydroxylation of styrene

A 2 dram vial with magnetic stir bar was charged with 1 equiv peroxide (0.17 mmol), 10 mol% catalyst (0.017 mmol). The vial was sealed with a rubber septum and sparged with N₂. Dry MeCN (1.7 mL) and styrene (0.87 mmol) were added. Reactions were stirred for 16 h. The reaction mixture was passes through a plug of silica gel and the solvent was removed *in vacuo*.

A.5 References

-
- (a) Michaelis, C. J.; Shaffer, C. J.; Yoon, T. P. "Copper(II)-Catalyzed Aminohydroxylation of Olefins" *J. Am. Chem. Soc.* **2007**, *129*, 1866–1867. (b) Michaelis, D. J.; Ischay, M. A.; Yoon, T. P. "Activation of *N*-Sulfonyl Oxaziridines Using Copper(II) Catalysts: Aminohydroxylations of Styrenes and 1,3-Dienes" *J. Am. Chem. Soc.* **2008**, *130*, 6610–6615. (c) Benkovics, T.; Du, J.; Guzei, I. A.; Yoon, T. P. "Anionic Halocuprate(II) Complexes as Catalysts for the Oxaziridine-Mediated Aminohydroxylation of Olefins" *J. Org. Chem.* **2009**, *74*, 5535–5552. (d) Benkovics, T.; Guzei, I. A.; Yoon, T. P. "Oxaziridine-Mediated Oxyamination of Indoles: An Approach to 3-Aminoindoles and Enantiomerically Enriched 3-Aminopyrrolindolines" *Angew. Chem. Int. Ed.* **2010**, *49*, 9153–9157. (e) DePorter, S. M.; Jacobsen, A. C.; Partridge, K. M.; Williamson, K. S.; Yoon, T. P. "*N*-Nosyl oxaziridines as terminal oxidants in copper(II)-catalyzed olefin oxyaminations" *Tetrahedron Lett.* **2010**, *51*, 5223–5225. (f) Williamson, K. S.; Yoon, T. P. "Iron-Catalyzed Aminohydroxylation of Olefins" *J. Am. Chem. Soc.* **2010**, *132*, 4570–4571.
 - (a) Michaelis, D. J.; Williamson, K. S.; Yoon, T. P. "Oxaziridine-Mediated Enantioselective Aminohydroxylation of Styrenes Catalyzed by Copper(II) Bis(Oxazoline) Complexes"

-
- Tetrahedron* **2009**, *65*, 5118–5124. (b) Williamson, K. S.; Yoon, T. P.; “Iron Catalyzed Asymmetric Oxyaminations of Olefins” *J. Am. Chem. Soc.* **2012**, *134*, 12370–12373.
3. Yuan, C.; Axelrod, A.; Varela, M.; Danysh, L.; Siegel, D. “Synthesis and reaction of phthaloyl peroxide derivatives, potential organocatalysts for the stereospecific dihydroxylation of alkenes” *Tetrahedron Lett.* **2011**, *52*, 2540–2542.
 4. (a) Griffith, J. C.; Jone, K. M.; Picon, S.; Rawling, M. J.; Kariuki, B. M.; Campbell, M.; Tomkinson, N. C. O. “Alkene Syn Dihydroxylation with Malonyl Peroxides” *J. Am. Chem. Soc.* **2010**, *132*, 14409–14411. (b) Jones, K. M.; Tomkinson, N. C. O. “Metal-Free Dihydroxylation of Alkenes using Cyclobutane Malonyl Peroxide” *J. Org. Chem.* **2012**, *77*, 921–928. (c) Picon, S.; Rawling, M.; Campbell, M.; Tomkinson, N. C. O. “Alkene Dihydroxylation with Malonyl Peroxides: Catalysis Using Fluorinated Alcohols” *Org. Lett.* **2012**, *14*, 6250–6253. (d) Rawling, M. J.; Rowley, J. H.; Campbell, M.; Kennedy, A. L.; Parkinson, J. A.; Tomkinson, N. C. O. “Mechanistic insights into the malonyl peroxide *syn*-dihydroxylation of alkenes” *Chem. Sci.* **2014**, *5*, 1777–1785.
 5. Issues regarding the purity and safety of the preparation of **A.10** were experienced. **A.10** was synthesized using the same method as Tomkinson (see ref. 4a) for the preparation of cyclic peroxides. See section A.4.
 6. (a) Johnson, J. S.; Evans, D. A. “Chiral Bis(oxazoline) Copper(II) Complexes: Versatile Catalysts for Enantioselective Cycloaddition, Aldol, Michael, and Carbonyl Ene Reactions” *Acc. Chem. Res.* **2000**, *33*, 325–335. (b) Alexakis, A.; Bäckvall, J. E.; Krause, N.; Pàmies, O.; Diéguez, M. “Enantioselective Copper-Catalyzed Conjugate Addition and Allylic Substitution Reactions” *Chem. Rev.* **2008**, *108*, 2796–2823. (c) Stanley, L. M.; Sibi, M. P. “Enantioselective Copper-Catalyzed 1,3-Dipolar Cycloadditions” *Chem. Rev.* **2008**, *108*, 2887–2902. (d) Shibasaki, M.; Kani, M. “Asymmetric Synthesis of Tertiary Alcohols and α -Tertiary Amines via Cu-Catalyzed C–C Bond Formation to Ketones and Ketimines” *Chem. Rev.* **2008**, *108*, 2853–2873.

Appendix B. Brønsted Acid Catalysis using Cysteic Acids

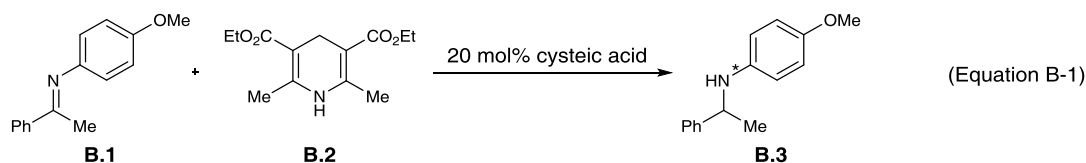
B.1 Introduction

Enantioselective synthesis of organic molecules is a large area of research in the realm of organic chemistry, and as such, many approaches to enantioenriched compounds have been developed. One of these approaches is chiral Brønsted acid catalysis. Over the past decade, the use of strong Brønsted acid catalysts has been explored, however, the majority of this research has focused on binaphthyl (BINOL) derived phosphoric acids.¹ As such, only a small range of acidity is attainable, which limits the possible reactivity.² To increase the acidity of these catalysts, the phosphoric acid has been replaced with more acidic compounds such as phosphoramides, sulfonamides, and sulfonic acids.

In the Yoon group, we are interested in developing strongly acidic chiral Brønsted acid catalysts for enantioselective organocatalysis. Intrigued by the use of peptides as chiral ligands and catalysts in other organic transformations,³ we wondered if we could design a strong Brønsted acid catalyst based on a peptide backbone. We hypothesized that a peptide containing a cysteine amino acid residue could be oxidized to the sulfonic acid (cysteic acid) and thus form a strong Brønsted acid. This appendix details the investigation of cysteic acids as chiral Brønsted acids in the enantioselective reduction of imines.

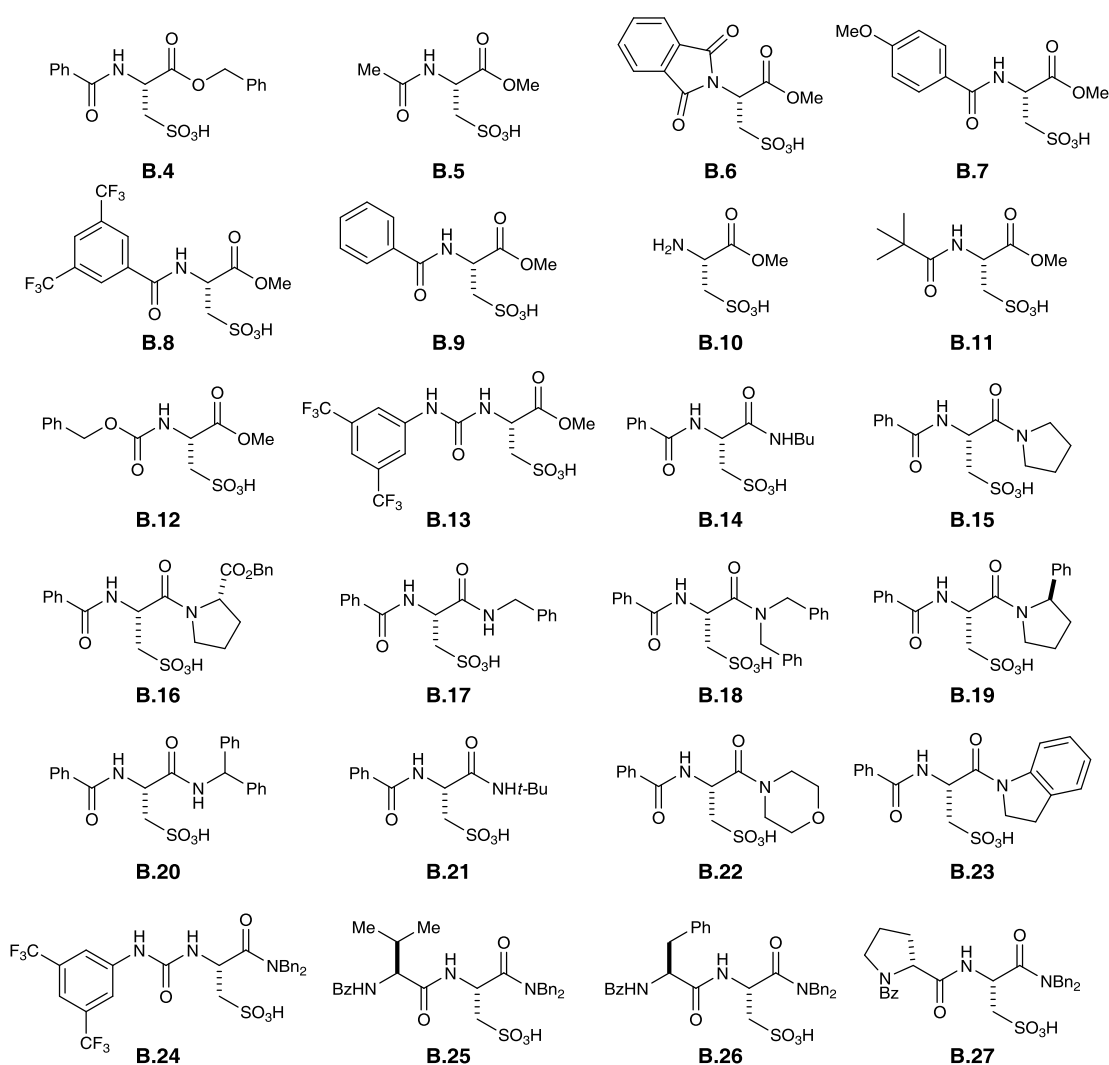
B.2 Results and Discussion

To begin, the reduction of imine **B.1** to amine **B.3** with Hantzsch ester **B.2** as the stoichiometric reductant (Equation B-1) was chosen to test the cysteic acid catalysts for both reactivity and enantioselectivity. This reaction was chosen as it has previously been reported with chiral BINOL phosphoric acids as the Brønsted acid.⁴



Cysteic acids were synthesized from oxidation of the corresponding cystine with performic acid. The cystines were readily derivatized using well-known peptide coupling techniques. A total of 24 cysteic acids were investigated (Figure B-1).

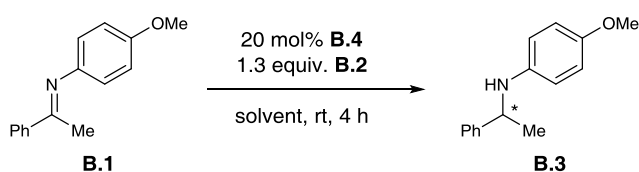
Figure B-1. Structure of the cysteic acids



In Brønsted acid catalysis, the solvent choice is crucial as the strength of the interaction of the acid catalyst with the substrate is dependent upon solvent polarity. Table B-1 details a

screening of solvents using cysteic acid **B.4** in the reduction of **B.1**. Halogenated solvents (chloroform and dichloromethane) yielded the highest product yield after 4 h but resulted in no stereoselectivity. Hexane and ether, likely due to poor solubility of **B.4**, resulted in little to no yield of amine **B.3** and thus the stereoselectivity could not be determined. While toluene, benzene and tetrahydrofuran resulted in moderate yields of **B.1**, a minor amount of enantioselectivity was observed. Due to the low enantioselectivities observed, it is difficult to draw any trends due to solvent polarity at this time. Benzene was chosen for further study as it was the highest yielding of solvents that showed any stereoselectivity.

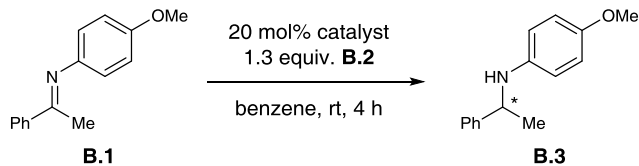
Table B-1. Solvent screen for the reduction of imines



Entry	solvent	B.3 (%) ^b	ee (%) ^c	B.1 (%) ^b
1	hexane ^d	0	n/a	86
2	ether ^d	3	nd	79
3	toluene ^d	24	2	58
4	benzene ^d	40	2	48
5	tetrahydrofuran	20	2	55
6	chloroform	65	0	28
7	dichloromethane	65	0	25

^a Reaction conducted using 0.07 mmol **B.1**, 0.014 mmol **B.4**, 0.09 mmol **B.2** and 1.2 mL solvent. ^b Yields determined by ¹H NMR spectroscopy with respect to CH₂Br₂ as standard. ^c Enantiomeric excess determined by SFC. ^d Heterogeneous reaction mixture.

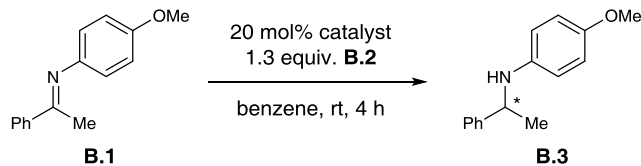
Upon determining the solvent, the effect of substituents on the *N*-terminus of the cysteic acid was investigated (Table B-2). Enantioselectivities remained low (-3–5% ee) and no clear trend was observed. It was noted that a protecting group on the nitrogen was necessary; the unprotected catalyst **B.10** resulted in no formation of product. Urea containing catalyst **B.13** generated product in the highest selectivity (5% ee) albeit at the expense of reactivity (5% yield).

Table B-2. Alteration of the *N*-terminus of the cysteic acid catalyst

Entry	catalyst	B.3 (%) ^b	ee (%) ^c	B.1 (%) ^b
1	B.5	11	nd ^d	82
2	B.6	11	nd ^e	46
3	B.7	23	0	58
4	B.8	22	2	51
5	B.9	15	2	82
6	B.10	0	n/a	99
7	B.11	31	-3	44
8	B.12	22	1	56
9	B.13	5	5	77

^a Reaction conducted using 0.07 mmol **B.1**, 0.014 mmol catalyst, 0.09 mmol **B.2** and 1.2 mL benzene. ^b Yields determined by ¹H NMR spectroscopy with respect to CH₂Br₂ as standard. ^c Enantiomeric excess determined by SFC. ^d In CH₂Cl₂, 1% ee. ^e In CH₂Cl₂, 5% ee.

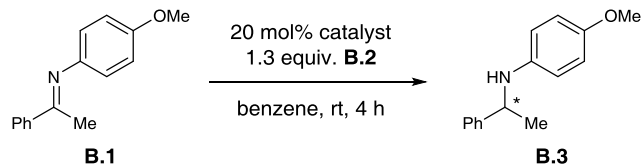
The effect of changing *C*-terminus was also investigated (Table B-3). Enantioselectivities were higher when there was no amide N–H present (2–7% vs. -2–1% ee). Dibenzylamine (**B.18**) and morpholine (**B.22**) capped cysteic acids gave the highest enantioselectivities. A combination of the terminus with the best enantioselectivities from Table B-2 and Table B-3, was also attempted (**B.24**); however no selectivity was observed (18% yield of **B.3**, 0% ee).

Table B-3. Alteration of the C-terminus of the cysteic acid catalyst

Entry	catalyst	B.3 (%) ^b	ee (%) ^c	B.1 (%) ^b
1	B.14	25	-1	53
2	B.15	17	4	55
3	B.16	27	2	56
4	B.17	18	1	52
5	B.18	25	7	52
6	B.19	13	5	61
7	B.20	15	0	58
8	B.21	15	-2	63
9	B.22	7	7	70
10	B.23	11	4	61

^a Reaction conducted using 0.07 mmol **B.1**, 0.014 mmol catalyst, 0.09 mmol **B.2** and 1.2 mL benzene. ^b Yields determined by ¹H NMR spectroscopy with respect to CH₂Br₂ as standard. ^c Enantiomeric excess determined by SFC.

We were particularly interested in testing peptide versions of the catalyst as a means of creating more chiral space around the cysteic acid. In a preliminary screen, three dipeptide catalysts were synthesized and tested under the imine reduction conditions (Table B-4). The extra amino acid was added on the *N*-terminus and capped with a benzoyl group while the *C*-terminus was capped with dibenzylamine. While the valine (**B.25**) and phenylalanine (**B.26**) containing dipeptides resulted in little or no enantioselectivity, the proline dipeptide catalyst (**B.27**) resulted in very little ee.

Table B-4. Examination of dipeptide catalysts

Entry	catalyst	B.3 (%) ^b	ee (%) ^c	B.1 (%) ^b
1	B.25	14	0	66
2	B.26	16	2	67
3	B.27	14	5	65

^a Reaction conducted using 0.07 mmol **B.1**, 0.014 mmol catalyst, 0.09 mmol **B.2** and 1.2 mL benzene. ^b Yields determined by ¹H NMR spectroscopy with respect to CH₂Br₂ as standard. ^c Enantiomeric excess determined by SFC.

B.3 Conclusions and Future Directions

Even though yields and enantioselectivities are low, we have demonstrated that cysteic acids can be used in Brønsted acid catalysis. Further investigations are needed before a synthetically useful method is achieved. These data have shown that there is promise for the use of cysteic acids in asymmetric Brønsted acid catalysis. One of the reason peptide backbones were chosen was their amenity to high throughput screening techniques such as solid phase synthesis⁵ and split-pool methods.⁶ With solid phase synthesis, peptides of lengths more than two can be synthesized more readily than with traditional peptide coupling chemistry. Furthermore, these catalysts can be screened more efficiently using split-pool techniques. Indeed, the future direction of this project is to use the split-pool method to screen larger peptides. Additionally, the identity of the test reaction (*i.e.* imine reduction) will also be accessed.

B.4 Experimental

B.4.1 Synthesis of cysteic acids

Cysteic acids **B.4–B.27** were synthesized by the oxidation of either the analogous cystine or the cysteine (see general method below). Cystines and cysteines were synthesized using standard peptide coupling procedures.

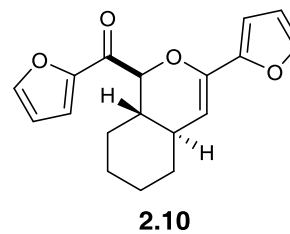
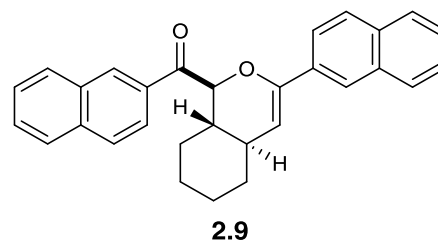
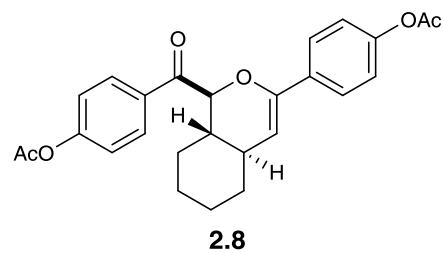
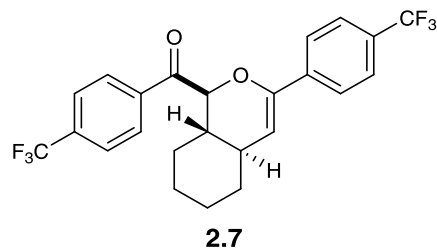
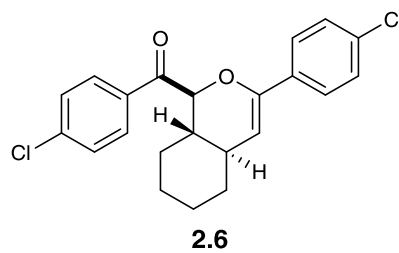
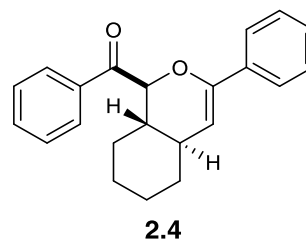
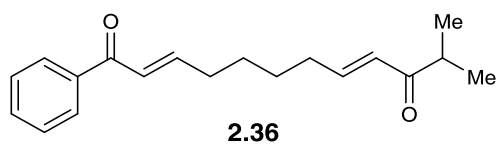
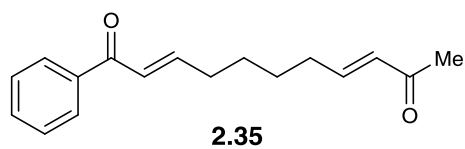
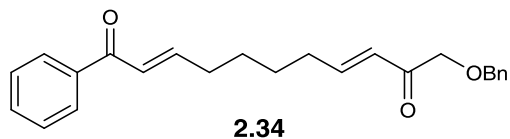
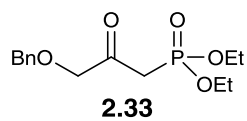
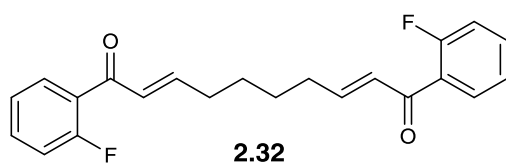
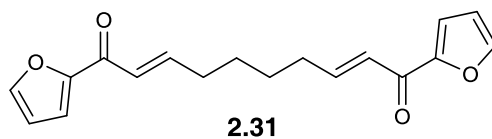
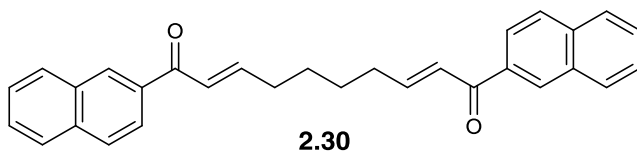
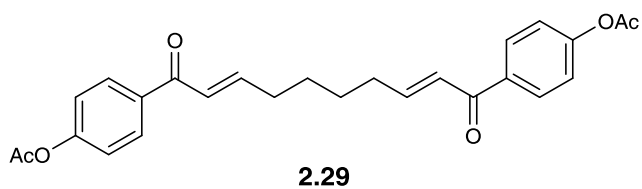
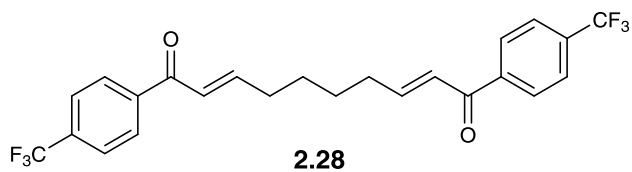
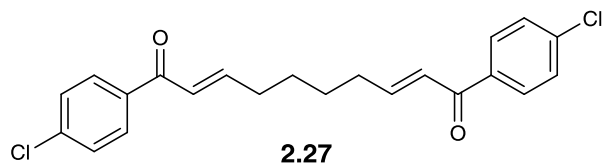
General method for the oxidation of cystine and cysteine to cysteic acid: Oxidation of cystine and cysteine to the cysteic acid was performed using modified procedure reported by Lim.⁷ Performic acid was prepared by mixing 9.7 mL of formic acid with 0.3 mL of 30% hydrogen peroxide and letting the solution sit for 1 h. The performic acid (0.1 M) was chilled in an ice bath and added to a chilled vial containing the cystine or cysteine. The reaction was stirred in an ice bath for 2 h. Solvent was removed *in vacuo*. H₂O was added and removed *in vacuo*. Cysteic acid was used without further purification.

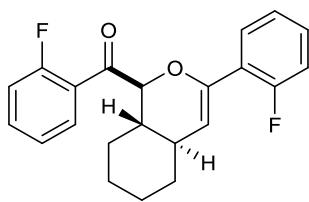
B.5 References

1. (a) Akiyama, T.; Itoh, J.; Fuchibe, K. "Recent Progress in Chiral Brønsted Acid Catalysis" *Adv. Synth. Catal.* **2006**, *348*, 999–1010. (b) Akiyama, T. "Stronger Brønsted Acids" *Chem. Rev.* **2007**, *107*, 5744–5758. (c) Terada, M. "Chiral Phosphoric Acids as Versatile Catalysts for Enantioselective Transformations" *Synthesis* **2010**, *12*, 1929–1982.
2. (a) Christ, P.; Lindsay, A. G.; Vormittag, S. S.; Neudörfl, J.-M.; Berkessel, A.; O'Donoghue, A. C. "pK_a Values of Chiral Brønsted Acid Catalysts: Phosphoric Acids/Amides, Sulfonyl/Sulfonyl Imides, and Perfluorinated TADDOLs (TEFDDOLs)" *Chem. Eur. J.* **2011**, *17*, 8524–8528. (b) Rueping, M.; Nachtsheim, B. J.; Ieawsuwan, W.; Atodiresei, I. "Modulation the Acidity: Highly Acidic Brønsted Acids in Asymmetric Catalysis" *Angew. Chem. Int. Ed.* **2011**, *50*, 6706–6720. (c) Yang, C.; Xue, X.-S.; Jin, J.-L.; Cheng, J.-P. "Theoretical Study of the Acidities of Chiral Phosphoric Acids in Dimethyl Sulfoxide: Hints for Organocatalysis" *J. Org. Chem.* **2013**, *78*, 7076–7085.
3. (a) Hoveyda, A. H.; Hird, A. W.; Kacprzynski, M. A. "Small peptides as ligands for catalytic asymmetric alkylations of olefin. Rational design of catalysts or of searches that lead to them?" *Chem. Commun.* **2004**, 1779–1785. (b) Colby Davie, E. A.; Mennen, S. M.; Xu, Y.; Miller, S. J. "Asymmetric Catalysis Mediated by Synthetic Peptides" *Chem. Rev.* **2007**, *107*, 5759–5812.
4. (a) Hoffman, S.; Seayad, A. M.; List, B. "A Powerful Brønsted Acid Catalyst for the Organocatalytic Asymmetric Transfer Hydrogenation of Imines" *Angew. Chem. Int. Ed.* **2005**, *44*, 7427–7427. (b) Rueping, M.; Sugiono, E.; Azap, C.; Theissmann, T.; Bolte, M. "Enantioselective Brønsted Acid Catalyzed Transfer Hydrogenation: Organocatalytic Reduction of Imines" *Org. Lett.* **2005**, *7*, 3781–3783.
5. Merrifield, B. "Solid Phase Synthesis" *Science* **1986**, *232*, 341–347.
6. Lam, K. S.; Lebl, M.; Krchňák, V. "The 'One-Bead-One-Compound' Combinatorial Library Method" *Chem. Rev.* **1997**, 411–448.
7. Seo, H.; Lim, D. "Total Synthesis of Halicylindramide A" *J. Org. Chem.* **2009**, *74*, 906–909.

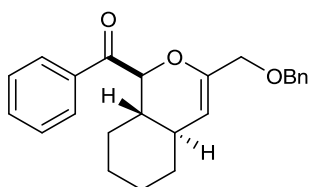
Appendix C. ^1H NMR and ^{13}C NMR spectra for new compounds

C.1 List of Compounds for Chapter 2

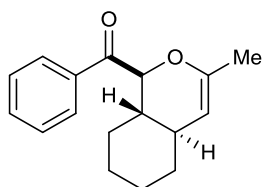




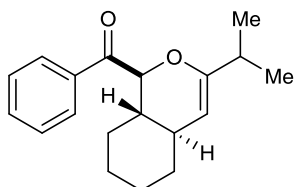
2.11



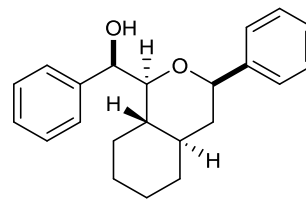
2.13



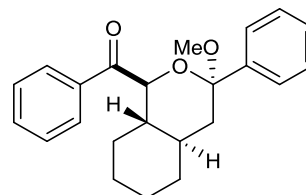
2.14



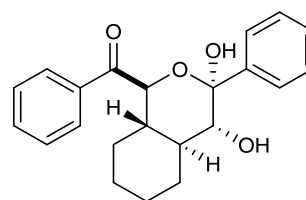
2.15



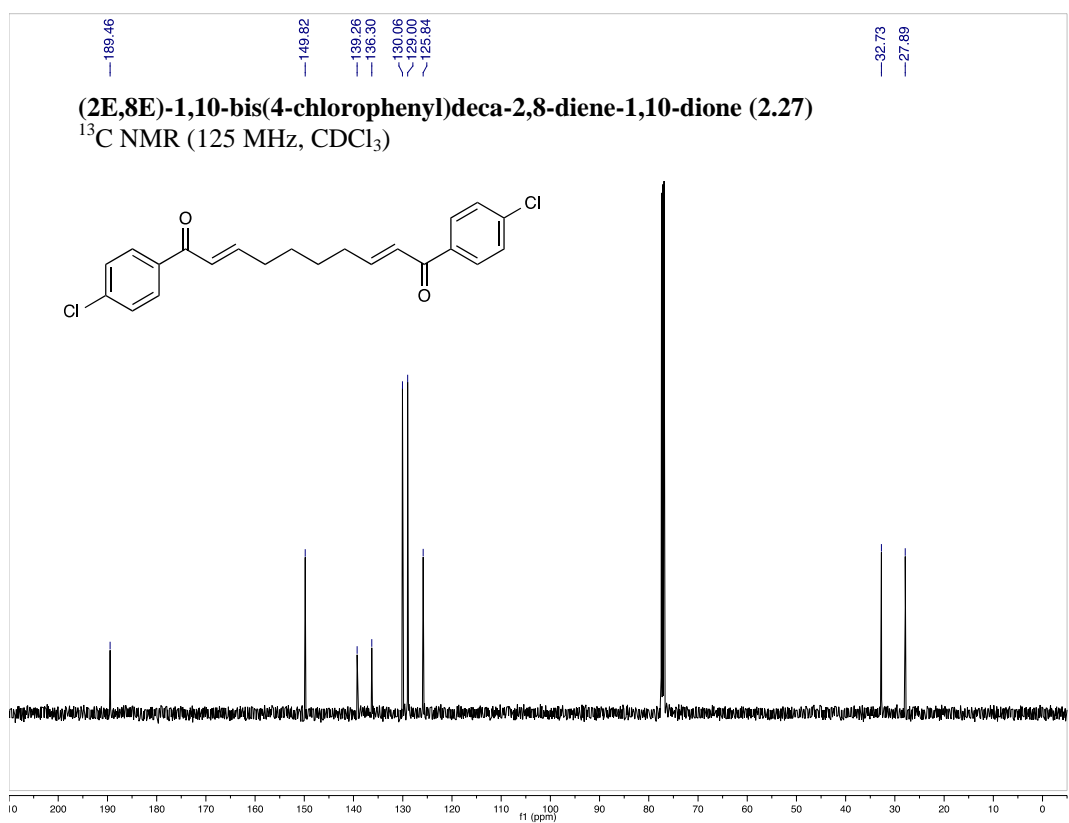
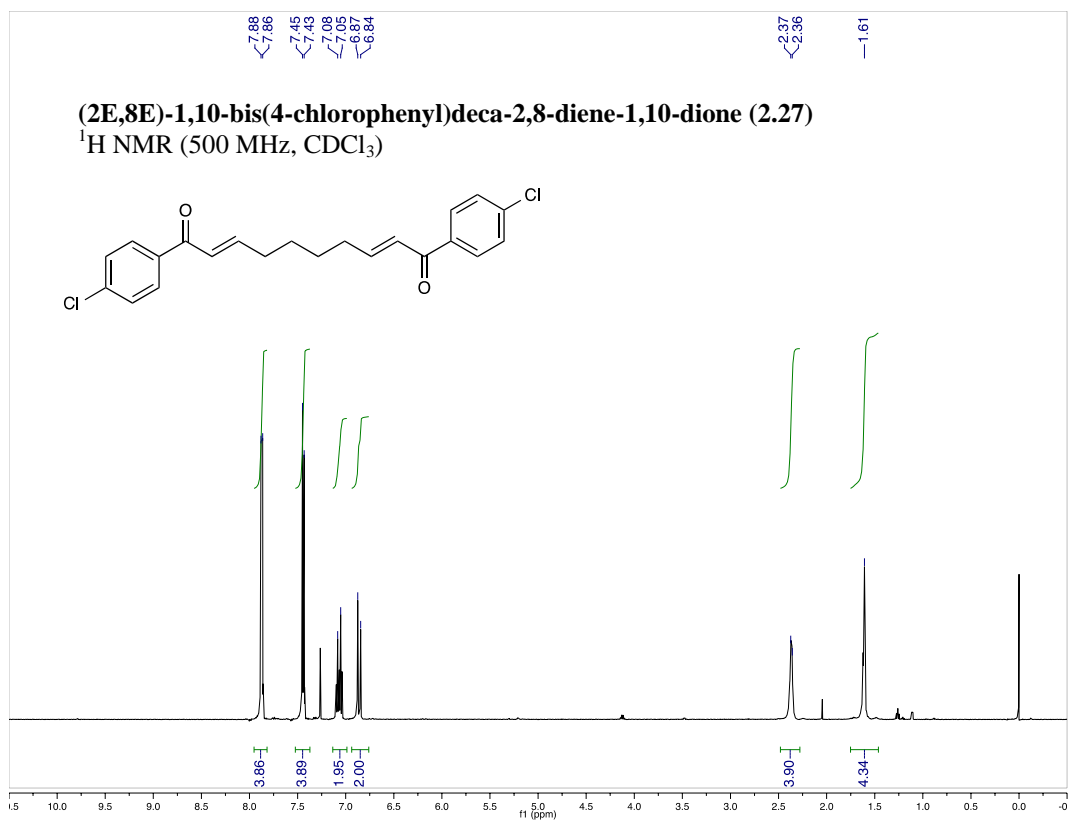
2.24

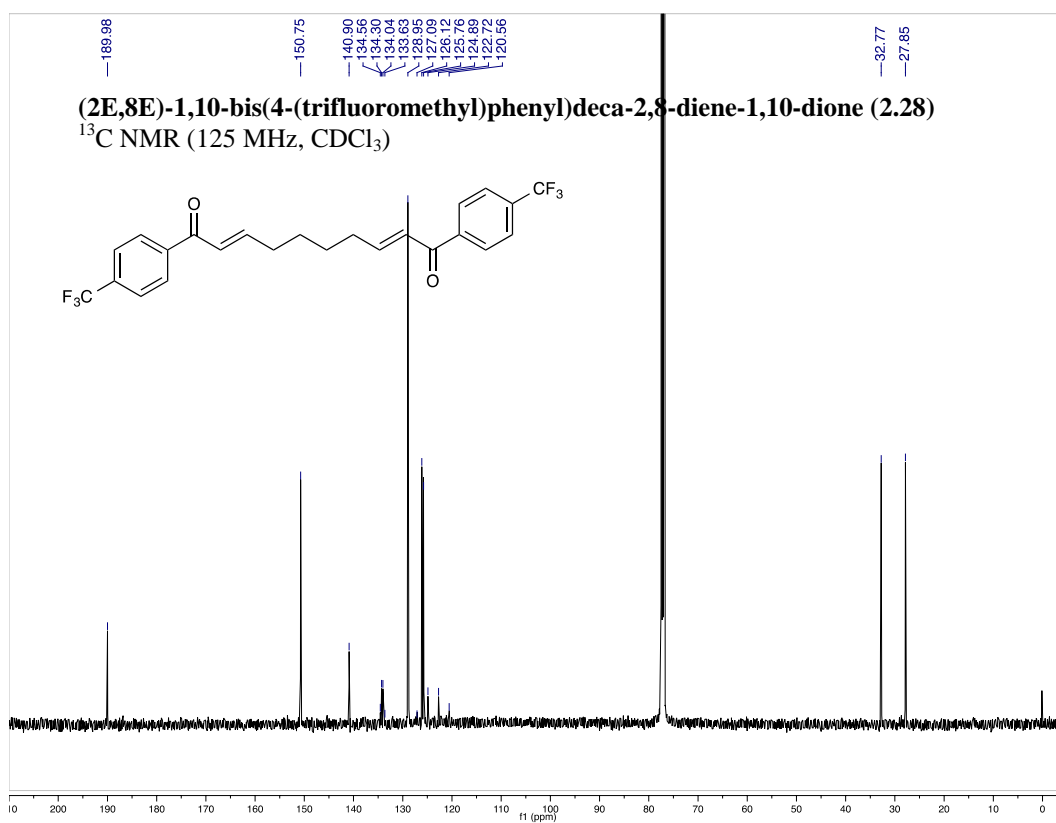
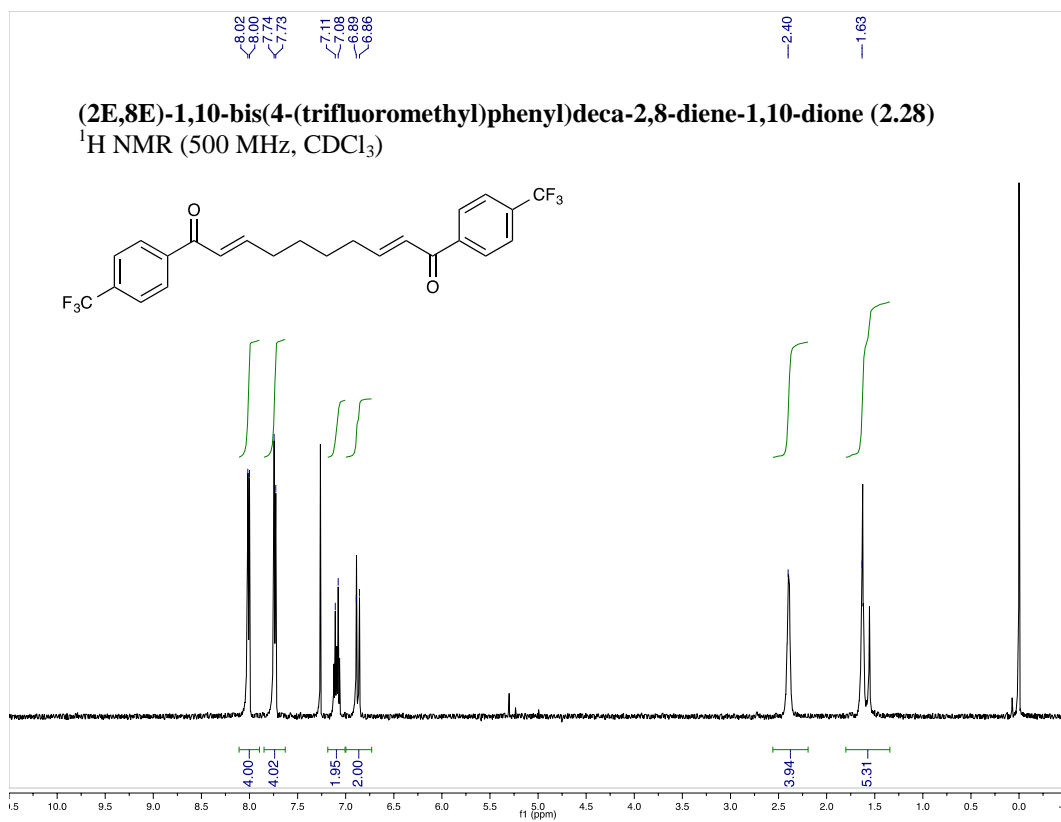


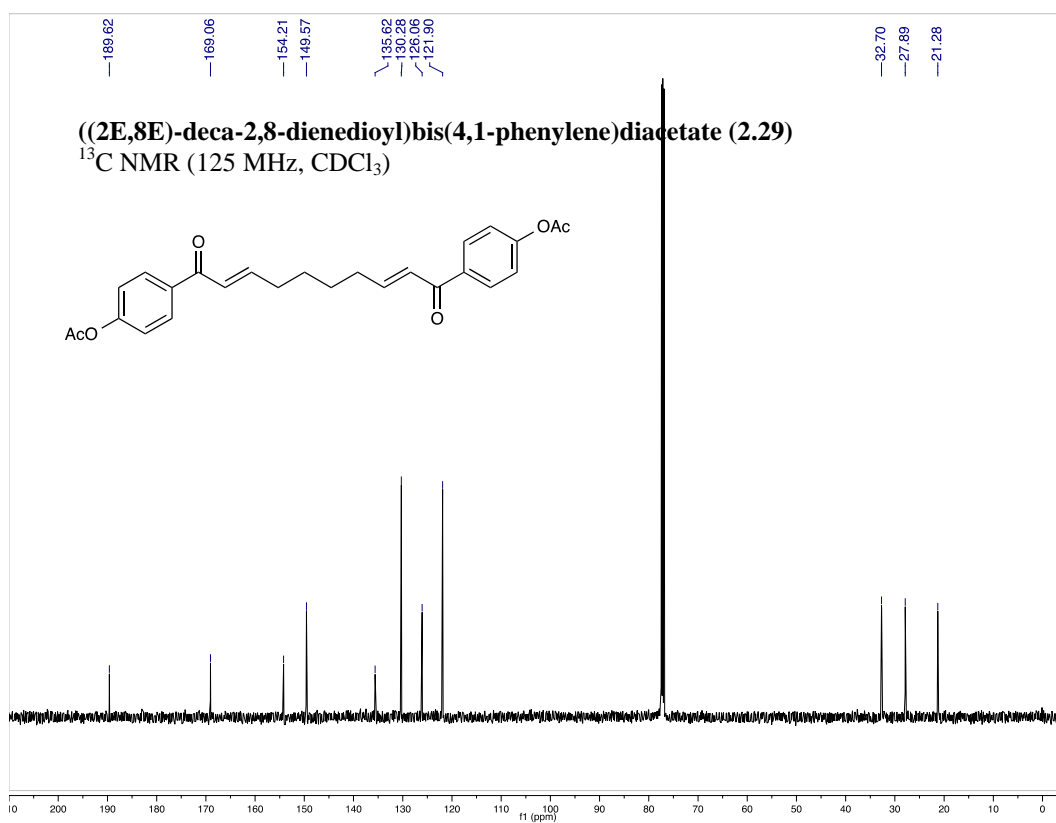
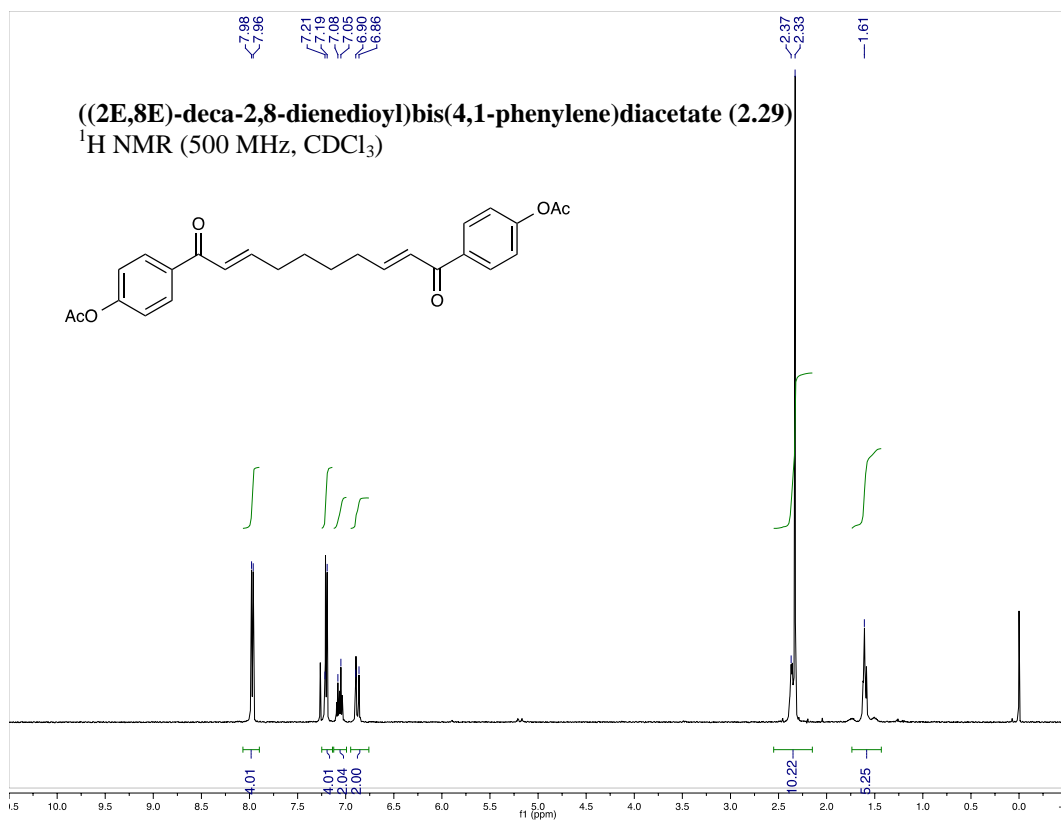
2.25

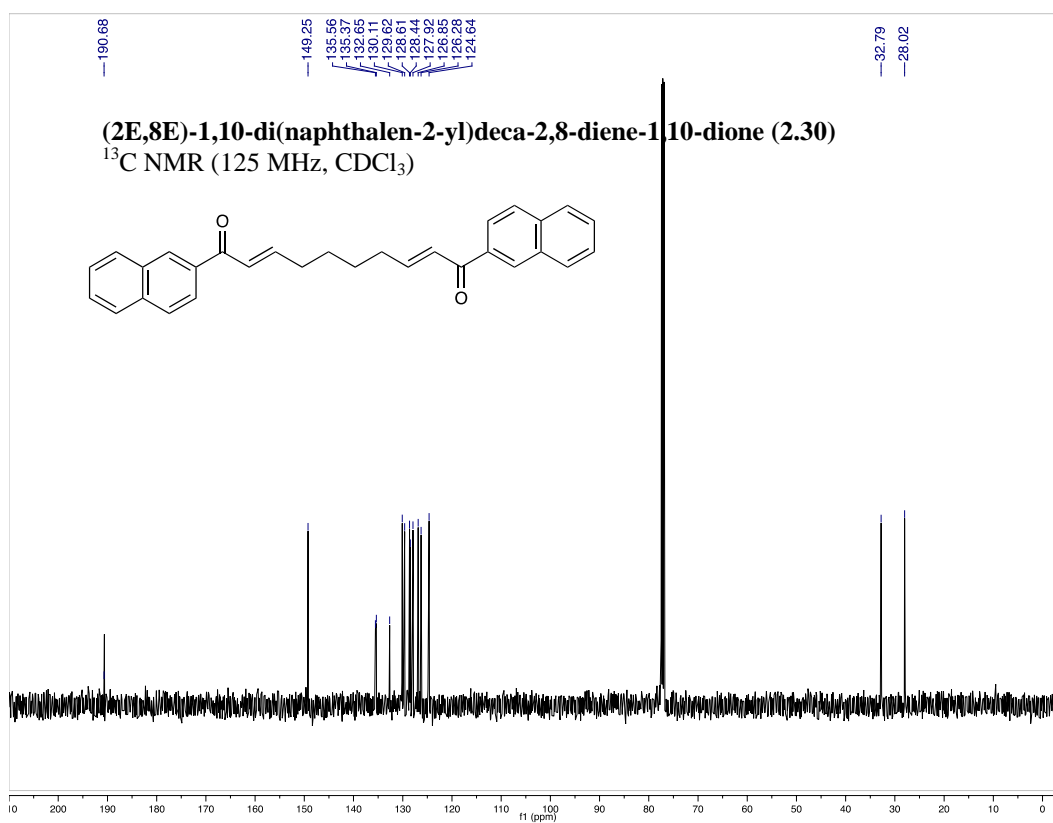
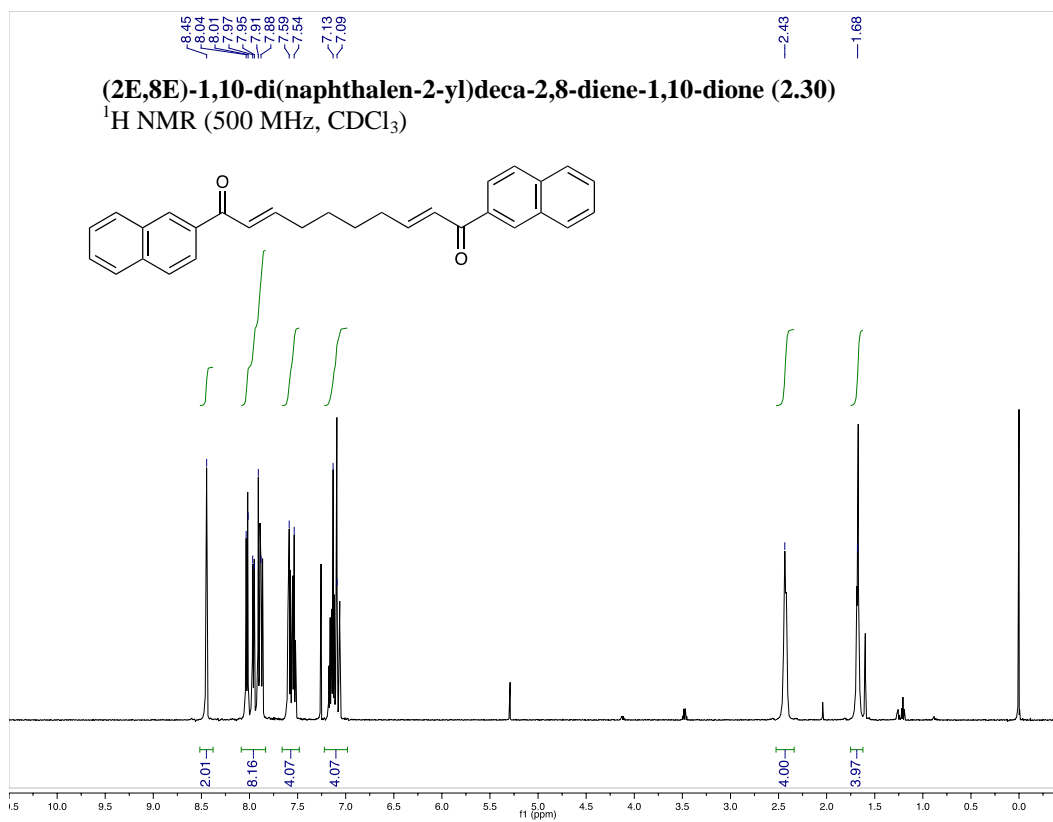


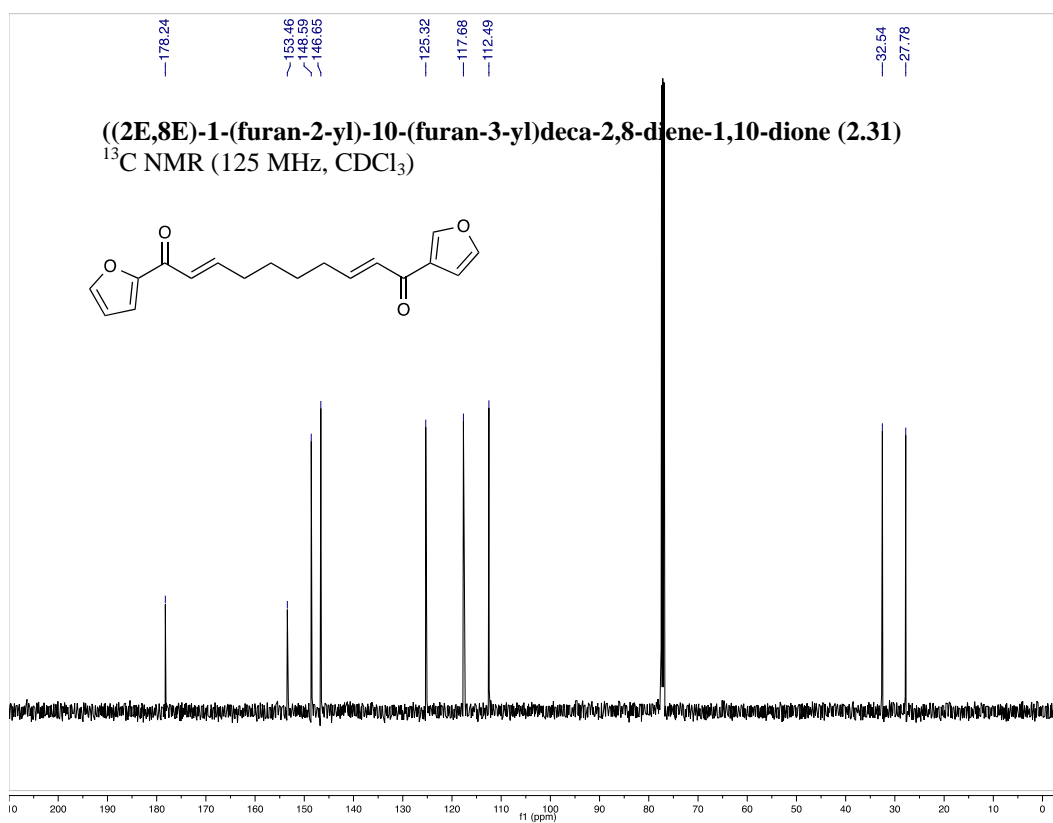
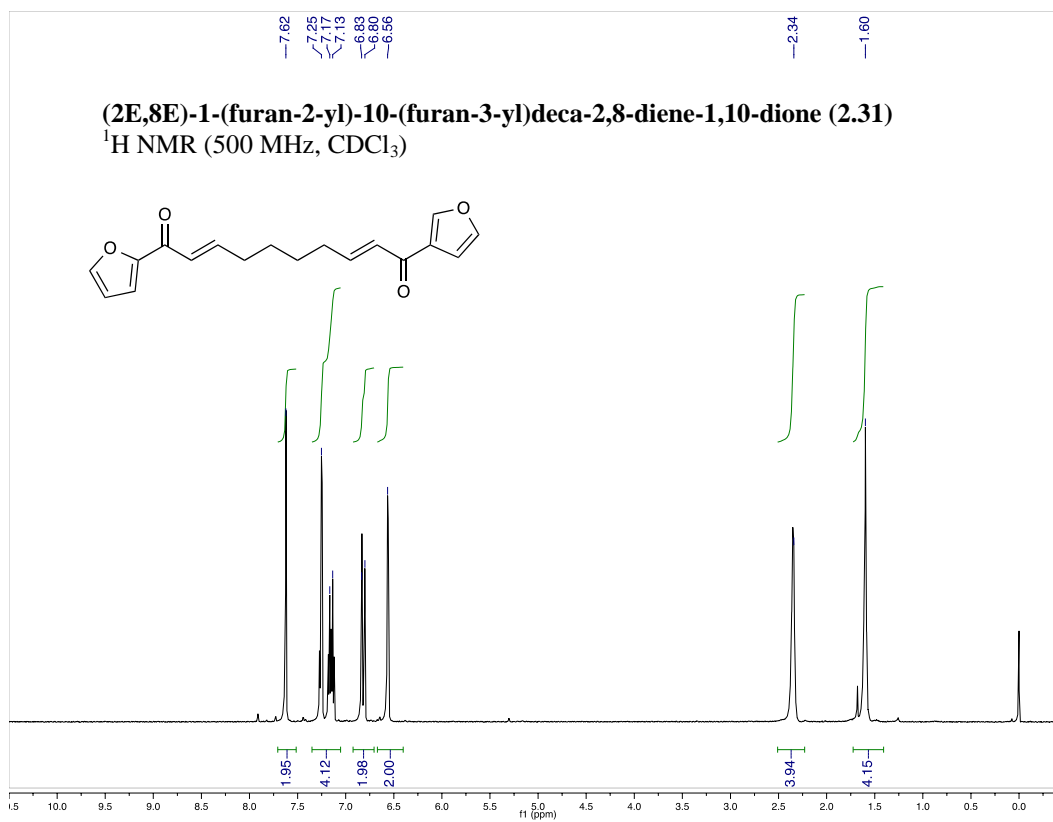
2.26

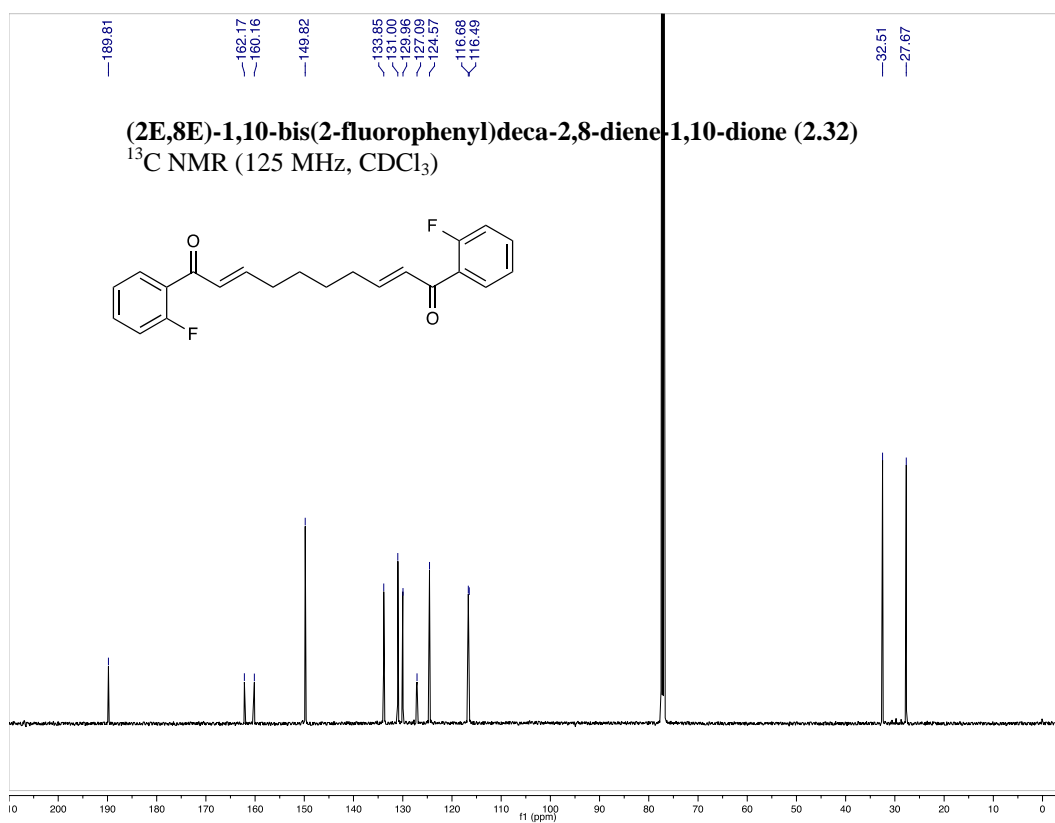
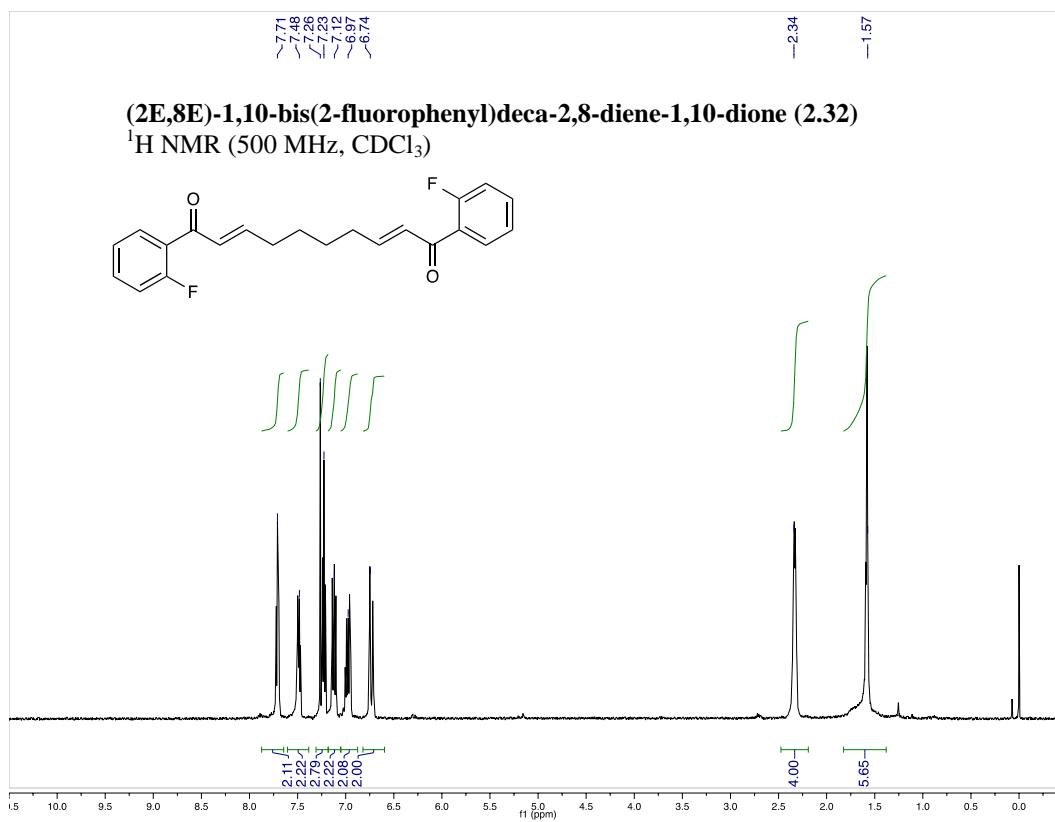


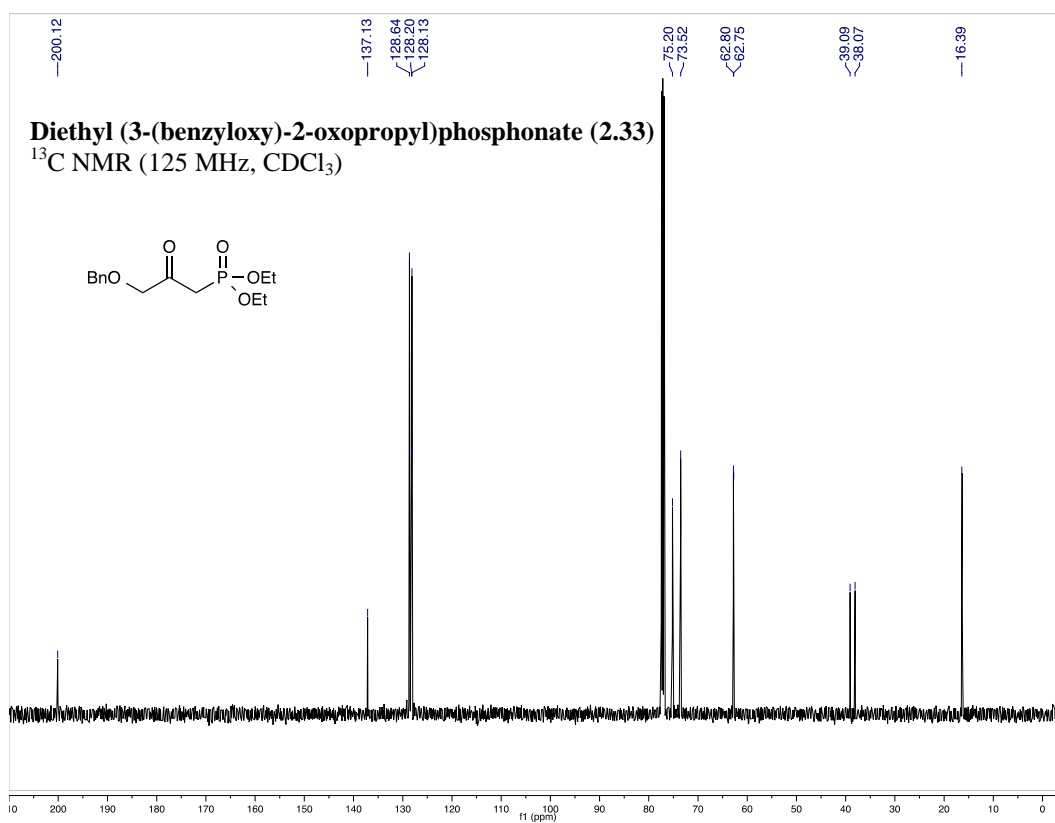
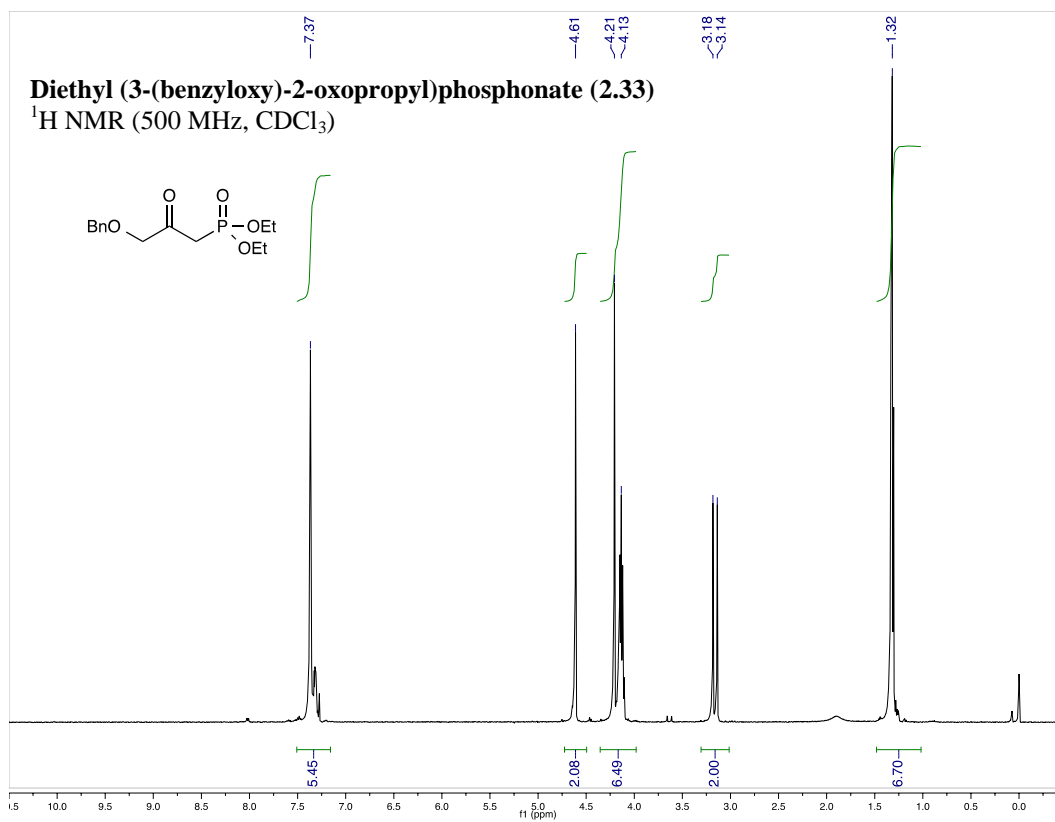


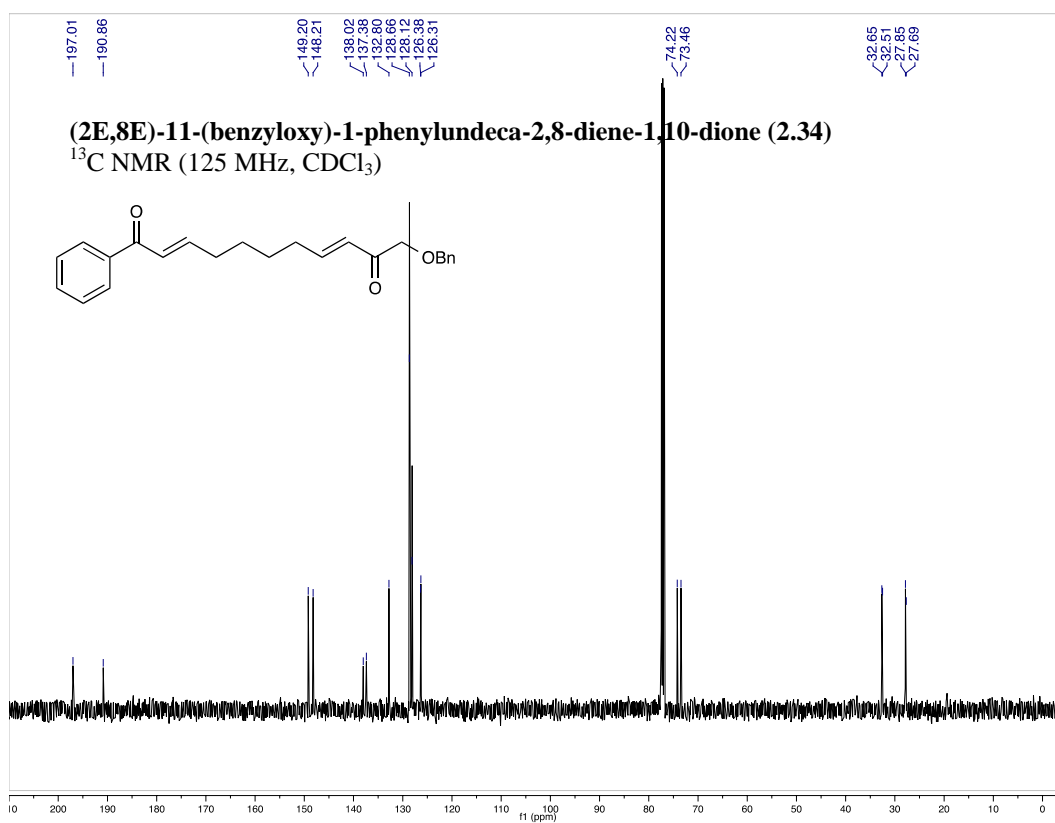
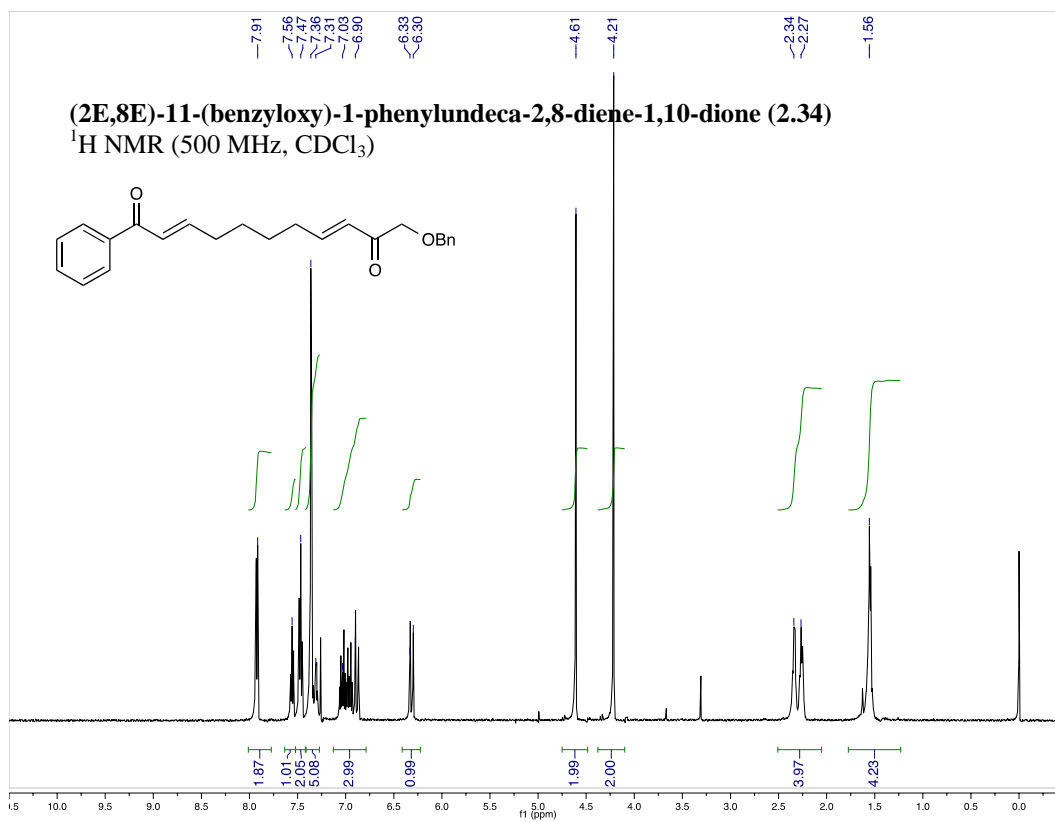


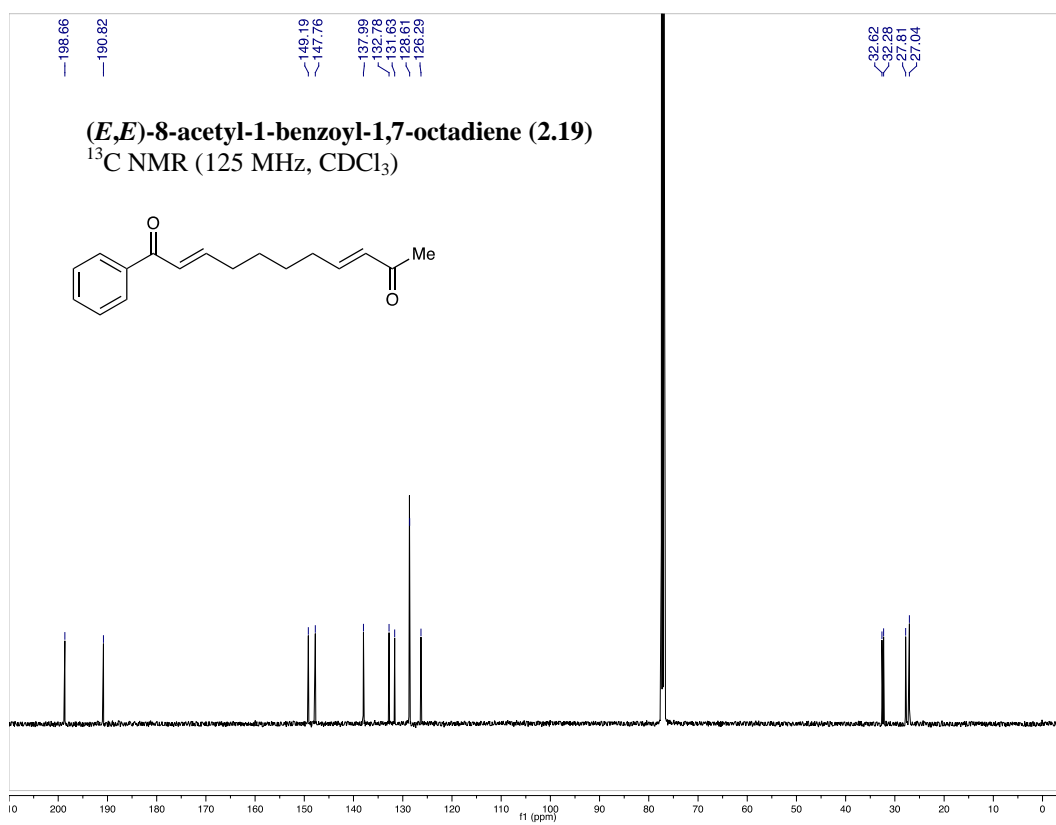
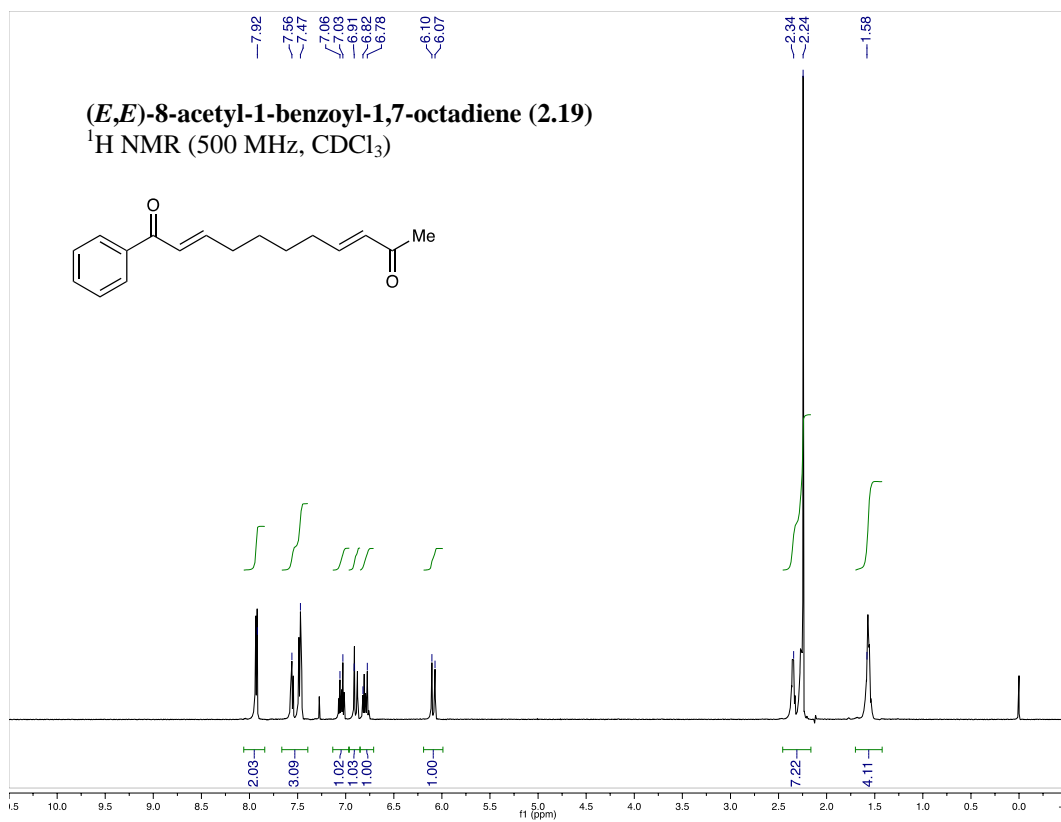


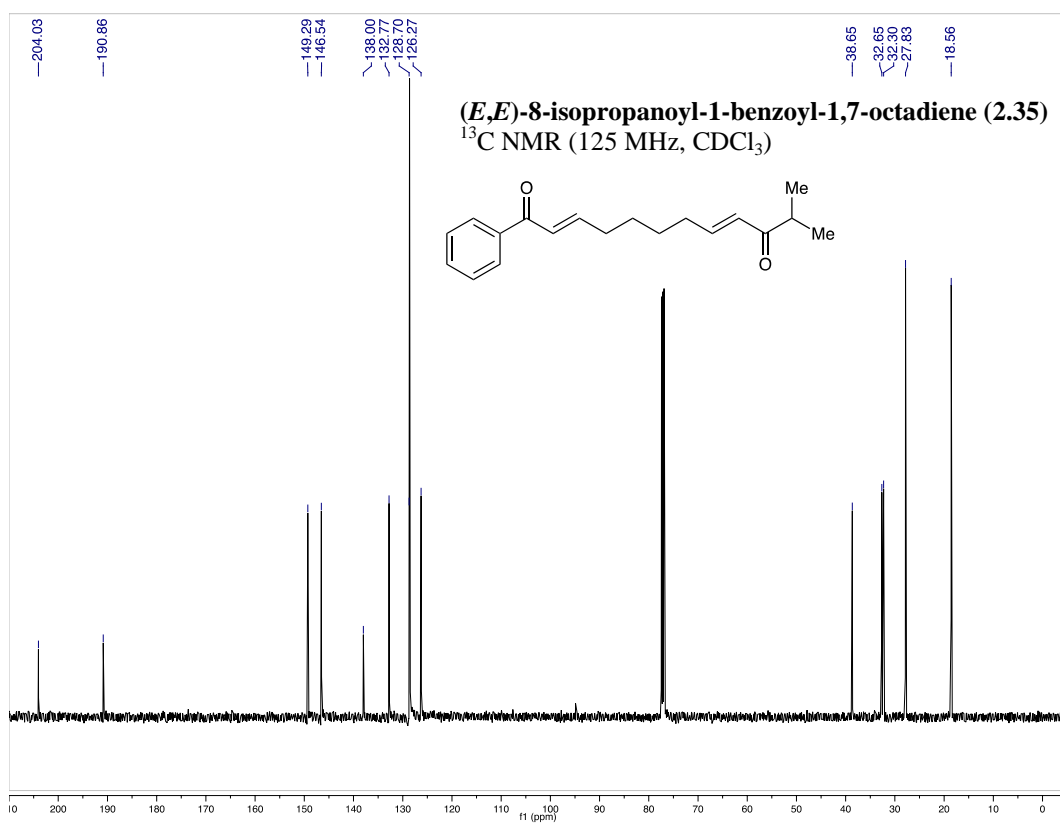
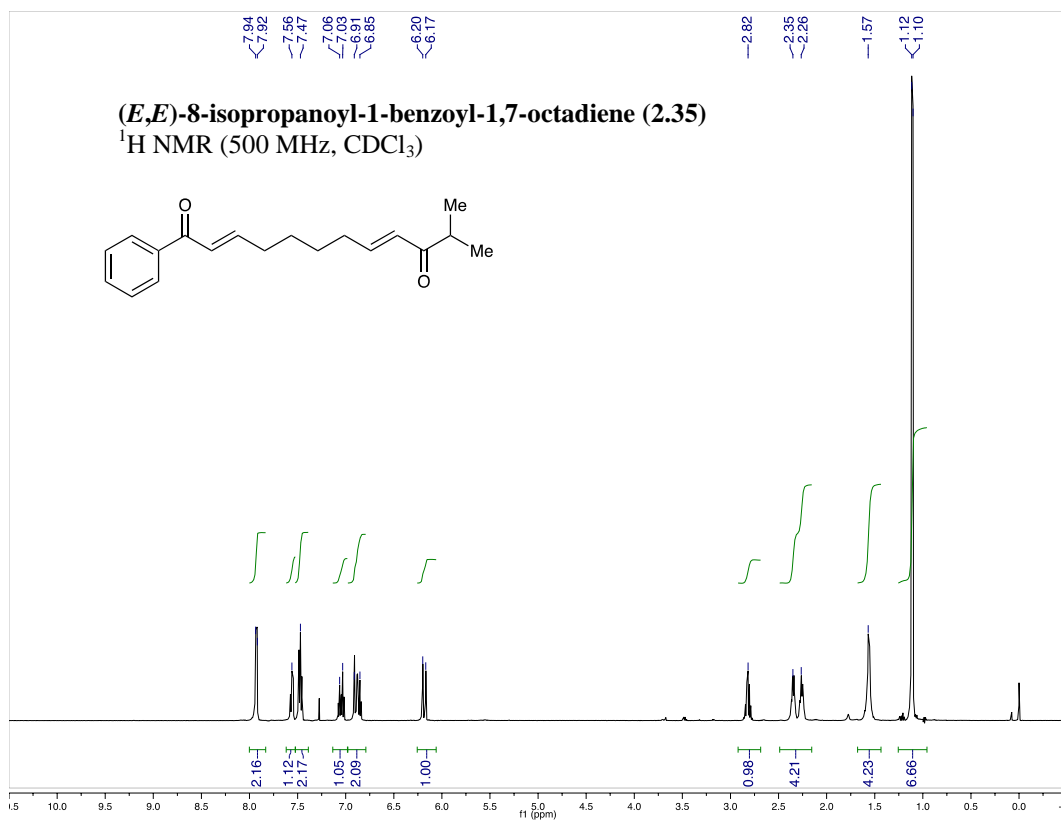


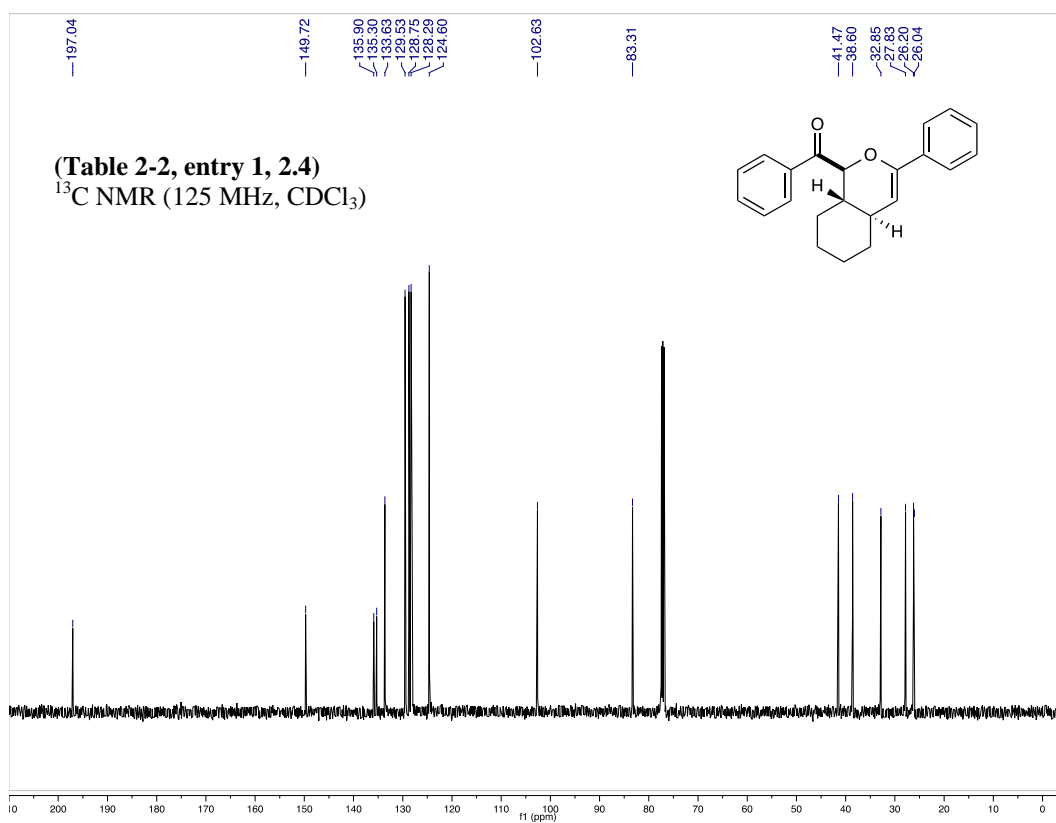
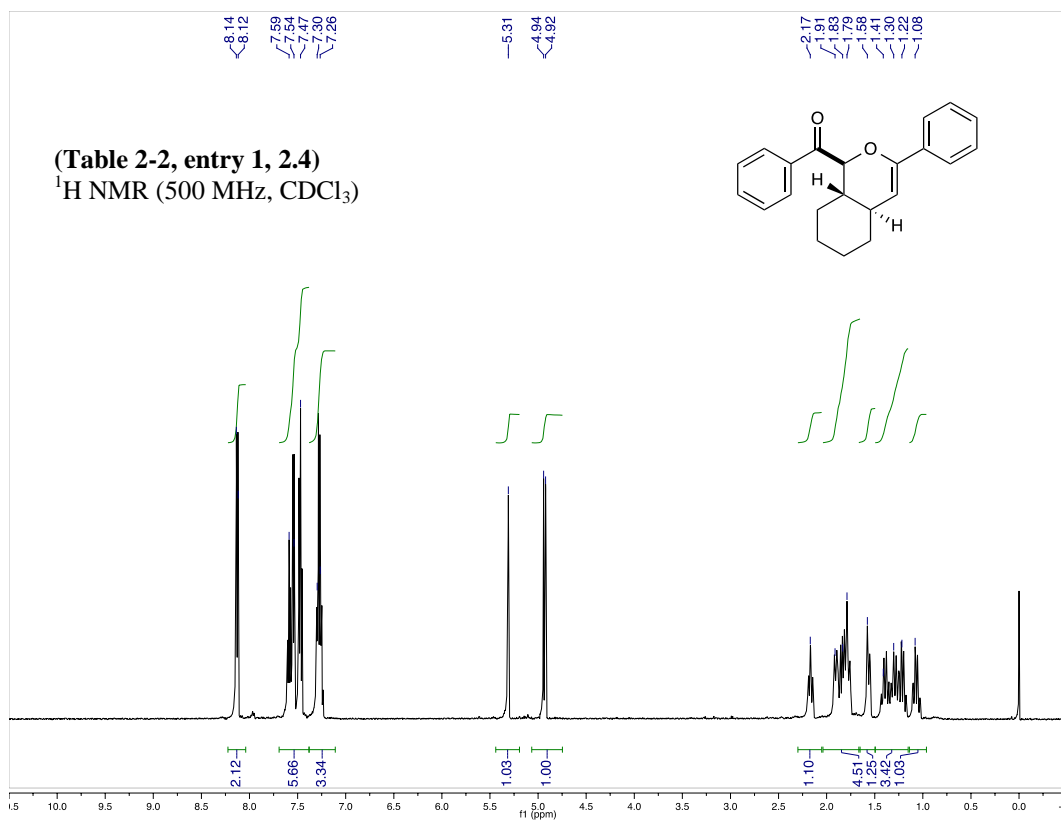


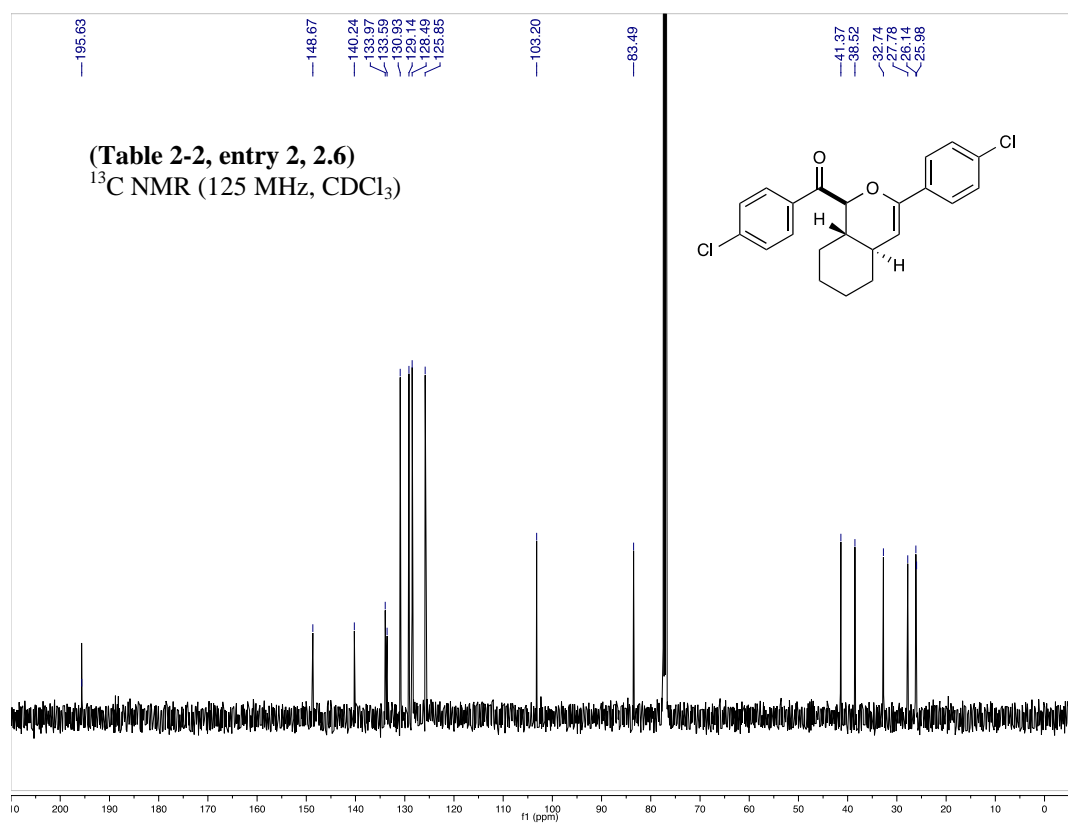
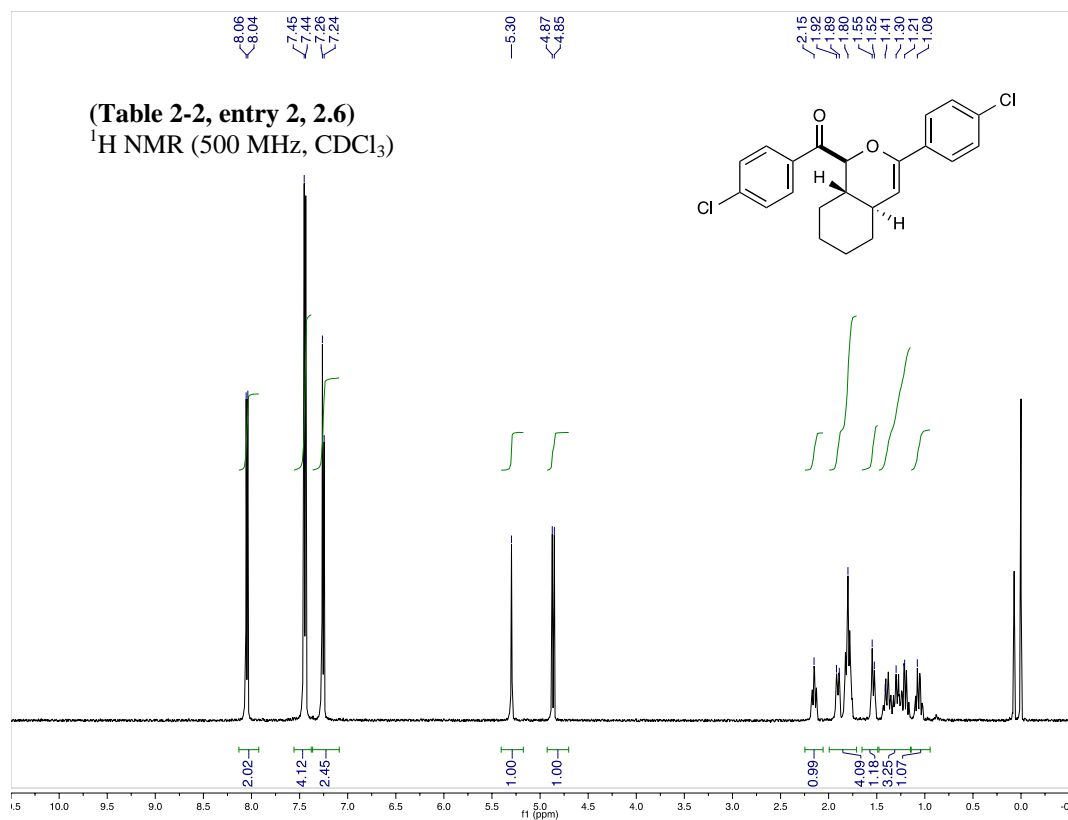


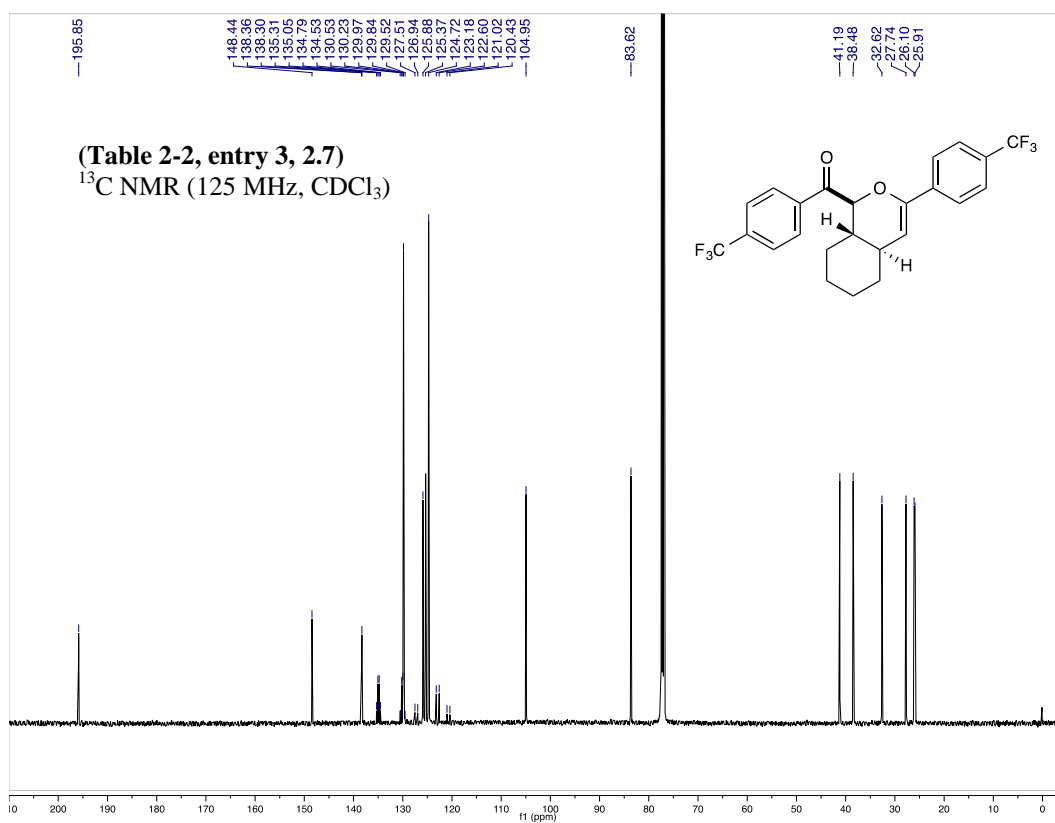
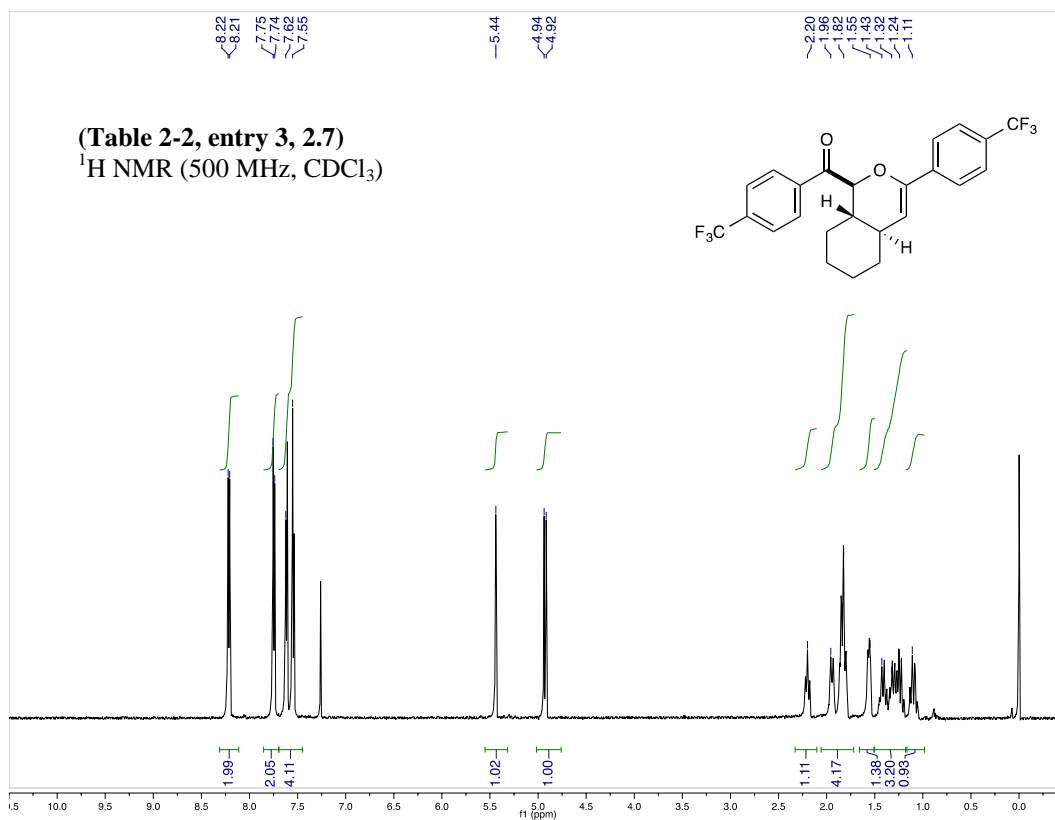


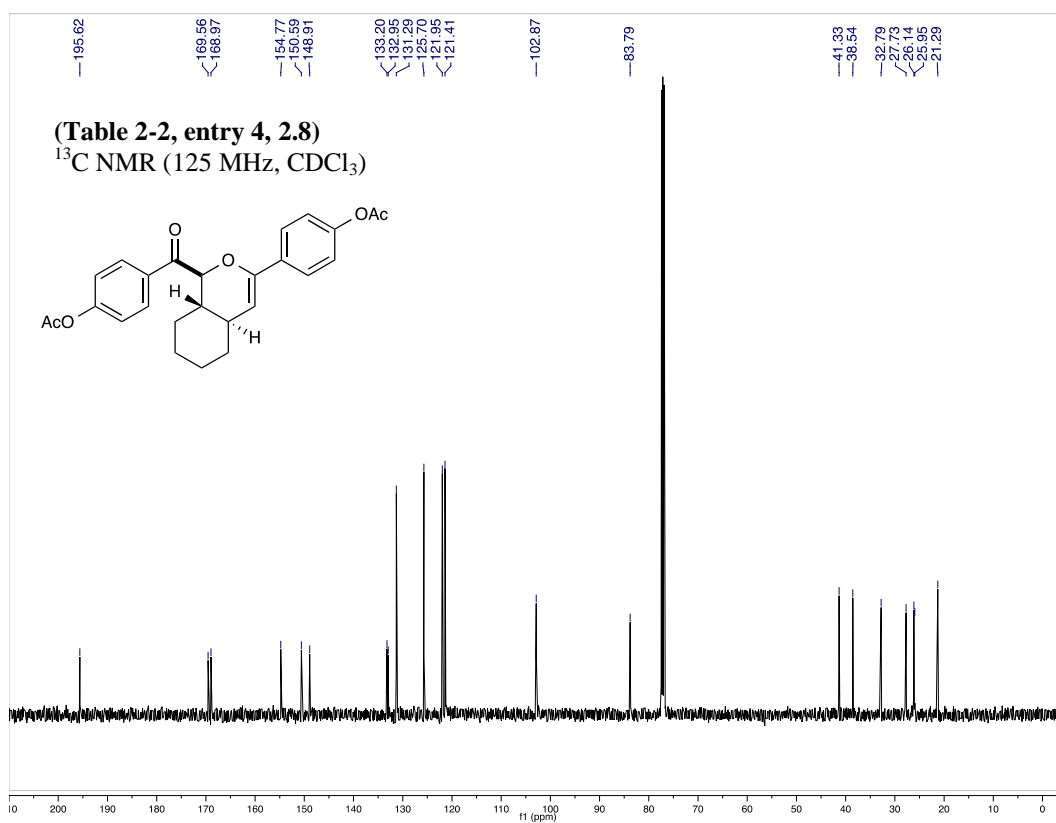
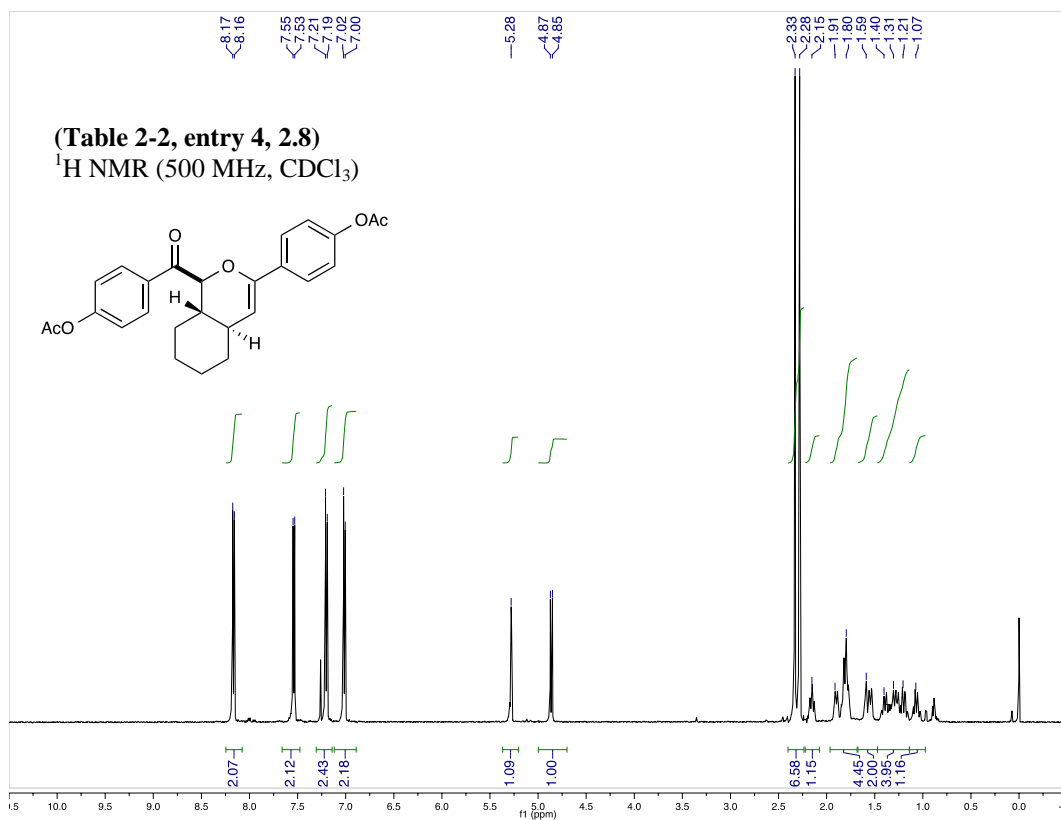


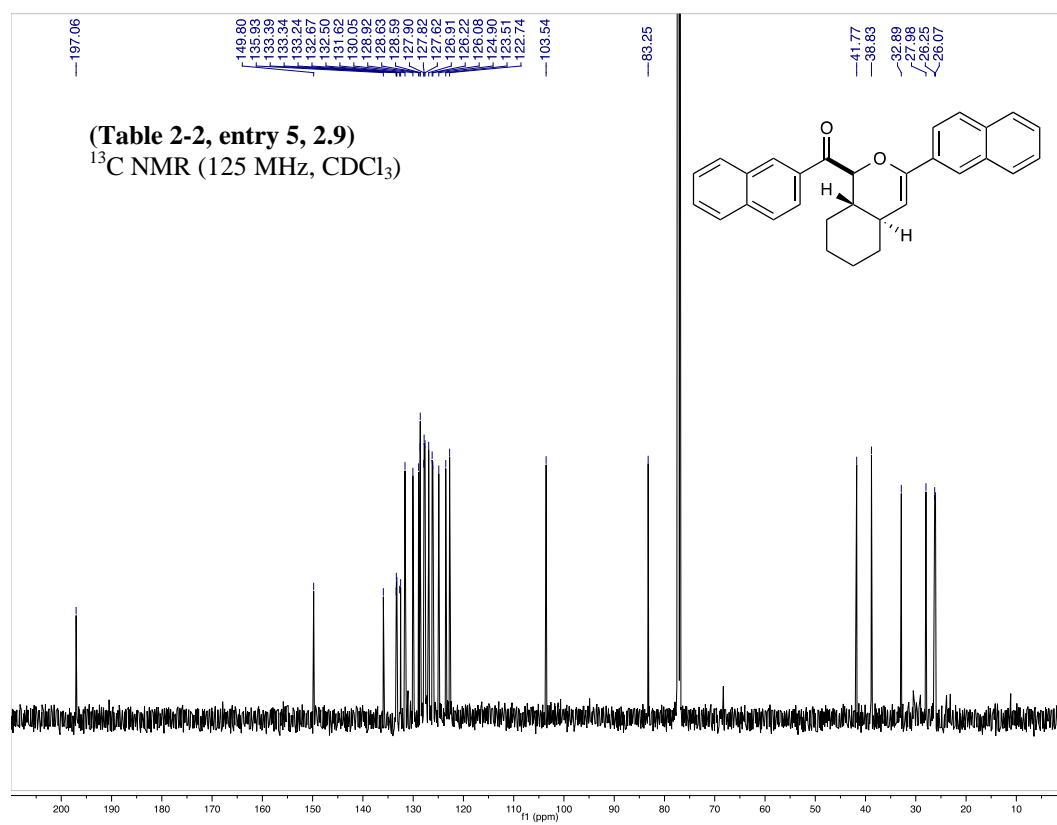
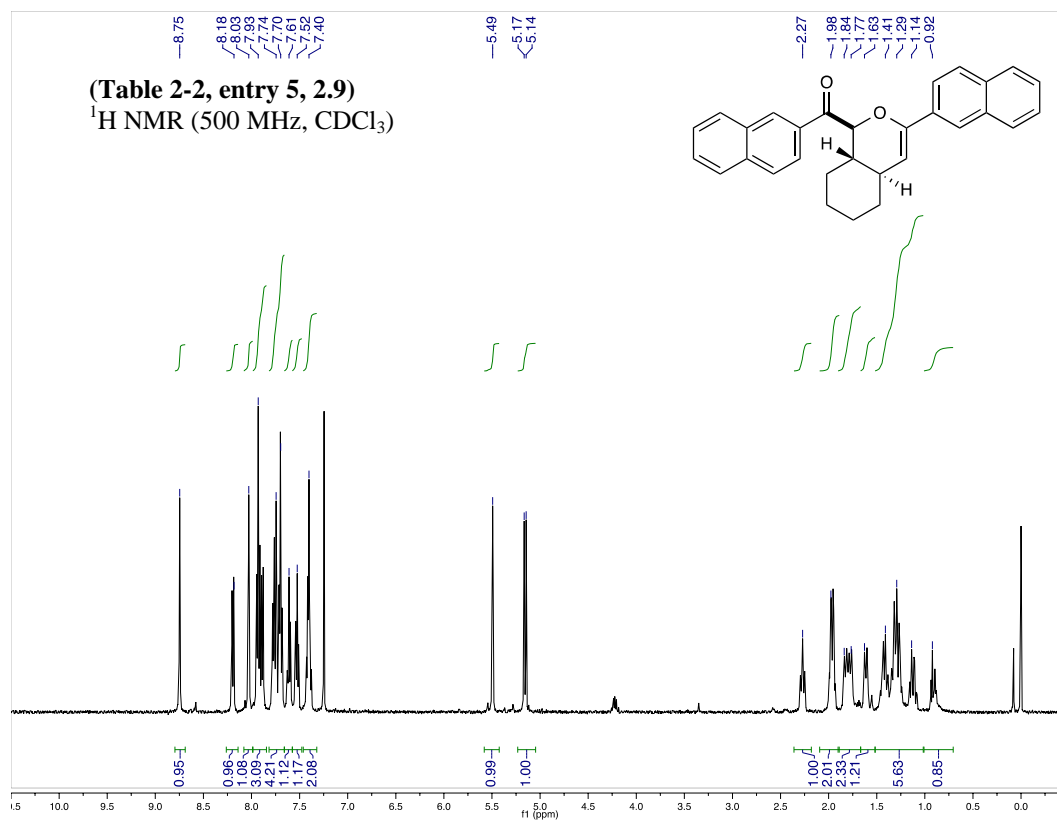


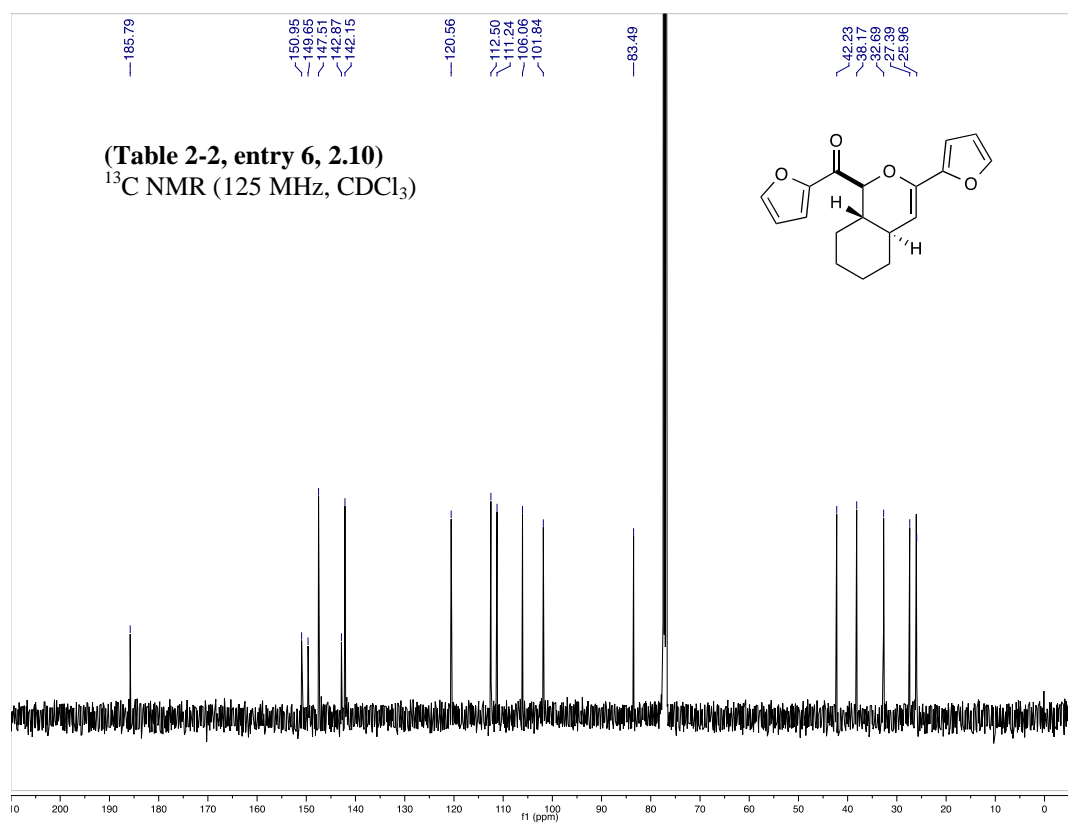
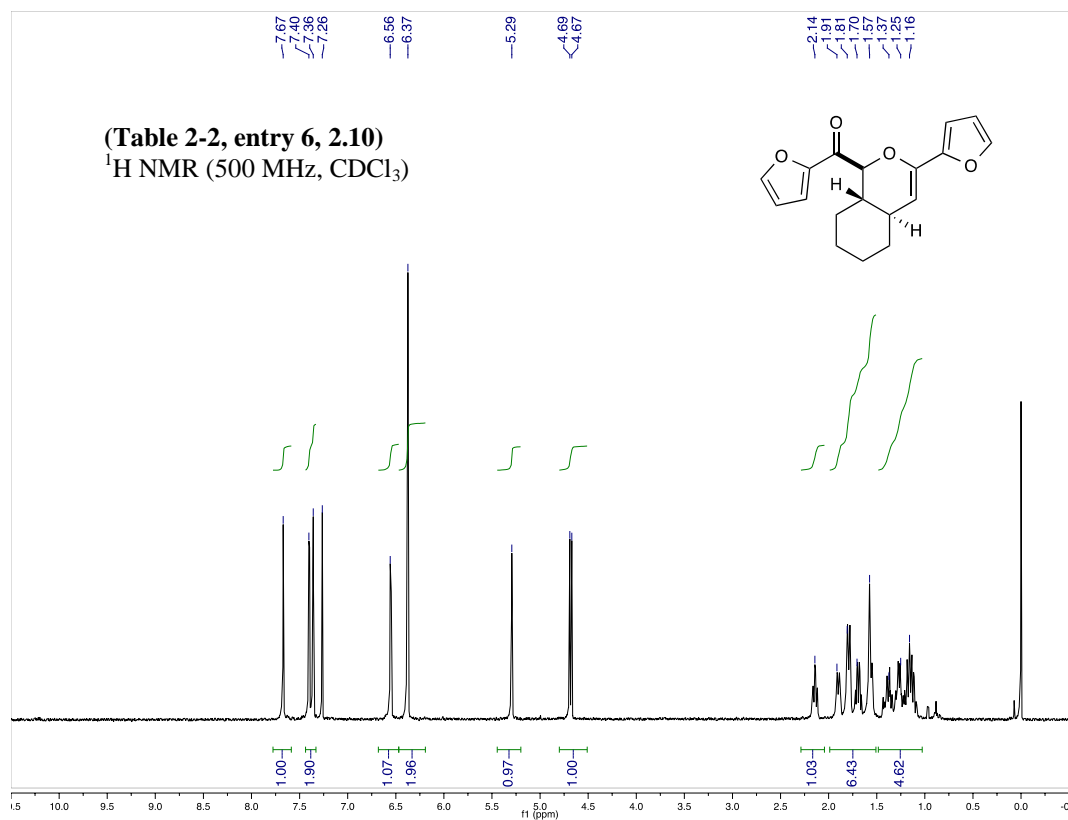


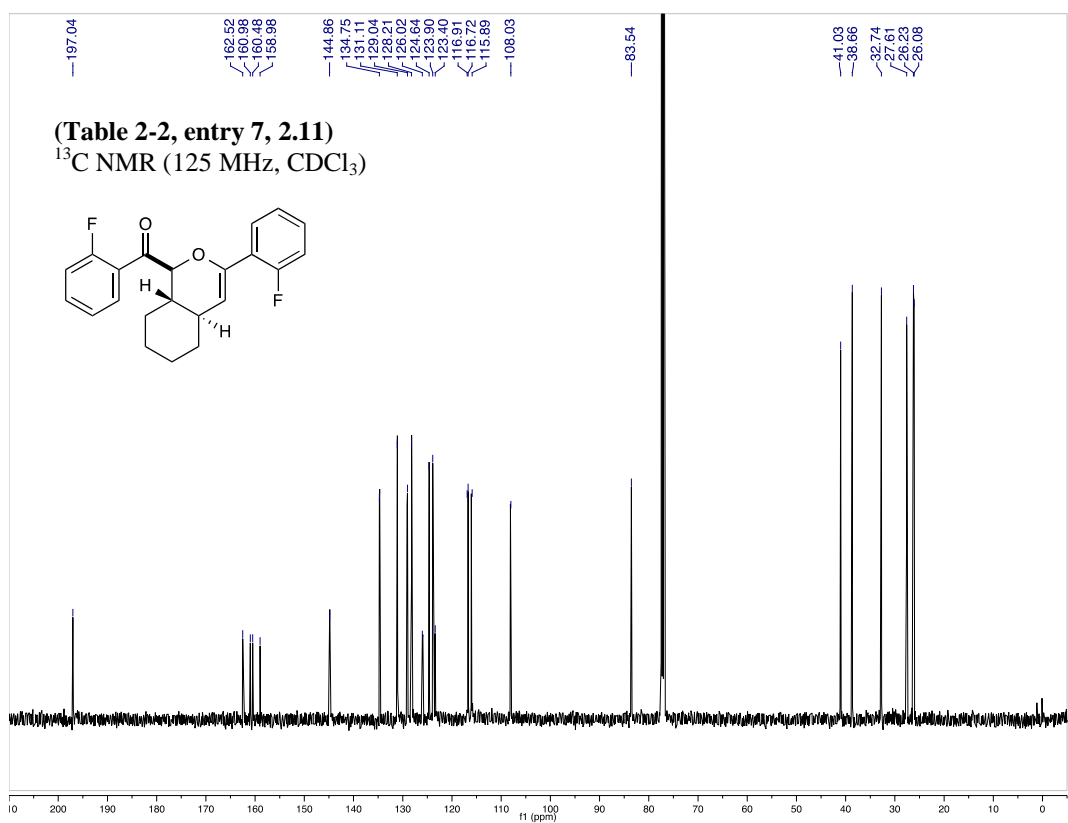
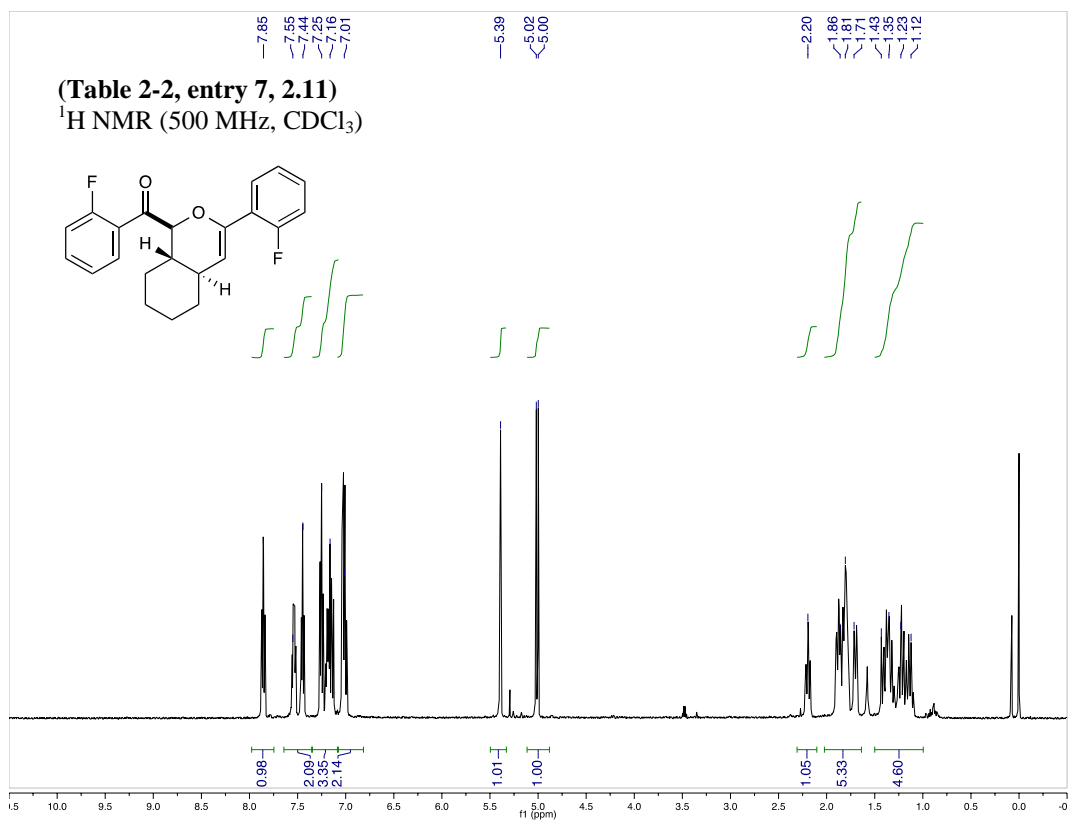


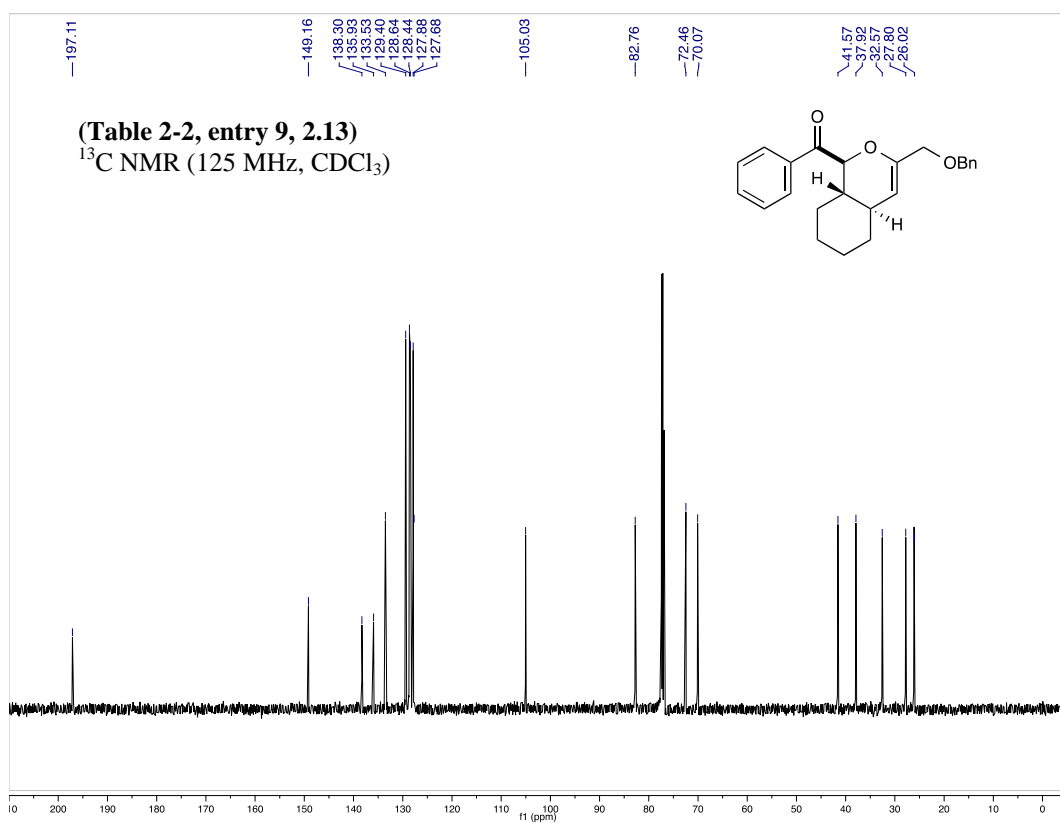
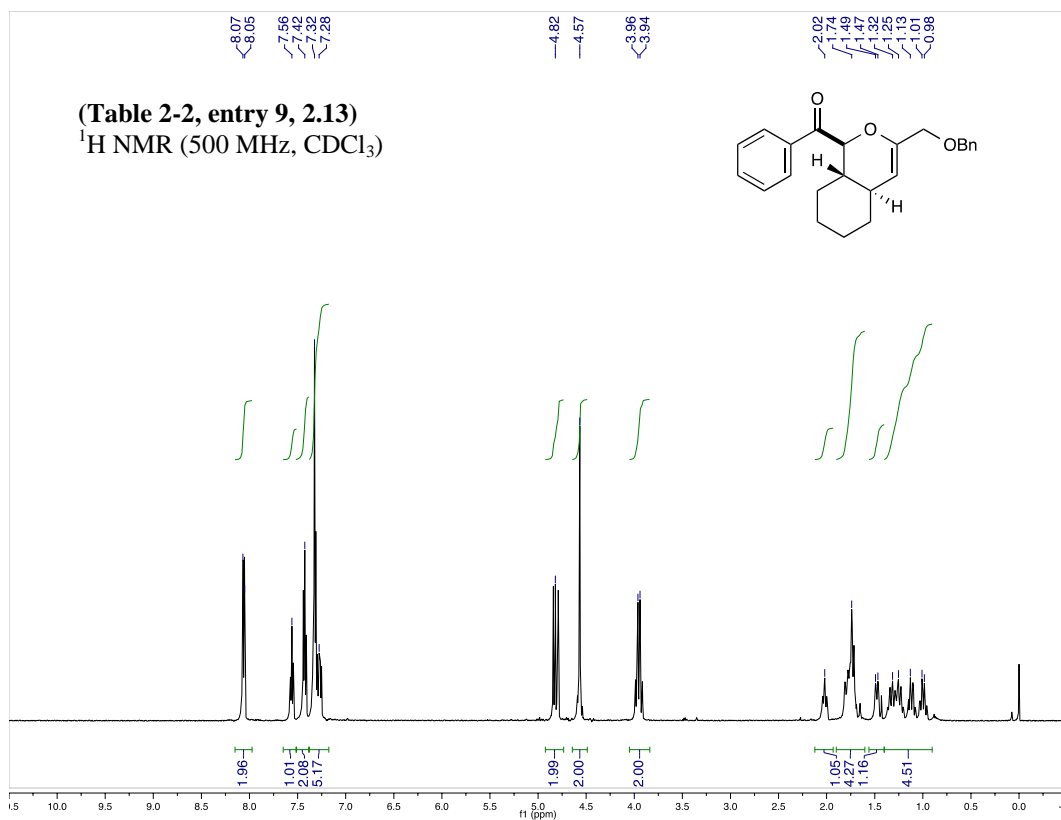


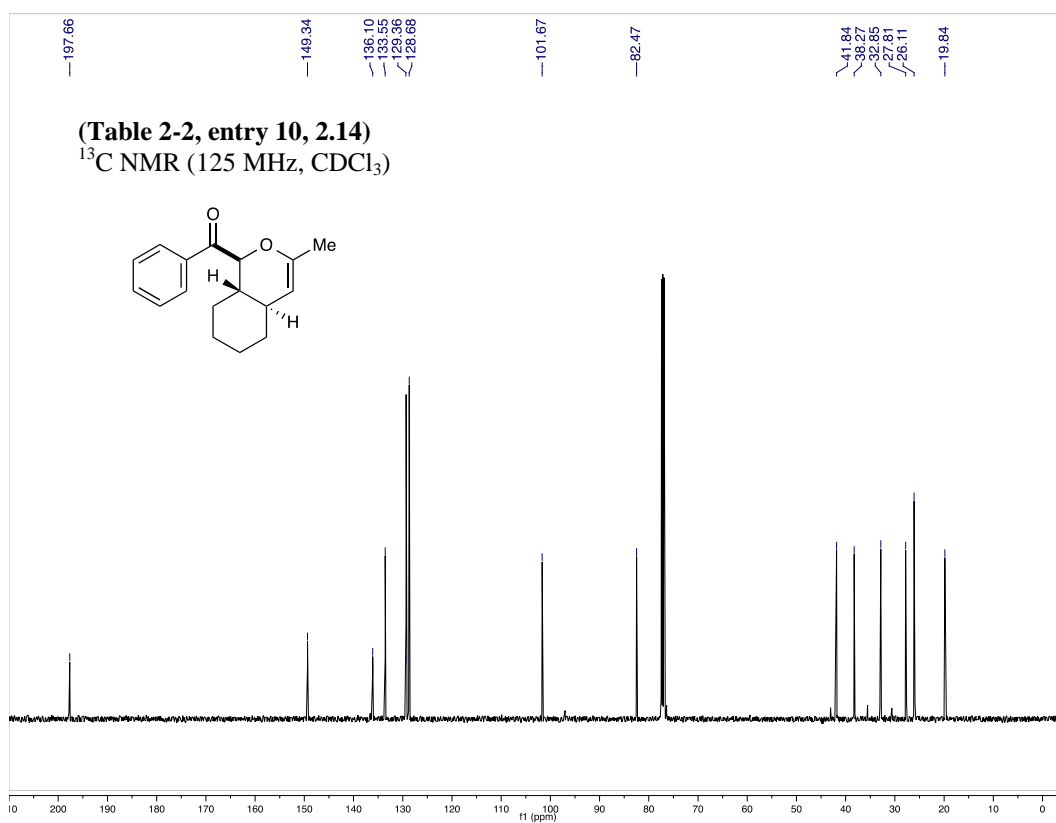
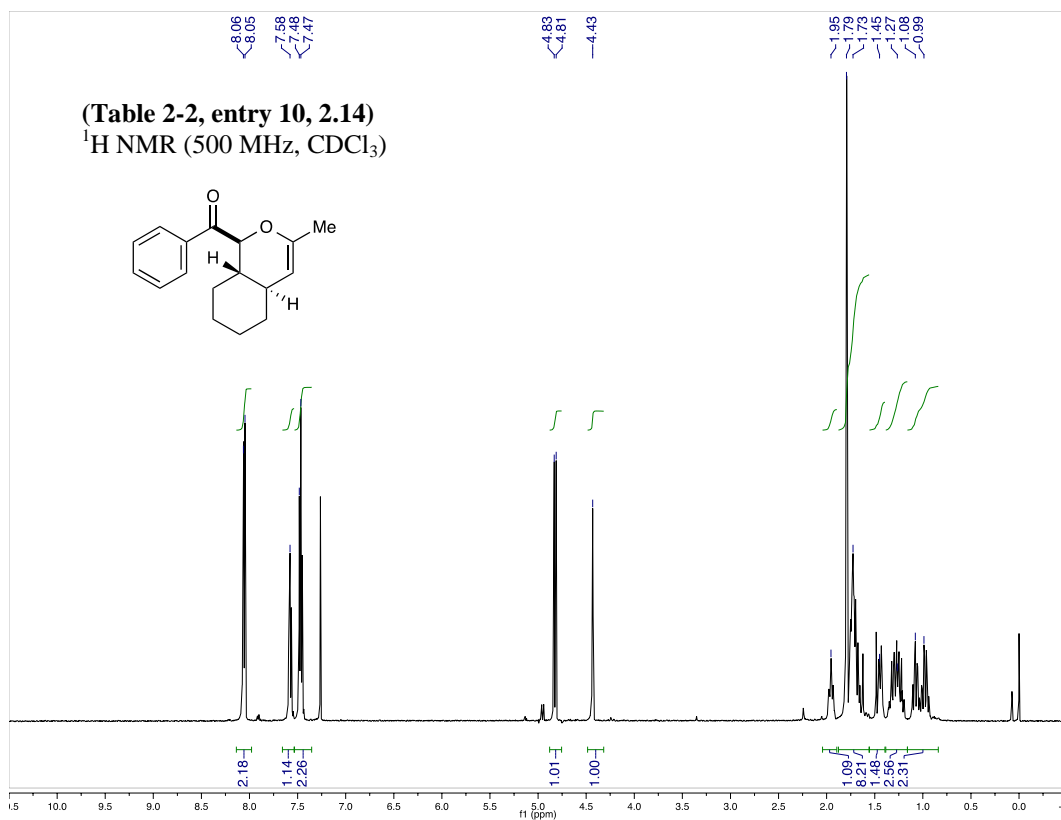


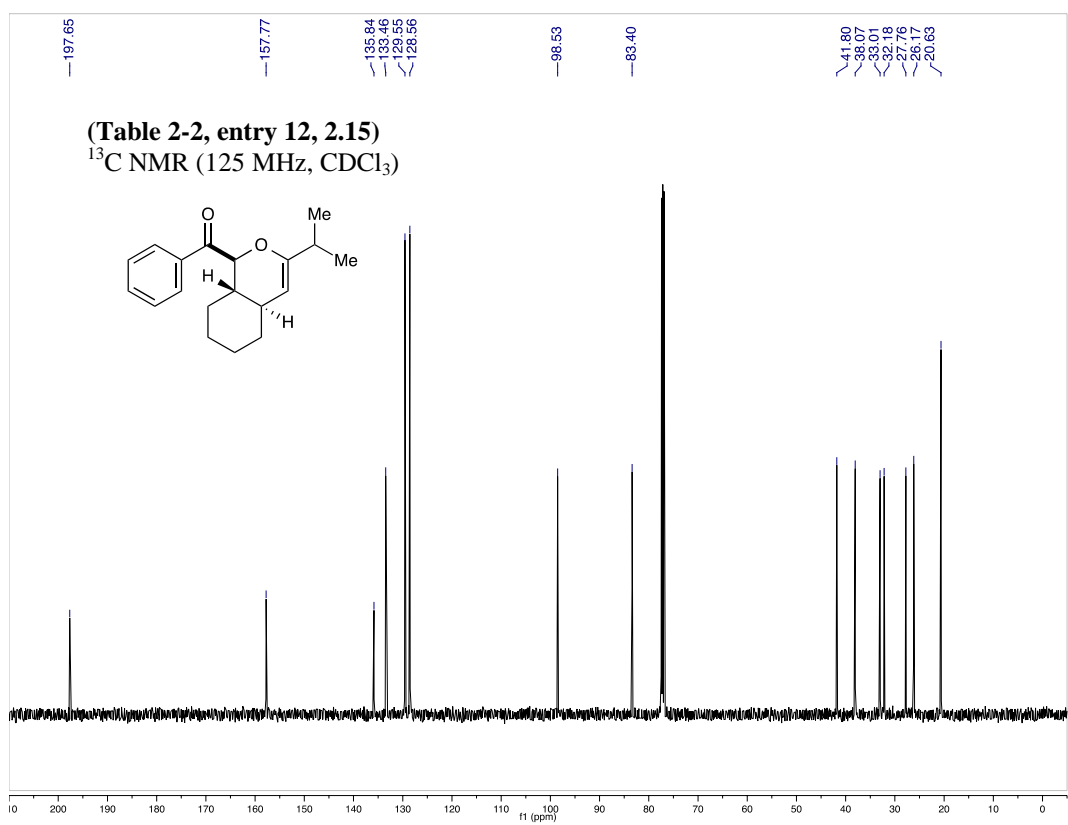
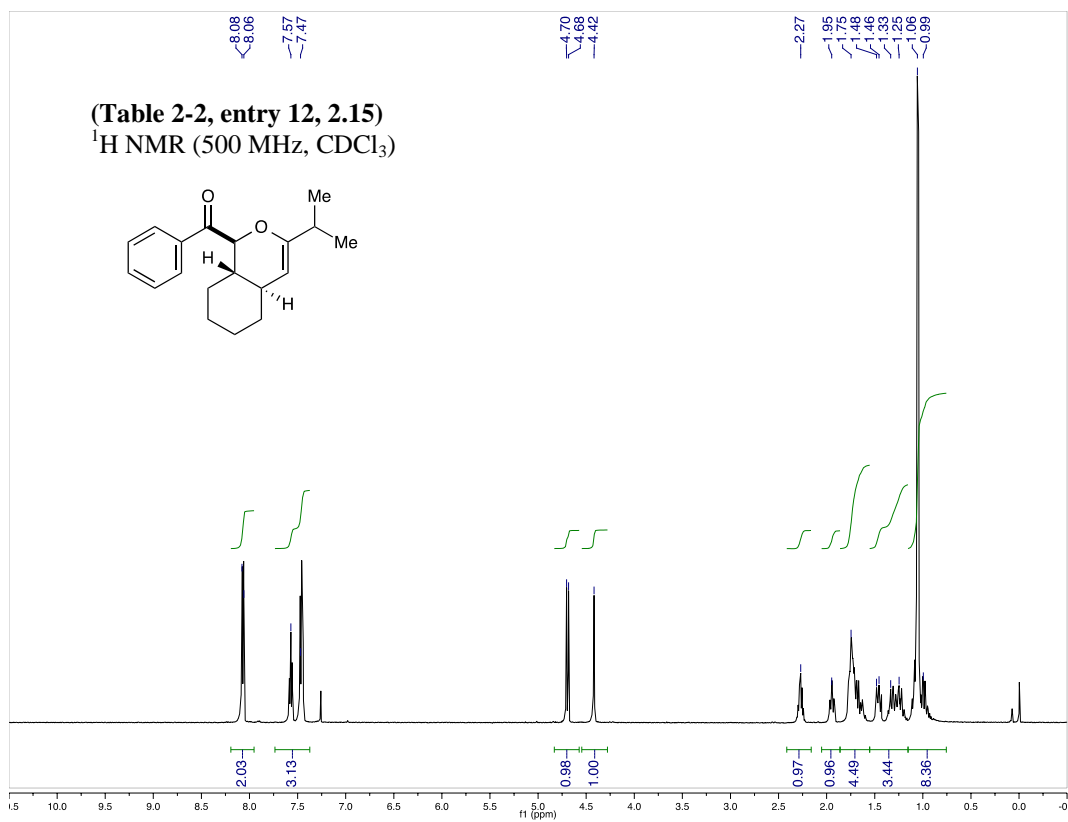


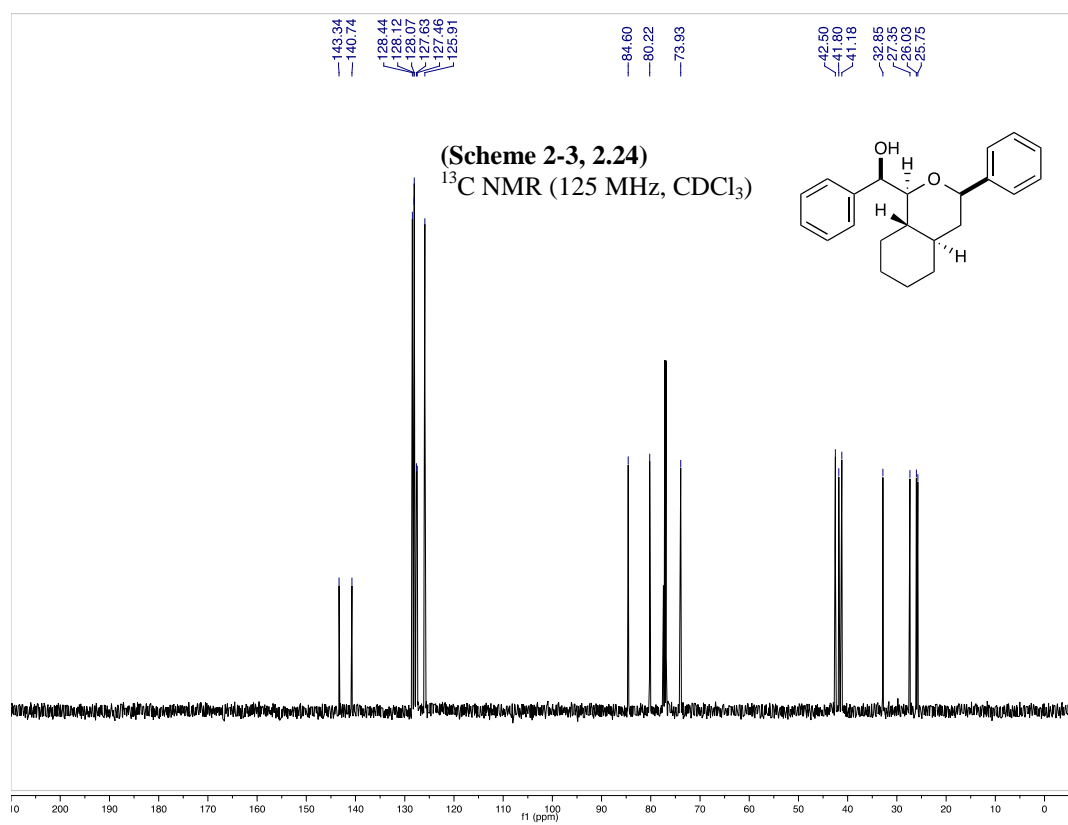
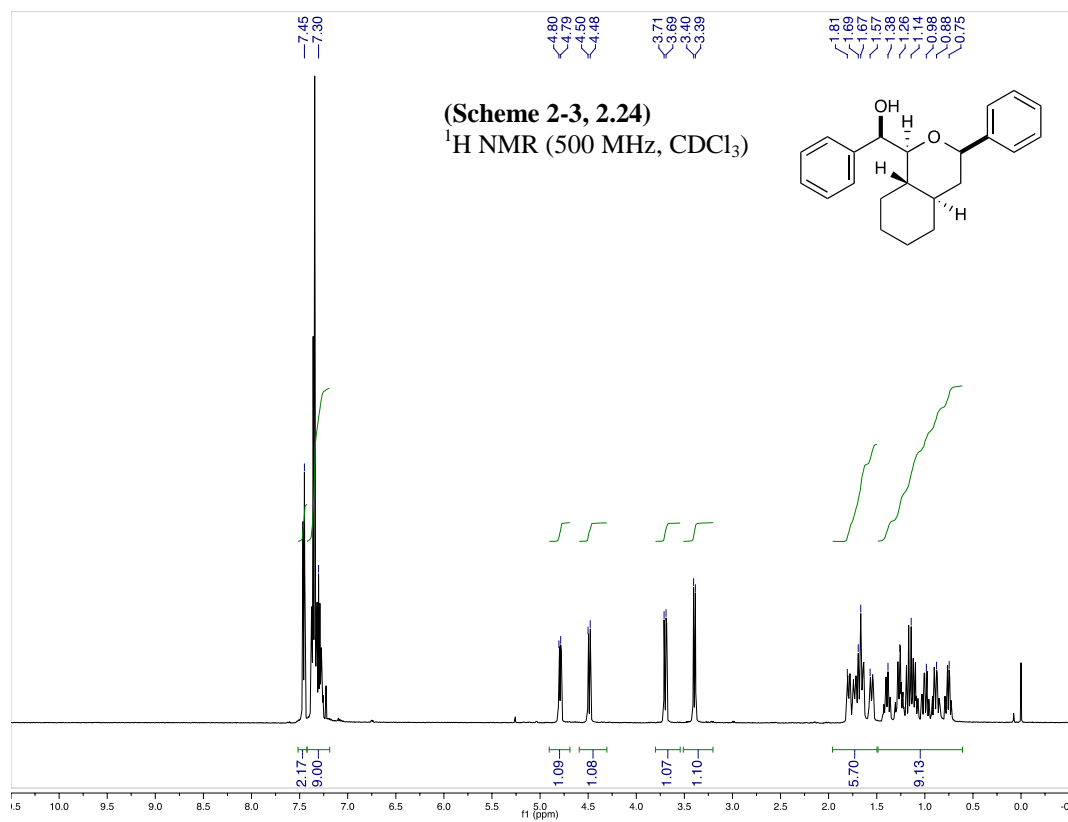


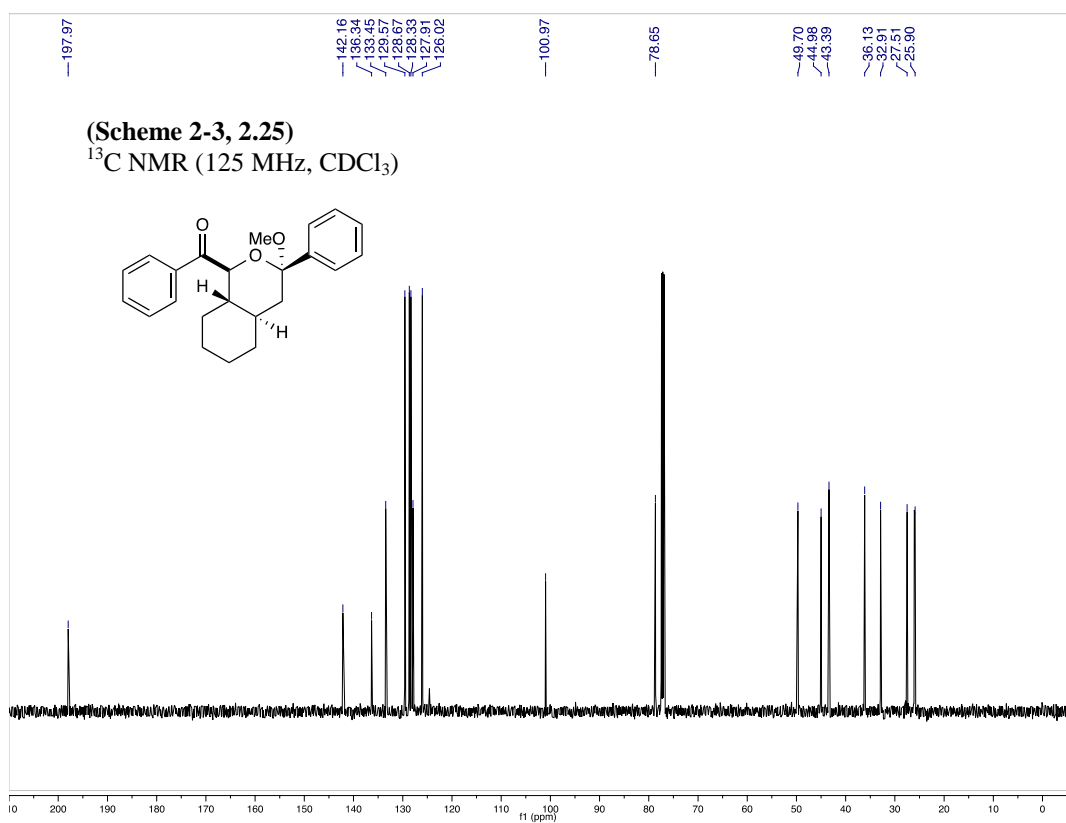
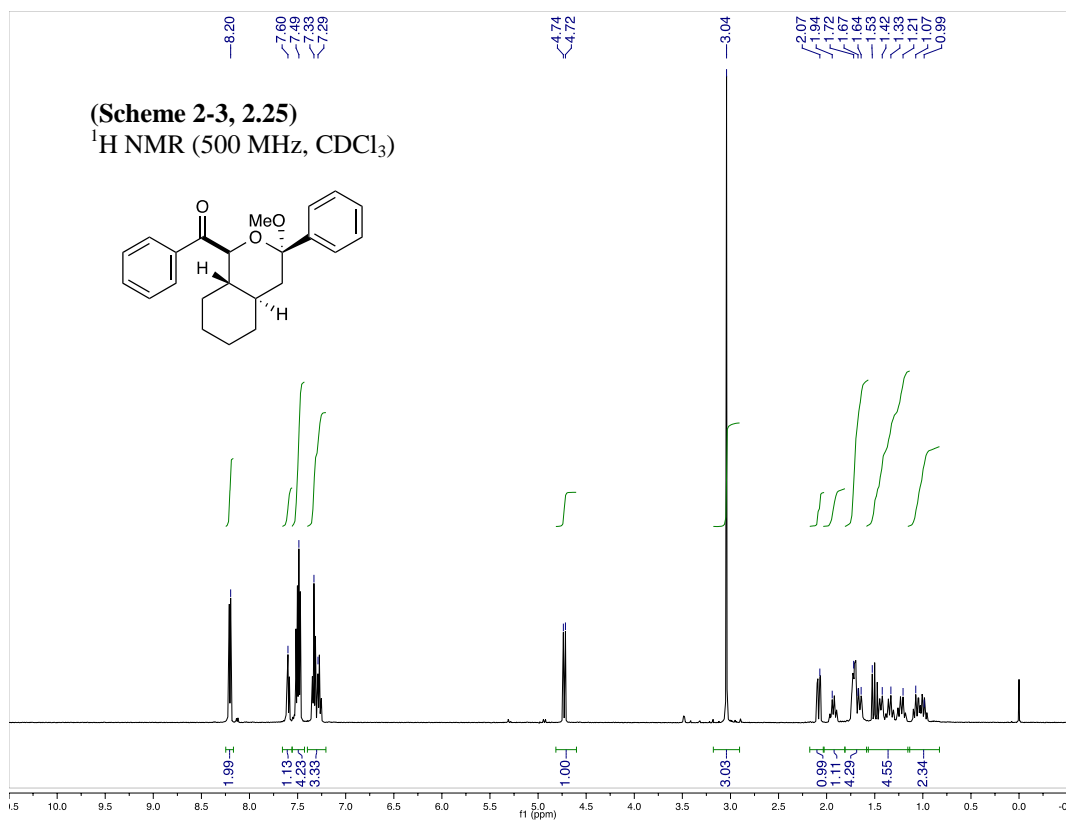


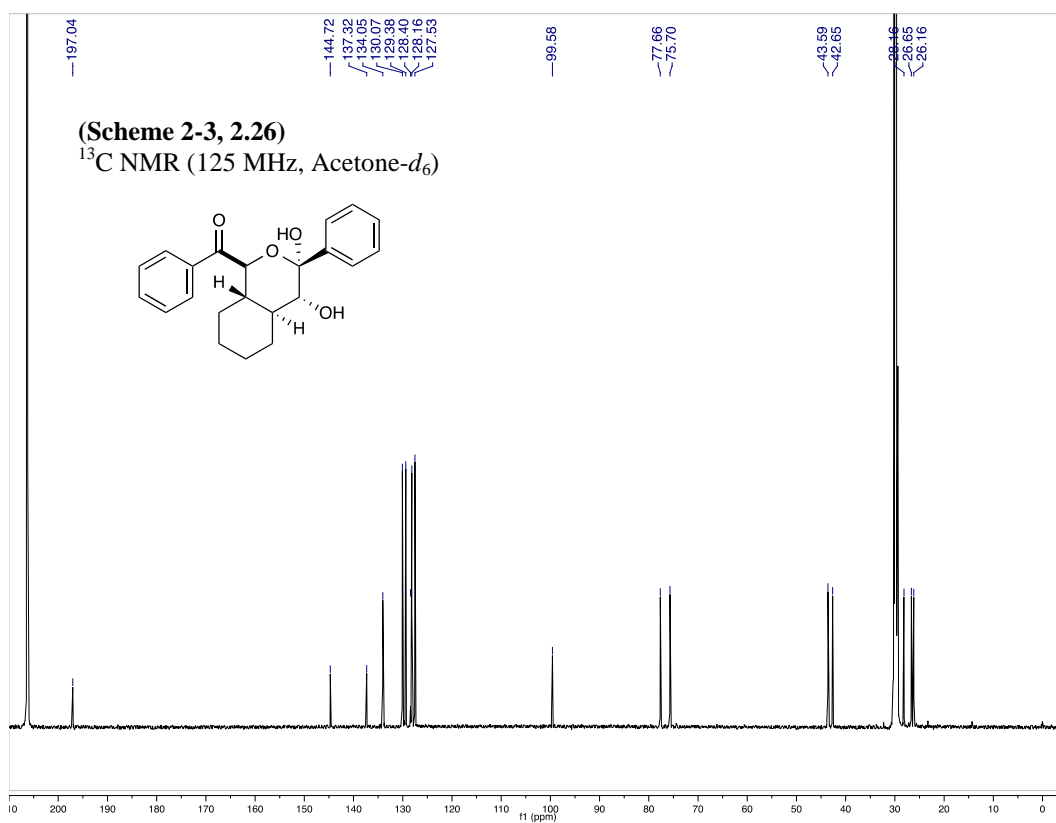
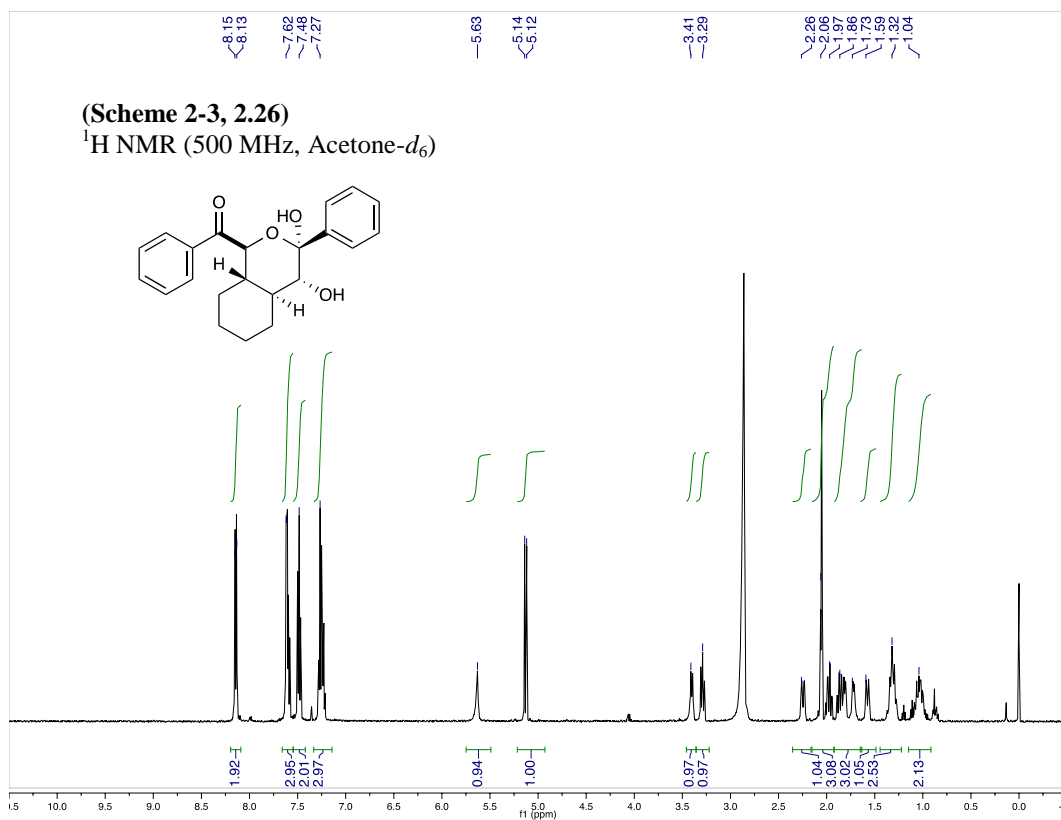


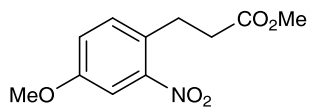
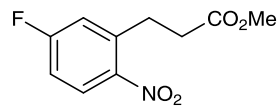
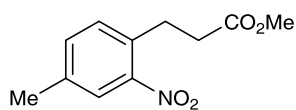
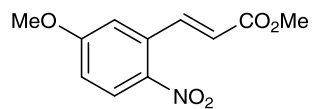
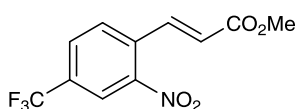
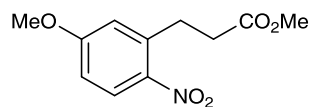
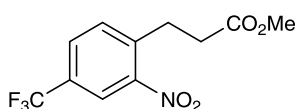
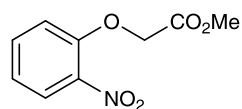
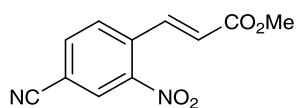
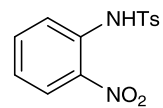
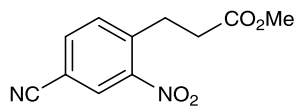
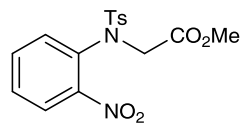
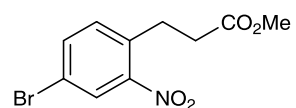
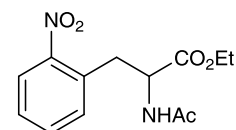
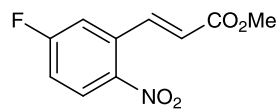


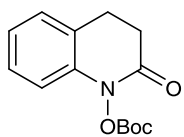




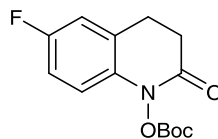




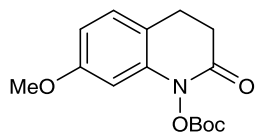
C.2 List of New Compounds for Chapter 3**3.17****3.26****3.19****3.27****3.20****3.28****3.21****3.29****3.22****3.30****3.23****3.31****3.24****3.32****3.25**



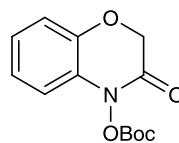
3.13



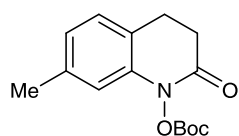
3.38



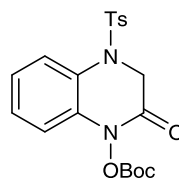
3.33



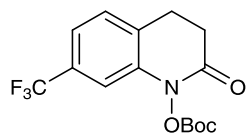
3.39



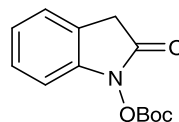
3.34



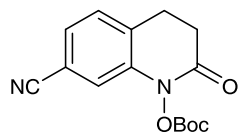
3.40



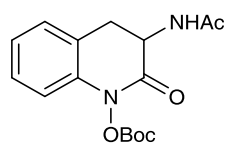
3.35



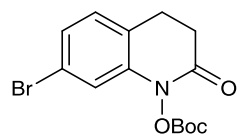
3.41



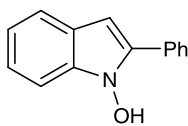
3.36



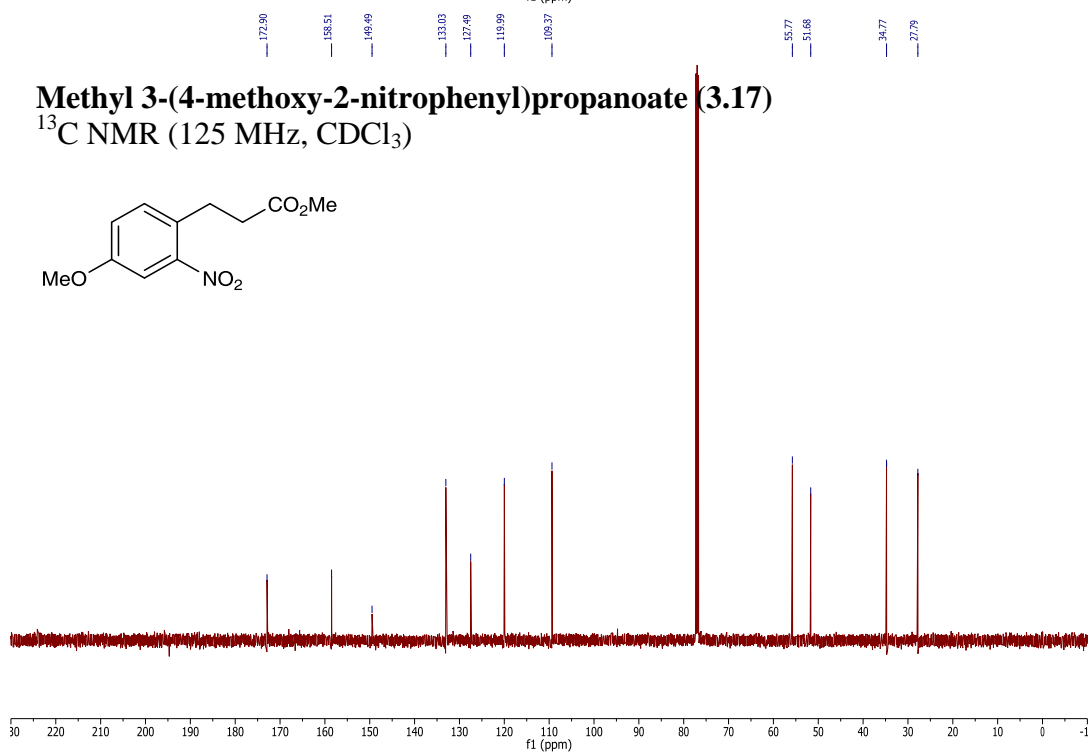
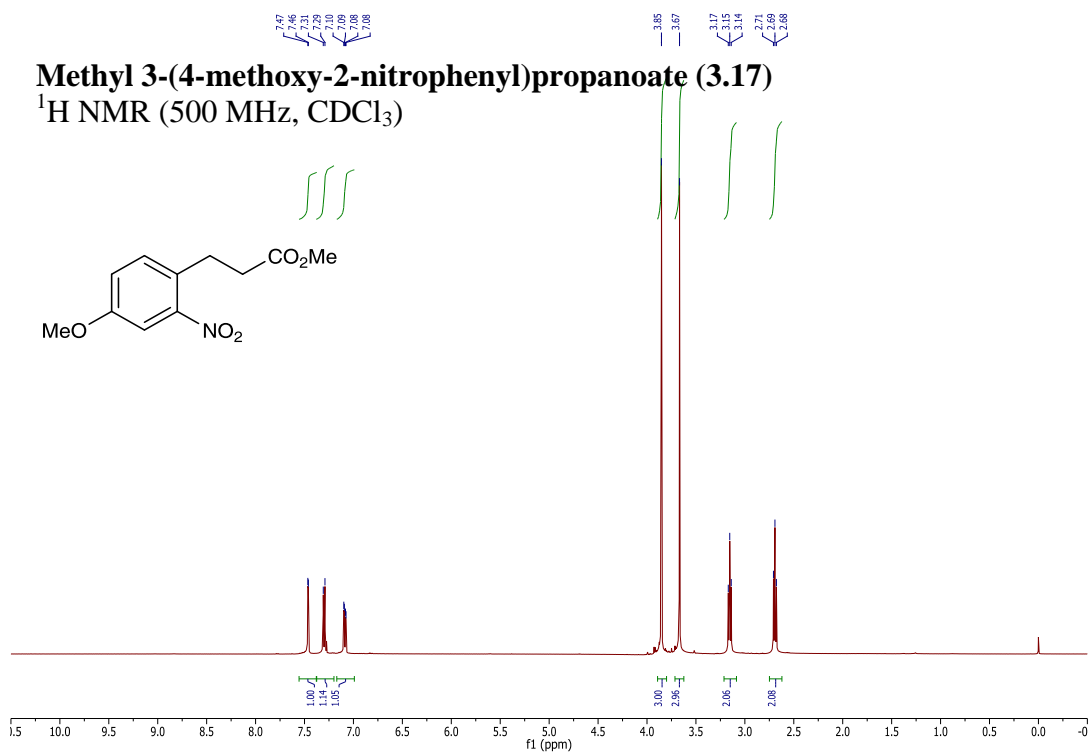
3.42

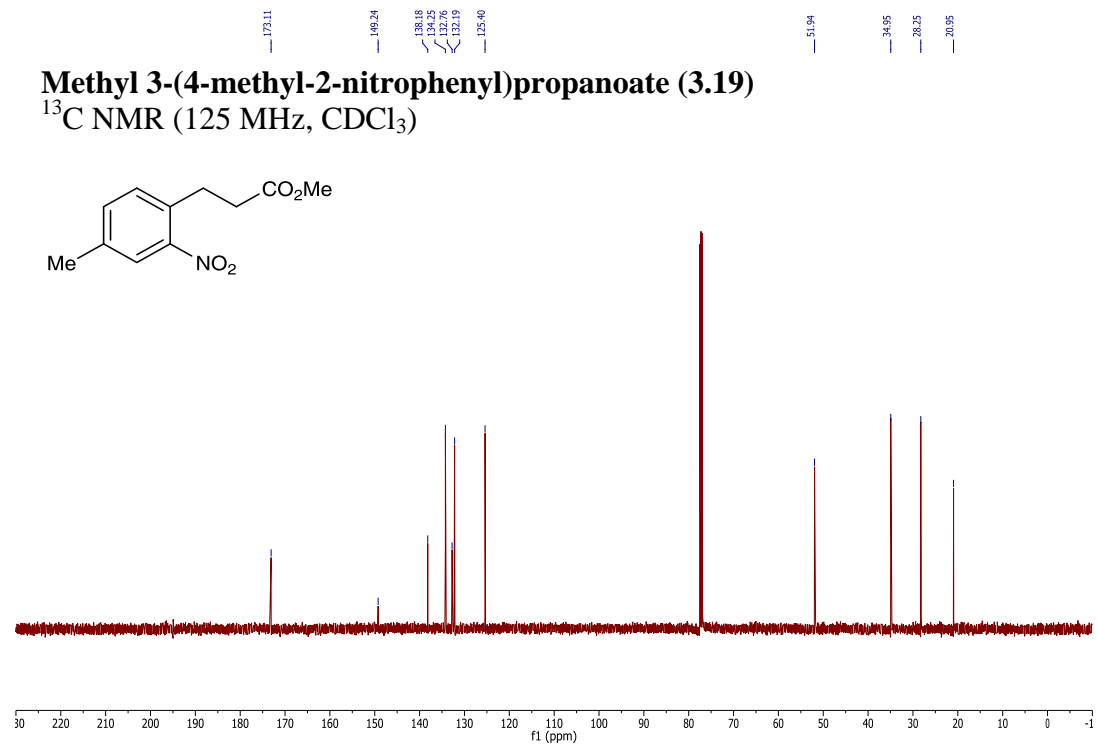
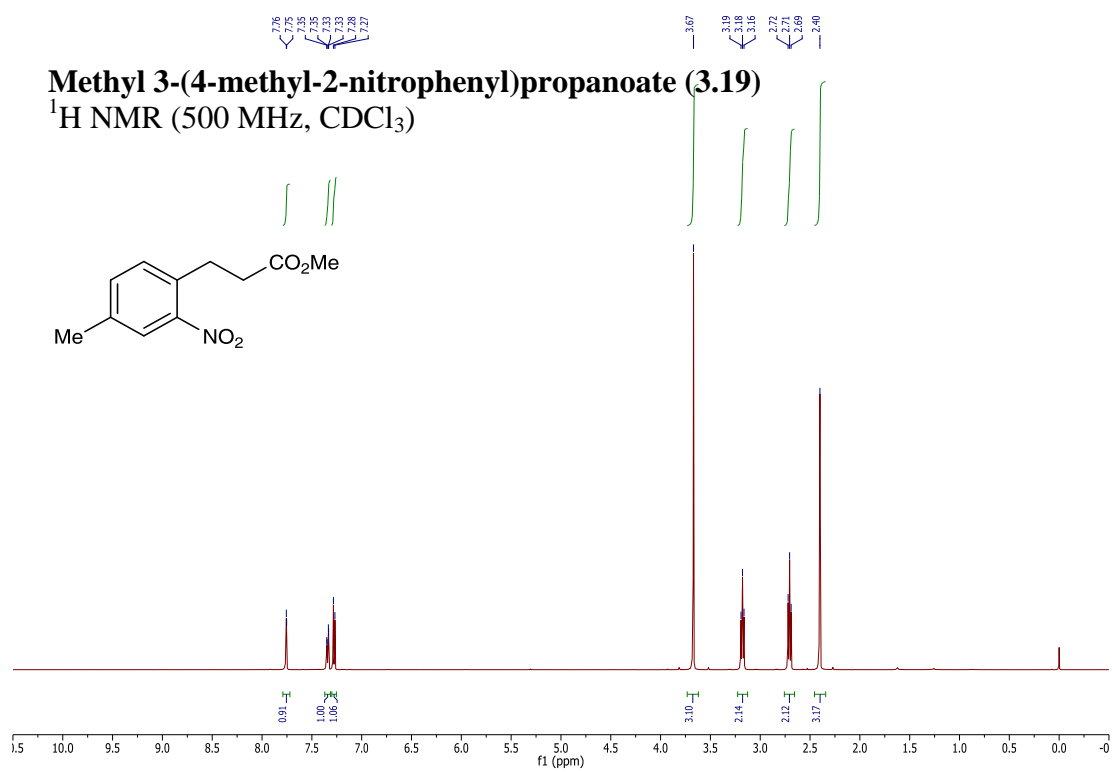


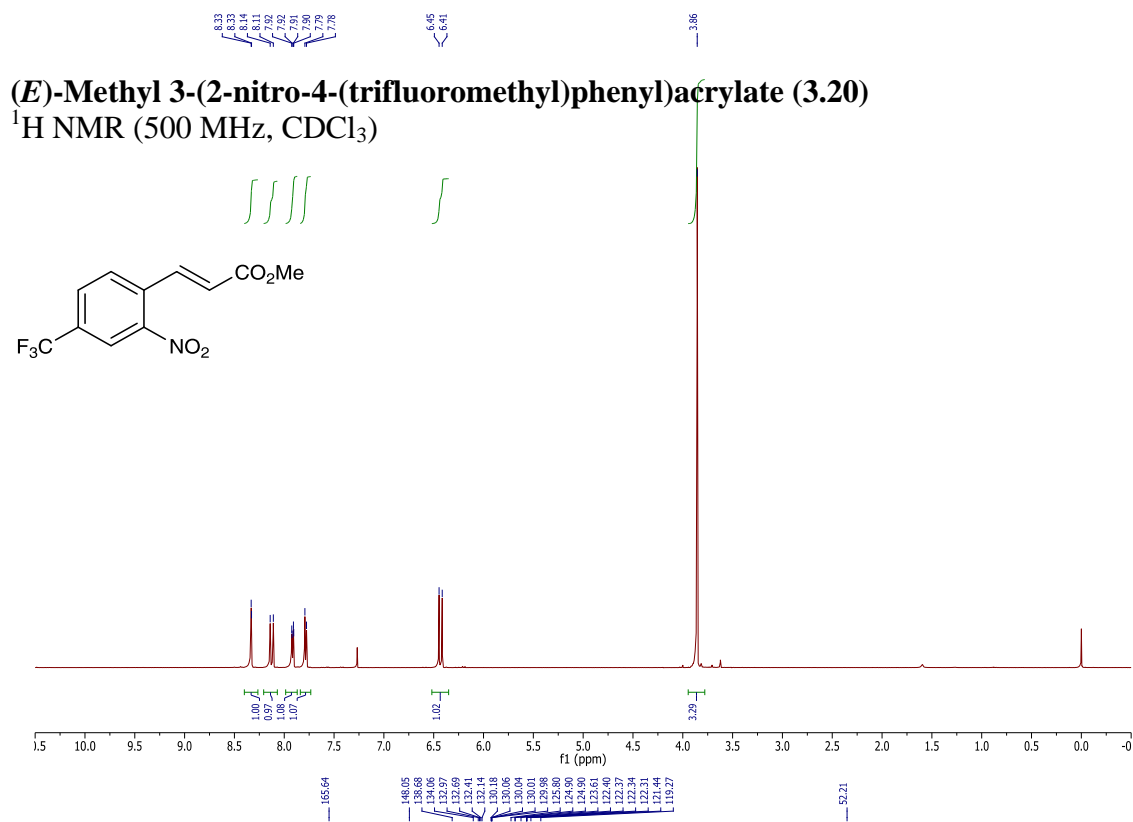
3.37



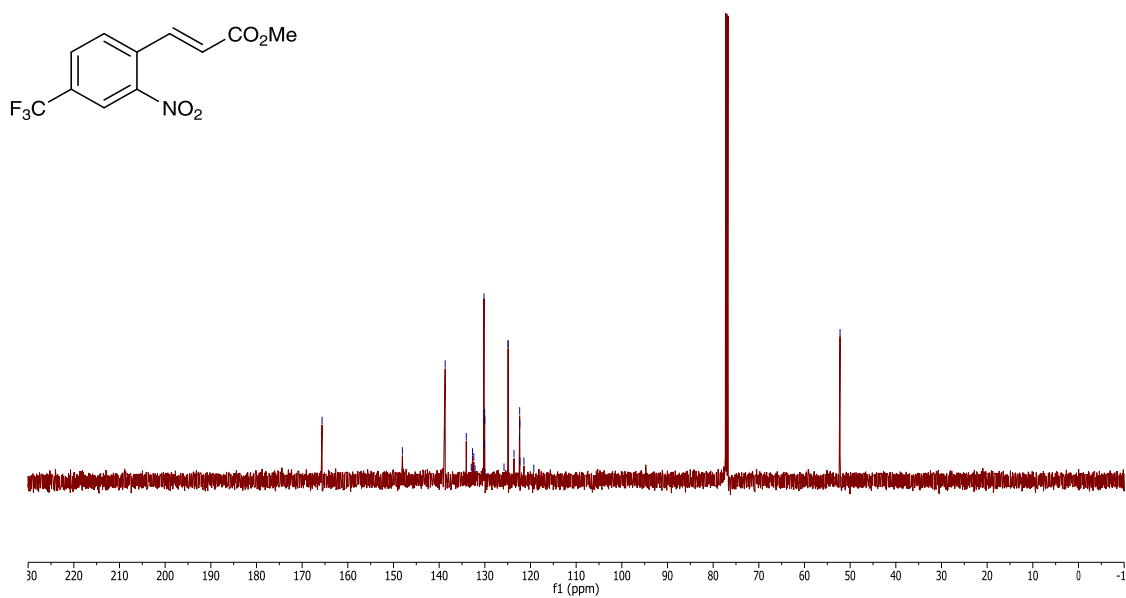
3.12

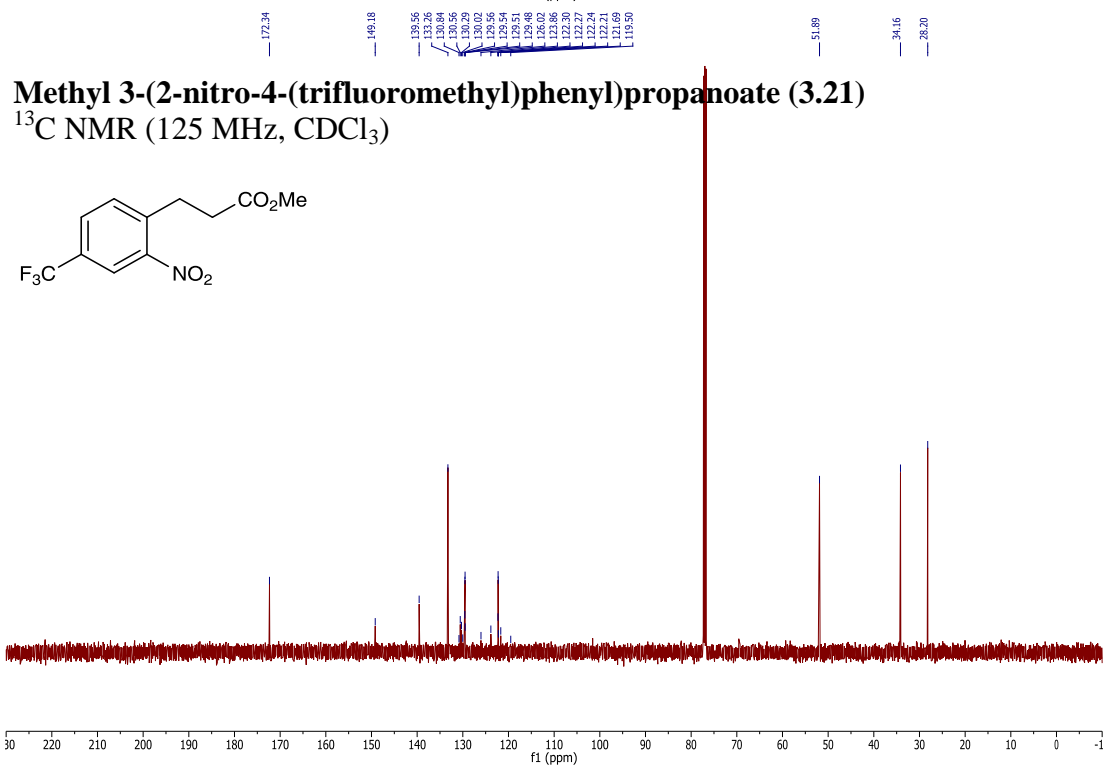
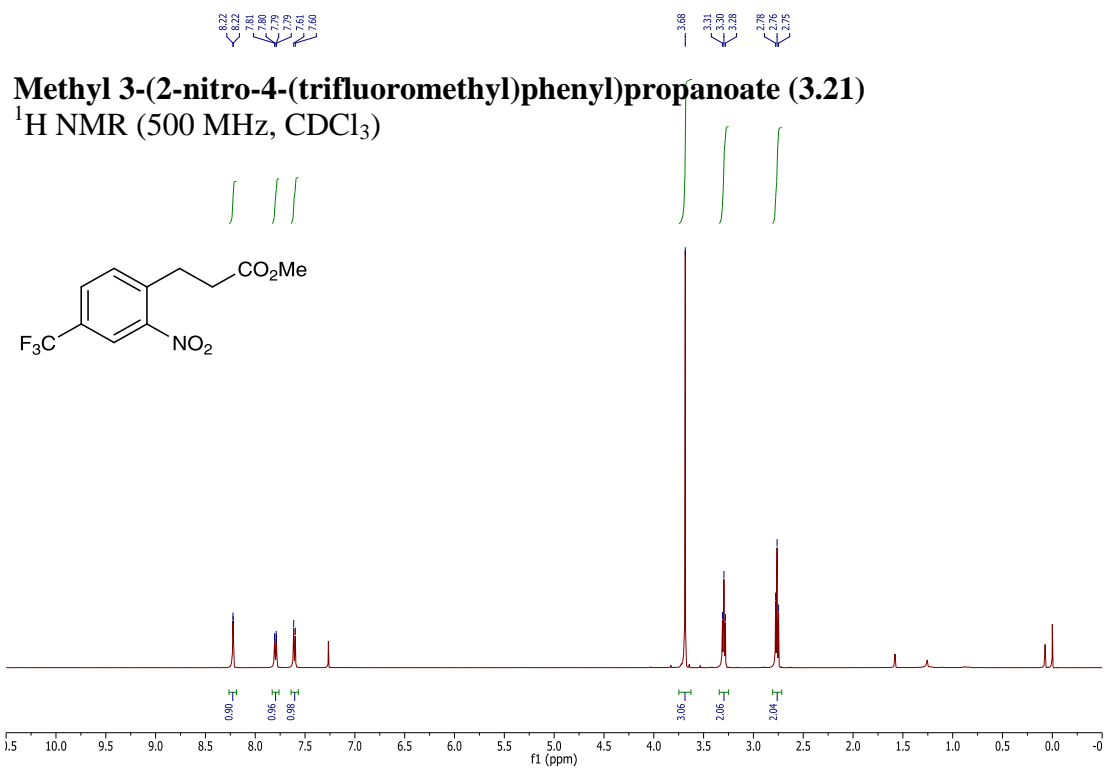


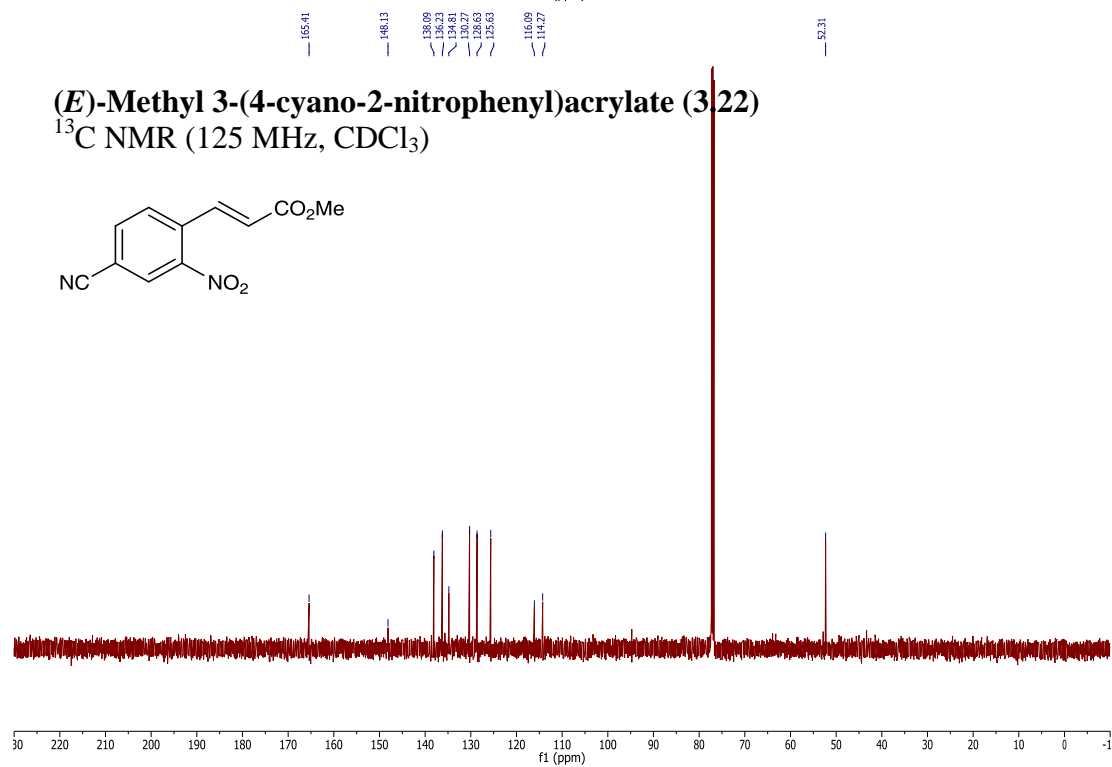
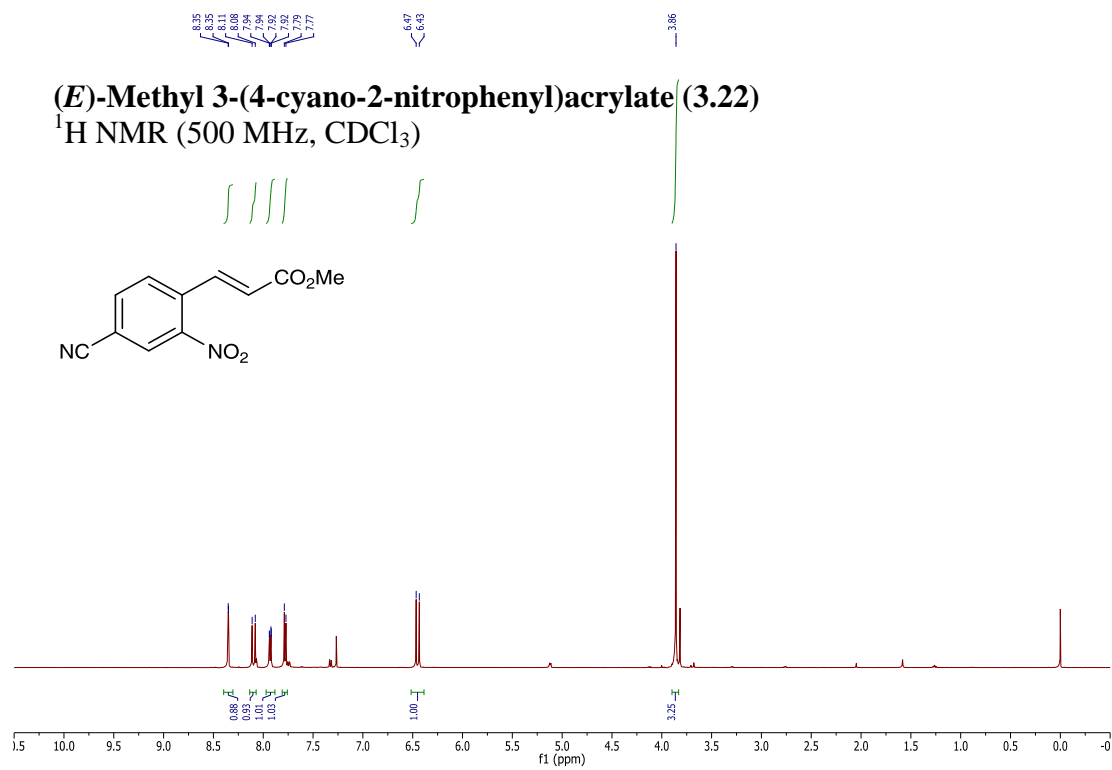


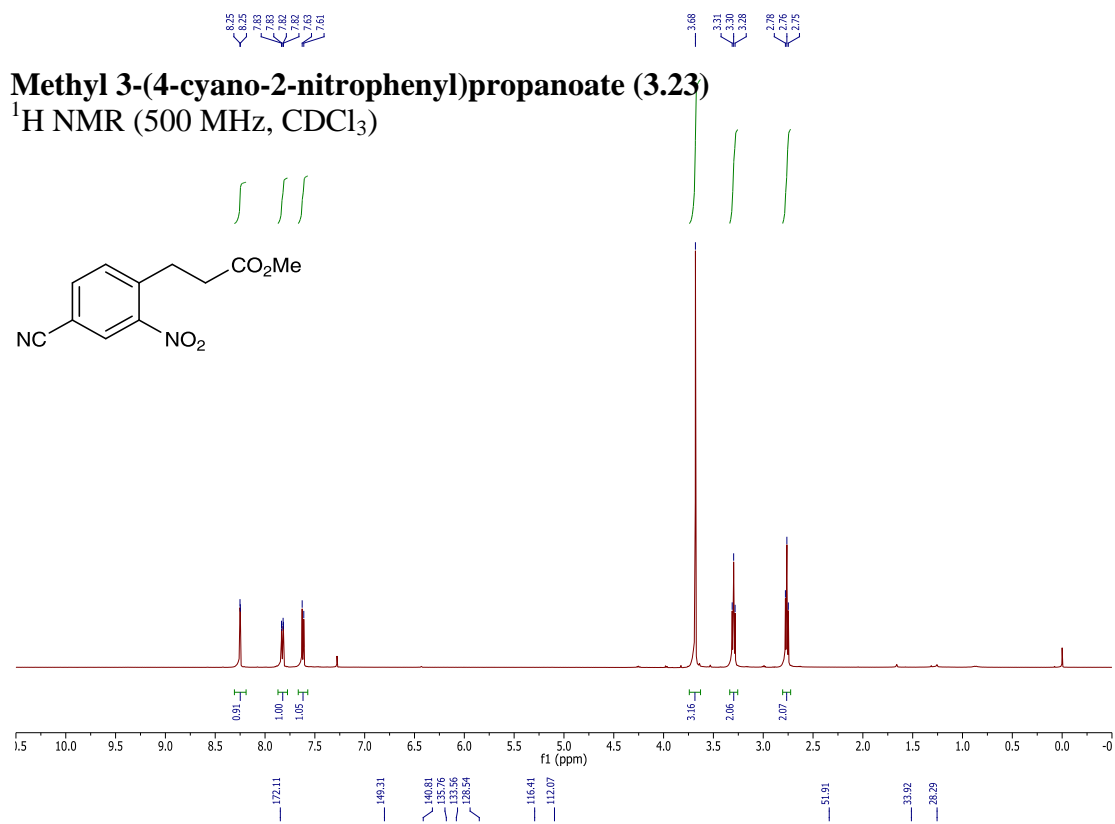


(E)-Methyl 3-(2-nitro-4-(trifluoromethyl)phenyl)acrylate (3.20)
¹³C NMR (125 MHz, CDCl₃)

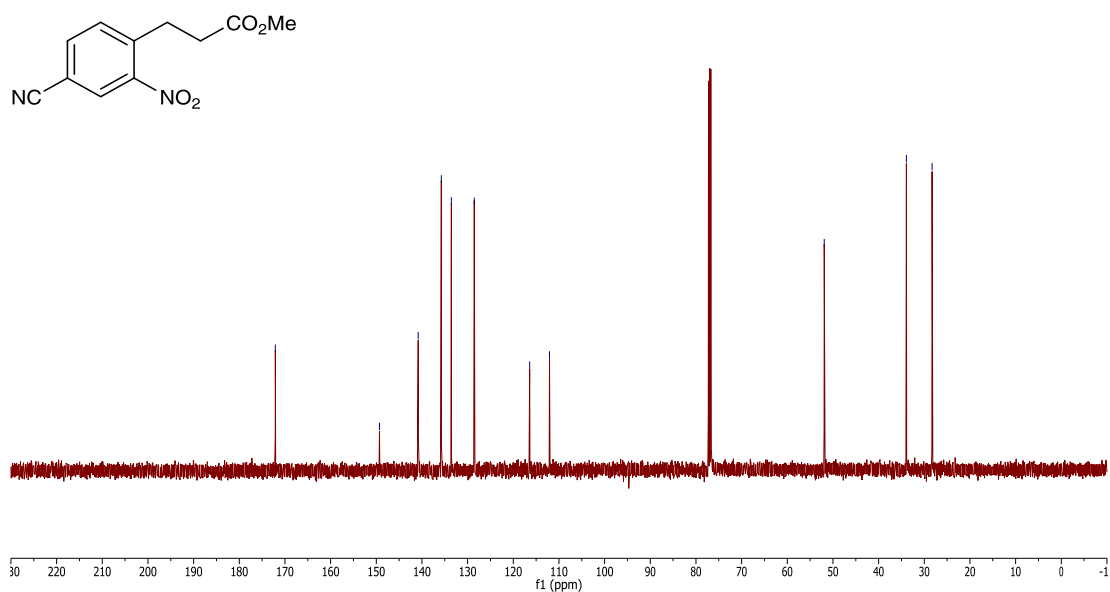


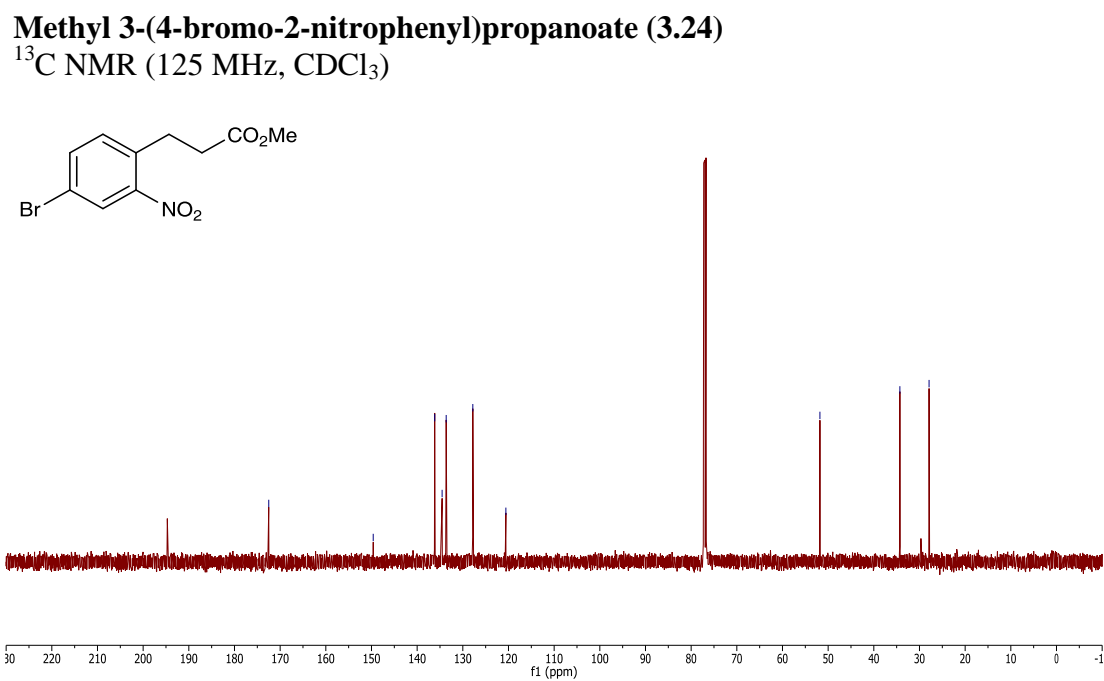
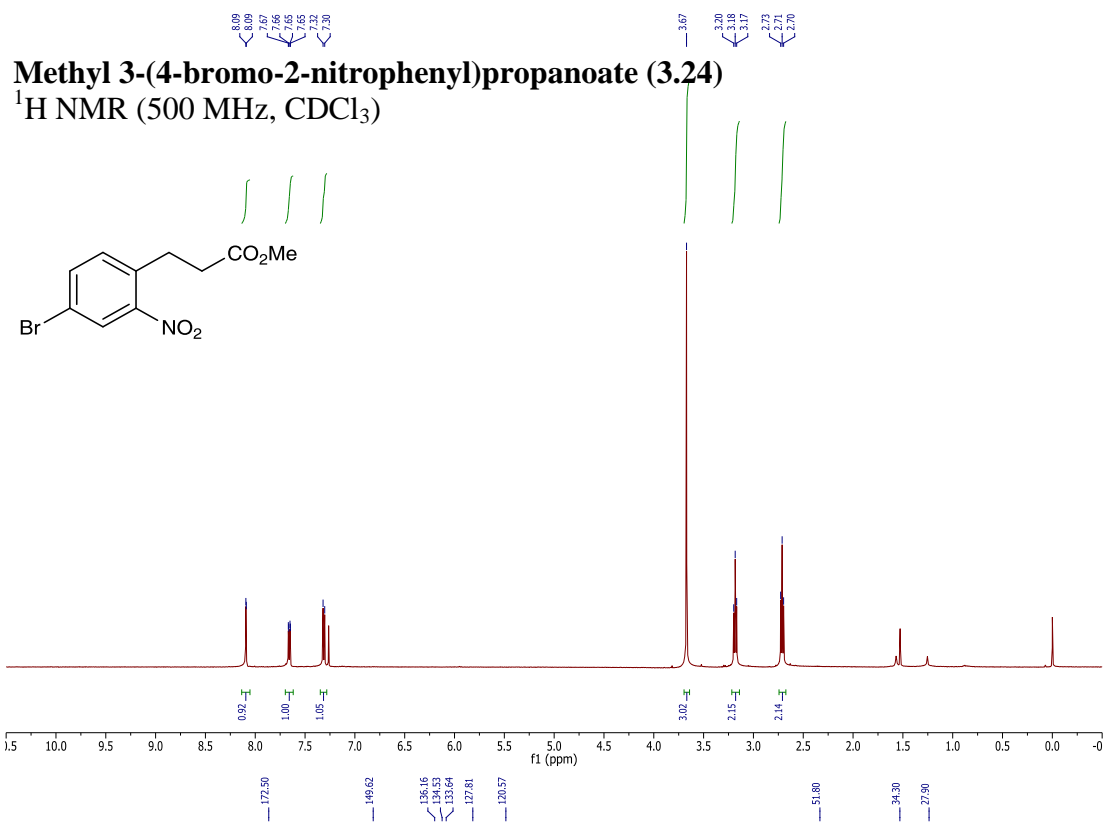


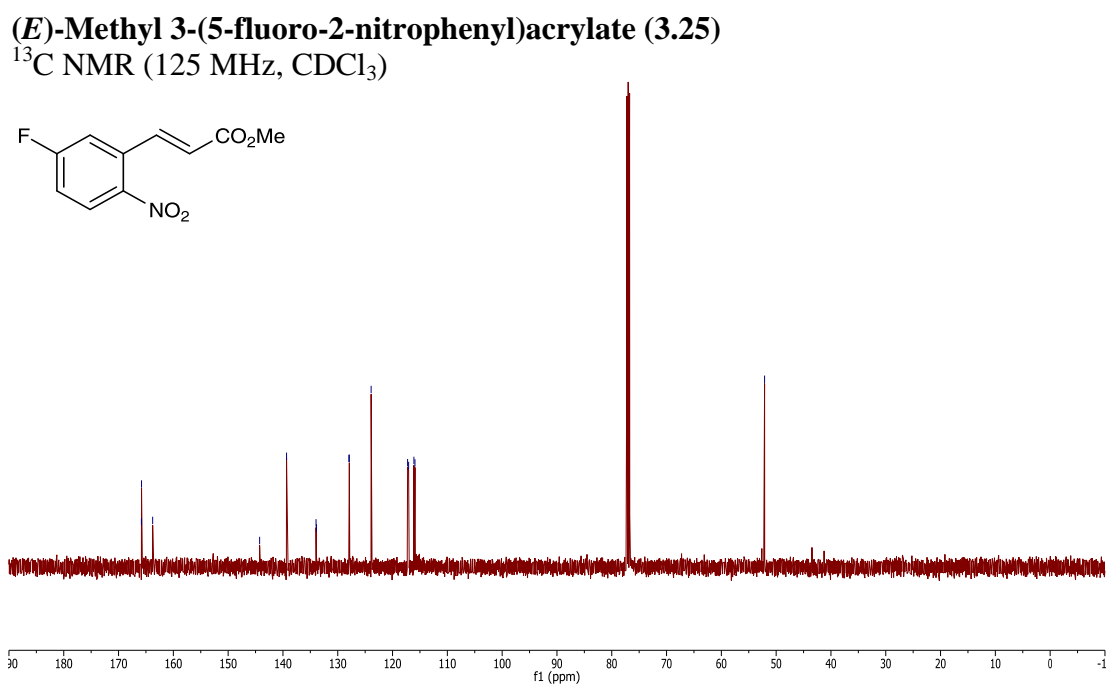
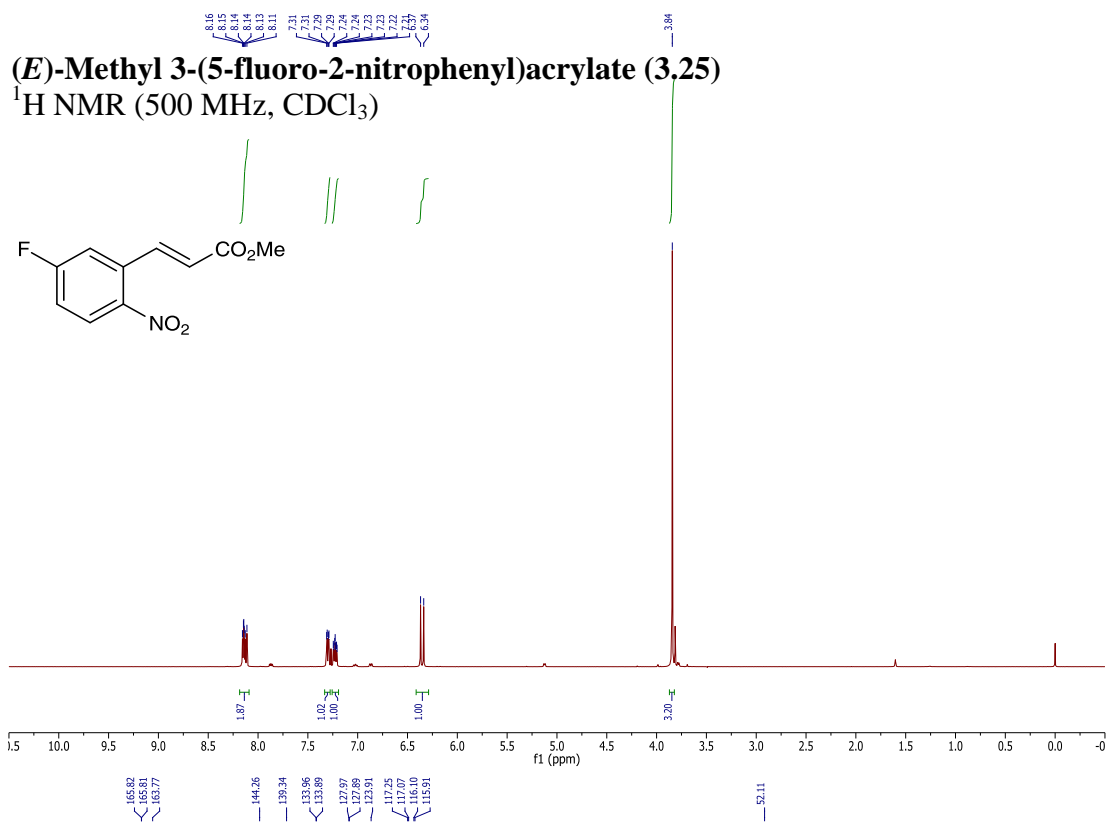


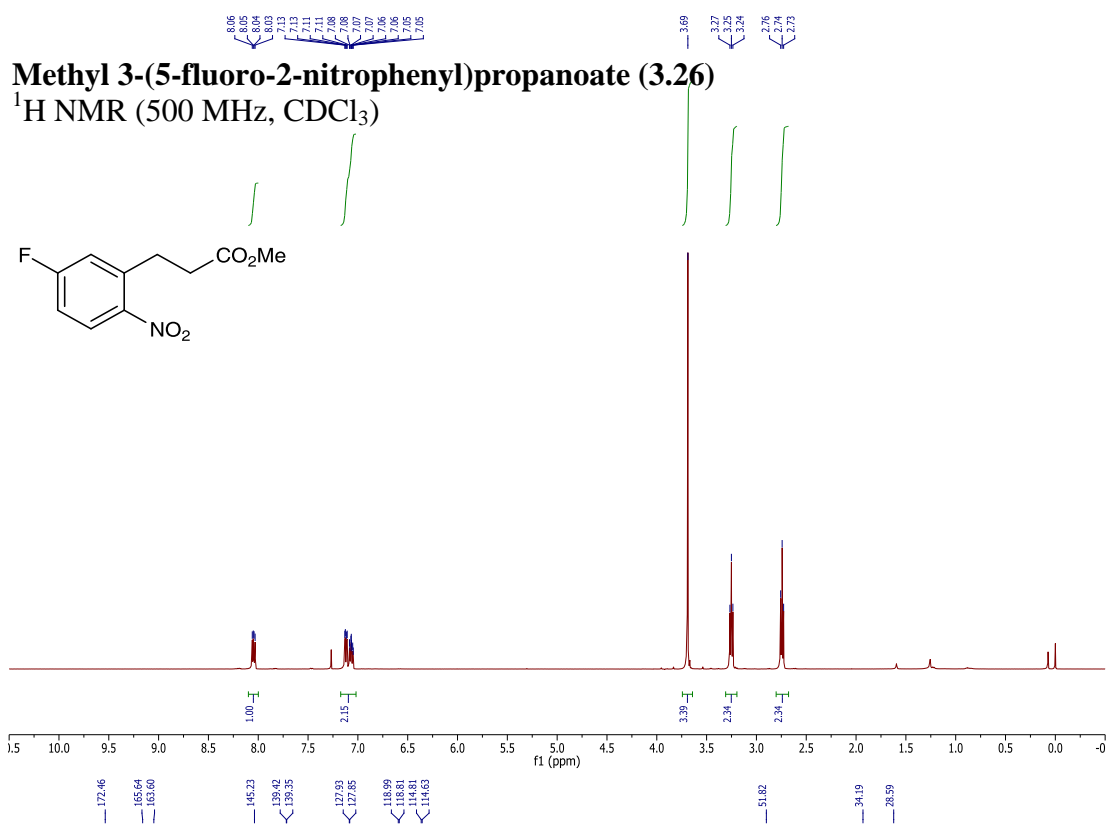


Methyl 3-(4-cyano-2-nitrophenyl)propanoate (3.23)
¹³C NMR (125 MHz, CDCl₃)

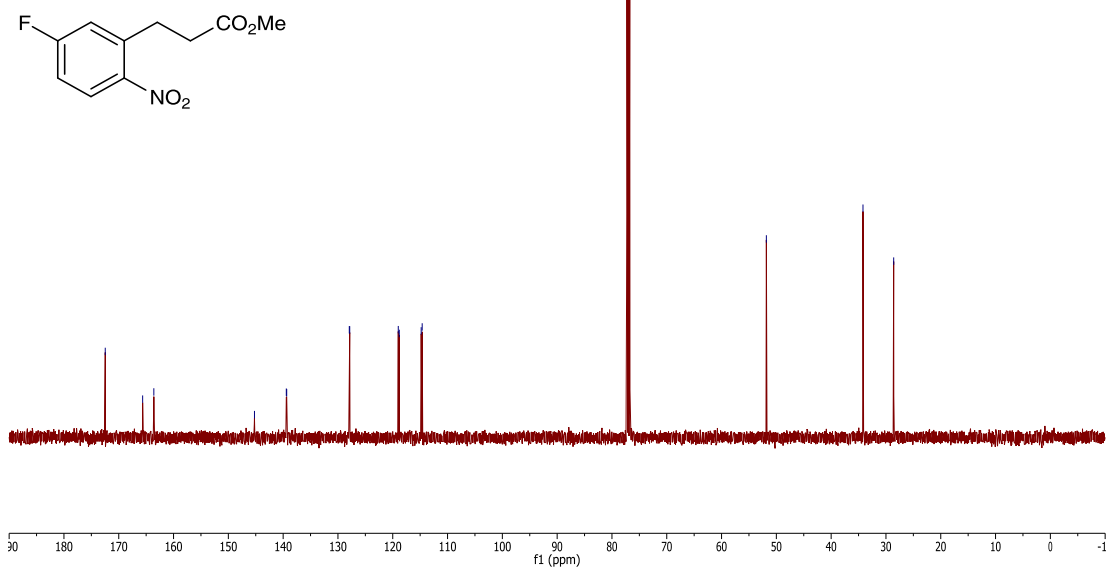


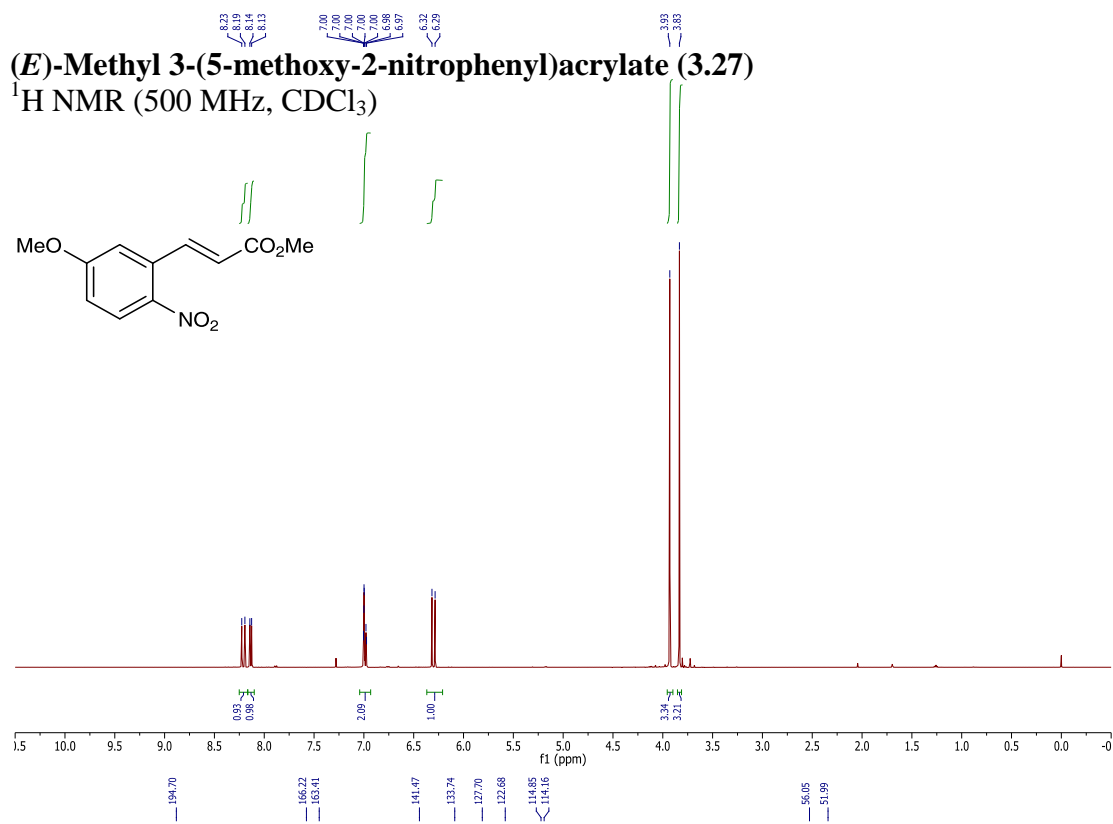




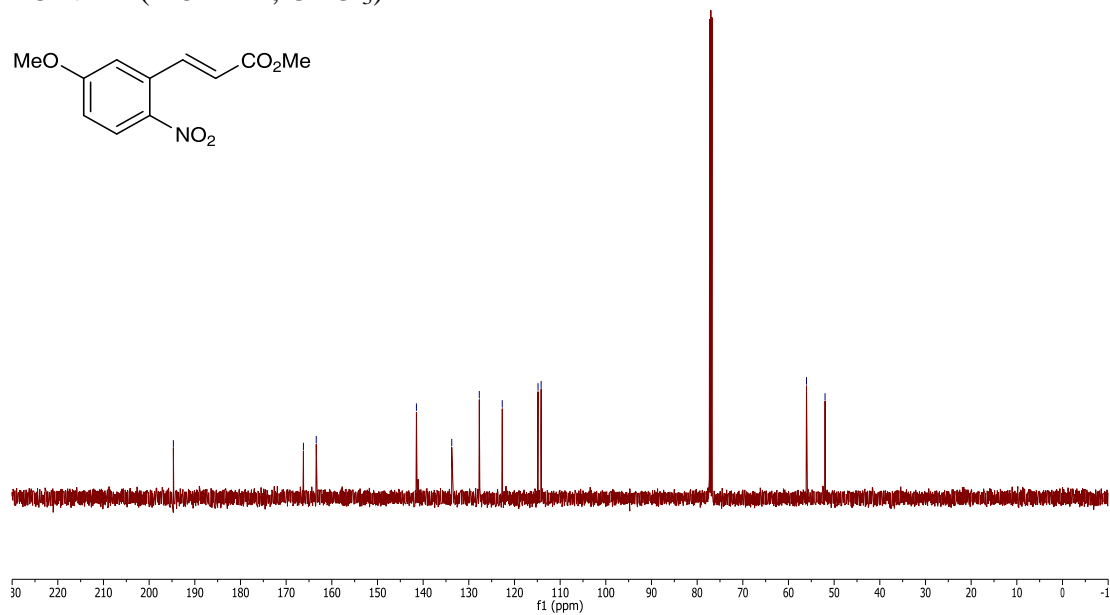


Methyl 3-(5-fluoro-2-nitrophenyl)propanoate (3.26)
 ^{13}C NMR (125 MHz, CDCl_3)

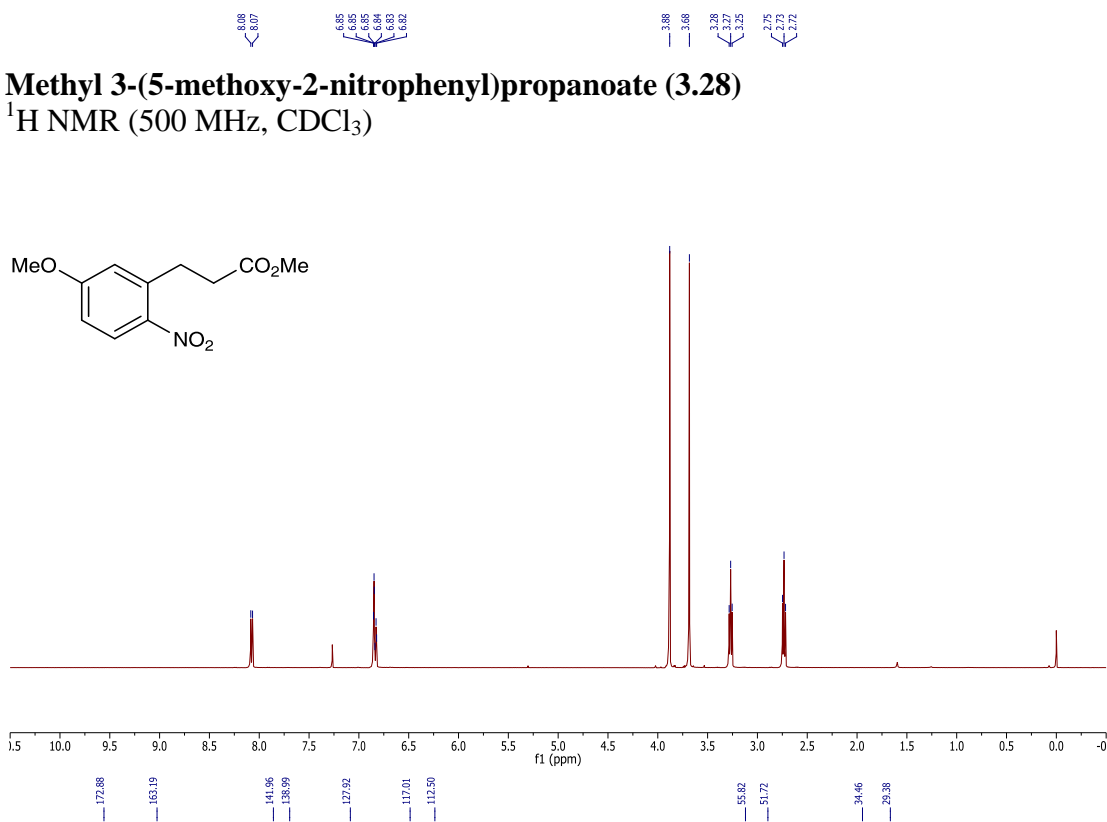




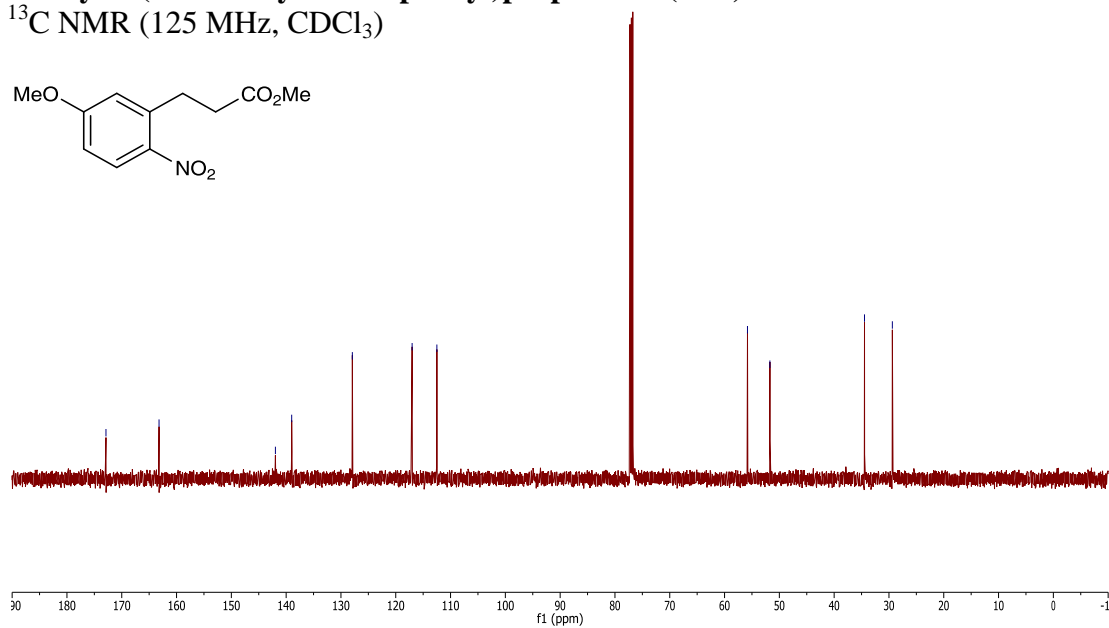
(E)-Methyl 3-(5-methoxy-2-nitrophenyl)acrylate (3.27)
 ^{13}C NMR (125 MHz, CDCl_3)

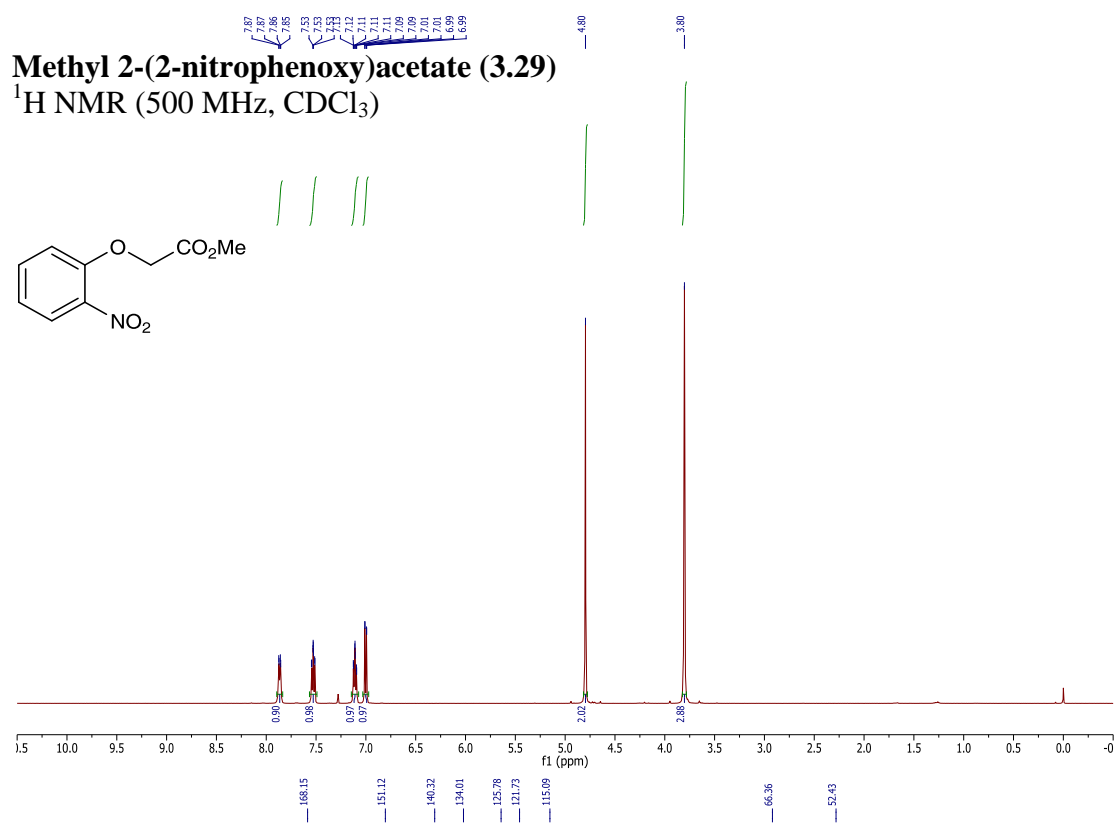


Methyl 3-(5-methoxy-2-nitrophenyl)propanoate (3.28)
 ^1H NMR (500 MHz, CDCl_3)

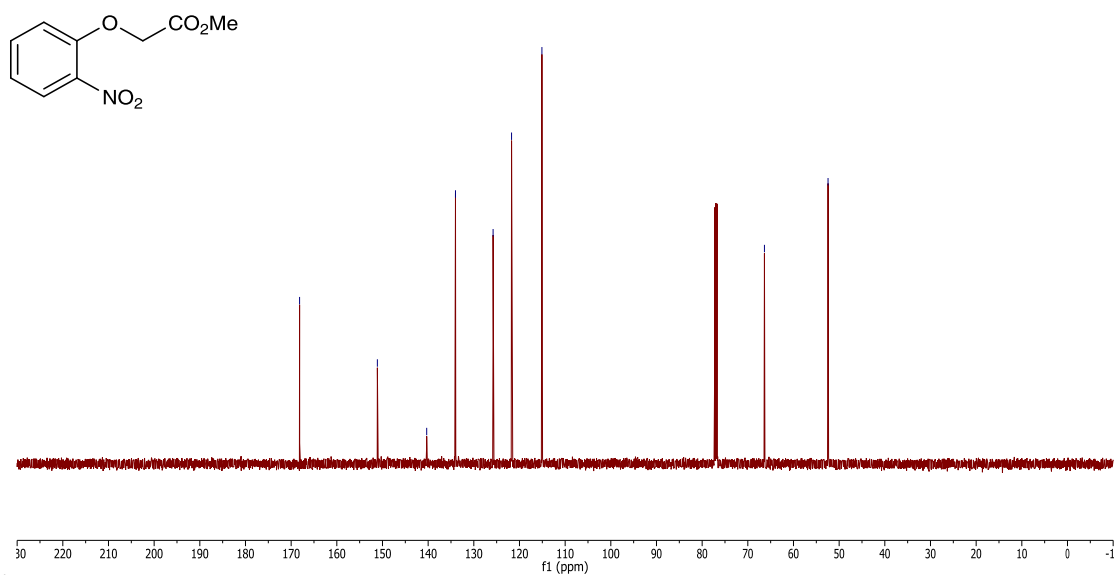


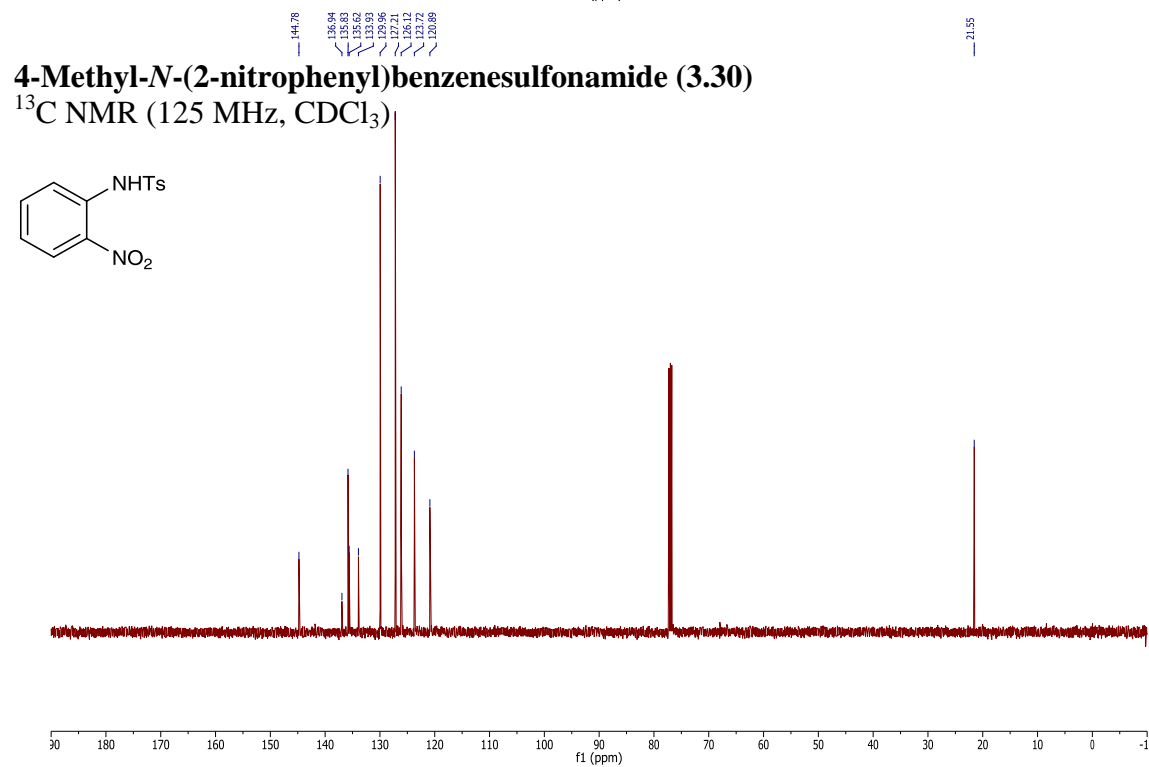
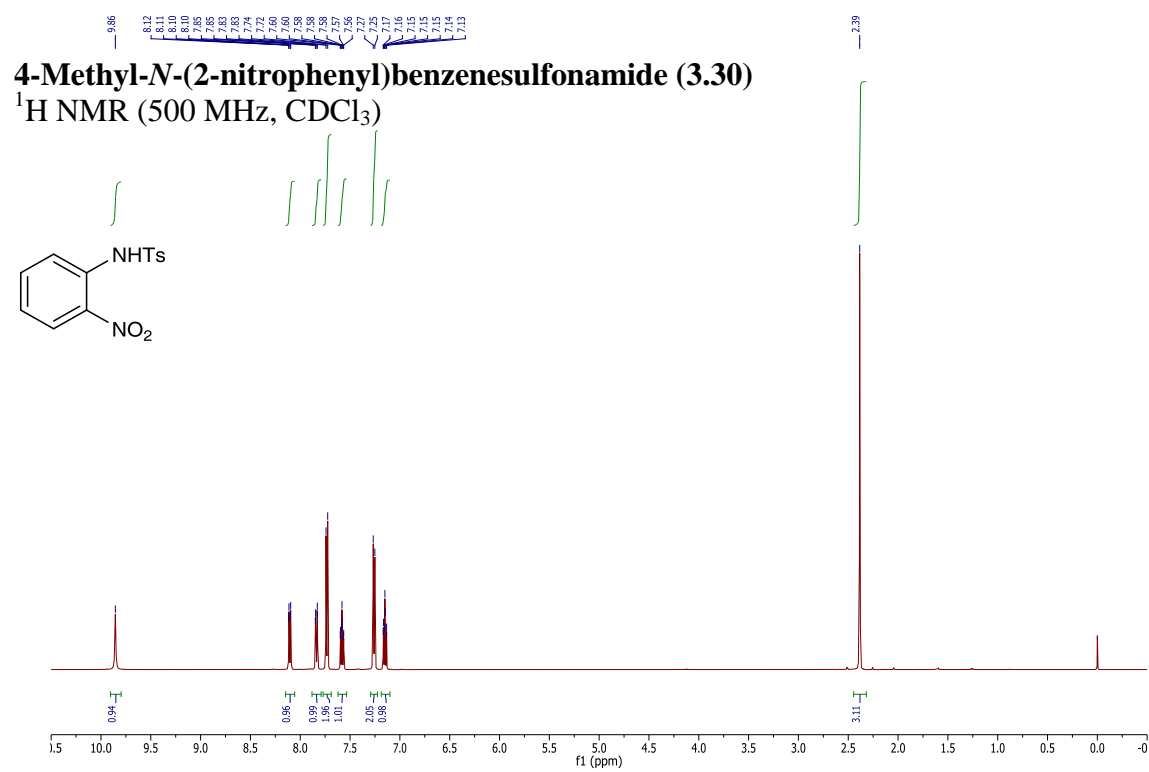
Methyl 3-(5-methoxy-2-nitrophenyl)propanoate (3.28)
 ^{13}C NMR (125 MHz, CDCl_3)





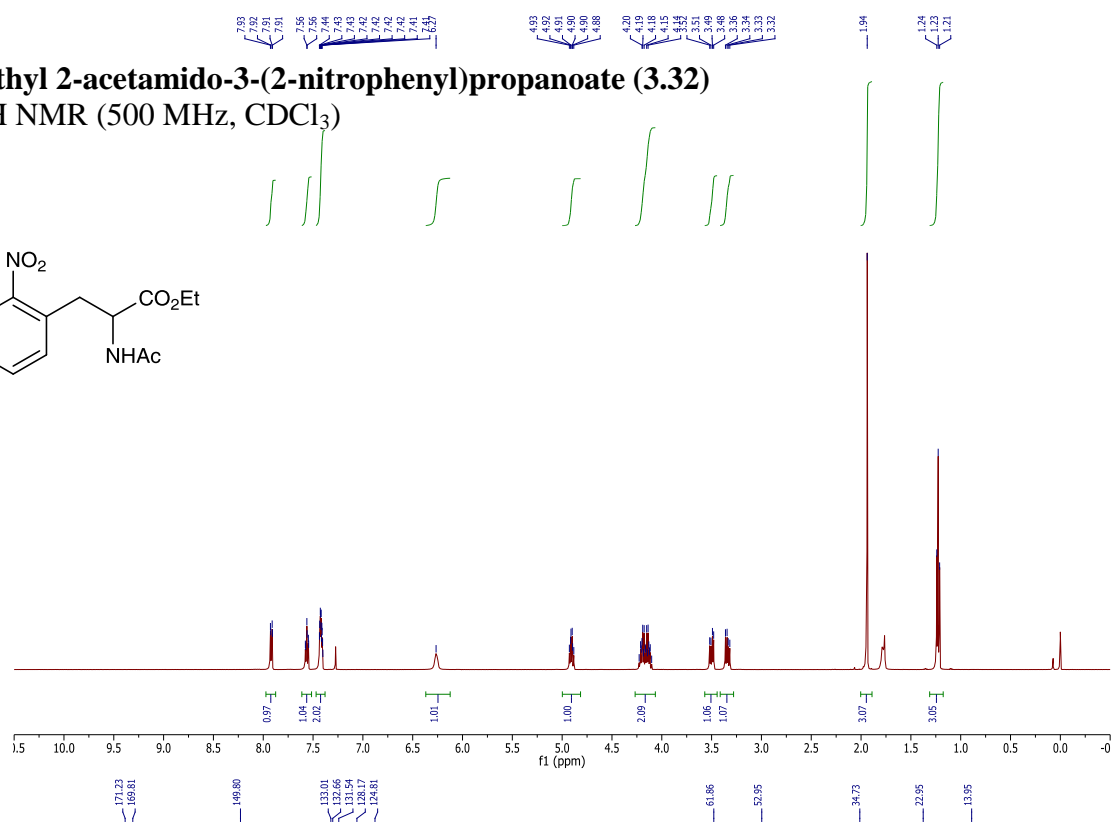
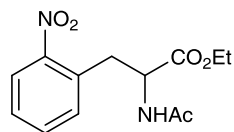
Methyl 2-(2-nitrophenoxy)acetate (3.29)
 $^{13}\text{C NMR}$ (125 MHz, CDCl_3)





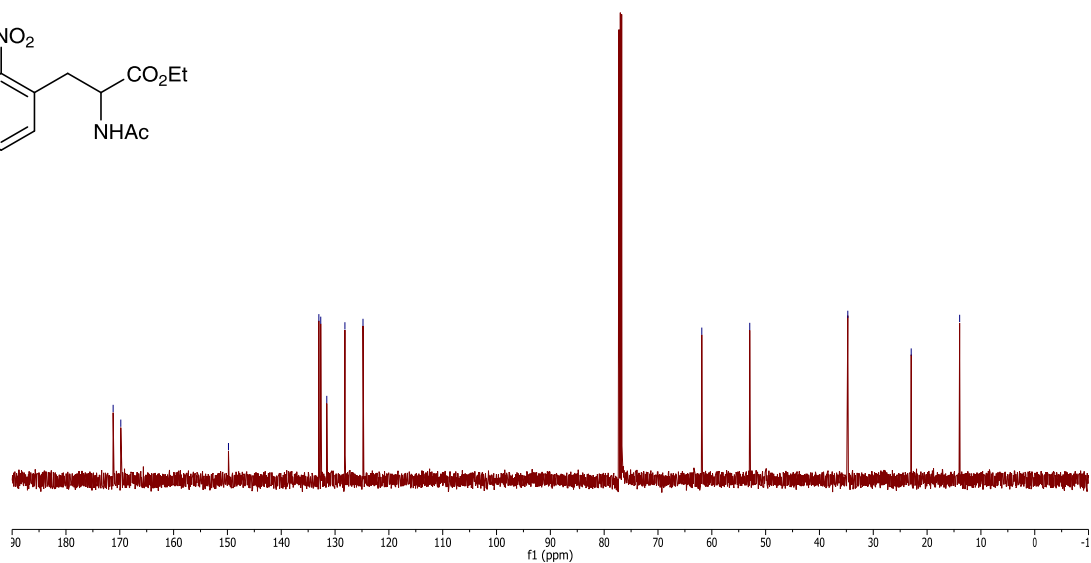
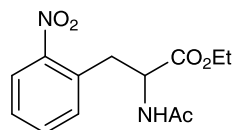
Ethyl 2-acetamido-3-(2-nitrophenyl)propanoate (3.32)

$^1\text{H NMR}$ (500 MHz, CDCl_3)

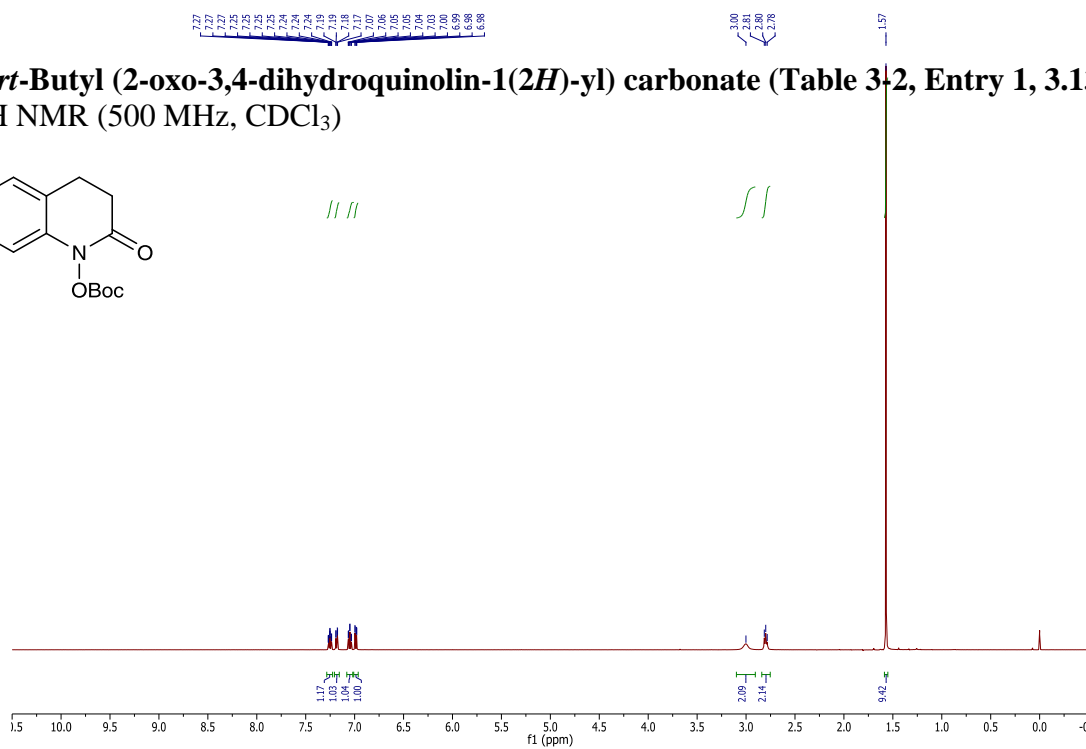
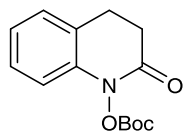


Ethyl 2-acetamido-3-(2-nitrophenyl)propanoate (3.32)

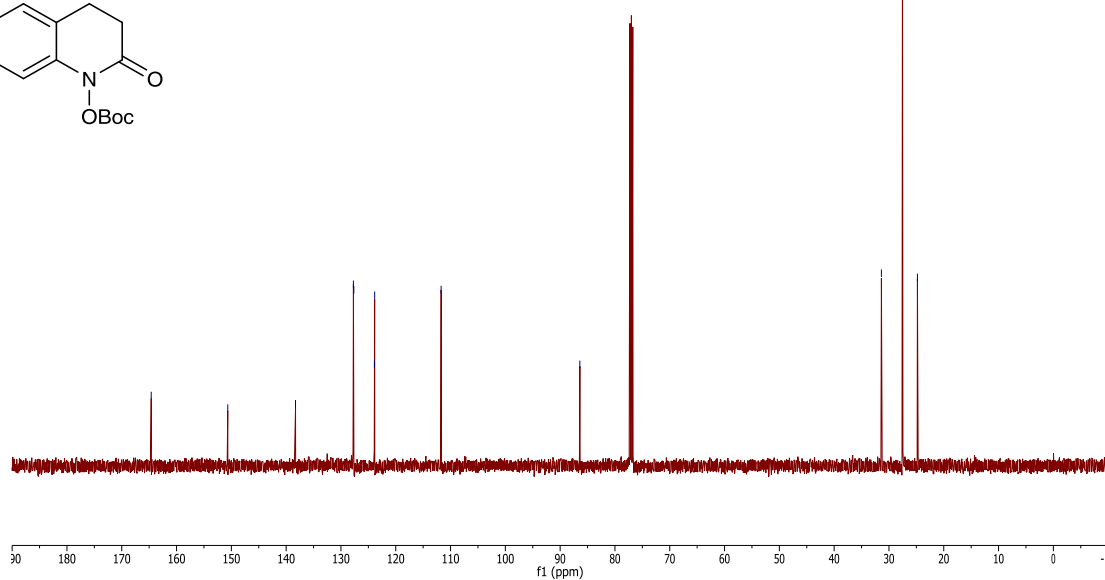
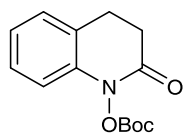
$^{13}\text{C NMR}$ (125 MHz, CDCl_3)



***tert*-Butyl (2-oxo-3,4-dihydroquinolin-1(2*H*)-yl) carbonate (Table 3-2, Entry 1, 3.13)**
¹H NMR (500 MHz, CDCl₃)

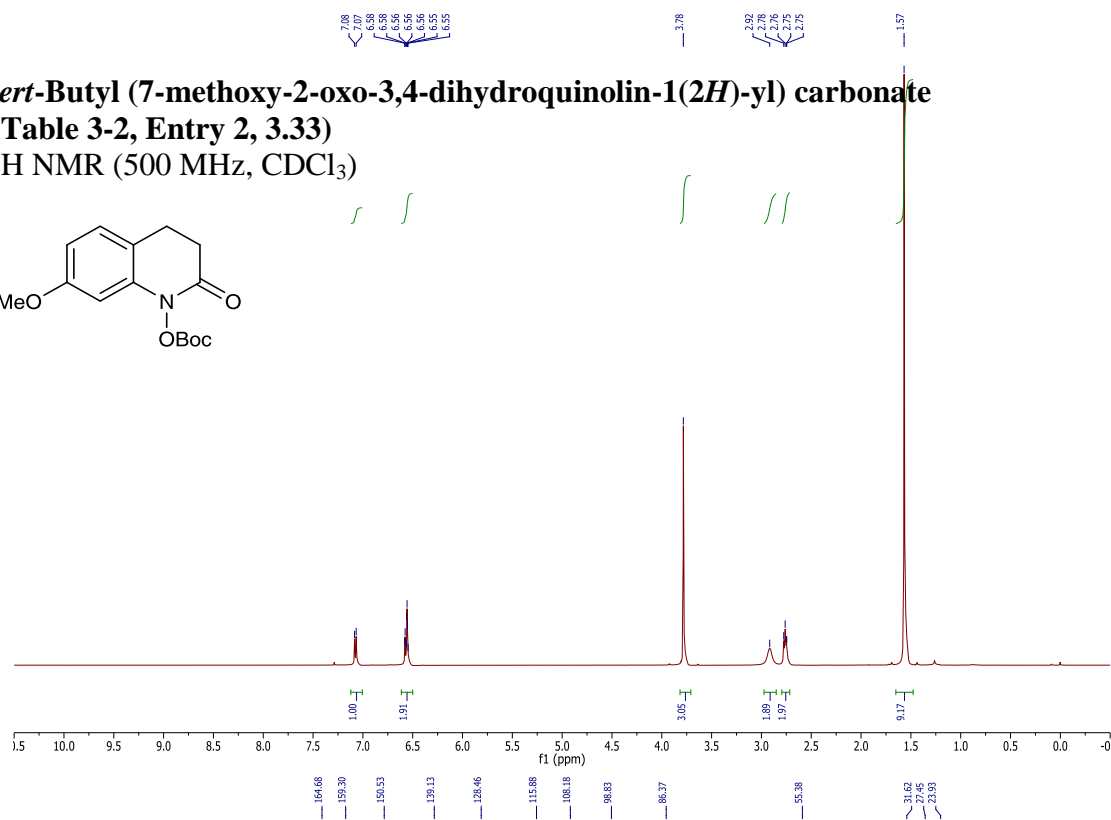
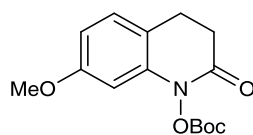


***tert*-Butyl (2-oxo-3,4-dihydroquinolin-1(2*H*)-yl) carbonate (Table 3-2, Entry 1, 3.13)**
¹³C NMR (125 MHz, CDCl₃)



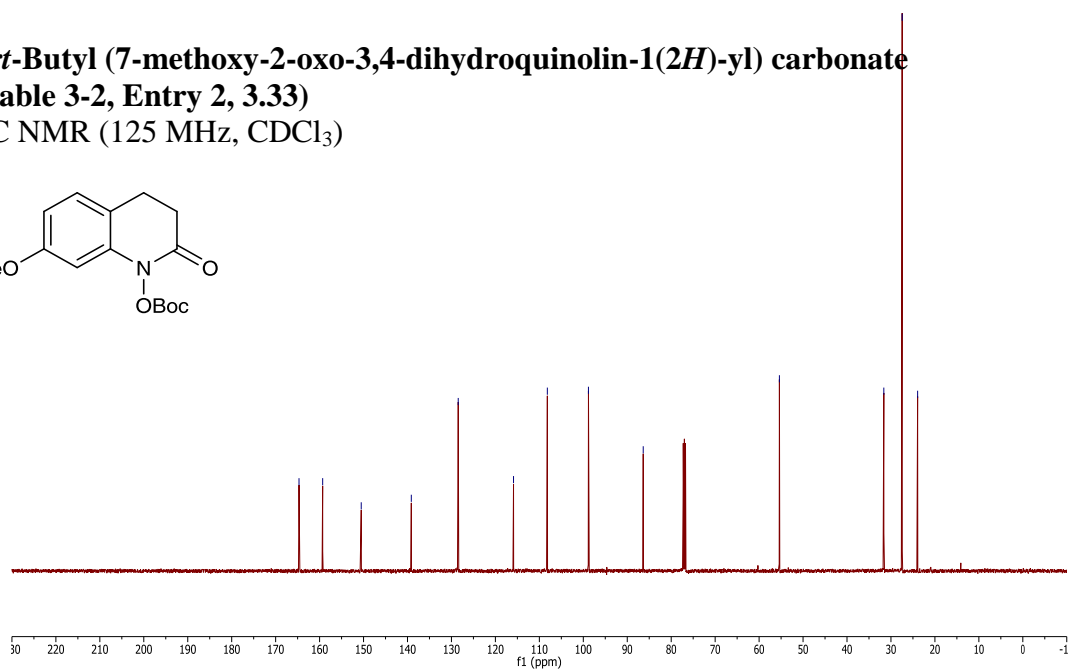
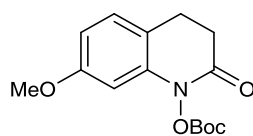
***tert*-Butyl (7-methoxy-2-oxo-3,4-dihydroquinolin-1(2*H*)-yl) carbonate**
(Table 3-2, Entry 2, 3.33)

^1H NMR (500 MHz, CDCl_3)



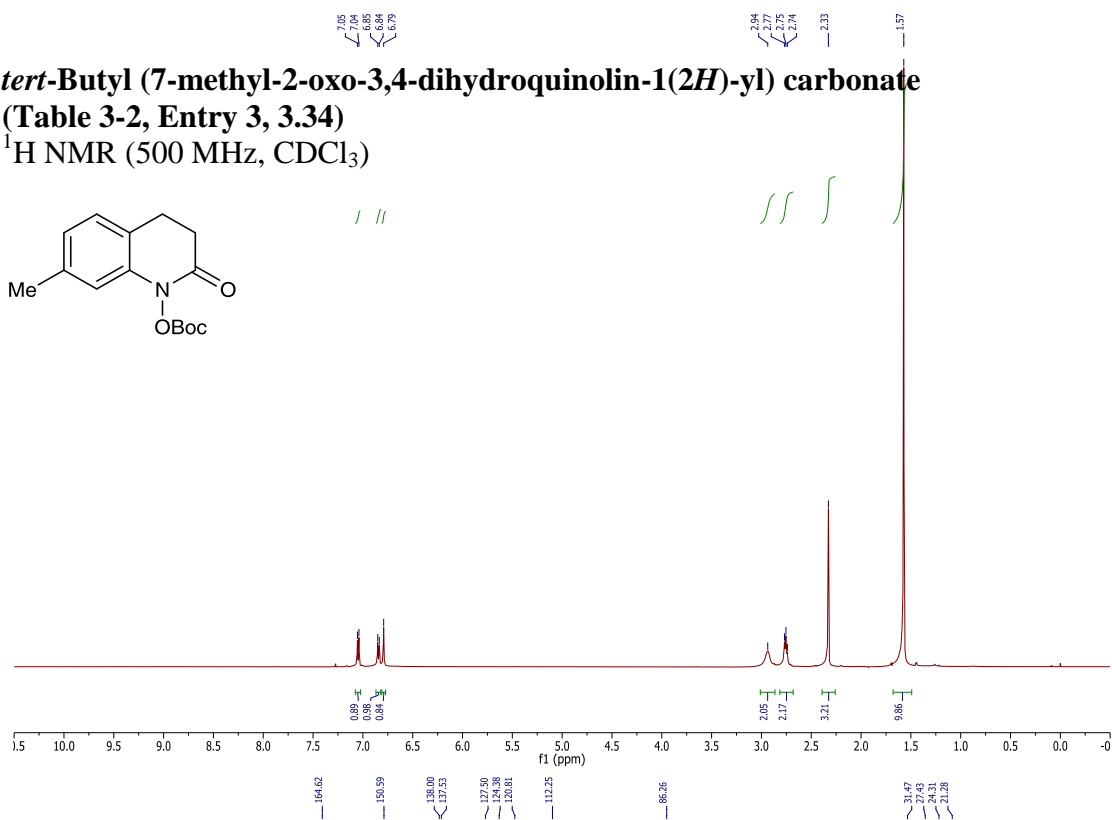
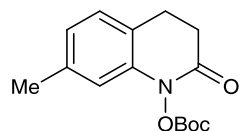
***tert*-Butyl (7-methoxy-2-oxo-3,4-dihydroquinolin-1(2*H*)-yl) carbonate**
(Table 3-2, Entry 2, 3.33)

^{13}C NMR (125 MHz, CDCl_3)



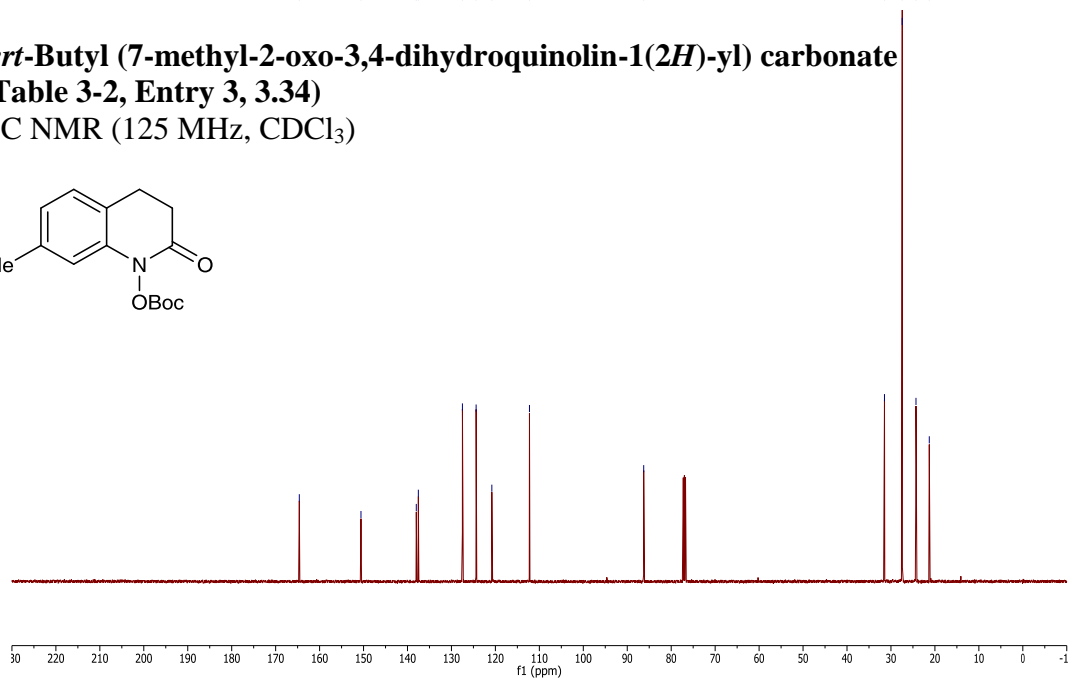
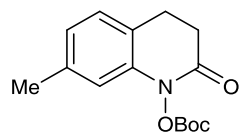
***tert*-Butyl (7-methyl-2-oxo-3,4-dihydroquinolin-1(2*H*)-yl) carbonate**
(Table 3-2, Entry 3, 3.34)

^1H NMR (500 MHz, CDCl_3)

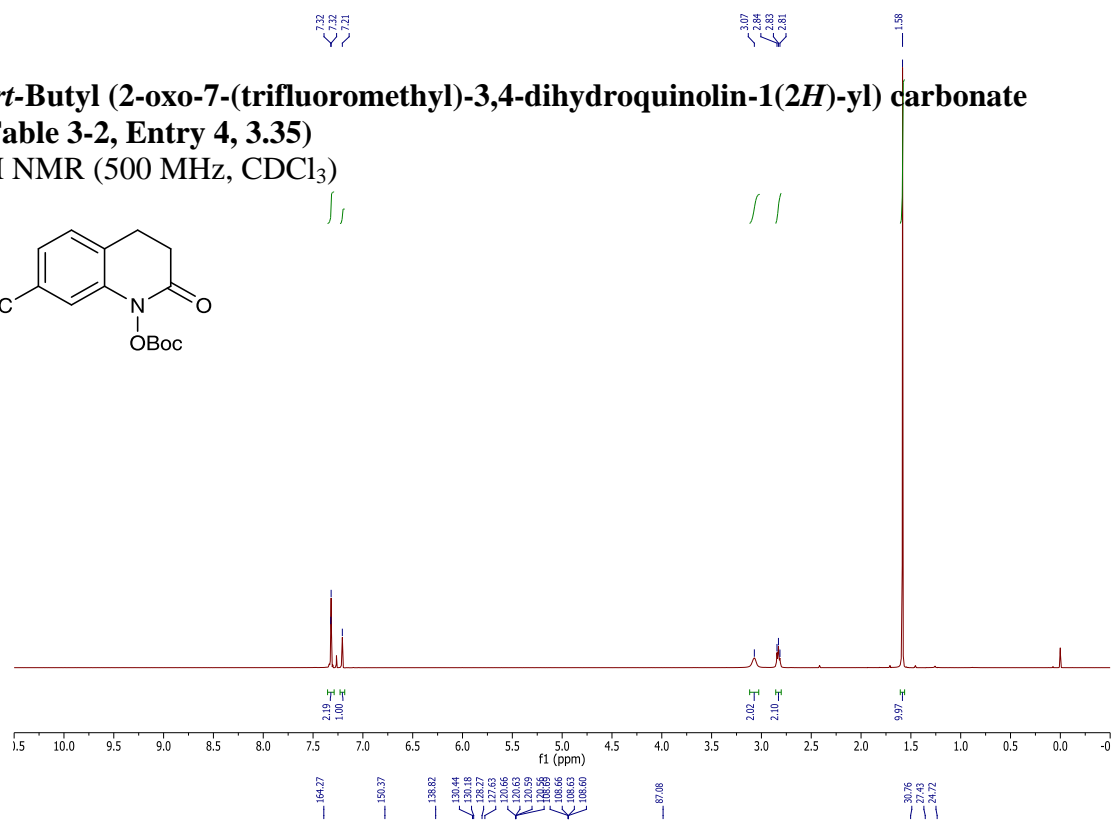
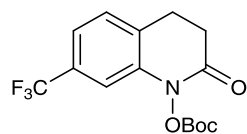


***tert*-Butyl (7-methyl-2-oxo-3,4-dihydroquinolin-1(2*H*)-yl) carbonate**
(Table 3-2, Entry 3, 3.34)

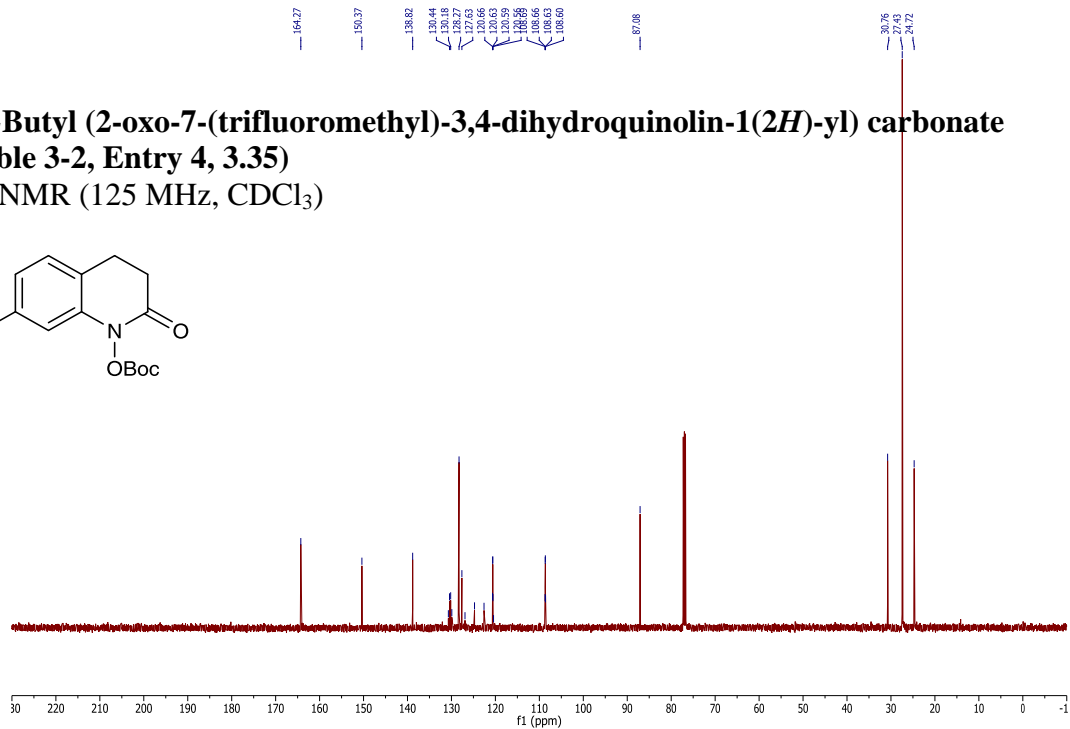
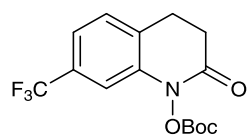
^{13}C NMR (125 MHz, CDCl_3)



***tert*-Butyl (2-oxo-7-(trifluoromethyl)-3,4-dihydroquinolin-1(2*H*)-yl) carbonate**
 (Table 3-2, Entry 4, 3.35)
¹H NMR (500 MHz, CDCl₃)

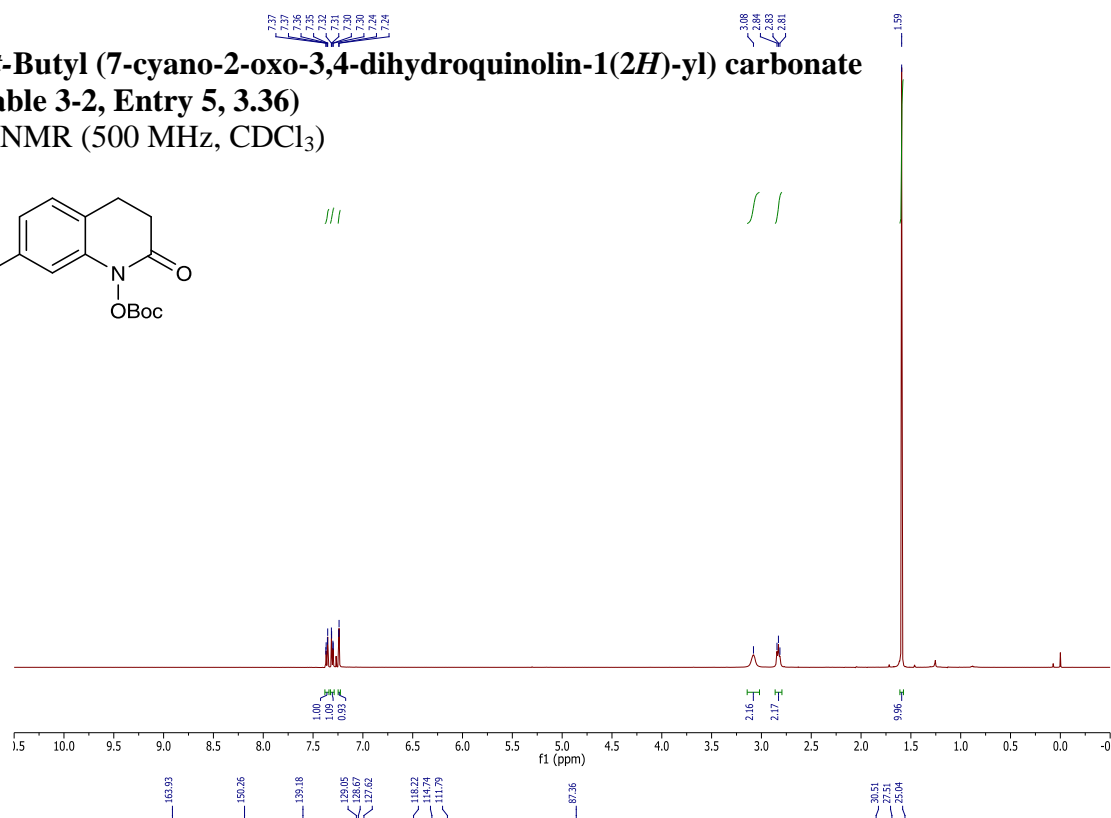
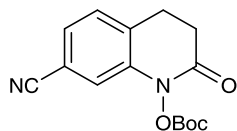


***tert*-Butyl (2-oxo-7-(trifluoromethyl)-3,4-dihydroquinolin-1(2*H*)-yl) carbonate**
 (Table 3-2, Entry 4, 3.35)
¹³C NMR (125 MHz, CDCl₃)



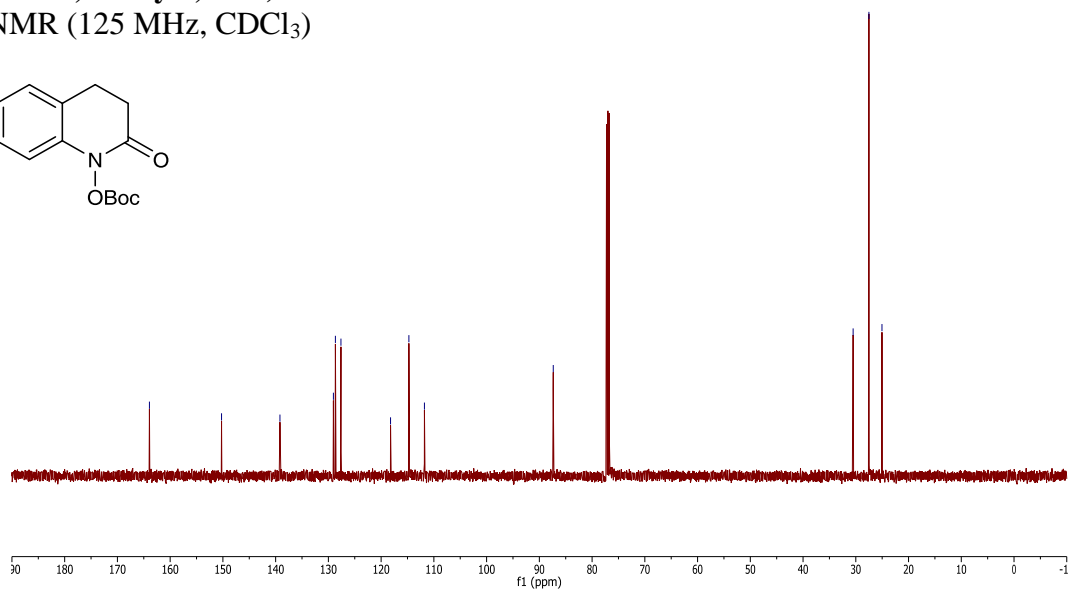
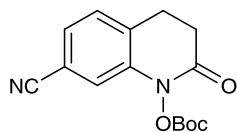
***tert*-Butyl (7-cyano-2-oxo-3,4-dihydroquinolin-1(2*H*)-yl) carbonate**
(Table 3-2, Entry 5, 3.36)

¹H NMR (500 MHz, CDCl₃)

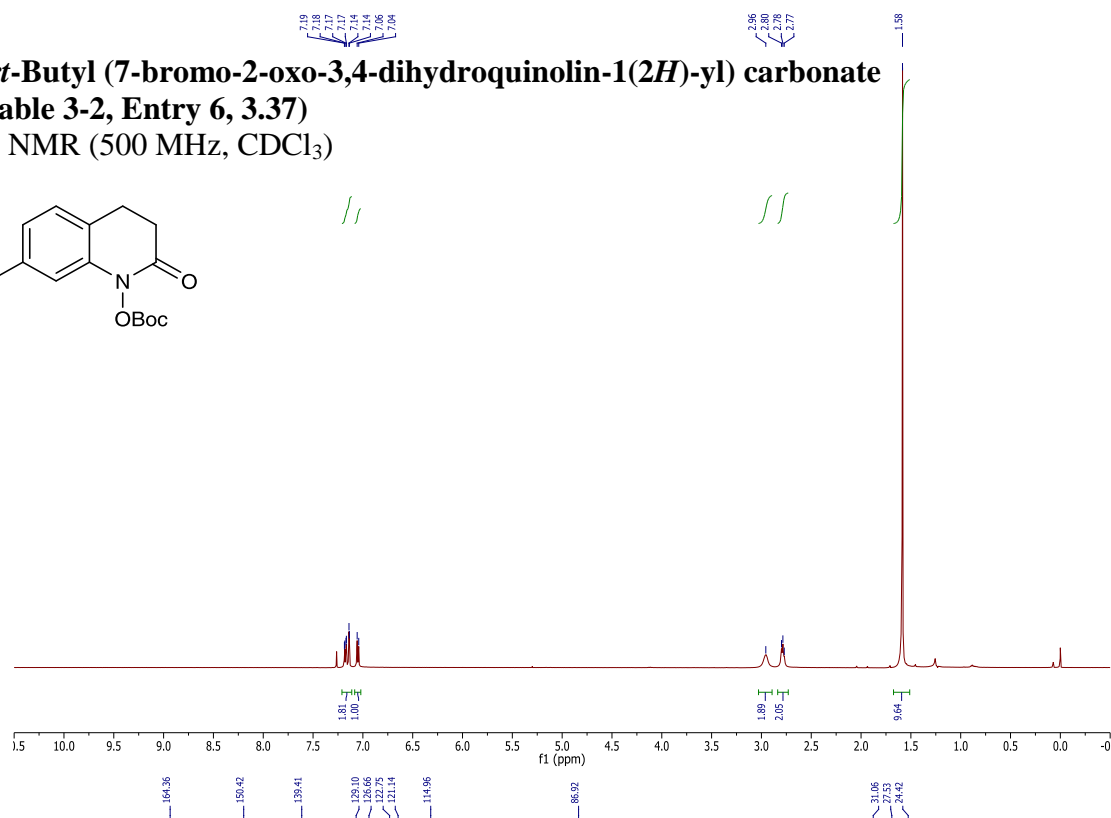
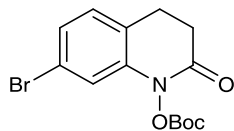


***tert*-Butyl (7-cyano-2-oxo-3,4-dihydroquinolin-1(2*H*)-yl) carbonate**
(Table 3-2, Entry 5, 3.36)

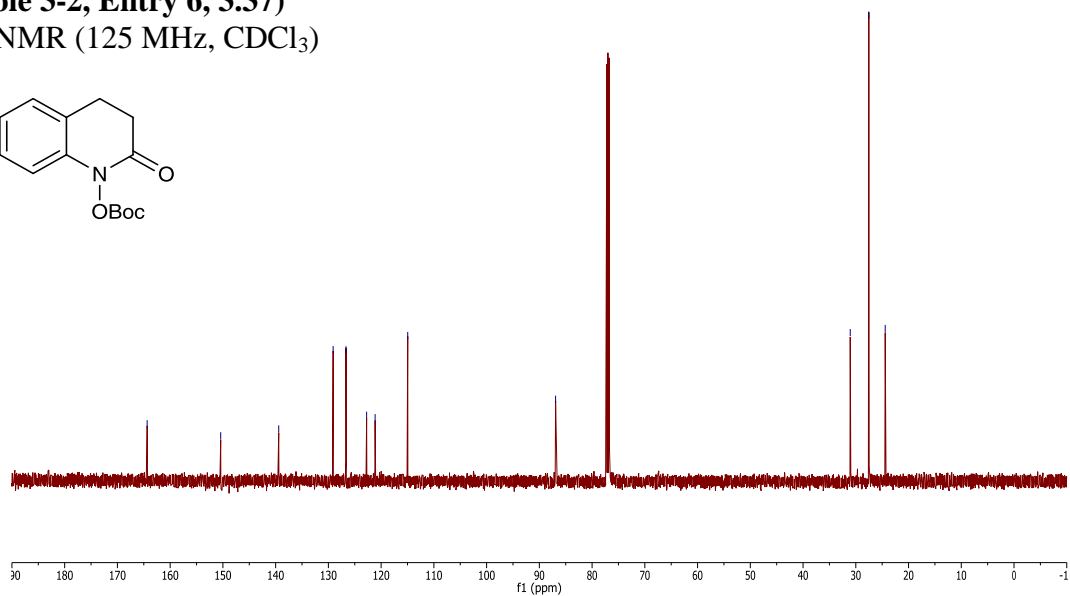
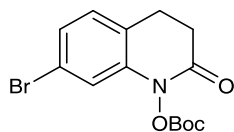
¹³C NMR (125 MHz, CDCl₃)



***tert*-Butyl (7-bromo-2-oxo-3,4-dihydroquinolin-1(2*H*)-yl) carbonate**
 (Table 3-2, Entry 6, 3.37)
¹H NMR (500 MHz, CDCl₃)

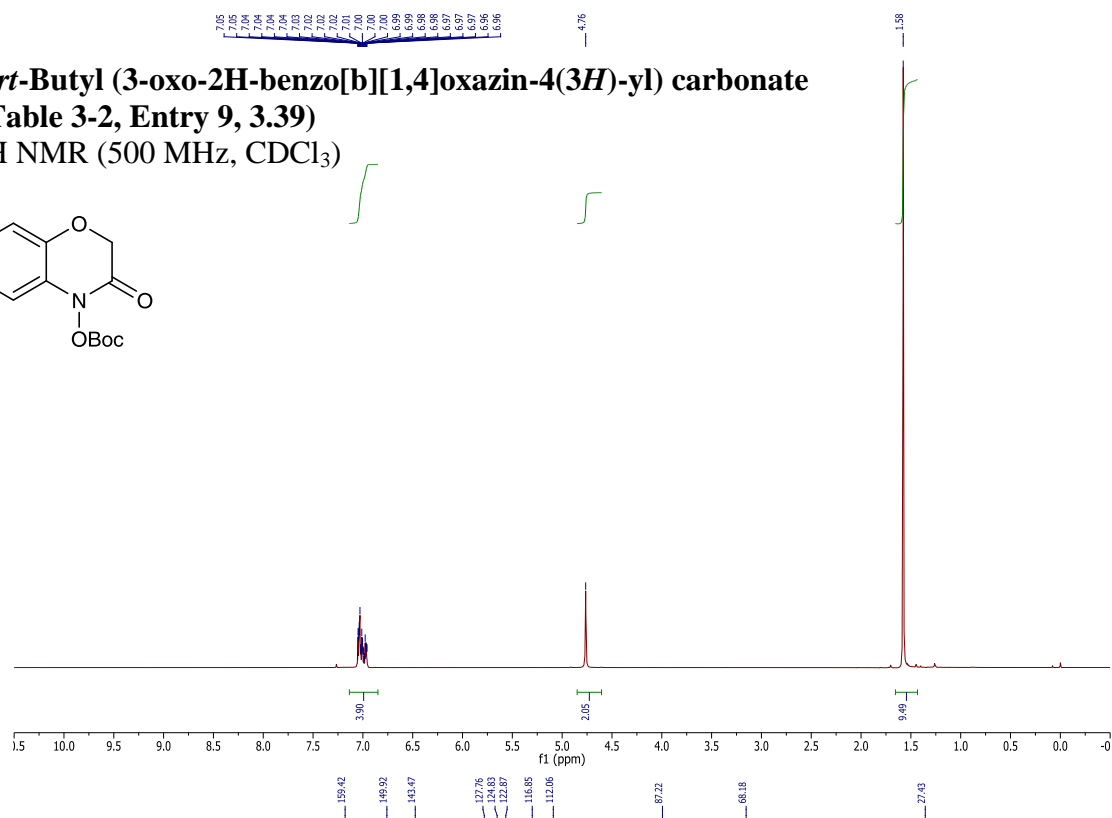
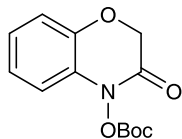


***tert*-Butyl (7-bromo-2-oxo-3,4-dihydroquinolin-1(2*H*)-yl) carbonate**
 (Table 3-2, Entry 6, 3.37)
¹³C NMR (125 MHz, CDCl₃)



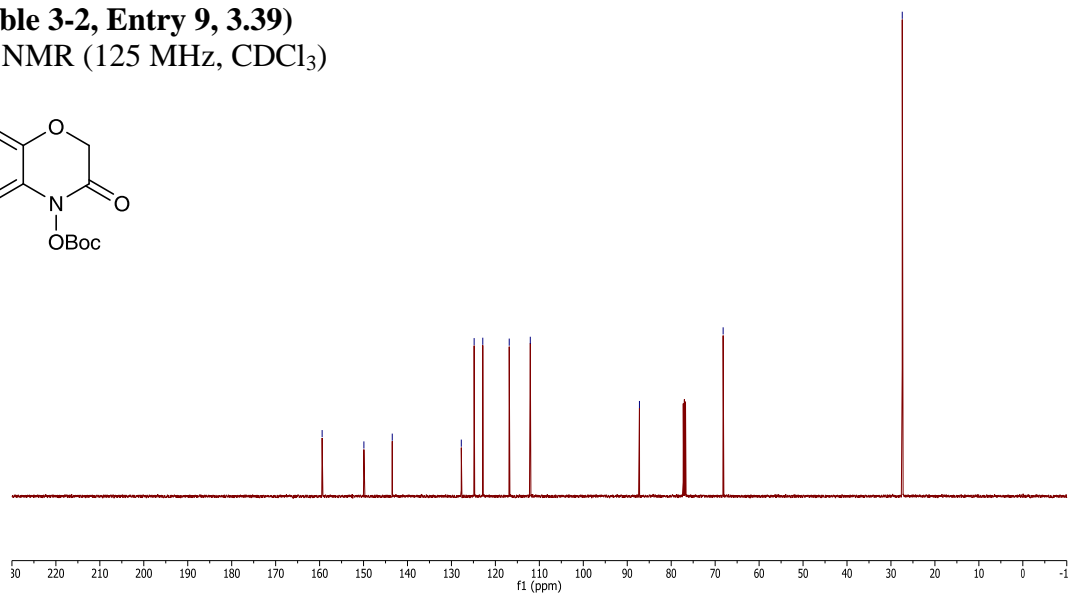
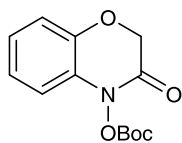
***tert*-Butyl (3-oxo-2H-benzo[*b*][1,4]oxazin-4(3*H*)-yl) carbonate**
(Table 3-2, Entry 9, 3.39)

¹H NMR (500 MHz, CDCl₃)



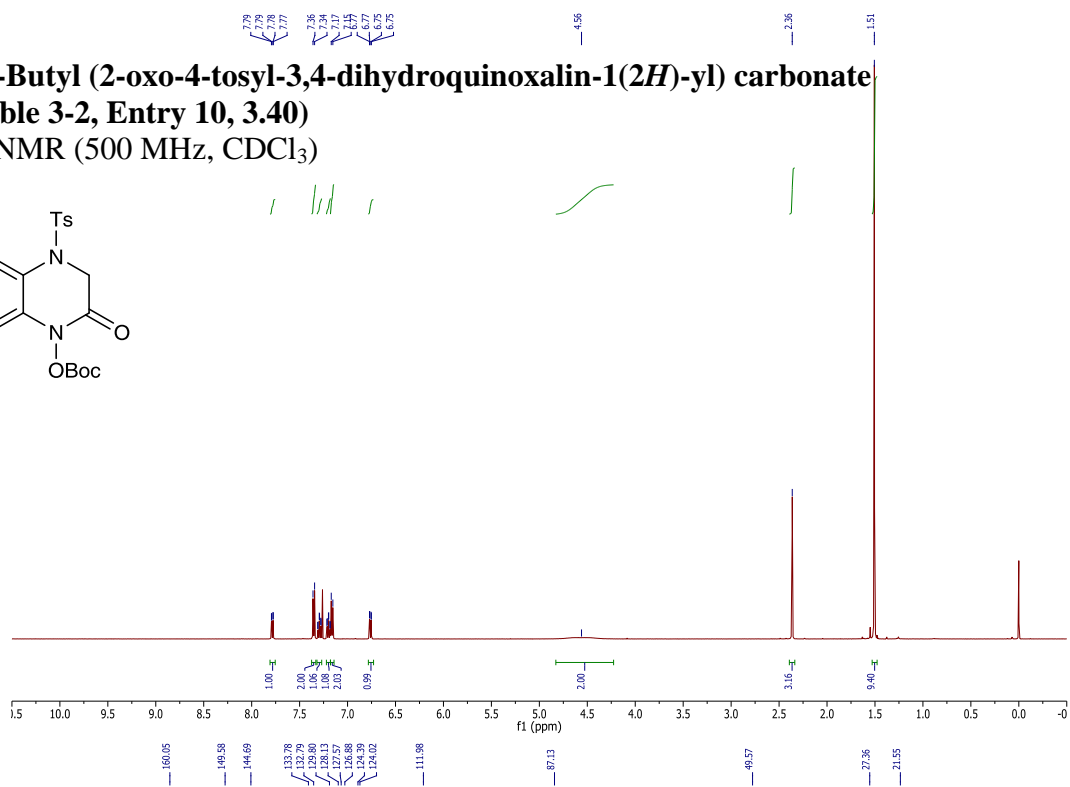
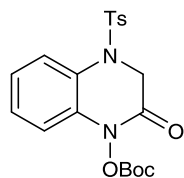
***tert*-Butyl (3-oxo-2H-benzo[*b*][1,4]oxazin-4(3*H*)-yl) carbonate**
(Table 3-2, Entry 9, 3.39)

¹³C NMR (125 MHz, CDCl₃)



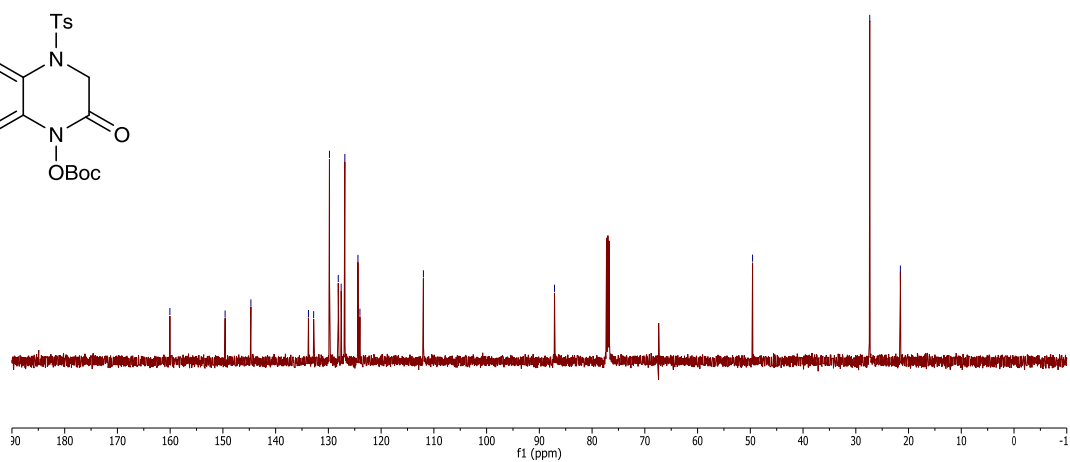
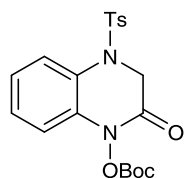
***tert*-Butyl (2-oxo-4-tosyl-3,4-dihydroquinoxalin-1(2*H*)-yl) carbonate**
(Table 3-2, Entry 10, 3.40)

^1H NMR (500 MHz, CDCl_3)



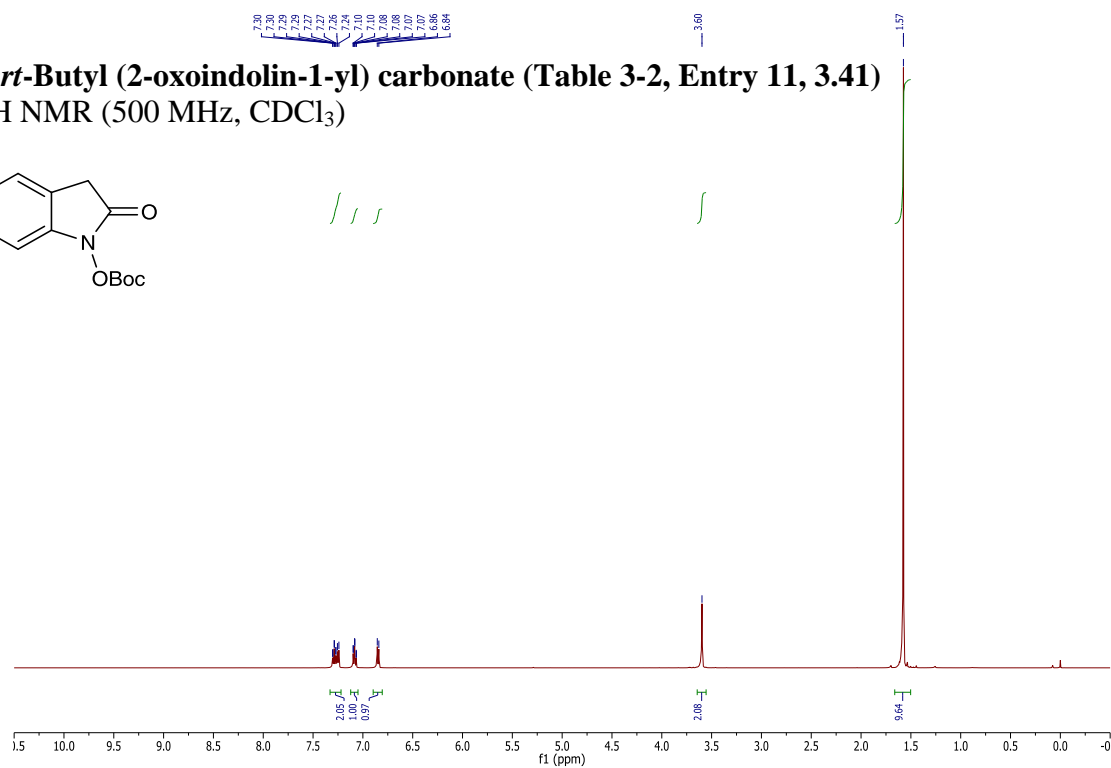
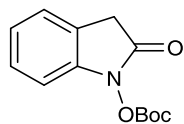
***tert*-Butyl (2-oxo-4-tosyl-3,4-dihydroquinoxalin-1(2*H*)-yl) carbonate**
(Table 3-2, Entry 10, 3.40)

^{13}C NMR (125 MHz, CDCl_3)



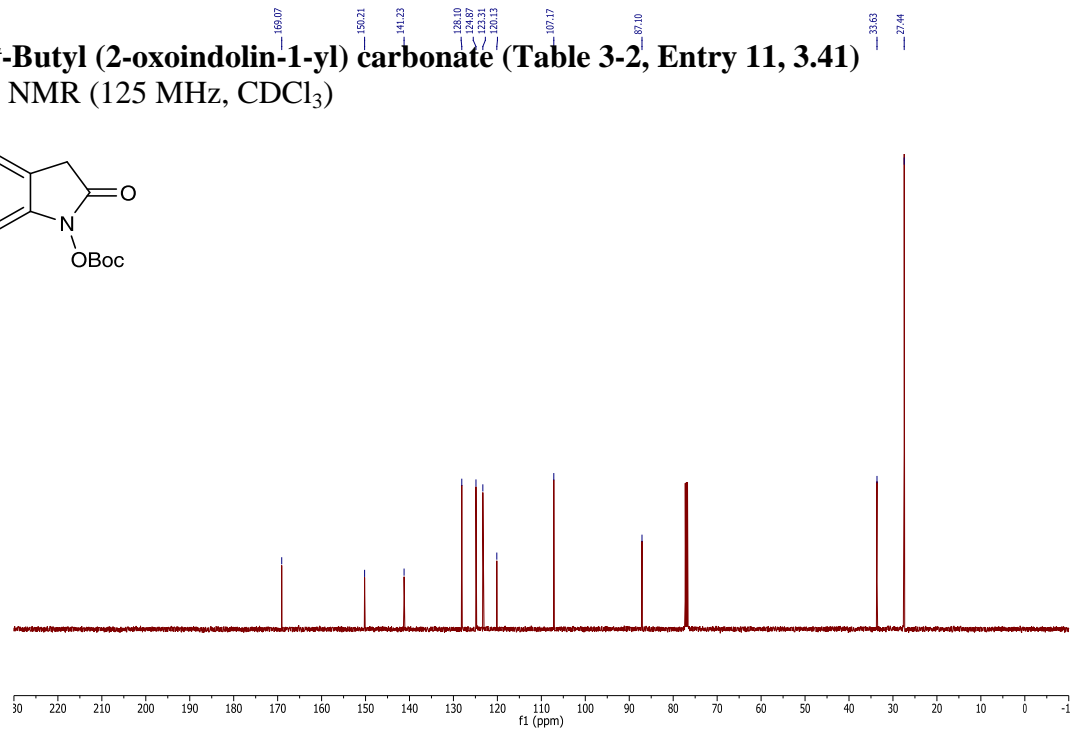
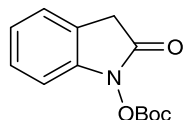
***tert*-Butyl (2-oxoindolin-1-yl) carbonate (Table 3-2, Entry 11, 3.41)**

^1H NMR (500 MHz, CDCl_3)

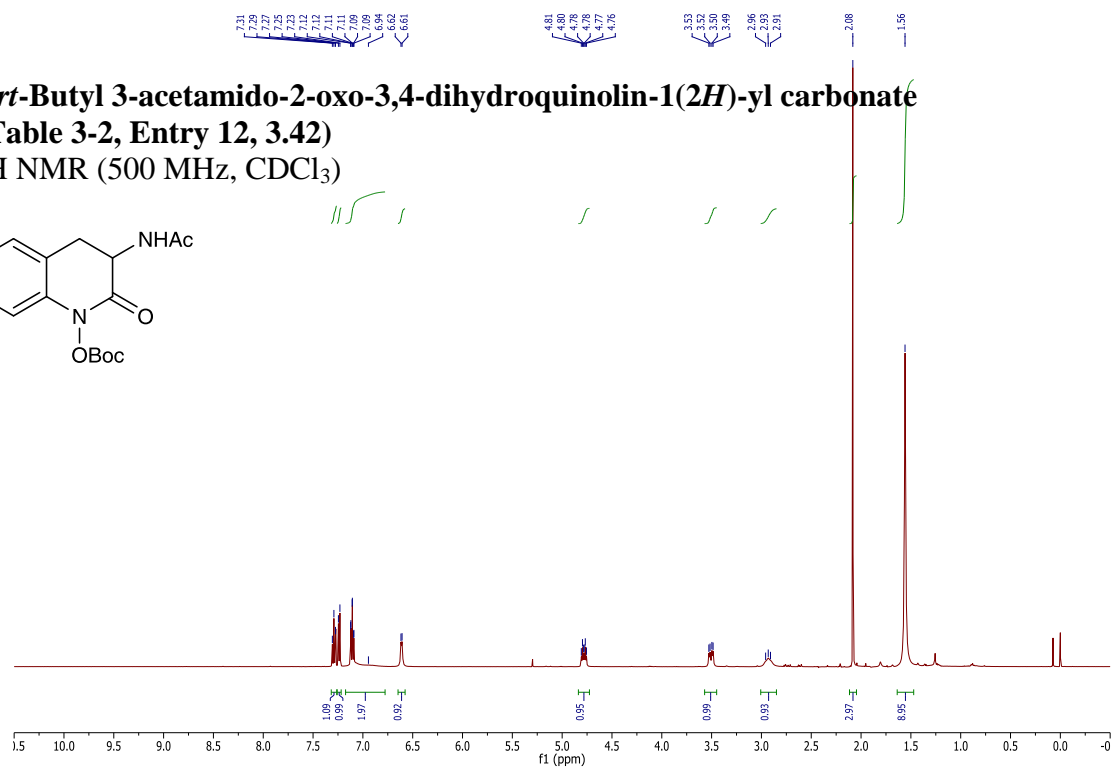
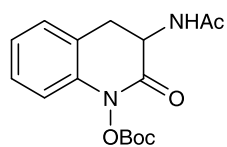


***tert*-Butyl (2-oxoindolin-1-yl) carbonate (Table 3-2, Entry 11, 3.41)**

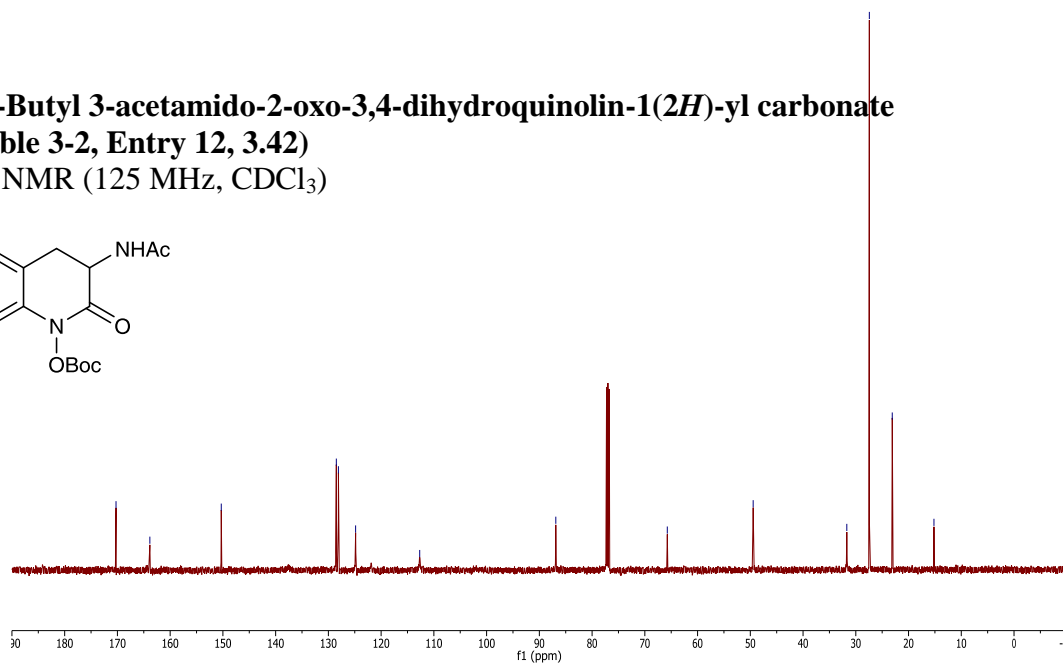
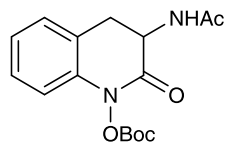
^{13}C NMR (125 MHz, CDCl_3)

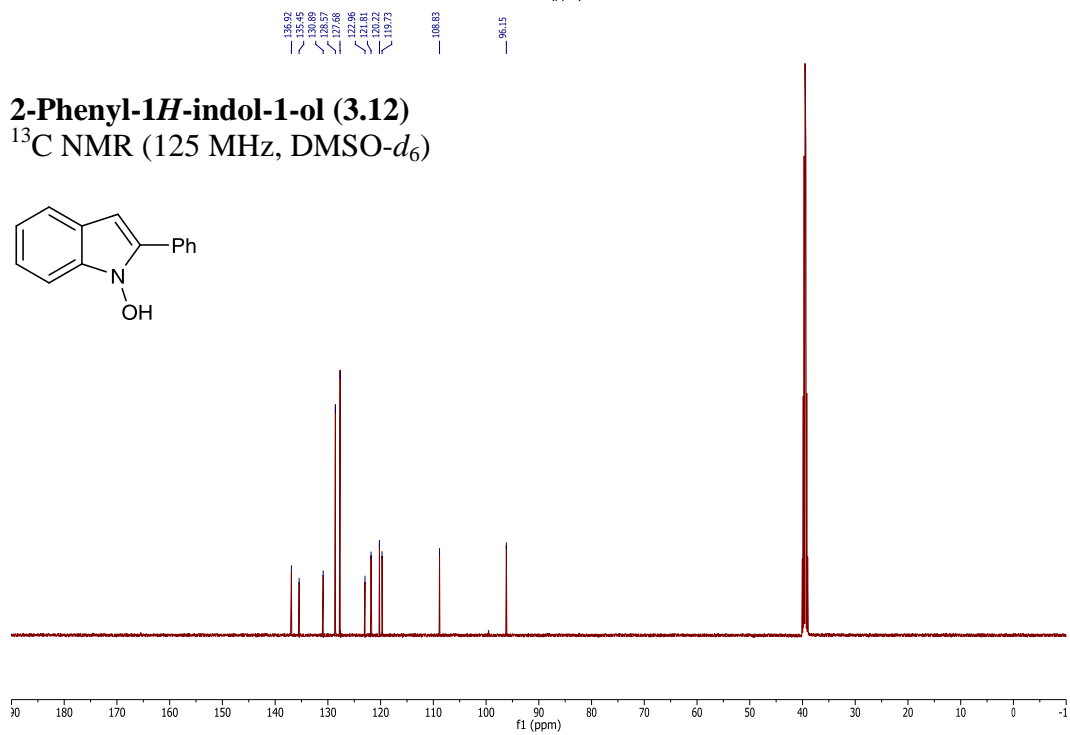
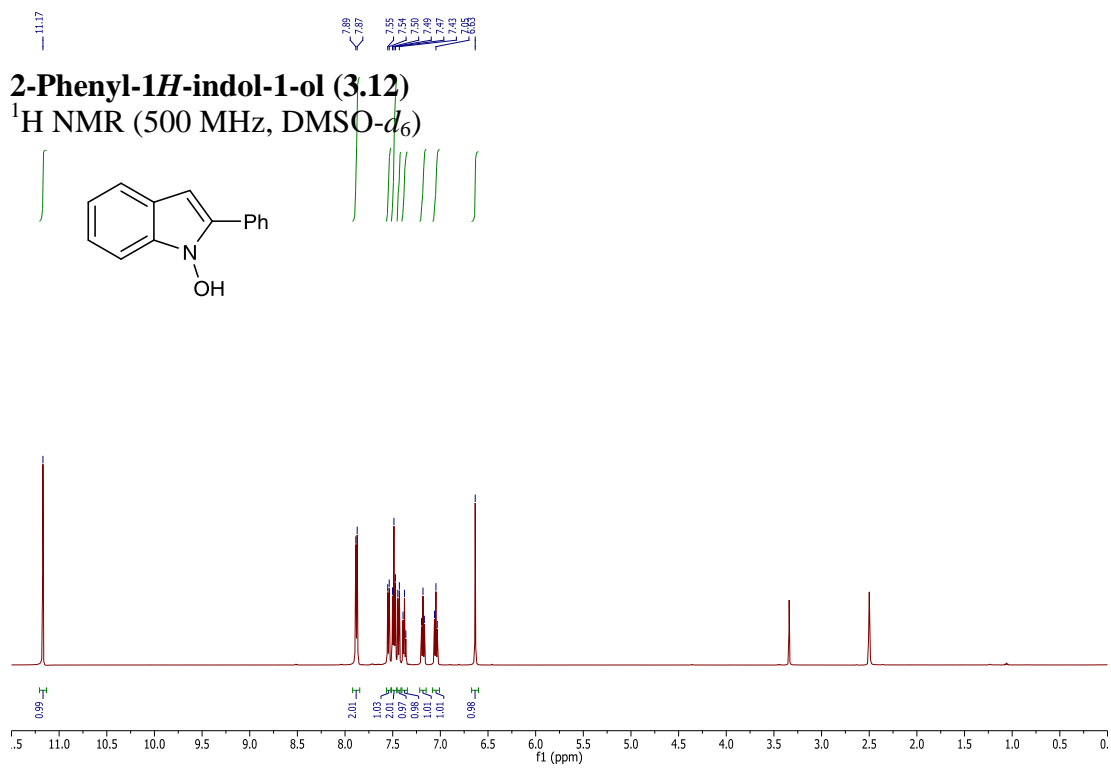


***tert*-Butyl 3-acetamido-2-oxo-3,4-dihydroquinolin-1(2*H*)-yl carbonate**
 (Table 3-2, Entry 12, 3.42)
¹H NMR (500 MHz, CDCl₃)

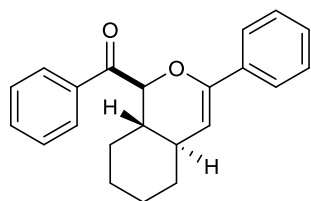


***tert*-Butyl 3-acetamido-2-oxo-3,4-dihydroquinolin-1(2*H*)-yl carbonate**
 (Table 3-2, Entry 12, 3.42)
¹³C NMR (125 MHz, CDCl₃)

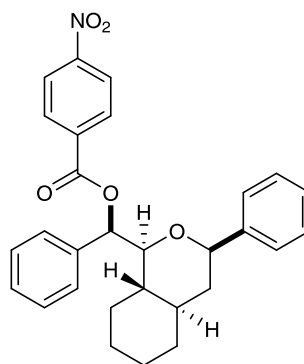




Appendix D. X-ray Crystallographic Data

Compounds characterized by X-ray diffraction analysis

2.4
(yoon15)



D.1
(yoon27)

D.1 Characterization of cycloadduct 2.4 (yoon15)

Data Collection

A colorless crystal with approximate dimensions $0.54 \times 0.22 \times 0.12 \text{ mm}^3$ was selected under oil under ambient conditions and attached to the tip of a MiTeGen MicroMount©. The crystal was mounted in a stream of cold nitrogen at 100(2) K and centered in the X-ray beam by using a video camera.

The crystal evaluation and data collection were performed on a Bruker SMART APEXII diffractometer with Cu K_α ($\lambda = 1.54178 \text{ \AA}$) radiation and the diffractometer to crystal distance of 4.03 cm.

The initial cell constants were obtained from three series of ω scans at different starting angles. Each series consisted of 50 frames collected at intervals of 0.5° in a 25° range about ω with the exposure time of 5 seconds per frame. The reflections were successfully indexed by an automated indexing routine built in the APEXII program. The final cell constants were calculated from a set of 9941 strong reflections from the actual data collection.

The data were collected by using the full sphere data collection routine to survey the reciprocal space to the extent of a full sphere to a resolution of 0.82 \AA . A total of 43215 data were harvested by collecting 15 sets of frames with 0.7° scans in ω with an exposure time 6-12 sec per frame. These highly redundant datasets were corrected for Lorentz and polarization effects. The absorption correction was based on fitting a function to the empirical transmission surface as sampled by multiple equivalent measurements.¹

Structure Solution and Refinement

The systematic absences in the diffraction data were uniquely consistent for the space groups $P2_1/n$ that yielded chemically reasonable and computationally stable results of refinement.²

A successful solution by the direct methods provided most non-hydrogen atoms from the E -map. The remaining non-hydrogen atoms were located in an alternating series of least-squares cycles and difference Fourier maps. All non-hydrogen atoms were refined with anisotropic displacement coefficients. All hydrogen atoms were refined with independent isotropic displacement coefficients.

There are two symmetry independent molecules (mirror-image-related stereoisomers) in the asymmetric unit.

The final least-squares refinement of 565 parameters against 6146 data resulted in residuals R (based on F^2 for $I \geq 2\sigma$) and wR (based on F^2 for all data) of 0.0543 and 0.1574, respectively. The final difference Fourier map was featureless.

The molecular diagrams are drawn with 50% probability ellipsoids.

References

1. Bruker-AXS. (2007) APEX2, SADABS, and SAINT Software Reference Manuals. Bruker-AXS, Madison, Wisconsin, USA.
2. Sheldrick, G. M. (2008) SHELXL. *Acta Cryst.* **A64**, 112-122.
3. Pennington, W.T. (1999) Diamond. *J. Appl. Cryst.* **32**(5), 1028-1029.
4. Dolomanov, O.V.; Bourhis, L.J.; Gildea, R.J.; Howard, J.A.K.; Puschmann, H. "OLEX2: a complete structure solution, refinement and analysis program". *J. Appl. Cryst.* (2009) **42**, *in print*.

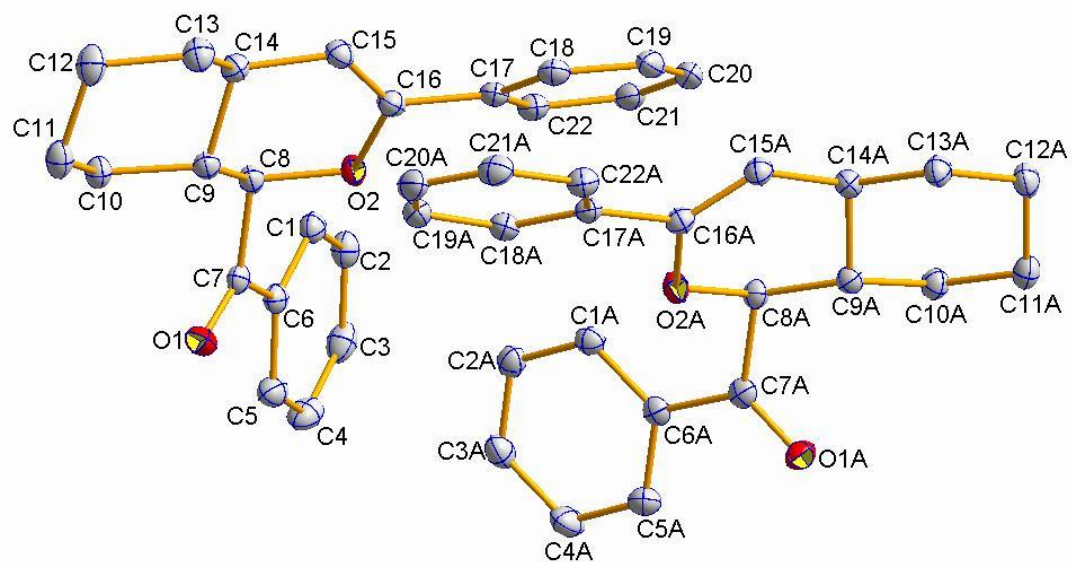


Figure D-1. A molecular drawing of yoon15. All H atoms are omitted.³



Figure D-2. The two stereoisomers of yoon15 superimposed (one molecule had to be inverted). All H atoms are omitted.⁴

Table D-1. Crystal data and structure refinement for yoon15

Identification code	yoon15	
Empirical formula	C ₂₂ H ₂₂ O ₂	
Formula weight	318.40	
Temperature	100(2) K	
Wavelength	1.54178 Å	
Crystal system	Monoclinic	
Space group	P2 ₁ /n	
Unit cell dimensions	a = 9.6022(3) Å	α = 90°.
	b = 18.1549(6) Å	β = 97.663(2)°.
	c = 19.5359(6) Å	γ = 90°.
Volume	3375.22(19) Å ³	
Z	8	
Density (calculated)	1.253 Mg/m ³	
Absorption coefficient	0.616 mm ⁻¹	
F(000)	1360	
Crystal size	0.54 x 0.22 x 0.12 mm ³	
Theta range for data collection	3.34 to 69.72°.	
Index ranges	-11<=h<=11, -21<=k<=21, -23<=l<=23	
Reflections collected	43215	
Independent reflections	6146 [R(int) = 0.0276]	
Completeness to theta = 67.00°	97.6 %	
Absorption correction	Empirical with SADABS	
Max. and min. transmission	0.9319 and 0.7304	
Refinement method	Full-matrix least-squares on F ²	
Data / restraints / parameters	6146 / 0 / 565	
Goodness-of-fit on F ²	1.034	
Final R indices [I>2sigma(I)]	R1 = 0.0543, wR2 = 0.1479	
R indices (all data)	R1 = 0.0613, wR2 = 0.1574	
Largest diff. peak and hole	0.703 and -0.227 e.Å ⁻³	

Table D-2. Atomic coordinates ($\times 10^4$) and equivalent isotropic displacement parameters ($\text{\AA}^2 \times 10^3$) for yoon15. $U(\text{eq})$ is defined as one third of the trace of the orthogonalized U_{ij} tensor.

x	y	z	$U(\text{eq})$	
O(1)	7009(1)	8752(1)	1858(1)	22(1)
O(2)	7582(1)	7601(1)	3131(1)	19(1)
C(1)	9830(1)	7422(1)	2222(1)	19(1)
C(2)	10659(2)	6963(1)	1875(1)	22(1)
C(3)	10431(2)	6920(1)	1159(1)	26(1)
C(4)	9371(2)	7336(1)	786(1)	26(1)
C(5)	8547(2)	7796(1)	1131(1)	22(1)
C(6)	8768(1)	7844(1)	1852(1)	17(1)
C(7)	7857(1)	8354(1)	2195(1)	17(1)
C(8)	7980(1)	8350(1)	2989(1)	17(1)
C(9)	7065(1)	8919(1)	3287(1)	17(1)
C(10)	7488(2)	9717(1)	3162(1)	19(1)
C(11)	6501(2)	10248(1)	3467(1)	23(1)
C(12)	6484(2)	10110(1)	4239(1)	25(1)
C(13)	6142(2)	9307(1)	4379(1)	23(1)
C(14)	7151(1)	8790(1)	4068(1)	18(1)
C(15)	6934(2)	7991(1)	4214(1)	18(1)
C(16)	7140(1)	7463(1)	3762(1)	18(1)
C(17)	6954(1)	6664(1)	3862(1)	17(1)
C(18)	5917(2)	6402(1)	4240(1)	20(1)
C(19)	5748(2)	5650(1)	4330(1)	24(1)
C(20)	6623(2)	5150(1)	4058(1)	26(1)
C(21)	7661(2)	5406(1)	3689(1)	24(1)
C(22)	7818(2)	6157(1)	3582(1)	20(1)
O(1A)	1963(1)	4665(1)	1847(1)	22(1)
O(2A)	2493(1)	5799(1)	3133(1)	19(1)
C(1A)	4786(1)	5989(1)	2255(1)	18(1)
C(2A)	5659(2)	6435(1)	1922(1)	20(1)
C(3A)	5540(2)	6439(1)	1208(1)	24(1)
C(4A)	4547(2)	5993(1)	821(1)	27(1)
C(5A)	3664(2)	5554(1)	1151(1)	22(1)
C(6A)	3774(1)	5547(1)	1870(1)	17(1)
C(7A)	2812(1)	5052(1)	2197(1)	17(1)
C(8A)	2901(1)	5052(1)	2989(1)	16(1)
C(9A)	1980(1)	4476(1)	3274(1)	16(1)
C(10A)	2428(2)	3684(1)	3146(1)	19(1)
C(11A)	1424(2)	3144(1)	3430(1)	21(1)
C(12A)	1356(2)	3275(1)	4197(1)	22(1)
C(13A)	1014(2)	4078(1)	4350(1)	20(1)
C(14A)	2040(1)	4598(1)	4054(1)	17(1)
C(15A)	1827(1)	5396(1)	4208(1)	17(1)
C(16A)	2055(1)	5930(1)	3767(1)	17(1)
C(17A)	1922(1)	6730(1)	3890(1)	17(1)
C(18A)	2773(2)	7233(1)	3596(1)	19(1)
C(19A)	2689(2)	7984(1)	3734(1)	22(1)
C(20A)	1733(2)	8242(1)	4151(1)	25(1)
C(21A)	868(2)	7746(1)	4435(1)	24(1)
C(22A)	960(2)	6999(1)	4309(1)	20(1)

Table D-3. Bond lengths [\AA] and angles [$^\circ$] for yoon15

O(1)-C(7)	1.2154(17)	O(1A)-C(7A)	1.2158(17)
O(2)-C(16)	1.3795(16)	O(2A)-C(16A)	1.3811(16)
O(2)-C(8)	1.4494(16)	O(2A)-C(8A)	1.4496(15)
C(1)-C(2)	1.390(2)	C(1A)-C(2A)	1.389(2)
C(1)-C(6)	1.3980(19)	C(1A)-C(6A)	1.3982(19)
C(1)-H(1)	1.003(17)	C(1A)-H(1A)	0.955(17)
C(2)-C(3)	1.389(2)	C(2A)-C(3A)	1.383(2)
C(2)-H(2)	0.972(19)	C(2A)-H(2A)	0.954(18)
C(3)-C(4)	1.392(2)	C(3A)-C(4A)	1.395(2)
C(3)-H(3)	1.017(19)	C(3A)-H(3A)	0.992(18)
C(4)-C(5)	1.385(2)	C(4A)-C(5A)	1.383(2)
C(4)-H(4)	0.945(19)	C(4A)-H(4A)	0.954(19)
C(5)-C(6)	1.3994(19)	C(5A)-C(6A)	1.3956(19)
C(5)-H(5)	0.974(18)	C(5A)-H(5A)	0.992(18)
C(6)-C(7)	1.4935(19)	C(6A)-C(7A)	1.4921(19)
C(7)-C(8)	1.5390(18)	C(7A)-C(8A)	1.5386(18)
C(8)-C(9)	1.5209(19)	C(8A)-C(9A)	1.5213(18)
C(8)-H(8)	0.977(17)	C(8A)-H(8A)	1.000(17)
C(9)-C(10)	1.5317(18)	C(9A)-C(10A)	1.5302(18)
C(9)-C(14)	1.5362(18)	C(9A)-C(14A)	1.5336(18)
C(9)-H(9)	0.961(17)	C(9A)-H(9A)	0.970(17)
C(10)-C(11)	1.5289(19)	C(10A)-C(11A)	1.5307(19)
C(10)-H(10B)	0.994(18)	C(10A)-H(10D)	1.000(17)
C(10)-H(10A)	0.995(17)	C(10A)-H(10C)	0.978(17)
C(11)-C(12)	1.531(2)	C(11A)-C(12A)	1.528(2)
C(11)-H(11A)	0.994(19)	C(11A)-H(11D)	0.988(18)
C(11)-H(11B)	0.991(19)	C(11A)-H(11C)	0.977(18)
C(12)-C(13)	1.527(2)	C(12A)-C(13A)	1.5326(19)
C(12)-H(12B)	0.997(19)	C(12A)-H(12D)	0.984(18)
C(12)-H(12A)	0.998(19)	C(12A)-H(12C)	0.997(18)
C(13)-C(14)	1.5311(19)	C(13A)-C(14A)	1.5316(19)
C(13)-H(13A)	0.994(18)	C(13A)-H(13C)	0.985(17)
C(13)-H(13B)	0.989(18)	C(13A)-H(13D)	0.965(18)
C(14)-C(15)	1.4992(19)	C(14A)-C(15A)	1.5001(18)
C(14)-H(14)	0.999(17)	C(14A)-H(14A)	0.985(17)
C(15)-C(16)	1.336(2)	C(15A)-C(16A)	1.334(2)
C(15)-H(15)	0.940(17)	C(15A)-H(15A)	0.941(17)
C(16)-C(17)	1.4774(18)	C(16A)-C(17A)	1.4803(18)
C(17)-C(22)	1.398(2)	C(17A)-C(18A)	1.3998(19)
C(17)-C(18)	1.400(2)	C(17A)-C(22A)	1.402(2)
C(18)-C(19)	1.389(2)	C(18A)-C(19A)	1.393(2)
C(18)-H(18)	0.957(18)	C(18A)-H(18A)	0.988(18)
C(19)-C(20)	1.390(2)	C(19A)-C(20A)	1.388(2)
C(19)-H(19)	0.920(19)	C(19A)-H(19A)	0.990(18)
C(20)-C(21)	1.386(2)	C(20A)-C(21A)	1.388(2)
C(20)-H(20)	0.990(19)	C(20A)-H(20A)	0.992(19)
C(21)-C(22)	1.391(2)	C(21A)-C(22A)	1.385(2)
C(21)-H(21)	0.980(19)	C(21A)-H(21A)	0.947(19)
C(22)-H(22)	0.981(18)	C(22A)-H(22A)	0.956(18)
C(16)-O(2)-C(8)	117.54(10)	C(3)-C(2)-C(1)	120.05(14)
C(2)-C(1)-C(6)	120.13(13)	C(3)-C(2)-H(2)	120.1(10)
C(2)-C(1)-H(1)	121.3(10)	C(1)-C(2)-H(2)	119.9(10)
C(6)-C(1)-H(1)	118.6(10)	C(2)-C(3)-C(4)	120.27(14)

C(2)-C(3)-H(3)	118.7(10)	C(16)-C(15)-C(14)	122.11(13)
C(4)-C(3)-H(3)	121.1(10)	C(16)-C(15)-H(15)	117.6(10)
C(5)-C(4)-C(3)	119.75(14)	C(14)-C(15)-H(15)	120.2(10)
C(5)-C(4)-H(4)	120.5(11)	C(15)-C(16)-O(2)	123.45(13)
C(3)-C(4)-H(4)	119.8(11)	C(15)-C(16)-C(17)	125.83(13)
C(4)-C(5)-C(6)	120.51(14)	O(2)-C(16)-C(17)	110.71(11)
C(4)-C(5)-H(5)	119.4(10)	C(22)-C(17)-C(18)	118.89(13)
C(6)-C(5)-H(5)	120.0(10)	C(22)-C(17)-C(16)	120.42(13)
C(1)-C(6)-C(5)	119.28(13)	C(18)-C(17)-C(16)	120.69(13)
C(1)-C(6)-C(7)	122.57(12)	C(19)-C(18)-C(17)	120.32(14)
C(5)-C(6)-C(7)	118.15(12)	C(19)-C(18)-H(18)	120.0(11)
O(1)-C(7)-C(6)	121.02(12)	C(17)-C(18)-H(18)	119.5(11)
O(1)-C(7)-C(8)	120.35(12)	C(18)-C(19)-C(20)	120.44(14)
C(6)-C(7)-C(8)	118.61(11)	C(18)-C(19)-H(19)	120.1(12)
O(2)-C(8)-C(9)	112.56(11)	C(20)-C(19)-H(19)	119.5(12)
O(2)-C(8)-C(7)	102.12(10)	C(21)-C(20)-C(19)	119.55(14)
C(9)-C(8)-C(7)	114.31(11)	C(21)-C(20)-H(20)	120.1(10)
O(2)-C(8)-H(8)	108.6(10)	C(19)-C(20)-H(20)	120.3(10)
C(9)-C(8)-H(8)	108.8(10)	C(20)-C(21)-C(22)	120.48(14)
C(7)-C(8)-H(8)	110.2(10)	C(20)-C(21)-H(21)	122.0(11)
C(8)-C(9)-C(10)	113.69(11)	C(22)-C(21)-H(21)	117.5(11)
C(8)-C(9)-C(14)	108.64(11)	C(21)-C(22)-C(17)	120.29(14)
C(10)-C(9)-C(14)	108.84(11)	C(21)-C(22)-H(22)	119.9(10)
C(8)-C(9)-H(9)	107.8(10)	C(17)-C(22)-H(22)	119.8(10)
C(10)-C(9)-H(9)	109.4(10)	C(16A)-O(2A)-C(8A)	117.24(10)
C(14)-C(9)-H(9)	108.4(10)	C(2A)-C(1A)-C(6A)	120.15(13)
C(11)-C(10)-C(9)	110.07(12)	C(2A)-C(1A)-H(1A)	121.3(10)
C(11)-C(10)-H(10B)	109.9(10)	C(6A)-C(1A)-H(1A)	118.5(10)
C(9)-C(10)-H(10B)	108.0(10)	C(3A)-C(2A)-C(1A)	120.06(13)
C(11)-C(10)-H(10A)	111.6(10)	C(3A)-C(2A)-H(2A)	119.9(10)
C(9)-C(10)-H(10A)	111.1(10)	C(1A)-C(2A)-H(2A)	120.0(10)
H(10B)-C(10)-H(10A)	106.0(14)	C(2A)-C(3A)-C(4A)	120.20(14)
C(10)-C(11)-C(12)	111.67(12)	C(2A)-C(3A)-H(3A)	118.4(10)
C(10)-C(11)-H(11A)	108.0(10)	C(4A)-C(3A)-H(3A)	121.4(10)
C(12)-C(11)-H(11A)	108.8(10)	C(5A)-C(4A)-C(3A)	119.86(14)
C(10)-C(11)-H(11B)	111.3(10)	C(5A)-C(4A)-H(4A)	121.3(11)
C(12)-C(11)-H(11B)	108.2(10)	C(3A)-C(4A)-H(4A)	118.9(11)
H(11A)-C(11)-H(11B)	108.7(14)	C(4A)-C(5A)-C(6A)	120.41(13)
C(13)-C(12)-C(11)	111.32(12)	C(4A)-C(5A)-H(5A)	120.6(10)
C(13)-C(12)-H(12B)	108.6(11)	C(6A)-C(5A)-H(5A)	119.0(10)
C(11)-C(12)-H(12B)	110.5(11)	C(5A)-C(6A)-C(1A)	119.32(13)
C(13)-C(12)-H(12A)	109.6(11)	C(5A)-C(6A)-C(7A)	117.91(12)
C(11)-C(12)-H(12A)	110.7(10)	C(1A)-C(6A)-C(7A)	122.76(12)
H(12B)-C(12)-H(12A)	106.0(14)	O(1A)-C(7A)-C(6A)	121.04(12)
C(12)-C(13)-C(14)	110.56(12)	O(1A)-C(7A)-C(8A)	120.55(12)
C(12)-C(13)-H(13A)	110.7(10)	C(6A)-C(7A)-C(8A)	118.41(11)
C(14)-C(13)-H(13A)	109.6(10)	O(2A)-C(8A)-C(9A)	112.74(11)
C(12)-C(13)-H(13B)	112.2(10)	O(2A)-C(8A)-C(7A)	102.40(10)
C(14)-C(13)-H(13B)	108.5(10)	C(9A)-C(8A)-C(7A)	114.30(11)
H(13A)-C(13)-H(13B)	105.2(14)	O(2A)-C(8A)-H(8A)	107.9(9)
C(15)-C(14)-C(13)	113.98(12)	C(9A)-C(8A)-H(8A)	110.3(9)
C(15)-C(14)-C(9)	110.28(11)	C(7A)-C(8A)-H(8A)	108.8(10)
C(13)-C(14)-C(9)	110.34(11)	C(8A)-C(9A)-C(10A)	113.32(11)
C(15)-C(14)-H(14)	109.0(9)	C(8A)-C(9A)-C(14A)	108.57(11)
C(13)-C(14)-H(14)	105.6(9)	C(10A)-C(9A)-C(14A)	108.87(11)
C(9)-C(14)-H(14)	107.4(9)	C(8A)-C(9A)-H(9A)	108.4(10)

C(10A)-C(9A)-H(9A)	109.7(10)	C(13A)-C(14A)-C(9A)	110.24(11)
C(14A)-C(9A)-H(9A)	107.9(9)	C(15A)-C(14A)-H(14A)	107.8(10)
C(9A)-C(10A)-C(11A)	109.83(11)	C(13A)-C(14A)-H(14A)	106.5(10)
C(9A)-C(10A)-H(10D)	107.2(10)	C(9A)-C(14A)-H(14A)	107.5(9)
C(11A)-C(10A)-H(10D)	109.6(10)	C(16A)-C(15A)-C(14A)	122.21(13)
C(9A)-C(10A)-H(10C)	112.2(10)	C(16A)-C(15A)-H(15A)	118.1(10)
C(11A)-C(10A)-H(10C)	111.4(10)	C(14A)-C(15A)-H(15A)	119.6(10)
H(10D)-C(10A)-H(10C)	106.4(14)	C(15A)-C(16A)-O(2A)	123.41(12)
C(12A)-C(11A)-C(10A)	111.52(11)	C(15A)-C(16A)-C(17A)	125.63(13)
C(12A)-C(11A)-H(11D)	110.0(10)	O(2A)-C(16A)-C(17A)	110.94(11)
C(10A)-C(11A)-H(11D)	108.2(10)	C(18A)-C(17A)-C(22A)	118.60(13)
C(12A)-C(11A)-H(11C)	110.0(10)	C(18A)-C(17A)-C(16A)	120.45(12)
C(10A)-C(11A)-H(11C)	111.1(10)	C(22A)-C(17A)-C(16A)	120.95(12)
H(11D)-C(11A)-H(11C)	105.9(14)	C(19A)-C(18A)-C(17A)	120.45(14)
C(11A)-C(12A)-C(13A)	112.24(12)	C(19A)-C(18A)-H(18A)	119.7(10)
C(11A)-C(12A)-H(12D)	108.8(10)	C(17A)-C(18A)-H(18A)	119.9(10)
C(13A)-C(12A)-H(12D)	109.1(10)	C(20A)-C(19A)-C(18A)	120.27(14)
C(11A)-C(12A)-H(12C)	110.6(10)	C(20A)-C(19A)-H(19A)	122.3(10)
C(13A)-C(12A)-H(12C)	108.7(10)	C(18A)-C(19A)-H(19A)	117.4(10)
H(12D)-C(12A)-H(12C)	107.3(14)	C(19A)-C(20A)-C(21A)	119.59(13)
C(14A)-C(13A)-C(12A)	110.28(12)	C(19A)-C(20A)-H(20A)	118.5(11)
C(14A)-C(13A)-H(13C)	109.2(10)	C(21A)-C(20A)-H(20A)	121.8(10)
C(12A)-C(13A)-H(13C)	111.5(10)	C(22A)-C(21A)-C(20A)	120.55(14)
C(14A)-C(13A)-H(13D)	108.9(11)	C(22A)-C(21A)-H(21A)	120.0(11)
C(12A)-C(13A)-H(13D)	112.3(10)	C(20A)-C(21A)-H(21A)	119.5(11)
H(13C)-C(13A)-H(13D)	104.5(14)	C(21A)-C(22A)-C(17A)	120.52(14)
C(15A)-C(14A)-C(13A)	114.01(12)	C(21A)-C(22A)-H(22A)	120.7(11)
C(15A)-C(14A)-C(9A)	110.53(11)	C(17A)-C(22A)-H(22A)	118.7(11)

Symmetry transformations used to generate equivalent atoms:

Table D-4. Anisotropic displacement parameters ($\text{\AA}^2 \times 10^3$) for yoon15. The anisotropic displacement factor exponent takes the form: $-2p^2[h^2 a^*2U^{11} + \dots + 2 h k a^* b^* U^{12}]$

U^{11}	U^{22}	U^{33}	U^{23}	U^{13}	U^{12}	
O(1)	23(1)	22(1)	20(1)	3(1)	-1(1)	2(1)
O(2)	27(1)	14(1)	17(1)	0(1)	7(1)	-2(1)
C(1)	20(1)	17(1)	20(1)	1(1)	4(1)	-4(1)
C(2)	21(1)	19(1)	28(1)	0(1)	5(1)	-2(1)
C(3)	27(1)	22(1)	30(1)	-6(1)	11(1)	-4(1)
C(4)	29(1)	31(1)	19(1)	-5(1)	8(1)	-7(1)
C(5)	23(1)	25(1)	19(1)	1(1)	2(1)	-5(1)
C(6)	16(1)	17(1)	18(1)	1(1)	3(1)	-4(1)
C(7)	16(1)	15(1)	19(1)	2(1)	2(1)	-5(1)
C(8)	17(1)	15(1)	18(1)	2(1)	1(1)	-1(1)
C(9)	16(1)	16(1)	18(1)	1(1)	1(1)	0(1)
C(10)	20(1)	15(1)	22(1)	1(1)	3(1)	0(1)
C(11)	22(1)	16(1)	31(1)	1(1)	5(1)	1(1)
C(12)	28(1)	17(1)	32(1)	-3(1)	10(1)	2(1)
C(13)	26(1)	21(1)	22(1)	-1(1)	7(1)	1(1)
C(14)	19(1)	18(1)	17(1)	-1(1)	2(1)	0(1)
C(15)	20(1)	19(1)	16(1)	2(1)	3(1)	0(1)
C(16)	18(1)	19(1)	16(1)	2(1)	1(1)	0(1)
C(17)	19(1)	17(1)	14(1)	2(1)	-2(1)	0(1)
C(18)	20(1)	22(1)	18(1)	2(1)	-2(1)	0(1)
C(19)	25(1)	26(1)	20(1)	7(1)	-4(1)	-8(1)
C(20)	34(1)	18(1)	22(1)	4(1)	-9(1)	-5(1)
C(21)	30(1)	19(1)	19(1)	-2(1)	-6(1)	2(1)
C(22)	23(1)	20(1)	16(1)	0(1)	-2(1)	-1(1)
O(1A)	22(1)	22(1)	20(1)	-3(1)	1(1)	-4(1)
O(2A)	27(1)	14(1)	17(1)	0(1)	8(1)	2(1)
C(1A)	19(1)	18(1)	17(1)	0(1)	2(1)	3(1)
C(2A)	19(1)	18(1)	24(1)	1(1)	1(1)	0(1)
C(3A)	24(1)	22(1)	26(1)	7(1)	4(1)	-1(1)
C(4A)	30(1)	31(1)	19(1)	7(1)	2(1)	-4(1)
C(5A)	23(1)	24(1)	19(1)	1(1)	-1(1)	0(1)
C(6A)	16(1)	16(1)	19(1)	0(1)	2(1)	3(1)
C(7A)	15(1)	15(1)	19(1)	-1(1)	2(1)	4(1)
C(8A)	18(1)	14(1)	18(1)	-1(1)	3(1)	1(1)
C(9A)	16(1)	16(1)	17(1)	0(1)	1(1)	1(1)
C(10A)	20(1)	16(1)	21(1)	-1(1)	3(1)	1(1)
C(11A)	21(1)	15(1)	26(1)	-1(1)	3(1)	-1(1)
C(12A)	26(1)	17(1)	25(1)	3(1)	5(1)	-3(1)
C(13A)	24(1)	18(1)	19(1)	0(1)	5(1)	-4(1)
C(14A)	19(1)	16(1)	16(1)	2(1)	2(1)	0(1)
C(15A)	20(1)	17(1)	16(1)	-1(1)	4(1)	0(1)
C(16A)	16(1)	18(1)	16(1)	-2(1)	2(1)	0(1)
C(17A)	19(1)	16(1)	14(1)	-1(1)	-1(1)	0(1)
C(18A)	21(1)	19(1)	16(1)	2(1)	0(1)	0(1)
C(19A)	25(1)	18(1)	21(1)	3(1)	-3(1)	-3(1)
C(20A)	32(1)	18(1)	23(1)	-2(1)	-3(1)	2(1)
C(21A)	27(1)	23(1)	20(1)	-4(1)	2(1)	5(1)
C(22A)	20(1)	21(1)	18(1)	-1(1)	2(1)	0(1)

Table D-5. Hydrogen coordinates ($\times 10^4$) and isotropic displacement parameters ($\text{\AA}^2 \times 10^3$) for yoon15.

x	y	z	U(eq)	
H(1)	9973(17)	7457(9)	2739(9)	23
H(2)	11398(19)	6671(10)	2135(9)	27
H(3)	11037(18)	6573(10)	917(9)	31
H(4)	9224(19)	7306(10)	299(10)	31
H(5)	7809(19)	8086(10)	867(9)	27
H(8)	8956(18)	8427(9)	3190(8)	20
H(9)	6111(18)	8841(9)	3081(8)	20
H(10B)	8467(19)	9789(9)	3390(9)	23
H(10A)	7509(18)	9812(9)	2661(9)	23
H(11A)	5540(20)	10173(10)	3221(9)	27
H(11B)	6779(18)	10768(10)	3407(9)	27
H(12B)	7420(20)	10232(10)	4505(9)	30
H(12A)	5789(19)	10438(11)	4424(9)	30
H(13A)	5158(19)	9189(10)	4184(9)	27
H(13B)	6199(18)	9201(10)	4878(9)	27
H(14)	8113(18)	8938(9)	4283(8)	22
H(15)	6687(18)	7843(9)	4644(9)	22
H(18)	5283(19)	6742(10)	4409(9)	25
H(19)	5057(19)	5479(10)	4574(9)	29
H(20)	6519(18)	4615(10)	4135(9)	31
H(21)	8296(19)	5071(10)	3487(9)	28
H(22)	8552(18)	6332(9)	3317(9)	24
H(1A)	4886(17)	5958(9)	2747(9)	22
H(2A)	6358(19)	6731(10)	2185(9)	24
H(3A)	6177(18)	6762(10)	984(9)	29
H(4A)	4497(19)	5995(10)	329(10)	32
H(5A)	2953(19)	5235(10)	881(9)	26
H(8A)	3904(18)	4984(9)	3192(9)	20
H(9A)	1018(18)	4552(9)	3064(8)	19
H(10D)	3397(18)	3618(9)	3397(9)	23
H(10C)	2490(18)	3591(9)	2658(9)	23
H(11D)	483(19)	3206(9)	3164(9)	25
H(11C)	1695(18)	2634(10)	3356(9)	25
H(12D)	2269(19)	3145(10)	4460(9)	27
H(12C)	634(19)	2951(10)	4365(9)	27
H(13C)	45(18)	4207(10)	4155(9)	24
H(13D)	1052(18)	4172(10)	4838(9)	24
H(14A)	2989(17)	4458(9)	4271(8)	21
H(15A)	1562(17)	5533(9)	4637(9)	21
H(18A)	3463(18)	7055(9)	3302(9)	23
H(19A)	3340(18)	8315(10)	3530(9)	26
H(20A)	1723(19)	8776(11)	4257(9)	30
H(21A)	222(19)	7923(10)	4723(9)	28
H(22A)	332(18)	6659(10)	4484(9)	24

Table D-6. Torsion angles [°] for yoon15

C(6)-C(1)-C(2)-C(3)	-0.3(2)	C(6A)-C(1A)-C(2A)-C(3A)	-0.6(2)
C(1)-C(2)-C(3)-C(4)	0.0(2)	C(1A)-C(2A)-C(3A)-C(4A)	-0.3(2)
C(2)-C(3)-C(4)-C(5)	0.3(2)	C(2A)-C(3A)-C(4A)-C(5A)	1.1(2)
C(3)-C(4)-C(5)-C(6)	-0.3(2)	C(3A)-C(4A)-C(5A)-C(6A)	-1.0(2)
C(2)-C(1)-C(6)-C(5)	0.3(2)	C(4A)-C(5A)-C(6A)-C(1A)	0.1(2)
C(2)-C(1)-C(6)-C(7)	-179.13(12)	C(4A)-C(5A)-C(6A)-C(7A)	-178.79(13)
C(4)-C(5)-C(6)-C(1)	0.0(2)	C(2A)-C(1A)-C(6A)-C(5A)	0.7(2)
C(4)-C(5)-C(6)-C(7)	179.43(13)	C(2A)-C(1A)-C(6A)-C(7A)	179.51(12)
C(1)-C(6)-C(7)-O(1)	174.78(13)	C(5A)-C(6A)-C(7A)-O(1A)	0.27(19)
C(5)-C(6)-C(7)-O(1)	-4.63(19)	C(1A)-C(6A)-C(7A)-O(1A)	-178.55(13)
C(1)-C(6)-C(7)-C(8)	-7.08(18)	C(5A)-C(6A)-C(7A)-C(8A)	-178.68(11)
C(5)-C(6)-C(7)-C(8)	173.52(12)	C(1A)-C(6A)-C(7A)-C(8A)	2.51(18)
C(16)-O(2)-C(8)-C(9)	-36.52(15)	C(16A)-O(2A)-C(8A)-C(9A)	37.74(15)
C(16)-O(2)-C(8)-C(7)	-159.56(10)	C(16A)-O(2A)-C(8A)-C(7A)	161.04(10)
O(1)-C(7)-C(8)-O(2)	116.84(13)	O(1A)-C(7A)-C(8A)-O(2A)	-115.56(13)
C(6)-C(7)-C(8)-O(2)	-61.31(14)	C(6A)-C(7A)-C(8A)-O(2A)	63.39(13)
O(1)-C(7)-C(8)-C(9)	-5.01(17)	O(1A)-C(7A)-C(8A)-C(9A)	6.69(17)
C(6)-C(7)-C(8)-C(9)	176.83(11)	C(6A)-C(7A)-C(8A)-C(9A)	-174.36(11)
O(2)-C(8)-C(9)-C(10)	178.42(10)	O(2A)-C(8A)-C(9A)-C(10A)	-178.15(10)
C(7)-C(8)-C(9)-C(10)	-65.65(14)	C(7A)-C(8A)-C(9A)-C(10A)	65.44(14)
O(2)-C(8)-C(9)-C(14)	57.08(14)	O(2A)-C(8A)-C(9A)-C(14A)	-57.06(14)
C(7)-C(8)-C(9)-C(14)	173.01(10)	C(7A)-C(8A)-C(9A)-C(14A)	-173.47(10)
C(8)-C(9)-C(10)-C(11)	179.08(11)	C(8A)-C(9A)-C(10A)-C(11A)	-178.41(11)
C(14)-C(9)-C(10)-C(11)	-59.69(14)	C(14A)-C(9A)-C(10A)-C(11A)	60.68(14)
C(9)-C(10)-C(11)-C(12)	56.88(15)	C(9A)-C(10A)-C(11A)-C(12A)	-56.61(15)
C(10)-C(11)-C(12)-C(13)	-54.10(16)	C(10A)-C(11A)-C(12A)-C(13A)	53.11(16)
C(11)-C(12)-C(13)-C(14)	54.40(16)	C(11A)-C(12A)-C(13A)-C(14A)	-53.27(16)
C(12)-C(13)-C(14)-C(15)	176.99(12)	C(12A)-C(13A)-C(14A)-C(15A)	-177.28(11)
C(12)-C(13)-C(14)-C(9)	-58.29(15)	C(12A)-C(13A)-C(14A)-C(9A)	57.73(15)
C(8)-C(9)-C(14)-C(15)	-48.12(14)	C(8A)-C(9A)-C(14A)-C(15A)	47.46(14)
C(10)-C(9)-C(14)-C(15)	-172.39(11)	C(10A)-C(9A)-C(14A)-C(15A)	171.25(11)
C(8)-C(9)-C(14)-C(13)	-174.92(11)	C(8A)-C(9A)-C(14A)-C(13A)	174.42(11)
C(10)-C(9)-C(14)-C(13)	60.81(14)	C(10A)-C(9A)-C(14A)-C(13A)	-61.80(14)
C(13)-C(14)-C(15)-C(16)	146.18(14)	C(13A)-C(14A)-C(15A)-C(16A)	-146.33(13)
C(9)-C(14)-C(15)-C(16)	21.43(18)	C(9A)-C(14A)-C(15A)-C(16A)	-21.50(18)
C(14)-C(15)-C(16)-O(2)	0.9(2)	C(14A)-C(15A)-C(16A)-O(2A)	0.5(2)
C(14)-C(15)-C(16)-C(17)	179.90(12)	C(14A)-C(15A)-C(16A)-C(17A)	-177.56(12)
C(8)-O(2)-C(16)-C(15)	6.61(18)	C(8A)-O(2A)-C(16A)-C(15A)	-8.50(18)
C(8)-O(2)-C(16)-C(17)	-172.57(10)	C(8A)-O(2A)-C(16A)-C(17A)	169.78(10)
C(15)-C(16)-C(17)-C(22)	-146.37(14)	C(15A)-C(16A)-C(17A)-C(18A)	148.82(14)
O(2)-C(16)-C(17)-C(22)	32.78(16)	O(2A)-C(16A)-C(17A)-C(18A)	-29.42(16)
C(15)-C(16)-C(17)-C(18)	33.3(2)	C(15A)-C(16A)-C(17A)-C(22A)	-30.3(2)
O(2)-C(16)-C(17)-C(18)	-147.52(12)	O(2A)-C(16A)-C(17A)-C(22A)	151.49(12)
C(22)-C(17)-C(18)-C(19)	-0.44(19)	C(22A)-C(17A)-C(18A)-C(19A)	1.74(19)
C(16)-C(17)-C(18)-C(19)	179.85(12)	C(16A)-C(17A)-C(18A)-C(19A)	-177.37(12)
C(17)-C(18)-C(19)-C(20)	1.3(2)	C(17A)-C(18A)-C(19A)-C(20A)	-1.6(2)
C(18)-C(19)-C(20)-C(21)	-0.7(2)	C(18A)-C(19A)-C(20A)-C(21A)	0.5(2)
C(19)-C(20)-C(21)-C(22)	-0.8(2)	C(19A)-C(20A)-C(21A)-C(22A)	0.6(2)
C(20)-C(21)-C(22)-C(17)	1.7(2)	C(20A)-C(21A)-C(22A)-C(17A)	-0.4(2)
C(18)-C(17)-C(22)-C(21)	-1.06(19)	C(18A)-C(17A)-C(22A)-C(21A)	-0.72(19)
C(16)-C(17)-C(22)-C(21)	178.65(12)	C(16A)-C(17A)-C(22A)-C(21A)	178.38(12)

Symmetry transformations used to generate equivalent atoms:

D.2 Characterization of D.1 (yoon27)

Data Collection

A colorless crystal with approximate dimensions $0.68 \times 0.51 \times 0.48 \text{ mm}^3$ was selected under oil under ambient conditions and attached to the tip of a MiTeGen MicroMount©. The crystal was mounted in a stream of cold nitrogen at 100(1) K and centered in the X-ray beam by using a video camera.

The crystal evaluation and data collection were performed on a Bruker SMART APEXII diffractometer with $\text{Cu K}\alpha$ ($\lambda = 1.54178 \text{ \AA}$) radiation and the diffractometer to crystal distance of 4.02 cm.

The initial cell constants were obtained from three series of ω scans at different starting angles. Each series consisted of 41 frames collected at intervals of 0.6° in a 25° range about ω with the exposure time of 2 seconds per frame. The reflections were successfully indexed by an automated indexing routine built in the APEXII program. The final cell constants were calculated from a set of 9982 strong reflections from the actual data collection.

The data were collected by using the full sphere data collection routine to survey the reciprocal space to the extent of a full sphere to a resolution of 0.81 \AA . A total of 26521 data were harvested by collecting 27 sets of frames with 0.7° scans in ω with an exposure time 3-7 sec per frame. These highly redundant datasets were corrected for Lorentz and polarization effects. The absorption correction was based on fitting a function to the empirical transmission surface as sampled by multiple equivalent measurements.¹

Structure Solution and Refinement

The systematic absences in the diffraction data were consistent for the space groups *Ia* and *I2/a*. The *E*-statistics suggested the non-centrosymmetric space group *Ia* that yielded chemically reasonable and computationally stable results of refinement.²⁻⁴

A successful solution by the direct methods provided most non-hydrogen atoms from the *E*-map. The remaining non-hydrogen atoms were located in an alternating series of least-squares cycles and difference Fourier maps. All non-hydrogen atoms were refined with anisotropic displacement coefficients. All hydrogen atoms were included in the structure factor calculation at idealized positions and were allowed to ride on the neighboring atoms with relative isotropic displacement coefficients.

The final least-squares refinement of 318 parameters against 4270 data resulted in residuals *R* (based on F^2 for $I \geq 2\sigma$) and *wR* (based on F^2 for all data) of 0.0284 and 0.0759, respectively. The final difference Fourier map was featureless.

The molecular diagram is drawn with 50% probability ellipsoids.

References

1. Bruker-AXS. (2007) APEX2, SADABS, and SAINT Software Reference Manuals. Bruker-AXS, Madison, Wisconsin, USA.
2. Sheldrick, G. M. (2008) SHELXL. *Acta Cryst.* **A64**, 112-122.
3. Dolomanov, O.V.; Bourhis, L.J.; Gildea, R.J.; Howard, J.A.K.; Puschmann, H. "OLEX2: a complete structure solution, refinement and analysis program". *J. Appl. Cryst.* (2009) **42**, 339-341.
4. Guzei, I.A. (2006-2008). Internal laboratory computer programs "Inserter", "FCF_filter", "Modicifer".

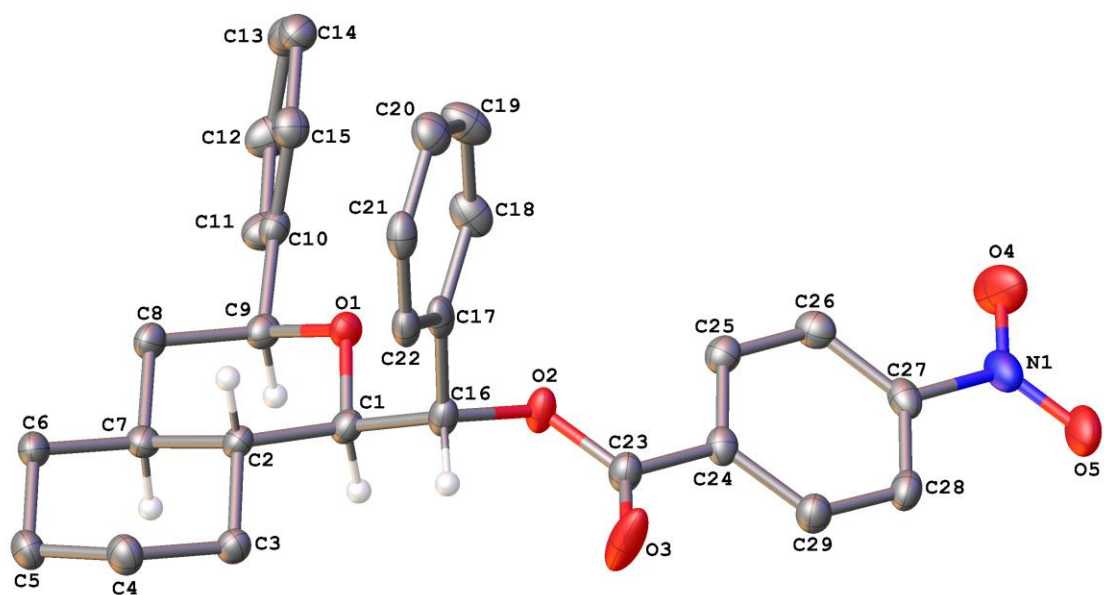


Figure D-3. A molecular drawing of yoon27. The H atoms on the non-chiral C atoms are omitted.

Table D-7. Crystal data and structure refinement for yoon27

Identification code	yoon27	
Empirical formula	C ₂₉ H ₂₉ N O ₅	
Formula weight	471.53	
Temperature	100(2) K	
Wavelength	1.54178 Å	
Crystal system	Monoclinic	
Space group	Ia	
Unit cell dimensions	a = 8.7727(2) Å	α = 90°.
	b = 27.9624(7) Å	β = 91.8390(10)°.
	c = 9.8321(4) Å	γ = 90°.
Volume	2410.63(13) Å ³	
Z	4	
Density (calculated)	1.299 Mg/m ³	
Absorption coefficient	0.717 mm ⁻¹	
F(000)	1000	
Crystal size	0.68 x 0.51 x 0.48 mm ³	
Theta range for data collection	3.16 to 71.67°.	
Index ranges	-10 ≤ h ≤ 10, -34 ≤ k ≤ 33, -11 ≤ l ≤ 12	
Reflections collected	26521	
Independent reflections	4270 [R(int) = 0.0237]	
Completeness to theta = 67.00°	99.8 %	
Absorption correction	Numerical with SADABS	
Max. and min. transmission	0.7257 and 0.6426	
Refinement method	Full-matrix least-squares on F ²	
Data / restraints / parameters	4270 / 2 / 318	
Goodness-of-fit on F ²	1.051	
Final R indices [I > 2σ(I)]	R1 = 0.0284, wR2 = 0.0758	
R indices (all data)	R1 = 0.0285, wR2 = 0.0759	
Absolute structure parameter Flack x	-0.08(12)	
Absolute structure parameter Hoof t y	-0.02(3)	
Extinction coefficient	0.00075(10)	
Largest diff. peak and hole	0.193 and -0.182 e.Å ⁻³	

Table D-8. Atomic coordinates ($\times 10^4$) and equivalent isotropic displacement parameters ($\text{\AA}^2 \times 10^3$) for yoon27. $U(\text{eq})$ is defined as one third of the trace of the orthogonalized U_{ij} tensor.

x	y	z	U(eq)	
O(1)	8132(1)	3644(1)	5502(1)	20(1)
O(2)	5462(1)	3717(1)	6859(1)	25(1)
O(3)	3763(2)	3352(1)	8160(2)	52(1)
O(4)	3220(2)	5917(1)	8909(1)	50(1)
O(5)	1843(1)	5608(1)	10463(1)	37(1)
N(1)	2716(2)	5577(1)	9520(1)	29(1)
C(1)	7593(2)	3241(1)	6234(1)	20(1)
C(2)	8181(2)	2771(1)	5646(1)	18(1)
C(3)	7660(2)	2327(1)	6418(1)	22(1)
C(4)	8235(2)	1870(1)	5750(2)	25(1)
C(5)	9968(2)	1874(1)	5641(2)	27(1)
C(6)	10521(2)	2327(1)	4942(1)	24(1)
C(7)	9934(2)	2782(1)	5616(1)	20(1)
C(8)	10461(2)	3235(1)	4911(1)	22(1)
C(9)	9760(1)	3679(1)	5545(1)	20(1)
C(10)	10176(2)	4130(1)	4798(1)	21(1)
C(11)	11327(2)	4427(1)	5318(1)	28(1)
C(12)	11771(2)	4833(1)	4619(2)	31(1)
C(13)	11049(2)	4950(1)	3387(2)	28(1)
C(14)	9902(2)	4657(1)	2868(2)	26(1)
C(15)	9466(2)	4248(1)	3558(1)	24(1)
C(16)	5853(2)	3270(1)	6182(1)	21(1)
C(17)	5133(1)	3274(1)	4767(2)	22(1)
C(18)	5099(2)	3691(1)	3980(2)	28(1)
C(19)	4467(2)	3687(1)	2674(2)	33(1)
C(20)	3840(2)	3270(1)	2130(2)	28(1)
C(21)	3849(2)	2856(1)	2902(2)	25(1)
C(22)	4500(2)	2858(1)	4210(1)	22(1)
C(23)	4385(2)	3705(1)	7768(1)	23(1)
C(24)	4007(2)	4201(1)	8240(1)	20(1)
C(25)	4558(2)	4603(1)	7582(1)	22(1)
C(26)	4130(2)	5055(1)	7999(2)	24(1)
C(27)	3175(2)	5092(1)	9083(1)	23(1)
C(28)	2618(2)	4700(1)	9764(1)	24(1)
C(29)	3035(2)	4249(1)	9325(1)	24(1)

Table D-9. Bond lengths [Å] and angles [°] for yoon27

O(1)-C(1)	1.4258(15)	C(10)-C(11)	1.3918(19)
O(1)-C(9)	1.4315(15)	C(11)-C(12)	1.389(2)
O(2)-C(23)	1.3216(17)	C(11)-H(11)	0.9500
O(2)-C(16)	1.4603(15)	C(12)-C(13)	1.387(2)
O(3)-C(23)	1.1976(18)	C(12)-H(12)	0.9500
O(4)-N(1)	1.2159(19)	C(13)-C(14)	1.381(2)
O(5)-N(1)	1.2250(18)	C(13)-H(13)	0.9500
N(1)-C(27)	1.4821(16)	C(14)-C(15)	1.3899(19)
C(1)-C(16)	1.5275(19)	C(14)-H(14)	0.9500
C(1)-C(2)	1.5311(17)	C(15)-H(15)	0.9500
C(1)-H(1)	1.0000	C(16)-C(17)	1.5100(19)
C(2)-C(3)	1.5337(17)	C(16)-H(16)	1.0000
C(2)-C(7)	1.5398(17)	C(17)-C(22)	1.3931(19)
C(2)-H(2)	1.0000	C(17)-C(18)	1.3990(19)
C(3)-C(4)	1.5288(18)	C(18)-C(19)	1.382(2)
C(3)-H(3A)	0.9900	C(18)-H(18)	0.9500
C(3)-H(3B)	0.9900	C(19)-C(20)	1.388(2)
C(4)-C(5)	1.527(2)	C(19)-H(19)	0.9500
C(4)-H(4A)	0.9900	C(20)-C(21)	1.385(2)
C(4)-H(4B)	0.9900	C(20)-H(20)	0.9500
C(5)-C(6)	1.5283(19)	C(21)-C(22)	1.391(2)
C(5)-H(5A)	0.9900	C(21)-H(21)	0.9500
C(5)-H(5B)	0.9900	C(22)-H(22)	0.9500
C(6)-C(7)	1.5301(18)	C(23)-C(24)	1.5009(18)
C(6)-H(6A)	0.9900	C(24)-C(25)	1.3913(19)
C(6)-H(6B)	0.9900	C(24)-C(29)	1.394(2)
C(7)-C(8)	1.5231(18)	C(25)-C(26)	1.3855(18)
C(7)-H(7)	1.0000	C(25)-H(25)	0.9500
C(8)-C(9)	1.5272(18)	C(26)-C(27)	1.380(2)
C(8)-H(8A)	0.9900	C(26)-H(26)	0.9500
C(8)-H(8B)	0.9900	C(27)-C(28)	1.383(2)
C(9)-C(10)	1.5098(17)	C(28)-C(29)	1.3843(19)
C(9)-H(9)	1.0000	C(28)-H(28)	0.9500
C(10)-C(15)	1.3902(19)	C(29)-H(29)	0.9500
C(1)-O(1)-C(9)	112.77(10)	C(2)-C(3)-H(3A)	109.5
C(23)-O(2)-C(16)	118.11(10)	C(4)-C(3)-H(3B)	109.5
O(4)-N(1)-O(5)	124.42(12)	C(2)-C(3)-H(3B)	109.5
O(4)-N(1)-C(27)	117.78(13)	H(3A)-C(3)-H(3B)	108.0
O(5)-N(1)-C(27)	117.80(12)	C(5)-C(4)-C(3)	111.51(12)
O(1)-C(1)-C(16)	106.73(10)	C(5)-C(4)-H(4A)	109.3
O(1)-C(1)-C(2)	111.48(10)	C(3)-C(4)-H(4A)	109.3
C(16)-C(1)-C(2)	112.45(10)	C(5)-C(4)-H(4B)	109.3
O(1)-C(1)-H(1)	108.7	C(3)-C(4)-H(4B)	109.3
C(16)-C(1)-H(1)	108.7	H(4A)-C(4)-H(4B)	108.0
C(2)-C(1)-H(1)	108.7	C(4)-C(5)-C(6)	111.69(11)
C(1)-C(2)-C(3)	113.53(10)	C(4)-C(5)-H(5A)	109.3
C(1)-C(2)-C(7)	109.85(10)	C(6)-C(5)-H(5A)	109.3
C(3)-C(2)-C(7)	109.83(10)	C(4)-C(5)-H(5B)	109.3
C(1)-C(2)-H(2)	107.8	C(6)-C(5)-H(5B)	109.3
C(3)-C(2)-H(2)	107.8	H(5A)-C(5)-H(5B)	107.9
C(7)-C(2)-H(2)	107.8	C(5)-C(6)-C(7)	112.23(11)
C(4)-C(3)-C(2)	110.93(11)	C(5)-C(6)-H(6A)	109.2
C(4)-C(3)-H(3A)	109.5	C(7)-C(6)-H(6A)	109.2

C(5)-C(6)-H(6B)	109.2	O(2)-C(16)-H(16)	109.1
C(7)-C(6)-H(6B)	109.2	C(17)-C(16)-H(16)	109.1
H(6A)-C(6)-H(6B)	107.9	C(1)-C(16)-H(16)	109.1
C(8)-C(7)-C(6)	112.54(10)	C(22)-C(17)-C(18)	118.52(13)
C(8)-C(7)-C(2)	110.07(10)	C(22)-C(17)-C(16)	120.37(12)
C(6)-C(7)-C(2)	110.05(10)	C(18)-C(17)-C(16)	121.11(12)
C(8)-C(7)-H(7)	108.0	C(19)-C(18)-C(17)	120.50(13)
C(6)-C(7)-H(7)	108.0	C(19)-C(18)-H(18)	119.7
C(2)-C(7)-H(7)	108.0	C(17)-C(18)-H(18)	119.7
C(7)-C(8)-C(9)	111.04(11)	C(18)-C(19)-C(20)	120.48(13)
C(7)-C(8)-H(8A)	109.4	C(18)-C(19)-H(19)	119.8
C(9)-C(8)-H(8A)	109.4	C(20)-C(19)-H(19)	119.8
C(7)-C(8)-H(8B)	109.4	C(21)-C(20)-C(19)	119.70(14)
C(9)-C(8)-H(8B)	109.4	C(21)-C(20)-H(20)	120.2
H(8A)-C(8)-H(8B)	108.0	C(19)-C(20)-H(20)	120.2
O(1)-C(9)-C(10)	107.46(10)	C(20)-C(21)-C(22)	119.90(13)
O(1)-C(9)-C(8)	110.27(10)	C(20)-C(21)-H(21)	120.1
C(10)-C(9)-C(8)	111.97(10)	C(22)-C(21)-H(21)	120.1
O(1)-C(9)-H(9)	109.0	C(21)-C(22)-C(17)	120.90(13)
C(10)-C(9)-H(9)	109.0	C(21)-C(22)-H(22)	119.6
C(8)-C(9)-H(9)	109.0	C(17)-C(22)-H(22)	119.6
C(15)-C(10)-C(11)	118.68(12)	O(3)-C(23)-O(2)	125.46(12)
C(15)-C(10)-C(9)	121.07(11)	O(3)-C(23)-C(24)	123.61(13)
C(11)-C(10)-C(9)	120.21(12)	O(2)-C(23)-C(24)	110.92(11)
C(12)-C(11)-C(10)	121.14(12)	C(25)-C(24)-C(29)	120.44(12)
C(12)-C(11)-H(11)	119.4	C(25)-C(24)-C(23)	121.24(12)
C(10)-C(11)-H(11)	119.4	C(29)-C(24)-C(23)	118.27(12)
C(13)-C(12)-C(11)	119.77(13)	C(26)-C(25)-C(24)	119.95(13)
C(13)-C(12)-H(12)	120.1	C(26)-C(25)-H(25)	120.0
C(11)-C(12)-H(12)	120.1	C(24)-C(25)-H(25)	120.0
C(14)-C(13)-C(12)	119.34(13)	C(27)-C(26)-C(25)	118.26(13)
C(14)-C(13)-H(13)	120.3	C(27)-C(26)-H(26)	120.9
C(12)-C(13)-H(13)	120.3	C(25)-C(26)-H(26)	120.9
C(13)-C(14)-C(15)	121.02(13)	C(26)-C(27)-C(28)	123.17(12)
C(13)-C(14)-H(14)	119.5	C(26)-C(27)-N(1)	118.00(12)
C(15)-C(14)-H(14)	119.5	C(28)-C(27)-N(1)	118.82(12)
C(14)-C(15)-C(10)	120.04(12)	C(27)-C(28)-C(29)	118.03(13)
C(14)-C(15)-H(15)	120.0	C(27)-C(28)-H(28)	121.0
C(10)-C(15)-H(15)	120.0	C(29)-C(28)-H(28)	121.0
O(2)-C(16)-C(17)	108.45(10)	C(28)-C(29)-C(24)	120.13(13)
O(2)-C(16)-C(1)	106.24(10)	C(28)-C(29)-H(29)	119.9
C(17)-C(16)-C(1)	114.76(11)	C(24)-C(29)-H(29)	119.9

Symmetry transformations used to generate equivalent atoms:

Table D-10. Anisotropic displacement parameters ($\text{\AA}^2 \times 10^3$) for yoon27. The anisotropic displacement factor exponent takes the form: $-2p^2[h^2 a^*2U^{11} + \dots + 2 h k a^* b^* U^{12}]$

	U ¹¹	U ²²	U ³³	U ²³	U ¹³	U ¹²
O(1)	17(1)	20(1)	24(1)	2(1)	4(1)	0(1)
O(2)	24(1)	18(1)	34(1)	-4(1)	13(1)	0(1)
O(3)	71(1)	21(1)	68(1)	-6(1)	52(1)	-6(1)
O(4)	85(1)	21(1)	45(1)	-2(1)	15(1)	7(1)
O(5)	44(1)	34(1)	33(1)	-10(1)	3(1)	15(1)
N(1)	38(1)	24(1)	25(1)	-6(1)	-5(1)	10(1)
C(1)	21(1)	20(1)	18(1)	-1(1)	4(1)	0(1)
C(2)	18(1)	20(1)	16(1)	0(1)	4(1)	1(1)
C(3)	22(1)	21(1)	22(1)	2(1)	5(1)	1(1)
C(4)	26(1)	21(1)	30(1)	0(1)	3(1)	2(1)
C(5)	27(1)	24(1)	30(1)	2(1)	4(1)	8(1)
C(6)	21(1)	26(1)	23(1)	3(1)	4(1)	7(1)
C(7)	20(1)	24(1)	18(1)	2(1)	0(1)	3(1)
C(8)	17(1)	26(1)	23(1)	2(1)	4(1)	2(1)
C(9)	17(1)	25(1)	19(1)	1(1)	1(1)	0(1)
C(10)	17(1)	24(1)	21(1)	-2(1)	4(1)	1(1)
C(11)	26(1)	35(1)	23(1)	2(1)	-2(1)	-5(1)
C(12)	29(1)	36(1)	28(1)	0(1)	0(1)	-13(1)
C(13)	29(1)	25(1)	30(1)	3(1)	8(1)	-1(1)
C(14)	24(1)	30(1)	25(1)	3(1)	1(1)	3(1)
C(15)	19(1)	26(1)	27(1)	-2(1)	0(1)	-1(1)
C(16)	20(1)	16(1)	27(1)	-1(1)	9(1)	0(1)
C(17)	13(1)	21(1)	32(1)	0(1)	7(1)	2(1)
C(18)	25(1)	20(1)	40(1)	1(1)	-3(1)	-3(1)
C(19)	30(1)	26(1)	44(1)	10(1)	-6(1)	-3(1)
C(20)	22(1)	31(1)	32(1)	1(1)	-1(1)	2(1)
C(21)	16(1)	22(1)	37(1)	-6(1)	5(1)	1(1)
C(22)	17(1)	19(1)	30(1)	0(1)	8(1)	3(1)
C(23)	23(1)	21(1)	27(1)	-2(1)	6(1)	1(1)
C(24)	17(1)	22(1)	23(1)	-4(1)	0(1)	2(1)
C(25)	21(1)	24(1)	21(1)	-3(1)	1(1)	-1(1)
C(26)	27(1)	21(1)	24(1)	0(1)	-2(1)	-1(1)
C(27)	23(1)	22(1)	24(1)	-5(1)	-6(1)	6(1)
C(28)	22(1)	29(1)	22(1)	-4(1)	3(1)	5(1)
C(29)	23(1)	22(1)	26(1)	0(1)	4(1)	1(1)

Table D-11. Hydrogen coordinates ($\times 10^4$) and isotropic displacement parameters ($\text{\AA}^2 \times 10^{-3}$) for yoon27

	x	y	z	U(eq)
H(1)	7962	3267	7204	23
H(2)	7778	2745	4686	22
H(3A)	8054	2342	7372	26
H(3B)	6532	2320	6428	26
H(4A)	7930	1590	6294	30
H(4B)	7755	1838	4830	30
H(5A)	10288	1591	5118	32
H(5B)	10448	1852	6564	32
H(6A)	10173	2323	3975	28
H(6B)	11650	2331	4973	28
H(7)	10342	2789	6577	25
H(8A)	10162	3220	3932	26
H(8B)	11587	3257	4988	26
H(9)	10131	3706	6514	24
H(11)	11817	4351	6166	34
H(12)	12566	5030	4983	37
H(13)	11340	5228	2905	33
H(14)	9405	4737	2026	31
H(15)	8682	4049	3183	29
H(16)	5432	2996	6703	25
H(18)	5514	3979	4346	34
H(19)	4461	3972	2146	40
H(20)	3408	3270	1231	34
H(21)	3411	2571	2538	30
H(22)	4512	2572	4732	26
H(25)	5226	4567	6848	26
H(26)	4485	5333	7551	29
H(28)	1969	4738	10511	29
H(29)	2657	3973	9764	29

Table D-12. Torsion angles [°] for yoon27

C(9)-O(1)-C(1)-C(16)	176.13(10)	O(1)-C(1)-C(16)-O(2)	-61.44(12)
C(9)-O(1)-C(1)-C(2)	-60.72(13)	C(2)-C(1)-C(16)-O(2)	176.02(10)
O(1)-C(1)-C(2)-C(3)	178.77(10)	O(1)-C(1)-C(16)-C(17)	58.38(13)
C(16)-C(1)-C(2)-C(3)	-61.41(14)	C(2)-C(1)-C(16)-C(17)	-64.16(14)
O(1)-C(1)-C(2)-C(7)	55.36(13)	O(2)-C(16)-C(17)-C(22)	-140.96(12)
C(16)-C(1)-C(2)-C(7)	175.19(10)	C(1)-C(16)-C(17)-C(22)	100.46(14)
C(1)-C(2)-C(3)-C(4)	177.91(10)	O(2)-C(16)-C(17)-C(18)	39.67(17)
C(7)-C(2)-C(3)-C(4)	-58.67(14)	C(1)-C(16)-C(17)-C(18)	-78.92(16)
C(2)-C(3)-C(4)-C(5)	56.08(15)	C(22)-C(17)-C(18)-C(19)	-0.8(2)
C(3)-C(4)-C(5)-C(6)	-52.91(15)	C(16)-C(17)-C(18)-C(19)	178.57(14)
C(4)-C(5)-C(6)-C(7)	53.33(15)	C(17)-C(18)-C(19)-C(20)	0.7(2)
C(5)-C(6)-C(7)-C(8)	-179.10(11)	C(18)-C(19)-C(20)-C(21)	0.1(2)
C(5)-C(6)-C(7)-C(2)	-55.94(13)	C(19)-C(20)-C(21)-C(22)	-0.7(2)
C(1)-C(2)-C(7)-C(8)	-51.69(13)	C(20)-C(21)-C(22)-C(17)	0.7(2)
C(3)-C(2)-C(7)-C(8)	-177.24(10)	C(18)-C(17)-C(22)-C(21)	0.12(19)
C(1)-C(2)-C(7)-C(6)	-176.28(10)	C(16)-C(17)-C(22)-C(21)	-179.27(12)
C(3)-C(2)-C(7)-C(6)	58.17(13)	C(16)-O(2)-C(23)-O(3)	5.4(2)
C(6)-C(7)-C(8)-C(9)	175.88(10)	C(16)-O(2)-C(23)-C(24)	-173.47(10)
C(2)-C(7)-C(8)-C(9)	52.73(13)	O(3)-C(23)-C(24)-C(25)	-168.25(15)
C(1)-O(1)-C(9)-C(10)	-177.25(10)	O(2)-C(23)-C(24)-C(25)	10.62(17)
C(1)-O(1)-C(9)-C(8)	60.46(13)	O(3)-C(23)-C(24)-C(29)	9.2(2)
C(7)-C(8)-C(9)-O(1)	-56.28(13)	O(2)-C(23)-C(24)-C(29)	-171.94(12)
C(7)-C(8)-C(9)-C(10)	-175.88(10)	C(29)-C(24)-C(25)-C(26)	-0.47(18)
O(1)-C(9)-C(10)-C(15)	-44.53(16)	C(23)-C(24)-C(25)-C(26)	176.92(11)
C(8)-C(9)-C(10)-C(15)	76.70(15)	C(24)-C(25)-C(26)-C(27)	0.94(18)
O(1)-C(9)-C(10)-C(11)	137.97(13)	C(25)-C(26)-C(27)-C(28)	-0.45(19)
C(8)-C(9)-C(10)-C(11)	-100.80(15)	C(25)-C(26)-C(27)-N(1)	-179.69(11)
C(15)-C(10)-C(11)-C(12)	-0.3(2)	O(4)-N(1)-C(27)-C(26)	-0.83(19)
C(9)-C(10)-C(11)-C(12)	177.27(13)	O(5)-N(1)-C(27)-C(26)	178.48(12)
C(10)-C(11)-C(12)-C(13)	0.7(2)	O(4)-N(1)-C(27)-C(28)	179.89(13)
C(11)-C(12)-C(13)-C(14)	-0.5(2)	O(5)-N(1)-C(27)-C(28)	-0.79(18)
C(12)-C(13)-C(14)-C(15)	-0.2(2)	C(26)-C(27)-C(28)-C(29)	-0.51(19)
C(13)-C(14)-C(15)-C(10)	0.6(2)	N(1)-C(27)-C(28)-C(29)	178.72(12)
C(11)-C(10)-C(15)-C(14)	-0.4(2)	C(27)-C(28)-C(29)-C(24)	1.0(2)
C(9)-C(10)-C(15)-C(14)	-177.89(12)	C(25)-C(24)-C(29)-C(28)	-0.51(19)
C(23)-O(2)-C(16)-C(17)	102.98(13)	C(23)-C(24)-C(29)-C(28)	-177.98(12)
C(23)-O(2)-C(16)-C(1)	-133.17(12)		

Symmetry transformations used to generate equivalent atoms: